Helicobacter pylori: Cellular Immunity and Protection from Multiple Sclerosis

Harry Hassan Jenkins

Thesis submitted to the University of Nottingham for the degree of Doctor of Philosophy

July 2021

Declaration

Unless otherwise stated, the work presented in this thesis is my own. No part has been submitted for another degree at this, or any other institute of learning.

Harry Jenkins

July 2021

Dedicated to my family, especially my mum whose struggle with MS inspired this thesis.

To my Gran, who always supported me, I wish you were here to see this.

With a special dedication to my best friend, I miss you.

Acknowledgements

First and foremost, I would like to say thank you to my supervisor, Karen Robinson, for her guidance and support through my Ph.D.

I would like to thank the *Helicobacter* group; Dr Kazuyo Kaneko, Dr Darren Letley, Joanne Rhead, and our PhD and post-doctoral researchers

Dr Marie Dittmer, and Professor Denise Fitzgerald for their efforts and advice with our collaborative work

Jeni Luckett, for her assistance and advice with the imaging experiments

The Nottingham Digestive Diseases Biomedical Research Unit, staff, and patients who donated samples for my research

The Medical Research Council, and particularly the IMPACT Doctoral Training Partnership for giving me this opportunity

Abstract

Helicobacter pylori colonises the stomachs of almost half the world's population, subverting host immunity to usually establish a life-long infection. Although asymptomatic in most cases, peptic ulcer disease and gastric cancer develop in a minority of those colonised. Recently, more evidence is emerging that the reducing prevalence of infections in developed countries is linked with the stark rise of allergy, asthma, and autoimmune diseases such as multiple sclerosis (MS).

The 'Old friend's hypothesis', suggests that the lack of exposure to certain microbes, likely by increasing antibiotic use and improved sanitation, causes dysregulated immunity leading to immune and inflammatory conditions. The microbiota also regulates host immunity, during homeostasis and in the response to infection and susceptibility for disease development. The induction of tolerogenic dendritic cells and IL-10-producing regulatory T-cells, is an important *H. pylori* persistence mechanism. In the literature, these responses are also linked to the mitigation of extra-gastric diseases. Inadequate Treg responses are associated with a negative prognosis, especially in MS. This is the most common neurological condition affecting young adults, causing chronic progressive disability with a devastating impact on quality of life. Using the mouse model experimental autoimmune encephalomyelitis (EAE), the research group previously reported a reduced severity of EAE when infected with *H. pylori*.

For the current studies, it was hypothesised that protection from MS may be mediated through *H. pylori* modulation of the T-helper response. Gastric mucosal inflammation induced by *H. pylori* may alter lymphocyte homing patterns and reduce infiltration to the central nervous system. The regulatory T-cell response has previously been shown to facilitate repair in a demyelinated central nervous system by the secreted factor CCN3. This was proposed as a potential mechanism for *H. pylori* to mediate a protective effect in EAE or MS. Murine glia were cultured with CD4 supernatants to investigate the myelinating capacity of oligodendrocytes.

Firstly, differences in the peripheral blood T-helper and cytokine responses were investigated between infected and uninfected patients, and infected patients before and after *H. pylori* eradication therapy. Differences in IL-17A, IL-12p70 and IL-10 concentrations were detected according to presence of *H. pylori* infection and gastro-duodenal pathology. The $CD4^+$ T-helper cytokines *IL10* and *IL17A* were differentially expressed at the mRNA level in PBMCs between infected and uninfected patients. *IL10* mRNA was elevated following *H. pylori* eradication, concurrent with a reducing anti-*Hp* humoral IgG response. This indicates that the infection exerts important effects on the immune system.

Using the EAE model, a strain-specific mitigation of disease severity was observed when infected with *H. pylori* strain SS1 compared to PMSS1, independently of the CD4 T-helper subsets quantified. A fluorescence-based technique was developed for *in vivo* imaging of EAE $CD4^+$ T-cells adoptively transferred to infected or uninfected recipient mice. The $CD4^+$ T-cell populations from the spleens and mesenteric lymph nodes of *H. pylori* infected mice contained higher frequencies of both pro- and anti-inflammatory T-helper subsets. CCN3 *mRNA* was markedly elevated in cells from infected mice. There was a marked increase in myelin production from glia treated with supernatants from CD4 cells, and this was slightly higher using the cell supernatants from infected mice. The differences observed were modest, and further work is required to confirm and expand on these preliminary findings.

Table of Contents

Figures

Tables

Presented Research

Oral presentations

Peripheral Blood Cytokine Expression in *Helicobacter pylori* Infection and Disease
Harry Jenkins, Jody Winter, Darren Letley, John Atherton, Karen Robinson
13th International workshop on Pathogenesis and Host Response in *Helicobacter* Infections, Helsingor, Denmark; 2018
* Awarded the 'Best Oral Presentation' prize

Characterising Peripheral Immune Responses During *Helicobacter pylori* Infection and Eradication: Impact on the Potential Protection Associated with Infection?
Harry Jenkins, Jody Winter, Akanksha Thakkar, Kazuyo Kaneko, Darren Letley, John Atherton, Karen Robinson
Microbiology Society Conference, 2019, Belfast

Poster presentations

Characterising Peripheral Immune Responses During *Helicobacter pylori* Infection and Eradication: Impact on the Potential Protection Associated with Infection?

Harry Jenkins, Jody Winter, Akanksha Thakkar, Kazuyo Kaneko, Darren Letley, John Atherton, Karen Robinson
Microbiology Society Conference, 2019, Belfast

Peripheral Blood Cytokine Expression in *Helicobacter pylori* Infection and Disease
Harry Jenkins, Jody Winter, Darren Letley, John Atherton, Karen Robinson
13th International workshop on Pathogenesis and Host Response in *Helicobacter* Infections, Helsingor, Denmark; 2018

***Helicobacter pylori*: The Effect of Infection, and Eradication, on Host Immunity and Immunological Disease**
Harry Jenkins, Jonathan White, Darren Letley, Kazuyo Kaneko, Dona Reddiar, Bruno Gran, John Atherton, Karen Robinson
Microbiology Society Conference, 2018, Birmingham

Towards an Understanding of the Immune Response to *Helicobacter pylori* Infection & Models of Multiple Sclerosis: How Can Protection be Mediated?
Harry Jenkins, Joanna Stephens, Kazuyo Kaneko, Darren Letley, Joanne Rhead, John Atherton, and Karen Robinson
Nottingham Molecular Pathology Node, Annual Meeting 2018

Table 1: Abbreviations

AhR	Aryl Hydrocarbon Receptor	MΦ	Macrophage
APC	Antigen Presenting Cell	NFAT	Nuclear Factor of Activated T-cells
BabA	Blood-Group Antigen-Binding Adhesin	NO	Nitric Oxide
BAFF	B-cell activating factor of TNF family	NSAID	Non-Steroidal Anti-inflammatory Drug
BBB	Blood-Brain Barrier	NTC	Non-Template Control
BCR	B-Cell Receptor	OMP	Outer Membrane Proteins
CagA	Cytotoxin Associated Gene A	PA	Pernicious Anaemia
CagA	Cytotoxin Associated Gene A	PAMP	Pathogen-Associated Molecular Patterns
CAM	Cell Adhesion Molecule	PBMC	Peripheral Blood Mononuclear Cells
CD	Crohn's Disease	PGE2	Prostaglandin E2
CD25	Cluster of Differentiation 25	PLP	Proteolipid Protein
CD4	Cluster of Differentiation 4	PML	Progressive Multifocal Leukoencephalopathy
cDNA	Complementary DNA	PPAR	Peroxisome Proliferator-Activated Receptors
CNS	Central Nervous System	PPI	Proton Pump Inhibitors
COX2	Cyclooxygenase 2	PPMS	Primary-progressive MS
CT	Cycle Threshold	PRR	Pattern Recognition Receptors
CTLA4	Cytotoxic T-Lymphocyte Associated Protein 4	PUD	Peptic Ulcer Disease
DC	Dendritic Cells	qPCR	Quantitative Polymerase Chain Reaction
DNA	Deoxyribonucleic Acid	RA	Retinoic Acid
DupA	Duodenal Ulcer-Promoting A	RhA	Rheumatoid Arthritis
E	Efficiency (PCR)	RNA	Ribonucleic Acid
EAE	Experimental Allergic Encephalomyelitis	ROR	Retinoic Acid Orphan Receptor
EBV	Epstein-Barr Virus	ROS	Reactive Oxygen Species
EDSS	Expanded Disability Status Scale	RRMS	Relapsing-Remitting MS
GAPDH	Glyceraldehyde 3-Phosphate Dehydrogenase	RT	Reverse Transcriptase
GC	Gastric Cancer	SabA	Sialic-Acid Binding Adhesin
GEC	Gastric Epithelial Cells	SCFA	Short-Chain Fatty Acids
GGT	Gamma-Glutamyl Transpeptidase	SH2	Src-homology 2 domain
GOI	Gene of Interest	SHP-2	SH2 domain containing tyrosine phosphatase 2
Hp	*Helicobacter pylori*	SNP	Single Nucleotide Polymorphisms
Hp-I	*Helicobacter pylori* Infection	SPMS	Secondary-progressive MS
IBD	Inflammatory Bowel Disease	STAT3	Signal transducer and activator of transcription 3
ICOS	Inducible T-cell Co-Stimulator	T4SS	Type IV Secretion System
ICOSL	Inducible T-cell Co-Stimulator Ligand	TCR	T-Cell Receptor
IDO	Indoleamine 2,3-Dioxygenase	Teff	Effector T-cells
IFN	Interferon	TF	Transcription Factor
IFNG	Interferon Gamma (Gene)	Th	T-helper Cells
IFNγ	Interferon Gamma (Protein)	TLR	Toll-Like Receptor
IL	Interleukin	Tmem	Memory T-cells
Kyn	Kynurenine	TNF	Tumour Necrosis Factor
L-Arg	L-Arginine	Tr1	Type-1 Regulatory T-cell
LPS	Lipopolysaccharide	Treg	Regulatory T-cells
MALT	Mucosal Associated Lymphoid Tissue	UC	Ulcerative Colitis
MAMP	Mucosa-Associated Molecular Patterns	VacA	Vacuolating Cytotoxin Gene A
MBP	Myelin Basic Protein	WT	Wild-Type
MIP-3a	Macrophage Inflammatory Protein-3a		
MOG	Myelin Oligodendrocyte Glycoprotein		
mRNA	Messenger RNA		
MS	Multiple Sclerosis		

Chapter 1

A General Introduction

A brief review of the field of *Helicobacter pylori*, discussing the current knowledge and debating the evidence and controversies of a protective influence in multiple sclerosis.

1.1 – *Helicobacter pylori*

The bacterium *Helicobacter pylori* is arguably amongst the most successful human pathogens, infecting over half of the world population and exhibiting strategies which can enable persistent infection for the lifetime of the host [1]. Chronic gastritis develops in nearly all infected individuals, although the majority of these will remain asymptomatic. Despite this, *H. pylori* infection is a major risk factor for the development of gastroduodenal diseases such as peptic ulcer disease (PUD) and gastric cancers (GC); currently the fifth leading cause of global cancer deaths [2].

In 1875 German scientists Bottcher and Letulle first demonstrated that bacteria were present in the margins of duodenal ulcers. In 1889 Jaworski identified the presence of spiral-shaped organisms from gastric washings which he named *Vibrio rugula* [3]. Around 100 years later in 1979 the Australian pathologist Robin Warren noticed the occurrence of similar organisms in tissue samples from patients with gastrointestinal disease. He studied the microbes with colleague Barry Marshall in the early 1980s and successfully cultured the bacteria somewhat serendipitously in 1982 when a culture was left for an extended period over the Easter break [3]. They followed with several publications describing the organism as a curved bacterium present in chronic gastritis and peptic ulcers [4-6]. The bacterium was named *Campylobacter pyloridis* as it appeared similar to the curved *Campylobacter* genus, however in 1989 sequencing of the

genome revealed that it was in fact a distinct species and subsequently renamed to *Helicobacter pylori* [7].

The notion that peptic ulceration was caused by bacterial infection contrasted greatly with the long-held belief from gastroenterologists that ulcers were caused by excess acidity and stress. To demonstrate causation, Barry Marshall drank a live culture of *H. pylori* to infect himself aiming to show an initiation of gastritis [8]. In 1994, *Helicobacter pylori* was classified as a class 1 human carcinogen by the World Health Organisations' International Agency for Research on Cancer (IARC) for its role in the development of gastric adenocarcinoma and MALT lymphoma [9]. Marshall and Warren were awarded the Nobel Prize for Medicine in 2005 for the discovery and characterisation of *Helicobacter pylori*.

1.1.1 – General features and epidemiology

H. pylori is a Gram-negative, microaerophilic bacterium measuring around 2.5-5µm by 0.5-1µm. The organisms have up to 6 polar flagella covered by a membranous sheath with characteristic terminal bulb [10,11]. *H. pylori* is found globally in the stomachs of humans but can infect some non-human primates [12]. The infection is acquired in early life and persists, often asymptomatically, for the lifetime of the host. The major routes of transmission for *H. pylori* are not well defined however the three mechanisms thought to enable the spread of infection are Faecal-Oral, Oral-Oral, and gastro-oral [2,13-15]. In developing nations, the incidence of infection can be around 70-90%, in Nigeria the rate is 87.7% however in developed and western countries that figure drops markedly to around 20-40%, with the lowest being 18.4% in Switzerland [16]. This declining prevalence is likely to continue as fewer than 5% of children are becoming infected in western regions [17]. Within the population of developed nations, the incidence of *Helicobacter* infection appears higher amongst citizens of a lower socio-economic status [11,18]. Current data indicates that *H. pylori* prevalence is still declining throughout the world. Theories to explain this trend include improved hygiene, environmental or dietary factors, as well as lifestyle aspects such as less crowded living conditions [11]. However, perhaps the greatest factor is the modern worlds' use of antibiotics, especially during childhood. In opposition to the declining incidence of the

infection comes a rise in the prevalence of immune-mediated diseases including allergy, asthma, and autoimmune conditions like multiple sclerosis [19]. A protective role for *H. pylori* in mouse models has been convincingly demonstrated to reduce asthma and allergic responses [20-24]. Furthermore, infection has been associated with a protection from several autoimmune diseases [17]. The importance of this pathogen in human diseases is largely based on correlative data. The role of *H. pylori* in human health and disease appears diverse and provides key insights into the symbiotic relationship humans have with our resident microorganisms.

1.1.2 – Evolutionary genetics and strain variation.

Genetic studies on *H. pylori* diversity in strains from around the world revealed patterns which closely followed human ancestry. From these data we can infer that the bacterium has colonised the stomach since the early origin of our species and followed human migration out of Africa and over the globe [25,26]. *H. pylori* possesses marked genetic diversity both between and within strains. The high rate of mutation and recombination in the *H. pylori* genome is one advantage for survival and adaptation in the varying conditions of the hosts' microenvironment [27]. There are 7 major families of *H. pylori* strains named by the region in which they are prevalent and denoted '*hp*[region]', within these groups there can be sub classifications denoted '*hsp*[region]' [28], a phylogenetic tree is presented in *Figure 1.* The genetic variation between strains can confer a different pathogenic potential, for instance strains from Europe are associated with a higher incidence of disease and cancer risk in comparison to African strains [29]. This is partly due to variation in human genetics such as polymorphisms in immune-related genes, but also due to strain-specific variance in the *H. pylori* genome and the inclusion of virulence determinants. These virulence factors include adhesive outer membrane proteins vital for colonisation, and secreted toxins such as CagA and VacA (described in detail later).

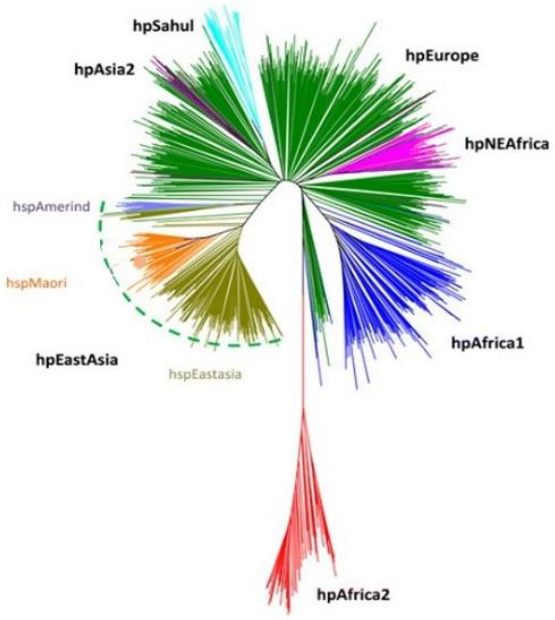

Figure 1 The phylogenetic tree of H. pylori regional strains.

Graphical representation of regional *H. pylori* strain variation. *H. pylori* strains are classified into 7 major groups. Some with further sub-populations defined. The different strains possess distinct genetic profiles, with varied potential of gastric pathogenicity depending on the colonising strain. *Figure modified from Miftahussurur, et al. (2014)* [28]

1.1.3 – Outer membrane proteins and adhesins.

Outer membrane proteins (OMPs) of *H. pylori* are divided into families including the 'major OMP family' called Hop (*Helicobacter* Outer Membrane Porins) with 21 members, and the 'Hop-related family' of 12 members, called Hor (Hop-related Proteins) [27,30]. The Hop family contain numerous proteins with adhesive function, these include BabA, SabA, HopZ, OipA, AlpA and AlpB. Adhesins reported to be important for colonisation of the gastric epithelium include blood-group antigen-binding adhesin A (BabA) which can bind Lewis b antigens (Le^b) and sialic acid-binding adhesin (SabA) which can bind sialylated Lewis X antigens (Le^X). HopZ is important for adhesion to gastric epithelial cells (GEC) during early infection whilst HopQ, similarly to other OMPs including BabA, has been postulated to enhance CagA translocation via the T4SS [31]. The inclusion of adhesins in the *H. pylori* genome are crucial for initiation of colonisation in the epithelium and can regulate the level of inflammation [31], and as such can be predictors of strains with pathogenic potential.

1.1.4 – Colonisation of the gastric epithelium.

H. pylori must survive the low pH of the stomach lumen and navigate through the mucus layer before colonising the gastric epithelium. *H. pylori* has several specialisations which enable quick navigation and migration. Initially the bacterium requires navigational cues to direct movement. These occur in the form of pH-sensing ability and chemoreceptors enabling chemotaxis towards chemical gradients provided by urea, or bicarbonate and sodium which are concentrated beneath the mucus layer; urea is provided from the bloodstream to the capillary beds beneath the mucus layer, sodium bicarbonate is released by transporters from parietal cells on the epithelium. Urea gradients are sensed through chemoreceptors such as TlpB [32].

Some *H. pylori* proteins adhere to the outer bacterial membrane including urease and HspB which are found to be co-localised [33,34]. The function of adsorbed urease is proposed to be three-fold; firstly, it hydrolyses urea to produce ammonia and thus buffers acid pH in the immediate environment. Secondly it is proposed that urease enables the use of urea as a nitrogen source for amino acid synthesis. In addition, urease-derived ammonium may function similarly as in *Ureaplasma urealyticum* which uses this conversion to create an ammonium chemical potential to act as an energy source for powering flagella [35,36]. Autolysis and release of urease has been proposed to occur to maintain a permissive environment for colonisation by buffering gastric acid [33,34]. Autolysis could be utilised by *H. pylori* as a means of presenting virulence factors and cytoplasmic protein directly to the gastric mucosa. Interestingly, autolysis may be a mechanism of immune subversion by *H. pylori* by releasing an overwhelming number of cytoplasmic protein antigens [37], or by acting to conceal outer membrane proteins so host immune surveillance is unable to recognise bacterial antigens [34].

1.1.5 – Gastric mucus and mucins.

The mucous forms a gel-like adherent ultrastructure, predominantly water with around 5% proteins (3% mucins, 2% other molecules such as IgA) [38]. Mucins are glycosylated proteins secreted from goblet cells and Paneth cells [39]. The mucous not only serves to protect the epithelium from the acidity of the stomach lumen but also functions as one of the first barriers against opportunistic microorganisms containing

antimicrobial molecules such as lysozyme and beta-defensins [40]. Paneth cells in humans express 2 β-defensins [41], whereas in mice they can express around 20 [42]. *H. pylori* can subvert these mechanisms, infection can alter the expression of β-defensins [43], and the *H. pylori* urease (UreB) can inhibit opsonisation by antimicrobial peptides, including the complement protein C3b [44]. Penetration of the mucous is aided by the helical morphology of the bacterium, motility is provided by the bundle of 4-6 flagella powered by proton motive force allowing quick movement at low pH [35].

Mucins themselves are targets for *H. pylori* adhesion during colonisation, which can be mediated through the adhesins, BabA, SabA and LabA [45,46]. BabA has been well documented to bind Le^b structures on the gastric mucin MUC5AC, to which *H. pylori* is often found to co-localise and is important for colonisation [47]. *H. pylori* affects the biosynthesis and expression of mucins in the stomach [48-51]. This can promote increased inflammation and the development of pre-neoplasms [50,52]. The reduction of gastric mucins (MUC1, MUC5AC, and MUC6) and the increase of intestinal mucin MUC2 (associated with intestinal metaplasia) can be restored after eradication of *Helicobacter* [52,53]. As mucins act as receptors for microbial adhesins, reduced expression can prevent *H. pylori* binding and lower the colonisation density. The gastric epithelium has several cell-surface mucins such as MUC1, MUC3, MUC4, MUC12-17 which can function as receptors for microbial adhesins [39]. These can also block pathogens from establishing direct contact with the epithelial cells, which is a crucial requirement for the deployment and activation of microbial secretory systems such as the type-IV secretion system (T4SS) of *H. pylori* [39]. MUC1 can bind to the SabA and BabA adhesins to entrap microbes causing MUC1 to shed away from the cell surface acting as a releasable decoy which can prevent *H. pylori* binding to GECs [46]. Indeed, polymorphisms in MUC1 can confer an increased risk of infections, worsening gastritis, and the development of gastric cancer in a *H. pylori*-infected gastric mucosa [39,54]. Some mucins have intrinsic antimicrobial effects; MUC6 contains an α1,4-*N*-acetylglucosamine (α1,4-GlcNAc) residue which has been shown experimentally to inhibit *H. pylori* from synthesising the important membrane components, cholesterol-α-glucosides [39,55,56]. This has detrimental effects on *H. pylori* growth and a relevance to phagocytosis, discussed in the context of macrophages later in this review.

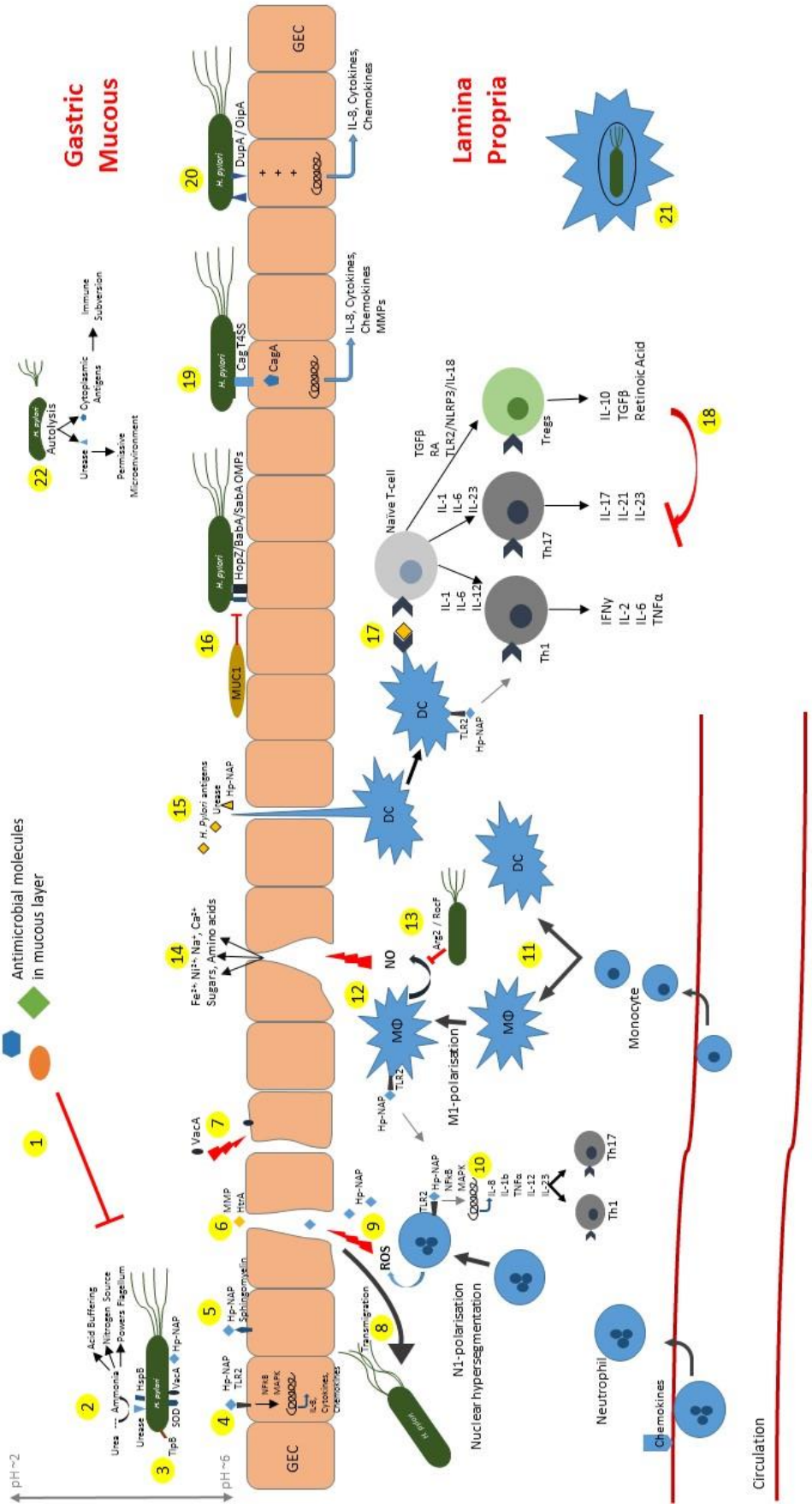
Gastric Mucous
Lamina Propria
Antimicrobial molecules in mucous layer
pH ~2
pH ~6
GEC
Acid Buffering
Nitrogen Source
Powers Flagellum
Urea → Ammonia
HspB
TipB
SOD
VacA
Hp-NAP
TLR2
NFκB
MAPK
IL-8, Cytokines, Chemokines
Sphingomyelin
MMP
HtrA
VacA
Fe²⁺, Ni²⁺, Na⁺, Ca²⁺
Sugars, Amino acids
H. Pylori antigens
Urease
Hp-NAP
MUC1
HopZ/BabA/SabA OMPs
CagT4SS
CagA
DupA/OipA
IL-8, Cytokines, Chemokines MMPs
Autolysis
Cytoplasmic Antigens
Immune Subversion
Urease
Permissive Microenvironment
Transmigration
ROS
NO
Hp-NAP
TLR2
NFκB
MAPK
IL-8
IL-1b
TNFα
IL-12
IL-23
N1-polarisation
Nuclear hypersegmentation
M1-polarisation
MΦ
DC
Vgr2 / RocF
Naïve T-cell
TGFβ
RA
TLR2/NLRP3/IL-18
IL-1
IL-6
IL-23
IL-1
IL-6
IL-12
Th17
Th1
Tregs
IL-17
IL-21
IL-23
IFNγ
IL-2
IL-6
TNFα
IL-10
TGFβ
Retinoic Acid
Monocyte
Neutrophil
Chemokines
Circulation

Figure 2 Schematic of the major events during H. pylori infection.

(1) Gastric mucus contains anti-microbial compounds which act as a first defence against infectious microbes. **(2)** *H. pylori* urease-derived ammonia functions three-fold; it can buffer gastric acid promoting *H. pylori* survival; it provides a nitrogen source; ammonia gradients can power flagella. **(3)** *H. pylori* migrates towards urea gradients using chemoreceptors such as TlpB. Urea will be concentrated towards the epithelium under the mucus layer. **(4)** The secreted *Hp*-NAP can activate TLR2 and initiate inflammatory cytokine and chemokine expression via NFkB and MAPKs in GECs. **(5)** *Hp*-NAP can form adhesions to sphingomyelins on host cells. **(6)** *H. pylori* factors are secreted. *Hp*-NAP activates neutrophils and promotes Th1 responses and GEC damage. MMPs and HtrA can cause the disruption to cell-cell junctions and cell polarity promoting both metaplasia and GC. They also allow dissemination of secreted factors through the epithelial barrier. **(7)** VacA can adsorb to the outer membrane of *H. pylori* in addition to being secreted and acid activated. VacA can insert to host cell membranes causing vacuolation, disruption to cell signalling and antigen presentation, inhibition of phagocytosis, mitochondrial membrane depolarisation and cytochrome C release causing apoptosis. **(8)** Barrier disruption allows transmigration of *H. pylori* to the lamina propria. **(9)** Neutrophils recruited to the inflamed mucosa display nuclear hypersegmentation and N1-polarisation in *H. pylori* infection. **(10)** Hp-NAP can bind neutrophil TLR2 and cause activation and expression of inflammatory genes including IL-8, IL-1, IL-12, IL-23, CXCL8 and TNFα promoting Th1/Th17 responses. Activated neutrophils produce ROS which lead to GEC damage. **(11)** Monocytes are recruited to the inflamed mucosa and can differentiate into macrophage or dendritic cells. **(12)** M1-polarised macrophages contribute to GEC damage through the secretion of inflammatory mediators and cytotoxic compounds including nitric oxide (NO) via the enzyme iNOS. **(13)** *H. pylori* can inhibit NO production in macrophages as a means of immune subversion. Induction of arginase Arg2 and *H. pylori* derived RocF can inhibit iNOS through competition for the substrate L-Arginine. **(14)** VacA-mediated gastric epithelial damage and apoptosis can provide a survival advantage through the release of nutrients to the microenvironment. These nutrients can include sugars, amino acids, minerals, or ions and can be scavenged by *H. pylori*. **(15)** Dendritic cells project dendrites through the epithelial barrier and can present *H. pylori*-derived antigens to naïve T-cells. **(16)** Bacterial adhesion to the epithelium is crucial for colonisation and utilises outer membrane proteins (OMP) including BabA, SabA and HopZ. Gastric mucins, specifically the GEC surface residing MUC1 inhibit adhesins from tethering to the GECs preventing colonisation. **(17)** Antigen-presenting DCs can activate effector T-cells; a mixed Th1/Th17/Treg is induced. Hp-NAP and urease can activate TLR2 and promote NLRP3 inflammasome assembly. This has been shown to induce Tregs in an IL-18-dependent manner and provides a means of immune evasion and tolerance which can provide protection against asthma. **(18)** *H. pylori* induced Tregs can suppress the Th1/Th17 response. Treg induction by *H. pylori* will usually cause sufficient suppression to Th1/Th17 responses that the infection is never cleared, allowing persistent infection. **(19)** The Cag type 4 secretion system (T4SS) injects CagA into host cells whereby it may alter the phosphorylation and activation of host cellular signalling proteins promoting inflammatory gene expression (notably IL-8) and disrupting cell junctions and motility which promotes metaplasia and GC. CagA can limit toxicity of VacA thereby protecting the GECs to which *H. pylori* are tethered. **(20)** The expression of virulence factors including DupA and OipA are associated with increased inflammation and higher risk of gastric atrophy and disease. **(21)** *H. pylori* can survive within host cells including monocytes and macrophages. Bacterial persistence and even replication has been observed within structures termed megasomes formed through phagosome fusion. This can be because of VacA-mediated inhibition to phagocytosis. **(22)** Autolysis of *H. pylori* has numerous benefits. It can release factors such as urease in the local vicinity therefore creating a more permissive environment for colonisation. It has been proposed that the release of an overwhelming number of antigens can work as a means of immune escape.

1.2 – *H. pylori*-Associated Diseases & Their Determinants

H. pylori can be a causative factor in the development of gastric diseases including chronic gastritis, peptic ulcer disease, gastric adenocarcinoma, and MALT lymphoma[57].

1.2.1 – Gastro-duodenal Diseases

A chronic infection with *H. pylori* results in chronic gastritis, usually asymptomatic. In some cases, particularly with virulent strains it can lead to the development of peptic ulcer disease (PUD), comprising gastric and duodenal ulceration (GU/DU) [57]. In the longer-term inflammation can contribute to the development of gastric adenocarcinoma and MALT lymphoma [57]. Although GC only occurs in a small proportion of infected individuals, considering that half the world population carry *H. pylori* this translates to a significant number of cancer deaths [58].

The development of symptomatic disease is dependent on many factors including bacterial strain, human genetics, dietary, and environmental influences. *H. pylori* infection is still the largest risk factor for the development of gastric cancer (GC) which occurs in around 1-5% of infected people [58]. Gastric cancer presents a considerable burden to human health, being the fifth highest cause of cancer-related deaths globally [59]. After successful eradication, the presentation and recurrence of peptic ulcers are reduced [11,60]. Furthermore, eradication of *H. pylori* has been shown to improve the manifestations of atrophic gastritis including recovering acid secretory function [61]. Meta-review of published literature suggest that screening and eradication of *H. pylori* reduces the incidence of gastric cancers and burden to public health [59,62].

In the UK, the National Institute for Health & Care Excellence (NICE) recommends a 7-day course of twice-daily treatment with a proton pump inhibitor (PPI) drug, and antibiotics; amoxicillin with either clarithromycin or metronidazole as the first line treatment regimen following a positive diagnosis of *H. pylori* infection. Testing for *H. pylori* infection is usually performed using a biopsy urease test, a Carbon-13 urea breath test (^{13}C-UBT), a stool antigen test, or in some cases serological analysis (NICE Clinical Guidance; CG184).

1.2.1.1 – Peptic ulcer disease (PUD).

Peptic ulcers are ruptured regions of the gastric epithelial layer penetrating through the mucosa [11]. Commonly, ulcers develop at the antral-corpus transitional region, but this distribution is affected by other factors [11]. The two largest risk factors for PUD are *H. pylori* colonisation and non-steroidal anti-inflammatory drugs (NSAIDs) [36,45,57,63]. In combination this risk is further augmented and NSAIDs are the largest cause of gastric ulcer bleeds and hospital admissions after *H. pylori* [63]. PUD is associated with virulent strains inducing higher levels of inflammation and gastric epithelial damage [36]. Elevated levels of gastric acid can also contribute to ulcer formation [36]. Peptic ulcers can often remain asymptomatic but can present as upper abdominal pain and can be life-threatening in the event of a rupture and gastrointestinal haemorrhage. Eradication of *H. pylori* can lead to ulcer healing and the prevention of recurrence [45].

1.2.1.2 – Gastric cancer (GC).

Over time, in a relatively small number of cases *H. pylori* infection can lead to the development of gastric adenocarcinoma and MALT lymphoma [58]. *H. pylori* is considered to be the leading cause of gastric cancer worldwide and the fifth leading cause of total cancer deaths [45]. Metaplasia and atrophic gastritis caused by chronic inflammation, pan-gastritis, and the virulence factor CagA can lead to the development of gastric cancer [45]. Adenocarcinoma and MALT lymphoma similarly to PUD tend to regress following *H. pylori* eradication [45,59,60]. Although gastric cancer is perhaps the most important consequence of *H. pylori* infection it is not within the scope here, but well reviewed in the literature [58,64,65].

1.2.1.3 – Chronic gastritis

H. pylori colonisation will always induce marked inflammation in the gastric mucosa (chronic gastritis), the distribution and severity of which is determined by acid balance, host gene polymorphisms, or virulence factors [11]. Cytotoxic molecules including reactive oxygen species (ROS) and nitric oxide (NO) derived from infiltrating neutrophils and macrophages, and bacterial-derived toxins can damage GECs increasing the risk of secondary disease. Strains with higher potential to cause

disease possess a functional *cag* pathogenicity island (*cag*PAI) and other virulence factors including CagA, VacA and OipA [36]. The virulence factors of *H. pylori* are discussed in detail later.

1.2.1.4 – Autoimmune gastritis (AIG).

There are two major forms of gastritis; type A, autoimmune gastritis (AIG) which occurs in the corpus and fundus; and type B antral-predominant gastritis [66-68]. Infection with *H. pylori* is traditionally associated with type B antral gastritis but can induce AIG through molecular mimicry. AIG may well be asymptomatic until the level of gastric atrophy causes the presentation of either iron-deficiency anaemia, or B12 deficiency (pernicious anaemia, PA), in addition to changes in the production of gastric secretions such as pepsinogen, gastrin and gastric acid [66]. In the longer term this favours the development of PUD and GC [66,67].

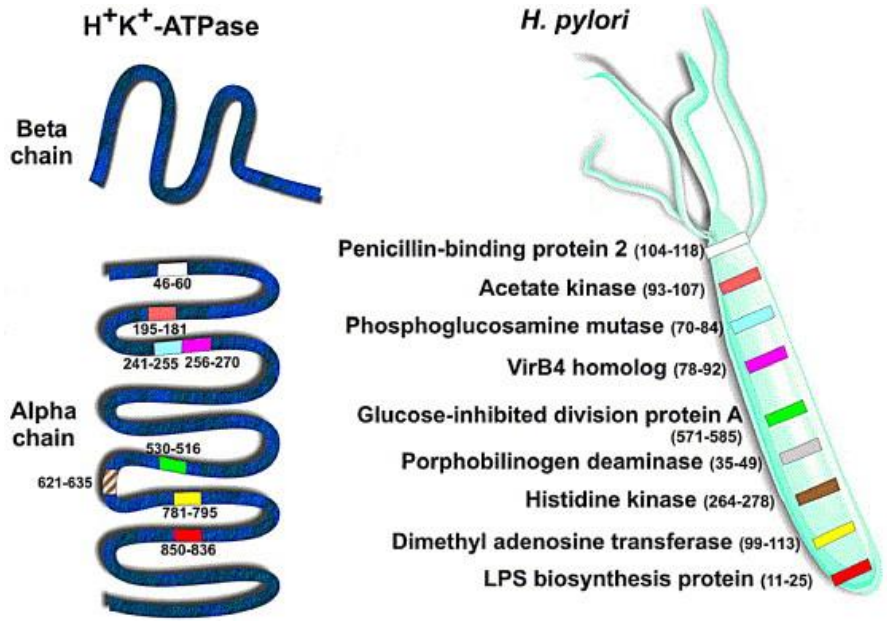

Figure 3 Molecular mimicry between H. pylori and human H^+K^+-ATPase.

The screening of $CD4^+$ T-cell clones that proliferate to both H^+K^+-ATPase and *H. pylori* lysate has enabled the precise definition of the epitope specificity within the H^+K^+-ATPase molecule of autoreactive or cross-reactive T-cell clones. Bioinformatics has predicted series of at least nine cross-reactive peptides belonging to different *H. pylori* proteins. The cross-reactive peptides of *H. pylori* are depicted with the corresponding epitopes in the H^+K^+-ATPase. These data represent the basis for a mechanism of molecular mimicry in the genesis of gastric autoimmunity. *Figure used unmodified from; M.M. D'Elios et al., Microbes and Infection 6 (2004) 1395–1401* [68].

AIG results from autoimmunity against epitopes from gastric epithelial and parietal cells [67]. *H. pylori* specific Th1 cells can aberrantly recognise epitopes from the human H^+/K^+-ATPase proton pump on parietal cells suggesting *H. pylori* as a causal factor [67,68]. These cross-reactive T-cells have been isolated from patients with AIG and shown to possess affinity for epitopes in *H. pylori* lysates [67,68]. At least 9 proteins of *H. pylori* share epitopes with the H^+/K^+-ATPase pump (*Figure 3*). This infiltration of the cross-reactive Th1 cells occurs concurrently with increased expression of pro-inflammatory molecules [67].

1.2.1.5 – Gastritis-related nutrient deficiencies.

H. pylori infection and atrophic gastritis are often accompanied by the presentation of cobalamin deficiency (B12-deficiency, pernicious anaemia) and iron-deficiency anaemia [66,69]. Destruction of parietal cells through *H. pylori*-mediated gastric atrophy impairs the secretion of intrinsic factor, an essential requirement for the acquisition of cobalamin from the pro-vitamin form [66]. The loss of gastric glands and parietal cells also reduces acid secretion which correlates to lower ferrous iron availability [70]. Low gastric pH is required for the activation of ascorbate-mediated iron transport, thus hypochlorhydria prevents iron absorption [70]. Eradication of *H. pylori* restores diminished ascorbate and acid levels [71]. Previous studies have identified *H. pylori* infection as a major risk factor for the presentation of anaemias in children and that this correlates to deficits in growth rate both as young children and during puberty [69,72,73]. Both iron and B12 deficiencies can cause abnormalities in neurogenesis and CNS development. In fact, B12 deficiency impairs myelin synthesis and leads to the incorporation of aberrant lipids [74,75]. It may therefore be interpreted that B12 deficiency secondary to *H. pylori* infection is a risk factor for MS. It would be interesting to determine if *H. pylori*-mediated iron or cobalamin deficiency can alter the formation or composition of CNS myelin resulting in differential susceptibility to CNS pathologies such as MS.

1.2.2 – Extra-gastric disease.

In contrast to the contribution to gastro-duodenal pathology, *H. pylori* can also influence the course of extra-gastric diseases. The over-arching aim of this thesis is

to investigate proposed protective associations for such conditions. This is likely a result of either direct- or indirect interference between common immunological pathways. Much of the evidence in the literature would suggest that *H. pylori* can exert a suppressive rather than a cumulative effect to the immunopathology of these diseases. Examples of these include inflammatory bowel diseases (IBD), allergic responses, cardiovascular, neurological, gynaecological, and hematologic conditions [17,76-79]. Of particular interest here is the crosstalk which may occur between the immunological mechanisms of *H. pylori* and multiple sclerosis, discussed in detail later.

1.2.2.1 – Inflammatory bowel diseases (IBD).

H. pylori infection is negatively correlated to the incidence of inflammatory bowel diseases (IBD) which comprise Crohn's disease (CD) and ulcerative colitis (UC) [17,80-83]. IBD is a chronic inflammatory disease of the gastrointestinal tract. The incidence of IBD is high in developed nations with around two million patients in Europe alone, however rates are also increasing in developing nations [84], conversely to declining incidence of *H. pylori* infection [82], perhaps attributable to the 'hygiene hypothesis' proposed by Strachan [85]. Genetic susceptibility, environmental triggers, dysregulated microbiota, and imbalances of inflammatory and anti-inflammatory immunity are all considered risk factors for IBD [84], indeed numerous inflammatory cytokines and chemokines are upregulated in IBD patients [86]. Several susceptibility genes are reported in the literature to affect IBD including tight junction-related E-cadherin, NOD2, and genes involved in the host immune response involving the IL-23/Th17 pathway [87]. Dysregulation or to the gut microbiota may influence IBD occurrence; *Proteobacteria* and *Actinobacteria* are elevated in opposition to a reduced proportion of *Bacteroidetes* and *Firmicutes* species in CD/UC patients highlighting the importance of gut bacteria in the wider context of human health [87,88].

Furthermore, eradication of *H. pylori* could induce the development of CD [17,89], and the regional rates of IBD elevate in accordance with the initiation of *H. pylori* eradication therapy for PUD in those populations [83]. Whether this effect is mediated directly by *H. pylori*, or indirectly by modification to the gut microbiota

(consequentially from antibiotic eradication therapy) remains to be proven. In animal models, *H. pylori* infection can protect from experimentally induced colitis through tolerising effects on dendritic cells and Treg induction[17], conversely IBD is exacerbated by a sub-optimal Treg response [17]. Interestingly, non-*pylori Helicobacter* species *H. bilis* and *H. hepaticus* can confer opposing biological effects and induce experimental colitis and GI inflammation in mouse models through selective Th1 and Th17 stimulation [83].

1.2.2.2 – Allergy and asthma.

Diseases of dysregulated and excessive immune responses such as asthma and hayfever are increasingly common in developed nations, in parallel to the decline of infections, especially during childhood [85,90]. The literature suggests an inverse correlation between asthma and allergy and *H. pylori* infection [20-22,91-94]. This has been attributed to tolerised DC's, regulatory T-cell induction, and the anti-inflammatory cytokine IL-10. This topic is discussed in more depth in the context of Tregs. Briefly, asthma can be characterised as a Th2/Th17 mediated disease resulting in inflammation of the airway and lung, infiltration of eosinophils, mast cells, and a pronounced elevation of IgE as a product of the Th2-derived cytokines IL-4, 5, 9 and 13 [20,90].

The dynamic balance between Th1 and Th2 responses was initially proposed to mediate this protection whereby the responses of one type can counteract the other [90]. In this regard, the absence of Th1-polarising infections such as *H. pylori* in childhood leads to unrestrained Th2 hyper-responsiveness manifesting as asthma and allergies [90,92]. The Th1/Th2 paradigm is also proposed to form the basis from which to explain the protection from Th1-mediated disease with a concurrent Th2-polarising helminth infection [90], convincingly shown to mitigate EAE and MS severity [95-98]. However, the matter is complicated as asthma is exacerbated by the Th1-derived cytokine IFNγ [99]. The mechanism may instead be primarily mediated via tolerogenic DC and regulatory T-cell responses [20,21,90].

Increased prevalence of the gut commensals *Bifidobacterium* and *Lactobacillus* also favour Treg induction, and suppress asthma, supporting the premise of the gastrointestinal microbiota being intricately involved in maintaining immune homeostasis [90]. Infectious and commensal organisms alike may both modulate airway inflammation. Commensal species may induce regulatory T-cell populations able to suppress Th2 hyper-responsiveness, mediated by tolerising effects on dendritic cells favouring an induction of regulatory T-cells, IL-10 or TGFβ, supportive of a suppression of Th2 and IgE responses [17,90]. In contrast, infectious microbes may activate the Toll-Like Receptors (TLR) 4, 5 and 9 or provide bacterial LPS to stimulate Th1 responses which could subsequently inhibit Th2 cellular activity. There are studies suggesting the activation of TLR4 by *H. pylori* may be involved in the protection from allergic asthma [94], by inducing tolerogenic DC's [100]. The effect of *H. pylori* on the immunology of asthma have been thoroughly investigated in the literature and are discussed in detail in relation to the Treg response to *H. pylori* infection.

1.2.3 – Factors which influence the risk of disease

To better understand the mechanisms behind the protection from such diseases we must appreciate the external factors which can influence them.

1.2.3.1 – Gastric acid balance.

Acid secretion is a key factor modulating the course of a *H. pylori* infection and associated pathologies, Including gastric atrophy, colonisation density, antral/corpus-predominant gastritis, and ulcer distribution [57,101] (*Figure 4*). Lifestyle factors that affect gastric acid secretion include high-salt diets, smoking, stress, and NSAID's; the second leading cause of PUD after *H. pylori* [36,57]. Lifestyle changes including the cessation of smoking or medical interventions such as proton pump inhibitors (PPI's) can reduce acid load thus modifying the incidence of further gastric disease [36]. Eradication of *H. pylori* has been demonstrated to restore the acid balance in the gastric mucosa [102].

Antral-predominant gastritis is associated with the loss of somatostatin-secreting D-cells [57]. Somatostatin is essential in the control of other gastric secretions, inhibition can lead to unrestrained secretion of G-cell-derived gastrin (hypergastrinemia), causing elevated acid secretion from parietal cells (hyperchlorhydria) [45]. Elevated levels of urease-derived ammonia or the inflammatory cytokines TNFα, IL-1β, and IL-8 can affect the regulation of these secreted factors [101]. Indeed, IL-1β is upregulated in the *H. pylori*-infected gastric mucosa and potently inhibits parietal cell acid secretion [11,45,101,103-105]. The more virulent *cag* PaI/CagA+ strains can lead to elevated levels of these inflammatory cytokines and have an augmented effect on gastric acid regulation [11,45].

Reduced pH predisposes to antral-predominant gastritis, duodenal metaplasia, lower colonisation density, and duodenal ulcers [45]. The corpus may be protected from colonisation by the low pH unless other factors such as cytokines, atrophy or medications cause a reduction of acid production. Lowering the pH also precipitates bile-acids which are inhibitory to *H. pylori* colonisation [36]. Furthermore, damage to the epithelium can impair the secretion of bicarbonate which contributes to a reduced pH [36]. In contrast, pan-gastritis is associated with atrophy and loss of the acid-secretory parietal cells, attenuating acid secretion (hypochlorhydria), predisposing to gastric ulcers, higher colonisation densities, increased atrophy, intestinal metaplasia, and adenocarcinoma [11,45,101,106].

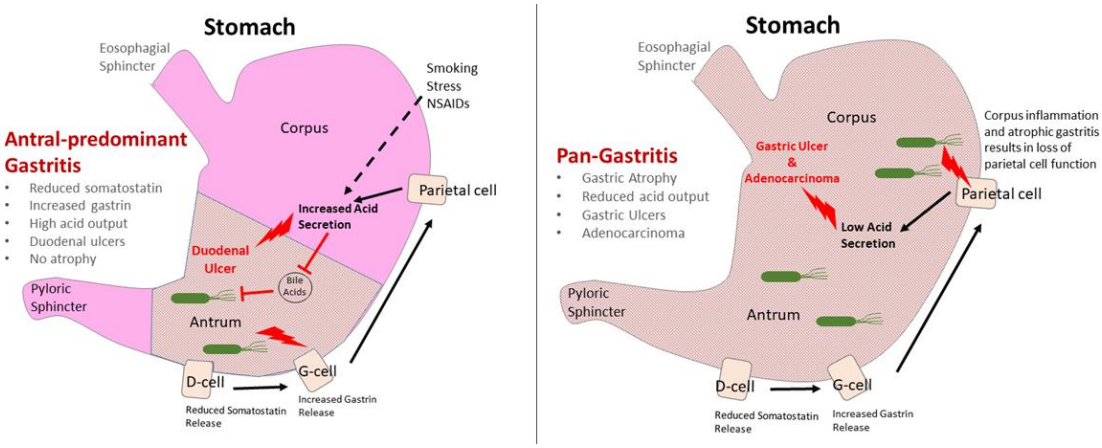

Figure 4 Acid balance in the H. pylori-infected stomach

Antral gastritis can result in the inhibition of D-cell-derived somatostatin secretion, this results in increased gastrin release from G-cells and a subsequent increase of acid secretion by parietal cells. High gastric acid output is thought to protect the corpus from infection but is associated with duodenal ulcers. Bile acids are inhibitory to *H. pylori* colonisation, low pH precipitates bile acids and increasing bacterial burden. Smoking, stress and NSAIDs contribute to increased acid production. Conversely, pan-gastritis can occur if acid secretion is low. This can be due to the loss of parietal cells because of atrophic gastritis, or by some medications such as proton pump inhibitors. This can result in gastric ulcers, higher colonisation density, increased atrophy, and a higher risk of adenocarcinoma.

1.2.3.2 – Host gene polymorphisms.

Gastro-duodenal disease occurs with a higher frequency in those with polymorphisms in immune-related genes. Many of these gene polymorphisms increase the risk of gastric cancer to a greater extent than the risk of peptic ulceration [106], including IL-1β, IL-2, IL-10, and toll-like receptor (TLR) genes [101,106]. A selection of polymorphisms and their associated risks are presented in *Table 2*.

Polymorphisms in the IL-1 gene cluster resulting in elevated gene expression are associated with hypochlorhydria, gastric atrophy and increased risk of cancer development [107]. Activation of the IL-1β pro-peptide is mediated through NLRP3 inflammasome assembly which is influenced by the *H. pylori* virulence factors VacA and *cag* PaI [105]. Polymorphism in this gene may lead to a higher expression and a lower risk of acquiring *H. pylori* infection [103].

IL-10 is an anti-inflammatory cytokine characteristic of regulatory T-cells (Tregs) with a wide range of cellular sources, and with importance to *H. pylori* infection, persistence, and disease (discussed in more detail later). There have been at least 4 single nucleotide polymorphisms (SNPs) in the *IL10* gene proposed as risk factors for *H. pylori* pathogenesis, whereas a further 8 would appear to augment IL-10, thus suppressing inflammation [101].

TNFα is an inflammatory cytokine mediating a wide range of cellular responses. SNPs affecting the TNFα promoter region have produced contrasting results regarding its influence on *H. pylori* infection, with positive, negative and no associations being reported [101,108]. At least two SNPs in the IL-12 gene correlate to increased risk of adenocarcinoma however not to the development of ulcers [101].

Table 2 Host Gene Polymorphisms & their consequences

Host Gene	Biological Effect of Polymorphism	Reference
IL-1β	Hypochlorhydria, increased gastric atrophy, increased GC risk	*Chan FKL, 2002; Tseng FC, 2006; El-Omar, 2001; Santos JC, 2012; Semper RP, 2014*
IL-1α	Lower risk of *H. pylori* infection in children	*Tseng FC, 2006*
IL-10	Increased risk of *H. pylori* infection, increased gastric inflammation	*Chan FKL, 2002*
TNFα	Varied effects reported. Increased risk of GC	*Chan FKL, 2002.* *Roesler BM, 2014*
IL-12	Increased risk for gastric adenocarcinoma	*Chan FKL, 2002*
IL-2	Varied effects reported between regional groups	*Chan FKL, 2002*
MUC1	Increased incidence of infection, increased gastritis, increased GC risk, associated to Crohn's disease	*Wen R, 2015; McGuckin MA, 2011*
NOD1	Increased susceptibility to *H. pylori* infections including enteroinvasive *E. coli* and *L. pneumophila.*	*Caruso R, 2014*
NOD2	Mutations in NOD2 associated with Crohn's disease, increased susceptibility to infections including enteroinvasive *E. coli* and *L. pneumophila.*	*Abraham C, 2009; Caruso R, 2014*

1.2.4 – Virulence factors of *H. pylori*.

H. pylori possesses several key determinants of survival and pathogenesis termed virulence factors which include Cytotoxin Associated Gene A (*cagA*); Vacuolating Cytotoxin A (VacA); Duodenal Ulcer-Promoting Gene A (*dupA*); Outer Inflammatory Protein A (OipA); the blood antigen binding protein A and B OMP's (BabA and BabB);

and SabA. One of the most important factors that confers increased virulence potential to *H. pylori* is the *cag* Pathogenicity Island (*cag*PAI) which encodes a type IV secretion system (T4SS). Those infected with *cag*PAI-positive strains have an increased likelihood of symptomatic infection and the development of secondary diseases. A wider array of expressed virulence factors results in a more aggressive phenotype and disease-promoting potential. Strains with mutated, non-functional, or absent virulence factor genes may have drastically altered characteristics, pathogenicity, or survival capacity within the host. Two of the best studied virulence factors, and those which can markedly affect the severity of *H. pylori* infection, are CagA and VacA which are discussed in more detail below.

1.2.4.1 – *cag* pathogenicity island (*cag*PAI) / CagA

The *cag*PAI is a region of DNA around 40Kb in size encoding 27-31 proteins which in complex form the components of a type IV secretion system and additional accessory proteins [11,109]. The T4SS is a bacterial 'syringe'-like delivery system, which is utilised for the purpose of injecting bacterial protein directly into the cytosol of GEC in addition to playing an important role in bacterial adhesion to the epithelium. Strains lacking *cag*PAI or with non-functional mutated alleles display a greatly reduced capacity for colonisation establishment, persistence and pathogenicity to the host [11].

A major function of the T4SS is to enable the CagA protein to be delivered into GEC's where it is subsequently phosphorylated by host Src-dependent kinases. Translocation of CagA into host cells is dependent on CagL binding to $\alpha_5\beta_1$-integrin on host GEC's which is essential for the activation of the *cag* T4SS. This acts as an anchor for *H. pylori* on host cells, induces These full assembly of the T4SS, and activates Src-family kinases to perform the phosphorylation of CagA [110-112]. CagL binding is enabled through an RGD motif (Arg-Gly-Asp) which is exposed after acid-induced conformational changes in the stomach [110,111]. The CagL-GEC interaction can activate the gastrin promoter and contribute to hypergastrinemia associated with *H. pylori* infection [111]. Following delivery and phosphorylation in host cell cytosol CagA activates Src homology protein 2 (SHP-2) which proceeds to dephosphorylate numerous host proteins initiating changes in cellular signalling, activity and morphology [108]. CagL-integrin binding

initiates signalling cascades in GEC's that result in NFκB activation and IL-8 expression in addition to the activation of focal adhesion kinase (FAK), epidermal growth factor receptor and MAPK signalling [111,113].

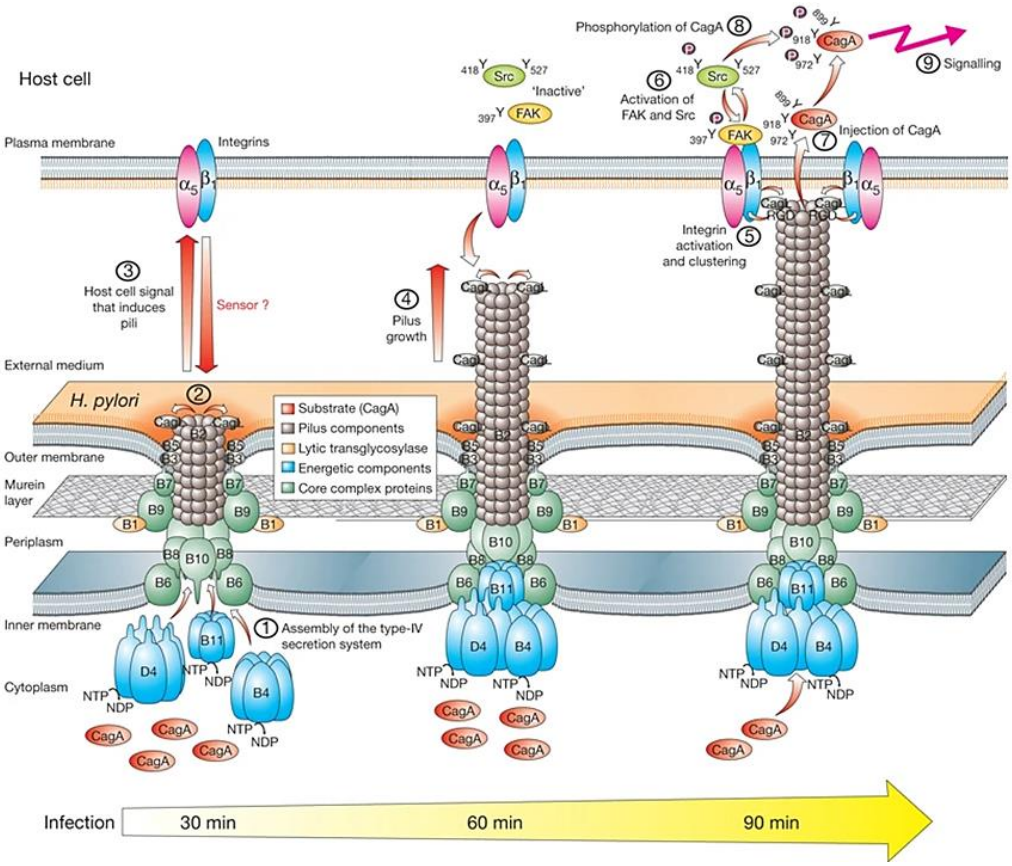

Figure 5 Formation of the cag type IV secretion system.

(1) In the early stages of infection, the T4SS subunits are assembled to span the *H. pylori* membrane. (2, 3, 4) The polymerisation of the pilus causes projection toward host cellular surfaces. (5) CagL is a protein located at the tip of the pilus, CagL binding to α5β1-integrins on the host cell allows full assembly of the T4SS. (6) CagL:integrin association activates host kinases including FAK and Src. (7) CagA can be translocated into the host cytosol upon integrin activation. (8) CagA is phosphorylated by host kinases. (9) CagA phosphorylation leads to altered host signalling which causes cytoskeletal rearrangement, disruption of cell-cell junctions and inflammatory gene expression, notably IL-8. *Figure adapted from; Kwok, et al. (2007); Nature 449(7164):862-6. DOI: 10.1038/nature06187* [112].

The stimulation of GEC-derived IL-8, serves as an inflammatory mediator and potent recruiter of neutrophils, potentiating gastric inflammation. It is also responsible for the dysregulation of β-catenin and cell-cell junctions which may promote epithelial to mesenchymal transition, motility, and increased risk of GC development [114,115]. Through such changes, cells adopt a 'hummingbird phenotype'. As such, it can be

considered that CagA is a functional oncoprotein, the presence of which leads to a phenotype supportive of gastric malignancies [108]. CagA-positivity is a risk factor for both GU and GC in *Hp*Europe strains however *Hsp*EAsia strains do not show similar associations [108,116]. CagA+ strains usually also have a pathogenic type *vacA*-s1/m1/i1 allele. On the other hand, strains with no *cag*PAI in the genome are often asymptomatic and with a non-toxic *vacA*-s2/m2 type. The allelic variants of *vacA* are discussed in the next section.

CagA is polymorphic and can contain distinct repeat sequences in the 3' region in a series of EPIYA (Glu-Pro-Ile-Tyr-Ala) repeats, which provide tyrosine phosphorylation sites. The number of EPIYA motifs differs and EPIYA-A, -B, -C and -D segments are reported, defined by the sequence following the primary EPIYA site. Two main species predominate between European and East Asian strains; EPIYA-ABC which are mainly European strains; and EPIYA-ABD which are East Asian [117,118]. Phosphorylation of CagA in the EPIYA segments enables the binding of SHP-2 via the SH2 domain resulting in downstream effects to host cellular signalling [108,116,118]. Therefore, the effect on host cells and to disease risk is highly dependent on the organisation and quantity of the EPIYA sequences of *cagA* in different regional strains. The EPIYA-A and -B repeats are not as important as the EPIYA-C and -D segments in terms of activity, with EPIYA-C and -D repeats phosphorylated more readily than -A and -B regions [108,116-118]. East Asian (EPIYA-ABD^{+}) strains carry a higher risk of GU and GC than European (EPIYA-ABC^{+}) strains [116]. Within EPIYA-ABC genotypes, the number of C-sequence repeats is correlated to cancer risk amongst European strains. This is likely to be an effect of having extra available phosphorylation sites [119]. In contrast, the A and B type segments are found singularly and not in repeating units [117]*Helicobacter* strains with ABCC and ABCCC repeats are associated with increased levels of phosphorylated CagA, IL-8 secretion, GEC damage and GC [117-120]. A representation of the function of CagA and the organisation of EPIYA sequences are shown in *Figure 6*. The function of CagA can be mitigated or augmented by the specific allelic variant of another important virulence factor, VacA, and thus these two proteins appear to function in tandem at conferring virulence [108].

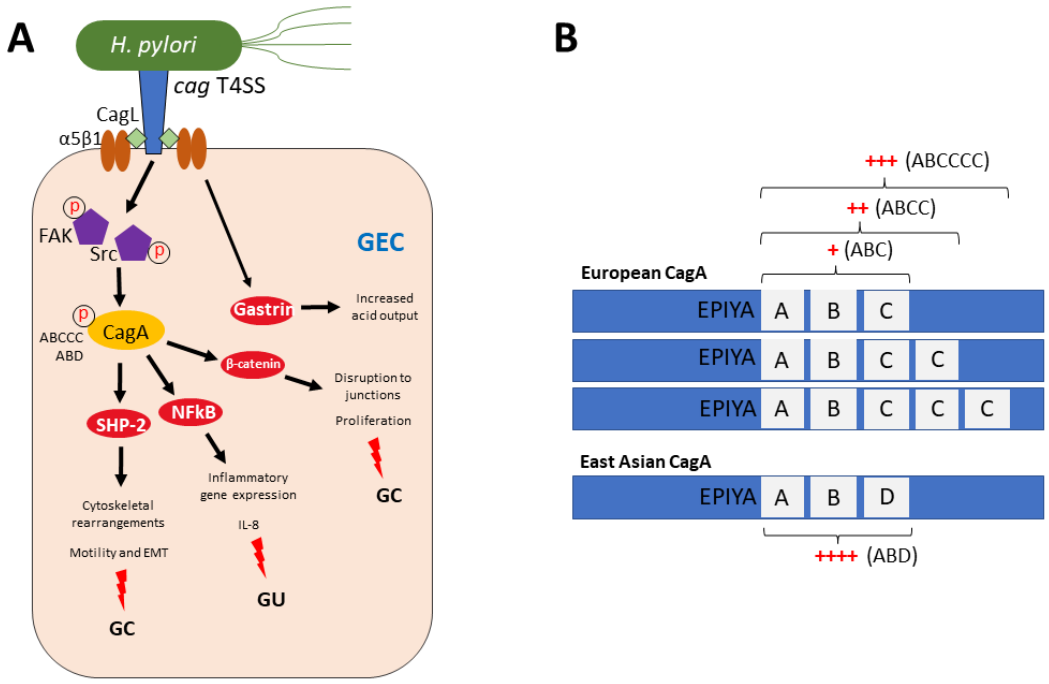

Figure 6 The structure and functions of CagA in H. pylori infection.

(A) A simplified representation of the major functions for the cag T4SS and CagA in host gastric epithelial cells. The RGD motif of CagL is exposed after acid-induced conformational changes. CagL recognises the α5β1-integrin via the exposed RGD motif. CagL:integrin binding is essential for the full assembly and activation of the T4SS and results in the phosphorylation of focal adhesion kinase (FAK) and Src, along with the translocation of CagA (and other bacterial constituents such as peptidoglycan) into the host cytosol. CagL binding to α5β1-integrin has been suggested to activate transcription at the gastrin promotor thus contributing to high acid load. CagA can be phosphorylated at EPIYA sites by host kinases. Phosphorylated CagA activates SHP-2 which can lead to altered phosphorylation of host proteins. Downstream effects of CagA include disruption to cell-cell junctions, β-catenin-mediated transcription, proliferation, motility, EMT and cytoskeletal rearrangements, together these can increase the risk of gastric cancer (GC). CagA can also induce NFkB-mediated inflammatory gene expression including IL-8, increases the risk of gastric ulcers (GU). (B) A representation of the structure of CagA EPIYA segments between European and East Asian strains. East Asian strains contain clusters A, B and D following the EPIYA site, these are considered the most pathogenic strains. European strains contain A, B and C clusters following the EPIYA site. The C-cluster can be found in repeating units to produce ABC, ABCC or ABCCC forms, strains with higher numbers of C-clusters have a higher pathogenic potential.

1.2.4.2 – Vacuolating cytotoxin A (VacA).

The multitude of functions exhibited by VacA are diverse and include vacuolation of host cells; interference with endosomal maturation; ion channel formation; cytochrome C mediated apoptosis; mitochondrial membrane disruption; cytoskeletal disruption; initiation of autophagy mechanisms; and modulation of effector T-cell activity [108,116,121,122]. *vacA* is always present in *H. pylori* irrespective of strain, however it is polymorphic resulting in different pathogenic potentials [108,116]. Initially translated as a 140kD peptide VacA is cleaved to yield a functional protein of around 88kDa

comprised of 2 associated subunits p37 and p58 (sometimes referred to in the literature as p33 and p55 fragments), both of which are required for functionality [57,123,124]. The larger p58 portion facilitates the binding to host cells whereas the p37 portion contains hydrophobic domains to allow insertion into cell membranes and mediate the vacuolating activity and ion channel formation [57,122,124]. Secreted VacA can adsorb to the outer membrane of *H. pylori* or can form soluble 'snowflake'-shaped hexameric oligomers (*Figure 7*). The non-covalent associations of VacA hexamers may be influenced by the gastric pH allowing VacA to be acid-activated [122,124,125].

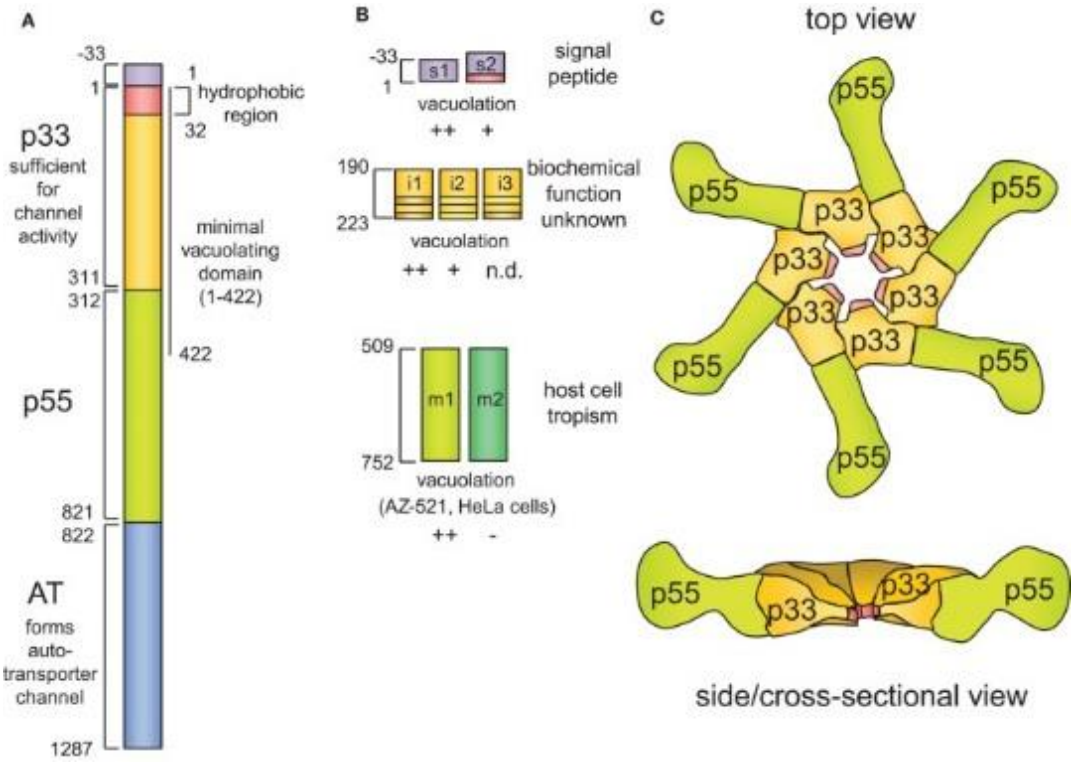

Figure 7 The structure of VacA

(A) Schematic VacA structure. Each domain is denoted by a different colour and by the first and last amino residue of that domain. The name of each domain is denoted in bold, and its function (if known) is described. (B) The polymorphic nature of the vacA gene is emphasized by highlighting the three major allele families, which are in the signal region (s region), the intermediate region (i region), and the mid-region (m region). (C) The proposed structure of the VacA oligomeric assembly, based on the crystal structure of a portion of p55 [Gangwer *et al.* (2007)] and electron microscopy imaging of VacA oligomers [El-Bez *et al.* (2005)]. *Figure used unmodified from: Kim, et al., 2012; Front. Cell. and Infect. Microbiol., March, Vol* ***2,*** *Art.37; doi:10.3389/fcimb.2012.00037* [124].

There are three characteristic regions of variance in the *vacA* gene; the signal region (s); intermediate region (i); and middle region (m). Regional variance in strains give rise to distinct potentials for cellular toxicity. The two most studied sites of variance are in

the signal (s) and middle (m) region which produce either s1/s2 or m1/m2 forms. The s1 region may be further classified as s1a, s1b and s1c [124]. The combination of *s* and *m* regions within the genome influences the activity of VacA and thus the pathogenicity of that strain *in vivo* [57,125]. The signal region is at the N-terminus of the smaller p37 subunit and is cleaved upon export to yield the mature VacA protein [57,122]. The *s*2 form differs from *s*1 by the inclusion of 12 amino acids to the signal peptide resulting in an altered cleavage site, that leaves N-terminal hydrophilic residues which impede membrane insertion, this causes the reduced vacuolating activity noted in s2-containing strains [57,122,126]. The middle region is in the larger p58 subunit and can mediate binding to host cells. Strains with the *m*1 form are capable of binding to a wider range of cells, the reduced binding capacity of m2 forms mediates the lower pathogenicity of *m*2-containing strains [57,108,122,125]. The type 1 forms confer increased cytotoxicity, s1/m1 variants of VacA are highly pathogenic with increased vacuolating activity; s2/m2 variant reduces vacuolating function and toxicity [57,108]. In Japan *H. pylori* strains are nearly all *vacA*-s1/m1 and there is an increased risk of gastric adenocarcinoma and PUD associated with these strains [57].

The more recently described intermediate (i) region is located between the s and m regions and has i1, i2 and i3 variants. The i-region contains additional clusters of variances termed cluster A, B and C. Polymorphism in these clusters can alter the toxicity of VacA. Regarding disease risk, the intermediate region influences the activity of VacA, and *i*1-containing strains have a higher vacuolating activity, inflammation and are associated with PUD and GC [122,124,127,128]. The *i*1 region is suggested to the best VacA-associated indicator of disease risk. Indeed, alleles containing the *i*2 variant will lose vacuolating ability even in *s*1/*m*1 strains [121,124,125,127,128]. Taken together, we see highly polymorphic proteins each able to confer varying pathogenic potential to the strains which express them. The *H. pylori* strains expressing *vacA*-s1/m1/i1 are the most harmful in terms of contributing to disease and gastric insult, whereas *vacA*-s2/m2/i2 would produce markedly less active and non-toxic proteins [57,122,125].

The oligomerisation of secreted VacA monomers is influenced by pH, in fact VacA is acid-activated and thus the gastric niche provides an optimum environment [122,124].

VacA can bind to host cells using a variety of receptors including receptor protein tyrosine phosphatase (RPTPα and RPTPβ), epidermal growth factor receptor (EGFR), leukocyte functional antigen-1 (LFA-1) and sphingomyelins [57,122,125]. There are many functions of VacA besides the characteristic vacuolation for which it was named. The cellular processes shown to be affected by VacA include pore and anion channel formation, cellular apoptosis, host signalling cascades, antigen processing, phagosome formation, and T-cell activation [57,122]. Some of the known VacA functions in host cells are presented in *Figure 8.*

The permeablisation of cell membranes by VacA gives the bacterium access to nutrients including urea, bicarbonates and sugars which provide a survival advantage [57]. Disruption to the endocytic processes causes VacA-mediated disruption to antigen processing [125]. The formation of anion channels allows the efflux of ions including Fe^{2+} and Ni^{2+} and influx of Ca^{2+} which can regulate calcium dependent signalling and cause disruption to the membrane potentials [122,124]. When VacA binds to cells it becomes internalised although the exact mechanisms of internalisation are debated in the literature [125]. The disruption to membrane potentials in mitochondria by VacA is a contributory mechanism to induce apoptosis. This may occur by reducing ATP production, modulation of host signalling, or by the release of cytochrome C; ablation of channel-forming activity can prevent cytochrome C-mediated apoptosis [122,125]. Other effects of VacA include reducing gastric mucin production, parietal cell acid secretion, and pancreatic enzyme secretion [125].

Modulation of host cell signalling has downstream consequences on the cell-cycle and expression of inflammatory genes [122]. It has been demonstrated that particularly s1/m1 variants upregulate the expression of cytokines including TNFα, IL-1, IL-6, IL-10 and IL-13 [122]. The dysregulation of calcium caused by channel formation can lead to the induction of IL-8 and other inflammatory genes through NFkB and p38/MAPKs and activate calcium-dependent cytoskeletal activity [122,124]. Furthermore, COX2 which increases the PGE2-dependent secretion of bicarbonate is elevated by VacA. Bicarbonate release serves to neutralise the gastric acid in the immediate environment and activation of COX2/PGE2 also influences the Th1/Th2 polarisation to favour

tolerance, discussed in a later section. Notably, others have reported the opposite occurring in mouse models, here VacA appears to inhibit PGE2-mediated bicarbonate and promote PUD [122,124]. In addition, VacA interacts with the PI3K/Akt/GSK3β-axis resulting in increased β-catenin and expression of cell cycle-related genes involved in the development of GC [122].

H. pylori can survive intracellularly within phagosomes, and that this is dependent on the inhibition of phagosome maturation and lysosome fusion. VacA has been demonstrated to modulate these processes by disrupting phagosome maturation through the retention of coronin-1 [122]. Interestingly, VacA did not appear to affect the ability of *H. pylori* to persist within phagosomes and instead would appear to promote the formation of megasomes through monotypic fusion [122]. An important effect of VacA in terms of immune modulation is the associated inhibition of antigen presentation [122]. Furthermore, VacA-mediated inhibition of both B- and T-cell proliferation has been reported, and VacA can internalise to migratory activated T-cells through binding to the cell surface molecules CD18/LFA-1 [122]. Within T-cells, VacA attenuates the expression of IL-2 and IL-2Rα by inhibiting the phosphorylation and subsequent nuclear translocation of the transcription factor of activated T-cells (NFAT). This is thought to occur via calcium efflux through the formation of membrane channels and blocks T-cell activation and effector function [122,124]. Additionally, inhibition of T-cell proliferation may occur via the anion channel-forming function of VacA independently of both NFAT and IL-2, utilised as a mechanism to prevent the expansion of *H. pylori*-specific activated T-cells [129].

Many strains that express the more virulent *vacA*-m1/s1 alleles are $CagA^+$, however strains carrying the less pathogenic *vacA*-m2/s2 alleles are often $CagA^-$ suggesting a relationship between these two factors [108]. Within cells CagA and VacA can exert antagonistic effects, one such example is with the NFAT pathway. Here, CagA can cause increased phosphorylation and activation of NFAT in a PLCγ/calcinurin-mediated pathway, however VacA-mediated calcium efflux can block this process [122,124]. In addition, CagA can counteract VacA-mediated apoptosis in both phosphorylated and non-phosphorylated forms. CagA has been demonstrated to protect from apoptosis in

2 ways; blocking the transport of VacA intracellularly, in addition to increasing expression of anti-apoptotic Bcl2 [122,124,130]. Taken together, CagA would appear to exert a certain protection over VacA-mediated cytotoxicity. Others have suggested that the injection of CagA to cells to which *H. pylori* is adhered to can prevent them from succumbing to VacA toxicity. This can maintain the gastric niche and protect cells directly supporting the bacterium [122,124,130].

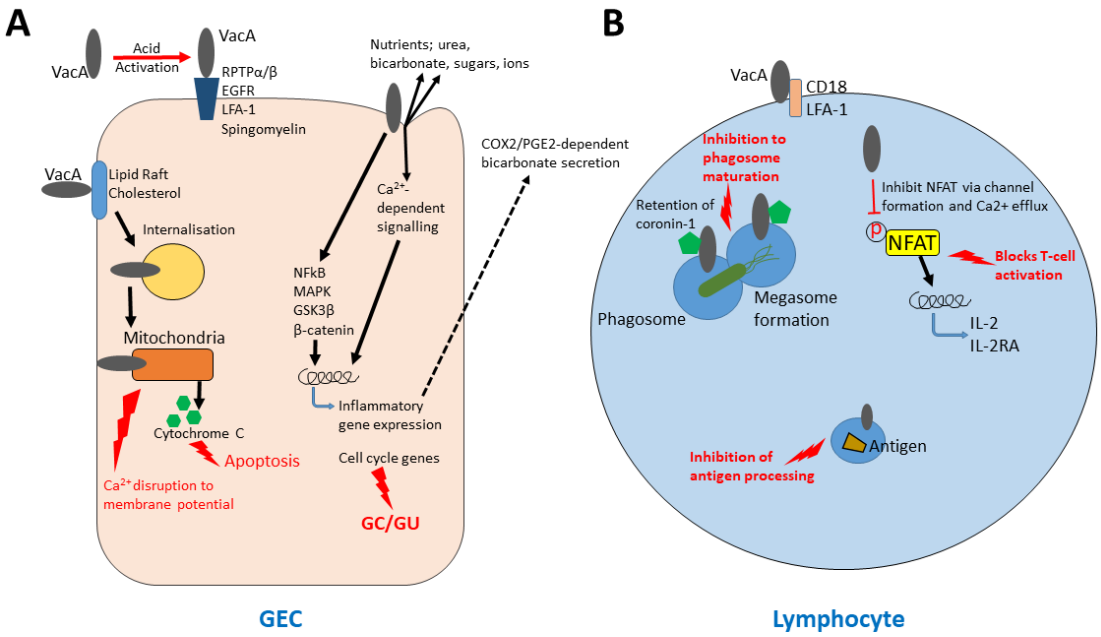

Figure 8 The major effects of VacA on GECs and lymphocytes.

(A) In GECs, VacA can be adsorbed to *H. pylori* outer membrane, or secreted where it forms hexameric oligomers. VacA is acid activated and can bind to host receptors including RPTPα/β, epidermal growth factor receptor (EGFR), leukocyte functional antigen-1 (LFA-1) and sphingomyelins. VacA binds in vicinity of lipid rafts and internalised in cholesterol-dependent mechanisms. Internalised VacA can insert to mitochondrial membranes forming channels and causing Ca2+ efflux. This results in disruption to membrane potentials, cytochrome C release and apoptosis. VacA can also exert effects on the GSK3β/β-catenin-axis resulting in the expression of cell cycle-related genes and promote gastric cancer. The channel forming ability of VacA allows nutrient efflux from host cells and disruption to calcium signalling and downstream expression changes of cytoskeletal and inflammatory genes. VacA activates signalling through NFkB to increase expression of inflammatory genes. VacA increases expression of COX2 which results in the PGE2-dependent secretion of bicarbonate, neutralising gastric acid and creating a permissive microenvironment for *H. pylori* survival. (B) In immune cells, VacA can bind to cell surface receptors including LFA-1 and CD18. VacA can cause the inhibition to endocytosis and phagosome maturation, possibly involving the retention of coronin-1. Attenuated phagosomes can undergo homotypic fusion to form megasomes, capable of supporting the survival and replication of *H. pylori* internally. VacA can inhibit the phosphorylation and activation of the nuclear factor of activated T-cells (NFAT) which abrogates IL2 and IL-2Rα expression thus inhibiting T-cell effector function. Interestingly, CagA appears to activate NFAT and thus CagA and VacA have opposing functions in some respects.

1.2.4.3 – Additional virulence factors of *H. pylori*

Duodenal ulcer-promoting gene A (*dupA*) has a higher prevalence amongst cases of duodenal ulcer (DU) but may be a protective factor for GC [35, 46]. Potentially this may be due to *dupA*-positive strains showing a trend for increased acid secretion [131]. Overall, the prevalence of *dupA* is higher among Western than Asian strains. Interestingly, the presence of *dupA* has a significant association with the failure of *H. pylori* eradication therapy [116]. The 5' end of the *dupA* reading frame can have two forms with either the presence or absence of a 600bp sequence which confers altered functionality to the expressed protein [116], the longer form of *dupA* can be indicative of gastric disease risk [116,132]. The *dupA* locus is flanked either side by *Vir* genes [116]., the *vir* cluster forms a functional T4SS which may influence disease development [132]. Mutation in or around the *dupA/vir* cluster may prevent a secretion-system being formed thus reducing the risk of disease [116].

OipA, otherwise referred to in the literature as HopH, is an OMP that can facilitate adhesion to the gastric epithelium. OipA is associated with increased secretion of IL-8 by GEC, higher inflammation, and the presentation of PUD, although this is disputed by others [116,133]. In a meta-analysis, functional OipA was shown to be a significant risk for peptic ulcer (PU) and GC [134]. OipA status (ON, or OFF) may be related to the expression of other *H. pylori* virulence factors; *oipA*-ON is associated with *cagA*+/vacA-type1 alleles; whilst *oipA*-OFF is associated with *vacA*-type 2 variants [133]. OipA could also influence the phosphorylation of proteins integral to *cag*PAI-related signalling pathways causing elevations of IL-8 secretion and inflammation [116]. An *oipA*$^{-/-}$ mutant strain of *H. pylori* resulted in lower levels of the inflammatory cytokines IL-1β, IL-17, IL-18 and TNFα in a Mongolian gerbil infection model, it was concluded that OipA status may be a better predictor of disease outcomes than *cag*PAI, but this is debated [116]. Conversely, OipA can inhibit the maturation of dendritic cells (DC) by reducing expression of co-stimulatory molecules CD40 and CD86, and MHC-II thus suppressing the activation of effector T-cells, enabling bacterial persistence. However, in the infected mucosa, DC-derived IL-10 was significantly reduced in the presence of OipA but no change found in IL-12 to support

a reduction of effector responses [135]. A summary of some of the virulence factors of *H. pylori* and their biological functions is presented in *Table 3*.

The scope of this review does not allow for in-depth analysis of the functions of further virulence factors. It is however important to understand the nature of *H. pylori* pathogenesis and how the distinction between asymptomatic and pathogenic infections are mediated and regulated, through the presence, absence, or functional status of such entities.

Table 3 Virulence factors of H. pylori and their associated biological effects

Virulence Factor	Biological Function	Reference
***cag*PAI**	Encodes T4SS required for CagA translocation into host cells	*Kusters J, 2006*
CagA	Translocated to host cells via T4SS, phosphorylated by host kinases, activates host SHP-2, causes dephosphorylation of host proteins and altered cellular function.	*Naumann M, 2017; Roesler BM, 2014; Bonsor DA, 2015; Cover T, 2012; Scott-Algood HM, 2006; Peek Jr. RM, 2010;*
VacA	Pore-formation, vacuolation, interrupts phagosome maturation, interrupts antigen processing, inhibit T-cell activation via NFAT pathway.	*Roesler BM, 2014; Shiota S, 2013; Jones KR, 2011; Jones KR, 2010; Atherton JC, 2006; Papini E, 2001; Kim IJ, 2012*
DupA	Higher prevalence in western strains, associated with duodenal ulcer, flanked by the *vir* loci encoding a secretion system, increased acid secretion, negatively associated with GC risk.	*Roesler BM, 2014; Shiota S, 2013; Abadi ATB, 2014; Imagawa, 2010*
OipA	HopH, functions in adherence, associated with increased IL-8 secretion and inflammation, associated with VacA/CagA-positive strains.	*Shiota S, 2013; Dossumbekova A, 2006; Kudo T, 2004; Liu J, 2013; Yamaoka Y, 2002*
BabA/SabA	Bind to blood group antigens, lewis B antigens (BabA) and sialylated lewis antigens (SabA), important for adhesion to gastric epithelium, essential for colonisation, can enhance CagA translocation via *cag*T4SS	*Matsuo Y, 2017; Odenbreit S, 2009; Alm R, 2000.*

1.3 - Host Immune Response to *H. pylori*

1.3.1 – Innate Immune Response to *H. pylori*

Infection and inflammation of the gastric mucosa stimulates an infiltration of innate and adaptive lymphocytes. Macrophage activation and neutrophil infiltration is of a large scale and persists throughout the infection, secreting inflammatory chemokines and cytokines contributing to a highly immunogenic microenvironment. They also produce cytotoxic molecules such as reactive oxygen species (ROS) and nitric oxide (NO) which can damage host epithelial cells, contributing to gastric pathogenesis. The inflammatory milieu orchestrates the activation of adaptive immune responses.

1.3.1.1 – PRR/PAMP Signalling

Recognition of pathogen-associated molecular patterns (PAMPs) by pattern recognition receptors (PRRs) initiates immune responses to clear an identified infection [114,136-139]. *H. pylori* has evolved strategies to avoid PRR-mediated detection, including the modification of recognisable constituents such as flagellin and LPS which leaves TLR4 and TLR5 only weakly activated [45,106,114,140]. The major PRR activated in response to *H. pylori* is TLR2 which can promote NLRP3 inflammasome assembly and NFkB-activation. This can result in the expression of genes including IL-1β, IL-8, IL-18, IFNs, NOS, and defensins [23,140,141]. Naïve T-cells may express both IL-1R and IL-18R and the effector subtype induced during activation can be influenced by this balance. Briefly, after *H.pylori*-mediated TLR2 activation and NLRP3-inflammasome assembly in dendritic cells, high IL-1β can initiate differentiation to a Th1 lineage, whereas high IL-18 may result in tolerance promoting Tregs [23]. This balance has relevance to the protection from certain diseases mediated by *H. pylori*, discussed later.

NOD1 recognises constituents of peptidoglycan (PGN) from gram-negative bacteria such as *H. pylori*. Human NOD1 has specificity for PGN fragments containing GlcNAc-MurNAc diaminopimelic acid tripeptide (GM-TriDAP), and derivatives thereof. PGN can enter cells through phagocytosis, endocytosis, transport across junctions from neighbouring cells, bacterial outer membrane vesicles (OMVs) or directly into cells through secretion systems such as the *H. pylori cag* PaI T4SS [106,140,142,143]. NOD1

activation induces the NFkB and MAPK signalling pathways producing cytokines and inflammatory mediators [64,142-144]. In Nod1$^{-/-}$ and Nod2$^{-/-}$ models, mice show an increased susceptibility to microbial infections including *H. pylori* [142]. *H. pylori* can modify PGN by N-deacetylation as a means of evading NOD-mediated detection [142].

1.3.1.2 – Neutrophils.

Neutrophils are amongst the first responders to an infection infiltrating in large numbers. When activated they produce chemokines important for the recruitment of a further immune response [145]. They also contribute to GEC damage through degranulation and the secretion of cytotoxic molecules such as ROS and NO through the respiratory burst [106]. Human neutrophil peptides; HNP-1 to -4 are α-defensins expressed by human neutrophils, making up around 50% of granulated proteins [146], however are absent in mice [41,42]. Depletion of neutrophils resulted in deficient clearance of *H. pylori* and reduced Th1 cell responses in mouse models, suggesting neutrophils to play an essential role in the propagation of the host T-cell response to *Helicobacter* infection [146].

Neutrophils are recruited to the site of infection by the production of local IL-8 (CXCL8) a potent neutrophil chemotactic factor, upregulated in GECs in response to infection. Activation of PRRs by *H. pylori*-derived ligands induces inflammatory signalling thus further increasing the expression of IL-8 [45]. In addition, virulence factors of the colonising strain can have marked effects on the levels of IL-8 induced; CagA+ strains induce higher levels of IL-8, augmenting neutrophil infiltration and consequentially increasing GEC pathology [106].

A virulence factor of *H. pylori* is a potent neutrophil activator; the *H. pylori* neutrophil-activating protein (*Hp*-NAP) can both recruit other neutrophils and facilitate adhesion to the epithelium [145]. It can activate TLR2 inducing expression of IL-12 and IL-23 in neutrophils and monocytes augmenting Th1 and Th17 adaptive responses [145,147]. Further reported function of Hp-NAP include the binding of free iron and protection of DNA from damage and can be localised to the bacterial outer membrane and may function in adhesion to mucins or sphingomyelins.[145].

1.3.1.3 – Monocytes.

Monocytes can differentiate into macrophage or dendritic cells thus being a major source of recruited phagocytes in response to infection [148]. They can act counter-productively in some instances by assisting the spread of pathogens. It has been demonstrated that *Listeria monocytogenes* gains entry into the bone marrow and CNS by travelling inside monocytes [148]. Monocytes may express inflammatory molecules including TNFα, NO and IL1β, engage in phagocytosis and co-ordinate adaptive immune responses through the activation of T-cells [148,149]. *H. pylori* can achieve persistence inside monocytes by inhibiting phagosome maturation, and functional deficits and the early apoptosis of monocytes associated with *H. pylori*-related factors is a mechanism contributing to immune evasion by the bacterium [150].

1.3.1.4 – Macrophages.

Macrophages recognise and ingesting microbes, present antigen, and secrete a diverse array of inflammatory molecules to orchestrate further adaptive cellular responses. The macrophage response is a major obstacle for invading bacteria and one which must be subverted for a chronic infection to be established. There are numerous strategies hypothesised by which *H. pylori* can accomplish this, including alterations to NO metabolism, inhibition to phagosome maturation, and modifications to cellular PAMPs to avoid PRR activation [1,151].

Macrophages are important sources of nitric oxide (NO) produced using the enzyme iNOS (inducible NO synthase). *H. pylori* infection causes an upregulation of iNOS in both GEC's and macrophages [115,151-153]. Subversion of NO toxicity is crucial to allow *H. pylori* to survive and establish a persistent infection. The *H. pylori*-derived arginase RocF and macrophage-derived Arg2 are upregulated by *H. pylori*. Together both Arg2 and RocF are in direct competition with iNOS for the common substrate L-arginine and exert a cumulative inhibition of host NO production, limiting the clearance of *H. pylori* and providing a mechanism of phagocyte evasion [115,151-155].

H. pylori has been shown to interfere with phagosome fusion and maturation thus preventing the deposition of lytic enzymes and antimicrobial compounds [106,151]. Defective phagosomes have also been demonstrated to permit intracellular survival of *H. pylori*, multiple phagosomes may undergo homotypic fusion to form enlarged shared compartments termed megasomes [151]. Mechanistically there is debate, some report that the interference to phagocytosis by *H. pylori* is dependent on the virulence factors CagA and VacA, whereas others propose this to occur independently of these [151,156].

The cell wall of *H. pylori* contains a notable proportion of cholesterol glucosides which affect bacterial growth and survival. The cholesterol-α-glucosyltransferase enzyme of *H. pylori* (CapJ), functions in the acquisition and α-glycosylation of cholesterol from host cell membranes. Several groups have provided evidence that α-glycosylation of cholesterol in this manner attenuates phagocytosis of *H. pylori* thus evading the immune response [157,158].

1.3.1.5 – Dendritic cells.

Dendritic cells (DC's) are professional antigen presenting cells and transduce signals to T-cells stimulate effector responses in both immature and mature states. This is of relevance with regards to immune tolerance to non-harmful or self-antigens, discussed later in this section. The culture of DCs in the presence of *H. pylori* has been demonstrated to cause the expression of a range of both anti- or pro-inflammatory cytokines which can be dependent on many variables such as bacterial strain and environmental stimuli [106]. It is well documented that *H. pylori* infection can initiate a profound inflammatory immune response involving primarily Th1 and Th17 lymphocytes. If DC uptake antigen in an environment lacking inflammatory stimuli, or indeed if they are desensitised by *H. pylori*-derived factors, they fail to elicit effector T-cell differentiation and can instead promote tolerance and cause an expansion of regulatory T-cell populations, described later.

Gastric tissues of *H. pylori*-infected individuals have increased numbers of DCs presenting a tolerogenic phenotype [45]. Recently, *H. pylori* has been shown to

interfere with DC maturation and suppress effector T-cell responses by reducing co-stimulatory molecules and T-cell polarising factors, skewing cytokine production towards an anti-inflammatory type upon stimulation [159,160]. Furthermore, *Lactobacillus acidophilus* is a Th1-polarising pathogen known to induce M1-macrophage/Th1 responses. A reduction in co-stimulatory molecules CD80/86 and notably lower levels of inflammatory cytokines IL-12, IFNy, TNFα and IL-6 were found when DCs or macrophages had been co-cultured with *H. pylori* in an *L. acidophilus* infection model [159]. *H. pylori* can drive Treg differentiation by inducing DC-derived IL-18 [20,21]. In the gut, DC's have been observed to induce Treg cells via the secretion of retinoic acid (RA) and TGFβ [161,162]. This provides evidence of *H. pylori*-mediated suppression of these inflammatory responses mediated primarily through dendritic cells and with effector T-cell function as the immediate affecter. This *H. pylori*-mediated suppression of DCs, can occur through both VacA and CagA –dependent and –independent mechanisms [160,163].

1.3.2 – Adaptive immune response to *H. pylori* infection.

H. pylori infection initiates a robust inflammatory response predominated by Th1 cells, although the adaptive response is usually insufficient to clear the infection. The scale of this response is a contributory factor to the extent of gastric pathogenesis through the chronic expression of cytokines causing inflammation, acid imbalance, gastric epithelial-barrier dysfunction, and the apoptosis of GECs [45,57,106,164]. Infection results in phagocyte infiltration and activation, M1-polarisation in macrophages, and an environment enriched in inflammatory cytokines including IL-1β, IL-6, IL-8, IL-12, IFNy, IL-18 and TNFα [45,141]. The cytokine milieu created during *H. pylori*-associated gastric inflammation influences the adaptive T-cell responses.

1.3.2.1 – Th1-mediated responses.

The Th1-associated cytokines IFNy, TNFα, IL-12 and IL-18 are upregulated in the infected mucosa [45] and the expression of the transcription factor T-bet (which drives Th1 differentiation) is expressed in a greater proportion of lymphocytes in the gastric mucosa and peripheral blood in *H. pylori*-infected individuals [165]. Several *H. pylori* factors including urease and Hp-NAP can induce stronger Th1 responses and

increased cytokine secretion [145]. This is also greater in virulent *cag*+ strains as compared to *cag*- strains and the extent of gastritis can be influenced by the scale of this response [106]. Th1 cytokines promote increased inflammation, macrophage M1 polarisation and activity, causing epithelial cell toxicity [45].

In Th1/IFNγ-incompetent mouse models there is a significant reduction of gastric atrophy and increased colonisation density demonstrating the importance of the Th1 response against *H. pylori* [45,57,106]. In contrast, a robust Th1 response leads to lower colonisation densities but increasing severity of gastritis as a result [166]. Interestingly, although contributing to gastric pathogenesis, a robust Th1 response may serve as a protective factor against the development of gastric cancer due to an increased anti-tumour efficiency [45].

Despite a strong Th1 response in most cases *H. pylori* can evade and persist. There are several mechanisms proposed by which this could occur. VacA can prevent Th1 activation through interference to the TCR and IL-2 calcineurin-dependent signalling pathways and blocking the translocation transcription factor NFAT [140,141,165]. Strains carrying the *cag*PAI can induce T-cell apoptosis and cell cycle arrest through the induction of Fas ligand FasL [165]. The enzyme gamma-glutamyl transpeptidase (GGT) of *H. pylori* induces T-cell death through the production of ROS, and cell cycle arrest [140,165]. In the infected gastric mucosa, cyclooxygenase-2 (COX-2) is upregulated in response to LPS and the cytokines IL-1β and TNFα [167]. COX-2 can mediate the production of prostaglandin E2 (PGE2) which can suppress innate immune responses, and thus reduce Th1-polarisation and IFNγ production [167,168]. On the other hand it is suggested that it may induce Th17 and Treg responses [168]. Th1 inhibition by PGE2 in the context of *H. pylori* infection is mediated via blockade of IL-2 signalling and modulation of dendritic cells [165,168,169]. *Helicobacter* can alter the expression of Lewis antigens in a phase-variable manner and these can bind the C-type lectin receptor DC-SIGN on DCs rendering them ineffective at Th1 induction [57].

Alternatively, the enzyme indoleamine 2,3-dioxygenase (IDO) is a regulator of the tryptophan catabolic pathways and the production of metabolites such as kynurenine. IDO is upregulated in *H. pylori*-infected gastric tissue, this has been associated with a reduction in IFNγ and T-bet in infected individuals; inhibition to IL-

2 signalling; activation of Aryl hydrocarbon receptors (AhR); and inducing Tregs in a CTLA4-dependent mechanism [170-172] [165]. An environment deficient in tryptophan can inhibit T-cell replication and increase T-cell apoptosis. Kynurenine (Kyn) is a major IDO-derived metabolite of tryptophan and has anti-inflammatory and immunosuppressive potential [171-173].

1.3.2.2 – Th2-mediated responses.

The Th2-assoiciated cytokines IL-4 and IL-5 are found at low abundance [45,165,174], concurrently with an increase in Th1-associated cytokines IL-2 and IL-12 during *H. pylori* infection [45,165]. This pro-inflammatory skewing of the Th1/Th2 balance may limit Th2 responses and mediate protection from allergy and asthma, which has been observed in response to *H. pylori.* In contrast, Th2-polarising conditions such as intestinal helminth infection can abrogate the Th1 response to *H. pylori,* reducing gastritis severity but permitting higher colonisation densities due to a reduced protective immunity [106].

Interestingly, the response to *H. pylori* in African patients has on occasion been reported by others as being Th2-biased, in opposition to the Th1-biased responses seen in European and Japanese individuals [106]. This is demonstrative of the effect of both bacterial strain and host genetics in orchestrating the immune response against the infection. The Th2-biased response in these instances could partially explain the reduced incidence of secondary disease and gastric cancer in African populations, a paradox termed the 'African enigma' [175].

1.3.2.3 – Th17-mediated responses.

The immune response to *H. pylori* is often described as being Th1-mediated. More specifically, it is Th1-dominant but with a substantial Th17 component. The differentiation of the Th17 lineage is driven by the transcription factor RORγT and Th17 cells secrete the signature cytokines IL-17, IL-21, IL-22, IL-6 and TNFα [176-179]. Th17 activation induces the recruitment of innate immune cells and contributes to the secretion of pro-inflammatory cytokines, chemokines, and antimicrobial molecules. Th17 differentiation is induced by the polarising factors such as IL-1β, IL-

6, TGFβ, and IL-23 secreted by antigen presenting cells in response to pathogen [177]. On the other hand, STAT3-dependent expression of the orphan nuclear receptor RORα can also promote Th17 differentiation in the absence of RORγT [180]. Interestingly TGFβ supports the production of FOXP3 driving the Treg specification, however when IL-6 is present FOXP3 is inhibited and instead favours Th17 induction. Alternative induction of the Th17 lineage can produce cells with non-pathogenic regulatory functions (Treg17 cells) [179]. It has been reported by others, that Th17 cells may under certain conditions transdifferentiate into regulatory-like cells that display an anti-inflammatory phenotype resembling FOXP3- type-1 regulatory T-cells (Tr1) and lose expression of IL-17 [181,182]. Conversely, Treg cells may adopt a Th17 phenotype in certain inflammatory conditions [183].

Activated Th17 cells are characteristically responsive to fungal infection but are intricately involved in the response to many infections and autoimmune diseases. In the *H. pylori*-infected gastric mucosa Th17 cells and IL-17 are upregulated and contribute to inflammation and gastric pathogenesis [176-178]. The secretion of B-cell activating factor of TNF family (BAFF) by *H. pylori*-activated macrophages is important for the generation of Th17 cells [45]. In mice, inflammation is sustained in models of Th1-ablation suggesting a potentially crucial role for Th17 cells in propagating and sustaining *H. pylori*-mediated gastritis [165]. The neutralisation of IL-17 in IFNγ$^{-/-}$ mouse models totally abrogates protective immunity to *H. pylori* [165]. Furthermore, IL-17 induces the secretion of pro-inflammatory cytokines and chemokines including IL-8 in the infected mucosa [184], in addition to antimicrobial molecules from gastric epithelial cells such as β-defensins [185].

There are conflicting data in the literature regarding the Th17 response after *H. pylori* eradication. Some report the numbers of Th17 cells to be sustained post-eradication, whereas others note a rapid decline [184,186].

1.3.2.4 - Immunometabolism as a modulator of T-cell Regulation

As the literature demonstrates, immune responses can be modulated metabolically [187-189]. Glycolysis drives T-effector functions, whereas Tregs favour fatty acid oxidation [189]. In other instances, a deficiency of available glutamine during CD4+ T-cell receptor activation can induce Treg differentiation even when under Th1-

polarising conditions [189]. On the other hand, high-salt environments favour skewing the Th17/Treg balance towards inflammatory Th17 cells [189]. The glycolytic pathway has been shown to modulate the expression of the alternate splice variants of FOXP3, which can support either Treg or Th17 effector functions [188,190]. A mechanism Tregs use to suppress T-effector responses is through the metabolism of ATP to AMP through CD39/CD73. Interestingly, one of the mechanisms of action of the MS therapeutic drug dimethyl fumarate, is mediated through inhibition of the glycolytic enzyme GAPDH [187]. Taken together, the balance between T-effector and regulatory T-cells can be shaped by the metabolic state and nutrient availability in the immediate environment and should be considered to regulate T-cell driven responses.

1.4 – Regulatory T-cells: Function and Mechanisms

A subset of suppressive $CD4^+$ T-cells with the ability to dampen pro-inflammatory effector T-cell responses and maintain tolerance to non-pathogenic and self-antigens are regulatory T-cells (Tregs). Broadly, Tregs may be grouped into two major categories; thymic-derived 'natural' Tregs (nTregs), a $CD4^+CD25^+FOXP3^+$ T-cell subset produced during thymocyte development in response to a strong T-cell receptor (TCR) affinity to self-antigens during selection; and 'inducible' Tregs (iTregs), arising from $FOXP3^-$ conventional T-cells in the periphery, adopting a regulatory phenotype in response to certain stimuli which can be $FOXP3^+$ (Th3 cells) or $FOXP3^-$ (Tr1 cells) both characteristically producing IL-10 and TGFβ [90,191-195]. Many biological processes may be differentially affected by the activity of Tregs. These include autoimmunity, tumour immunity, and tolerance to transplanted tissues [90].

1.4.1 – Natural Regulatory T-cells (nTregs)

Naturally arising nTregs develop when antigen is presented to T-cells without the necessary co-stimulatory signals to induce an effector response, or in the thymus as part of central tolerance in developing thymocytes with TCR specificity to self-antigen expressed as part of the thymic AIRE-mediated tolerance mechanism [196]. The autoimmune regulator protein (AIRE) is expressed in medullary and cortical thymic epithelial cells (mTEC/cTEC) and functions as a master transcription factor facilitating

the presentation of self-antigen to developing thymocytes [196]. Thymocytes with TCR specificity to antigens expressed in this manner will undergo clonal deletion or will differentiate to suppressive Tregs [196]. The nTregs constitutively express the major lineage-defining transcription factor FOXP3 [192]

These regulatory lineage T-cells were first proposed by Gershon & Kondo *circa* 1970-75 [195,197-199]. It was in the 1990's that Tregs, acting through secretion of anti-inflammatory cytokines including TGFβ and IL-10, were beginning to be properly described in the literature through seminal work by Sakaguchi *et al.* [200]. The emergence of Tregs was largely due to observations that distinct T-cell populations were responsible for either the development or protection of autoimmunity in mouse models, leading to the hypothesis that there were suppressive T-cells restraining inflammatory responses [201].

The first cellular marker identified to distinguish Tregs was the IL-2 receptor alpha chain (IL-2Rα), or cluster of differentiation 25 (CD25) by Sakaguchi *et al.* 1995 [201]. These $CD25^{+}CD4^{+}$ T-cells were crucial for the maintenance both of self-tolerance and suppression of effector responses to non-self-antigens. They were dependent on IL-2 and could suppress by contact dependent mechanisms [200,201].

In 2001, Brunkow *et al.* [202] identified a mutation in the *foxp3* gene as being the causative factor for the autoimmune condition observed in *Scurfy* mice. The similar human condition, immune dysregulation Polyendocrinopathy enteropathy X-linked syndrome (IPEX) was also linked to *FOXP3* mutation by Bennett *et al.* (2001) [203]. Both these mouse and human conditions cause spontaneous autoimmune development in multiple tissues [200,202]. After the identification of FOXP3 as a crucial determinant of Scurfy and IPEX, Fontenot *et al.* (2003) [204] reports that *FOXP3* was in fact the master transcription factor responsible for the development and function of the newly described TGFβ- and IL-10-secreting $CD25^{+}CD4^{+}$ Treg cells.

By the early turn of the millennium, immunologists now had a clearer understanding of a population of thymic-derived T-cells with a suppressive capacity, driven by *FOXP3*, expressing high levels of CD25, dependent on IL-2, and could function both through secretion of suppressive cytokines IL-10 and TGFβ as well as through

contact-dependent mechanisms utilising surface peptides as CTLA-4. These cells had been shown to possess the ability to restrain effector T-cell responses and to be crucial for the maintenance of self-tolerance, with autoimmunity developing when these cells were inhibited or deficient.

1.4.2 – Type 1 Regulatory T-cells (Tr1)

Tr1 cells were first described by Roncarolo *et al.* in 1998 [205]. Tr1 cells are distinct from FOXP3^{+} Tregs[206]. Discerning between Tr1 or non-Tr1 cells is not a straightforward matter. This can be done by characterising cellular markers and by assessing the suppressive capacity of the cells. It is proposed by Roncarolo, *et al.* (2018) [206], that there are 4 requirements to correctly define a Tr1 cell. First, the main proteins to be expressed will be IL-10 and TGFβ; secondly, unlike other IL-10 secreting cells, Tr1 cells will secrete IL-10 and concurrently possess a FOXP3-independent suppressive capacity against effector T-cells; thirdly, the signature Tr1 surface markers LAG-3 and CD49b can also be expressed by other cell lineages and so additional markers must be used when gating, these can include ICOS, PD-1, CTLA-4, CCR5, and TIGIT; finally, although a transient expression is possible, Tr1 cells are considered to be constitutively FOXP3- and thus distinct from FOXP3+ nTregs or Th3 cells [206].

Tr1 cells can be induced from T-cells in the presence of anti-inflammatory polarising factors such as IL-10, TGFβ, IL-27, and IFNα, they may also be trans-differentiated from activated effector memory T-cells [181]. Trans-differentiation can occur from Th1 and Th17 cells through TGFβ/IL-27/AhR-dependent mechanisms [206].

A major mechanism for the generation of Tr1 cells is mediated by IL-10-producing tolerogenic dendritic cells (DC-10) which can be induced by TGFβ, IL-10 and IL-27 from peripheral monocytes [206]. Although IL-10 is a major driver of Tr1 induction, it is not essential as others report the ability of naïve T-cells to adopt a Tr1-like phenotype when exposed to IL-27, TGFβ, IFNα, and IL-6 in various combinations, in addition to activation of ICOS and CD46 [206].

The generation of Tr1 cells from originally pro-inflammatory lineages is most likely a mechanism by which the inflammatory cascade is resolved when infection is

eliminated [206]. Trans-differentiation of activated effector T-cells into Tr1 cells is noted from Th1 cells in malaria infection, from Th2 cells in allergic patients and from Th17 cells in the intestine [206].

Tr1 cells have the capacity to suppress pathogenic T-cell responses in models of type-1 diabetes (T1D), rheumatoid arthritis (RA) and multiple sclerosis (MS) [206]. This suppression is exerted in multiple ways, largely overlapping with those of the nTregs. Primarily, secretion of the suppressive cytokines IL-10, TGFβ, and IL-35 [191,207]. Suppression can also be mediated by inducing cytolysis of Tcells and antigen presenting cells by the release of the bioactive molecules Granzyme A or B (GZMA/GZMB) and perforin [191,206,207]. There are contact-dependent mechanisms utilising CTLA-4 and PD-1, as well as CD73/CD39-mediated suppression by limiting available ATP. Modification of environmental cytokine concentrations such as with IL-2 deprivation, inhibits T effector function [191]. Modulation of dendritic cell function can be achieved through CTLA4 and CD80/86 activation, this stops T-cell activation by APCs [191,207]

These two major suppressive regulatory T-cell lineages are distinct in tissue compartmentalisation, phenotype, and function but act co-operatively in biological scenarios [206]. To distinguish Tregs and Tr1 cells, the surface proteins LAG3 and CD49b are useful but imperfect markers expressed by Tr1 but not constitutively by Tregs [208]. Given the similar expression profiles and the inter-diversity between T-cell lineages, identification between subsets is not always straightforward.

As we see, here builds a complicated picture of heterogenous populations of regulatory T-cells, with poorly characterisable (and often overlapping) markers, which may often possess markedly different suppressive capacity and biological function both *in vivo* and *vitro*. It is very important to note, that the heterogeneity amongst Treg subsets may be complicating the picture we see from the literature. Here, different research groups do not always use the same cellular markers to discern Treg populations. Some use FOXP3 and CD25, however these studies may miss very biologically relevant Tr1 populations. Others focus on IL-10 secretion; however, the secretion of suppressive cytokines does not consider the contact-dependent mechanisms.

Additionally, many studies identifying Tregs with flow cytometry gate populations based on CD4 expression, however here we may not account for regulatory subsets such as regulatory CD8 cells and regulatory B-cells. Another consideration is that categorising subsets as being either high or low for the expression of specific markers is not in itself reproducible. There will always be populations of cells in the 'mid' range with no clear and defined boundaries between groups. Currently there is no way of unifying these data, so until there is a consensus signature of Treg subsets, these discrepancies must be considered when assessing data in the literature.

There is also a need to consider the means of Treg suppression *in vivo*. Much of the research over the years into the mechanisms in which Tregs supress effector responses has been done using *in vitro* suppression assays, and as such there is little assurance that these mechanisms will be fully recapitulated when considering an *in vivo* environment [191,207]. Indeed, *in vitro* assays at their best can give us clues as to the functional capability of Tregs, but as Treg function is so inexplicably dependent on the microenvironment they cannot fully reproduce the *in vivo* context, with regards to polarising factors and surrounding cellular populations present.

1.4.3 – The Function of Tregs: Markers, Mechanisms, and Modulation

There are numerous reported studies focussing on the function of Tregs during infection and there are several microbes including bacteria and viruses which appear to elicit an increase in Treg populations [193,194]. It has been suggested that the production of iTregs in this manner may be dependent on secreted TGFβ or indeed TGFβ-homologues secreted by certain pathogens [194]. Functionally, the induction of iTregs in these incidences may act two-fold; firstly it may limit tissue damage caused by the inflammatory effector T-cells recruited to the site, and secondly this may lead to inefficient clearance of the pathogen resulting in chronic infection [194]. Modulation of co-stimulatory signalling may be utilised by microbial pathogens such as *H. pylori* to promote persistence and immune evasion, and thus may provide one mechanism for the protection against autoimmune conditions. Further elucidation of how, or at least if, *H. pylori* alters these signalling pathways within T-cells or APCs may be important.

1.4.3.1 – Cellular Markers of Regulatory T-cells

CD25 is expressed on T-cells during development but maintained on regulatory lineages. CD25 is the alpha-chain for the IL-2 receptor (IL-2Rα) and its presence is critical for both maintenance and function of Tregs [192]. The functional significance of CD25 is the binding of IL-2 necessary for the maintenance of Treg populations, the major source of IL-2 is from other T-cells where a feedback circuit is created. IL-2 from effector T-cells maintains the population of Tregs to subsequently downregulate IL-2 and prevent excessive Teff responses [192].

The characteristic transcription factor directing the development of the nTreg lineage is FOXP3, a member of the forkhead-box family of winged-helix TFs. FOXP3 is responsible for controlling the development and regulatory T-cells and ablation or mutation of FOXP3 leads to autoimmune complications as exemplified by IPEX (Immunodysregulation Polyendocrinopathy Enteropathy X-linked Syndrome) [192].

Attenuation of CTLA-4 (cytotoxic T-lymphocyte-associated protein 4) is comparable to that of Treg ablation and causes increased autoimmunity [192]. CTLA-4 (CD152) is a cell surface-expressed molecule present constitutively on naturally arising thymic-derived nTregs, and upregulated on effector T-cells upon activation [209]. It exerts negative regulation of effector T-cell (Teff) signalling and promotes suppression [192]. CTLA-4 provides a primary mechanism for Tregs to mediate their suppression through inhibition of the CD28:CD80/CD86 interaction between APC's and T-cells. CTLA-4 has affinity for CD80/CD86 expressed on antigen presenting cells, as does the cell-activating CD28 molecule. CTLA-4 has a higher affinity for CD80/86 and thus can competitively inhibit activation of Tcells via this pathway [209]. In $FOXP3^{+}$ nTregs CTLA-4-mediated contact-dependent suppression is a primary function. CTLA-4 restrains T-cell proliferation which is conversely increased with CTLA-4 depletion [209,210]. In fact, *ctla4*$^{-/-}$ mice develop lymphoproliferative disease replicating that of *foxp3*$^{-/-}$ models showing its importance in Treg homeostasis and function [211]. The loss of CTLA-4 leads to an impaired suppressive potential of Tregs [209], and administration of neutralising antibodies against CTLA-4 has an efficacy in augmenting the anti-tumour immune

responses as a result of enhancing T-cell proliferation [210]. Mechanistically, CTLA-4 activation both blocks CD28, and inhibits the synthesis of the essential T-cell survival factor IL-2 causing cell cycle arrest preventing propagation of an immune response [212]. CTLA-4 may act through modulation of the Tryptophan metabolic pathway by inducing IDO expression in an IFNγ-dependent mechanism in APCs, downregulating T-cell activation [213].

Glucocorticoid-induced TNFR-related protein (GITR) is expressed constitutively by nTregs, low-level expression in other T- and B-lineages increases upon activation similarly to CTLA4. GITR is thought to play additional co-stimulatory roles and inhibition of GITR results in conditions comparative to Treg depletion [192].

Helios is a transcription factor belonging to the Ikaros family often absent from iTregs but constitutively present on nTregs [194]. Helios$^{-/-}$ cells do not appear to have a reduction in suppressive capacity nonetheless can be used to discern nTregs and iTregs.

Neuropilin-1 (Nrp1) is a protein localised on the cell surface of Treg cells and under control of Foxp3 [194]. Nrp1 can function as a co-receptor for semaphorins and is upregulated in cancer cells, it might also act as a TGFβ co-receptor [194]. Nrp1 is not present when iTregs are induced at mucosal sites but characteristic of thymic-derived Foxp3+ nTregs.

The Inducible Co-stimulator (ICOS) is a co-stimulatory molecule, homologous to CD28, expressed widely on CD4^{+} T-helper cells including Treg cells [214]. ICOS binding to its sole ligand B7RP-1 (ICOSL) on antigen presenting cells (APC) and B-cells can exert differential effects on T-cell functionality [214-216]. The ICOS:ICOS-L interaction mediates T-cell survival and proliferation independently of the CD28 pathway, in Tregs this leads to the production of the cytokines IL-10, 4, 5, and GM-CSF [90]. Indeed, ICOS is an important determinant of T-cell propagation and size of the total pool [214]. Of the reported functions of ICOS are the proliferation of effector Th1 and Th2 cells, enhancing the formation of germinal centres, and the attenuation of Th17 responses

in EAE [90,216-218]. On the other hand, others have shown that ICOS-deficient mice display impaired Treg responses, inadequate B-cell humoral responses, and higher susceptibility to the development of EAE [90,214,216]. With regards to asthma, deficiency of ICOS leads to attenuated IgE responses, Th2 cytokine expression and airway inflammation suggesting ICOS is crucial to the generation of allergic responses [90].

1.4.5 – Regulatory T-cell Response to *Helicobacter pylori*

Helicobacter pylori has been well documented to induce an expanded regulatory T-cell population in the host. Early-life infection may be an important factor for an efficient Treg response as infection during adulthood results in a lesser regulatory response, higher Th1 and Th17 activity and elevated disease risk [140,219]. The major transcription factor and cytokines associated with the Treg lineage are FOXP3, IL-10 and TGFβ which are expressed in a higher proportion of cells in the mucosa and peripheral blood of infected individuals [45]. *H. pylori* persistence is abolished in IL-10$^{-/-}$ mice demonstrating the importance of this cytokine for *H. pylori* [220]. Notably, the development of secondary diseases such as peptic ulcers is more likely in individuals with an inadequate Treg response [45,166,220].

The induction of Tregs has been demonstrated experimentally to suppress both Th1- and Th2-mediated cellular responses [45,165]. In the context of *H. pylori*-mediated protection from allergy, individuals with a stronger Treg response in peripheral blood had significantly reduced IgE levels, these levels were restored with inhibition of IL-10. In addition it was noted that IgE concentration was reduced to a greater extent when infected with virulent CagA+ *H. pylori* strains [219]. Tregs can exert suppressive influence through the secretion of anti-inflammatory cytokines; by contact-dependent mechanisms involving CTLA-4; the CD39/CD78-mediated generation of adenosine; and the secretion of cytotoxic molecules such as granzyme B [106]. Suppression of Th1/Th17 responses is a mechanism by which *H. pylori* can subvert the protective immunity of the host and establish a persistent infection in the stomach. It has also been proposed to confer a protection from extra-gastric diseases including inflammatory bowel diseases [140].

Previous work by others has provided evidence that *H. pylori* infection can protect from asthma, this has been convincingly demonstrated in the literature [20-22,24]. This

protection was greatest when mice were infected in early life and diminished after *H. pylori* eradication [20,140]. In these studies, an accumulation of Tregs was observed in the lungs. Depletion of Tregs attenuated the protection, whilst adoptive transfer of Tregs from *H. pylori*-infected mice was seen to transfer the protection to uninfected donors [20]. Asthma protection was associated with CagA+ seropositivity yet not dependent on the translocation of CagA to host cells as seen with strains lacking a functional *cag* T4SS [20]. Furthermore, it has been postulated previously that CagA+ strains induce more profound Treg responses [166].

There have been several mechanisms reported by which *H. pylori* can induce Tregs through tolerising effects on dendritic cells. This process would appear to be dependent on the secretion of IL-18 in dendritic cells as it does not occur in either $IL18R^{-/-}$ or $IL\text{-}18^{-/-}$ models [21,23]. In this regard, we have discussed previously that *H. pylori* can activate TLR2 and induce NLRP3 inflammasome assembly and caspase-1 activation, subsequently activating IL-1β [23]. DCs express IL-18 constitutively, in combination with IL-1β derived from activated PRRs this can drive the production of Th1/Th17 effector cells. In contrast, with insufficient IL-1β, possibly due to inadequate PRR activation as a result of *H. pylori* PAMP modification, predominant IL-18 instead favours the generation of regulatory FOXP3+ Tregs [24]. Tolerised dendritic cells maintain a semi-mature phenotype which lack expression of a full complement of co-stimulatory molecules and thus lose the ability to initiate inflammatory T-cell activation, instead promoting Tregs. In the context of asthma, the depletion of DCs abrogated the protection [21,24]. *H. pylori*-tolerised DCs appear capable of skewing the Treg/Th17 balance to promote a dominant suppressive state in a TGFβ- and IL-10-dependent manner [140,221], and numbers of semi-mature tolerised DCs are increased in the infected mucosa [24].

Alternatively, *Helicobacter* can alter the expression of Lewis (Le) blood group antigens in a phase-variable manner, these can bind the C-type lectin dendritic cell-specific ICAM grabbing non-integrin (DC-SIGN) on DCs [222]. Binding to DC-SIGN can induce tolerogenic phenotype in DCs and reduced expression of co-stimulatory molecules which renders them inefficient for Th1 recruitment [57]. Lewis antigen

binding to DC-SIGN is associated with lower levels of IL-6 and IL-12 and upregulation of DC-derived IL-10, whereas Le^- strains have been demonstrated to display increased Th1 responses [114,165,222,223]. Much is still unknown regarding the exact mechanisms and there is a great need for further research to elucidate the necessary stimuli or criteria for this to occur.

1.4.7 – Regulatory T-cells in MS and EAE

The emergence of auto-reactive lymphocytes in MS could be due to inadequate Treg responses or dysfunctional tolerance in antigen presenting cells such as DCs [224]. Viglietta *et al.* (2004) first postulated that an impaired suppressive function of peripheral blood-derived Tregs may be involved in the pathogenesis of MS [225], a finding supported by others [226]. In these studies, Tregs derived from MS patients displayed a reduced capacity to suppress Th1 responses, IFNy secretion, and MOG-specific T-cell proliferation as compared to healthy controls. Interestingly, the defect of suppressive function would appear to be confined to RRMS as similar observations were not apparent in patients with secondary-progressive disease [227]. It was observed that there were no significant changes in the frequency of Tregs between patient or control groups mediating the reduced capacity for suppression [225,226]. The existence of myelin-reactive T-cells in MS is not specific to individuals with disease as they can be found ubiquitously at lower levels in healthy controls [228,229]. Therefore, it is likely that disease is caused instead by ineffective suppressive responses to control them.

Using the animal model EAE, studies have shown that myelin specific Tregs are generated after MOG immunisation, and do populate the CNS during EAE, however fail to prevent the onset of disease [230]. In other studies the administration of Tregs to EAE mice mediated a marked reduction in disease activity, whilst depletion of Tregs increased severity and prevented remission [228].

More recently, expression of the ectonuclosidase CD39 has been shown to mediate the suppression of Th17 responses and IL-17 production [231]. CD39 hydrolyses ATP to ADP and AMP, further to adenosine by CD73. Limitation of available ATP is inherently

suppressive for T-effector activity. Importantly, $CD39^+$ $FOXP3^+$ Tregs are deficient in MS patients [231].

Furthermore, a factor derived from the commensal microbe *B. fragilis*, polysaccharide A (PSA), can activate TLR2 on Tregs and induce expansion of CD39+ Treg populations [232]. This data has shown *B. fragilis*-derived PSA to confer a protection from CNS demyelination in EAE, whilst ablation of CD39 abrogates the effect of PSA. The expression of CD39 may be important in the protection from EAE as $CD39^-$ cells drive further progression of disease [232]. This demonstrates a direct interaction of a microbial products in the regulatory capacity of host Treg function in autoimmune disease.

TLR2 activation has been shown to induce a Th17-biased skewing of the Treg/Th17 balance in MS patients. TLR2 expression was higher in MS patients compared to controls and this was suggested as a possible contributory factor to the defective ability of Tregs to suppress Th17-mediated inflammation and MS pathogenesis [233]. In contrast, activation of TLR2 by *H. pylori*-derived factors including urease can induce the expansion of Tregs through the TLR2/NLRP3/IL-18 axis [23]. This demonstrates the importance and multi-functionality of TLR2-related signalling in the maintenance of immune homeostasis and function.

There are many studies addressing the involvement of the microbiota in both MS severity and Treg homeostasis. Numerous microbes have been shown to have a beneficial or detrimental effect on MS in studies in specific pathogen free (SPF) or germ-free (GF) mice. Indeed, being germ-free alone has a significant impact on EAE which demonstrates an important link between severity of disease and the complexity of the gut microbiota, the exact mechanism for this is still unknown.

In the recent literature, Tregs have been demonstrated to improve the capacity for oligodendrocyte differentiation and subsequent CNS remyelination [234]. The study found that mice deficient in Tregs had a markedly reduced capacity for remyelination, which was reversed after *ex vivo* transfer of Tregs. The effect on oligodendrocytes was found to be dependent on the expression of CCN3 by Tregs. [234]. Importantly, this study provides a mechanism for Treg-mediated protection from

autoimmune demyelination, which is distinct from immunosuppression, and instead suggestive of a stimulation of regeneration and repair, discussed in chapter 5.

It is noteworthy that some therapeutics which have efficacy in MS, e.g., IFNβ, glucocorticoids and Finglolimod, have been shown to affect Treg homeostasis and function, which may contribute to their therapeutic effects [235-237]. CTLA-4 was identified to be differentially expressed on Tregs between MS patients and controls and the expression of both CTLA-4 and FOXP3 was increased after a course of IFNβ treatment in patients. This was concurrent with an increase in Th2-related cytokine expression [235]. It has been demonstrated that glucocorticoid treatment, a commonly associated therapy for MS, is associated with an increase in the numbers of $CD25^{+}FOXP3^{+}$ and IL-10-secreting Tregs in RRMS patients [236]. In addition, the number of CD39+ Tregs has been observed to increase in response to administration of the sphingosine-1-phosphate inhibitor and immunosuppressant Finglolimod, surprisingly considering the mechanism of action (discussed in chapter 4) [237].

Taken together, the data convincingly demonstrate that a deficit in Treg function and homeostasis may be a contributory factor to the pathogenesis of MS, although mechanistically there is much to be elucidated. It is therefore of great importance to further our understanding of regulatory lineage T-cells, the involvement they have in autoimmune diseases such as MS, and how the microbiota, specifically *H. pylori* can influence this activity.

1.5 – Multiple Sclerosis

1.5.1 – Background to Multiple Sclerosis

Multiple sclerosis (MS) was first described by Charcot in 1868 [238,239], followed by Pasteur (*circa* 1900), and Rivers (1933). MS is a demyelinating and neurodegenerative disease of the central nervous system (CNS) propagated by auto-reactive CD4 and CD8 T-cells targeting proteins in oligodendrocyte myelin. T-cells specific for epitopes of myelin basic protein (MBP), myelin oligodendrocyte glycoprotein (MOG) and proteolipid protein (PLP) are frequently found elevated in MS [240]. This results in large

scale inflammation of the brain and spinal cord by monocyte/macrophage, neutrophils, T-cells, along with the activation and polarisation towards an inflammatory phenotype of CNS-resident microglia and astrocytes (termed reactive gliosis). There is also a pronounced B-cell mediated humoral response with upregulated IgG production. The net result of this substantial inflammatory cascade is the characteristic destruction of oligodendrocytes, demyelination, and axonal degeneration. The loss of the insulating glia in this manner leads to disrupted neural conduction which manifests as motor dysfunction, cognitive impairment, and progressive disability in affected individuals [224]. Around 50% of patients will require permanent use of wheelchair by 25 years after an initial diagnosis [224].

The presentation of MS in patients can vary on an individual basis, largely a result of the spatial distribution of demyelination [224]. Neurotoxic molecules such as ROS and NO secreted from infiltrating macrophages and neutrophils facilitate the stripping of myelin from the axon and results in lesion formation. Reactive astrocytes populate these regions and form glial scars, that can be visualised using magnetic resonance imaging (MRI) [224]. MS is usually suspected after a first report of clinically isolated syndrome (CIS) which is a spontaneous acute demyelinating event with no known causation. Clinically, MS is a diagnosis now made according to the McDonald criteria [241], which assesses the spatio-temporal dissemination of lesions using MRI; whereby the requirements are for two distinct lesions to form over at least two separate attacks [241,242].

The disease can be categorised into distinct phases; relapsing-remitting (RRMS), secondary progressive (SPMS), primary progressive (PPMS), and more rarely progressive-relapsing (PRMS) [243]. A majority of those affected (85-90% [244]) present with a relapsing-remitting disease course (RRMS). This phase is characterised by attacks of demyelination followed by a period of remission and partial recovery. Patients will often maintain a RRMS course for decades after initial diagnosis. Secondary-progressive MS develops in most patients consequentially from chronic RRMS as the threshold between autoimmunity and neurodegeneration is crossed. Here, periods of remission become less frequent to absent and result in a

progressively worsening disability with no periods of recovery. Occasionally, around 10-15% of patients may present with a progressive course from the onset, which is termed primary-progressive [244]. The transition to progressive MS may represent a point at which the endogenous myelin repair mechanisms fail, these mechanisms are responsible for facilitating recovery during remission in RRMS patients.

The classification of MS disability in a clinical setting is made according to the expanded disability status scale (EDSS) revised by Kurtzke [245]. Briefly, this scoring system assesses the extent of cognitive and motor dysfunction across a range of biological functions and physical manifestations, such as impaired ambulation. The EDSS is scored in 0.5 increments on a scale of 0-10, with 10 being mortality [245].

1.5.2 – Epidemiology of MS

1.5.2.1 – The prevalence of MS

MS is currently the most common neurological disability to affect young adults. An estimated 2.8 million people are affected globally, and a new diagnosis is estimated to be made every 5 minutes [246]. The global prevalence of MS is around 60-200 per 100,000 in high-risk areas including Europe and North America, and around 6-20 per 100,000 in lower risk areas such as Japanese and Asian populations. The rates of MS are rising sharply within European nations, from an average of 104 per 100,000 in 2013, to 146 per 100,000 in 2020; a rise of over 30% in the last 7 years [246]. In the UK, the incidence of MS is estimated to be 196 per 100,000 people, with incidence increasing by around 2.4% per year [244,246-248]. The regional increase of MS is in parallel to that of other immunological disease, and concurrent with reducing exposure to allergens and infections in those populations. The hygiene hypothesis [85], or more recently referred to as the old friends hypothesis [249,250] is a likely candidate to explain the trends in prevalence, and there is evidence that many commensal or pathogenic organisms can regulate the immune system with consequences for immunological diseases.

1.5.2.2 – Risk factors for developing MS

The exact cause of MS is still an unknown and the focus of much research worldwide. There is no single causative factor yet identified to initiate MS, however extensive studies in the literature highlight several key determinants of risk for MS. These include several microbial, genetic, hormonal, and environmental factors which are associated with MS development [224]. There is a clear bias for MS to develop predominantly in females as compared to males, this bias approaches 3:1 [244,251]. This observation may implicate the sex hormones as factors influencing MS risk, which are known to have an immunomodulatory role [251-253]. Furthermore, the age of onset occurs in most instances after puberty, and symptoms and relapse frequencies are noted to remit during pregnancy and recur post-partum or during menstruation [244,251]. Higher oestrogen levels have efficacy in moderating EAE severity, whilst mouse models lacking functional oestrogen receptors lose this effect [254].

Studies amongst families and between twins indicate increased incidence of MS when a family member is affected, lending weight to an underlying genetic factor influencing susceptibility. Indeed, there are certain genetic fingerprints associated with MS risk [244]. Genetic susceptibility factors are largely restricted to immune-related genes such as those encoding TGFβ, TNFα, IL-1, and CTLA-4, and the IL-2 and IL-7 receptors in addition to factors involved in the IFN and NFkB signalling pathways [224,228,244,255]. There is a particular association with polymorphism in the major histocompatibility complex (MHC, or human leukocyte antigen; HLA) genetic cluster [244,256]. Up to 60% of the genetic risk for MS comes from the HLA cluster. The two most closely associated alleles linked to MS risk are *HLA-DR1501* and *HLA-DQ0601* [244,256]. Of course, the MHC class II alleles being associated to susceptibility supports the premise of a primarily $CD4^+$ T-cell-driven disease [255].

The distribution of MS prevalence globally suggests certain environmental factors can influence the risk of developing the disease. The incidence of MS is affected by geography, being markedly more common in higher latitudes [257-259]. This is hypothesised to relate to ultraviolet (UV) exposure or vitamin D, both of which have been reported to affect the incidence and course of MS and exhibit inherent

immunomodulatory influences[244,258,260]. Interestingly, vitamin D levels can affect the levels of Tregs and IL-10 [260]. Furthermore, there are polymorphisms in the vitamin D receptor that can confer increased risk for these diseases [244], and melatonin levels and circadian regulation is suggested to affect susceptibility [224,244]. Indeed, no direct causal link has been established through genetic factors alone suggesting a complex multi-factorial causation. This is likely comprised of a combination of genetic susceptibility coupled with environmental or microbial triggers and/or hormonal influences.

Wilkin, *et al.* [261,262] hypothesised that the autoimmune response in MS is a secondary outcome resulting from a primary pathogenic event in the CNS, termed the 'primary lesion theory' [261,262]. In this model, a prior pathogenic event within the CNS could be an initiating factor in MS, supporting an idea of chronic viral involvement. The viral hypotheses are based around research performed in non-human primate MS models in which chronic asymptomatic herpesvirus infection produced potentially cross-reactive T-cells which could later be activated by molecular mimicry with self-antigens [263]. Furthermore, Epstein-Barr virus infections are strongly associated with MS incidence [263], and with higher EBV-specific antibody levels correlating with elevated MS risk [224]. Potentially, CNS antigens in draining lymph nodes (resulting from the primary lesion), could be cross-reactive with virus antigen-specific T-cells, causing reactivation of the immune repertoire and subsequent migration of these cells to the CNS and propagating further inflammation. In this scenario, those patients with inadequate immune regulatory mechanisms, or genetic predisposition for hyper-responsive immunity would be more likely develop to MS, which may not develop in others [263]. The dependence of individual genetic factors for MS incidence is supported in the literature by the susceptibility genes with immunological functions reported in the literature. Viruses such as herpesvirus-6 (HHV6) and particularly Epstein-Barr virus (EBV) are noteworthy examples which have been investigated [244,264,265]. It has indeed been shown that MS incidence is higher in those patients with a history of infectious mononucleosis as a result of EBV infections [265], and MS patients are found almost exclusively to have evidence of EBV infected B-cells, however EBV infection is also common in the healthy population, being

acquired during childhood and establishing asymptomatic chronic infection of the B-cellular compartment through life [265].

Viral triggers of MS may propagate their effects through molecular mimicry, generating auto-immune cellular and humoral immune responses. Another possibility is that myelin-reactivity is generated aberrantly to an immune response against a distinct neural antigen through the phenomena of epitope spreading. Epitope spreading is observed in the EAE model whereby induction of EAE using MBP generates auto-reactive T-cells with specificity for both distinct epitopes of MPB, as well as other myelin proteins such as PLP and MOG [266-268].

To date, evidence of a causal link between viral infection and MS development is insufficient. However, human endogenous retroviruses (HERVs) have been suggested as candidates. The W-family of HERVs (HERV-W) includes; multiple sclerosis-associated retrovirus (MSRV), and ERVWE1 [264]. Both of which are present in MS patients, and detected at higher levels during relapse [264]. Importantly, other viral infections can result in demyelinating events in the CNS, which provides a precedent for the viral trigger hypothesis. The papovavirus JC causes progressive multifocal leukoencephalopathy (PML), which incidentally is a serious side-effect of the MS drug Natalizumab. The measles virus can result in post-infectious encephalopathy [244]. Similar examples exist in animal models, such as the Theiler's murine encephalomyelitis virus (TMEV), mouse hepatitis virus (MHV), Semliki Forest virus (SFV), and canine distemper virus [244,269,270]. In fact, TMEV is utilised in some virally induced MS models in mice, whereby it elicits an EAE-like course like primary-progressive MS [270,271].

1.5.3 – Cellular mechanisms of MS pathology

1.5.3.1 – A proposed model to describe MS development

The exact aetiology of MS is not clearly understood, however current paradigms of MS autoimmunity defines a 3-compartment 'response-to-damage' model, proposed by t'Hart *et al.* (2009) [263]. These compartments are; the afferent compartment comprising the lymph nodes and spleen, the target compartment of the central

nervous system, and the draining compartment of the cervical or lumbar lymph nodes [263]. Firstly, the afferent compartment is the site of which auto-reactive T-cells are primed in the periphery by APCs. In MS the initiating epitope is not known, it may be due to an infectious trigger, in EAE it is induced by immunisation. These primed autoreactive cells would then proceed along a migratory pathway toward the target compartment, the CNS. When in the target compartment, interaction of the autoreactive cells with CNS-resident antigen presenting cells (APCs) initiates a re-activation of the primed T-cells, the ensuing inflammatory cascade then results in the hallmark demyelination and inflammation.

CNS lesions produce antigens from myelin breakdown products which are taken up by resident APCs and drained via the interstitial or cerebrospinal fluids. Finally, the efferent compartment comprises the draining lymph nodes for the target compartment, the cervical lymph nodes (CLN) or lumbar lymph nodes (LLN). Here, breakdown products from the target site lesion such as myelin-laden macrophage present antigen and prime further T-cell response [263,272-274].

1.5.3.2 – Cellular mediators

There is a large CNS infiltrate active in MS, comprised of CD4 and CD8 T-helper lineages, B-cells, large numbers of activated CNS-resident astrocytes and microglia, and infiltrating monocyte macrophages [224]. Monocyte macrophage, dendritic cells, microglia, and neutrophils are observed to congregate in regions of demyelination and the numbers of these cells correlates with increasing pathology and clinical scores [224]. Macrophages are a prominent feature in active lesions secreting cytotoxic molecules, chemokines, inflammatory cytokines , and containing myelin debris [228].

As the disease progresses from relapsing-remitting to a secondary progressive phenotype the scale of infiltrate reduces but does not cease [224]. This is thought to reflect a shift in the underlying disease mechanisms, changing from a primarily inflammatory-mediated pathology to a more intrinsically neurodegenerative pathology. This may be supported by age-related changes in the CNS or immune function as patients age, or perhaps developing after a threshold of CNS damage has been reached [224]. This is still to be proven.

T-cells specific for multiple myelin peptide targets are present in MS [224], however also from non-MS individuals [224]. Self-reactive CD4 T-cells isolated from MS patients can have cross-reactivity with other myelin antigens. For instance, MBP-specific T-cells demonstrated a certain degree of affinity for epitopes of MOG and PLP [228]. Furthermore, there is a reduced specificity of TCRs on T-cells from MS patients and this redundancy may mediate epitope spreading or cross-reactivity to other myelin antigens thus facilitating a propagation of the response [228]. CD8 T-cells can outnumber CD4 cells at lesion sites, however $CD4^+$ are critical for the propagation of the disease. Indeed, the animal model can be induced by adoptive transfer of encephalitogenic $CD4^+$ cells (passive EAE), but not similarly effectively with CD8 cells. Furthermore, the association of the genetic risk of MHC-II alleles with MS would favour the CD4-dominant model. The inflammatory cytokines produced by activated CD4 T-cells augments infiltration of innate leukocytes and activation of CNS-resident microglia and astrocytes to a polarised inflammatory phenotype [275].

The major $CD4^+$ T-cell lineages contributing to MS pathology are the Th1 and Th17 cells. The central role these subtypes have in MS is supported by the observation that adoptive transfer EAE can be induced by either Th1 or Th17 encephalitogenic cells alone [275,276]. Reduction, of the Th1/Th17 responses has beneficial consequences. Indeed it is considered that skewing towards a Th2-biased response is a mechanism of action of some of the leading MS therapies including IFNβ (Rebif™) [224]. This is also hypothesised as being a primary mechanism for the protection from MS conferred by intestinal helminths [97]. These subsets characteristically secrete the signature IFNγ and IL-17, respectively, in addition to numerous other pro-inflammatory cytokines [224]. These signature Th1 and Th17 cytokines have been demonstrated in either loss- or gain- of function models to mediate the inflammation in MS [275,276].

IFNγ can stimulate the upregulation of MHC molecules on APCs and the secretion of inflammatory cytokines from polarised macrophages and resident CNS glia; microglia and astrocytes [275,276]. Interestingly, IFNγ has been shown to exert differential effects on MS between the brain or spinal cord whereby inflammation in the spinal cord was enhanced, but reduced in the brain [275]. There are indeed non-pathogenic roles reported for this cytokine including downregulation of microglial responses at certain

disease phases, and the inhibition of EAE development if administered during the induction [275]. These complex biological functions are still being elucidated.

IL-17 is elevated in MS patients and proposed to be correlated to severity [277], however the importance of IL-17 is disputed by others [278]. The pro-inflammatory properties of IL-17 can augment ROS generation serves as a stimulator of chemokine secretion which elevates CNS infiltrates whilst participating in the breakdown of the blood-brain barrier through induction of MMPs [276,277]. The secretion of inflammatory cytokines by CNS-resident glia is upregulated by IL-17 [275]. Furthermore, the Th17-derived cytokine IL-21 supports B-cell activation and antibody production, and another Th17-derived factor IL-23 is essential to sustain an inflammatory phenotype of Th17 cells. Interestingly, IL-17 by itself would appear non-essential to disease propagation as seen with experimental abrogation of its function [278]. Furthermore, it has been demonstrated that it is IL-23 which conferred a pathogenic potential to IL-17, whereby without IL-23, Th17 cells lost pathogenicity despite maintaining IL-17 production [275,279]. In other studies IL-17 neutralisation was sufficient to suppress the development using the mouse model [277]. The roles of cytokines in the processes of MS and EAE are still being fully elucidated.

A wide repertoire of lymphocytes are active in MS as well as the $CD4^+$ lineages; including $CD8^+$ cells and B cells [228]. $CD8^+$ T-cells are present in large numbers at the regions of demyelination, usually concentrated at the lesion edge as compared to CD4 cells which reside deep within lesions [280]. A proportion of these CD8 cells can express IL-17 [224,281] and are correlated with increasing lesion burden, often outnumbering $CD4^+$ cells in post-mortem MS tissue [276,281].

B-cells are important mediators of myelin pathology, supported by Th17-cell derived cytokines including IL-21. Increased levels of IgG in the cerebrospinal fluid (CSF) are associated with higher inflammatory responses in MS and greater demyelination. Both opsonisation with IgG and complement subsequently attract further macrophage-mediated damage directed to myelin [282]. B-cells populate the inflamed CNS forming germinal centres in the meninges, they can also contribute to the inflammatory milieu and secrete IL-6 and TNFα [276]. Furthermore, CD20-directed therapies have efficacy in treating MS [224,282], demonstrating the importance of B-cells

maintaining and propagating the inflammation in MS. On the other hand, B-cells can also secrete IL-10 and IL-35 which are anti-inflammatory and shown experimentally to reduce symptoms of EAE [283]. Recently, it was reported that gut-derived IgA and IL-10-sereting plasma cells could migrate to the inflamed CNS and suppress EAE, discussed in chapter 4.

1.5.4 – Therapeutic Interventions for Multiple Sclerosis

There is currently no cure for MS. There are 15 approved treatments aimed at patients in the relapsing stages, these include interferon beta (IFNβ), fingolimod, glatiramer acetate (GA), and natalizumab (NTZ) which all possess a certain efficacy for the management of early relapsing MS [284-287]. Many of these therapies work by a broad non-specific immunosuppression, such as inhibiting lymphocyte ingress to the CNS, or egress from lymphoid tissue. IFNβ can reduce antibody production, BBB permeability, and suppress inflammatory cytokines thus favouring a Th2 polarisation [288]. Glatiramer acetate is a combination of synthetic polymers that mimic the structure of MBP; Th2-polarisation is a proposed mechanism of action in this instance also [289].

However, none of these confer an efficacy in the later stages of progressive disease. In fact, only two pharmacological interventions have been recently licensed for progressive MS within Europe; Siponimod (Mayzent; Novartis) and Ocrelizumab (Ocrevus®; Genentech/Roche Pharmaceuticals™) [284]. The mechanism of action of these drugs is primarily immunosuppression. Siponimod alters lymphocyte trafficking in the lymphatics (discussed in chapter 4), whilst ocrelizumab depletes $CD20^+$ B-cells. The progressive phase of MS develops around 2 decades after the first clinically identified relapse. This stage may mark a distinct change in the underlying disease mechanisms, from an autoimmune to a primarily neurodegenerative basis [244]. Indeed, progressive MS patients often have fewer autoreactive $CD4^+$ cellular infiltrates in the CNS but maintain a chronic response at a lower level. It would appear there is a damage threshold which when crossed leads to axonal degeneration independently of an ongoing autoimmune attack. This may be sequalae of the endogenous repair mechanisms failing [224]. During MS remission there is evidence

that an amount of repair occurs at a lesion site; oligodendrocyte precursors migrate to the lesion site and proliferate however fail to differentiate. Problematically, although these broad immunosuppressants have been shown to have efficacy in slowing the rate of the progression they also inherently lead to an increased risk of infection, there have also been incidences of serious side effects including progressive multifocal leukoencephalopathy (PML) which can result in mortality [224].

Probably the most important area in which new drugs are required is to promote and facilitate effective remyelination in the CNS. The lack of potential therapies thus far to slow or reverse progressive MS has necessitated this research, and the number of studies for remyelination has increased markedly in the last 10 years [290]. The primary readouts for these studies generally fall into three categories: quantification of remyelination, numbers of oligodendrocyte precursors (OPC), or numbers & differentiation state of oligodendrocytes (OGC) [290]. From 39 studies in which the outcome measure was remyelination, none of them gave markedly increased remyelination (maximum point estimate <1.66 [290]) whereas several had a detrimental effect. Interestingly, the statin Simvastatin scored amongst the worst with a point estimate of -3.63 [290]. As statins are one of the most widely prescribed medication in the UK, the effect of these on MS warrants further investigation. Simvastatin was approved for use in a phase IV trial for RRMS as an add-on therapy to IFNα (Avonex) by Biogen Idec (Clinical Trial Identifier: NCT00492765), which concluded there was little or no effect. High-throughput methods are often used to screen large volumes of novel small molecule drug candidates for biological effect. In this regard, micropillar arrays have been used to screen compounds for differentiation-promoting effects on pre-OGCs [291,292]. Physically, these arrays consist of a series of 25µm tall conical pillars which provide a 'scaffold' for which oligodendrocytes may wrap similarly to an axon. The use of these arrays has led to the identification of several novel drug candidates. Of these, clemastine, and benztropine have been identified as having an efficacy for the promotion of oligodendrocytes, at least *in vitro* [291].

Benztropine is an approved pharmaceutical therapy for Parkinsons' disease but has been found to promote OGC differentiation. The mechanism of action of Benztropine is through antagonism of the M1 and M3 muscarinic receptors but also has dopamine reuptake inhibitory activity [292,293]. When administered in the PLP-EAE model to rodents, benztropine was found to markedly decrease the EAE severity score as compared to untreated mice, and to a greater extent than currently approved MS therapies fingolimod and IFNβ [293]. This reduction in severity score is coupled with an increase in the number of myelinated axons. The effect on remyelination was investigated using cuprizone-mediated demyelinating *in vitro* models which confirmed the pro-remyelinating effect [293].

Clemastine is an anti-histaminergic and M1/M3 muscarinic receptor antagonist which has been found to promote myelination and OGC differentiation in an M1-muscarinic receptor-dependent antagonistic manner [292]. Clemastine has been studied for efficacy in MS in a phase 2 clinical trial (ReBUILD; NCT02040298) [292]. Here, administration of clemastine was effective in stimulating repair to the optic nerve myelin. Given this effect on the optic nerve, a phase 2 clinical trial (ReCOVER; NCT02521311) sees clemastine given to 90 optic neuritis patients with similar outcome measures, this trial is still on-going with no results yet to report [294].

The amphoterin-induced gene and open reading frame-3 (AMIGO3), and the leucine rich repeat and immunoglobulin-like domain-containing protein 1 (LINGO1) are negative regulators of axonal regeneration and myelination [295-299]. Inhibition to these negative regulators of myelination may therefore provide a potential therapeutic target. Using *in vitro* models, Mi *et al.* have eloquently shown that antagonising the function of LINGO1 both through interfering RNA (RNAi) or with anti-LINGO1 neutralisation, results in improved OGC differentiation and remyelination [295-298]. Furthermore, using the EAE model to investigate this occurrence *in vivo*, LINGO1 knockout mice had substantially reduced clinical severity scores [296]. However, in a human phase 2 clinical trial (SYNERGY; NCT01864148) [300], administration of anti-LINGO1 in combination with Avonex™ (IFNβ1) to RRMS patients reported anti-climactic results, with no significant effect observed compared to placebo [300]. The

failure to translate results from the EAE model to the human condition is a common trend. Indeed, numerous anti-CD19 and anti-CD20 therapies showed great efficacy in mitigating EAE severity but failed to confer a benefit in human trials.

1.6 – The Microbiota: A Major Regulator of Immune Homeostasis, Gut-Brain Communication, and Health & Disease

The regional increase of MS is in parallel to that of other immunological disease, and concurrent with reducing exposure to allergens and infections in those populations. The hygiene hypothesis [85], or more recently referred to as the old friends hypothesis [249,250] is a likely candidate to explain the trends in prevalence, and there is evidence that many commensal or pathogenic organisms can regulate the immune system. The gut microbiota has a profound effect on the development and function of lymphocytes and shaping the relative frequencies of inflammatory or anti-inflammatory cellular responses [301]. Communication between the CNS and the gut can occur via several mechanisms including signalling through the vagus nerve, endocrine-mediated crosstalk, microglial metabolites such as SCFA and kynurenine metabolites, and gut-derived neurotransmitters including serotonin and gamma-aminobutyric acid (GABA) [302-308]. A function of the vagal fibres is the chemo-sensing of gut luminal compounds such as dietary metabolites, bacterial components, and hormones [309]. Interestingly, in the case of gamma-aminobutyric acid (GABA) levels, an inhibitory neurotransmitter produced by microbes including *Bacteriodes* and *Escherichia spp*., has been shown to have a correlation to depression [310]. There are GABA receptors expressed on T-cells and macrophages, whereby GABA signalling results in inhibitory effects to cellular activation [311]. There are reports of the inhibitory GABA activity having a beneficial effect in type-1 diabetes and rheumatoid arthritis and EAE [311].

In fact, several neurotransmitters and neuro-active molecules are produced by various human commensal species including serotonin, acetylcholine, GABA, dopamine, noradrenaline, and histamine [310,312-314]. This is in addition to hormones such as noradrenaline, leptin, ghrelin, and cortisol [313]. Both SCFA's and Tryptophan

metabolites of the Kynurenine pathway have been attracting more attention in the literature in recent years and are the subject of much research [314]. Interestingly, the expression of indoleamine dioxygenase (IDO) is enhanced in *H. pylori* infected individuals [315]. Here, the level of IDO protein in the gastric mucosa of infected individuals was correlated with reductions in Th1, Th17, and Th22 cells, and a concurrent increase in Tregs [315]. Furthermore, IDO protein level within the mucosa was negatively correlated to the presence of peptic ulcer disease [315]. Similar observations are made by others, Larussa *et al.* report that IDO expression is increased in the infected gastric mucosa in parallel with a reduction of IL-17 [316]. Others propose that IDO expression in response to *H. pylori* infection is regulated through TGFβ and CTLA-4 and represents a mechanism of immune suppression mediated via the augmented Treg response induced by *H. pylori* [317].

To sustain our evolutionary symbiotic relationship with our resident microbes, tolerance to commensal-derived antigens must be established. Immunological systems are often dysfunctional in germ-free animal models which suggests the vital importance of the microbiota in the development of these mechanisms [90]. Relating to MS, effects are noted such as altered disease course and relapse frequency, in addition to unexplained sudden outbreaks of MS in confined communities [244]. There are also clear differences in EAE mice housed in either specific pathogen-free conditions compared to germ-free and controls [244]. Deconvoluting the complex interactions between microbiota-host in the context of immunological development, tolerogenicity, and disease-specific effects is a daunting task. Nonetheless, in the literature we see such delineations starting to be presented.

1.6.1 – The microbiota and multiple sclerosis

In recent years there have been a wealth of published studies in which the gut microbiome modifies the severity of MS and EAE. Indeed, germ-free mice appear to possess an inherent resistance to the development of EAE [318], however their immune systems are not fully mature. A protection which could be attenuated by restoring a commensal SPF-free microbiome [318]. The same effect is apparent in transgenic mice with a TCR specific for MBP, development of EAE is abrogated if they are housed in

SPF conditions [244]. Quantification of the gut microbiota in MS patients administered disease modifying drugs for MS; glatiramer acetate (GA) or di-methyl fumarate (DMF) observed changes to gut microbial composition which may relate to their therapeutic effect [319].

Chen *et al.* [320] investigated the faecal microbiome composition between MS patients and healthy controls. Here it is observed that distinct population differences are apparent between groups. Specifically, the microbial species *Pseudomonas, Mycoplana, Haemophilus, Blautia*, and *Dorea* were found over-represented in MS patients. The species *Parabacteroides, Adlercreutzia* and *Prevotella* were reduced as compared to healthy controls.

Berer *et al.* [318] found that germ-free mice would appear to have an inherent resistance to EAE induction using the relapsing-remitting SJL mouse model [318]. Further to this, supplementing germ-free mice with a faecal microbiota derived from MS patients was sufficient to induce the development of spontaneous EAE in the recipient mice, not apparent with a non-MS microbiota [321]. Analyses of the microbiome from faeces highlighted increased abundance of *Akkermansia* and decrease in the tolerogenic *Sutterella* from MS patient's microbiota as compared to the microbiome of a non-MS twin. When transferred to germ-free mice this faecal microbiota was able to induce spontaneous EAE at a rate not observed in transferred microbiota from non-MS individuals [321]. Systematic review of the gut microbiome in MS concludes that between MS patients and healthy controls no significant changes in overall microbiome diversity are observed, in agreement with the work of others. However, changes in individual bacterial taxa of *Bacteriodes, Prevotella, Akkermansia*, amongst others were indeed supported [322].

Erny *et al.* [303] have presented supporting evidence; that ameliorated or reduced complexity to the gut microbiota can alter both the numbers and phenotype of microglia. Furthermore, microglia from germ-free mice fail to propagate inflammatory signalling upon activation, this could be reversed with administration of SCFA's suggesting interplay between these two factors [303,308]. The major

differences were found within inactive microglia which indicates changes to the cells function during homeostasis in the absence of a complex microbiota [303]. This is further supported by gene expression analysis which indicates cytokine and chemokine pathways are attenuated in the GF microglial cells [303]. Interestingly, reintroduction of microbial complexity, and SCFAs supplemented to drinking water would appear to rescue microglial phenotype and function [303].

Similar effects were reported by Rothhammer *et al.* [306] who find microglial function can be modulated through microbial-derived metabolites of Tryptophan acting through the AhR pathway, which can further modulate the function of astrocytes [306,307,323]. Here, deletion of AhR in microglia or astrocytes worsened EAE and led to increased demyelination and innate immune response, independently of the T-cell response. Whereas administration of *Trp* or *Trp*-metabolites in mice fed a *Trp*-depleted diet reduced the severity of EAE[306].

Shahi *et al.* [324,325], showed that colonisation of the gut microbiota with the commensal *Prevotella histocola* (*P. histocola*) was at lower abundance in MS patients. When investigating this microbe using the EAE model, *P. histocola* colonisation had the astounding effect of conferring protection from EAE severity on a scale comparable with the leading DMD's; Copaxone™ (glatiramer acetate) and interferon-beta (IFNβ) [322,324,325]. This EAE-limiting effect was attributed to reduction in Th1 and Th17 response concurrent with an increased abundance of regulatory $CD4^{+}FoxP3^{+}$ cells.

Rojas *et al.* [326], show selective colonisation of controlled microbiota in mice with *Trichuris muscalinis* (*T. mu*) has been shown to reduce both EAE and MS severity. Intriguingly this was attributed to intestinal IL-10- and IgA-producing regulatory B-cells migrating to the CNS and is discussed in chapter 4 [326]. In contrast, the literature also contains opposing reports of *T. mu* infection augmenting the Th1 and Th17 immune responses and worsening experimental colitis [327].

Numerous and often conflicting reports are published in the literature focussed on the role of the microbiota in EAE. In one study, inoculation of EAE mice with *Lactobacillus reuteri* (*L. reuteri*) was sufficient to reduce the development of Th1 and Th17 cells and downregulate the severity of EAE, this effect was proposed to be mediated through alterations to microbiota diversity [328]. This finding was replicated by Johanson *et al.* [329] who also demonstrate a protection from EAE after *L. reuteri* supplementation. On the other hand, others find that colonisation of germ-free mice with *L. reuteri* worsened EAE severity through induction of Th1 and Th17 responses and increasing their frequency in CNS lymphocytic infiltrates, an effect inferred because of molecular mimicry to human MOG [330]

Intestinal helminths such as hookworm have been demonstrated to reduce the severity of EAE in animal models [95,97]. Helminthic worms similarly to *H. pylori*, have co-evolved with human beings for thousands of years and have evolved mechanisms to modulate the host responses in order to persist [95]. These persistence strategies can involve the preferential induction of anti-inflammatory IL-10 and TGFβ-producing Tregs [95]. An estimated 25% of the human population are infected with helminths, the incidence of which is biased towards populations of lower socio-economic status [95], in the same manner as *H. pylori* infections are distributed globally, infections with helminths are inversely correlated to the incidence of allergic and immunological diseases within those populations [95]. The case of helminth infections lends weight to the old friends' hypothesis. Several studies have investigated the therapeutic effects of helminth immunotherapy (HIT) with relevance to multiple sclerosis, with most agreeing that HIT confers a resistance to mice against the severity of EAE [95,97,98]. This effect was seen only when administered prophylactically and did not suppress an already established EAE immune response [98].

A clinical trial from esteemed colleagues within this institution, Tanasescu *et al.* (Clinicaltrials.gov identifier: NCT01470521) investigated the effect of therapeutic hookworm infection in MS patients. The primary readout for this study was the development of new lesions or relapse frequency. Although this trial reported a non-significant effect on currently established MS, they did observe a trend for a reduced

relapse rate in the infected group concurrent with an increase in Tregs [96]. Infection of MS patients with such parasites has been associated with alteration to gut microbial diversity, this may contribute to the observed therapeutic effect [331]. In the same regard, first-line MS treatments including IFNβ and NTZ would seem to cause shifts in the microbiome diversity. A study by Jenkins *et al.* (Clinicaltrials.gov identifier NCT00630383) found that in MS patients infected with hookworm, no relapses were reported during the study period, and an increase of microbial taxa with immunoregulatory-promoting ability were observed, especially for the *Bacteriodes* phyla and corresponding to increased frequency of regulatory T-cells [331]. Although HIT is currently an emerging concept, data would appear to support a clinical benefit for individuals to harbour such parasitic infections.

Detailed analysis of the microbiota in either MS patients or EAE mice is not an aim of the work in this thesis, however the impact of the gut microbiome in the incidence and severity of MS is supported widely in the field. When considering the impact of both parasitic helminth infections and microbiome composition in modulating the incidence and severity of EAE and MS, a role for *H. pylori* is supported.

Although much is still to be elucidated regarding the exact mechanisms for microbiota-mediated regulation of immune responses, commensal microbes may induce inflammatory responses detrimental to EAE, or favour immune tolerance through release of TGFβ, retinoic acid (RA) or IL-18 or IL-10 promoting Treg development [162]. This can suppress Th1, Th2, and Th17 lineage cells, such as those involved with allergy, asthma and autoimmune conditions like IBD, diabetes and MS [192].

1.7 – Evidence of *H. pylori* Protection from MS

In recent years there have been several reports in the literature hypothesising that infection with *H. pylori* can confer a degree of protection from the incidence or severity of MS [280,332-337]. An inverse correlation is observed between *H. pylori*

seropositivity and MS progression, as measured by the expanded disability status scale (EDSS), a well-established scoring system for multiple sclerosis.

In support of this hypothesis, *H. pylori* has been shown to have a similar protective effect on other immune mediated diseases. Both asthma and allergy are caused by aberrant/hyper-responsive immune reactions. Infection with *H. pylori* has been shown to reduce the severity of these conditions. In this regard, some potential mechanisms have been identified and reported [20-22,24,219].

Importantly, the protection from asthma has been attributed to *H. pylori*'s ability to induce suppressive regulatory T-cells (Tregs) in the host [20,219]. Tregs may contribute to this protection through the secretion of anti-inflammatory mediators such as TGFβ and IL-10. Furthermore, previous work by this research group has demonstrated that IgE levels are reduced in the serum of *H. pylori*-infected patients as compared to uninfected individuals [219]. The suppression of IgE was increased further still when the infecting strain was of a more virulent *cagA*+ genotype. CagA+ *Hp* strains are indeed capable of inducing larger numbers of regulatory T-cells and subsequently produced more circulating IL-10.

A dysfunction of Tregs has been suggested as a contributing factor for the development of MS and EAE [225,226,228,230,231,338-341]. Similarly, administration of Tregs would appear to suppress disease severity in experimental models [342]. These effects are likely mediated by the Treg-induced suppression of inflammatory Th1 and Th17 cells either via contact-dependent mechanisms or through the actions of secreted anti-inflammatory factors such as IL-10 [342].

Li *et al.* (2007) first provided evidence that *H. pylori* infection could provide a protection form MS [333]. This study included patients with both conventional MS (CMS) in addition to a variant, opticospinal MS (OSMS) from a Japanese population. The study included 52 patients with CMS, 53 with OSMS, and 85 healthy controls. *H. pylori* status was determined by serology and seropositivity was found to be significantly lower in the CMS group as compared to healthy controls (22.6% and 42.4% respectively, p=0.018). Notably, EDSS scores were found to be markedly lower

in *H. pylori*-positive individuals, but this effect was only observed in patients with conventional MS.

Mohebi *et al.* (2013) conducted an analysis amongst a cohort of 163 MS patients and 150 age- and sex-matched controls from an Iranian population [336]. In this study assays for anti-*H. pylori* IgG and IgM antibodies were used to determine *H. pylori* seropositivity in patients, the EDSS was used in evaluation of MS progression. These analyses determined that *H. pylori* seropositivity was significantly reduced in MS patients compared to the control group (54% to 73% respectively, p=0.001). In addition, EDSS scores were significantly lower in *H. pylori*-seropositive patients as compared to seronegative individuals (p=0.017). These data suggest that incidence of MS is less frequent amongst *H. pylori*-positive individuals, and that MS patients with concurrent *H. pylori* infection had a reduced severity of disease.

Following from this, Pedrini *et al.* (2015) conducted similar observations amongst an Australian cohort [280]. In this study 550 MS patients and 299 age- and sex-matched controls were included. *H. pylori* status was determined by serology for *H. pylori*-specific IgG, and the EDSS used to evaluate MS disease progression. These analyses agreed with previous data that *H. pylori* seropositivity was less frequent amongst MS patients compared to healthy controls (14% to 22% respectively, p=0.027). However, in contrast, this difference was determined to be significant only in females. The seropositive females also displayed lower disability scores (p=0.049) in agreement with the findings of others.

On the other hand, Gavalas *et al.* (2015) reported the opposite [337]. Their study consisted of 44 MS patients and 20 matched controls from a Greek cohort. *H. pylori* status was determined by histology and EDSS used to evaluate MS patients. The authors concluded that *H. pylori* infection was significantly more frequent amongst MS patients than the controls (86.4% to 50% respectively, p=0.002), which is in direct contrast to previous findings by others. Furthermore, they reported that *H. pylori*-mediated pathologies such as duodenal ulcer were exclusively present within the MS group. These findings are therefore very controversial.

Recent meta-analyses have been performed to clarify conflicting results from previous findings regarding the association between *H. pylori* prevalence and MS. Work by Yao *et al.* (2016) included a total of 1553 MS patients and 1252 healthy controls from nine eligible studies [335]. They reported and confirmed that *H. pylori* infection was less common in MS patients compared to healthy controls (24.66% to 31.84% respectively, p=0.0001). However, interestingly this effect was determined to only be statistically significant in Western countries (p=0.01) and not Eastern populations (p=0.2) [332].

Recently, Cook *et al.* (2015) analysed the relationship between *H. pylori* and MS [334]. This study assessed 71 MS patients from a Nottingham cohort and 42 matched healthy controls. *H. pylori* status was determined by serology. This study reported that the prevalence of *H. pylori* was twice as high amongst healthy controls compared to MS patients (42.9% to 21.1% respectively, p=0.018). A similar trend was observed from work published by others in the field [280,332,335,337,343]. In addition, the effect of *H. pylori* infection was assessed in the animal model EAE [334]. EAE was scored according to an established and previously validated scoring system. The severity of EAE was found to be reduced in mice previously infected with *H. pylori* (p=0.012).

Advancing from this, $CD4^+$ T-cells were harvested from the spleen and CNS of the EAE study animals. In T-cell proliferation assays, a significant reduction of MOG-specific proliferation was observed in *H. pylori* infected EAE mice (p=0.001). In flow cytometry analyses, splenocytes from *H. pylori*-infected EAE mice compared to uninfected EAE mice contained significantly reduced numbers of CD4 cells expressing the cytokines IFNγ (0.58% to 13.7% respectively, p=0.0043) or IL-17 (0.82% to 46.2% respectively, p=0.0043) or the transcription factors Tbet (0.93% to 28.8% respectively, p= 0.0051) and RORγt (0.36% to 3.88% respectively, p=0.0051).

In CD4 cells isolated from the CNS, *H. pylori*-infected EAE mice also had significantly reduced proportions of these Tbet/$IFN\gamma^+$ or RORγt/$IL\text{-}17^+$ expressing $CD4^+$ cells as compared to controls ($Tbet^+$, 40% to 74%; $ROR\gamma t^+$ 18.2% to 42%; $IFN\gamma^+$, 28.6% to 48.4%; $IL\text{-}17^+$, 15.4% to 28.1% respectively). Interestingly, although *H. pylori*-mediated immune suppression is associated with increased Treg responses, these

data did not find a significant change in the number of $FOXP3^+$ cells, neither was there a higher level of T-cell apoptosis amongst the *H. pylori* infected mice to explain the inhibition of effector T-cell responses. It is an important consideration that FoxP3 is representative of thymic-derived natural Tregs, however there are subsets of suppressive regulatory T-cells which can be FoxP3- such as the IL-10 and TGFβ-producing type 1 regulatory cells (Tr1). These cells can arise through trans differentiation from distinct T-helper subsets and have a variable and remarkably plastic expression profile making them tricky to reliably account for.

Table 4 Evidence that *H. pylori* infection provides a protection from MS

Study	Cohort	Incidence of *Hp* Infection	Results	*Significance*	Disease Severity	*Significance*
Li, *et al.* (2007)	52 MS 85 HC	Hp seropositivity lower in MS	22% to 42% MS/HC	p= 0.018	EDSS lower in Hp+	n/s
Mohebi, *et al.* (2013)	163 MS 150 HC	Hp seropositivity lower in MS	54% to 73% MS/HC	p= 0.001	EDSS lower in Hp+	p= 0.017
Pedrini, et al. (2015)	550 MS 299 HC	Hp seropositivity lower in MS	14% to 22% MS/HC	p= 0.027	EDSS lower in Hp+	p= 0.049
Yao, *et al.* (2016)	1552 MS 1252 HC	Hp seropositivity lower in MS	24% to 31% MS/HC	p= 0.0001	----	----
Cook, *et al.* (2015)	71 MS 42 HC	Hp seropositivity lower in MS	21% to 42% MS/HC	p= 0.018	EAE severity lower in Hp+	p= 0.012

1.8 – Differences of the human and murine immune response to *H. pylori* infection & between MS and EAE

Mouse models of human immune responses are not a perfect recapitulation. For MS & EAE there are important underlying differences (described in section 3.1.5). Some of these include the CD4/CD8 dichotomy and the antigens responsible for induction (MOG in EAE, unknown in MS). Other disparities are the age of onset (~30 years of age in humans) and disease duration (decades in humans, 3 weeks in mice). Indeed, numerous therapeutic innovations identified with EAE have not translated to MS showing the importance of these differences. For *H. pylori,* important disparities (*Table 5*) are that humans are colonised in childhood when immunity is naive and inefficient, these infections favour Tregs and lead to lower inflammation; the response in adulthood may not be comparable. Indeed, infection in adulthood leads to a response skewed toward inflammatory effectors and greater gastric pathology [140,219,344]. It cannot be assumed that a decades-long process to develop gastric disease in humans is reproduceable in a short-term murine model, and infection of C57BL6 mice does not cause gastric cancer. The gastric microbiota composition, pH, and mucous layer are also different between human and mouse [345], affecting both colonisation and disease mechanisms [345]. Importantly, *H. pylori* does not naturally colonise mice; Lee *et al.* discovered the mouse-competent Sydney strain 1 (SS1) [346], however the *cag* T4SS is non-functional and unable to translocate CagA. Additionally, *vacA* is present in the lesser-inflammatory type 2 form (*S2/i2/m2*); however, murine T-cells are resistant to *vacA*. In humans, *H. pylori* infection induces a marked neutrophilic response & expression of IL-8; although homologues are present in mice (MIP-2 and KC), IL-8 is not [347,348]. FOXP3 is expressed as alternatively spliced isoforms in humans, generated by exon skipping at exon 2 [347,348]. These isoforms can modulate Treg/Th17 subsets and are differentially expressed in some autoimmune disorders including rheumatoid arthritis, IBD, and MS [188,190,347]. These variants have not been observed in mice [348]. Furthermore, there are differences in the presence or expression of TLRs, CCL chemokines, interleukins, and complement proteins between the human and mouse [349].

Table 5 Major differences between human and mouse models of H. pylori infection and MS/EAE

Factor	Human	Mouse
T-cell response to MS or EAE	$CD8^+$ Dominant	$CD4^+$ Dominant
Specific antigen	Unknown; numerous myelin peptides	MOG fragment 35-55
Initiating event	Unknown; viral origin, infectious trigger, molecular mimicry?	Immunisation (Freund's adjuvant, *Pertussis* toxin, MOG).
Disease course	Onset ~30 years of age. Duration of several decades.	Onset at 7 d.p.i. Peak at 14d.p.i Maximal at 21d.p.i.
H. pylori Infection	Natural colonisation	Few mouse-competent strains (*i.e.* SS1)
Cellular response	Neutrophil dominant	Lymphocyte dominant
vacA genotype	*vacA* type 1 and 2 Inhibits human T-cell activation	*vacA* type 2 Mouse T-cells resistant to *vacA*
cagA genotype	Risk factor for gastric cancer	No cancer development
*cag*PAI functionality	Strain dependent	SS1: non-functional, PMSS1: functional
Gastric niche	High acid output (pH ~1-2) Thick mucous	Lower acid output (pH ~3-4) Thinner mucous
Gastric microbiota	Highly variable within groups	Vender-specific
FOXP3/foxp3	Splicing variants	Full-length only
Gastric cancer	Adenocarcinoma, MALT lymphoma	No cancer
Neutrophil defensins	4 expressed	Not expressed

1.9 – Aims of My Research

1.9.1 – Characterisation of the human peripheral immune response to *H. pylori* infection and eradication

From *H. pylori* infected individuals, plasma cytokine concentrations were stratified to the severity of gastroduodenal disease to investigate potential prognostic biomarkers for disease risk. In *H. pylori*-infected donors undergoing *a regimen of* eradication therapy, we measured the anti-*H. pylori* and anti-CagA plasma IgG concentrations from donor blood. RT-qPCR was used to quantify the relative expression of the T-helper subset cytokines: IFNγ (Th1), IL-4 (Th2), IL-17A (Th17), and IL-10 (Tregs) in human peripheral blood mononuclear cells (PBMC). Blood samples were taken at 5 intervals over a 24-month period from pre- to post-eradication. It is important to understand how the host immune response changes upon removal of *H. pylori*. In some instances, eradication of *H. pylori* is associated with rapid change in immune response whilst others report a sustained effect after eradication [186]. If *H.*

pylori can be protective in certain circumstances, eradication may remove the source of that protection. I aimed to investigate this by analysing changes in peripheral immune signatures in our cohort.

1.9.2 – *H. pylori*-mediated immunomodulation in Experimental Autoimmune Encephalomyelitis (EAE)

A previous study from this research group was the first to demonstrate a protection from EAE severity in a mouse model of *H. pylori* infection (Cook, *et al.* [334]). This study identified substantially reduced EAE severity scores in the infected mice. In parallel with this was a marked reduction of Th1 and Th17 cells in both the spleens and central nervous system of these mice after infection with *H. pylori*.

It was important to both confirm this finding in an independent experimental set-up, but also to expand on the previous data to propose and identify potential mechanisms. An aim of this work was to evaluate whether they are differences in the protection from EAE between two strains of *H. pylori*: SS1 and PMSS1. These two strains differ in their ability to secrete CagA into host cells. Hussain *et al.* [219] found that the more virulent PMSS1 was associated with higher circulating IL-10, and this was correlated to lower IgE concentration. Suppressed IgE may translate to better protection from allergic and atopic diseases, potentially through elevated IL-10. It was hypothesised that the protection from EAE may be differential depending on the colonising *H. pylori* strain. In such a situation, these differences should be apparent through reduced clinical severity scores and should be measurable through changes in T-cell populations and cytokine production in the spinal cord, the levels of which are known to correlate to the neurological damage. To establish this, flow cytometry was used primarily as a technique to characterise lymphocyte populations in the spleen and central nervous system, according to the presence of transcription factors and cytokine expression.

1.9.3 – Differential lymphocyte trafficking in *H. pylori*-infected and uninfected mice

Previous work in this group has identified the chemokine receptor CCR6 and the cognate ligand CCL20 as important mediators of T-cell migration to the gastric mucosa in the context of *H. pylori* infection [219]. Interestingly, in multiple sclerosis the

majority of pathogenic myelin specific Th17 cells express CCR6. Furthermore, CCL20 has been demonstrated to be upregulated in the inflamed CNS mediating infiltration of leukocytes which correlate to MS severity score. We hypothesised that *H. pylori*-mediated induction of CCL20 expression in the stomach may modify $CD4^+$ T-helper lymphocyte trafficking and potentially divert pathogenic cells towards the gastric mucosa and away from the CNS. This may be a mechanism whereby *H. pylori* infection is able to mitigate CNS pathology in MS.

To investigate this, CD4 cells were extracted from EAE mice in the pre-symptomatic priming phase of EAE, preceding CNS accumulation. These cells were labelled with a fluorescent dye before adoptive transfer into groups of *H. pylori*-infected or uninfected mice. Differential homing patterns between groups were analysed using an IVIS *in vivo* imaging system at 24 hours post-transfer. Tissues from the recipient mice were collected and used in a flow cytometry analysis to characterise the distribution of T-helper subtypes and phenotypes according to the markers which they express.

1.9.4 – *H. pylori*, Oligodendrocyte differentiation, and Remyelination

Regulatory T-cells have been demonstrated to facilitate CNS regeneration and axonal remyelination in the demyelinated CNS. This effect was proposed to be mediated through the secreted central communication network protein 3 (CCN3). Given that Treg-induction is a hallmark of *H. pylori* infection, it was hypothesised that active gastric infection may result in a greater proportion of Tregs and a richer source of Treg-derived factors, which may translate to elevated potential to remyelinate axons. To assess this, we gathered $CD4^+$ T-cells from the spleens and mesenteric lymph nodes of *H. pylori* PMSS1-infected or uninfected mice. These $CD4^+$ cells were characterised using flow cytometry to quantify the expression of T-helper subset signature transcription factors. We also produced CD4-conditioned cell culture supernatants containing secreted factors of CD4 cells. The cytokine composition within these was quantified by ELISA. These supernatants were then incubated with murine mixed glia, whereby the proliferation and differentiation of the remyelinating oligodendrocytes was measured using fluorescent immunostaining.

1.10 – Overarching Aims & Hypotheses

1.10.1 – Hypotheses proposed

This thesis aims to investigate the overarching hypothesis that in a subset of patients, infection with *Helicobacter pylori* can confer some protection against immunological conditions such as the autoimmune disease, multiple sclerosis (MS).

I hypothesised that this protection may be mediated through modulation to the $CD4^+$ T-helper cells; specifically, through the induction of the immunosuppressive regulatory T-cells (Tregs) and the anti-inflammatory cytokine IL-10.

Protection may arise from a suppression of inflammatory T-effector cell responses, modulation to lymphocyte trafficking, or by facilitating a CNS environment conducive to remyelination and repair.

1.10.2 – Aims

I aimed to address these hypotheses by performing quantification and analysis of $CD4^+$ T-cell populations in infected and uninfected human cohorts, *H. pylori* infected mice, and in EAE mice, the animal model of MS.

1.10.3 – Objectives

The specific objectives of the studies conducted were:

1. To quantify the $CD4^+$ T-cell signature cytokines in the peripheral blood of *H. pylori* infected human participants, when infected, and following a course of antibiotic eradication of *H. pylori*.
2. To use the mouse model of MS to investigate how infection with *H. pylori* influenced the course or severity of EAE. This was done by comparing clinical severity scores between infected and uninfected groups, and characterising the frequencies of Th1, Th2, Th17 and Treg subsets.
3. To ascertain if the $CD4^+$ T-cell pool in *H. pylori* infected mice is polarised towards a pro-regenerative state, through the induction of Tregs and the associated secreted factor CCN3, and whether this can facilitate the differentiation of oligodendrocytes with a subsequent production of myelin protein.

Chapter 2

The Human Immune Response to *H. pylori* Infection and the Effects of its Eradication

Chapter 2: Investigating the cellular and humoral immune response in peripheral blood of patients infected with *H. pylori* and after antibiotic-mediated eradication.

2.1 – Introduction

2.1.1 – Gastric Pathogenesis of *H. pylori* Infection

H. pylori infection induces a robust inflammatory cell infiltrate in the gastric mucosa. Marked infiltration of neutrophils is an early hallmark, and this persists chronically. The neutrophils produce inflammatory molecules such as interleukin-8 (IL-8), nitric oxide (NO) and reactive oxygen species (ROS), which recruit and maintain further leukocyte responses but also contribute to gastric pathology and disease risk [106,350]. Chronic inflammation is observed as macrophages, neutrophils and dendritic cells populate the mucosa, B-cells produce *H. pylori*-specific IgG and IgA neutralising antibodies and $CD4^+$ T-helper lymphocytes co-ordinate the further immune response directed against the pathogen [106,351]. All infected individuals will develop a chronic gastritis however in most cases (around 80% or more of infected individuals) this will be asymptomatic and can persist lifelong without clinical consequence [106]. A minority of infected patients, around 10-15%, will proceed to develop a symptomatic condition and present with a gastric pathology such as peptic ulcer disease (PUD) [11,58,106]. In the most severe cases (around 1-5% of infected individuals), chronic inflammation and oxidative stress result in atrophic gastritis, dysplasia and metaplasia thus facilitating a progression to gastric cancer [11,58,64,115].

The most common presentation of *H. pylori* infection is localised to the anatomical region of the gastric antrum, however a pan-gastritis affecting the gastric corpus is present in some patients [11]. Colonisation of the gastric corpus is associated with impaired acid secretion, thus creating more favourable conditions for *H. pylori* to colonise the corpus [11]. Loss of acid-secretory function can occur as a result of cytokines produced in response to *H. pylori* infection such as IL-1β and TNFα, and in some instances is caused through autoimmune gastritis (AIG) initiated through the phenomena of molecular mimicry between antigenic regions of the *H. pylori* urease subunit B (UreB) and the human gastric H^+K^+-ATPase [67,68,174,352]. Pan-gastritis leads to an increased overall chance of further pathogenesis, destruction of the acid-secreting parietal cells thus further attenuating acid-secretion. Atrophic gastritis resulting from chronic *H. pylori* infection is a precursor event leading to dysplasia and metaplasia thereby facilitating the progression to the development of gastric cancer [11].

2.1.2 – Immune Responses to *H. pylori* Infection

There is an influx of $CD19^+$ B-cells in gastric mucosal tissue and *H. pylori*-specific IgG and humoral and antibody response is insufficient to clear the infection [11,106,114,174]. The T-cell mediated response in the gastric mucosa comprises a predominantly $CD4^+$ Th1 inflammatory component with a notable Th17 cellular contribution, as well as cytotoxic $CD8^+$ T-cells [106,351,353]. Indeed, the Th1-associated cytokines IFNγ, TNFα, IL-2, IL-12 and IL-18 are upregulated markedly during infection and support the Th1-dominant paradigm [106,351,352]. The Th1/Th17 response results in the secretion of inflammatory cytokines and chemokines marking the infected mucosa for leukocyte migration. However, they also contribute to the degree of gastric pathology and the incidence of complications such as peptic ulcer disease (PUD) and gastric cancer (GC).

Crucially, there is also a marked presence of suppressive regulatory T-cells (Tregs) characterised by expression of $CD4^+CD25^{hi}FOXP3^+$ and secreting anti-inflammatory factors such as TGFβ and IL-10 [106,221]. The induction of Tregs provides one mechanism by which *H. pylori* is believed to exploit to enable persistence lifelong in the host and attenuate efficient clearance of the infection [1,106].

2.1.3 – Beneficial Sequalae of *H. pylori* Infection

In recent years evidence has begun to emerge that infection with *H. pylori* is associated with protection against immune-mediated diseases, including allergies, asthma, and autoimmunity [20,22,91-94,219,334,354]. This protection is thought to be at least partially dependent on the *H. pylori*-induced suppressive Treg response and anti-inflammatory factors such as IL-10 [20,219]. This research group has shown previously that reduced IgE concentrations correlated to increased levels of IL-10. This relationship was stronger in the presence of more virulent CagA^{+} *H. pylori* strains, which induce larger numbers of Tregs [219]. The work of Arnold & Oertli *et al.* supports these data with mouse models, and provides preliminary mechanisms by which this occurs, via tolerising effects on dendritic cells resulting in an attenuated ability to induce pro-inflammatory immunity [20-22,24,354].

There is currently no published data on whether the proposed *H. pylori*-mediated protection is dependent on a current active infection, or if it is induced in early life as the immune system is developing and then becomes permanent. The former scenario would be supported mechanistically by the known ability of *H. pylori* to actively induce a robust regulatory T-cell response in the infected host through the production of bioactive mediators inducing tolerogenicity to dendritic cells [21,24]. This suppressive response is theorised to either directly or indirectly modulate the activity and frequency of pro-inflammatory cellular subsets which can mediate exacerbations of chronic immune diseases. The latter scenario would be supported by paradigms such as the 'hygiene hypothesis'; or perhaps more accurately and currently referred to as the 'old friends' hypothesis' [355,356]. These hypotheses suggest that once-commensal microbes are being lost from the microbiomes of individuals in the modern world, as a likely result of increasing antibiotic administration through childhood, and better sanitation through life. This disruption to the canonical human microbiota perhaps leads to aberrant responses in later life through dysregulation of immune homeostasis and development during childhood and contributing to the rise of allergic and immunological disease [355,356].

2.1.4 – Extra-gastric Diseases Affected by *H. pylori* Infection and Eradication.

In addition to gastro-duodenal conditions, *H. pylori* infection has been linked to extra-gastric disorders such as asthma, inflammatory bowel diseases (IBD - comprising Crohn's disease; CD, and ulcerative colitis; UC) and chronic immune thrombocytopenia (cITP) [22,219,334,357-359]. In some instances, such as in the case of asthma, these extra-gastric associations can be of a protective nature [20,22,81,219,332,334,335,357]. Importantly, the effect of *H. pylori* eradication on these extra-gastric diseases, and the host systemic immune response in general, has not been well studied to our knowledge to date.

2.1.4.1 – Chronic Immune Thrombocytopaenia (cITP)

The autoantibody mediated condition chronic immune thrombocytopenia (cITP) is characterised by an antibody response mounted against antigens of blood platelet glycoproteins. This results in reduced platelet counts and disorders affecting blood clotting. *H. pylori* is associated with an exacerbation of this condition [357]. Mechanisms underlying this are not well understood or characterised.

One study by Rocha *et al.* [357] has investigated the effect of *H. pylori* eradication therapy on the manifestations of cITP, and the plasma cytokine concentrations associated with the activity of the $CD4^+$ T-helper cell subtypes, Th1, Th2, Th17, and Tregs. Here, when patients were administered triple therapy to eradicate the bacterium, remission from cITP was observed in 28.8% of the patients. Remission was not observed in two patients who failed eradication therapy and remained *H. pylori* positive by ^{13}C-UBT. Before eradication therapy, the baseline levels of the cytokines IL-1β, IL-6, IL-12p70, TGFβ1, and TNFα were all higher in the *H. pylori*-positive patients as compared to uninfected individuals.

Amongst the patients in whom eradication of infection had resulted in cITP remission, there was a reduction in the pro-inflammatory cytokines associated with Th17 and Th1 T-helper subsets (IL-1β, IL-6, IL-17A, IL-23A, TNFα, or IL-2, IL-12p70, IFNγ respectively) and a concurrent increase in the anti-inflammatory cytokines associated with Th2 and Treg cells (IL-4; or IL-10 and TGFβ1 respectively). This effect was sustained at a timepoint of 6 months post-eradication. In the patients who did

not display a remission from cITP (as determined by recovering platelet counts) there was a mild but non-significant trend in these same cytokines. The authors conclude that infection with *H. pylori*, and subsequent eradication can result in notable changes to cytokine profiles by which the manifestations of cITP can be modulated. Only ~29% of patients observed a cITP remission after *H. pylori* eradication in this cohort which highlights those human participants are subject to many external influences which can modulate their immune response. However, within the responders (those who entered a cITP clinical remission) significant cytokine differences were indeed reported because of *H. pylori* eradication.

2.1.4.2 – Inflammatory Bowel Diseases (IBD)

Inflammatory bowel diseases (IBD) comprising Crohns' disease (CD) and ulcerative colitis (UC) have been suggested to be negatively correlated to *H. pylori* infection [358,359]. Review of the available data reports that there is a significant negative association between *H. pylori* infection and the incidence of IBD in which only 26.5% of IBD patients had a concurrent *H. pylori* infection as compared to 44.7% of healthy controls (*p=0.001*) [80]. Other studies agree, and report that in those *H. pylori*-infected patients who did present with IBD, the age-of-onset was significantly later (circa 40 years of age c.f. 30 years of age in *H. pylori*-naïve patients) suggesting a mitigation or at least modulation in the disease course [81]. Taking this, it is possible that eradication of *H. pylori* may result in worsening of the symptoms of IBD [17].

2.1.4.3 – Allergy and Asthma

Allergies and asthma are atopic conditions in which *H. pylori* infection has been repeatedly reported to confer a protective influence in both humans and mouse models [20,91-93,219]. This is especially noted when the colonising strain is a more virulent *cagA*$^{+}$ or *vacA-i1* genotype, or in those individuals with stronger Treg responses mediated by IL-10 [20,92,219]. An emerging concept is that this protection is associated with *H. pylori*-induced regulatory immunity. In fact, Tregs and the anti-inflammatory IL-10 are inversely correlated to IgE levels in human plasma [20,219]. Other groups have investigated the mechanism by which this occurs and have identified tolerising

effects on dendritic cells in the induction of Tregs. This is hypothesised to be in a manner dependent on the activation of the NLRP3 inflammasome and secretion of IL-18 in APCs [20,23,358].

2.1.4.4 – Multiple Sclerosis (MS) and the animal model experimental autoimmune encephalomyelitis (EAE)

Protection from MS has been proposed by numerous studies based on inverse correlations of *H. pylori* infection in MS patients as compared to healthy individuals [280,332,333,335,336,343]. Work by Ranjbar *et al.* 2019 [343] demonstrates that amongst MS patients, those serologically positive for *H. pylori* present with significantly decreased inflammatory cytokine levels (IFNγ, TNFα, IL-6, and IL-17; *p=<0.001*) in plasma, coupled with increased anti-inflammatory IL-10 and IL-4; *p=<0.001*) [343]. Indeed, this research group has presented evidence previously (Cook *et al.* 2015 [334]) showing that only 21.1% of MS patients were *H. pylori*-infected as compared to 42.9% of healthy volunteers (*p=0.018*) [334]. This trend is similarly observed in the work of other research groups [280,332,333,335,336,343]. To investigate this further using the animal model EAE, we showed a significant reduction in the maximal EAE disease severity score. This was in concordance a lower frequency of inflammatory Th1 and Th17 cells in the spleens and central nervous systems of infected mice, determined by flow cytometry [334]. To my knowledge, we are the only group to show a direct suppression of EAE by *H. pylori* infection to-date. Further work identifying the mechanism behind this would fill a notable gap within the current literature. With the global prevalence of autoimmune and allergic conditions rising, this is an important field of study for diseases which significantly impact the quality of life of many individuals.

2.1.5 – Rationale and Hypotheses for this study

Attenuation of the inflammatory and immune responses after eradication of *H. pylori* explains the mitigation of on-going gastric inflammation and recovery from pre-existing gastric pathology. However, attenuation of a chronic stimulation of Treg responses is a matter of interest particularly for the work within this thesis, as it has been hypothesised that protection can be mediated through Treg cells and the

secreted anti-inflammatory cytokines including IL-10. Taking this, we must consider that eradication of the bacterium may therefore remove the source of protection and lead to worsening immunological diseases in cases of atopy and autoimmunity. As such, eradication may not always be the most beneficial treatment option for an infected individual. This proposal is controversial especially in ethical terms. To consider advising a patient to not eradicate a bacterial infection with known associations to serious and potentially fatal implications such as gastric cancer is a bold statement, and one that should be made only if founded on solid mechanistic evidence and clinically definable characteristics. A persons' risk of developing disease from their *H. pylori* infections must be evaluated and considered alongside the potential benefit they may receive if they suffer with allergy or autoimmunity. For such a decision to be made, it would be beneficial to develop a blood-based test to determine disease risk. For this, peripheral cytokine levels could be used as a prognostic biomarker for the risk of developing serious *H. pylori*-associated disease. Such a blood test could inform physicians on treatment strategies and may identify groups of individuals in which eradication of infection may not be the most viable course of action.

2.1.5.1 – Peripheral Blood Cytokines as Prognostic Biomarkers for Gastric Disease

It was hypothesised that more severe clinical manifestations of *H. pylori*-mediated disease would be associated with higher inflammatory plasma cytokine concentrations. These markers may be used to infer changes in immune cell activity, therefore inform on individuals' risk of gastric cancer development.

2.1.5.2 – The peripheral blood immune response to *H. pylori* infection, before and after antibiotic eradication

It was hypothesised that the peripheral blood $CD4^+$ T-helper responses would be affected after a patient is subject to the standard regimen of triple therapy and subsequent eradication of *H. pylori*. Data quantifying the host immune response in the periphery after such a medical intervention is lacking in the literature.

2.2 – Aims

2.2.1 – Quantification of plasma cytokines across disease associated variables.

- To stratify plasma cytokine concentrations from *H. pylori* infected or uninfected individuals (quantified previously by Winter *et al.*, 2013; unpublished data) by *H. pylori* associated gastro-duodenal pathology.
- To evaluate the dataset to identify potential blood-based cytokine biomarkers which may be used for prognostic applications to determine an individuals' risk of developing *H. pylori*-associated disease.

2.2.2 – Changes in the peripheral blood antibody response and T-helper cell subsets before and after *H. pylori* eradication

- To measure the concentrations of plasma anti-*H. pylori* IgG antibodies in a cohort of patients who had undergone a regimen of *H. pylori* eradication therapy.
- To quantify T-helper subsets Th1, Th2, Th17 and Treg in peripheral blood by flow cytometry, using signature transcription factors and cytokines.
- To quantify PBMC cytokine mRNA expression in the above T-helper subsets using RT-qPCR assays.
- To evaluate the datasets and determine if significant differences in T-helper subtypes are apparent following the eradication of *H. pylori.*
- To determine the CagA virulence type of the colonising strains by quantifying anti-CagA antibodies.

2.3 – Materials and Methods

2.3.1 – Plasma Cytokine Quantification & Analysis

Samples were obtained from 29 *H. pylori* infected and 47 uninfected donors attending routine upper GI endoscopy at the Queens' Medical Centre, Nottingham, with informed written consent. Ethical approval was granted from the Nottingham

Ethical Committee 2 (reference 08/H0408/195). Plasma cytokine concentrations were determined using high-sensitivity electro-chemiluminescence assays (Meso Scale Discovery®; MSD), by Dr. Jody Winter and Dr. Karen Robinson, University of Nottingham. These cytokine concentration data were stratified by; *H. pylori* infection status, Sydney score (grouped as low or high scores, 0-1 and 2-3) for the scale of gastric mononuclear cell inflammation, neutrophil infiltration, extent of gastric atrophy (scored at 0, 1, 2, or 3), extent of intestinal metaplasia, *vacA* Signal region type (S1 or S2), *vacA* mid region type (M1 or M2), *vacA* intermediate region type (I1 or I2), *cagA* status, age, and sex. This was to investigate associations of these variables with the levels of cytokines in peripheral blood. Sections from antral and corpus biopsies were scored by a qualified histopathologist who was blinded to the study data, using the Sydney scoring system to score inflammation, activity (neutrophil infiltration), atrophy, and intestinal metaplasia.

2.3.2 – Eradication Study

2.3.2.1 – Clinical samples

Peripheral blood was collected from patients attending the Queens Medical Centre, Nottingham for a routine upper GI tract endoscopy, most commonly to investigate symptoms of dyspepsia. Clinical samples were donated with informed written consent and approval from the Nottingham Research Ethical Committee 1 (REC Ref: 12/EM/0446). Exclusion criteria include patients regularly taking NSAIDs, proton pump inhibitors, antibiotics, or immunosuppressive therapies in the preceding 4 weeks, who were not asked to donate samples for the research. The use of probiotics and/or H2 receptor blockers were not included in the exclusion criteria. To our knowledge, no donors were diagnosed with additional co-morbidities that may result in immune dysregulation. The age range of the study participants was 18-70 with a mean age of 55. None of the donors had clinically diagnosed allergy or asthma requiring medical intervention, however 18% (9/50) had some history of sub-clinical atopy, and 6% (3/50) had some history of adult asthma. Data on age, sex, relevant disease history (including peptic ulcer disease) were collected for all enrolled

participants. *H. pylori* infection status was determined using a ^{13}C-urea breath test (^{13}C-UBT) and biopsy based confirmatory test.

Enrolled participants provided blood at the initial visit (month 0; infected). Patients were then administered the first-line triple therapy (Amoxicillin, PPI, clarithromycin/metronidazole; 7-day course) and returned 2 months post-treatment initiation. Eradication was defined by providing a negative ^{13}C-UBT. Proceeding this, they returned to provide blood samples at 3 further timepoints (6, 12, and 24 months) over a 2-year follow-up period. In the event of a failure to eradicate, a subsequent altered regimen of antibiotics was prescribed as required until a negative ^{13}C-UBT was provided at 2-month post-therapy. Blood was collected in vacutainer tubes containing EDTA anti-coagulant (Greiner). Peripheral blood mononuclear cells (PBMCs) were purified by density gradient centrifugation and aliquoted for subsequent flow cytometry and RNA analysis. Blood was processed by Dr. Jonathan White, Dr. Karen Robinson, Dr. Dona Reddiar, Dr. Darren Letley, and Dr. Kazuyo Kaneko, and Harry Jenkins, University of Nottingham.

Table 6 presents the demographics of the eradication study participants.

Table 6 Patient demographics for the *H. pylori* eradication study.

Patient Demographics for the Study	
Number of patients	50
Male: Female Ratio	24:26
Mean Age (years)	55.5 (18-70)
Non-smoker	52% (26/50)
Ex-smoker	20% (10/50)
Smoker	28% (14/50)
Allergy/atopy	18% (9/50)
Adult asthma	6% (3/50)
Peptic ulcer disease (PUD)	20% (10/50)
Multiple eradication attempts	14% (7/50)

2.3.2.2 – Purification of PBMCs from whole blood.

Following centrifugation of whole blood at 200 x *g* for 10 minutes plasma was collected, aliquoted, and stored at -80^{o}C. Cell culture medium was prepared from

RPMI-1640 (Sigma) with the addition of 100 $U.ml^{-1}$ penicillin with 100$\mu g.ml^{-1}$ streptomycin, P/S (Sigma), 10% *v/v* foetal bovine plasma (Invitrogen) and 2mM L-glutamine (Invitrogen). Leucosep™ tubes were spun at 200 x *g* for 5 minutes to clear any bubbles. Blood was poured into 50ml falcon tubes with the addition of 20ml culture medium. 20mls of this mixture was poured into Leucosep™ tubes and spun at 800 x *g* for 15 minutes. The supernatant containing the PBMC layer was distributed evenly to two 20ml universal tubes each with the addition of 20ml culture medium and centrifuged at 200 x *g* for 5 minutes. Supernatants were discarded and the resulting pellet was resuspended in 20ml medium. This wash step was performed in triplicate. After the final washing step, the pelleted cells were resuspended in 5ml culture medium and kept on ice.

2.3.2.3 – Cell counting.

Cell suspensions were diluted with Trypan Blue solution to exclude dead cells (which will appear blue). An aliquot was applied to a haemocytometer slide and cells were counted before resuspension in culture medium at a concentration of $1x10^6ml^{-1}$.

2.3.2.4 – RNA isolation

$5x10^6$ PBMCs were added to a universal tube and centrifuged at 200 x *g* for 5 minutes. The supernatant was discarded. From the cell pellets, total RNA was isolated using an RNeasy mini kit (QIAGEN, Cat. No. 74104) according to the manufacturer's instructions. RNA preparations were treated with Turbo DNase (Invitrogen) as per the manufacturers' instructions. Eluted RNA was quantified using a NanoDrop™-ND1000 spectrophotometer (NanoDrop™ technologies). The RNA was diluted to $20ng.\mu l^{-1}$ in DNase/RNase-free water for use in subsequent RT-qPCR reactions.

2.3.2.5 – *H. pylori*-negative patient PBMC Samples

PBMCs were purified from the blood of 12 *H. pylori*-negative donors. RNA was isolated and reverse transcribed (as described above) before being pooled. Pooled *H. pylori*-negative cDNA was used as a comparator sample for subsequent RT-qPCR analyses.

2.3.2.6 – cDNA Preparation

The cDNA synthesis was performed from 100ng template RNA using SuperScript II Reverse Transcriptase (Invitrogen; Cat. No. 18064), oligo(dT)$_{12-18}$ primer (Invitrogen; Cat. No. 18418-012) with addition of RNaseOUT (Invitrogen; Cat. No. 10777-019) according to the manufacturer's instructions. For each sample a minus RT (-RT) control (using water in place of reverse transcriptase enzyme) was prepared to assess potential genomic DNA (gDNA) contamination. The cDNA samples were stored at -20°C for use in subsequent qPCR analyses.

2.3.2.7 – Reverse Transcription-Quantitative Polymerase Chain Reaction (RT-qPCR)

RT-qPCR for the target genes *IFNG*, *IL4*, and the reference gene *GAPDH*, was performed on a RotorGene 3000 (Corbett Research) using RotorGene SYBR green PCR mixture (Qiagen; Cat No. 204074) and Quantitect™ primer assays (QIAGEN; *IFNG*: QT00000525, *IL4*: QT00012565; sequences not disclosed). PCR cycling conditions are detailed in *Table 7*. The amplifications were performed in 20µl reaction volumes according to the manufacturer's instructions, or as described previously, Robinson *et al.* (2008) [166]. Each run included no-template controls using RNase/DNase-free water in place of template cDNA to check for contamination of the reaction mixture. A melt analysis was performed to assess the specificity of the primer assays. To confirm that no genomic DNA contamination was present in the samples, a minus RT control was included from the reverse transcription using water in place of reverse transcriptase and run in parallel to the samples. A positive control was included using commercially available oligo(dT)-primed total human reference cDNA (Clontech; Cat No. 636692). Samples were run in duplicate. For comparison, pooled cDNA from *H. pylori*-negative donors was produced and assayed in triplicate. Sample and comparator results were normalised to the housekeeping gene, of glyceraldehyde-3-phosphate dehydrogenase (*GAPDH)* which should remain stably expressed irrespective of experimental conditions. PCR reaction efficiencies were calculated from standard curves produced by plotting the Ct values of serially diluted cDNA. All assay efficiencies were >1.93 and <2.01. Data analyses were performed using the Pfaffl method [360] to generate relative expression ratios.

Table 7 RT-qPCR Cycling conditions: IFNG, IL4, GAPDH

PCR Procedure	Cycling Steps
Hold – 95°C for 5 mins	
Cycling (45 cycles)	95°C for 5 secs
	60°C for 15 secs
Hold – 60°C for 5 mins	
Melt Curve (60-95°C)	
Hold 72°C for 5 mins	

To maintain consistency with previous work (Hussain, *et al.* 2016 [219]; White, 2016 [361]), RT-qPCR analysis of *IL10* mRNA expression used alternative conditions. The procedure was as described in section 2.3.2.6 with the following modifications. Reactions were performed in a final volume of 20µl using DyNAmo HS qPCR mixture (New England Biolabs; Cat No. F410L) according to the manufacturer's instructions and using 0.15µM final primer concentrations. Primer sequences are described in *Table 8*. The PCR cycling conditions are detailed in *Table 9* . Reaction efficiencies were 1.82 for *GAPDH* and 2.04 for *IL10*.

Table 8 PCR Primer Sequences; IL10, GAPDH

Gene	Primer	Sequence	Tm	Product length
GAPDH	Forward	5'- CCACATCGCTCAGACACCAT-3'	Tm= 66.3	114 b.p.
	Reverse	5'- GGCAACAATATCCACTTTACCA -3'	Tm= 65.8	
IL10	Forward	5'- GCTGGAGGACTTTAAGGGTTACCT – 3'	Tm= 65.3	109 b.p.
	Reverse	5'- CTTGATGTCTGGGTCTTGGCT -3'	Tm= 65.3	

Table 9 PCR cycling conditions; IL10, GAPDH

PCR Procedure	Cycling Steps
Hold – 95°C for 15 mins	
Cycling (45 cycles)	Denaturation: 95°C for 15 secs
	Annealing: 62°C for 30 secs
	Extension: 72°C for 30 secs
Hold – 72°C for 10 mins	
Melt Curve (72-95°C)	
Hold 72°C for 5 mins	

The qPCR assay had been inconsistent for *IL17A* using the above conditions, and across multiple candidate primer pairs. The analyses of *IL17A* were therefore performed using amended protocols. For this, cDNA was synthesised using 500ng

template RNA, primed with 250ng of random hexamers (Invitrogen) and 1 unit SuperScript II reverse transcriptase (Invitrogen). The resulting cDNA was used at 50ng per 20µl qPCR reaction volume. These analyses used TaqMan primers and probes in place of SYBR Green-based chemistry. For this, reactions were performed using commercial primer/probe assays (Applied Biosystems) and TaqMan Fast Universal Master Mix (Applied Biosystems) according to manufacturers' instructions. Both *GAPDH* and *IL17A* assays were duplexed in the same reaction.

As *IL17A* will be expressed at a much lower level than the housekeeping gene *GAPDH*, we used primer-limited assays for the housekeeping gene to reduce the consumption of reaction components before the target gene amplification began. Fluorescence was detected from 520-536nm for FAM (*IL17A*) and 560-580nm for VIC (*GAPDH*). Assay information is given in *Table 10*. PCR cycling conditions in *Table 11*.

Table 10 TaqMan Assay Information; IL17A, GAPDH

Target	Dye	Sequence / Information	Tm	Product length
GAPDH	Vic (PL)	**Assay: Hs99999905_m1** [Undisclosed Sequence] **Details:** Amplicon spans exon boundary **Amplicon Location:** Exon 2-3 **Assay Location:** 229	60	122 b.p.
IL17A	FAM	**Assay: Hs00936345_m1** [Undisclosed Sequence] **Details:** Probe spans exon boundary **Amplicon Location:** Exon 1-2 **Assay Location:** 76	60	88 b.p.

Table 11 PCR cycling conditions; IL17A, GAPDH

PCR Procedure	Cycling Steps
Hold – 50°C for 2 mins	
Hold – 95 C for 20 sec	
Cycling (40 cycles)	Denaturation: 95°C for 3 secs
	Anneal/Extend: 60°C for 30 secs (Acquiring)

2.3.2.8 – Agarose Gel Electrophoresis

PCR products were visualised on 100ml agarose gels consisting of 3.5% *w/v* agarose in 1x Tris-Borate-EDTA (TBE) running buffer. Gels were electrophoresed at 110v until the dye reached 75% down the gel. GelRed stain (Biotium; Cat. No. 41002) was

included at 5µl per 100ml. All gels were imaged under UV light. All amplicons were of the expected molecular weight and the same in the comparator and study samples.

2.3.2.9 – RNA Integrity Analysis

Quality control and analysis of RNA integrity was performed using a TapeStation 4200 instrument (Agilent), using the RNA ScreenTape kit (Agilent; Cat. No. 5067-5630) according to the manufacturers' instructions. Briefly, RNA samples were thawed on ice before both samples and ScreenTape reagents were vortexed briefly and centrifuged before use. 5µl of RNA ScreenTape sample buffer (Cat No. 5067-5577) was mixed with 1µl of RNA sample in a 200ul reaction tube (Agilent; Cat No. 401428) and sealed. The sample was mixed by vortex at 1000 x *g* for 1 min at room temperature before centrifugation for 1 minute. The reaction mixture was then heated at 72°C for 3 mins to resolve any secondary structure before being placed on ice for 2 minutes to prevent it reforming. Here, the samples were spun for 1 minute to collect condensates to the bottom of the tube. Tubes were then loaded into the TapeStation instrument for automated analysis.

2.3.3 – Human Plasma anti-*H. pylori* IgG ELISA

The IgG antibody response was quantified from human plasma using a commercially available ELISA kit (BioHit™ Cat. No. 601040) according to the manufacturers' instructions. Plasma was diluted 1:200 for use in ELISA. Quantification was performed using a standard curve of known concentrations and the optical density was measured using a BioTek plate reader instrument.

IgG concentrations were determined in plasma samples from the *H. pylori* eradication study at 5 timepoints (Month 0, 2, 6, 12, and 24) over a 24-month period from patients undergoing *H. pylori* eradication therapy. IgG levels were analysed for statistical significance using the Wilcoxon matched-pairs test; significance attributed where $p = <0.05$.

2.3.4 – Human plasma anti-CagA IgG ELISA

The presence of antibodies to the *H. pylori* virulence factor CagA was determined using commercially available ELISA kits according to the manufacturer's instructions (Genesys Diagnostics; Cat. No. GD033). Plasma was diluted 1:200 prior to use in ELISA assays. Optical density was quantified with a BioTek plate reader and comparing the result with two internal positive and negative controls. A positive test result was attributed to a sample if the optical density was >2.1x higher than the internal negative control.

2.3.5 – Statistical analysis

Data analysis was performed using GraphPad Prism™ software. Normality and distribution of the data were evaluated using a Shapiro-Wilks test. Grouped analyses were performed using ANOVA, or Kruskal-Wallace tests. Direct comparisons were performed using Mann-Whitney U-test or Wilcoxon Matched-pairs tests. Multiple comparisons corrections were applied where required using the Holm-Šídák's, Bonferroni, or Dunn's correction, as appropriate. In all instances, statistical significance was determined where $p = <0.05$.

2.4 – Results

2.4.1 – Determination of potential blood-based biomarkers for *H. pylori*-associated disease risk

Plasma from *H. pylori* positive and negative patients was assayed for cytokines and the only significant differences were in IL-17A and IL-12p70. These analyses observed a significant 1.7-fold increase in plasma IL-17A ($p=<0.0001$; Mann-Whitney *U*-test) in *H. pylori*-infected as compared to uninfected individuals; there was also a significant 2.1-fold decrease in plasma IL-12p70 concentrations ($p=0.01$, Mann-Whitney U-test) in *H. pylori*-infected as compared to uninfected individuals (*Figure 9; A & B*).

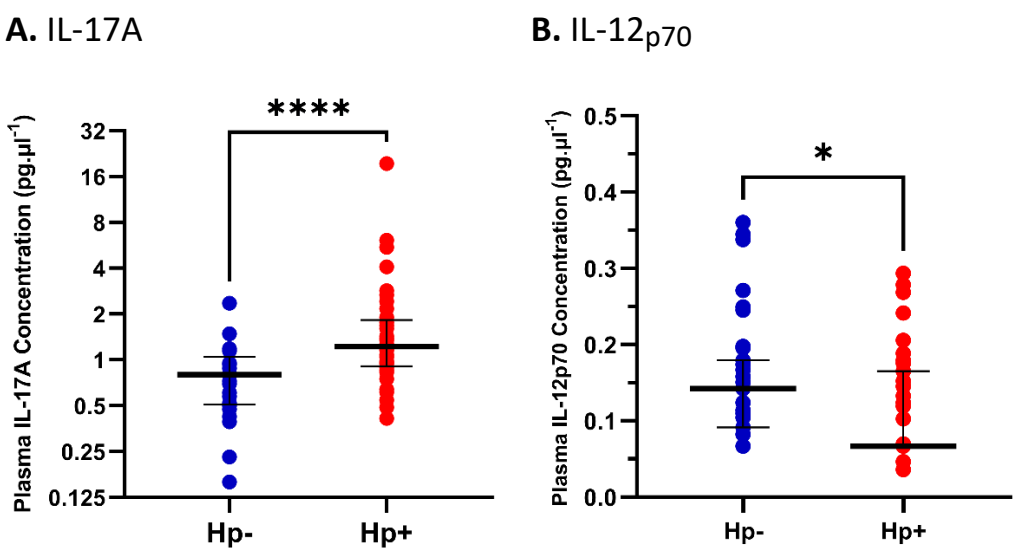

Figure 9 Plasma cytokine concentration in H. pylori-infected or uninfected individuals

Cytokine concentrations for (A) IL-17A, and (B) IL12p70, were measured in human plasma with high-sensitivity assays and stratified by *H. pylori* infection status; uninfected, Hp- (blue), or infected, Hp+ (red). Lines denote the median; error bars show the interquartile range. Mann-Whitney U-test; * p=0.01; **** p=0.0001.

Of the variables analysed, there were only significant differences in the concentrations of IL-17A and IL-10 (*Figure 10; A-C*). The plasma IL-10 concentration was modestly elevated by 1.4-fold (*p=0.01,* Mann-Whitney U-test) in patients who presented with higher Sydney scores for neutrophil infiltration (scores grouped as 2-3 on a scale of 0-3) in the gastric corpus as compared to patients with a low (0-1) score, but interestingly this was not recapitulated in the gastric antrum.

Similar results were observed for IL-17A concentrations, which were elevated 1.7-fold (*p=<0.004*) in patients presenting with a moderate/severe Sydney score for neutrophil infiltration (2-3) compared to those with mild scores (0-1) in the gastric corpus, but not significantly different in the gastric antrum. Additionally, plasma IL-17A was also elevated significantly 1.6-fold (*p=0.001*) in the gastric corpus (but not the antrum) in response to higher scores for the degree of mononuclear cell infiltration (score 2-3 on a scale of 0-3) as compared to individuals with a low score (0-1). Furthermore, IL-17A was significantly elevated in the plasma 1.7-fold (*p=<0.0001*) in *H. pylori*-infected as opposed to uninfected patients.

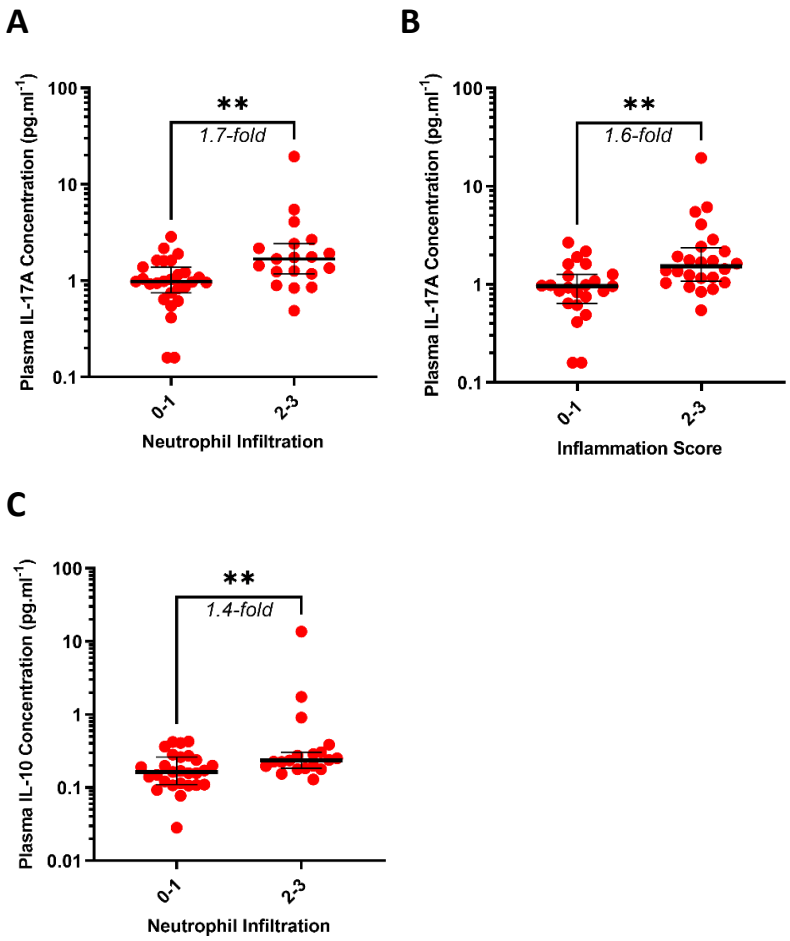

Figure 10 *Plasma cytokine concentration stratified by H. pylori infection status and gastro-duodenal pathology*

H. pylori infection status and disease-associated variables were used to stratify the concentration of cytokines in human plasma. Plots show those cytokines found to be significantly altered between groups. IL-17A was elevated in parallel with increasing Sydney scores for the infiltration of; (A) mononuclear cells; and (B) neutrophils, to the gastric corpus. (C) IL-10 was elevated in parallel to increased neutrophil infiltration to the gastric corpus. Dots represent individual patient levels; lines represent the median; error bars denote the interquartile range. *Mann-Whitney U-test; **p=<0.005*.

2.4.2 – The human peripheral blood immune responses to *H. pylori* eradication therapy

Plasma anti-*H. pylori* IgG and anti-CagA IgG antibody responses were assayed, in addition to the $CD4^+$ T-helper cell responses, in patients undergoing a course of *H. pylori* eradication.

2.4.3 - Plasma anti-*H. pylori* IgG Responses During Eradication Therapy

The plasma anti-*H. pylori* IgG responses were measured using a commercial ELISA before, and at four time-points after eradication therapy (*Figure 11; A*).

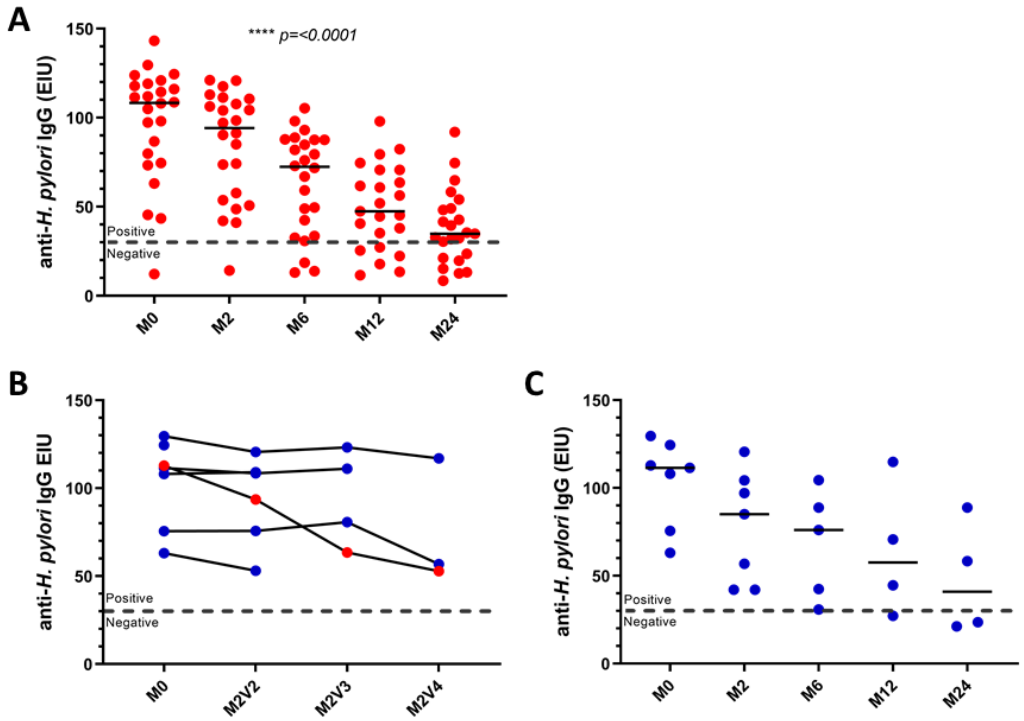

Figure 11 Quantification of anti-H. pylori IgG plasma concentration up to 24 months post antibiotic-mediated eradication therapy.

Eradication of *H. pylori* was anticipated to result in a reduction in circulating *H. pylori*-specific antibody levels. Commercial ELISA kits were used to quantify plasma IgG concentration in peripheral blood provided from the study cohort. Plasma IgG levels; (A) over 24 months post-eradication; (B) In treatment-resistant cases where eradication was not achieved; (C) In treatment-resistant cases after a successful eradication. Axis are measured in enzyme immunoassay units (EIU). Dotted line denotes the level of clinical sero-negativity. V2, V3, V4, represent repeat visits for further treatment regimens. Dots represent individual patients and lines denote the median. ANOVA test for linear trend; **** *p=0.0001.*

For most of the cohort, in which successful *H. pylori* eradication had been accomplished after the initial regimen of triple therapy, plasma IgG levels were significantly reduced over the 24-month period (*p=0.0001,* Wilcoxon matched-pairs analysis). Only 6 patients had antibody levels low enough to be considered serologically negative at 24 months post eradication. Interestingly, one patient had serologically negative levels of anti-*H. pylori* IgG in their blood from the start of the study.

In the five of the six patients who had one or more failed rounds of eradication therapy, plasma IgG levels remained constant (*Figure 11; B*). Upon a successful *H. pylori*-negative test result (by ^{13}C-UBT), samples from the subsequent timepoints contained reducing plasma anti-*H. pylori* IgG levels over the subsequent 24 months (*Figure 11; C*). Interestingly, patient T005 (blue dots on *Figure 11; B*) appeared to have reducing IgG concentrations whilst still repeatedly testing *H. pylori* positive.

2.4.4 – *H. pylori* Eradication Study - RNA Integrity Analysis and Quality Control

As this was a longitudinal study, it was important to confirm that the RNA samples were of a similar quality at the start and end of the study. Analysis of the RNA integrity between month 0 and month 24 from a selection of the cohort samples was performed using an Agilent TapeStation™ instrument (*Figure 12*). The TapeStation instrument assessed the estimated RNA integrity number (RIN^{e}), a measure of degradation, by running the sample through a gel matrix and observing bands corresponding to the 16S and 18S rRNA. In degraded samples these bands appear laddered. In addition to measuring RNA integrity, the instrument also provided the RNA concentration in the sample, which validated use of the NanoDrop readings. The RNA concentration was found to often be notably lower when measuring on the TapeStation that the concentration obtained via the NanoDrop.

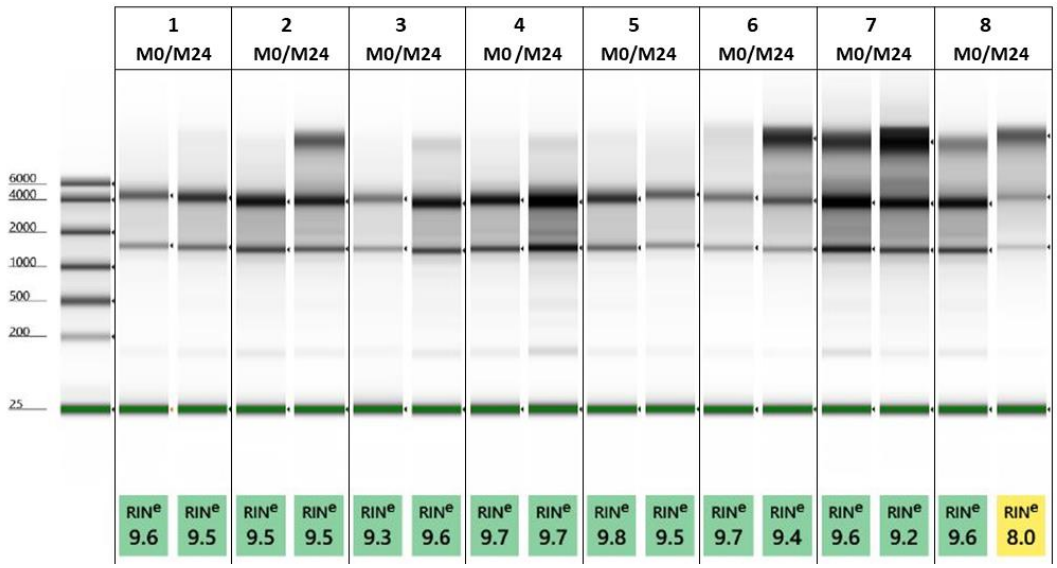

Figure 12 RNA integrity analysis of the eradication study PBMC samples

PBMC RNA samples from 8 randomly selected patients in the cohort were analysed on a TapeStation™ instrument to qualitatively assess samples for RNA integrity. Samples were chosen from month 0 and month 24 to assess degradation over time in storage. RNA integrity scores (RIN^e) are given below the gel images. Scores >9.0 are considered of high quality and with negligible degradation.

In total, 8 patients from the cohort (T003, 8, 11, 14, 19, 28, 37, 44 and T048) were randomly selected. Importantly, the RNA integrity (RIN^e) score indicated good quality RNA preparations (with RIN >9.0), for all but one of the samples (T048). No differences in integrity between months 0 and 24 were observed, apart from in the T048 samples (month 0, RIN=9.6; month 24, RIN=8.0. These data suggest that any observed differences in cytokine gene expression over the time course of the study are unlikely to be due to degradation in RNA quality over the 24 months (*Figure 12*). One patient (T035) was randomly selected and samples from all 5 timepoints from this patient were analysed in the same manner.

Two further randomly selected study participant samples were analysed between month 0 and 24 (lanes 2-5), along with 3 randomly selected *H. pylori* negative donor samples (lanes 6-8) to ascertain the integrity and quality of the RNA preparations which are used for comparison in these analyses *(Figure 13*).

As before, the RIN^e score for all the above was >9.0 indicating good quality RNA and there was no observable sample degradation over time, or within the comparator RNA samples.

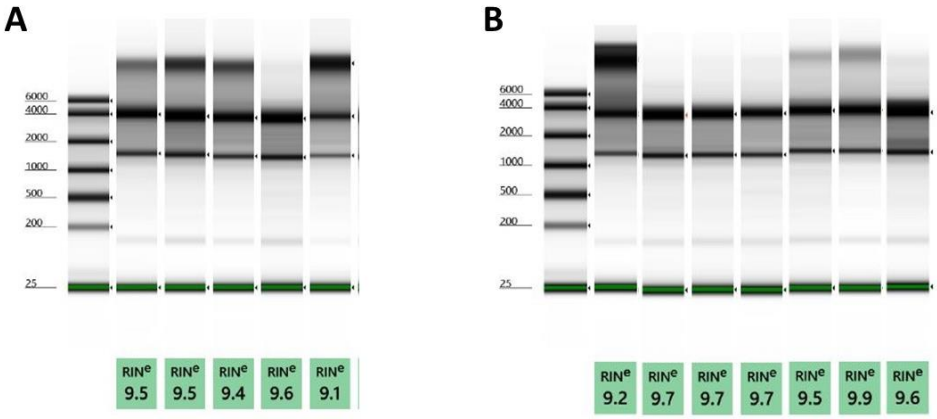

Figure 13 Quality control of RNA samples

PBMC RNA samples from a selection of patients in the cohort were analysed to qualitatively assess samples for RNA integrity. (A) Samples from a single patient (T035) for all 5 timepoints are in lanes 2-6; from left-right: M0, M2, M6, M12, M24. (B) Samples from 7 *H. pylori* negative donors were analysed to assess degradation in long term storage. RNA integrity scores (RIN^e) are given below the gel images. Scores >9.0 are considered of high quality and with negligible degradation.

2.4.5 – qPCR Assay Validation and Primer Efficiency Determination

In the first instance, the qPCR primers and probes were validated. Standard curves were produced for *GAPDH*, *IFNG*, *IL10* and *IL17A* (*Figure 14; A-F*) to determine the primer efficiency for each assay and the threshold value in which all subsequent quantification will be based. PCR reaction efficiencies ranged from the lowest of 1.85 (*IL17A*) to the highest at 2.04 (*IL10*). In qPCR, a perfect reaction will yield an exact doubling of PCR product during each cycle of PCR and would have an efficiency value of 2.0, ideal ranges are from 1.9 to 2.1, for multiplexed reactions 1.8-2.2 is acceptable. The lowest value of 1.85 here is still regarded as an appropriate range in which to proceed with the assays as the Pfaffl method [360] is used for quantification for which the mathematics accounts for differences in primer efficiencies. *Table 12* displays the efficiency, linearity, slope, and y-intercept of each qPCR assay.

Table 12 Efficiency and Linearity of the qPCR Assays

Target Gene	Efficiency (E)	Linearity (R^2)	Slope (M)	Intercept (B)
GAPDH	2.00	0.991	-3.33	19.47
IFNG	2.01	0.984	-3.30	21.85
IL4	1.93	0.950	-3.49	24.92
IL10	2.04	0.950	-3.40	28.18
**** GAPDH***	1.99	0.997	-3.34	18.36
**** IL17A***	1.85	0.985	-3.73	27.69

*Descriptive statistics for each qPCR assay used; determined from a standard curve using serially diluted cDNA. * Indicates assays were duplexed in the TaqMan reactions.*

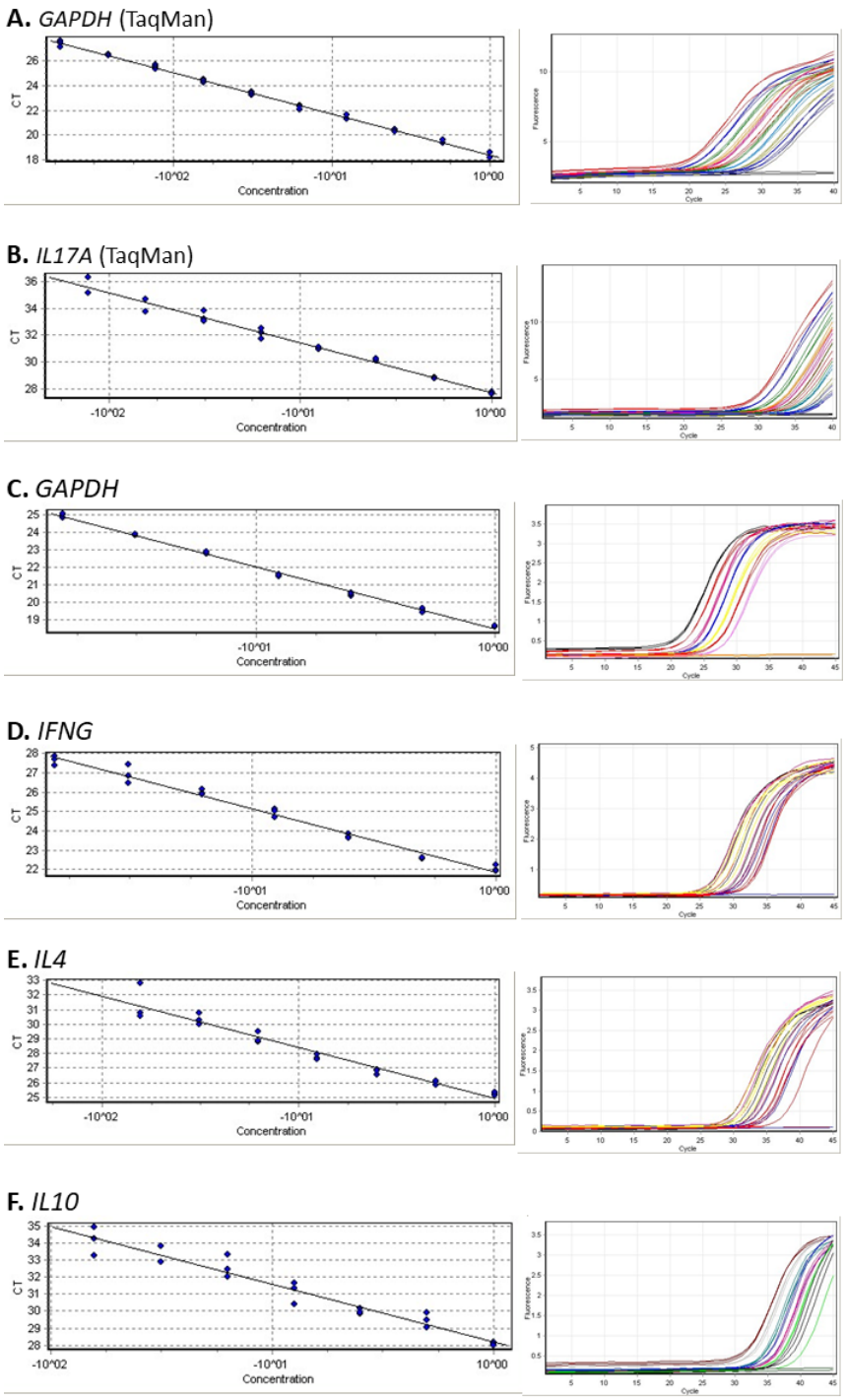

Figure 14 ***Dilution Series for the Calculation of PCR Efficiency and Linearity for each individual qPCR assay***

Each qPCR primer/probe assay was assessed for PCR efficiency, and linear range. Commercial total human reference cDNA was used as a standard and was analysed in a minimum of a 7-fold serial 1:2 dilution. Shown are the standard curves (left) and the raw amplification plots (right). Plots A and B use TaqMan probe-based assay, plots C-F use SYBR green chemistry. (A) *GAPDH*; (B) *IL17A*; (C) *GAPDH*; (D) *IFNG*; (E) *IL4*; (F) *IL10*. The efficiency (E), slope (m), and linearity (R^2) values are displayed in *Table 12.*

2.4.6 – Validation of Multiplexing qPCR Primers and Probes for the Duplex *GAPDH*/*IL17A* Assay

For the *IL17A* qPCR assay, a probe-based chemistry was used instead of the SYBR green-based chemistry used for the other gene targets. By using probe-based chemistry it is possible to include alternative reporter dyes on the probes allowing multiplexing of several gene targets within a single reaction. Before assays can be run as a multiplex, it was important to ascertain that the combination of primers and probes for multiple gene targets in a single reaction tube does not interfere or inhibit either qPCR assay. To determine the suitability to duplex the *IL17A* assay with the internal control *GAPDH* (housekeeping gene), reactions were run both as single probe assays and as a duplexed reaction and the change of Ct values (Ct; Threshold cycle, at which fluorescence raises above the baseline sufficiently to quantify) between the reactions was compared. A change of around 1 Ct is often expected when multiplexing probes, a change of 2 or more in Ct values would indicate that there is interference between the two primer-probe sets and would advise not to continue with the duplex setup. For all the reactions, a change of around 1 Ct was observed as expected and no differences greater than 2 were seen (*Figure 15; A & B*). As such the use of the duplex reaction was validated and this will be used for the *IL17A* analysis.

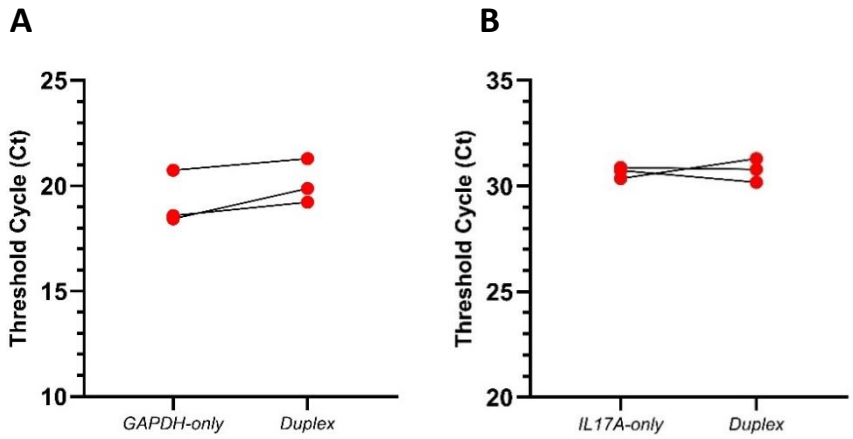

Figure 15 ***Comparison of single-target or duplexed TaqMan Assays***

To validate the suitability of duplexing primers and probes for *GAPDH* (A), and *IL17A* (B); 3 samples were tested using either single-plex or duplexed reaction conditions to assess any interference/inhibition that may have resulted from combining these assays in a single reaction.

2.4.7 – qPCR Product Validation

To verify that the amplicons produced during qPCR were of the expected size and there were no additional non-specific products amplified by the primers, an aliquot of the PCR reactions was taken from each gene target assay and run on agarose gels to visualise the nucleotide products present in the sample (*Figure 16*). The PCR reaction product was diluted 1:10 and a 5µl volume of this was run on a 3% *w/v* agarose TBE gel with 1x GelRed stain and electrophoresed at 120v until the dye had migrated 75% down the gel. The gel was imaged under UV light. No off-target products were seen indicating the assays are functioning as intended and specific to the intended target amplicons.

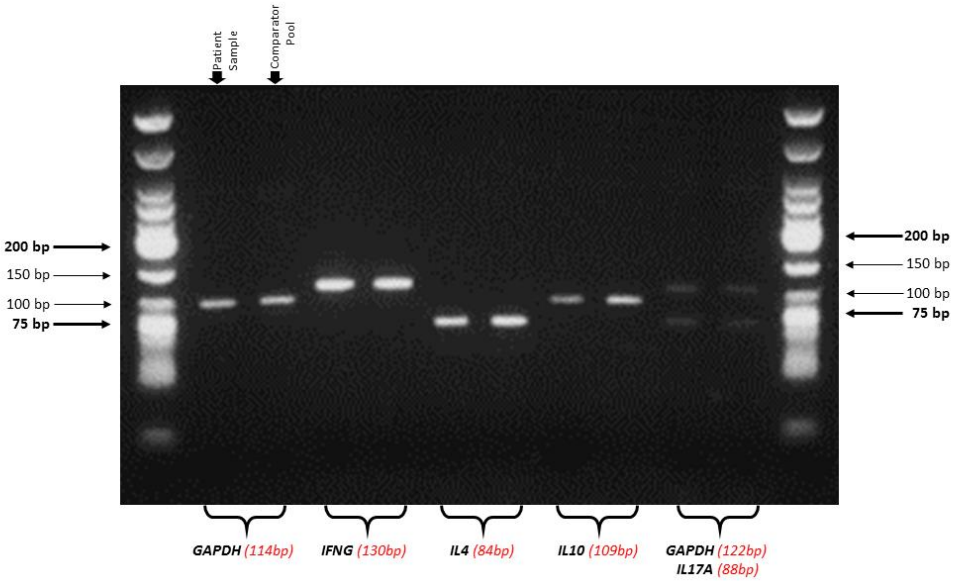

Figure 16 Agarose Gel Electrophoresis of qPCR Assay Amplicons

The PCR products from each assay were visualised on agarose gels to confirm only a single amplicon produced and of the correct size as the intended target. For this, PCR products were included from the comparator sample and a study sample to ensure no differences were apparent between the groups.

2.4.8 – qPCR Analysis of Cytokine mRNA Expression Levels in *H. pylori* negative comparator samples

Twelve *H. pylori* negative PBMC RNA samples were incorporated into a pooled standard comparator. To check whether there were any unusually high responses, the samples were assayed individually, using the pooled comparator as the reference. The median Ct from each of these should be equal to the value derived from the pool, giving an expression ratio of 1. Of the 12 samples, one (Sample 702)

was especially high in *IL10* mRNA and as such skewed the results for the pool (*Figure 17; A & B*). When this sample was removed, and the experiment repeated the median expression within the pool was 1 (as required). Sample 481 had a somewhat lower expression of *IL4* than the others and was also removed from the comparator pool (data not shown).

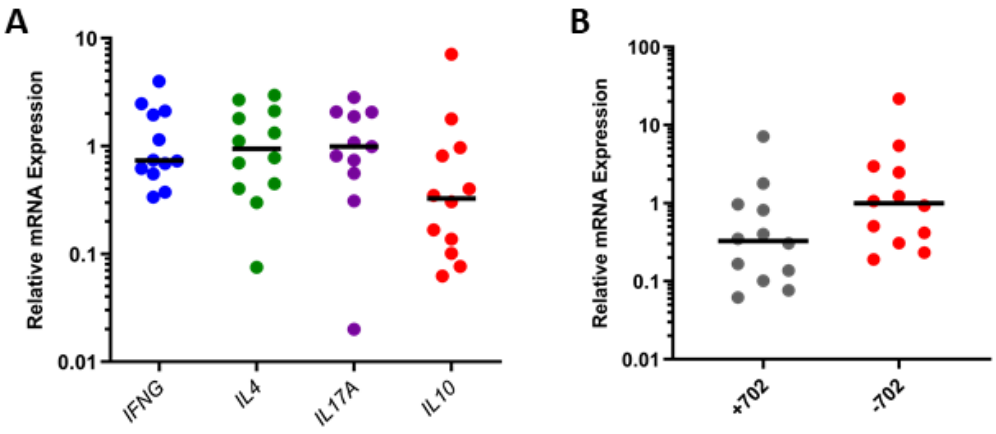

Figure 17 Relative mRNA expression in PBMCs from donors included in the H. pylori-negative comparator sample.

Expression ratios for individual *H. pylori*-negative samples are plotted normalised to *GAPDH* and relative to the pooled comparator sample. (A) mRNA expression ratio of *IFNG*, *IL4*, *IL17A*, and *IL10* in 12 uninfected donor PBMC samples. (B) The expression ratio of *IL10* after the removal of a high outlier from the comparator pool.

Similarly, as above, the *H. pylori* negative samples used in the comparator pool were assayed for expression of *IL17A* (this qPCR protocol was different to that of the other genes of interest due to difficulty detecting *IL17A* using a SYBR green based PCR, and as such performed separately). One of the 12 *H. pylori*-negative samples used previously was not available for use due to low RNA yield in the sample, as such the remaining 11 samples were tested. The distribution of the individual samples was wide indicating very variable expression of *IL17A* in all the *H. pylori*-negative patients.

To validate the qPCR assay for consistency and reliability, the same samples were assayed on three different occasions (on different days using different master mix each day) to determine run-to-run variability within the assays. Overall, the results were very consistent, and no substantial variability was observed (data not shown).

2.4.9 – PBMC Cytokine mRNA Expression in *H. pylori* Infected or Uninfected Patients

The relative expression of *IFNG*, *IL4*, *IL10* and *IL17A* in PBMC RNA was quantified and compared between 50 *H. pylori*-infected and 12 uninfected patients, using *GAPDH* as the housekeeping gene. No significant differences in *IFNG* or *IL4* PBMC mRNA expression were observed between the two groups. Interestingly, there was a significant reduction of 8.3-fold in the expression of *IL10* mRNA (*p=<0.0001*) and 2.6-fold of *IL17A* mRNA (*p=<0.03*) in the PBMC samples from *H. pylori*-infected patients compared to the pooled *H. pylori*-negative comparator (see *Figure 18*).

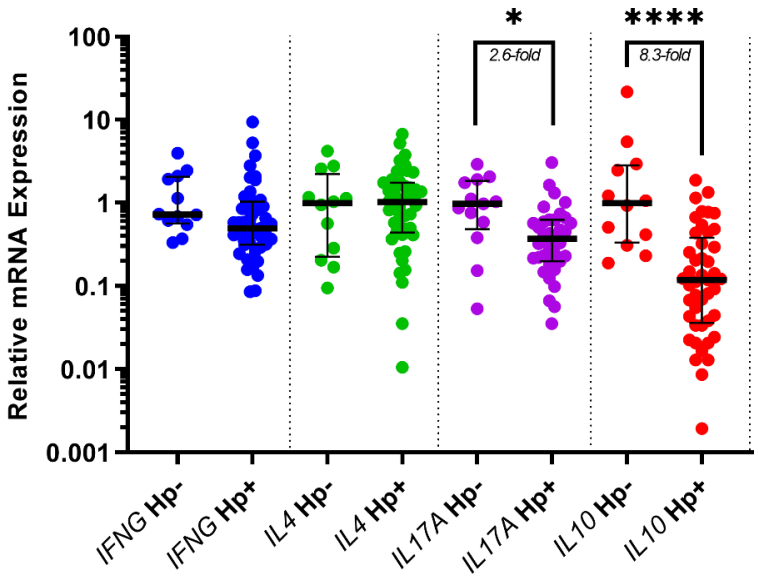

Figure 18 The relative expression ratio of Th1, Th2 Th17, and Treg signature cytokine mRNA in H. pylori infected or uninfected patient PBMC's.

The expression of the signature cytokines for the major T-helper cell lineages; *IFNG*, *IL4*, *IL17A*, and *IL10* from enrolled participants in the eradication study were quantified using RT-qPCR. The expression ratios in 50 *H. pylori* infected (Hp+) individuals are presented against the level from 12 uninfected (Hp-) donors. Data were normalised to the expression of the housekeeping gene *GAPDH* and expressed as a ratio relative to that of a pooled uninfected comparator sample. Lines represent the median; error bars denote the interquartile range. Kruskal-Wallace test with Dunn's correction; **p=0.03*; **** *p=<0.0001*.

2.4.10 – PBMC Cytokine mRNA Expression in Patients Who Failed or Responded to *H. pylori* Eradication Therapy.

Within the cohort, first-line eradication therapy failed in 6 out of the 50 patients enrolled in the eradication study at the 2-month post-treatment timepoint. There

were no biologically relevant differences in the expression of PBMC cytokine mRNA between these patients at month 2 and those who responded to the first regimen (*Figure 19*). There was a significant increase in *IL4* mRNA amongst those patients with successful eradication therapy (*p=0.006,* Mann-Whitney U-test).

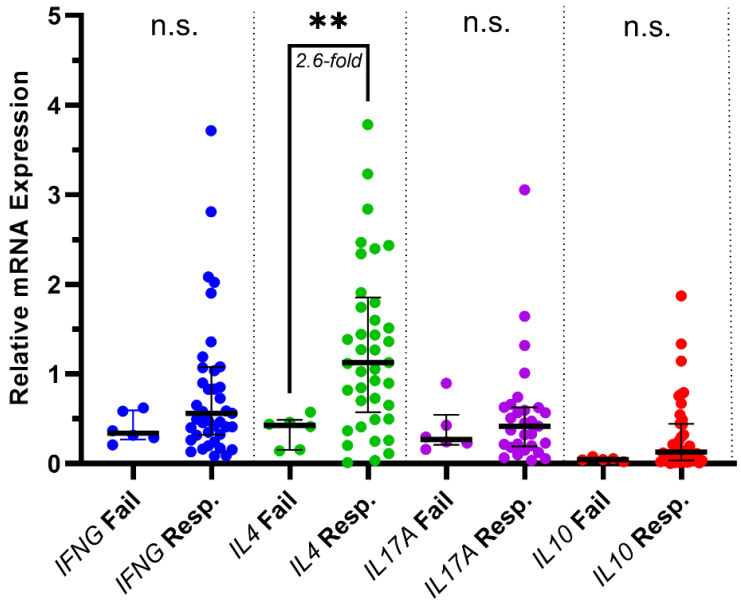

Figure 19 PBMC cytokine mRNA expression in patients whom either responded or failed eradication therapy

A small subset (12%) of the enrolled cohort did not successfully eradicate *H. pylori* in response to the first-line triple-therapy regimen prescribed. These patients required multiple rounds of treatment with alternate antibiotics to eradicate their infection. These patients were grouped as either responders (resp.) or failures (fail) to therapy and mRNA expression data was stratified according to these parameters to assess if antibiotic resistant colonising strains display differential expression of T-helper subset cytokines in peripheral blood. Mann-Whitney U-test; ** *p=0.006*).

In patients whom the first-line treatment was unsuccessful, PBMC cytokine mRNA was quantified by RT-qPCR and expressed relative to the expression of a stably expressed reference gene, *GAPDH* (*Figure 20; A-D*). No significant changes were observed from the baseline levels either during repeated antibiotic administrations or in subsequent samples collected up to 24 months post-eradication. There was a slight trend in *IL10* mRNA expression to fall after the first therapy attempt and recover over the subsequent months with no effect from repeated medication administrations. This difference was not statistically significant, and the trend recovered for the subsequent timepoints up to 24 months.

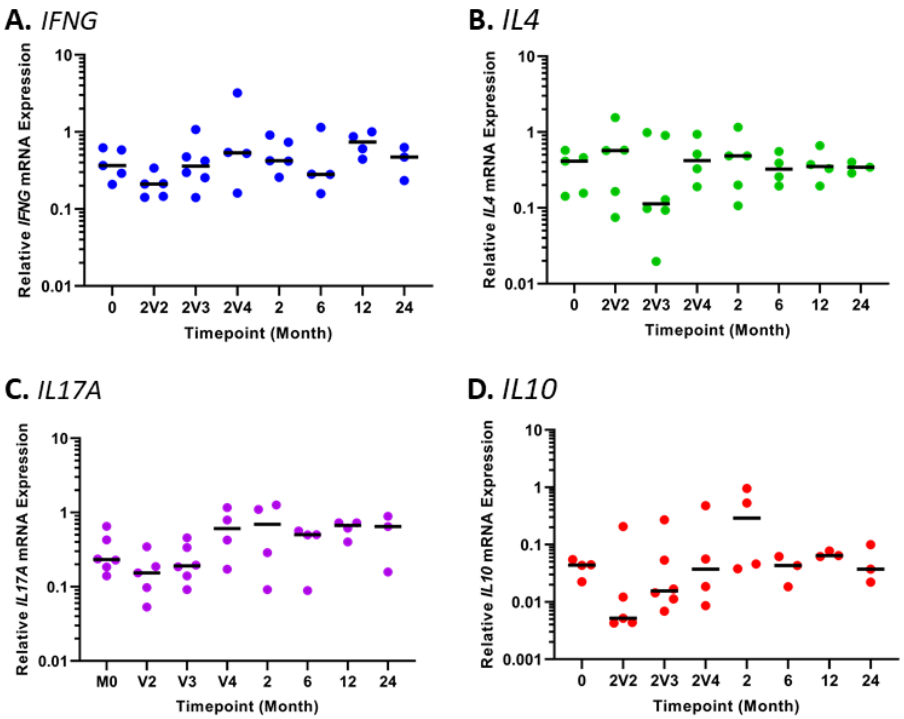

Figure 20 Human PBMC cytokine mRNA expression in patients who presented with antibiotic-resistant H. pylori infections.

The relative expression of PBMC cytokine mRNA in samples from 6 patients requiring multiple (between 2-5 different regimens) rounds of therapy to eradicate their infections, before and up to 24 months after successful eradication. Confirmation of eradication was made at month 2 post-treatment (M2), in the event of a positive ^{13}C-UBT, treatment was repeated, and the patient returned in a subsequent 2 months (2V2, 2V3 or 2V4). Plots show; (A) *IFNG;* (B) *IL4*; (C) *IL17A*; (D) *IL10.*

2.4.11 – PBMC Cytokine mRNA Expression in *H. pylori* Infected Patients through to 24 months post-Eradication of Infection

In the eradication study, there was a very high degree of variation between each individual's baseline expression of cytokines, which impeded the ability to see changes over time *(Figure 21; A-D*). The median expression levels at each timepoint were not markedly altered for *IFNG, IL4* and *IL17A* mRNA. There was no change in the median mRNA expression of *IL10* in the cohort from month 0 to month 12. At month 24 the mRNA expression of *IL10* had elevated 2.1-fold (*p=0.005*). Variation was high, from relative expression ratios of ~10 to <0.01.

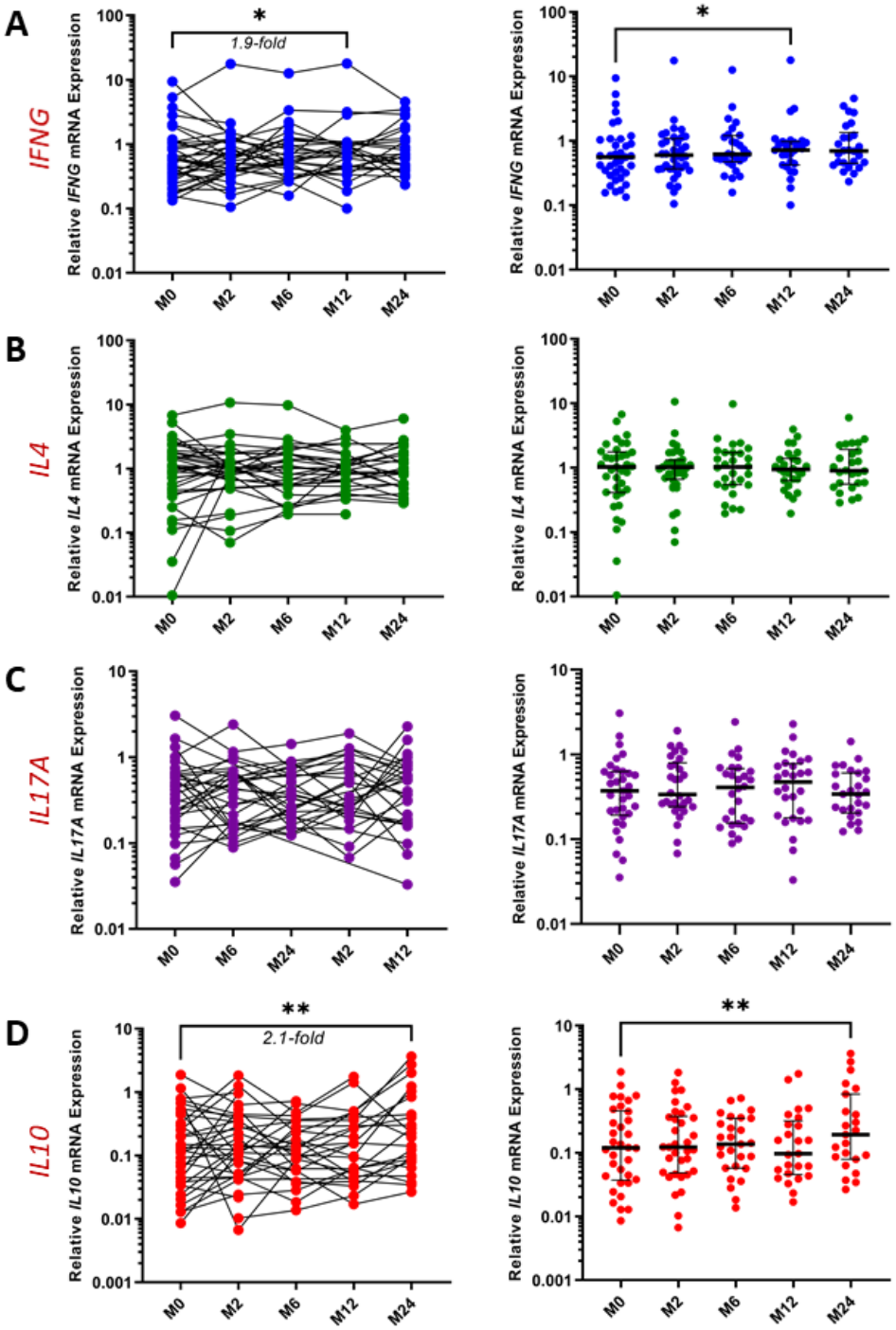

Figure 21 PBMC cytokine expression followed longitudinally in H. pylori-infected patients after a course of eradication therapy.

50 patients undergoing a course of *H. pylori* eradication therapy were recruited to the study. Blood was donated while still infected (month 0), after eradication (month 2), and on subsequent months 6, 12 and 24 after eradication. PBMC cytokine mRNA expression was quantified with RT-qPCR normalised to the housekeeping gene *GAPDH* and expressed relative to a pooled *H. pylori*-negative patient sample. Signature cytokines of the T-helper subsets; (A) Th1: *IFNG*; (B) Th2: *IL4*; (C) Th17: *IL17A*; and (D) Treg: *IL10*, were analysed. Wilcoxon matched-pairs test; *IFNG* M0-M12, * *p=0.04*; IL10 M0-M24, ** *p= 0.005.*

To better visualise differences in the expression levels, the data were analysed as a fold change from each patient's individual baseline level at month 0, prior to eradication of *H. pylori* (*Figure 22; A-D*). Observing the data in this manner, there appeared to be a notable increase in *IL10* mRNA expression at months 12 (2-fold; *p=0.0007*) and 24 (5-fold; *p=0.0003*) amongst the cohort. There were no major changes in the expression of *IFNG*, *IL4*, or *IL17A* throughout the 24-month period.

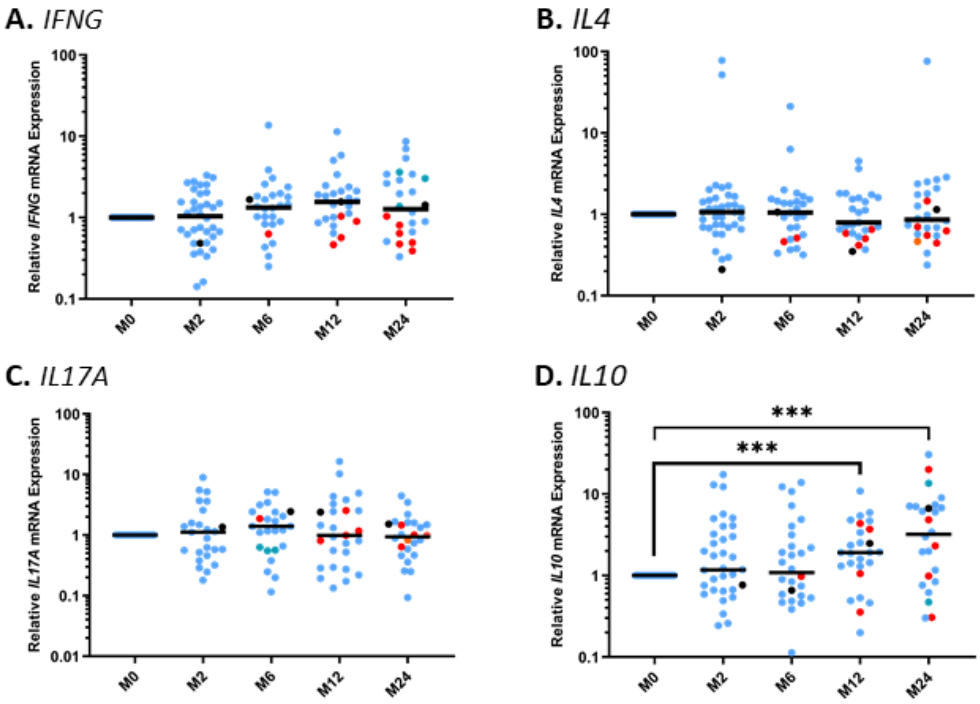

Figure 22 PBMC cytokine mRNA expression levels normalised to each individual baseline level in H. pylori-infected patients through 24 months post-eradication

To correct for high variation in the expression of cytokines within the cohort, each participant's expression level at month 0 (prior to *H. pylori* eradication) was used to normalise the subsequent results over time. (A) Th1 (*IFNG*); (B) Th2 (*IL4*); (C) Th17 (*IL17A*); and (D) Treg (*IL10*), The black-coloured point on each plot denotes patient T037 who was determined as having never been infected with *H. pylori*. The red points on each plot denote the patients who were attributed a serologically negative result for anti-*H. pylori* IgG ELISA by the timepoint. Lines denote the median; statistical analysis was performed using a Wilcoxon matched-pairs signed-rank test. M0-M12 *** *p=0.0007*; M0-M24 *** *p=0.0003.*

2.4.12 – PBMC Cytokine mRNA Expression Levels for a Single Patient Who Presented an inconclusive *H. pylori* Infection Diagnosis.

T037 is the single patient who appears to have presented with a positive *H. pylori* diagnosis by UBT at the start of the study but was negative for *H. pylori* serology (*Figure 23*). They also followed the trend of an increase of *IL10* mRNA from PBMCs at

month 24. No major changes were seen in the relative expression of *IFNG* or *IL4*, other than a drop at month 2 followed by a recovery.

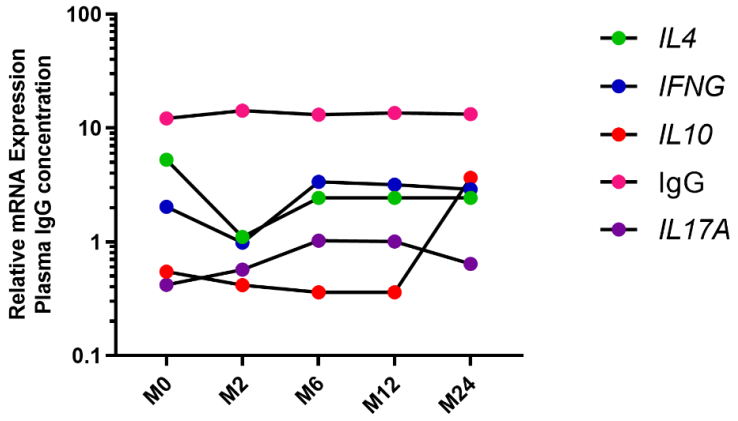

Figure 23 PBMC cytokine mRNA expression and plasma anti-H. pylori IgG concentration up to 24 moths post administration of triple therapy in a patient never infected with H. pylori

One patient (T037) presented with a positive UBT for *H. pylori* infection and was enrolled into this study yet was anti-*H. pylori* IgG seronegative. Plot shows the expression ratio of each cytokine in addition to IgG plasma levels up to 24 months post-eradication.

2.4.13 – CagA Virulence Type of the Infecting *H. pylori* Strains within the Cohort.

The virulence genotype of different *H. pylori* strains is known to have an impact on immune responses [106]. *cagA* positive *H. pylori* strains have been shown to induce an elevated regulatory T-cell response, which was correlated to a reduction in the concentrations of plasma IgE in human patients [219]. The presence of such a strain may therefore affect the response following eradication therapy. The *cagA* status of the colonising strains within the cohort was determined from the plasma samples collected at month 0 (infected), using a commercial anti-CagA IgG ELISA kit 38% (19 patients) of the samples were CagA- and 62% (31 patients) were CagA+.

CagA status of the patients in the cohort was used to stratify PBMC cytokine mRNA expression at month 0 of the study, but no significant differences were observed (*Figure 24; A-D*).

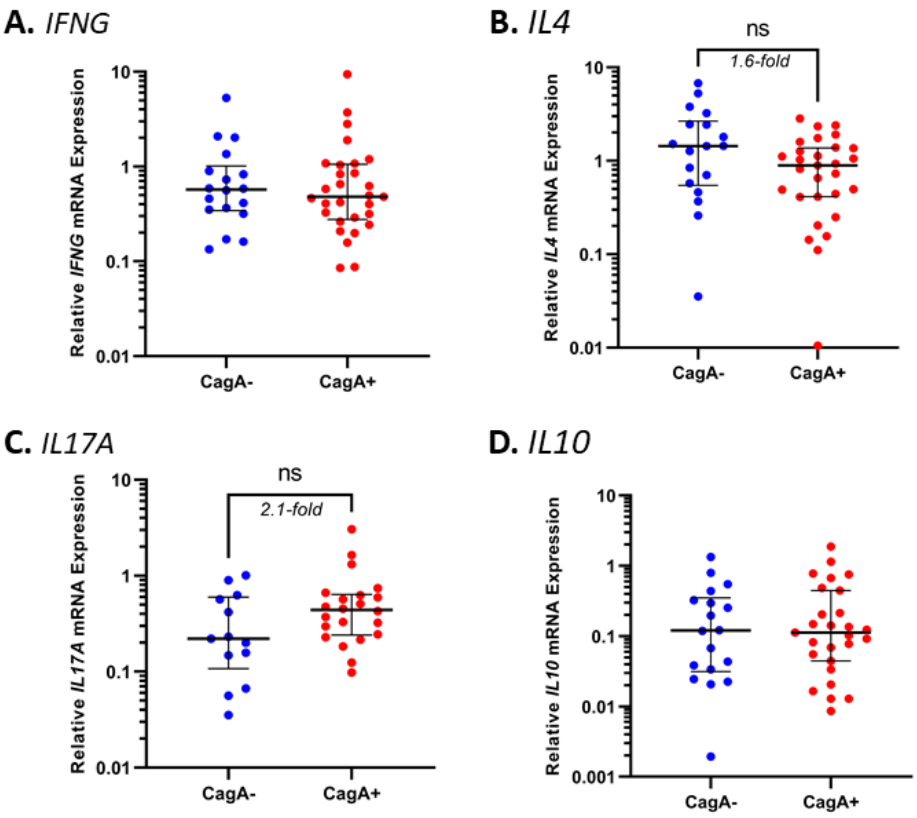

Figure 24 PBMC cytokine mRNA expression levels at Month 0, stratified by the CagA status of colonising H. pylori strains.

The expression ratios of T-helper cytokine mRNA in PBMCs from patients enrolled in the eradication study were stratified by the CagA status of the infecting *H. pylori* strains (as determined by ELISA). (A) Th1: *IFNG*; (B) Th2: *IL4*; (C) Th17: *IL17A*; and (D) Treg: *IL10*, Dots represent individual patients; lines show the group median expression; error bars denote the interquartile range. Mann-Whitney U-test.

CagA status was also used to group the patients' cytokine expression data throughout the whole study (*Figure 25; A-D*). No significant differences were observed.

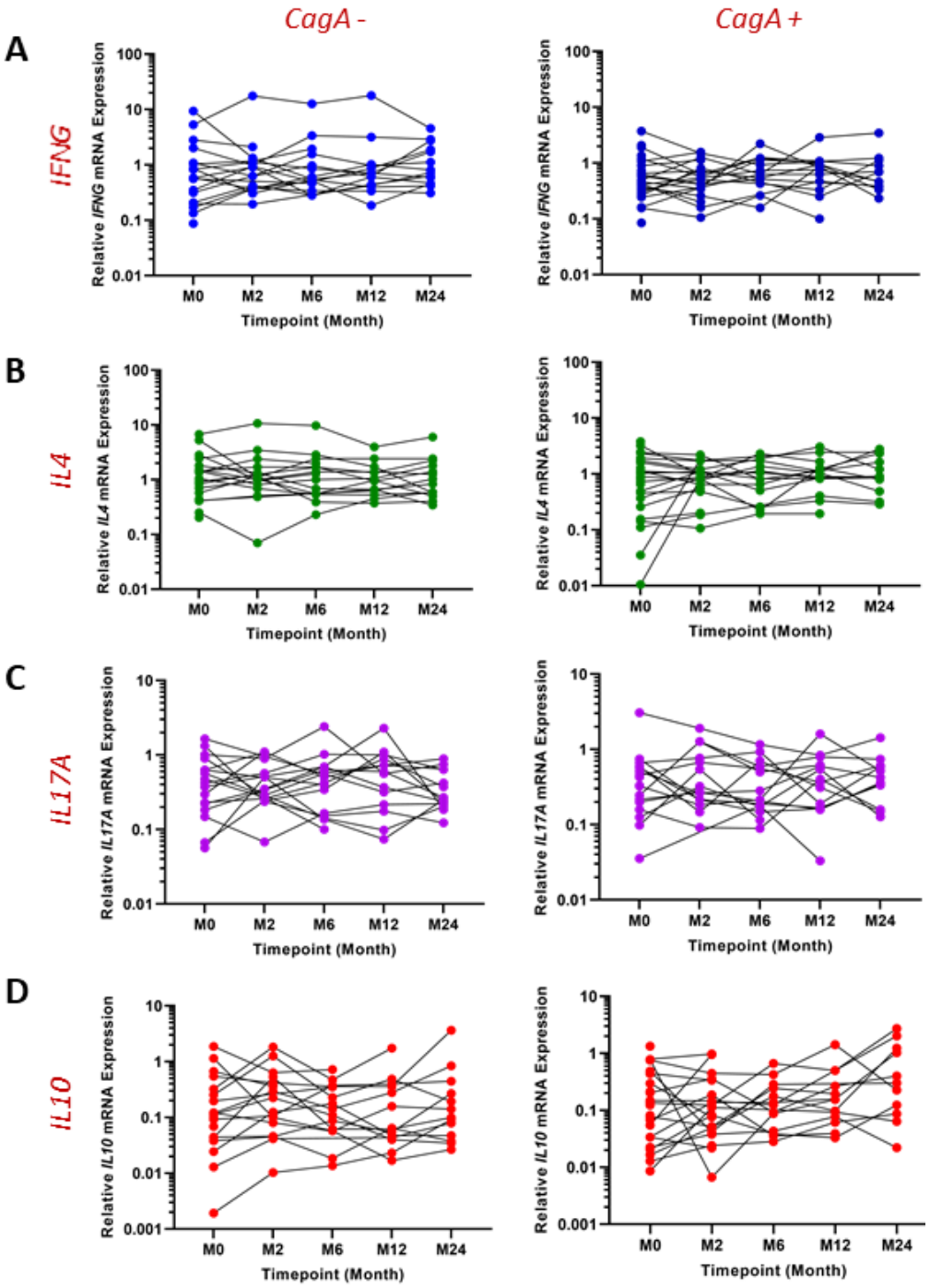

Figure 25 *Expression of PBMC cytokine mRNA through 24 months post-eradication of H. pylori infection stratified by the CagA status of the infecting strains.*

The expression of cytokine mRNA from PBMCs of the eradication study cohort at 5 timepoints over a 2-year follow-up period are plotted as CagA+ (left) and CagA- (right) groups, determined by ELISA. Expression ratios were normalised to *GAPDH* and relative to a pooled comparator sample from 11 *H. pylori* negative individuals PBMCs. (A) *IFNG*; (B) *IL4*; (C) *IL17A*; (D) *IL10*. Wilcoxon matched-pairs signed-rank test.

The CagA serological status of patients in the study had no observable impact on the levels of anti-*H. pylori* IgG in plasma at month 0, or throughout the longitudinal study.

PBMC cytokine mRNA expression levels were then stratified according to the presence, or absence, of peptic ulcer disease (PUD) at month 0. The expression of *IFNG*, *IL4* and *IL17A* were modestly elevated in PUD patients compared with those with no signs of gastric disease, however these differences did not reach statistical significance (*Figure 26; A-D*). There was no difference in the mRNA expression of *IL10* between those with or without peptic ulcer disease.

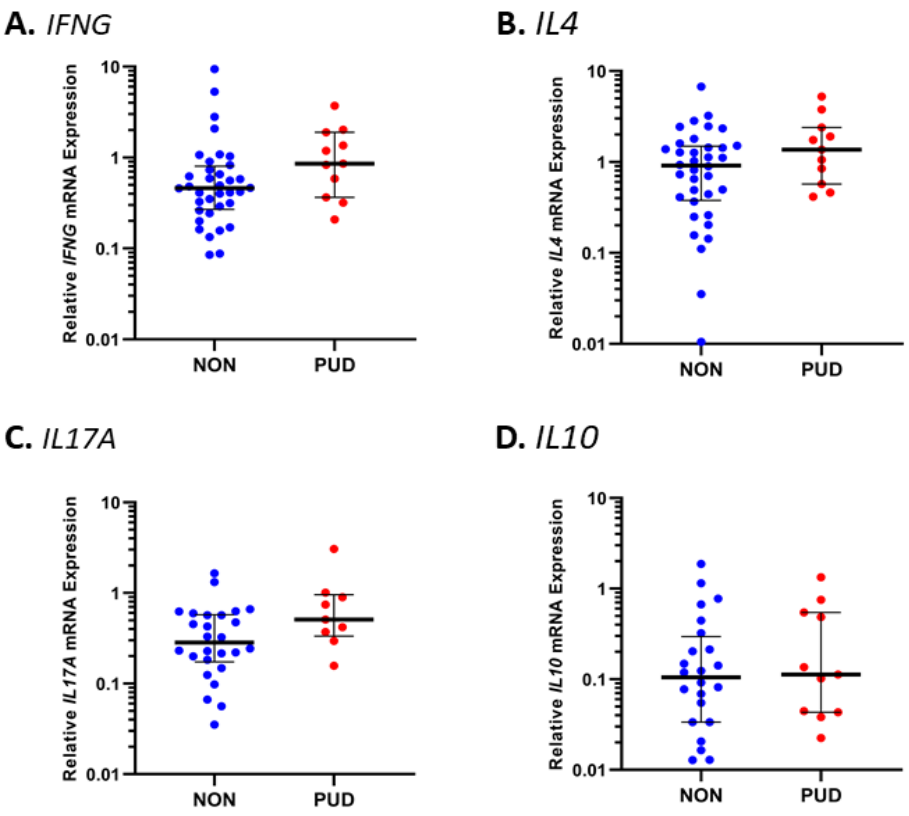

Figure 26 PBMC cytokine mRNA expression in patients infected with H. pylori (month 0)*, according to the presence or absence of peptic ulcer disease.*

PBMC cytokine expression data were stratified according to the presence or absence of clinically diagnosed peptic ulcer disease (PUD). (A) Th1: *IFNG*; (B) Th2: *IL4*; (C) Th17: *IL17A*; and (D) Treg: *IL10*, Dots represent individual patients; lines show the group median expression; error bars denote the interquartile range. Mann-Whitney U-test.

As smoking is a known risk factor for *H. pylori*-associated gastric disease, the smoking status (current, ex-smoker or non-smoker) of the participants in the eradication

study cohort was also used as a variable to stratify PBMCs cytokine mRNA expression. The expression of *IFNG* was halved (*p=0.02*) in current smokers compared to non- or ex- smokers at month 0 (*Figure 27; A-C*). Within the smoking group, this expression level rose (2.6-fold) after eradication of *H. pylori* to a level comparable of that of the non- and ex- smokers. No other significant differences were observed (data not shown).

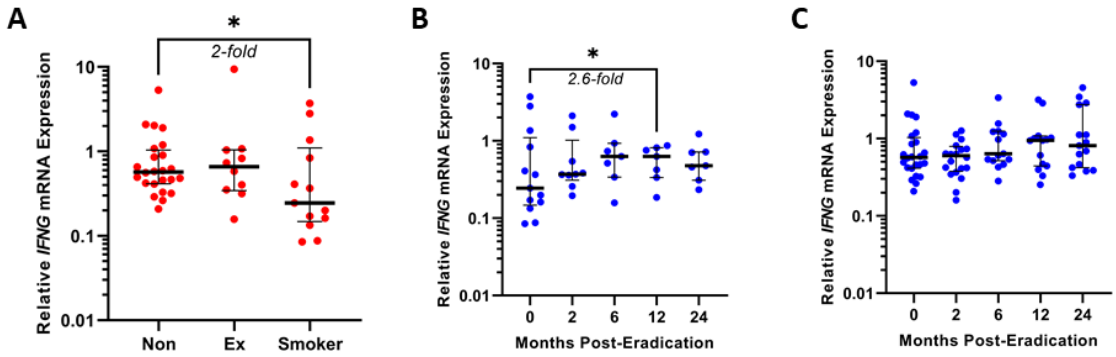

Figure 27 The effect of smoking status on the expression of IFNG mRNA in PBMCs through 24 months post-eradication of H. pylori infection

Cytokine mRNA expression is relative to a *H. pylori* negative pooled PBMC RNA sample, normalised to *GAPDH.* Dots represent individual patients. Lines represent the group median, with error bars denoting the interquartile range. **p=<0.05.*

Expression of the PBMC cytokines in the cohort was stratified according to gender with no differences between males and females (data not shown). Those individuals with history of allergy or atopy were analysed in a similar manner and found no differences in the expression of any cytokine in those with atopic history and those without (data not shown). There was also no difference found correlated to the level of inflammation in the gastric mucosa (data not shown).

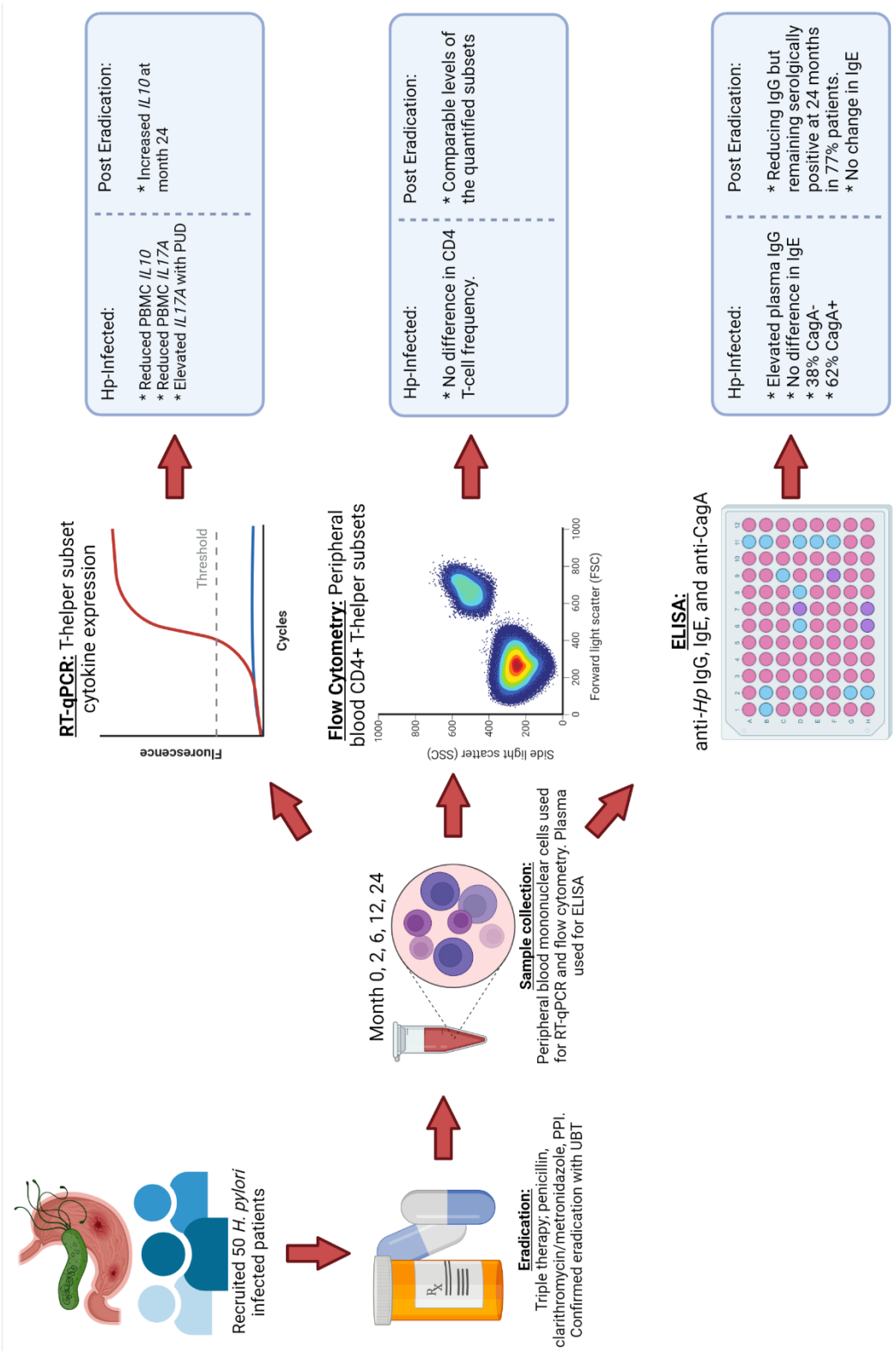

Figure 28 Schematic representation of the eradication study and summary of the data generated

H. pylori infected individuals presented with markedly reduced *IL17A* and *IL10* mRNA expression in peripheral blood mononuclear cells as compared to uninfected donors. In those infected, *IL17A* mRNA was modestly elevated where there was evidence of peptic ulcer disease. The expression of *IL10* was observed to rise notably over 24 months post eradication of *H. pylori*, concurrently with reducing plasma concentration of anti-*H. pylori* IgG. Figure created with BioRender.

2.5 – Discussion

A graphical summary of the study and data generated are given in *Figure 28*.

2.5.1 – Quantification of cytokine concentration in human plasma from *H. pylori*-infected individuals and their relationship to gastroduodenal disease

Summation of the Major Findings

- Plasma concentration of IL-17A was elevated in *H. pylori* infected as compared to uninfected individuals. Conversely, plasma IL-12p70 concentration was reduced in infected individuals.

- Plasma IL-17A concentration was further elevated with higher Sydney scores in the gastric corpus.

- IL-10 plasma concentration was modestly elevated in infected patients with higher mononuclear cell inflammation in the gastric corpus, however, was not significantly different between infected and uninfected groups.

The purpose of this investigation was to attempt to identify potential candidate biomarkers in peripheral blood with a prognostic value for discerning an individuals' risk of developing a *H. pylori*-associated gastric disease.

The plasma concentration of IL-17A was increased in *H. pylori*-infected as compared to uninfected individuals. The fold difference was modest, however and IL-17A is unlikely to be useful as a disease biomarker. To examine these data further the *H. pylori* infected group was stratified into subgroups based on the extent of gastroduodenal pathology present. There were no differences in plasma cytokine concentrations based on these stratifications with 2 exceptions. The plasma IL-10 concentration was modestly increased in infected patients presenting with a higher inflammation score in the gastric corpus. This was not recapitulated according to the

inflammation score of the gastric antrum. Our major finding was that of IL-17A. Plasma concentrations of IL-17A were increased modestly yet statistically significantly not just according to *H. pylori* infection status, but also higher inflammation and neutrophil infiltration in the gastric corpus. The finding of increased plasma IL-17A is unsurprising as the Th17 cellular response is reported in the literature to be increased in response to *H. pylori* infection [164,186]. The elevation of IL-17A in the gastric mucosa and in peripheral blood in response to *H. pylori* infection is a notable contributor to gastric pathogenesis and development of peptic ulcer disease and gastric cancer [362] and this study demonstrates that IL-17A, is also increased in the peripheral circulation of our cohort.

Reviewing the available literature, others also find increased IL-17A in those infected with *H. pylori* [176-178,186]. Arachchi *et al.* measured serum cytokine concentrations and reported both IL-17 and the Th17-associated IL-23 as being elevated significantly in *H. pylori* infected individuals. Furthermore, IL-17A, but not IL-23, concentration was greater in those with more severe gastritis [176]. Bagheri *et al.* reported Th17 cells and IL-17 also increased in infected patients, rising further in cases of peptic ulcer disease and in parallel to increased IL-8 [178]. This agrees with the findings from the current study which also demonstrate increased levels of IL-17 consequential of infection status, as well as higher Sydney scores for gastric mucosal neutrophilic and mononuclear cell infiltration in the corpus.

However, Serelli-Lee *et al.* investigated cytokine production in patients infected, uninfected, or with a previous infection with *H. pylori* [186]. Here, those with current infection had elevated IL-17 production from stimulated PBMCs than those naïve for *H. pylori*. However, these elevations were maintained in those with past-history of infection over *H. pylori*-naïve individuals. As these levels were apparently maintained in the absence of on-going infection it is unlikely, at least not on its own, to form a clinically useful test to diagnose future disease risk.

In contrast, plasma IL-12p70 was lower in *H. pylori*-infected patients to those uninfected. IL-12p70 is a heterodimer consisting of p40 and p35 subunits, produced primarily by monocyte/macrophages and dendritic cell subsets, with a major functionality of augmenting IFNγ-secreting Th1 cellular responses [363,364]. It is known

that *H. pylori* can induce tolerogenic dendritic cells, with an immature activation state resulting in attenuated inflammatory cytokine secretion and inefficient effector T-cell activation [21,24]. A shift in dendritic cell-derived IL-12 in favour of IL-18 is a mechanism proposed by Oertli *et al.* to facilitate Treg induction and subsequent atopic protection [21,24].

IL-12p40 was also quantified in our samples and was not found to be different between groups. Given the disparity between the levels of the IL-12-p70 heterodimer and p40 monomer quantified here, there may be wider effects on the related IL-12-family cytokines. Of course, IL-12p70 shares a subunit with the Th17-associated IL-23 [365]. Interleukin-23 is a heterodimer consisting of p40 and p19 subunits [366], a main function is supporting Th17 expansion conversely to IL-12p70 predominant effect supporting Th1 cells and IFNγ [367]. Interestingly, evidence from the literature suggests that p40 subunit deficiency in mice results in a resistance to the development of EAE [368,369]. Conversely, others report that deficiency of p35 subunit confers a susceptibility [370]. Cua *et al.* employed p19/p35/p40 knockout mouse models to investigate the contribution of these subunits to inflammation in the brain [371]. The authors propose that the p19 subunit is essential for the propagation of EAE, and thus IL-23 and not IL-12 is the most influential cytokine in this context. However, given that IL-12p70 was reduced in *H. pylori* infected individuals but not IL-12-p40, it would be logical to consider that p35 was lesser in our data (although not individually quantified). If so, this should have conferred a susceptibility not a protection from MS in those individuals, contrary to the hypothesis. Nonetheless, the changes in these subunits may indicate alterations to the ratios of IL-12 or IL-23; Th1/Th17 cells; or indeed other IL-12 family members. This remains to be seen and quantification of the other subunits; p40, p35, and p19 may be interesting to investigate in future work.

H. pylori infection is usually associated with antral-predominant colonisation in humans [57]. As has been described previously, pan-gastritis is often associated with a more severe gastric pathogenesis and predisposes to a greater incidence of ulceration and malignancy [57]. Given that pan-gastritis is a risk factor for the development of disease it is perhaps an important finding that this presentation

would appear to result in measurable differences in plasma IL-17A and IL12p70 concentrations where evidence of pan-gastritis was present. Taken together, these data suggest that these cytokines may be potential candidates on which to focus further investigation, however it must be stated that all the differences we observed in this study were modest and a clinical relevance of these findings is unlikely.

2.5.2 - Human anti-*H. pylori* IgG humoral immune response in patients for 24 months post triple-therapy mediated eradication of infections.

Summation of the major findings

- The plasma anti-*H. pylori* IgG response was reduced after confirmed eradication of the bacterium.

- Plasma IgG levels were unchanged in those individuals for whom the first-line treatment failed but were subsequently reduced after a successful eradication regimen.

- 77% of infected patients still had a seropositive plasma IgG response to *H. pylori* through 24 months post-eradication.

The plasma IgG ELISA data shows that within the cohort, the levels of anti-*H. pylori* IgG were decreased significantly over the 24-month period post eradication. However, most patients still presented with levels of anti-*H. pylori* IgG at the 24-month study endpoint which would be classified as serologically positive. No changes were observed in plasma IgG levels in the patients for whom the prescribed treatment failed to eradicate their infections in the first instance, and/or for subsequent eradication attempts. One exception to this was patient T005, here despite requiring multiple eradication attempts before providing a negative urea breath test the anti-*H. pylori* IgG levels dropped comparatively to the successfully treated participants. This may be a result of marked reductions in colonisation after treatment but falling short of total eradication, or indeed an eradication followed by

reinfection which cannot be discounted as no further confirmation of infection status was performed after the month 2 UBT. For the failed treatment group, upon a successful eradication (irrespective of the required number of attempts), IgG levels subsequently fell in a comparable manner to that observed in the initially successful treatment group.

This agrees with other published work in the literature. A study by Vonkeman *et al.* [372] investigated the anti-*H. pylori* IgG titres at baseline (infected) and then at 3 months and 12 months post-eradication therapy, as compared to a control group given placebo in place of triple therapy. Here, a median reduction of 55% was observed at 3 months in the treated group as compared to a median reduction of only 0.9% in the placebo group. At 12 months post eradication, a median 77% reduction in antibody levels were observed in the treated group compared to a median 22% reduction in the placebo treated group [372]. However, despite reductions in the median levels consistent with eradication of infection, within the cohort, 36% of the patients in the treated group reached serologically negative levels by the 12-month study endpoint compared with 10% in the placebo group. This is largely consistent with our own data, within our cohort we observed a 13% decrease in the plasma antibody levels at month 2, 33% at month 6, 56% at months 12, and 68% decrease at month 24. However only 8% of patients (2/24) were serologically negative at 6 months post eradication, 20% (5/24) at 12 months, and 25% (6/24) serologically negative at the study endpoint 24 months.

Interestingly, one patient (T037) was serologically negative for *H. pylori* from the start. The UBT is the gold standard method for *H. pylori* testing with over 93% accuracy, compared with only 80% for *H. pylori* serology, as reviewed by Best, *et al.* [373], thus our UBT result should be taken with more confidence than ELISA data. These statistics would lead to an expected false-positive figure of 3-4 patients in a cohort of 50 such as ours. Low colonisation densities can result from a stronger inflammatory immune response and low luminal pH, therefore predisposing to gastric diseases [11,57]. If there had been opportunity it would have been beneficial to confirm infection status in this patient by other methods such as a biopsy-based

culture or PCR method. Indeed, it is advisable to confirm infection status through more than one clinical test.

Taken together, the humoral immune response against *H. pylori* is indeed attenuated after antibiotic-mediated eradication as evidenced by a significant and consistent reduction of plasma antibody concentration in a temporal manner after treatment. Others report that IgG levels persist long term in a marked proportion of successfully eradicated patients [372,374]. Importantly, these data agree and suggest that the antibody response, at least the IgG response to *H. pylori* infection largely persists beyond 24 months. It would therefore be beneficial to perform longitudinal studies over a greater number of years than the 2 years follow-up in this study.

2.5.3 – Treatment failure and Antibiotic Resistance within the cohort

Summation of the major findings

- Eradication of *H. pylori* using the first-line regimen of triple-therapy was effective in 88% of patients within our cohort.

- 12% of patients were colonised with *H. pylori* strains with an inherent resistance to first-line antibiotics as seen by the failure to eradicate the infection in the first instance.

A growing global concern in the current literature is that of antibiotic resistance. Recent evidence would suggest that the rate of *H. pylori* resistance to clarithromycin or metronidazole within the European region is 18% and 32% respectively, however with little or no resistance to amoxicillin (1%) [375]. Within our cohort 12% of patients treated with amoxicillin and (either) clarithromycin or metronidazole in combination required multiple eradication attempts before a negative UBT was provided. When considering an estimated resistance to amoxicillin in Europe of 0-1% this is concerning. One patient (T048) required 5 eradication attempts. This is a concern not just for the field of *H. pylori* medicine but in a much wider context also. Indeed,

targeted antibiotic delivery and personalised precision regimens would be an essential step forward in this field of medicine.

It was hypothesised that the response to eradication therapy may be influenced not just by resistance of the colonising strain, but also by the host immune response. Indeed, we have discussed that *H. pylori* can suppress host immunity to enable persistent infections; those individuals with a more robust response result in lower colonisation densities, but the inflammation predisposes to increased pathogenesis [45]. However, in these cases lower initial colonisation densities may result in better efficacy of antimicrobials to eradicate the infection. In this regard, published literature supports this premise reporting increasing effectiveness of triple therapy in parallel to decreasing initial densities [376]. When patients in our cohort were grouped into eradication failures or responders (as determined by their successful eradication in the first instance, or the requirement for multiple rounds of therapy to eradicate their infection) there was no observable difference in the levels of the Th1, Th17 or Treg signature cytokines (*IFNG*, *IL10*, or *IL17A*) at the mRNA level. However, a trend was seen for the responders to have an elevated expression of *IL4* mRNA in peripheral blood. It would be expected that an increased Th2 response would result in a decrease to the Th1/Th2 ratio possibly increasing colonisation densities via ineffective clearance of infection by protective Th1-mediated immunity. This in turn may therefore predispose to higher rates of eradication failure, but this was not apparent from these data. Furthermore, there was no evidence that plasma IgG concentration was different in these patients as may be hypothesised if B-cell antibody secretion against *H. pylori* is augmented by elevated IL-4.

The variation in the basal expression levels of cytokines, and indeed the very small (6/50 patients, 12% of the total cohort) proportion of patients for which multiple attempts of eradication were required mean that this group size is not large enough for which to infer robust conclusions. A larger cohort of patients would be required to determine if this trend were recapitulated to an extent such as to suggest a biological relevance.

2.5.4 – T-helper cell cytokine mRNA expression in *H. pylori*-positive patients over a course of triple therapy-mediated eradication.

Summation of the major findings

- A notable reduction in the expression of PBMC-derived *IL10* and *Il17A* mRNA in *H. pylori* infected as compared to uninfected individuals was observed.

- Following patients' post-eradication, I observed no biologically relevant change in the levels of *IFNG, IL4 or IL17A mRNA in PBMC's* from the baseline through 24 months post-treatment.

- A trend for increased *IL10* mRNA transcripts at month 12 and 24 post-treatment was observed, as compared to baseline levels pre-treatment. With only 29 of 50 of the enrolled cohort completing the study this trend may not have been present with larger group sizes at later timepoints.

The current study enrolled 50 *H. pylori* positive individuals for the purpose of investigating how peripheral blood immune responses change after eradication of *H. pylori*. The literature would suggest that eradication results in reduced inflammatory cellular immune responses, and the healing and prevention of recurrence for peptic ulcer disease [60,377-379], gastric atrophy [61], and gastric cancer [60]. Considering the hypothesis that *H. pylori*-mediated regulatory immune response can confer a benefit to sufferers of extra-gastric immunological disease [91-94,334] it is of pertinence to know if eradication could remove the source of that protection. The peripheral expression of *IL10* and *IL17A* mRNA (signature cytokines for the Treg and Th17 T-helper cell subsets respectively) were found to be significantly decreased from *H. pylori*-infected as compared to uninfected patient PBMCs. These data are a notable deviation from the hypothesis and in disagreement the human plasma cytokine study presented in this chapter where IL-17A was the major effector cytokine to be changed in response to infection and disease. Others however do report reduced IL-17A in serum from infected individuals [380]. A possible cause for reduced IL-17A would be suppression of Th17 responses by Tregs or IL-10, however IL-10 was reduced to an even greater

extent. The balance of inflammatory to anti-inflammatory responses can influence the development of gastric disease [166]. The data from this study do not fit this paradigm, as we observe lower *IL10* and *IL17A* concurrently, and with no change in *IFNG* in infected patients. The human plasma cytokine data suggested IL-17A is increased in blood in cases of more severe disease, the lower levels observed in relation to uninfected people here would suggest the risk of disease is low. On the other hand, if we consider these data together, we observed greater reductions of IL10 than we did of IL17A in the infected patients, so perhaps tipping the balance towards inflammation in *H. pylori*-infected individuals.

Interleukin-10 (IL-10) is a signature anti-inflammatory cytokine expressed by Tregs, but also expressed by a plethora of other cellular lineages. *H. pylori*-negative patients in this analysis were selected from samples in the locally held in-house biobank, based on a similar age range (18-70) and sex ratio (48%:52%) as the study samples. As it would appear, by random misfortune these samples may not be the best representation of *H. pylori*-negative patients in general. Lower *IL10* mRNA production while infected, and subsequent elevation after eradication was unexpected. We hypothesised that *IL10* should be increased in *H. pylori*-infected patients as shown previously [20,219], and may decrease accordingly over time upon removal of the Treg-inducing bacterium. However, data from this cohort would not support either of these hypotheses.

There were no differences observed between infected or uninfected patients with regards to the peripheral expression levels of either the Th1 or Th2 cell signature cytokines *IFNG* and *IL4,* respectively. Nor was there any observable change in either cytokine mRNA up to 24 months post-eradication.

A previous qPCR analyses of human PBMC *IL10* expression was presented White, 2016 [361]. Here, samples were obtained from a cohort of patients attending routine endoscopy at the gastroenterology clinic of the Queens Medical Centre Nottingham, but distinct from the eradication study cohort (26 *H. pylori* negative; 91 *H. pylori* positive). *H. pylori* infection status was determined for these patients by ^{13}C-UBT and a biopsy-based rapid urease test. This work found that *IL10* mRNA expression was elevated in infected patients.

Previously published work by this research group, Hussain *et al.* 2016 [219] found a significant increase in *IL10* mRNA expression in freshly isolated PBMCs by qPCR in infected as compared to uninfected individuals. These data also find significant increases in the number of $CD4^{+}CD25^{hi}IL\text{-}10^{+}$ cells in infected c.f. uninfected individuals when analysing stimulated cells by flow cytometry.

Experimental work presented by Reddiar, 2016 [381], using flow cytometry to quantify CD4+IL-10+ and CD19+IL-10+ cells in stimulated PBMC's is an interesting comparison. These data are more consistent with the results presented here and show IL-10-producing $CD4^{+}$ cells were found to be higher in the *H. pylori*-negative patients, although by non-significant small differences. Furthermore, the lower number in *H. pylori* infected individuals was elevated after eradication therapy to a level comparable with the never-infected group. This finding contrasted with the frequency of Tregs (defined as $CD4^{+}CD25^{hi}$ cells) quantified by flow cytometry, which was elevated in infected as compared to uninfected individuals, and conversely reduced in successfully eradicated patients. No differences were seen in the proportion of $CD4^{+}CD25^{hi}$IL10+ Tregs between groups.

The disparity between $CD4^{+}CD25^{hi}$+ Tregs and IL-10-producing $CD4^{+}$ cells may be skewed by the reliance on CD25 as the characteristic marker for Tregs, as although expressed constitutively by Tregs CD25 is also unregulated and expressed transiently in activated effector T-cells, this distinction cannot be made in this study which may confound that data. These observations together would suggest that non-Treg $CD4^{+}$ lymphocytes expressing IL-10 are a confounding factor in this dataset. Foremost in the interpretation of the mRNA expression data as here we use *IL10* mRNA as a signature for Tregs, which may not appear to be an accurate measure, especially given the broad range of alternative cells which secrete this cytokine.

A logical summation of this would theorise that infection with *H. pylori* may augment IL-10+ expression in other $CD4^{+}$ T-helper lineages aside from the canonical Tregs. No work has been done to characterise this within this cohort and so only hypothetical scenarios can be proposed to explain this. There are indeed the $CD4^{+}CD25^{+/-}$FoxP3-IL-10-producing Tr1 lineages, or indeed trans-differentiated ex-effector $CD4^{+}$ cells such as $CD4^{+}RORγT^{+}IL\text{-}10^{+}$ or $CD4^{+}Tbet^{+}IL\text{-}10^{+}$ ex-Th1/17 cells. Indeed, IL-10 secretion

by effector T lineages are described in the literature most commonly as a mechanism of self-regulation and because of the resolution of inflammation [181]. Another rich source of IL-10 is from regulatory B-cells which were not quantified in these analyses, and indeed monocytes, macrophages, and dendritic cells also secrete IL-10, in addition to expressing CD4 [364,382-384].

It is important to also consider that the differences between infected, eradicated, and naive individuals seen in the analyses by Reddiar were derived from larger cohorts. The smaller group sizes in the current study may be insufficiently powered to observe differential IL-10 activity, as only 29 of 50 enrolled patients were still participating in the study by month 24. However, if this was the case one may expect to observe modest trends either way, which were apparent.

It is also notable that the variation observed within groups was substantial, with *IL10* mRNA expression ratios spanning several orders of magnitude, ranging from 0.001 to 100 as compared to the median of the comparator sample. This level of variation is unavoidable in human studies as per our diverse biologies and environments, however the variation will work to obscure trends, especially if these trends are small.

The qPCR data presented in the current study finds no changes in the expression of *IFNG* mRNA between infected and uninfected groups. The previous work of Hussain *et al.* also finds no difference in the frequency of $CD4^{+}IFN\gamma^{+}$ cells between groups by flow cytometry, however infected patients had a significantly elevated concentration of IFNγ in plasma when quantified by ELISA.

This study was powered on previous mRNA quantification from our research group which demonstrated differences in *IL10* mRNA transcript between infected and uninfected groups [361]. It was calculated that 42 patients should be sufficient a number to detect statistically relevant changes in expression. This power calculation factored in a 15% drop-out rate. In the current study of 50 individuals recruited, only 29 patients (58%) remained in the study to 24 months, as such the cohort may be too small to draw robust conclusions.

Although some modest statistical significances were reported, the variation in the groups and the very small changes in the expression levels would not assume a biological or at least a clinical relevance to these findings. However, when the expression data was normalised to individuals' baseline and the deviation over time quantified the trend for increased IL-10 was potentiated to a significant 2-fold increase at month 12 and 5-fold increase at month 24. This may be a direct result of antibiotic administration changing the composition of the microbiota; I do not have a control for such an occurrence in this study.

2.5.5 – CagA virulence genotyping of the infecting *H. pylori* strains within the eradication study patient cohort

Summation of the major findings

- The cohort was analysed for CagA seropositivity. 38% of patients harboured CagA- strains and 62% had CagA IgG. The data showed that CagA seropositivity affected peripheral blood T-helper cell responses. CagA+ seropositive patients had a 2.1-fold elevation in PMBC *IL17A* expression as compared to serologically CagA- patients. However, these differences were not statistically significant.

Major virulence determinants of *H. pylori* include the vacuolating cytotoxin gene A (*vacA*) and the cytotoxin-associated gene A (*cagA*) [57]. The presence of the *cag* PaI and CagA have previously been shown to result in an increased incidence of clinically symptomatic infections, including ulceration and the development of cancer [57]. On the other hand, previous published work by this research group and others have shown a *cagA+* status of a colonising strain to induce higher regulatory Tcell responses [219]. In fact, in the previous study by Hussain *et al.* plasma IgE levels, indicative of allergic response, were reduced in *H. pylori*-infected individuals and this effect was potentiated in CagA-secreting strains. This phenomenon was in parallel to an inverse increase in the frequency of Tregs and *IL10* mRNA in these patients. These

previous data would suggest these strains induce a stronger immune response and a concomitant stronger protective influence from immune-mediated diseases. Given this finding we analysed our patient cohort for CagA virulence type with commercially available ELISA kits using plasma derived from whole blood. Of the enrolled patients, 19 (38%) were CagA- and 31 (62%) were $CagA^+$.

The CagA status of each patients colonising strains was used to stratify the PBMC cytokine mRNA expression data into $CagA^+$ and CagA- groups. When infected with *H. pylori* (month 0) there was no statistically significant difference in the expression of T-helper cytokines between the groups, however *IL17A* expression was elevated 2.1-fold in CagA+ infections and *IL4* reduced 1.6-fold in the same group with no difference in *IFNG* or *IL10*. This is unusual as CagA is reported by others to be one of the major proteins facilitating an inflammatory response, predominantly Th1-polarised [385], we do not find differences in the Th1-associated cytokine IFNγ. However, others report that CagA suppresses inflammatory cytokine production *in vivo* by modulating the activity of downstream signalling molecules [386]. Following the trends in expression longitudinally there were no significant differences within each group. The concentration of IgE within this cohort has been analysed previously [361], with no differences in plasma IgE concentration attributable to *H. pylori* infection status, nor changes to these levels through the 24-month study period post-eradication. However, a reduction was reported when analysing a larger cohort separate to this study [361].

2.6 – Conclusions & Future Work

- Human plasma IL-17A and IL-12p70 concentrations are altered with infection status and disease severity

It would be an interesting expansion of the current work to quantify plasma levels of the other Th17-related or IL-12 family-related secreted factors which were not included in the current panel. These could include IL-21 and IL-23, which play crucial roles in Th17 cell lineage specification, RORγT transcription factor expression, and

providing feedback loops to control Th17 responses [387]; and/or the p40, p35, or p19 subunits of IL-12/IL-23. Of course, in addition to IL-17A there are indeed 6 other IL-17 family members, A to F, expressed by Th17 lineage cells [387]. These may be interesting to investigate. Taken together Th17 cells and their secreted factors may potentially have a value in prognosis of *H. pylori* risk to an infected individual.

- The humoral IgG response against *H. pylori* is reduced following eradication, but maintains sero-positivity past 24 months

We find the plasma IgG response declines after eradication but remains serologically positive in most patients. These data suggest that the use of serology in diagnostic applications should be used cautiously, or at least in combination with alternative approaches such as UBT, culture or PCR methodology.

- *IL10* mRNA is elevated at 12- and 24-months post-eradication

This study found no significant changes to individuals baseline levels of the Th1, Th2, or Th17 related cytokines from before to 24-months after eradication of *H. pylori* infection. The expression of IL-10, the anti-inflammatory cytokine produced primarily by Tregs shows signs of differential expression through this timeframe, however in the opposite manner to that hypothesised when commencing this study. Normalised to everyone's baseline expression level, *IL10* mRNA was elevated at month 12 and month 24 post-eradication.

The proportion of $CD4^{+}CD25^{hi}FOXP3^{+}$ Tregs, as determined by flow cytometry did not change, however the proportion of $CD4^{+}IL10^{+}$ lymphocytes were found to reduce from month 0 to month 24. There is disparity between the flow cytometry and qPCR data which cannot currently be explained.

We determined that patients with more virulent CagA+ infecting strains had 2-fold elevated *IL17A* in PBMCs, not reaching statistical significance.

The study would have benefitted by recalling patients for a longer-term sample donation, perhaps at 5 years post-eradication. However, with the rate of dropouts this 5-year group would likely consist of less than half of the initial enrolled cohort.

For future work of this nature, I would recommend larger group sizes in the first instance and factoring a larger proportion of dropouts than the 15% built into this study's power calculations.

It would be an interesting, and possibly quite important inclusion for similar work in the future to assess gut microbiota composition, perhaps with stool samples. This is especially pertinent when considering the certainty of antibiotics mediating disruption to these microbial communities. A likely scenario is that antibiotic-mediated disruption to the microbiome composition in treated individuals may have influenced the results we observed as the gut microbiome is intricately involved in shaping host immunology, the Th17/Treg balance especially. No work was performed to quantify the gastric or gut microbiota in this study.

Chapter 3

Investigating the Immunomodulatory Effects of *H. pylori* Infection in a Mouse Model of Chronic Autoimmunity

Chapter 3: Analysis of the differential $CD4^+$ T-cellular Activity in EAE, the animal model of multiple sclerosis (MS), in response to infection with *H. pylori*

3.1 – Introduction

3.1.1 – Experimental Autoimmune Encephalomyelitis (EAE)

The study of MS is somewhat hindered by the CNS-specific nature of the disease. Obtaining tissue is a major undertaking from living patients and available material is lacking. Much of the bio-banked tissue in existence is from MS patients' post-mortem. Due to the changing nature of MS from a relapsing to a progressive form over time, post-mortem tissue may not accurately reflect what is occurring during earlier active disease, at the stage where intervention is required. In these cases, researchers turn to the use of animal models. With MS being such a diverse disease in terms of biological pathways, creating experimental models is difficult [388]; currently the most widely used model of multiple sclerosis is experimental autoimmune encephalomyelitis (EAE) [269-272,388,389]. It is to-date, possibly the best model in which the autoimmune mechanisms that contribute to MS can be studied *in vivo* [269,272,388,390-392].

EAE was first observed unknowingly in the 1800's as reports of paralysis following Pasteur's rabies vaccine containing spinal cord homogenate [390]. In the first instance, the basis of EAE as a potential experimental model was documented by Koritschoner, *et al.* (1925) [393], and further described in the literature by Rivers *et al.* in 1933 whereby a similar injection of spinal cord homogenate (SCH) to rhesus monkeys

resulted in a demyelinating paralysis [394,395]. Later years started to elucidate specific peptide antigens within the SCH that could elicit this effect. The first protein with a specific encephalitogenic property was that of myelin basic protein (MBP) in 1962 by Einstein *et al.* [396].

3.1.2 – The flexibility of the EAE models

Active EAE is normally induced in study animals through an immunisation with myelin peptides in the presence of a strong adjuvant to generate a CD4-driven immune response mimicking that seen in MS (active EAE) [270,391,397]. EAE can also be induced in study animals through the adoptive transfer of encephalitogenic $CD4^+$ T-cells (passive EAE) [255,270,272,388,389,391,398]. Passive EAE can also be achieved with $CD8^+$ cells but to a lesser extent [388,399]. There are several peptides from CNS myelin able to facilitate autoimmunity in the model. MOG, PLP, and MBP are commonly used [269,388,389], however other proteins integral to myelin such as CNPase have been successfully used [388,398]. The choice of peptide, and/or the strain of mouse can be altered to induce distinct types of EAE which mimic different aspects or stages of MS [270,271,388,389,398].

The choice of model to use is dependent on the research question being asked [397]. To study a novel drug candidate aimed at RRMS one may want to use the $PLP_{139-151}$/SJL mouse model of relapsing-remitting MS to quantify relapse frequency between groups [271,272,388]. This model commonly affects the optic nerve and cerebellum and characterised by neutrophilic and lymphocytic infiltrates. The course will often resolve when M2-polarised macrophages loaded with myelin breakdown product populate the draining lymph nodes [272]

For study of the inflammatory processes in MS, immunisation can be performed with MBP, or indeed via *ex vivo* transfer of MBP-reactive T-cells. This model is often performed using B10.PL mice and Lewis rats where it will often not involve demyelination [272]. Although allowing specific focus on inflammation, it must be noted that in this model various important cellular signalling cues that play roles in disease may not be active without myelin breakdown. These include the anti-inflammatory cues reported from myelin-containing macrophages, and this must be considered when translating findings into human MS.

To study a more de-/re-myelination-specific topic toxin-induced demyelination can be performed using the chemical agents; cuprizone, lysolecithin, or ethidium bromide (EtBr) [269-271].

The TMEV model of viral-induced demyelination is a well characterised example of infectious interactions resulting in MS-like demyelination, axonal degeneration, and autoimmunity. A viral trigger for MS is a widely supported yet unproven hypothesis behind the induction of autoimmune response [263]. The TMEV model is characterised by an axonal damage due to viral infection and replication within neurons [269,270]. The damage to CNS axons is thus the trigger to stimulate a secondary autoimmune response [269]. Although not used as frequently, the TMEV-induced model may be a better recapitulation of the crucial factors in MS development.

To study chronic autoimmune mechanisms the MOG_{35-55}/C57BL6 model is the optimal model of progressive MS [271]. In our work, we have performed all EAE studies using the This model. MOG is expressed specifically on oligodendrocytes forming CNS myelin and has 3 epitopes known to be immunogenic in MS and EAE, fragment 1-22, 35-55, and 96-106 [397].

3.1.3 – Cellular Mechanisms of EAE Induction

It must be noted, that although the best model to-date for the study of MS, EAE is a far from perfect recapitulation of MS immunology. In EAE, CNS autoimmunity is driven largely by the generation of myelin-specific $CD4^+$ T-helper cells of the inflammatory Th1 and Th17 lineage [272,389,390,397]. These cells are primed in the periphery following immunisation and are subsequently re-activated when encountering cognate myelin antigen presented from APCs in the CNS draining lymph nodes [272]. The induction of inflammation, blood-brain barrier permeability, and mass infiltration of leukocytes of the innate and adaptive systems preceding demyelination and lesion formation are thought to occur in similar mechanisms described for MS in chapter 1, as such will just be described more briefly here. Indeed, in many instances the proposed mechanisms for MS (some of which are still debated) are inferred based on those observed in the EAE model.

The onset of disease in mice post-immunisation can occur around 9-12 days, however the subsequent clinical course and symptoms are subject to variability, depending on factors such as the site of injection, the animal model used, and inter-animal variation. EAE progresses in a 'bottom-up' manner, first affecting the tip of the tail with motor dysfunction spreading to hind legs, and front legs, the humane endpoint for laboratory animals is reached at signs of respiratory distress or when total limb paralysis is reached. The disease progression has a scoring system which ranges from 0-5 with increments of 0.5.

3.1.4 – Immunopathological Mechanisms

$CD4^+$ Th1 and Th17 cells mediate inflammation and neurological degeneration through the secretion of pro-inflammatory cytokines and chemokines upon re-activation in the CNS, leading to the recruitment and infiltration of monocyte macrophage and neutrophils in large numbers. Upregulation of the integrin VCAM-, production of CCL20 by the choroid plexus epithelial cells and astrocytes facilitates the homing of CCR6-expressing Th17. Further BBB disruption is supported by Th17 cells. Neutrophils and macrophages facilitate degradation of myelin from CNS axons, secrete potent cytotoxic molecules such as TNFα, ROS, NO and IL-1β to further support a robust immune response. Macrophages also present myelin breakdown antigens to prime further effector T-cell responses [398]. Reports in the literature show that removal of CNS-draining lymph nodes can reduce the frequency and extent of relapses in EAE [274]. This finding would implicate the draining cervical and lumber lymph nodes (cLN, lLN) as being a site of autoreactive priming and activation. Furthermore, these activated cells secrete matrix metalloproteinases MMP6 and MMP9 which help to disrupt the parenchymal barrier and support further lymphocytic infiltration into the CNS [400]. These inflammatory molecules contribute to the targeted destruction of insulating oligodendroglia. Reactive gliosis is induced in microglia and astrocytes whereby they are polarised to a pro-inflammatory phenotype, upregulating co-stimulatory and antigen-presenting molecules. Reactive astrocytes accumulate at the lesion and form the glial scar. Loss of oligodendrocytes and demyelination in this manner leads to the attenuated capacity for nerve impulses propagation, resulting in the hallmark symptoms of motor dysfunction. As the

disease progresses chronically this eventually results in the progressive disability observed in study animals.

3.1.5 – Considerations when translating EAE data to human MS

Although EAE is mediated through a similar T-cell driven autoimmune response against oligodendrocyte myelin, and characterises the inflammatory component of MS, there are stark differences. In MS, active lesion sites have a predominant number of CD8+ T-cells, whereby EAE is pre-dominantly CD4-driven [240,244,401]. It is notable that therapies that show efficacy in MS, target T-cells (of all subtypes) and B-cells together or just B-cells alone, however targeting only the $CD4^+$ T-cell population fails to control disease [401]. There are so far no animal models which efficiently reproduce the $CD4^+$ & $CD8^+$ T-cell and CD20+ B-cell contribution of MS, these models if developed would be of huge benefit to MS research. Development of MS is thought to be multifactorial, influenced by genetics, infectious triggers, microbiota, and environmental factors; of course, these potentially crucial factors are not reproducible in mouse models. Indeed, the genetic homogeneity of mice is not comparable to human cohorts. Nonetheless, it remains the best available method for immunologists and neurologist to try to deconvolute the plethora of complex factors causing MS.

3.1.6 – Rationale and Hypotheses

Taking the observations of others in the literature and supported by our own previous work in this field, I hypothesised that an active *H. pylori* infection in mice would suppress the development of pro-inflammatory T-cell responses in EAE mice and lead to a reduced incidence or severity of symptomatic EAE in the *Hp*-infected animals. I proposed that this protection may be mediated by the induction of Tregs, working through anti-inflammatory molecules including IL-10, in addition to contact-dependent inhibitory effects on inflammatory Th1 and Th17 cells, major drivers of EAE. This inhibition may occur within lymphoid tissue via the suppression of peripheral T-cell priming. It may be a result of alterations in the secretion of chemokines within the region of the gastric mucosa and thus cause aberrant T-cell trafficking in the infected host. It may occur via a distinct mechanism entirely.

In the first instance we conducted a pilot study to ensure that the EAE model worked in a reproducible way to previous experiments, when new batches of MOG peptide and adjuvants were used, and to obtain some preliminary data on the frequency of lymphocytes in EAE mice and non-EAE controls. A second study induced EAE in groups of mice infected with *H. pylori* strains SS1 or PMSS1, or sham-infected controls. This study endeavoured to ascertain whether *H. pylori* infection led to altered frequencies of T-cells in either the lymphoid compartment or the CNS, and if infected animals developed a less severe manifestation of EAE as compared to uninfected animals. Two *H. pylori* strains were used; SS1 (CagA+/*vacA* type 2, but with a non-functional *cag*PAI) and PMSS1 (CagA+/*vacA* type 2, and with a functional *cag*PAI). As the virulence factor CagA has been shown in humans to induce a more robust immune response, this comparison may help to inform on the potential effects of more virulent strains in protection against EAE.

3.1.7 – Hypotheses.

It was hypothesised that:

- The severity of EAE would be reduced in mice previously infected with *H. pylori.*
- The frequency of $CD4^+$ T-helper cell subsets Th1, Th2, Th17 and Treg would be altered in the infected EAE mice as compared to uninfected EAE animals.
- The frequency of inflammatory Th1 and Th17 cells infiltrating the CNS would be lower in the *H. pylori* infected animals as compared to uninfected mice.
- The frequency of Tregs would be increased in the spleen and mesenteric lymph nodes of *H. pylori* infected animals.
- The frequency of Tregs infiltrating the brain and spinal cord may be increased in *H. pylori* infected animals.
- The severity of EAE would be correlated to the level of inflammatory $CD4^+$ Th1 and Th17 cells infiltrating the CNS.
- More virulent CagA+ *Hp* PMSS1 strains would confer a greater amount of protection from CNS inflammation and EAE severity.

3.2 – Materials & Methods

3.2.1 – *H. pylori* culture and infection of C57BL/6 mice

H. pylori strain SS1 and PMSS1 were cultured on blood agar plates (Oxoid) from frozen stocks. Plates were passaged each 2 days. *H. pylori* growth was collected from the edges of the plates with a sterile swab and dispensed into 1.2ml of either Brucella broth (BB) or PBS at approximately $1x10^9$ bacteria per ml. 5-week-old female C57BL6 mice (Charles River), were dosed via oral gavage with 0.1ml of *Hp* inoculum or a medium-only sham control. Dosing of mice was performed every 2 days for a total of 3 doses. Animals were weighed weekly basis for a period of 3 weeks, prior to EAE induction.

3.2.2 – Induction of EAE in C57BL/6 mice

The chosen model used in our study was the MOG_{p35-55}-induced EAE in C57BL/6 mice, resembling a chronic progressive MS. Induction of disease was achieved through sub-cutaneous immunisation at 2 sites on the back/flank with an emulsion consisting of 250µg MOG peptide fragment p35-55 in complete Freunds' adjuvant (CFA) to an antigen-CFA ratio of 1:1. The inoculum emulsion was prepared by adding MOG_{p35-55} peptide (250µg in PBS) dropwise to pre-prepared CFA solution (4mg.ml^{-1} H37 Ra *M. tuberculin* in incomplete Freund's adjuvant; IFA). This was followed by an intra-peritoneal (I.P.) injection of 0.1ml *Pertussis* toxin (PTX) solution, containing 2µg.ml^{-1} PTX in PBS. The PTX injections were repeated 2 days after the initial immunisations.

Mice were checked for welfare and weighed at least once daily. An EAE severity score was assigned to each mouse according to a widely accepted and published EAE severity scoring criteria (O'Brien, 2010). This was used to assess the EAE clinical score daily from 1-20 days post-immunisation (d.p.i.). This scoring scale grades EAE severity from 0-5 based on the level of motor dysfunction and symptomatic paralysis. This criterion was used with modifications to allow for 0.5 increments as per previous work (pilot study) in response to non-definitive borderline scores being observed. Scores of 0; where no visible symptoms are apparent; score 1, first signs of a loss of tonus to the tail; score 2, impaired gait or righting-reflex; score 3, loss of mobility in one or both rear limbs; score 4, loss of mobility in front limbs. Score 5, quadriplegia.

The assignment of 0.5 increments were made whereby the animal did not categorically fall into either of the higher/lower categories.

After the onset of symptomatic EAE, mice were weighed and scored twice daily. With consideration to the welfare of the animals, refinements to housing conditions were made; powdered chow was rehydrated with water and placed into dishes. Freshly made batches were placed on the cage floor twice daily, to provide access to food and water for mice that may be experiencing motor deficits and paralysis as an expected outcome of the EAE model.

3.2.3 – Study termination and tissue collection

Animals were monitored twice daily and assessed against the pre-defined humane endpoints of the study. At the study endpoint of 21-days post immunisation, mice were humanely euthanised with CO_2 asphyxiation, confirmed with cervical dislocation. The spleens were collected into transfer medium (RPMI, 2% *v/v* FCS, 1% *v/v* penicillin/streptomycin) and kept on ice. Spinal cords were flushed from the spinal column via insertion of a pipette into the lower lumbar region and extracted hydraulically by flushing with PBS from a 5ml syringe. Cords were washed in sterile PBS, collected to transport medium, and kept on ice. Brains were extracted, washed in sterile PBS, and placed into a formalin solution in 5ml Bijous. Stomachs were halved lengthwise and cleaned of contents by gently washing with PBS. Half stomachs were placed into a urease solution to ascertain *Hp* infection status. The remaining half was pinned onto cork boards and placed into formalin solution.

3.2.4 – Processing of tissue for downstream assays

Spleens were homogenised to a single cell solution by rubbing through a 70µm cell strainer placed in a petri dish with 5mls washing medium (RPMI, 2% FCS, 1% pen/strep) using the end of a sterile 1ml syringe. Solutions were collected from the petri dish using a sterile Pasteur pipette and dishes were washed with a further 5ml washing medium to collect remaining cells. Cells were collected into a 20ml universal tube and centrifuged at 1000 x *g* for 5 minutes to pellet the cells. The pellets were resuspended and were further washed once more with 10mls washing medium before resuspension for counting in 10mls culture medium (RPMI, 10% FCS, 1% pen/strep)

Spinal cords were homogenised by rubbing through a 70µm cell strainer in 5mls washing medium (RPMI, 2% FCS, 1% pen/strep) in a petri dish as described above. Cells were collected to a 20ml universal tube and remaining cells washed from the dish and collected using a Pasteur pipette. The cell suspension, in 10mls washing medium was centrifuged at 1000 x *g* for 5 minutes and further washed once more. At this stage, lymphocytes were enriched from the crude spinal cord suspension using a Percoll density-gradient centrifugation. For this, neat Percoll solution was prepared by adding 1 part of 10x PBS to 9 parts Percoll. The spinal cord pellets were resuspended in 5mls of 30% *v/v* Percoll working solution (100% Percoll diluted to 30% *v/v* in Hanks' balanced salt solution; HBSS). The resuspended cells in 30% Percoll were slowly layered dropwise onto 4mls of 70% Percoll solution (100% Percoll diluted to 70% *v/v* in HBSS) in a 15ml Falcon tube. Tubes were centrifuged for 20 minutes at 500 x *g* to separate the cells. The cells of interest amass at the interface between the 30% and 70% Percoll layers and can be seen as a slightly opaque layer at the interface. These cells were extracted using a sterile Pasteur pipette carefully taking as little of the Percoll layers either side as possible. Extracted cells were suspended in culture medium at $1x10^6.ml^{-1}$.

3.2.5 – Flow cytometry cellular staining

Spleen cells were resuspended to a concentration of $1x10^6.ml^{-1}$ in culture medium. From each of these suspensions, 1ml was added to a 5ml FACS tube for flow cytometry panel staining. Spinal cord cells were similarly added to FACS tubes at the highest number possible from the number counted.

For cytokine analysis by flow cytometry, cells were stimulated for 6 hours at 37°C in the presence of a stimulation cocktail containing $1mg.ml^{-1}$ phorbol-12-myristate acetate (PMA), $1mg.ml^{-1}$ Ionomycin and $1mg.ml^{-1}$ PFA. For the first hour, tubes were incubated at 37°C with 5% CO_2 before the addition of $10mg.ml^{-1}$ Brefeldin A (BFA) to inhibit intracellular protein transport and secretion of cytokine. After the addition of BFA cells were transferred to a pre-warmed water bath at 37°C for a further 5 hours before keeping at 4°C for staining the following day.

Cells were pelleted at 300 x *g* and washed with sterile PBS before resuspending in viability staining buffer (100µl of PBS containing a 1:200 dilution of Zombie NIR viability dye; Biolegend) and incubated for 15 minutes at room temperature (RT) in the dark. Cells were then washed twice with PBA staining buffer (PBA, consisting of PBS with 0.01% bovine serum albumin (BSA) and 2% FCS) before addition of cell surface marker-specific antibodies. Surface marker staining was conducted on ice for 30 minutes before washing in duplicate with PBA (2% FCS). Here, tubes in which no intracellular staining was required were fixed with 0.5ml fixation buffer (Biolegend) for 20 minutes at RT in the dark before washing with PBA and finally resuspending in 0.5ml PBA for analysis (kept at 4°C).

For intracellular cytokine or transcription factor staining, tubes were incubated with either PBA-saponin or 1ml of 1x FoxP3 fixation/permeablisation buffer (eBioscience) for 30 minutes at RT in the dark. After two washes with 1ml of 1x permeablisation buffer (eBioscience) pelleted cells were incubated with staining antibodies for 30 minutes at RT in the dark. Cells were twice washed with 1x permeablisation buffer before being resuspended in 0.5ml of PBA staining buffer and kept at 4°C in the dark for subsequent analysis. For cytokine staining, the washing steps were performed using a PBA-Saponin buffer in place of fixation/permeablisation buffer, before finally resuspending in 0.5ml PBA staining buffer and kept at 4°C for analysis.

Fluorescence acquisition was performed using an Astrios Flow Cytometer (Beckmann-Coulter®). A target of 200,000 events falling within pre-defined lymphocyte gating parameters were collected for each sample. Gating was set according to isotype control antibodies. Representative gating strategy is shown in *Figure 29.*

Table 13 Flow cytometry specific antibodies used

Stain Used	Clone	Catalogue Num.	Quantity per test	Excitation	Emission
Zombie NiR	n/a	Biolegend; 423105	1:200	633	795/70
CD45:AF700	30-F11	Biolegend; 103128	0.25 µg	640	722/44
CD4:PCy7	RM4-4	Biolegend; 116015	0.2 µg	561	795/70
CD19:BV605	6D5	Biolegend; 115593	0.5 µg	405	614/20
CD11c:BV711	N418	Biolegend; 117349	0.06 µg	405	722/44
CCR6:AF647	29-2L17	Biolegend; 129807	0.25 µg	640	671/30
IFNG:FITC	XMG1.2	Biolegend; 505805	0.5 µg	488	513/26
IL4:BV421	11B11	Biolegend; 504119	0.1 µg	405	448/59
Tbet:AF647	4B10	Biolegend; 644803	1 µg	640	671/30
IL-17:PE	TC11-18H10	Biolegend; 506903	0.1 µg	488	576/21
IL-10:AF647	JES5-16E3	Biolegend; 505014	0.25 µg	640	671/30
Tbet:BV711	4B10	Biolegend; 644819	0.35 µg	405	722/44
GATA3:BV421	16E10A23	Biolegend; 653814	0.05 µg	405	448/59
RORγT:PE	B2D	eBioscience; 12-6981-82	0.25 µg	488	576/21
FoxP3:FITC	FJK-16S	eBioscience; 11-5773-80	0.5 µg	488	513/26
F4/80:PE	BM8	Biolegend; 123109	1 µg	488	576/21

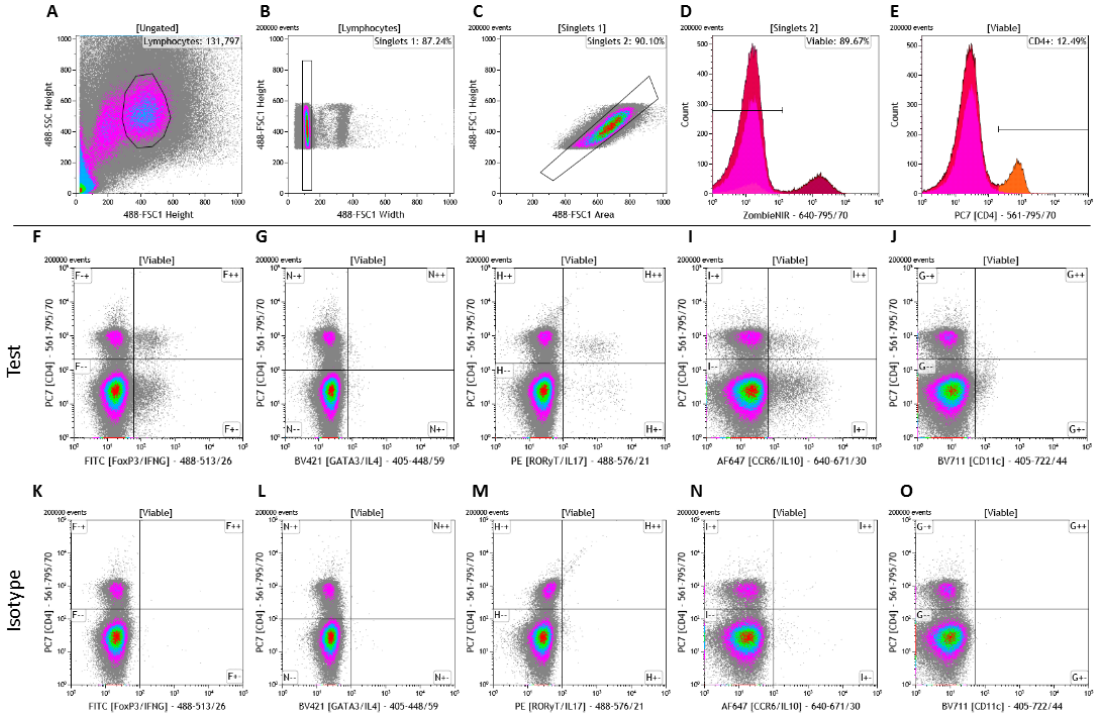

Figure 29 Representative gating strategy for flow cytometry analyses

Example of the flow cytometry gating parameters used in analyses. (A) lymphocytes gated accorded to forward and side scatter characteristics. (B & C) Debris and doublet exclusion. (D) Viable cells. (E) CD4. (F-J) Specific antibodies. (K-O) Isotype controls.

3.2.6 – Purification of $CD4^+$ cells

Remaining spleen cells were used to enrich $CD4^+$ cells for further analysis. Here, $CD4^+$ cells were purified using commercial positive selection kits according to the protocol previously described, and according to the manufacturers' recommendation using an EasyEights magnet in 5ml FACS tubes. After the purification, cells were resuspended in culture medium and counted using Trypan blue to exclude dead cells.

From the enriched $CD4^+$ cell suspensions, $1x10^6$ cells were added to a 5ml FACS tube for flow cytometry staining. These cells were stained according to the previous protocol for Zombie NIR, cellular surface markers, CD4, CD45, and CCR6 and T-helper transcription factors, Tbet, GATA3, RORyT and FoxP3.

The remaining cells were pelleted and resuspended in a serum-free media (XVIVO-15; Lonza). From these cells, $0.5x10^6$ were plated per well of a 24-well plate in a 0.5ml well volume of XVIVO-15 media. Mouse T-activator CD3/CD28 Dynabeads (Invitrogen) were washed with XVIVO-15 as described by the manufacturer and added to the plated cells at a bead:cell ratio of 1:1. The plates were incubated at 37°C in 5% CO_2 for 3 days for $CD4^+$ stimulation to occur. After 3 days, cell culture supernatants were aspirated from the wells into sterile 2ml tubes, and the cells were pelleted by centrifugation at 300 x *g* for 5 minutes. The supernatants were aspirated, transferred to a fresh tube, and further centrifuged at full speed for 5 minutes to pellet any residual debris or beads. The purified supernatant was transferred to a sterile 2ml tube before being frozen at -80°C for subsequent analysis. The cell pellets were frozen at -80°C for subsequent analysis.

After collection of the supernatants, a pooled sample of cells from each group was re-plated and restimulated with Dynabeads for a further 3 days in a 5% CO_2 incubator at 37°C. After which, the supernatants were collected in the method described above and frozen at -80°C. The pelleted cells from these restimulated samples were stained for Zombie NIR, CD4, CD25, Tbet, GATA3, RORyT, and FoxP3 for flow cytometry analysis to establish how the frequency of $CD4^+$ cell phenotypes have skewed after the repeated stimulation *in vitro.*

3.2.7 – Cytokine ELISA on stimulated CD4⁺ cell supernatants

The supernatants from the stimulated CD4⁺ cells were used to quantify CCN3, IL-10, IL-17A, IFNγ, and IL-4 concentration using commercially sourced ELISA kits, according to the protocols described previously.

3.3 – Results

3.3.1 – Pilot EAE experiment

A pilot experiment was performed to ensure the EAE model progressed with a course consistent with previous work by this research group and in line with expected outcomes according to the literature. For this pilot study, 6 mice per group were assigned to two groups, EAE and naïve. EAE was induced and allowed to progress to the pre-defined study endpoint of 24 d.p.i. Two of the EAE mice developed severe EAE, which fell under the pre-determined criteria requiring early termination form the study (an EAE score of >4 for 72 hours); two of the naïve mice developed severe ulceration at the injection site and were euthanised. In total, 4 mice per group completed the study. The first symptoms of a loss of tonus to the tail were apparent from 7-9 d.p.i and progressed to a peak EAE severity around 14-20 d.p.i. (*Figure 30*) Maximal EAE scores were relatively modest, but in line with others, reaching a maximum group mean of around 2.5.

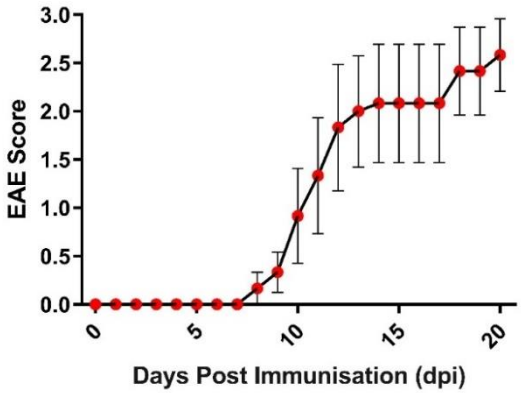

Figure 30 Mean EAE scores for mice in the pilot study.

The kinetics of EAE in the pilot study are shown. Four 5-week-old female C57BL6 mice were included in each group; naïve or EAE. The EAE group were assessed for welfare and scored for EAE severity once daily. Points represent the group mean EAE score, with error bars denoting the standard deviation.

EAE induces a robust immune response mediated by a wide range of cell types. CD4 T-cells, macrophage and dendritic cells infiltrate the CNS in large numbers, and this correlates with severity scores. There is also an activation of B-cell-mediated humoral responses.

In this study the numbers of $CD4^+$ T-cells, $CD4^+CD25^{Hi}$FoxP3 Tregs, $CD8^+$ T-cells, $CD19^+$ B-cells, $F4/80^+$ macrophage, and $CD11c^+$ dendritic cells were quantified from lymphocytes in the spleen using flow cytometry (*Figure 31; A*). Lymphocytes were gated according to forward and side-scatter characteristics. Macrophage and dendritic cells were gated on CD4-CD8- events. There was little difference in the frequencies of $CD4^+$, CD8+, F4/80+ or CD11c+ cells between the EAE and control groups in the spleen (*Figure 31; C*). However, there was a 1.4-fold decrease (*p=0.0001*) in the frequency of CD19 B-cells in the EAE group as compared to naïve control mice.

Within the lymph node both CD4 and CD8 T-cell frequency was reduced by 1.4-fold (n.s.) in parallel with an elevation in CD19 B-cell frequency (1.7-fold, *p=0.04*). F4/80+ macrophages increased 2.4-fold (n.s.) (*Figure 31; B*). No difference was observed for CD11c expressing dendritic cell lineages.

Spinal cord infiltrates were composed of 14-fold increases (from 1% to 15%) in $CD4^+$ T-cells in the EAE group as compared to the control mice (however this did not equate to a statistically significant difference with multiple comparisons correction). There were no marked changes in the frequency of $CD8^+$ or $CD19^+$ cells in the CNS between the groups. There were large elevations of $F4/80^+$ macrophage and $CD11c^+$ dendritic cells populating the CNS of EAE mice as compared to naïve mice ($F4/80^+$: 4-fold, *p=<0.0001*); $CD11c^+$: 13.5-fold, *p=<0.0001*). In comparison, one mouse which developed severe EAE (*Figure 32; A*) had 28% $CD4^+$ amongst CNS cells.

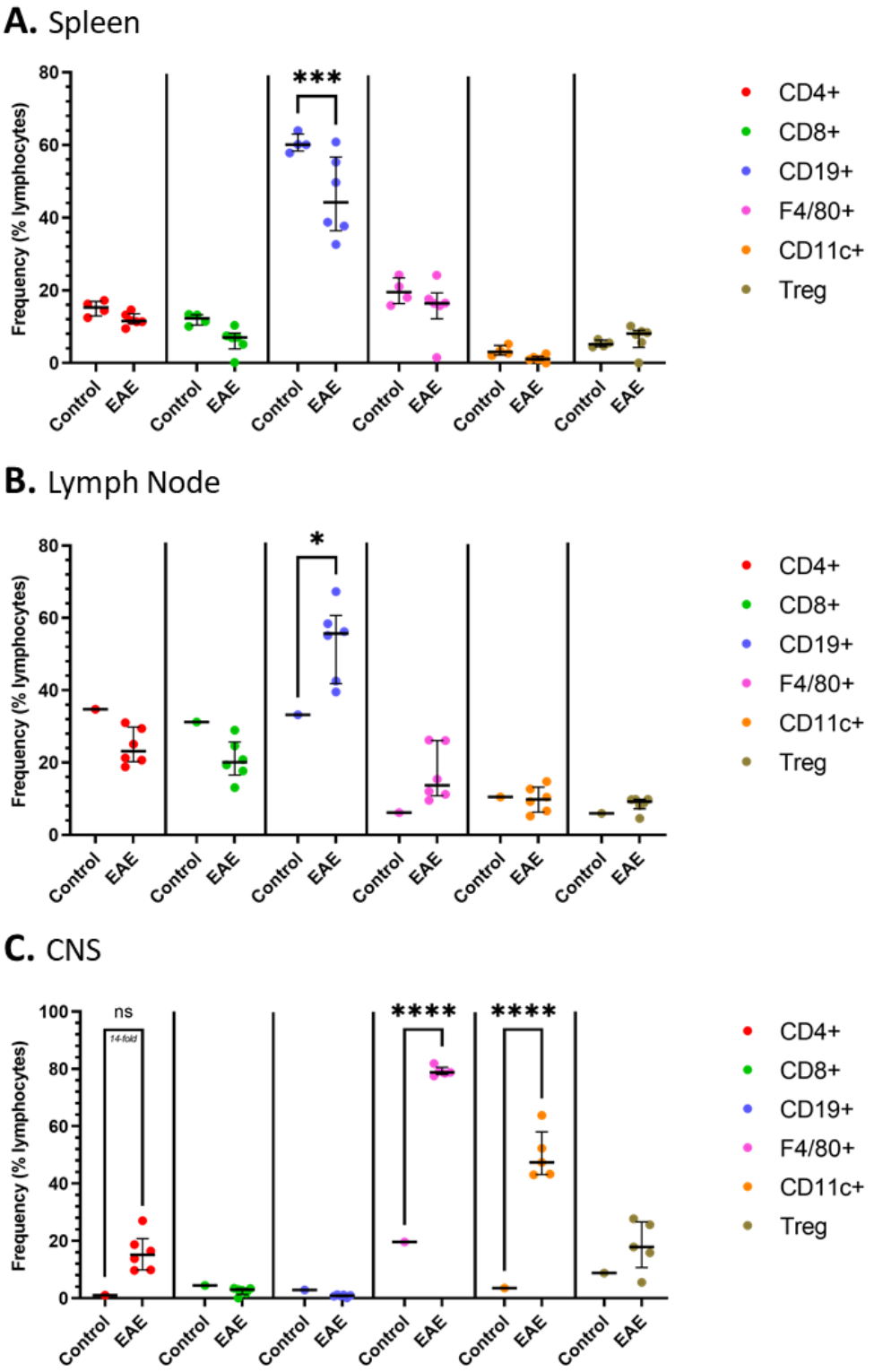

Figure 31 Quantification of the cellular infiltrates to the spleen, lymph nodes, and spinal cord of EAE and non-EAE mice analysed with flow cytometry.

The frequency of leukocyte subtypes was quantified using flow cytometry from the spleen (A), lymph nodes (B), and the spinal cord (C), of EAE mice compared to naïve non-EAE mice. Lymphocytes were gated by forward and side-scatter characteristics. Debris and doublets were excluded. Frequency is given as the percent of single cellular events analysed. Dots represent individual mice; lines show the median; error bars the interquartile range. Šídák's ANOVA; **p=0.04; ***p=0.0001; ****p=<0.0001.*

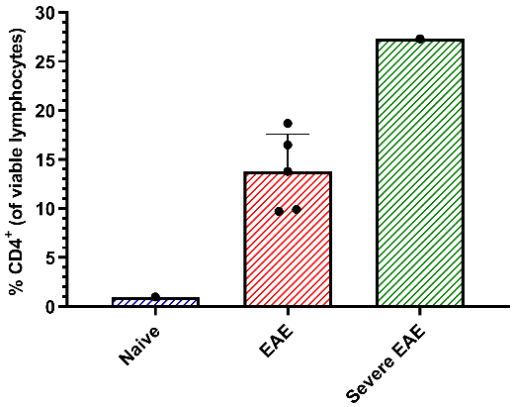

Figure 32 Frequency of CD4⁺ cells infiltrating the spinal cord of EAE mice or naïve control mice.

CD4⁺ cells were quantified from the spinal cords of EAE or non-EAE mice using flow cytometry. Debris, and doublets were excluded from the analysis. Single cellular events were gated, from which percent CD4+ was determined. Dots signify individual mice; bars represent the group median; error bars denote the interquartile range.

3.3.2 – *H. pylori* Infection as a modulator of EAE severity and kinetics

The EAE pilot had been successful and generated data in-line with expectations. As such, this model was taken forwards to a larger scale study whereby 3 groups of 8 mice were included; uninfected, infected with *H. pylori* strain SS1, or strain PMSS1. The two strains differ mainly in virulence, with PMSS1 inducing more rigorous immune responses, and shown previously to reduce plasma IgE potentially protecting from allergy. An aim of this work is to investigate a differential response in EAE from distinct strains. EAE was induced after an initial 3 weeks after the infections. At the study endpoint, half stomachs were used to establish the *H. pylori* colonisation status of mice in the study. *H. pylori* was not isolated from stomachs of the sham-infection group as expected. *H. pylori* was isolated from only 3 of the 7 mice administered with the PMSS1 strain, giving a colonisation success rate of 43%. There were 6 of 7 mice infected with strain SS1 from which *H. pylori* was successfully cultured giving a success rate of 86%.

In general, the kinetics of EAE progressed in a manner comparable to previous studies of this nature by this research group, following an expected and hypothesised trend (*Figure 33*). One noteworthy difference between this study and the previous pilot

study were that none of the groups in the current study reached the same EAE severity peak as the pilot study (mean EAE severity; pilot study: 2.5; Current study: BB and SS1: 1.57; PMSS1: 1.5). All 3 groups in the current study appeared to have comparable kinetics.

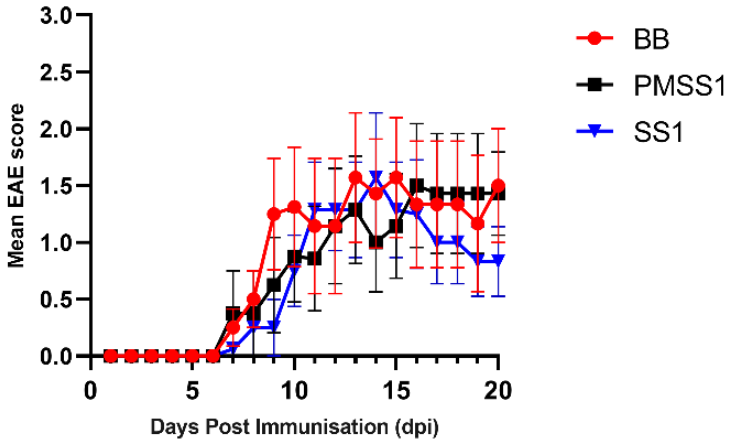

Figure 33 EAE severity scores of the current and previous EAE study

EAE severity was scored on a scale of 1-5 according to observable motor dysfunction daily as per published criteria. The 3 groups in the current study; uninfected mice sham-treated with *Brucella* broth (BB; red); *H. pylori* PMSS1-infected (PMSS1; black) and SS1-infected (SS1; blue) are plotted. Points plotted represent the mean scores for each group. Error bars denote the standard error of the means plotted.

In the current study, the day of onset (DoO) was defined as the day whereby the first signs of paralysis were observed (loss of tail tonus being the first sign). The DoO was comparable between groups (*Figure 34*). From each group, at least one mouse first presented with an EAE score at day 7, however the median DoO for the groups were slightly delayed in both the infected groups (PMSS1 and SS1, 10 d.p.i.) as compared to the uninfected control group (8.5 d.p.i.).

The peak severity for all groups was observed between days 13 and 17 (BB: 13d.p.i; PMSS1: 16d.p.i.; SS1: day 14 d.p.i). No notable differences were found between the BB, PMSS1 or SS1 groups (*Figure 34*). The mean peak EAE scores were 1.57 (BB), 1.50 (PMSS1), and 1.57 (SS1), respectively. At the stage of maximal EAE severity, the uninfected and PMSS1 infected groups then presented with a plateau in the scores

through to the study endpoint at day 20. However, in contrast, the SS1 infected group (blue) mean severity score continually dropped during the 14-20 d.p.i period.

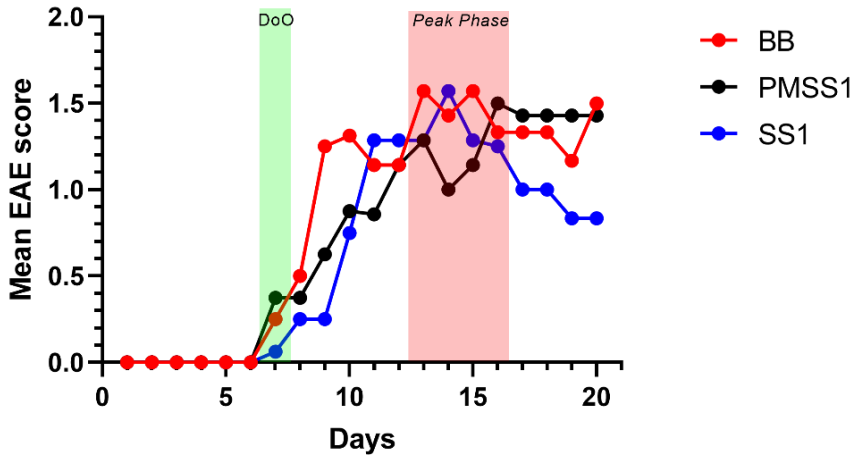

Figure 34 Mean EAE scores from mice infected with H. pylori strains HpSS1, HpPMSS1, or sham-treated control mice.

Mice were scored daily for EAE severity according to established criteria. Mean scores for the mice within each group are plotted. Uninfected (Brucella broth) BB; red, PMSS1; black, and SS1; blue. The day-of-onset (DoO) is overlayed in green. The peak phase is overlayed in pink.

Assessing the cumulative severity between the groups in the current study (*Figure 35*) found that the SS1 infected mice presented with a significant reduction of 1.7-fold (ANOVA, Tukey's test; *p= 0.0001*) at day 20 as compared to the uninfected group, and a lesser but significant reduction as compared to the PMSS1 group (1.4-fold, *p=0.02*).

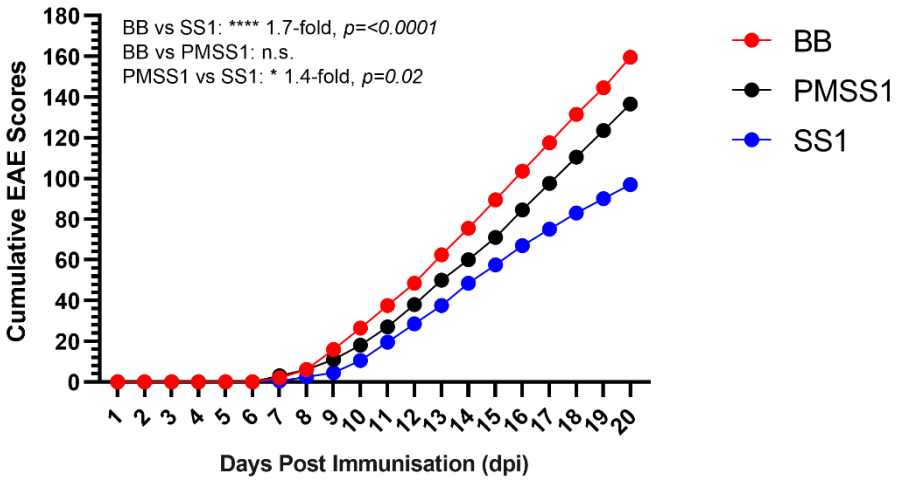

Figure 35 The cumulative EAE severity scores between groups of EAE mice, either previously infected with HpSS1, HpPMSS1, or sham-treated control EAE mice.

Mean cumulative EAE severity scores for each group are plotted. Red: Uninfected mice treated with Brucella broth (BB); black: *H. pylori*-PMSS1 infected; blue: *H. pylori* SS1-infected. Tukey's ANOVA; * p=0.02; **** p=<0.0001.

Day of onset, maximum EAE scores, and end severity scores were analysed for each group (*Figure 36; A-D*). The day of onset was similar between all groups at day 8-9 (*A*); maximum mean EAE scores for each group were comparable between the uninfected and PMSS1 infected groups (both with a group median score of 2.5), however the SS1 infected groups median maximum score was reduced to 1.5 (*B*). The group median EAE scores at the study endpoint of 20 d.p.i. were uninfected, 1.87; PMSS1, 1.67; SS1, 0.87 (*C*). Taking just mice which developed symptomatic EAE, median scores at the study endpoint were; uninfected, 3.0; PMSS1 infected, 2.0; SS1 infected, 1.0 (D).

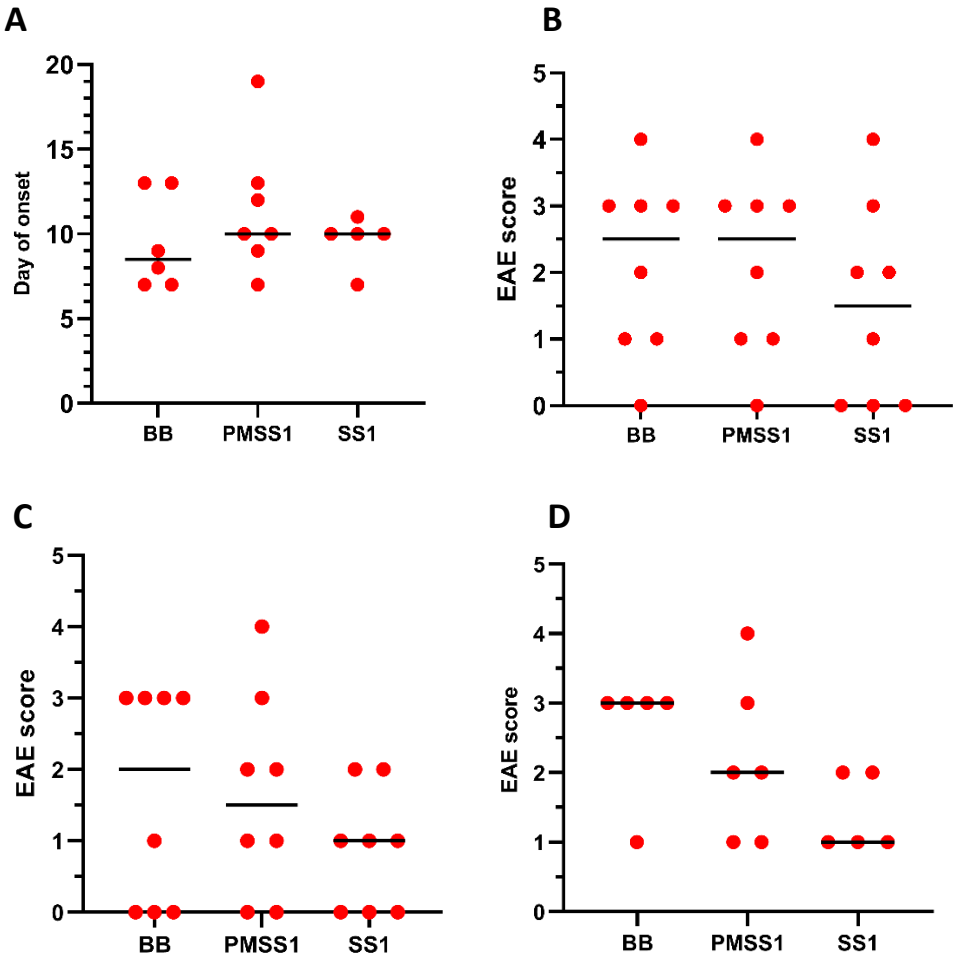

Figure 36 Day of onset, maximum EAE score, and final EAE scores from H. pylori infected or uninfected EAE mice

Mice were infected with *H. pylori* strain PMSS1, SS1, or sham-infected using *Brucella* broth-only (BB). Animals were scored daily after EAE induction for the remainder of the study period. (A) the day of onset for the first observable symptoms of EAE. (B) maximum EAE scores recorded for each mouse over the 20-day study period. (C) The final EAE score recorded on day of termination. (D) The final EAE scores on day of termination in those mice with symptomatic EAE. Dots represent individual mice; lines denote the median value.

3.3.3 – Distributions of lymphocytes in the spleens and spinal cords of *H. pylori* infected or uninfected EAE mice.

To quantify the relative frequencies of each of the cellular lineages in both the spleen and spinal cord, cells were stained with fluorochrome-conjugated antibodies and analysed by flow cytometry. The cells were stained for CD45 (leukocytes), CD4 (T-cells), CD19 (B-cells), CD11c (dendritic cells), CCR6 (CCL20-responsive cells). In addition, the cytokines IFNγ, IL-4, IL-17A, and IL-10 were stained after stimulation of the cells. These cytokines can be used to discern T-helper subtypes Th1, Th2, Th17,

and Treg when co-expressed with CD4. Discrimination of viable and non-viable cells was performed using a viability dye.

Lymphocytes were defined as cells falling under a predefined gate based on forward and side-scatter characteristics. The spinal cord contained a far more complex mixture of cell types and CD45 was used to distinguish lymphocytes from spinal cord cell solutions where clearly defined and dominant populations were not visually obvious.

No differences were observed in the frequency of CD4 T-cells, CD19 B-cells, or CD11c dendritic cells amongst splenocytes between groups (*Figure 37; A-C*). CD4 cells made up around 15% of the total splenocyte population in line with expectations. The dominant lineage was that of CD19 B-cells which account for around 50-60% of splenocytes in all groups. CD11c dendritic cells are defined as CD11c+ cells from CD4- CD19- splenocytes and account for <1% of splenocytes, comparable between all groups. T-helper subtypes were gated as $CD4^+$ cells co-expressing each of the signature cytokines (*Figure 37; D-G*). There were no differences observed in the frequency of any of the T-helper subtypes analysed between groups.

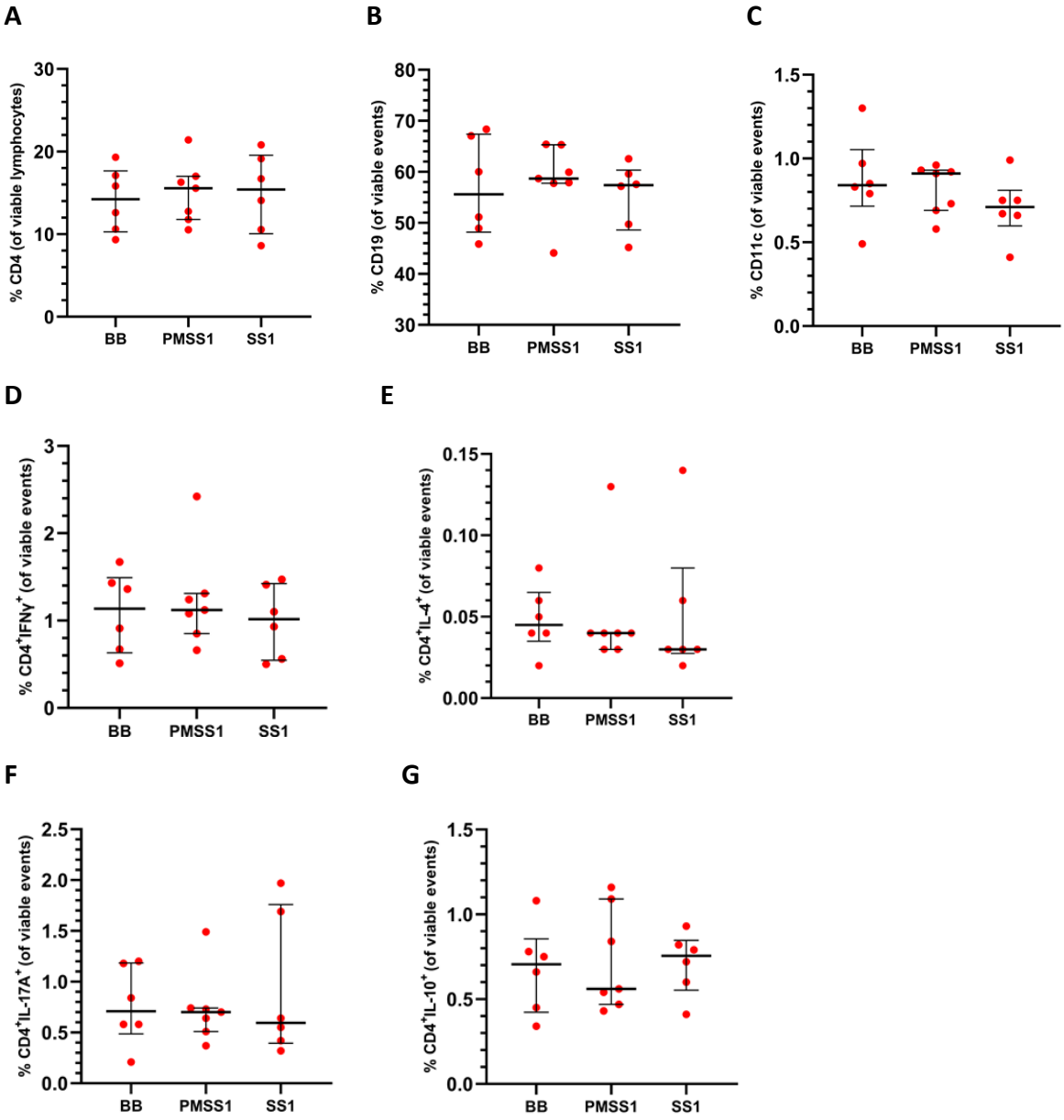

Figure 37 *Flow cytometry analysis of cellular populations in the spleens of H. pylori infected or uninfected EAE mice*

Splenocytes from *H. pylori*-infected or uninfected mice were analysed by flow cytometry. Lymphocytes were gated according to forward- and side-scatter characteristics, dead cells, debris, and doublets were excluded. Frequencies quoted are expressed as percent of viable cells. The cell surface markers for T-cells ($CD4^+$), B-cells (CD19+), and dendritic cells (CD11c) were quantified. From $CD4^+$ cells, those co-expressing the signature cytokines for the T-helper lineages; IFNγ (Th1); IL-4 (Th2); IL-17A (Th17); IL-10 (Treg) were also quantified. Dots represent individual mice; lines show the median; error bars denote the interquartile range.

Intracellular transcription factors characteristic of the T-helper lineages was also quantified between the uninfected and SS1-infected group (the two groups where a difference in disease severity was observed). The Th1, Th2, Th17, and Treg subtypes

were defined as CD45+CD4$^+$ cells expressing each of the 4 signature transcriptions factors, Tbet, GATA3, RORγT, and FoxP3, respectively. Total splenocytes from each mouse were enriched for CD4$^+$ cells using immunomagnetic separation. Enrichments were all in the order of 5-fold, from a starting CD4$^+$ frequency from total splenocytes of around 17% (from a single pooled sample per group) to purified CD4$^+$ frequencies of 90-95% from each individual mouse. Purified CD4$^+$ cells were then fixed, permeabilised and stained for the T-helper associated transcription factors.

In agreement with the cytokine data, no differences were observed across the groups in the relative frequencies of any of the T-helper types investigated, as determined by staining CD4$^+$ cells for the signature transcription factors (*Figure 38*). There was also no significant difference in the proportion of these subtypes expressing the CCL20-responsive homing receptor CCR6, which has been reported to direct migration of T-cells to the CNS in EAE and MS (*Figure 39*). However, interestingly the *H. pylori* SS1-infected mice had a median 50% reduction of CD45+CD4+CCR6+ cells in the spleen as compared to uninfected EAE mice.

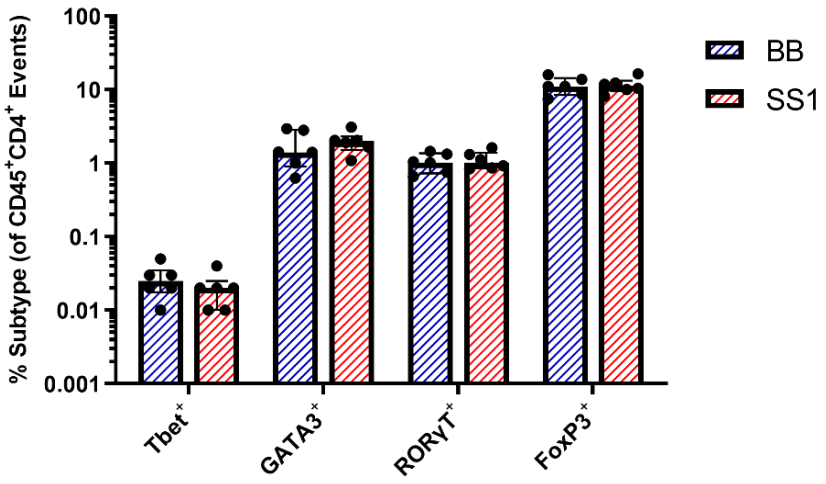

Figure 38 Quantification of the signature transcription factors of the major T-helper subsets within the spleen of infected or uninfected EAE mice.

Splenocytes from *H. pylori* strain SS1-infected (red bars) or sham-infected control mice (blue bars) were stained for CD45 and CD4 cell surface markers, and the intracellular transcription factors (TF's) characteristic of the 4 major T-helper subsets: Th1, Th2, Th17 and Treg (Tbet, GATA3, RORγT, and FoxP3, respectively). CD45$^+$ cells co-stained with both CD4 and one of the signature TFs are considered one of the T-helper subsets. Bars represent the median; error bars denote the interquartile range.

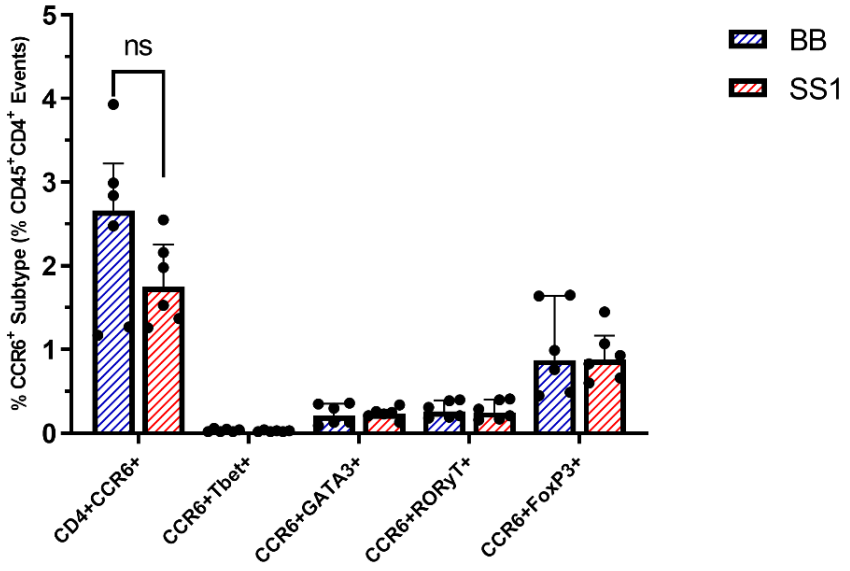

Figure 39 Splenocytes from H. pylori SS1-infected or uninfected EAE mice, stained for markers of T-helper subsets and the CCL20-responsive homing receptor CCR6.

To characterise the gut or CNS homing potential of the splenocytes from the infected or uninfected EAE mice, cells were stained for co-expression of CD4 with a subtype-specific transcription factor (Th1: Tbet, Th2: GATA3, Th17: RORγT, or Treg: FoxP3) to identify T-helper subtype. Cells were also stained for the cell surface chemokine receptor CCR6. Dots represent individual mice; bars denote the group median; error bars represent the interquartile range. Šídák's ANOVA; *p=0.06* (n.s.)

As anti-inflammatory immune responses can suppress the effector response, the major cellular sources of IL-10 production were investigated within the spleen. IL-10+ events were gated by co-expression of the main lineage-defining markers, CD4 (T-cell), CD19 (B-cell) and CD11c (dendritic cells). Dendritic cells were gated on CD4- and CD19- events. There was no difference in either the total frequency of splenocytes expressing IL-10, nor differences in the proportion of T-cells, B-cells, or CD11c cells positive for IL-10 between any of the groups (*Figure 40*). The major producers of IL-10 in the spleen were CD19+ B-cells, which represented 50-60% of IL-10-producing cells. Tregs, defined here as CD45+CD4+IL-10+ cells, accounted for 10-20% of IL-10-producing cells in the spleen. Insufficient cells were extracted from the spinal cords to quantify IL-10 expression between subsets in CNS infiltrate.

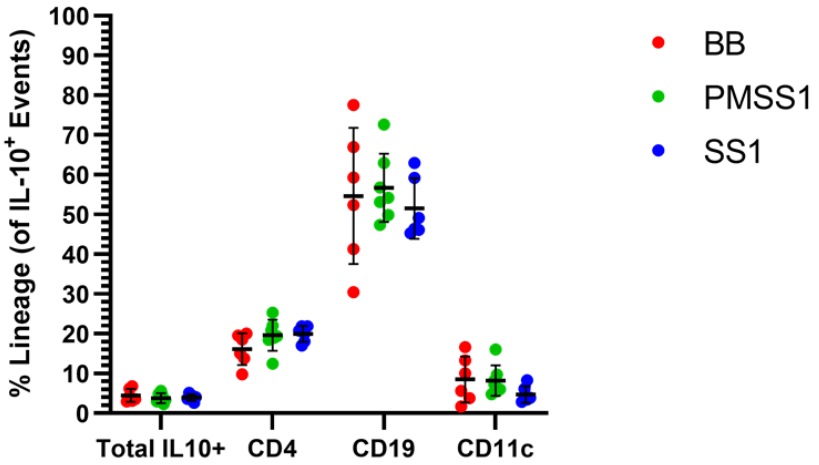

Figure 40 *Cellular sources of IL-10 within the spleen of H. pylori-infected or uninfected mice*

Splenocytes were analysed for IL-10 production by flow cytometry. Dead cells, debris, and doublets were excluded from the analysis. The percent of total gated cells expressing IL-10 is shown. Of T-cells, B-cells, and dendritic cells gated by the expression of cell surface markers CD4, CD19 and CD11c, respectively; the percentage of each of these lineages producing IL-10 are plotted. Dots represent individual mice; lines denote the group median; error bars show the interquartile range.

Cells extracted from the spinal cord were analysed in a similar manner, but with inclusion of CD45 to identify leukocytes in the non-lymphoid complex mixture. Total cell numbers per spinal cord, or CD45+CD4+ number per spinal cord were comparable between groups (*Figure 41*). There was an elevation in the frequency of $CD45^+$ cells in the spinal cords of both the PMSS1 and SS1 infected groups as compared to the sham-treated infection control group (*Figure 42; A*). This elevation was slight (around 1.4-fold, n.s.). Gating on just these $CD45^+$ events, there was no difference in the frequencies of $CD4^+$ T-cells, $CD19^+$ B-cells, $CD11c^+$ dendritic cells (*Figure 42; B-C*).

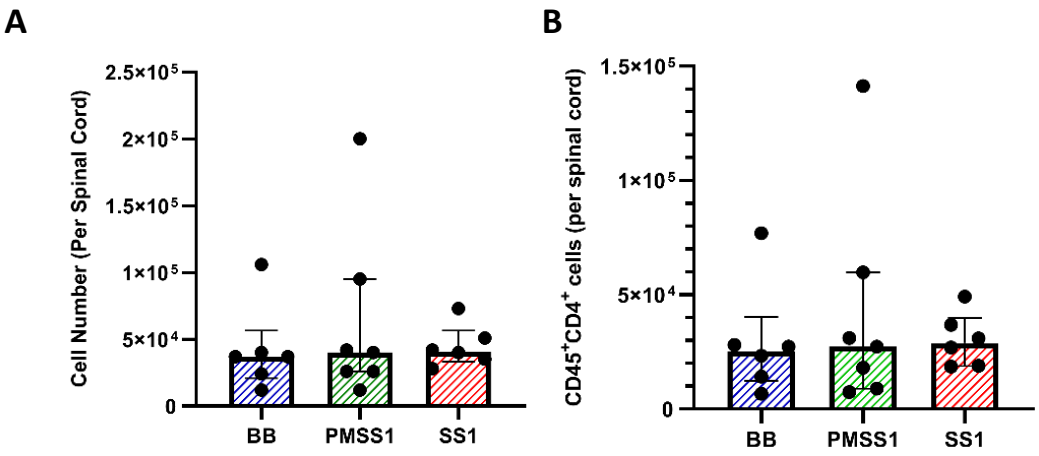

Figure 41 *Total cell numbers, and CD45+CD4+ lymphocyte numbers extracted from the spinal cords of EAE mice either infected with H. pylori strain PMSS1, SS1, or uninfected controls.*

Spinal cord cells from *H. pylori* infected or uninfected EAE mice were counted using Trypan blue exclusion of dead cells. Cell numbers per spinal cord are plotted. Dots show the individual mice; bars represent the group median; error bars denote the interquartile range.

The T-helper subtypes Th1, Th2, Th17 and Treg lineages were defined as $CD45^+$ cells co-expressing CD4 with a respective signature cytokine. There were no differences apparent between groups in the frequency of Th1, Th17 or Treg subtypes (*Figure 42; E-H*).

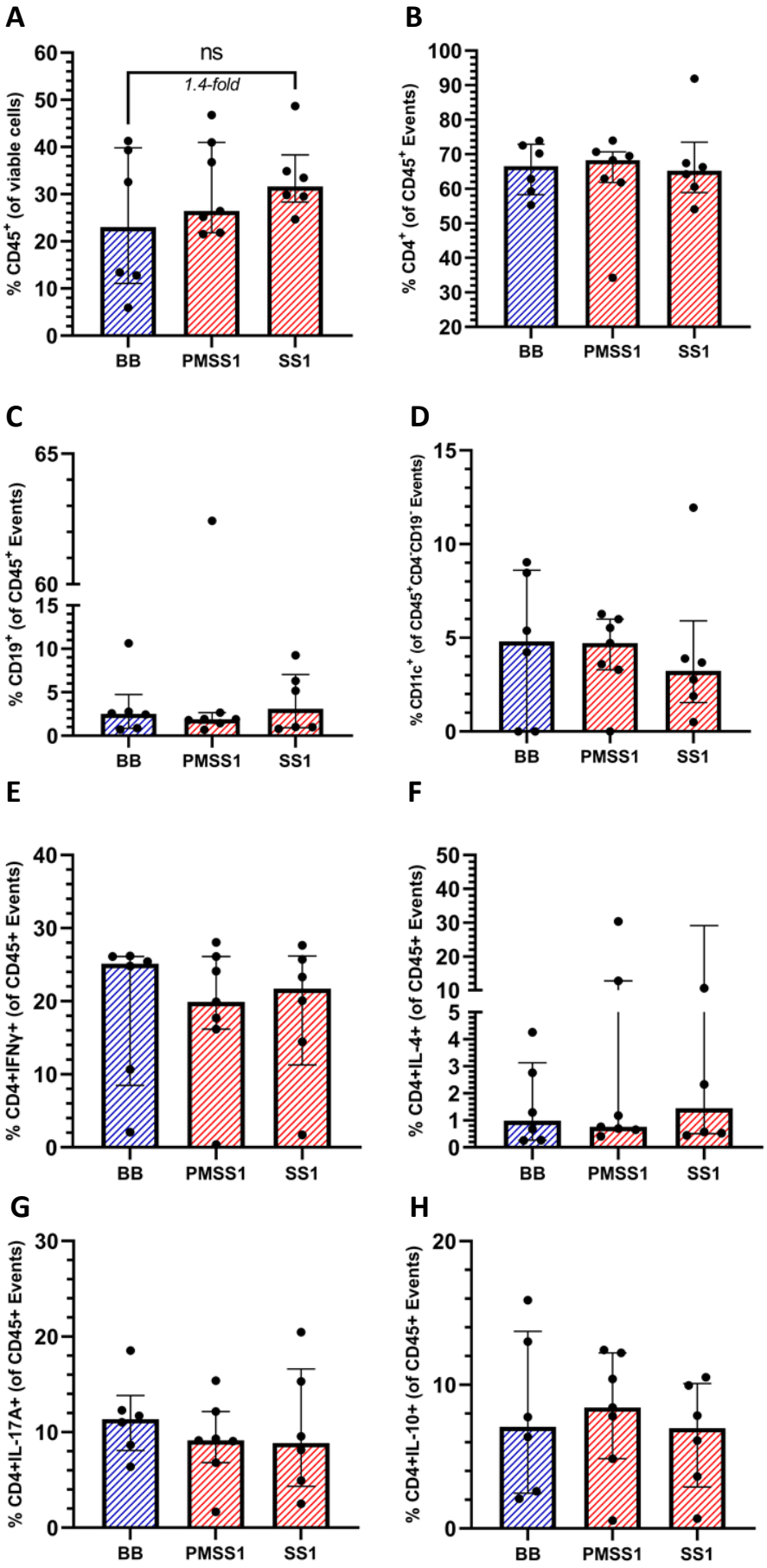
A
ns
1.4-fold
% CD45+ (of viable cells)
BB
PMSS1
SS1
B
% CD4+ (of CD45+ Events)
C
% CD19+ (of CD45+ Events)
D
% CD11c+ (of CD45+CD4-CD19- Events)
E
% CD4+IFNγ+ (of CD45+ Events)
F
% CD4+IL-4+ (of CD45+ Events)
G
% CD4+IL-17A+ (of CD45+ Events)
H
% CD4+IL-10+ (of CD45+ Events)

Figure 42 Flow cytometry analysis of lymphocyte frequency in the spinal cords of H. pylori infected or uninfected EAE mice.

EAE was induced in groups of 8 mice infected with either *H. pylori* strain PMSS1, SS1, or sham-infected controls. Upon termination of the experiment at 20 d.p.i. spinal cords were extracted, and cellular solutions were processed for flow cytometry staining of cell surface and intracellular markers. Lymphocytes were gated by forward and side-scatter characteristics. Dead cells, debris, and doublets were excluded from the analysis. Frequency of each marker is expressed as a percentage of total CD45+ lymphocytes. Cells were stained for markers of lymphocytes, CD45 (A); T-cells, CD4 (B); B-cells, CD19 (C); dendritic cells, CD11c (D), and the signature cytokines for the Th1, Th2, Th17 and Treg subsets, IFNγ (E), IL-4 (F), IL-17A (G), and IL-10 (H). Dots represent individual mice; bars represent the group median; error bars denote the interquartile range.

As the frequency of lymphocytes may remain constant despite changes in the overall scale of the CNS infiltrate, the total cell numbers for each of the investigated lineages were calculated from the total counts derived from tissue and the relative frequency determined by flow cytometry analysis (*Figure 43; A-G*). Of the signature T-helper cytokines quantified, no significant differences were observed between groups to explain the reduced cumulative disease severity.

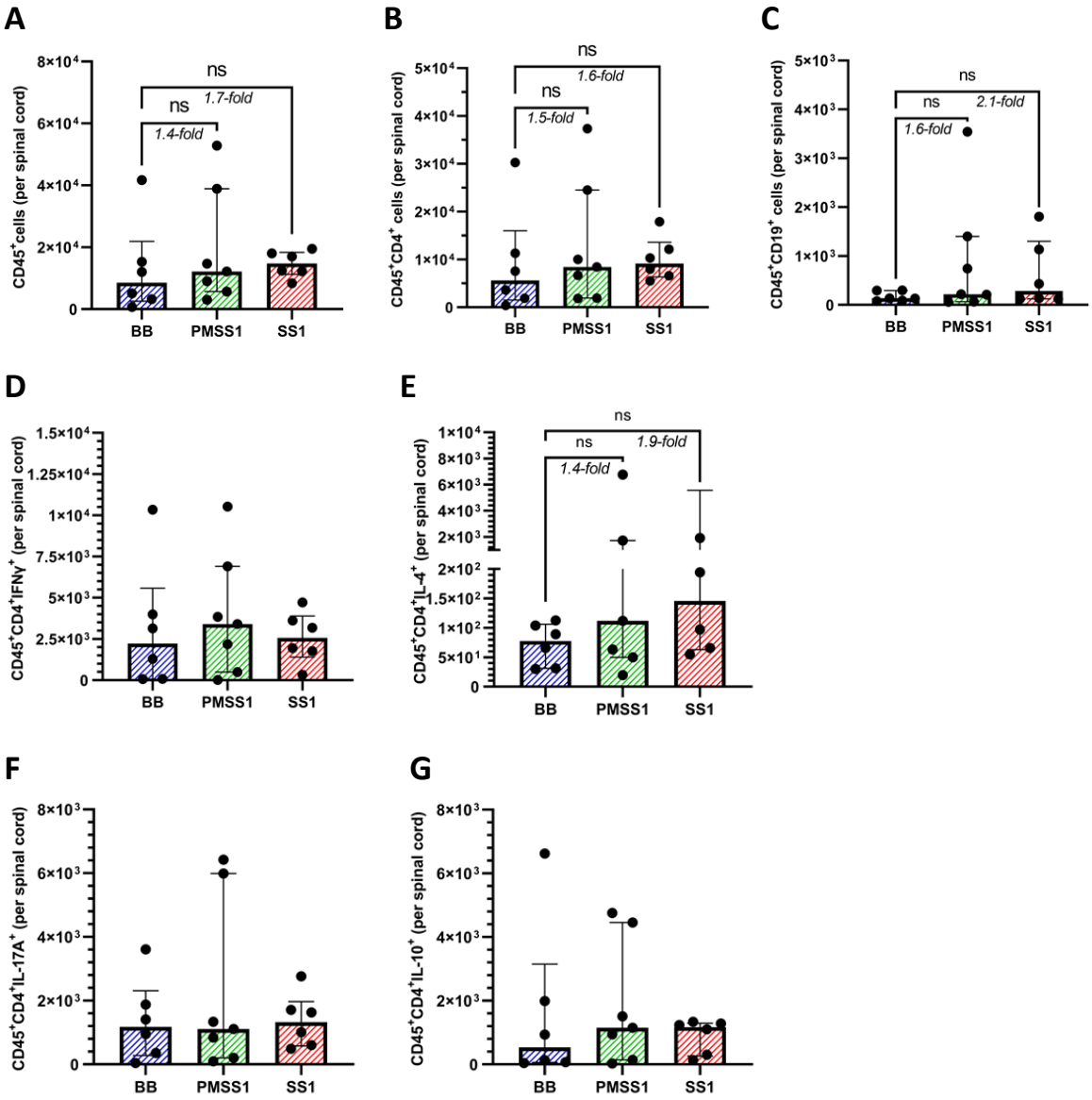

Figure 43 Absolute cell numbers of lymphocytes infiltrating the spinal cord of H. pylori PMSS1-infected, SS1-infected, or uninfected EAE mice.

The number of lymphocyte lineages infiltrating the spinal cord in *H. pylori* PMSS1 and SS1-infected, or uninfected EAE mice was quantified by flow cytometry and calculated against the total number of cells derived from tissue to give absolute cell numbers per spinal cord. Lymphocytes were gated by forward and side-scatter characteristics and stained positive for CD45. Dead cells, debris, and doublets were excluded from the analysis. Frequency of each marker is expressed as a percentage of total CD45+ lymphocytes. Cells were stained for CD45+, $CD4^+$ (CD4 T-cells), CD19 (B-cells), in addition to the signature cytokines of the T-helper lineages; Th1 (IFNγ), Th2 (IL-4), Th17 (IL-17A), and Treg (LI-10). Dots represent individual mice; bars represent the group median; error bars denote the interquartile range.

The expression of the cellular communication network protein 3 (CCN3) has been reported to stimulate CNS regeneration and remyelination with relevance to MS and

EAE [234], discussed in detail in chapter 5. Therefore, I hypothesised that CCN3 may be involved in the period of remission observed in the SS1-infected group. If CCN3 was differentially expressed between groups and influences disease severity then there may be a measurable difference between the BB and SS1 groups, where the greatest divergence of EAE clinical scores was apparent. In the first instance, I measured CCN3 concentration from plasma collected from naïve or EAE mice from the previous pilot study, and from stimulated CD4 supernatants derived from the uninfected and *H. pylori* SS1-infected groups in the current study.

CCN3 was reduced 2-fold in the EAE mice as compared to naïve untreated mice (*Figure 44; A*). Plasma was not collected in this study, however stimulated CD4 supernatants were produced, but CCN3 was not detected above the sensitivity of the ELISA kit in any samples tested (not shown). As CCN3 was not detectable from supernatants, but was present in murine plasma, CD4 cells were collected from culture and RNA was extracted for RT-qPCR. *Ccn3* mRNA expression (relative to *Gapdh*) was comparable between infected and uninfected EAE mice in supernatants after a 3-day stimulation. After a subsequent round of stimulation *Ccn3* mRNA was elevated in both groups (BB: 3.6-fold, n.s.; SS1: 6-fold, *p=0.0034*). Between the infected and uninfected groups, after 2 rounds of stimulation there was 1.9-fold higher (n.s.) expression of *Ccn3* mRNA in the *H. pylori* SS1-infected EAE group as compared to uninfected EAE mice (*Figure 44; B*).

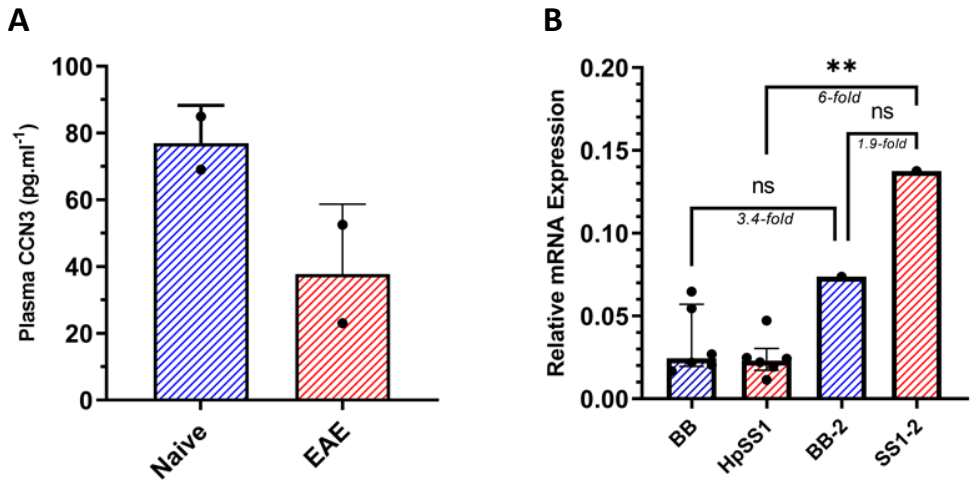

Figure 44 Abundance of CCN3 in plasma and CD4 cell supernatants from H. pylori-infected or uninfected mice with or without EAE

(A) CCN3 concentration in plasma was determined between naïve and EAE mice (without *H. pylori* infection). (B) From the current EAE study with concurrent *H. pylori* infection, $CD4^+$ cells were purified from the spleens of SS1-infected (SS1) or uninfected (BB) EAE mice, pooled within each group, and stimulated with anti-CD3/CD28 antibody for 3 days before being re-plated for a further 3 days with stimulation. Supernatants were collected and used to quantify CCN3 by ELISA. Cells were collected for RNA extraction to quantify *Ccn3* by RT-qPCR. *Bars represent the group median; error bars denote the interquartile range; Tukey's test ** p= <0.005*

3.3.4 – Does the severity of EAE influence the immune response in CNS tissue?

The severity of EAE should correlate to the accumulation of inflammatory CNS-infiltrating cells. Lymphocytes from the spinal cord were stratified according to EAE severity score irrespective of infection status (*Figure 45; A-H*).

With higher EAE scores there was an elevation of CD45+ cell frequency from <28% in mice with an EAE severity score of 0-1, rising to 40% at a score of 3 (n.s.). There were no differences in the frequency of $CD4^+$ cells amongst gated CD45+ events. No significant changes were observed for CD19+ B-cells. In mice with no observable EAE symptoms with a score of 0, there was <0.5% of cells expressing the dendritic cell marker CD11c whilst this rose markedly 10-fold in all mice with an EAE score assigned between 1-3 (n.s.).

There was no change in the total frequency of $CD4^+$ cells in parallel with EAE severity, however the proportions of these $CD4^+$ cells expressing the markers for the major T-helper subsets were differential when quantified. In mice with a score of zero, there was an elevation from a median frequency of $CD4^+$IFNγ+ (Th1) cells from 10%, to 20% at a score of 1 and 25% with scores of both 2 and 3 (n.s.). There was a concurrent drop in the frequency of $CD4^+$GATA3+ (Th2) cells from a median 7-8% frequency with a score 0, dropping to <1% in all mice with an assigned EAE score of 1-3 (n.s.). Interestingly, there were no substantial changes in the frequency of $CD4^+$IL-17A+ (Th17) cells according to EAE score. Somewhat counter-intuitively, there was a significant linear trend observed in the frequency of $CD4^+$IL-10+ (Tregs), for which the frequency increased according to EAE score from 3% at score 0; 7% at score 1; 10% at score 2; and 13% at score 3 (*p=0.026*). A similar analysis using splenocytes returned no notable differences in any of the cellular markers quantified according to the severity of EAE (data not shown).

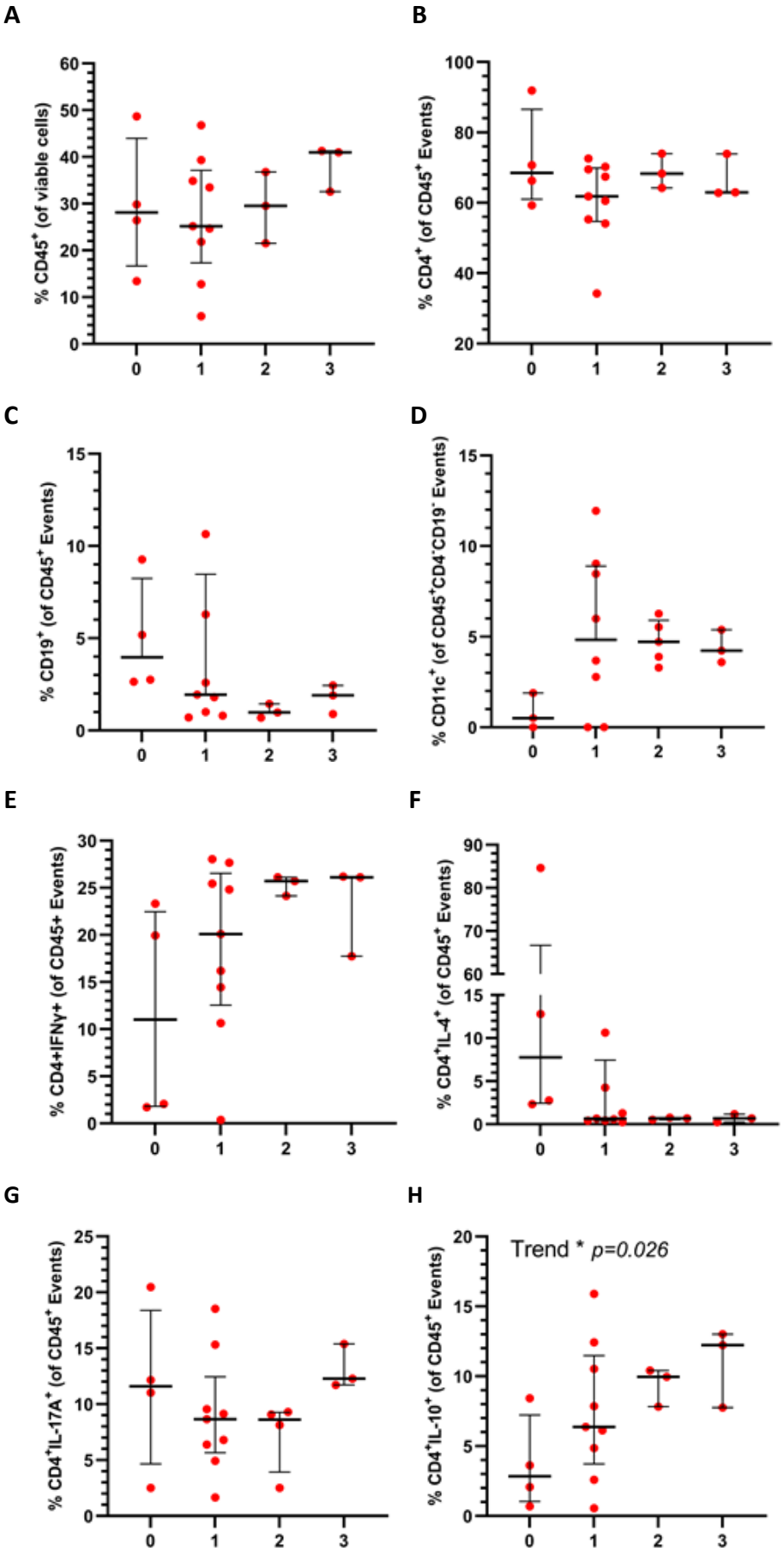
A
% CD45+ (of viable cells)
B
% CD4+ (of CD45+ Events)
C
% CD19+ (of CD45+ Events)
D
% CD11c+ (of CD45+CD4-CD19- Events)
E
% CD4+IFNγ+ (of CD45+ Events)
F
% CD4+IL-4+ (of CD45+ Events)
G
% CD4+IL-17A+ (of CD45+ Events)
H
% CD4+IL-10+ (of CD45+ Events)
Trend * p=0.026

Figure 45 CNS-infiltrating lymphocyte frequency stratified to EAE severity

Cell subsets present in the spinal cords of EAE mice were analysed using flow cytometry. Lymphocytes were gated by the expression of CD45; T-cells by the expression of CD45+CD4+; B-cells, CD45+CD19+; dendritic cells, CD45+CD4-CD19-CD11c+. T-helper subtypes were characterised by the co-expression of CD45+CD4+ and a signature cytokine (Th1: IFNγ; Th2: IL-4; Th17: IL-17A; Treg: IL-10). Lines represent the group median; error bars denote the interquartile range. ANOVA; ** p= <0.05*.

3.3.5 – The influence of *H. pylori* infection on spinal cord infiltrating leukocytes in EAE mice

For *H. pylori* to mediate a protection from EAE, it was hypothesised that there should be reductions in the CNS infiltrate in infected animals. The proportion of lymphocytes infiltrating the CNS was stratified to *H. pylori* infection status, irrespective of EAE score (*Figure 46; A-H*). There were only modest differences observed. There was a small increase in the frequency of CD45+ cells infiltrating the CNS in *H. pylori*-infected as compared to uninfected mice, *Hp*-: 22% c.f. *Hp*+: 30% (n.s.). The proportions of $CD4^{+}$IFNγ+ and $CD4^{+}$IL-17A+ (Th1 and Th17) cells infiltrating the CNS were modestly reduced in the *H. pylori*-infected EAE animals as compared to uninfected; Th1: Infected, 25% c.f. Uninfected, 20% (n.s.); Th17: Infected, 12% c.f. Uninfected 7% (n.s.). These small differences are unlikely to be clinically relevant. There were no notable differences in any of the markers analysed according to infection status (data not shown).

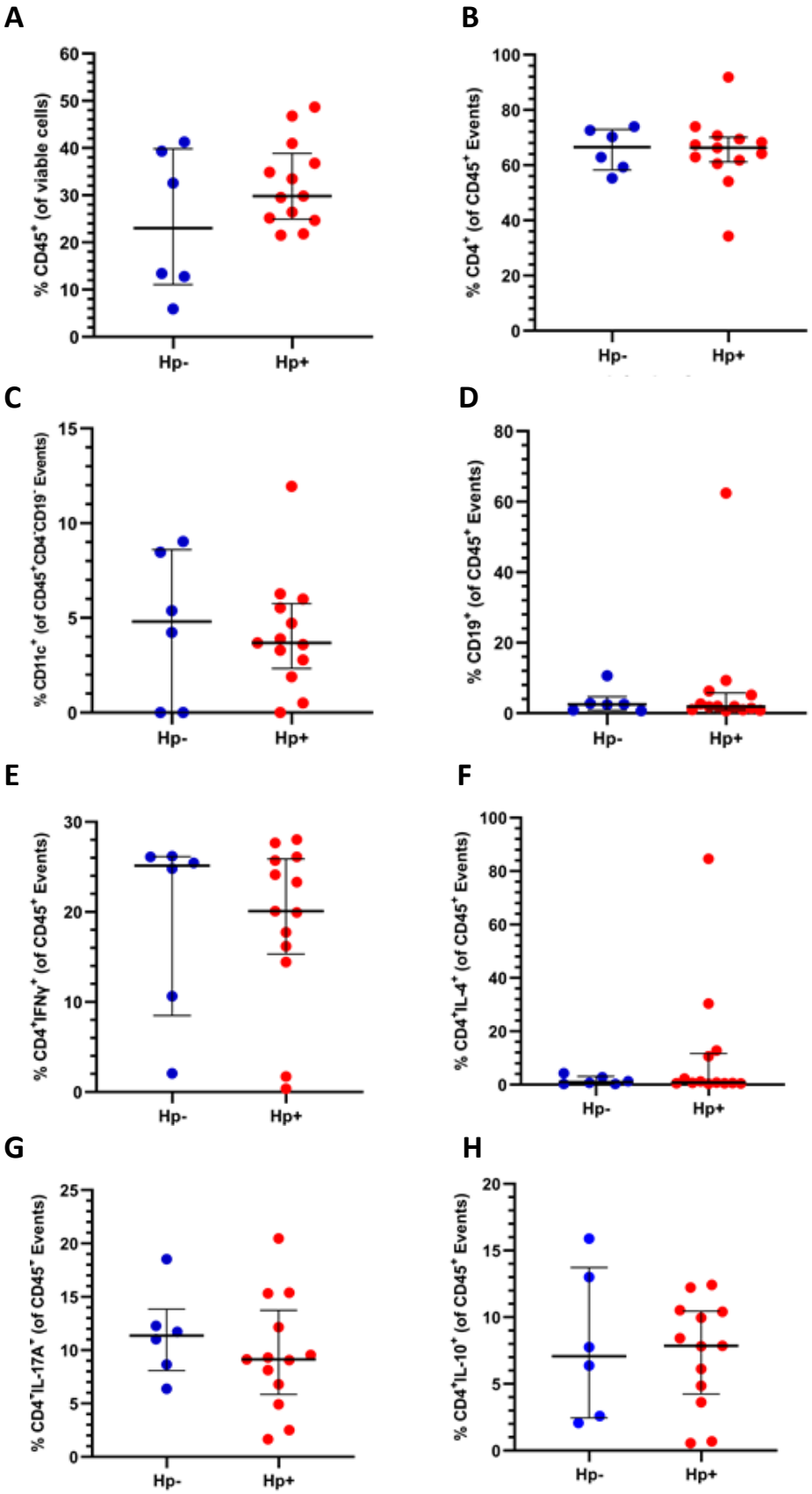
A
% CD45+ (of viable cells)
B
% CD4+ (of CD45+ Events)
C
% CD11c+ (of CD45+CD4-CD19- Events)
D
% CD19+ (of CD45+ Events)
E
% CD4+IFNγ+ (of CD45+ Events)
F
% CD4+IL-4+ (of CD45+ Events)
G
% CD4+IL-17A+ (of CD45+ Events)
H
% CD4+IL-10+ (of CD45+ Events)
Hp-
Hp+

Figure 46 Flow cytometry quantification of CNS infiltrating leukocytes in EAE mice stratified by H. pylori infection status

Spinal cord lymphocytes were characterised from EAE mice either infected with *H. pylori* or uninfected controls using flow cytometry. The *H. pylori* infected group consists of mixed *H. pylori* SS1 And PMSS1 infected animals. Dead cells, debris and doublets were excluded. From single viable cells, frequency is assigned as the percent of total CD45+ cells. Cells were stained for surface markers (A) CD45+; (B) CD4 (CD4 T-cells); (C) CD11c (dendritic cells); (D) CD19 (B-cells). T-helper subtypes were characterised by the co-expression of CD45+ $CD4^+$ with; (E) IFNγ (Th1); (F) IL-4 (Th2); (G) IL-17A (Th17); and (H) IL-10 (Treg) Dots represent individual mice; lines denote the median; error bars show the interquartile range.

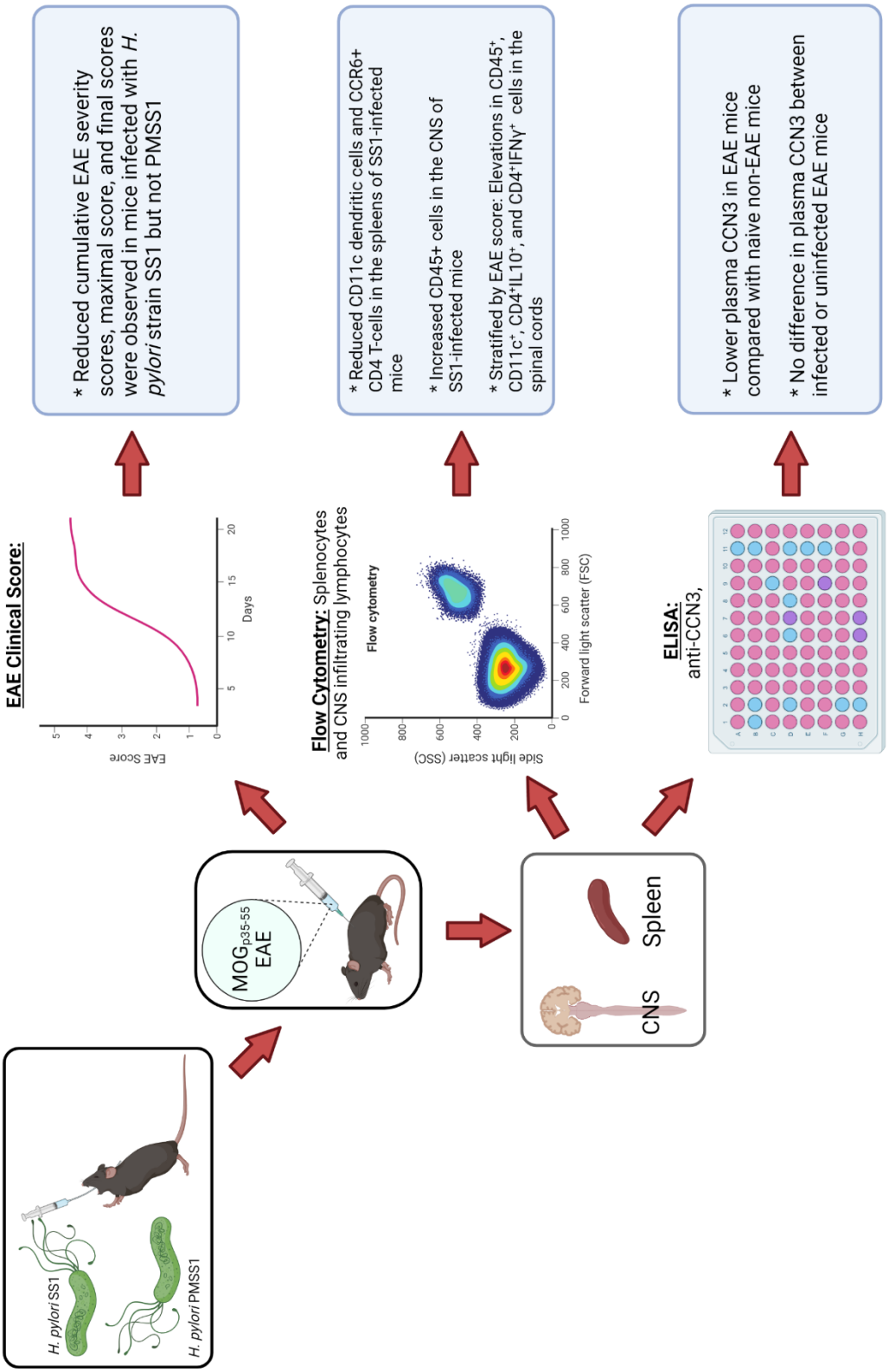

Figure 47 Schematic representation of the EAE study design and summary of the data generated

Mice were infected with either the SS1 or PMSS1 *H. pylori* strains prior to EAE induction. Mice were assessed daily and EAE severity scores recorded. At the endpoint, spleen and spinal cord were harvested for flow cytometry analysis of cellular populations. CCN3 concentration in plasma was quantified by ELISA between naïve or EAE mice. Figure created with BioRender.

3.4 – Discussion

A graphical summary of the study and data generated is shown in *Figure 47*.

3.4.1 – Summation of the major findings

- The pilot study found that $CD4^+$ cells, CD11c+ dendritic cells and F4/80+ macrophages were elevated substantially in the CNS of EAE mice as compared to non-EAE mice.

- In the main EAE study increasing EAE severity was associated with modest elevations of Th1 cells and CD11c dendritic cells, but not Th17 cells.

- The frequency of IL-10-producing $CD4^+$ cells (Tregs) elevated in parallel with increasing EAE severity scores in the CNS. The proportion of these cells was found to have a statistically significant correlation with increasing EAE scores.

- *H. pylori* infection status did not alter the proportion of Tregs in the CNS or spleen

- I observed a *H. pylori* SS1 strain-dependent effect of reducing the cumulative EAE severity scores.

- The reduced EAE severity observed was not coupled with any notable differences in lymphocyte frequencies in the CNS of EAE mice between infected or uninfected groups, nor between *H. pylori* strains.

- I did not reproduce the previous findings of Cook *et al.*

3.4.2 – Pilot EAE Experiment

In the first instance, I conducted a pilot EAE experiment without a concurrent *H. pylori* infection. The purpose of this study was twofold; firstly, it was necessary to ascertain that the protocol for EAE induction using new batches of adjuvant was successful prior to a larger-scale experiment; secondly, it would inform us of the nature of immune responses and whether the findings agreed with the published

literature. I quantified the major cellular lineages CD4, CD8, CD19, F4/80, and CD11c, but not T-helper subsets.

The EAE model used in this study is an established and well characterised model [272]. The consensus from the literature of the kinetics of EAE are for a predominantly $CD4^+$ T-cell-driven model with robust neutrophil, monocyte macrophage, and dendritic cell-mediated inflammatory and neurotoxic component [272,391,392]. The model is consistent in its' kinetics, which were characterised in detail by Caravagna *et al.* [402]. They reported elevated numbers T-cells and neutrophils in the blood at day 3, peaking at day 6, and subsiding after day 10, concurrently with accumulations in CNS tissues. CNS infiltrates initially consist of predominantly $CD4^+$ T-cells, dendritic cells, and macrophage lineages, following $CD4^+$ T-cell reactivation within the CNS and further blood-brain barrier disruption [392]. Axonal damage and clinical severity correlate to the scale in CNS infiltration of these cells and an activation of CNS-resident microglia [392,402,403]. Indeed, it was observed in this study that the development of severe EAE was associated with increased $CD4^+$ cell infiltration into the spinal cord. Predominantly $CD4^+$ T-cell, macrophage, and dendritic cell markers were elevated in the spinal cords of EAE mice. This supports the accepted hypothesis that these cell types are the major drivers of the model. The lymph nodes were enriched in CD19+ B-cells to the greatest extent, although I did not characterise the humoral anti-MOG responses in this study, a persistent antibody response is present [334,402].

When quantifying cellular lineages from tissues post-mortem, the spinal cords of EAE mice contained increased proportions of $CD4^+$ cells; an increase from baseline of 14-fold. Alongside this there were substantial elevations of F4/80+ macrophage and CD11c+ dendritic cells observed in parallel. The increased frequency of these cell types is in line with the consensus of the literature [269,272,391,402,403] . One mouse in the EAE group developed rapid and severe EAE resulting in early termination from the study. Interestingly, this mouse presented with a further increased frequency of CD4 cells in the CNS compared to the remainder of the EAE group, in addition to a reduced Treg:Teff ratio. Although no conclusions can be drawn from a single mouse, it is indeed expected that a higher number of lymphocytes infiltrating the CNS would be

associated with a more severe clinical presentation of EAE, and it is documented in the literature that inadequate Treg responses contribute to EAE pathogenesis [225,231,341].

When analysing the spleen and lymph nodes (LN), reductions in the relative frequencies of both $CD4^+$ and CD8+ cells in both tissues were noted. In the spleen, the frequency of all markers quantified was reduced in the EAE group. This may likely be a result of the efferent migration of cells from the spleen to the target compartments, which I see in our data.

As well as validating the use of the EAE model in our hands, these pilot data indicated that the $CD4^+$ cellular response is the major effector of EAE pathogenesis, at least in the context of adaptive cellular immunity.

3.4.3 – Immunomodulatory potential of *H. pylori* Infection in the Course and Severity of Experimental Autoimmune Encephalomyelitis

Previously published data from this research group was the first to report a reduction in EAE clinical scores in mice harbouring a gastric *H. pylori* infection [334]. The study reported a suppressed EAE severity score, and a marked reduction of $CD4^+$ Th1 and Th17 cells infiltrating the spinal cord of infected EAE mice as compared to uninfected EAE mice. This current study aimed to both confirm the previous findings and expand on this by assessing strain-specific variance in the protective effect between *H. pylori* strains SS1 and PMSS1. These two *H. pylori* strains differ in one major respect, by the presence of a functional *cag*PAI in strain PMSS1, and a non-functional *cag*PAI in strain SS1. Strains secreting CagA are more virulent, induce augmented inflammatory T-cell responses, peptic ulcer disease, and predispose to gastric cancer development [57]. On the other hand, previous work by both this research group and others found the more virulent CagA+ infecting strains also provided a greater level of protection from excessive immune responses, mediated through Tregs and IL-10 [21,24,219]. Infected mice may exhibit an altered course or attenuated severity of EAE, and those mice colonised with PMSS1 may mount a more robust immune response, importantly including the suppressive IL-10-secreting Tregs, and as such may confer a greater protection against EAE.

I hypothesised that I may observe reductions in EAE severity in the infected groups and aimed to perform detailed characterisation of the immune response. Reduced cumulative severity scores may indicate that there is a resistance to EAE development in the infected mice. This would infer that the first observable symptoms of EAE may be delayed as compared to the uninfected EAE mice. However, although both the infected groups did have a delayed day-of-onset (DoO) this was of just 1 day (Uninfected: median DoO, 8.5 d.p.i.; both PMSS1 and SS1-infected groups: DoO, 10 d.p.i.)

This is comparable to that observed in the previous study, and with expectations from the literature [272,402]. Protection from EAE severity is not necessarily associated with delayed onset, indeed, our previous study did not observe this [334]. The peak severity of EAE was reached between day 14-17, with all groups comparable in EAE severity, which reached a modest 1.5 mean score across all the groups. I hypothesised a reduced severity for *H. pylori* infected mice. However, for the uninfected EAE mice this was lower than the expected outcome and disagreed with previous findings which demonstrated a differential course between infected and uninfected EAE mice [334].

For this study, the dose of MOG used in the immunisations was lowered to 250ng from the 300ng used in the previous study. However, Aharoni *et al.* [404] have reported on the effects of titrating MOG concentration used in the EAE model and suggest that as low as 100ng is sufficient to induce a disease course comparable with the higher doses. In fact, it was only concentrations as low as 5ng which resulted in reduced peak scores. Rangachari *et al.* [405] suggest that doses of 200ng are sufficient for standard chronic non-remitting EAE induction, however report that doses of around 50ng can result in suppressed peak severity and even the presentation of relapses more like the PLP/SJL Relapsing-Remitting EAE model. Taken together it is unlikely that the slightly reduced dosage of MOG peptide used here would have been a causative factor in the stunted disease course which was observed.

3.4.4 – Differential cellular immune responses to EAE consequential of *H. pylori* infection.

I investigated whether the frequency of $CD4^+$ T-cell subsets was different between the infected and uninfected groups in either the spleen or CNS. Stronger Treg responses have been suggested as contributing to *H. pylori*'s protection from other diseases as discussed previously, and inadequate suppressive function of Tregs can exacerbate EAE and MS severity [225,226,230]. However, neither the study of Cook nor the current study found differences in FoxP3+ Tregs or IL-10-secreting $CD4^+$ cells in the spinal cords to explain the protection from disease severity. I did not observe a notable difference in the proportion of the Th1 or Th17 subsets, nor were there differences in the total cell number in the spleens to suggest a larger scale response. In the spinal cords, very few cells were recovered and were stained positive for Trypan blue. Given the poor recovery of cells it was not possible to know with confidence if numbers were accurate, but the percentage frequency won't inform of an increase in overall number. This is an unusual finding as both these cellular lineages are frequently reported in the literature to increase in the CNS and contribute a major driving force to the propagation of disease. Furthermore, there were astounding reductions of these lineages in the work of Cook [334], whereby these inflammatory subsets were reduced 2-fold in the CNS and nearly 20-fold in the spleens of *H. pylori* infected EAE mice. It may be that the frequency of subsets is constant but that the scale of the immune response is greater, leading to higher absolute cell numbers infiltrating the spinal cord. However, these data did not suggest differences in absolute cell counts between groups to support this.

3.4.5 – Differential cellular immune responses stratified by disease severity.

Stratifying these data to EAE score, there were non-significant trends for higher numbers of CD45+ cells, IFNγ-producing Th1 cells, and CD11c+ dendritic cells infiltrating the spinal cord in mice with higher EAE severity (as reported for the model by others [402,403]). Interestingly IL-10-producing Treg cells also followed this trend. The elevation of Th1 cells was opposed by a decline in Th2 cells, as is expected from the literature and the general Th1/Th2 dichotomy. Th17 cells are thought to be important drivers of EAE, however no difference in Th17 cells was observed per EAE

score in this study. This contrasts with the literature, as IL-17-producing $CD4^+$ cell responses are found higher in instances of more severe disease and with accumulation of these activated T-helper cells in the CNS [277].

The most notable of these differences were a 10-fold elevation in CD11c dendritic cells with EAE score 1-3 (similar across all scores) as compared to asymptomatic mice (score 0). Dendritic cells expand in the meninges and are recruited from blood during EAE, their numbers are correlated to severity [403]. In contrast, DC subtypes can promote tolerance and secrete anti-inflammatory IL-10 and TGFβ to suppress EAE [406]. I define DCs here as CD45+CD11c+ cells of the CD4- and CD19- lymphocyte populations. Of course, it must be noted that CD11c can also be expressed by CNS microglia upon activation as occurs during EAE [407].

Interestingly the only statistically significant difference observed was that of IL-10-producing $CD4^+$ Tregs, which were elevated in the spinal cord infiltrate in parallel with increased score, to a 4-fold increase at EAE score of 3 compared with 0. The consensus from the literature is that IL-10 elevations in the CNS are associated with a period of remission [408], and others demonstrate that CD4+IL-10+ cells in the CNS result in a suppression of inflammatory T-cell activity [409]. It could be supposed that the elevation of IL-10-secreting $CD4^+$ T-cells observed in this study could be a factor in the mild EAE severity observed. However, this would conflict with the trend for increasing LI-10 with increasing clinical score. Furthermore, there were no concurrent reductions in the inflammatory subtypes (Th1 and Th17) to further support this premise. Indeed, I hypothesised that Tregs may be elevated in *H. pylori* and play a role in the mitigation of disease severity, however I found no difference between infected or uninfected groups in this regard.

I did observe reductions in the cumulative EAE severity in the SS1-infected group as compared to both the PMSS1 group and control group. These data indicate that *H. pylori* strain SS1 had a more pronounced effect on the course of EAE than PMSS1, contrary to the hypothesis. Despite this deviation in the clinical course of disease my data did not find candidate cell types as a mechanism to explain this.

Interestingly, after peak EAE severity was reached, both the control and PMSS1-infected group remained at a similar severity through day 21 to the study endpoint. However, the SS1-infected mice appeared to display a physical reduction in the burden of paralysis, as measured by reducing EAE scores (from 1.5 to 0.8). It is not uncommon to see periods of slight recovery in the MOG-EAE model in C57BL6 mice [402], such as the superimposed periods of remission in MS. What is more noteworthy is that this was only the case in the SS1-infected EAE group. There are no other studies in the literature to my knowledge assessing the effect of different *H. pylori* strains on the clinical manifestation of EAE from which to compare these novel data. However, there is evidence of strain-specific effects on other immunological diseases such as allergy and asthma. Published work from this research group [219] found that the more virulent CagA+ *H. pylori* strains conferred a greater inhibition of IgE responses. Arnold *et al.* reported a similar scenario in experimentally induced asthma [20]. These studies suggest Tregs, and IL-10 are primary mediators in the mechanisms, however I did not observe such differences in the immune responses in this study to explain the current results. As I discussed in chapter 5, there is a potential for remyelination and repair to occur which may be able to investigate this protective and regenerative effect further.

3.4.6 – Evaluation, critique, and considerations for future work

One variable often underappreciated in the comparison of EAE scores from studies in the literature is the heterogenicity of the scoring systems used in different laboratories. For instance, I used a 0.5 increment system adapted from the 1-point increment system detailed in O'Brien 2010 [410]. The definition of each score/increment is variable between labs, for instance some count loss of tail tonus for the entire tail length, whereas some just for the proximal portion. There is also a high risk of potential subjective bias by the researcher performing the scoring. The variability in such scenarios has been reviewed by Takeuchi *et al.* [411].

The use of the EAE model is not without ethical concerns, currently it is generally agreed to be the best model for the study of MS. Nonetheless, it also presents a considerable burden to the animals used in these studies. Perhaps in future to best

assure the production of high-quality data from these studies, it may be of benefit to counter-intuitively increase group sizes in contrast to the general desire to reduce the numbers in accordance with the 3 R's. Fewer studies, consisting of larger groups would yield bigger datasets which would be protected somewhat from the detriment of losing some of the group early prior to the study endpoint. I noted drop-out rates of up to 20% of each group for the current study and 30% from the pilot study.

In terms of future optimisations to the methodology, I would consider longer initial *H. pylori* infection incubation periods. In this study, as with previous studies of this nature, after administration of *H. pylori* inoculum the mice were kept for 3 weeks to establish infections. In this study, as with some previous work, no difference in lymphocyte populations have been observed in the spleens. However, the infections performed in chapter 4 (migration study) and chapter 5 (remyelination study) were allowed to persist for 10-12 weeks, and statistically significant differences in splenocyte lineages were indeed observed.

EAE was induced in most of the mice, however they developed a clinically milder presentation than in the previous pilot study. This may have been mediated through microbiological differences in the mice. Importantly, it has been shown in the work of others that alterations in the composition of the murine gut microbiota, either through experimental selective colonisation, or indeed in germ-free models can have profound effects on the kinetics and severity of EAE. For instance, Gandy *et al.* reported differential relative abundances of *Bacteroidetes*, *Firmicutes*, and *Akkermansia* in EAE models [412]. Johansen *et al.* reported reductions in the ratio of *Lactobacillus* to *Clostridiaceae* after EAE induction [413]. Shahi *et al.* showed that colonisation with *Prevotella histocola* can mitigate the severity of EAE on a comparable scale with the leading pharmaceutical interventions of IFNγ and glatiramer acetate (GA). Berer *et al.* also further demonstrated the importance of the microbiota in EAE and MS by transferring microbiota from human MS patients to germ-free mice. Microbiota from the MS patients induced spontaneous EAE development in the recipient mice which did not occur of transferring microbiota from non-MS twins. Changes in the relative abundances of *Sutterella* and *Akkermansia* were identified between these microbiomes [321]. Indeed, the literature

is rich in evidence of a strong link between the microbiome and MS/EAE, for which conclusive mechanisms are noticeably absent.

In this regard, a potential reason for the inadequate exacerbation of EAE after induction in this study could indeed be due to the microbiota of the mice. Although specific pathogen free, of the same age and from the same supplier, the mice are not guaranteed to have a comparable microbiota between experiments. This is known to be readily modified with chow, housing, and supplier, although these variables were consistent in my experiments. Differences in the microbiomes of laboratory animals between different facilities is expected. However even when purchased from the same supplier it cannot be discounted that differences exist which may lead to a lack of reproducibility in animal disease models, especially those diseases inherently influenced by the microbiota [414]. It has been well reported that modifications to the microbiota, both in humans and in mice can have a profound impact on the severity or course of EAE or MS [321,324,325,412,413]. This supposition cannot be investigated as characterisation of the murine microbiomes was not performed in the work presented here, nor in the previous EAE study in the published work of Cook *et al.* for comparison. This confounding variable could be overcome by using mice with controlled microbiotas, or by characterising the microbiota experimentally as part of the study design in future work.

It may have been of benefit to test the *H. pylori* strains used in the original inoculum for viability. Bacteria were used freshly prepared from plates, and only taking colonies from around the edge of the growth to maximise viable cells. However, as I failed to culture *H. pylori* from the majority of the PMSS1 infected groups' gastric tissue it would be a useful reference to know they were confirmed as viable upon administration. Of course, it may instead be that we simply failed to culture *H. pylori* from tissue despite colonisation being present, which may have occurred in the event of very low colonisation density.

Many of the cells isolated from spinal cords using gradient separation were stained with Trypan blue dye indicating that they were dead or dying. This was not the case previously using the same experimental protocol, although a similar situation was seen in other work in this thesis (chapter 4; migration study). Optimisation of this

methodology, or identification of the problem, would be of benefit to ensure enough cells available for a robust downstream analysis.

Flow cytometry panels were kept to 8 colours to try to minimise the amount of post-acquisition compensation needed to be applied to the data to correct for overlap between fluorophore emissions. The technology available for such biological applications is constantly evolving. The University of Nottingham flow cytometry facility has recently acquired a full spectrum flow cytometer facilitating acquisition of markedly more fluorophores whilst avoiding the need for post-acquisition correction. This new technology would be of great benefit for our work and would enable larger panels to be stained whilst avoiding the negative impact it can confer to the dataset during analysis.

3.5 – Conclusions

- Infection with *H. pylori* strain SS1 resulted in a notable reduction in EAE clinical score as compared to both uninfected and PMSS1-infected mice.

- No substantial differences were observed in lymphocyte frequencies or numbers, either in the spleen or CNS to explain this reduction of severity.

- EAE can have a variable course between experiments with a potential to confound the comparison of data between separate studies.

- The mechanisms by which *H. pylori* can protect against EAE required further work to elucidate.

Chapter 4

Pilot Study to Investigate the Migration of CD4$^+$ T-Cells from EAE Mice, when adoptively transferred into *H. pylori* Infected Recipient Mice

Chapter 4: Development and optimisation of methodology for the non-invasive tracking of murine CD4$^+$ EAE lymphocytes *in vivo.* Proof of concept for a hypothesised differential trafficking in response to gastric *H. pylori* infection

4.1 - Introduction

The overarching hypothesis investigated in this chapter is that infection with *H. pylori* can induce alterations in T-cell trafficking in the infected host, which may function to attenuate autoimmune disease severity in the CNS. These changes to lymphocyte homing, through inflammatory and chemotactic stimuli in the infected gastric mucosa may divert the auto-reactive T-cells in EAE/MS away from the CNS, and instead cause them to home towards the inflamed stomach. In so doing, the number of pathogenic T-cells entering the brain and spinal cord and contributing to the progression of MS or the animal model EAE would be reduced. Therefore, providing a potential mechanism for *H. pylori*-mediated protection.

Furthermore, in accordance with previous findings from this research group and supported by published literature, the axis of the chemokine CCL20 and cognate receptor CCR6 are hypothesised as mediators of this mechanism.

4.1.1 – Cellular Trafficking

Cellular immunity requires a complex and orchestrated system to mount effective responses. The production of lymphocytes, their development, activation, and subsequent function takes place in distinct tissues and with a requirement for temporally coordinated signals and permissive microenvironmental conditions. For a cell to progress through these stages, and to be able to respond to stimuli where required, it must be able to migrate effectively to specific tissues in response to stimuli in a timely manner. The first description of this migration in the literature was made by Saxer in 1896 who described the phenomenon of "Wandering lymphocytes in emergent lymph nodes" [415,416].

To maintain effective immune surveillance under homeostatic conditions and efficient response to infections, T-cells must continually survey the plethora of antigens presented on APCs for those with specificity for the T-cell receptor (TCR). Only around 2% of human T-cells circulate in blood [417]. The remaining cells reside in tissue such as lymph, lungs, and skin, in prime positions to survey antigens and quickly respond when required.

T-cells have an intrinsic desire to explore, as encountering antigens is at the very core of their biology and migrating to target tissue is essential to their function. To search and encounter these antigens they must be highly mobile. The movement of lymphocytes during homeostasis/surveillance can be described as a series of little steps in an essentially random trajectory [418]. These 'random walks' can be described as 'diffusive' (Brownian-type), or 'super diffusive' (Levy-type) random walks [418]. However, when the necessary factors are present, for instance chemokines secreted at a site of infection, they can undergo 'ballistic' migration, which is essentially a directed migration orientated in a straight line towards a target [418]. A simplified overview of the major phases of cell migration is presented in *Figure 48*.

4.1.2 – Chemokines

The trafficking of lymphocytes is essential, and this is achieved in part by chemokines and chemokine receptors [419,420]. Chemokine secretion forms chemical gradients which act as navigational cues. Expression of chemo-attractants at a site of

inflammation are sensed through chemokine receptors, members of the 7 trans-membrane (7-TM) G-protein coupled-receptors (GPCRs), on leukocytes [421]. Receptor activation subsequently affects a multitude of intracellular signalling cascades which result in cell motility.

Chemokines are small protein molecules of around 8-15kDa in size, and 47 or more distinct but structurally related family members are identified [420,422]. Chemokines can be classified into two distinct functional groups; inflammatory or homeostatic [422]. The former, are expressed during inflammation to recruit leukocytes to tissue, such as IL-8 alternatively known as CXCL8, produced in response to inflammatory stimuli by macrophage and epithelial cells and induces the recruitment of neutrophils and T cells (which express the cognate receptors CXCR1 and CXCR2) to sites of inflammation. The homeostatic chemokines are constitutively expressed in tissues such as the lymph nodes, and aid cell migration to and within lymph for surveillance. Two such examples are CCL19 and CCL21 which are constitutively expressed within lymph nodes and recruit $CCR7^{+}$ lymphocytes [423,424]

4.1.3 – Mechanisms of Cell Migration

Lymphocytes travel through the circulatory systems until they encounter the inflamed tissues where they are recruited. The process of this migration from circulation into tissue was originally described in 3 steps; capture/rolling (mediated by selectins), activation (mediated by chemokines) and arrest (mediated by integrins and immunoglobulin-family cellular adhesion molecules; CAMS). These steps precede the migration through the vasculature. This process is somewhat expanded in detail; capture, rolling, slow-rolling, activation, arrest, adhesion, crawling, para/transcellular migration [425].

4.1.3.1 – The Role of Selectins

The initial capture is a process whereby lymphocytes first contact and tethers to the vascular endothelium. This is achieved through interactions between glycosylated ligands on lymphocytes with epithelial cell-expressed adhesion and homing molecules including P- and E-selectin. These can include PSGL1 (P-selectin

glycoprotein ligand 1, or CD162) which is expressed predominantly on lymphocytes, sialyl-Lewis^X moieties (CD15s) and the homing cell adhesion molecule, HCAM (CD44) [425,426]. Pools of intracellular P-selectin (CD62P) and E-selectin (CD62E) on epithelial cells are externalised in response to inflammatory events. There is also the potential for secondary tethering whereby captured/rolling lymphocytes can tether further free-flowing lymphocytes, achieved by the binding of PSGL-1 to L-selectin (CD62L). L-selectin on T cells also binds to adhesion molecules on the epithelium, for example MadCAM-1 facilitates entry of lymphocytes from the blood into mucosal-associated-lymphoid tissue [427,428].

The net effect of these interactions is the formation of low-affinity reversible bonds to the vasculature mediating the process of slow-rolling along the epithelium. The bonds are dynamically formed and broken to an extent which allows the cell to slow but not stop. These binding interactions are also referred to as 'catch bonds' which are affected by the shear stress caused by the blood flow itself [429].

4.1.3.2 – The Role of Integrins

As a result of slow rolling, the efficiency in which lymphocytes can become stimulated by the presence of chemokines around inflamed endothelia is increased. These chemokines are often expressed on the endothelium itself bound to heparin sulphate moieties or secreted as soluble factors [425]. Chemokine receptor activation and the GPCR signalling induced is the initiating factor for arrest and transmigration to occur. The chemokine-mediated activation of lymphocyte GPCRs leads to the upregulation of crucial integrins on the lymphocyte surface such as α4β1 (very-late antigen-4, VLA4 – CD49d), α4β7 (lymphocyte Peyers patch adhesion molecule-1; LPAM-1) and αLβ2 (leukocyte function-associated antigen 1; LFA1 – CD11a) [425]. These integrins can bind to the cell adhesion molecules such as ICAM1 (CD54) or VCAM1 (CD106) expressed on the inflamed epithelium. Within the CNS, VLA4:VCAM1-mediated adhesion is the major axis for T-cell migration, whereas α4β7:MadCAM1 interactions are the major mechanism in the gut mucosa [425]. In opposition to the low affinity selectin-mediated binding, integrins possess a far greater affinity for their counterpart adhesion molecules. These high affinity interactions result in the

lymphocyte coming to a near-halt in the target region, beginning a process of slow crawling on the vascular endothelium in search of the nearest cell junction to utilise as an entry point into tissue [425,426,430].

4.1.3.3 – Extravasation and Trans-endothelial Migration

This process of extravasation from the vasculature is termed trans-endothelial migration (TEM). Two types of TEM are utilised, paracellular TEM (pTEM) which involves migration between endothelial cells via junctions, and transcellular TEM (tTEM) in which lymphocytes pass through endothelial cell bodies [430]. In most cases pTEM is the primary mechanism. Interestingly, tTEM has been reported to occur at higher frequency in brain-derived endothelia, likely because of the specialised BBB cell-cell junctions in the brain [425,430,431]. Mononuclear cells can extravasate across the cerebral venules independently of cell junctions during EAE [432]. Activated T-cells, astrocytes, macrophages, and recruited neutrophils in the inflamed CNS can secrete inflammatory cytokines, chemokines and matrix metalloproteinases (MMPs) in MS and EAE which compromise junction integrity, BBB disruption, and facilitate further infiltration [431].

TEM is mediated by the integrin-CAM interactions of the firm-arrest phase. Binding of endothelial adhesion molecules such as VCAM-1 to lymphocyte integrins such as VLA-4 stimulates not only signalling cascades within the lymphocyte to allow crawling (for instance morphological/cytoskeletal remodelling and integrin clustering); but also signalling pathways within the endothelial cells. Ca^{2+} signalling, ROS generation and p38 MAPK signalling have roles influencing cell-cell junction integrity aiding extravasation from the vessel into target tissue [426,430,433].

Cell-cell junctions are held together structurally by numerous adhesion molecules of the cadherin, selectin, immunoglobulin, and integrin protein families [430]. The integrity of these junctions is compromised by the binding of adhesion molecules to integrins on lymphocytes, and by breaking the bonds between junctional proteins cells can migrate across endothelial junctions to the basal lamina and extra-cellular matrix (ECM).

4.1.3.4 – Guided Migration to a Target Site

Upon extravasation, T-cells reside within the interstitial layer amongst a complex mesh of the extracellular matrix (ECM). This meshwork is composed of numerous fibres, largely collagen and fibronectin. The T-cells utilise this framework to navigate through the matrix, primarily using Levy walks, but guided directionally by the gradients of chemokines and cytokines secreted at the target site [434]. T-cell integrins are utilised for this migration and will include importantly the αV-containing integrin subtypes [434]. Cells utilise a Levy-type random walks behaviour to navigate in search of antigen unless directional cues are provided by microenvironmental chemokine secretion. For instance, in the case of MS/EAE, upon extravasation through the BBB into the inflamed CNS, activated astrocytes and macrophage in the vicinity of tissue damage can secrete CCL20 to guide T-cells towards the primary lesion site through the CCL20/CCR6 axis [435]. During these journeys T-cells encounter tissue resident DCs and macrophages (or microglia in the context of the CNS) displaying antigen and can become re-activated in response to the specific stimuli, inducing the required immune response and creating permissive conditions for further recruitment of inflammatory cells [431].

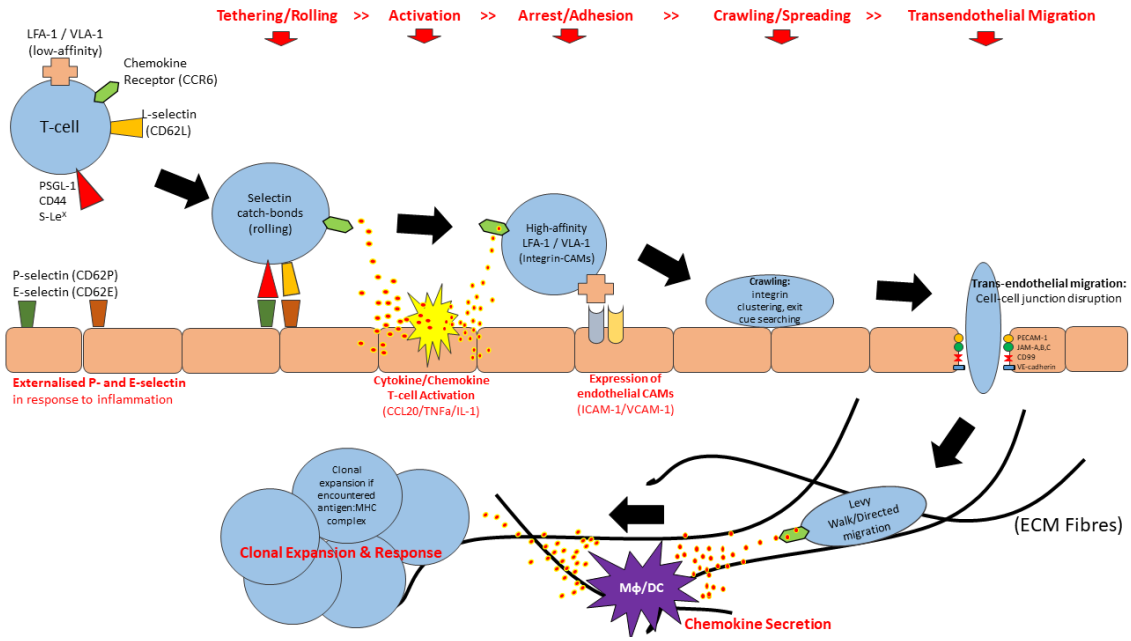

Figure 48 Schematic showing the major phases of leukocyte migration and response to stimuli

General schematic of the major processes involved in the trafficking and homing of T-cells. Lymphocyte-expressed L-selectin forms reversible catch-bonds with receptors on epithelial cells in the vasculature. These low affinity bonds result in the lymphocyte slowing and rolling along the walls of the vessels. While rolling, proximity to stimuli such as inflammatory cytokines and chemokines results in the externalisation of high-affinity bond-forming integrin molecules. In the case of MS and EAE, it is CCL20 expressed from Kolmer cells of the choroid plexus epithelium that acts as a stimulus for EAE cells entering the CNS. Integrins bind to cellular adhesion molecules (CAMs) on epithelial cells and cause the arrest of the lymphocyte at the target site. Cell-cell junctional molecules are affected by intracellular signalling cascades that occur consequentially of integrin:CAM binding, as well as weakened by activated immune cells already located within infected tissues. Increased permeability of the cell junctions allows the process of trans-endothelial cell migration into target tissue. Within target tissue, lymphocytes may encounter inflammatory cues and recognise cognate antigen presented by tissue resident macrophage. Re-activation of T-cells in this manner leads to the expansion and activation of a T-cell-mediated propagation of inflammation, secretion of bioactive molecules resulting in infiltration of neutrophils, macrophages, and monocytes to the stie of infection; forming the hallmark inflammation and cytotoxicity known to propagate the pathogenesis of MS and EAE

4.1.4 – Potential changes in T cell migration in *H. pylori*-infected MS patients

An infection in the gastric mucosa can lead to the expression of all the prerequisite molecules in the venules to stimulate T-cell extravasation. This may occur even in myelin-specific T-cells destined for the CNS. Therefore, it may be possible that highly pathogenic CNS-specific cells are diverted away from the stimuli in the CNS. Instead, these cells may extravasate the vasculature in the region of the gastric mucosa in

response to the *Hp* induced inflammatory molecules. Alternatively, due to the similarities in chemokines and receptors expressed by Treg and Th17 cells, *Hp*-specific Tregs may extravasate into the CNS rather than the gastric mucosa and contribute to suppression of pro-inflammatory cellular responses.

Several published studies show that infectious agents could reduce the severity of EAE. One such example is that of *Mycobacterium bovis,* strain bacillus Calmette-Guerin (BCG) [436,437]. Here, infection of C57BL6 mice with BCG 6 weeks prior to a MOG_{p35-55} EAE induction resulted in a 50% reduction in EAE incidence, and a 2-fold reduction in EAE clinical scores in the symptomatic infected animals compared to uninfected controls, and with a delayed onset of EAE. These observations were matched by no evidence of myelin pathology when staining spinal cord sections. BCG infected EAE mice had a 4-fold higher number of lymphocytes in the spleens, however a marked 3-fold reduction in the number of lymphocytes infiltrating the brain as compared to uninfected EAE mice. There was an absence of Th1 cells and a reduction in Th17 cells in the brain of infected animals, leading to the hypothesis that they were retained in the periphery which inhibited EAE progression. No differences in Treg cell frequency were observed infiltrating the brain or spinal cord [437].

On the other hand, related work by Lippens *et al.* [438] suggests a live BCG infection is not required to protect against EAE. Subcutaneous injections of freeze-dried BCG significantly reduced the severity and development of EAE in mice. This effect was attributed to the ability of BCG constituents to directly modulate dendritic cells and promote a tolerogenic IL-10-secreting Treg-inducing phenotype, in a mechanism like that of *H. pylori* in asthma models [21]. There were reduced numbers of MOG-specific CD45+, $CD4^+$, IFNy+, IL-17+, and GM-CSF+ T-cells infiltrating the spinal cord of BCG-treated animals. The numbers of CD103+ ICOS+ Tregs were increased in the lymph nodes and spleen, but importantly not the CNS. They hypothesised that BCG administration resulted in the modification of dendritic cells phenotype, leading to preferential induction of suppressive Tregs in the lymphoid tissues, inhibiting the development of pathogenic Th1 and Th17 responses in peripheral sites of priming and subsequent migration to the CNS.

To further support the hypothesis altered migration patterns in other lineages of gut-derived immune cells can affect the severity of both MS and EAE [326,352]. One such case in point is the identification of intestinal-derived IgA-producing and IL-10-secreting plasma cells/B-cells, found in the CNS in both EAE and MS, which confer a protection to disease severity [326]. This is interesting because intestinal IgA^+ cells are not unusually found within the brain, and it indicated that gut mucosal immune cells are attracted to this location and play a direct role in CNS inflammatory diseases. This supports the hypothesis that a GI tract bacterium such as *H. pylori* may be able to protect from MS.

4.1.5 – MS therapeutic drugs that act via modifying leukocyte migration.

There is also well documented evidence of pharmacological interventions affecting lymphocyte migratory pathways to be of benefit in MS. Three such examples licensed for use come in the form of Fingolimod (Gilenya™; Novartis Pharmaceuticals®), a spingosine-1-phosphate receptor (S1PR) modulator; Siponimod (BAF312 or Mayzent™; Novartis Pharmaceuticals®), a second-generation S1PR modulator similar to Fingolimod; and Natalizumab (Tysabri™; Biogen®), an anti-α4-integrin antibody [415]. All of which, when administered therapeutically have shown to have a clinical efficacy in the treatment of multiple sclerosis.

Gilenya™ or Fingolimod (FTY720) is a small molecule drug based on the fungal-derived amino acid myriocin. It functions as a shingosine-1-phosphate receptor suppressor, approved in some cases as an immunomodulatory treatment for relapsing-remitting forms of multiple sclerosis [286]. Shingosine-1-phosphate (S1P) is a blood-borne lipid mediator. S1P is found in higher concentrations in the blood than tissue fluids and hence gradients across these boundaries are formed and can be utilised in lymphocyte trafficking, affecting the ingress and egress between tissue and circulation. The S1P receptor (S1PR1) is a GPCR on lymphocytes. Activation of S1PR1 allows diapedeses from the tissue into the circulation. Fingolimod, or its biologically active form phospho-Fingolimod (Fingolimod-P), works by causing the internalisation of S1PR1. By inhibiting subsequent GPCR activation lymphocytes are rendered unable to egress from lymphoid tissue and are instead sequestered in lymph tissue. In the

case of MS, this has been demonstrated to reduce the number of inflammatory auto-reactive cells migrating to and infiltrating the CNS, thus preventing exacerbation of disease, and reducing the relapse rate [237,286,439]. A Cochrane systematic review of Fingolimod (La Mantia, *et al.* 2016 [286]), found that administration of the approved daily oral 0.5mg dose moderately increased the chance of being relapse-free at 24 months compared to placebo, and slightly increased the chance of being relapse-free at 12 months as compared to I.M. interferon-β1 (IFNβ1). However there was little or no evidence of halting disease progression in the long term, or efficacy treating progressive forms of MS [286].

In answer to this deficit, Novartis™ released Siponimod (Mayzent™ or BAF-312). Siponimod is a second-generation S1PR modulator which possesses affinity for a greater number of S1P receptors, S1PR-1 and -5, as opposed to Fingolimod solely targeting S1PR-1 [440]. Recently in 2020, the National Institute for Health and Care Excellence (NICE) issued their Technology Appraisal Guidance (NICE Guidance Number: TA656) in which the use of Siponimod for adults with secondary-progressive MS (SPMS) was approved in cases with evidence of active disease, being classed as the emergence of new lesions or an occurrence of relapse. In the phase 3 EXPAND clinical trial (Clinical Trials ID: NCT01665144), Siponimod was administered orally at 2mg daily against placebo [441]. The primary outcome measure was the proportion of patients with a confirmed disability progression (CDP) at 3-month intervals for a period of 36 months. Additional outcome measures included confirmed worsening of a 25-foot walk test; reducing increases of brain lesion volume; reduction in relapse rate; and reducing increases of brain atrophy. Results from the trial were reported by Kappos *et al.* [441], the EXPAND trial concluded that against the primary outcome measure of 3-monthly CDP, the Siponimod group had a relative risk reduction of 21% (*p=0.013*) compared to those given placebo, and 26% (*p=0.0058*) risk reduction for CDP at 6 months [441]. For the secondary outcome of total brain lesion load, the Siponimod-treated group had a mean 4.8-fold (*p=<0.0001*) reduction in new brain lesions (normalised to individuals' baseline) as compared to placebo, with 30% (*p=0.0002*) reductions in brain atrophy over 24 months [441]. Annualised relapse rate was similarly reduced in the Siponimod treated group 55% (*p=<0.0001*) compared to

placebo [441]. A Cochrane systematic review of Siponimod for MS (Cao, *et al.* 2020 [440]) is on-going but not published at the time of writing. Interestingly, other reports in the literature suggest an influence of Siponimod acting via the S1PR1 on astrocytes promoting glial repair and anti-inflammatory pathways in astrocytes (and oligodendrocytes via S1PR5), at least *in vitro* [442]. No work is yet published to my knowledge assessing the effect of Siponimod on the remyelinating potential of oligodendrocytes via S1PR5, as has been proposed for the related Fingolimod, this will be of interest to investigate.

Tysabri™, or Natalizumab, functions in somewhat the opposite manner, rather than blocking lymphocyte egress from the lymphatics, it prevents circulating lymphocytes from entry into the target tissue (the CNS). This is achieved through binding to the α4 subunit of very-late antigen-4 (VLA-4) the α4β1-integrin on lymphocytes. This results in an inhibition of the crucial interaction of VLA4 with the vascular cell adhesion molecule-1 (VCAM-1) expressed on the BBB during inflammation. In the case of MS and EAE, this prevents auto-inflammatory cells from gaining entry to the CNS through the BBB and mitigates disease exacerbations [415]. The use of monthly I.V. Natalizumab for the treatment of MS has been reviewed by Pucci, *et al.* [287]. Here, the use of Natalizumab either with or without co-therapy of IFNβ1a reduces the risk of experiencing a new relapse or inflammatory exacerbation at 48 months by 40% and reduces the risk of disease progression at the same time point by 25%.

The mode of action of these drugs contributes to the hypothesis that other interference to the lymphocyte migratory pathways, such as by infections, may be able to provide a protection from MS. Considering that the efficacy of the currently approved pharmacological interventions is largely restricted to relapsing-remitting MS, and fails to confer a clinically significant benefit to progressive and rapidly-worsening cases, there is a crucial need for the discovery and development of novel strategies to modulate the disease.

4.1.6 – The role of gut mucosal immunity in EAE and MS

To further complicate matters, $CD4^+$ T-cells in EAE home to and proliferate in the gut even in the absence of *Hp* infection. Duc *et al.* [427] found that Th17 cells homed to and proliferated within the colon during the pre-symptomatic phases of MOG_{p35-55}-induced EAE in C57BL6 mice. When *in vitro* generated MOG-specific Th17 cells were adoptively transfer to recipient mice, they developed symptomatic EAE and there was a significant accumulation of the injected cells in the colon. This was not observed with Th1 cells, indicating that gut homing is a function of Th17 lineage cells. The injected $Th17^{MOG}$ cells localised to the vessels in the colon and mesenteric lymph node. This indicated that during EAE $Th17^{MOG}$ cells initially migrate to the colonic lamina propria and mesenteric lymph nodes, proliferate, and upregulate CNS-specific homing molecules (such as α4β1-integrin) prior to extravasating through the colonic vasculature and trafficking to the CNS and subsequent onset of clinical symptoms of EAE.

From this same study, to investigate the contribution of the colonic homing to the development of EAE, the α4β7-integrin:MAdCAM-1 axis was investigated. $Th17^{MOG}$ cells were found to express the gut-homing α4β7 which was downregulated in parallel to upregulation of α4β1-integrin (CNS/VCAM-specific) immediately preceding CNS migration and symptomatic onset. By attenuating this gut homing the proportions of $Th17^{MOG}$ cells were reduced in the colonic tissue. This was paralleled by delayed onset and reduced severity of EAE, in addition to significantly reduced numbers of $Th17^{MOG}$ cells in the CNS. However, interestingly this effect was only apparent in adoptively transferred EAE. When a standard model of EAE induction was performed blocking the α4β7-integrin:MAdCAM-1 axis had no effect on the manifestation of clinical disease in the mice. The authors also report that the homing of these $Th17^{MOG}$ cells correlated to a shift in the colonic microbiota. Alterations to the microbiota composition through either $Th17^{MOG}$ injection, or antibiotic administration resulted in differential susceptibility to EAE development.

In summary, these data have major impacts on the work presented in this chapter. Firstly, it highlights once more the importance of the gut in lymphocyte homing patterns, specifically to EAE T-cells. Indeed, the gut microbiota, or dysregulation of

it, can have profound effects on the development or suppression of neurological inflammation and autoimmune disease. Secondly, it may suggest that these EAE T-cells home very differently in standard EAE to adoptive transfer EAE which needs to be considered upon analysing results from our models.

4.1.7 – Controversies in the role of the CCR6/CCL20 axis in EAE and MS

Previous SPECT-CT imaging data produced in this research group (Cook, *et al.* [443]) indicated that $CD4^+$ T-cells isolated from naïve donor mice and adoptively transferred into recipient *Hp*-infected mice, preferentially migrated towards the infected stomach and spleen. This led to the hypothesis that $CD4^+$ T-cells destined to migrate to the CNS during EAE may be diverted towards strong CCL20 chemokine gradients in the gastric mucosa arising from a *H. pylori* infection. The CCL20/CCR6 axis is also involved in MS and EAE, since myelin-specific Th17 and Treg cells express CCR6, and CCL20 expression is upregulated in the inflamed CNS [444-446].

Human Th17 cells differentiated from naïve T-cells *in vitro,* expressed CCR6, CCR9 and CXCR6 and migrated towards the respective ligands CCL20, CCL25 and CXCL16 respectively [447]. $CD4^+RORγT^+IL17^+$ (Th17) cells were almost exclusively $CCR6^+$. Together with the findings of Duc *et al.* that disrupting Th17-related gut-homing confers protection from EAE [427], and the known contribution Th17 cells have in EAE and MS [179,231], it is highly probable that this T-helper subtype is an important candidate to investigate in our work.

Previous work within this research group (Cook, *et al.* 2014 [448]), also showed that CCR6 was commonly expressed on $CD4^+CD25^+FoxP3^+$ murine Tregs, and that CCL20 was highly expressed in the inflamed gastric mucosa during *H. pylori* infection. These $CCR6^+$ Tregs were also observed to migrate towards recombinant rCCL20 *in vitro*. Intriguingly, this migration was observed in $CD4^+FoxP3^+$ but not $CD4^+FoxP3^-$ cells [448].

CCR6 is expressed on a wide range of $CD4^+$ cells in the EAE model perhaps most importantly the Th17 T-helper subset, but also by the Th1 and Treg lineages. Other studies in the literature have identified, in addition to Th17 and Th1, the $CD4^+$ GM-

CSF-only secreting cells to also be present in increased frequency in the CSF of MS patients, and to express CCR6 [449].

Several chemokines are expressed in the CNS during homeostasis and inflammation, including CXCL12, CCL19, CCL20 and CCL21 [421,450]. CCL20 is expressed constitutively in the choroid plexus epithelium under homeostatic conditions, and this area likely forms an initial entry point for T-cells performing immune surveillance in the CNS during the steady state [431,446]. Blood vessels of the 5th lumbar region of the spinal cord have been shown to host EAE/MS CD4^{+} T-cell accumulation and may serve as an additional entry point to the CNS as opposed to the choroid plexus; CCL20 is also expressed in this region [445,451]. The choroid plexus epithelial cells, called Kolmer cells, secrete CCL20 on the basolateral surface. The expression of CCL20 is upregulated during EAE, and further expressed by astrocytes once activated in response to CNS inflammation [435,444,446]. In fact, during the inflammatory conditions of EAE astrocytes are perhaps the largest producer of CCL20, induced by inflammatory cytokines including TNFα and IL-1β which can be produced by macrophage and neutrophils recruited to the lesion site [444]. It has been observed by others that mice deficient for the expression of CCR6 also possess a resistance to the development of EAE [446].

Reboldi, *et al.* [446] reported that CCR6-deficient mice had MOG-specific Th17 responses after immunisation in the EAE model, however they failed to develop EAE. It was concluded that CCR6 is redundant for T-cell migration to lymphoid tissue and initial priming in the preclinical phase of EAE, however is essential for subsequent trafficking into the CNS and initiation of inflammation. When the authors created a mixed (CCR6$^{-/-}$ / WT) Th17 cell solution composed of *in vitro* MOG-primed cells, the CCR6$^{-/-}$ cells were indeed found within the brain, however interestingly only at later timepoints as compared to the WT Th17 cells. This observation would infer that MOG-specific CCR6^{+} WT Th17 cells, and the CNS inflammation they induce, can then allow for a permissive inflammatory BBB microenvironment for subsequent CCR6$^{-/-}$ Th17 cell entry. This is important as it may suggest that CCR6 is primarily important for initial CNS infiltration, however, becomes redundant in active EAE when the BBB is already inflamed [446].

Elhofy *et al.* [452] also compared EAE induction in wild type or CCR6$^{-/-}$ mice. Surprisingly, they found the priming and induction of disease, day of onset, and peak severity was comparable between both groups [452]. The wild type mice had reduced clinical scores at day 21, which was sustained through day 35. The scores remained high in CCR6$^{-/-}$ group throughout, with no apparent recovery, and this correlated with numbers of lesions in the CNS. There were also significantly higher numbers of CD45^{+}CD4^{+} cells and CD45^{+}CD11b^{+} cells in the CNS of the CCR6$^{-/-}$ group compared to the wild type mice. The CCR6$^{-/-}$ mice also displayed significantly elevated IFNγ and IL-17 production in cells from the spleen and lymph nodes, but there no differences in either cytokine in the CNS. The attenuation of CCR6 in mice therefore appeared to worsen clinical scores and lesion load, as well as enhancing CD4 and macrophage infiltration to the CNS. [452].

From these observations, a hypothesis was presented that the abrogation of CCR6 may exert its modulatory effect on EAE not through inhibiting Th17 infiltration of the CNS, but rather by dysregulating the recruitment of regulatory T-cells to peripheral sites of EAE priming and thus preventing Treg-mediated suppression of the MOG-specific T-cell responses. However, upon investigation no differences in Foxp3^{+}, IL-10^{+} or TGFβ^{+} cells were found between groups in either the spleen or CNS. However, data was presented indicating that during the chronic phases of EAE, at the point where the CCR6$^{-/-}$ and WT groups diverged on clinical scores, there was a significant decrease in the number of PD-L1^{+} regulatory DCs in the spleen, but not the CNS or LN. Further to this finding, transfer of enriched PD-L1^{+} regulatory DCs to the CCR6$^{-/-}$ mice attenuated EAE suggesting that CCR6 may function in the regulation of migration of multiple cell types in EAE in addition to the previously identified CD4^{+} T-helper lineages thought primarily responsible [452].

Others have studied CCR6 expression specifically amongst inflammatory T-cell infiltrates of the CNS during active EAE [453]. Here, CCR6 expression was found preferentially on cells of the Th17-IL17^{+} lineage in agreement with others, also on Th1-IFNG^{+} and dual IFNG^{+}-IL17^{+} expressing CD4 cells, however not detected on CD8 T-cells. The chemokine CCL20, known to be expressed constitutively at the choroid plexus, was additionally upregulated on astrocytes corresponding to relapses. In

inflammatory infiltrates of the CNS, CCR6 expression was found to be co-localised to both $CD45^{high}$ and $CD45^{low}$ cells, to CD4 cells, but not CD8 cells.

4.1.8 – Rationale for the current study

A working hypothesis was formulated that crosstalk affecting the CCR6/CCL20 axis between these models of *H. pylori* infection and EAE may affect the T-cell response in the stomach or the CNS in a bi-directional manner. Firstly, pathogenic $CCR6^+$ Th17-EAE cells may be diverted away from the CNS and towards the *Hp*-infected stomach in response to high CCL20 expression in the gastric mucosa. Alternatively, $CCR6^+$ Treg-*Hp* cells generated during *Hp* infection may be able to respond to the CCL20 gradients in the inflamed CNS and migrate to the brain and spinal cord in the EAE model, thereby suppressing inflammatory responses in that tissue. Alternatively, disruption to the migration of cells to peripheral sites of EAE priming and induction which indirectly affect EAE severity may play a role.

To explore these hypotheses, we aimed to quantify cell subsets in tissues and quantify cytokine production from $CD4^+$ cell populations. We also aimed to track adoptively transferred cells *in vivo*. The previous study (Cook, *et al.* [443]) utilised SPECT-CT imaging to track cell migration. This option was no longer available and therefore, it was necessary to develop and optimise a method for tracking adoptively transferred and labelled cells *in vivo,* and non-invasively. The label selected would need to be suitable for imaging on the available equipment at the university which was the IVIS™ Spectrum imaging system (Perkin-Elmer®). For this we opted to try Xenolight DiR (Perkin-Elmer) as a potential cell labelling reagent. This reagent is a hydrophobic molecular dye which when added to a cell solution will embed into lipid bilayers and uniformly label all membranous structures within the solution to which it is added. There are considerations which need to be accounted for with the use of this regent. Firstly, staining is non-specific, and it will bind to any membrane including non-cellular structures such as exosomes which may be in the solution. It would therefore be crucial to first purify the cells of interest. For this purpose, commercial kits are readily available such as the $CD4^+$ T-cell selection kits (StemCell Technologies®). By staining pre-purified cells, there can be confidence that the label

is present only on the cells of interest. This will of course depend on the purity of the cells after selection.

4.2 – Aims & Hypotheses

4.2.1 – Hypotheses

We hypothesised that an active *H. pylori* infection can influence the trafficking of $CD4^+$ T-cells in the infected host.

This altered trafficking may, at least partially, be mediated by the chemokine CCL20 expressed in the gastric mucosa in response to *H. pylori*, and its cognate receptor CCR6 which is expressed on $CD4^+$ T-cells, including Th1, Th17 and Treg cells.

We hypothesised that interference in the CCL20/CCR6 axis and subsequent $CD4^+$ T-cell homing patterns may confer a benefit in cases of experimental autoimmune encephalomyelitis (EAE) the animal model of MS.

We proposed that after adoptive transfer, $CD4^+$ EAE T-cells may be diverted towards the inflamed gastric mucosa in infected animals, and away from the brain and spinal cord. This could contribute to the reduction in EAE disease severity previously observed in infected mice. This may provide a mechanism behind the reduced incidence of MS in humans infected with *H. pylori*.

By understanding how these protective effects occur, we may be able to identify new options for the treatment of MS.

4.2.2 – Aims.

- To validate a suitable reagent to use for fluorescently labelling purified murine $CD4^+$ cells.
- To design a pilot study in which $CD4^+$ splenocytes can be purified from EAE-induced mice, labelled, and then imaged *in vivo* after adoptive transfer to recipient *H. pylori* infected animals.
- To determine what future refinements are needed to the methodology to take forward to a larger scale experiment.

4.3 – Materials and Methods

4.3.1 – Cell Labelling using Xenolight DiR Reagent

Preliminary tests used the wide range of concentrations (1-320µM) of Xenolight DiR (Perkin-Elmer®; Cat No. 125964) as recommended by the manufacturer. Staining buffer was prepared by adding concentrations of 1, 5, 8.3, 15, 30, 50, 100, 320µM dye to a final volume of 1ml in 0.22µm sterile filtered PBS and mixed thoroughly. Staining buffer was freshly prepared each use. Murine splenocytes in culture medium (RPMI-1640 containing 100 $U.ml^{-1}$ penicillin, 100$µg.ml^{-1}$streptomycin (1% PS) and 10% *v/v* FCS) were counted on a haemocytometer with Trypan blue exclusion of dead cells. The cell suspension was centrifuged at 300x *g,* and the pellet was resuspended in washing medium (RPMI-1640, 2% FCS, 1% PS) to a concentration of $1x10^6$ cells per ml.

1ml of this solution was added to each of 8 tubes corresponding to the above dye concentrations. These tubes were centrifuged at 300x *g* to pellet the cells and washed in duplicate preceding media exchange for staining buffer. After the final wash, the pellet was loosened by flicking the tubes and the staining buffers were added at a volume of 1ml to each tube containing $1x10^6$ splenocytes, and thoroughly mixed. The cells in staining buffer were then incubated at 37°C and 5% CO_2 in a humidified incubator in the dark for a duration of 30 minutes, as described by the manufacturer's cited resources. After incubation, all tubes were diluted with 4ml serum-free RPMI-1640 and centrifuged at 300x *g* for 5 minutes to pellet the cells before resuspension in 2ml washing medium. The washing was performed in triplicate to ensure complete removal of residual dye from the cell solutions. After the final wash, the pellets which appeared visibly blue were resuspended in 1ml culture media and counted using a haemocytometer, with Trypan blue to exclude dead cells.

The additional optimisations performed used the above protocol with variations as required, described below. The temperature of the incubation step was optimised by performing staining at either 37°C, 4°C, or room temperature (RT). The duration of the incubation was tested at 5, 10, 20, or 30 minutes. The media used for the staining

buffer was tested using PBS, PBA, RPMI (both serum-free or 5% FCS), HBSS, and EasySep buffer (PBS, 2mM EDTA, 2% FCS). The initial concentration of cells added to the staining buffer was tested at 1, 2, 5, 10, 18, and 40 $x10^6.ml^{-1}$ (crude spleen homogenate).

4.3.2 – Flow cytometry to quantify fluorescence intensity.

Analysis of cellular fluorescence after labelling was quantified in the first instance using flow cytometry. Imaging was either performed immediately after labelling, or cells were fixed and imaged the next day where required. Additionally, some labelled cells were co-stained with anti-CD4:FITC antibody(Biolegend) immediately after Xenolight labelling. Stains used in flow cytometry are given in *Table 14*.

Table 14 Antibodies and acquisition information for flow cytometry analysis of labelled cells during optimisations.

Stain Used	Clone	Excitation	Emission	Filter Set
Xenolight DiR	n/a	640	795/70	FL25
CD4:FITC	RM4-4	488	513/26	FL17
CD45:AF647	30-F11	640	671/30	FL30

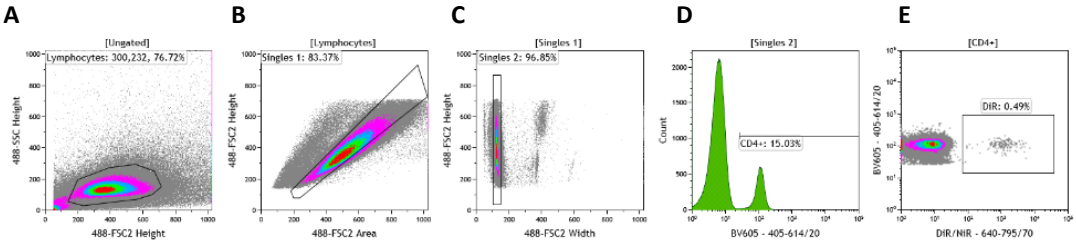

Figure 49 Gating strategy to identify $CD4^+$ DiR+ cells

Representative gating strategy for the identification of DiR-labelled $CD4^+$ cells. From left to right; lymphocytes; doublet and debris exclusion; $CD4^+$ cells; DiR-labelled cells.

For flow cytometry, after the final wash step post-labelling, cells were counted using Trypan blue to exclude dead cells and resuspended in culture medium to a concentration of $1x10^6.ml^{-1}$. This solution was used to aliquot 1ml volumes of the cell suspension into the required number of 5ml FACS tubes. For each acquisition, controls were included. Controls for flow cytometry consisted of unstained cells, and single stained cells, in addition to the co-stained cells, where applicable.

The FACS tubes containing $1x10^6$ cells were centrifuged at 300x *g* for 5 minutes to pellet cells. The pellets were resuspended in 1ml of PBA; PBS with 0.01% *w/v* bovine serum albumin (BSA) and 2% foetal calf serum (FCS). The cells were washed with PBA in duplicate. After the final wash, the pellet was loosened, and the required number of antibodies were added directly to the residual pellet volume (approximately 100µl) in the relevant tubes. These tubes were incubated on ice away from light for a period of 20 minutes. After the incubation, the cells were washed in duplicate with 1ml of PBA before finally resuspending in 0.5ml PBA for data acquisition.

For cells in which only Xenolight staining had been performed, these tubes were centrifuged at 300x *g* for 5 minutes to pellet the cells before washing with PBA in duplicate. After the final wash they were resuspended in 0.5ml PBA for acquisition. Occasionally where required, after the final wash the cells were resuspended in 0.5ml fixation reagent (Biolegend) and incubated at room temperature for 20 minutes in the dark. After this incubation, the fixed cells were washed in duplicate as described above and resuspended in 0.5ml PBA for acquisition.

Image acquisition was performed using an Astrios™ flow cytometer (Beckmann-Coulter®). A minimum of 50,000 events falling within the pre-defined lymphocyte gating parameters were recorded for each condition. The lymphocyte gate was placed based on the forward- and side-scatter characteristics of the cells being analysed. A representative example of this gating strategy is shown in *Figure 49.*

4.3.3 – Fluorescence Acquisition using TECAN® Plate Reader.

Cells co-stained for Xenolight and CD4:FITC were analysed using a fluorescent plate reader. Cells were stained according to the protocols described above for Xenolight DiR and anti-CD4:FITC (Biolegend) and plated at $1x10^6.ml^{-1}$ to give $0.1x10^6$ per well of a 96-well glass-bottomed TECAN plate. Images were acquired using bright-field, FITC (524nm wavelength), and Xenolight (760nm wavelength), presented in *Figure 55.*

4.3.4 – Animal Work

The study was conducted under the Home Office Licences 30/3298 and P9D20C785 held by Dr. Karen Robinson, in the Bio-support unit of the Queens' Medical Centre Medical School, Nottingham. All experiments were approved by the Animal Welfare and Ethical Review Body, University of Nottingham.

4.3.5 – *H. pylori* strain PMSS1 infection of recipient mice

4.3.5.1 – *H. pylori* Strain PMSS1 Culture

The *H. pylori* strain PMSS1 was recovered from frozen stocks. Bacterial aliquots of 50µl were placed onto blood agar (BA) plates (Oxoid) and tilted to spread the liquid. Plates were then cultured for 24 hours in a VAIN cabinet at 37°C under microaerophilic conditions. Fresh BA pates were inoculated with growth from the edges of the culturing plates and incubated for a further 48 hours, this was repeated for a further 48 hours. At the final passage, the growth was collected from plates using sterile swabs and suspended in sterile PBS. The final concentration for administration to study animals was determined at the point where a 1:10 dilution had an optical density of 1.0 at a wavelength of 600nm (equivalent to 1 x 10^9 colony forming units per ml).

4.3.5.2 – Infection of C57L/6 Mice with *H. pylori* Strain PMSS1

Here, 6–8-week-old C57BL/6 female mice (Charles River) were inoculated with 0.1ml of the above *H. pylori* PMSS1 suspension in PBS, providing 10^8 colony forming units per dose. In each group, 3 mice were infected, and 3 administered PBS-only as a sham infection control. Administration of inoculum was via oral gavage using a 1.5-inch straight gavage needle with a 2.5mm ball. Oral gavage was performed once each 48 hours for a total of 3 treatments. After the dosing schedule had been completed, mice were left for 12 weeks, recording their body weight once a week.

4.3.6 – Confirmation of *H. pylori* Infection

Prior to inducing EAE in the mice, tests were performed to confirm that they had been successfully infected. A stool antigen lateral flow test was used as per the manufacturers' instructions. Fecal DNA was extracted using a Fecal DNA MiniPrep Kit (Zymo Research; Cat No. D6010) according to the manufacturer's instructions.

Post-mortem tissue was obtained and weighed from half-stomachs by Dr. Darren Letley. Tissue was disrupted in 750µl iso-sensitest broth with 15% *v/v* glycerol and plated on Galaxo Selective Supplement A (GSSA) plates to culture *H. pylori* from gastric tissue. CFU counts were calculated per gram of tissue.

4.3.7 – EAE induction in donor mice

The EAE model was induced in 12-week-old female C57BL/6 mice. Induction was carried out by sub-cutaneous (S.C.) immunisation at 2 sites on the back/flank with 250µg MOG peptide fragment MOG_{p35-55} (AnaSpec; Cat. No. AS-63918) in 0.2ml complete Freunds' adjuvant containing 4mg.ml^{-1} H37Ra *M. tuberculin.* This was followed by an intraperitoneal (I.P.) injection of 200ng *Pertussis* toxin (PTX) working solution, repeated 2 days after the initial immunisations [410].

Mice were weighed and scored for EAE daily according to a published clinical scoring system [410]; 0—healthy, 1—flaccid tail, 2—impaired righting reflex and/or impaired gait, 3—partial hind-leg paralysis, 4—total hind-leg paralysis, 5—any sign of front-leg paralysis. This system was modified to include 0.5 increments for borderline symptoms. For this study, the defined endpoint was 7 days post-immunisation (d.p.i) which precedes the onset of observable symptoms in the animal.

4.3.8 – Tissue processing from donor mice

At a timepoint of 7 d.p.i. mice were humanely killed. Spleens were collected into RPMI-1640 containing 2% *v/v* foetal calf serum, 100 U.ml^{-1} penicillin G, and 100 µg.ml^{-1} streptomycin sulphate. Cell solutions were prepared by rubbing through a 70µm cell strainer. Cells were collected into a 20ml universal tube and centrifuged at 300 x *g* for 5 minutes to pellet cells. The medium was decanted, and cells were further washed once more with 10ml medium before resuspension for counting in 10ml culture medium (RPMI; 10% FCS, 1% p/s).

4.3.9 – Purification of $CD4^+$ EAE T-cells from donor mice

For CD4 selection, total spleen cell suspensions were counted using 3% acetic acid/ Methylene blue. At this stage, cells were pelleted and resuspended in the required volume of EasySep™ buffer (StemCell Technologies; Cat. No. 20144) to a concentration of 1x10^8.ml^{-1} where $CD4^+$ cells were enriched using negative selection kits (StemCell Technologies; Cat. No. 19852) as per the manufacturers' instructions.

4.3.10 – Labelling of purified $CD4^+$ T-cells

After the selection procedure, suspensions were counted using a haemocytometer with Trypan blue exclusion. Immediately after purification, the resulting CD4-

enriched cells were labelled with Xenolight DiR (Perkin-Elmer; Cat. 125964) according to the protocol optimised previously (*Section 4.3.1*).

4.3.11 – Adoptive Transfer of labelled $CD4^+$ EAE T-cells to recipient mice

Firstly, mice were moved to a heated chamber to allow dilating of the tail vein. Intravenous injection of 5 x 10^6 labelled $CD4^+$ cells in 75 µl sterile PBS, or PBS-only as a control, was performed by an experienced individual. After the injections, mice were replaced into their original cages and monitored for welfare for a period of 30 minutes.

4.3.12 – Imaging of donor mice

Animals were killed 24 hours post-injection; fur was removed, and organs dissected to be imaged individually using an IVIS Spectrum (Perkin-Elmer®) system. Image acquisition was performed at 710nm (excitation), and 760/80nm emission wavelengths, facilitating quantification in the near infra-red (NIR) channel. Fluorescence imaging was analysed using the LivingImage™ (Perkin-Elmer®) software package.

4.3.13 – Tissue Processing

After imaging was performed, the spleens, spinal cords, brains, and stomachs were obtained for downstream processing. Organs were collected into 5ml Bijoux in washing medium; RPMI-1640 with 5% FCS, 100 $U.ml^{-1}$ penicillin G, and 100 $\mu g.ml^{-1}$ streptomycin sulphate, and kept on ice.

Stomachs were halved lengthwise and residual food matter was washed out with sterile PBS. Half stomachs were pinned onto cork boards and washed thoroughly before placing onto blood agar plates (Oxoid®) for *H. pylori* culture. The remaining half stomach was cut into strips and placed into formalin solution for fixation for use in confocal microscopy.

Brains were halved to be used in both confocal microscopy and flow cytometry applications. A mid coronal section comprising both lobes was cut using a surgical blade and was placed into a 5ml Bijou containing 10% formalin solution for fixation. The remaining brain tissue was homogenised for the extraction of lymphocytes according to the protocol described for the spinal cords (below).

Spleens were homogenised to a single cell solution by rubbing through a 70µm cell strainer placed in a petri dish containing 5ml washing medium, using the end of a sterile 1ml syringe. Solutions were collected from the petri dish using a sterile Pasteur pipette and dishes were washed with a further 5ml wash medium to collect remaining cells. Cells were collected into a 20ml universal tube and centrifuged at 300x *g* for 5 mins to form a pellet. Cells were further washed once more with 10ml wash medium before resuspension for counting in 10ml culture medium.

Brains and spinal cords were both processed in the same manner. Tissue was homogenised by rubbing through a 70µm cell strainer in 5ml washing medium in a petri dish. Cells were collected to a 20ml universal and remaining cells washed from the dish and collected using a Pasteur pipette. The cell suspension was centrifuged at 300x *g* for 5 minutes and further washed once more with 10ml wash medium. Here, lymphocytes were isolated from the spinal cord suspension using Percoll™ density-gradient centrifugation. For this, a neat Percoll solution (100%) was prepared by adding 1-part of 10x PBS to 9-parts Percoll solution. From this solution, 70% and 30% solutions were prepared using HBSS as the diluent. The spinal cord cell pellets were resuspended in 5ml of 30% Percoll working solution (100% diluted to 30% *v/v* in HBSS). These resuspended cells were slowly layered dropwise onto 4ml of 70% Percoll solution (100% diluted to 70% *v/v* in HBSS) in a 15ml falcon tube. Tubes were then centrifuged for 20mins at 500x *g* to separate the cells. The cells of interest amass at the interface between the 30% and 70% Percoll layers and is seen as a visible, slightly opaque, cell layer at the interface. These cells were extracted using a sterile Pasteur pipette carefully taking as little of the Percoll layers either side as possible. Extracted cells were washed with complete medium before resuspending in 10ml culture medium for counting. Counts were performed using a haemocytometer and using Trypan blue to exclude dead cells.

4.3.14 – Flow Cytometry

Flow cytometry was performed on cells from the spleen, brain, and spinal cord of the recipient mice, extracted and processed as described above. For all conditions, $1x10^6$ cells (or as many as possible if cell numbers were low) were added to 5ml FACS tube. Cells were centrifuged at 300x *g* for 5 minutes and the medium decanted. The pellet

was resuspended by flicking the tube and was washed in duplicate by the addition of 1ml PBA (Sterile PBS, 0.01% *w/v* BSA, 2% *v/v* FCS) before pelleting and decanting the buffer. All tubes were kept on ice throughout.

Cells were stained for surface and intracellular markers (described in *Table 15*). For surface staining: after the PBA washes (described above) the pellets were loosened, and the required amount of antibody added to the residual pellet volume (approximately 100µl). Cells were incubated with antibody for a period of 30 minutes in the dark and kept on ice. After the incubation 1ml of PBA was added to each tube and centrifuged at 300x *g* for 5 minutes, the medium was decanted, and the pellet loosened by flicking the tube. Cells were washed in this manner in duplicate.

For intracellular staining, the FoxP3 Transcription Factor Staining Buffer Set (eBioscience; Cat. No. 00-5523) was used. The required tubes were centrifuged at 300x *g* for 5 minutes to pellet cells before resuspending the cells in 1ml of 1x Fixation/Permeablisation reagent and incubating on ice for 20 minutes away from light. The 1x Fixation/permeablisation reagent was prepared by mixing 1 part of 4x concentrate (eBioscience; Cat. 00-5123) with 3 parts of diluent (eBioscience; Cat. 00-5223) as described in the manufacturer's instructions. After the incubation, the cells were washed in duplicate with 2ml of 1x permeablisation buffer and centrifuged at 300x *g* for 5 minutes before decanting the buffer and loosening the pellet. After the final wash step, the required number of antibodies for transcription factors were added to the residual pellet volume. Cells were incubated with antibody on ice for a period of 30 minutes, away from light. After the incubation, the cells were washed in duplicate with 1x permeablisation buffer, as described above. After the final wash, the pellet was loosened and resuspended in 0.5ml PBA. Prior to analysing, all cell solutions were filtered.

Acquisition was performed using an Astrios™ flow cytometer (Beckmann-Coulter®). A target of 200,000 events were recorded, where possible. Analysis was performed using the Kaluza™ software package. A representative gating strategy is presented in (*Figure 50*)

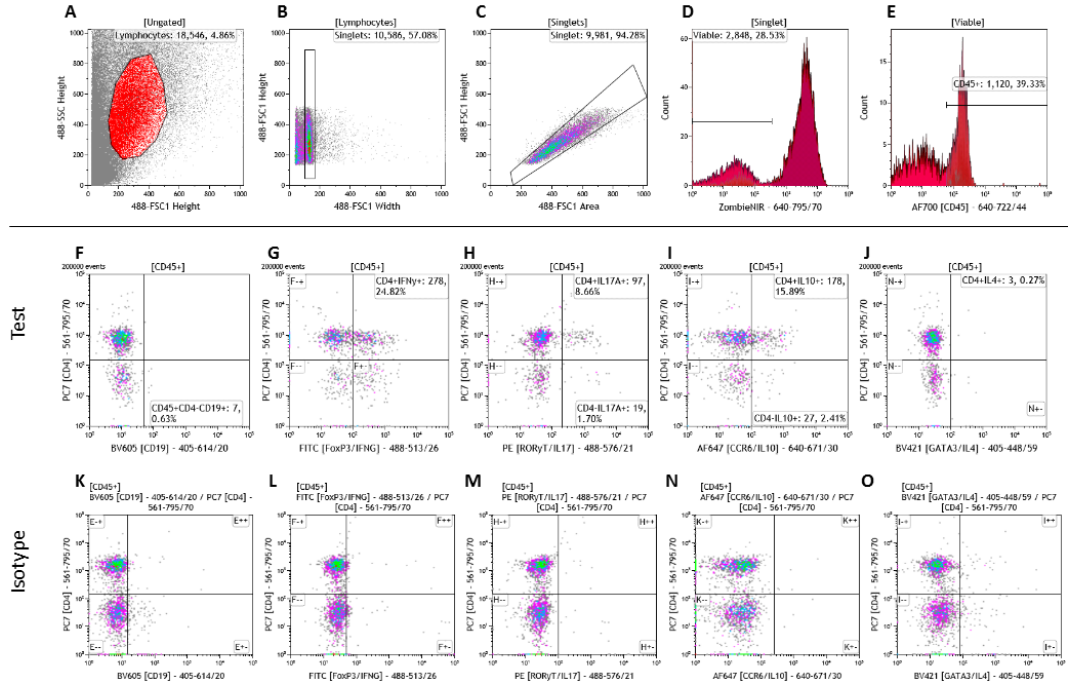

Figure 50 Example gating strategy for CNS cells

Splenocytes from C57BL6 mice were stained with Xenolight DiR reagent. Flow cytometry was used to quantify $CD4^+$ cells, and DiR-labelled $CD4^+$ cells amongst them. Gating, from left to right; lymphocytes according to forward and side scatter; doublet exclusion; debris exclusion; $CD4^+$ cells (histogram); Xenolight DiR-stained $CD4^+$ cells (dot-plot). Top panel: Identification of DiR-labelled cells. Plots A-J, gating strategy. Plots K-O, isotype controls. (A) Lymphocytes; (B-D) Debris, doublets, and dead cell exclusion; (E) CD45; (F-J) Specific antibodies; (K-O) Isotype control.

Table 15 Flow cytometry antibodies used in the analyses

Stain Used	Clone	Catalogue Num.	Quantity per test	Excitation	Emission	Filter
Xenolight DiR	n/a	Perkin-Elmer; 125964	10 µM	640	795/70	FL26
CD4:BV605	RM4-5	Biolegend; 100547	0.25 µg	405	614/20	FL8
CD45:BUV395	30-F11	BD Bioscience; 564279	0.1 µg	355	405/50	FL6
CCR6:BV421	29-2L17	Biolegend; 129817	1 µg	405	448/59	FL10
BV421 Isotype	HTK888	Biolegend; 400935	1 µg	405	448/59	FL10
Tbet:AF647	4B10	Biolegend; 644803	1 µg	640	671/30	FL12
AF647 Isotype	MOPC-21	Biolegend; 400167	0.5 µg	405	722/44	FL12
RORγT:PE	B2D	eBioscience; 12-6981-82	0.25 µg	488	576/21	FL18
PE Isotype	eBRG-1	eBioscience; 12-4301-81	0.25 µg	488	576/21	FL18
FoxP3:FITC	FJK-16S	eBioscience; 11-5773-80	0.5 µg	488	513/26	FL17
FITC Isotype	RTK2758	Biolegend; 400506	0.5 µg	488	513/26	FL17
CD19:BV605	6D5	Biolegend; 115593	0.5 µg	405	614/20	FL8
CD4:FITC	RM4-4	Biolegend; 116003	0.25 µg	488	513/26	FL17
CD11c:BV711	N418	Biolegend; 117349	0.06 µg	405	722/44	FL12
BV711 Isotype	MPC-11	Biolegend; 400963	0.06 µg	405	722/44	FL12
F4/80:PE	BM8	Biolegend; 123109	1 µg	488	576/21	FL18
PE Isotype	RTK2758	Biolegend; 400507	1 µg	488	576/21	FL18
Zombie NiR	n/a	Biolegend; 423105	1:200	633	795/70	FL25

Anti-mouse fluorochrome-conjugated antibodies used in flow cytometry. Clone used; catalogue numbers; volumes per test (defined as per tube, or million cells); and excitation and emission wavelengths are described.

4.4 - Results

4.4.1 – Flow Cytometry Analysis and Gating Parameters

Flow cytometry was used to assess the labelling of cells. Forward- and side-scatter characteristics were used to identify and gate lymphocytes. Doublets and debris were excluded. An example gating strategy for quantification of CD4, and DiR-positive cells is shown in *Figure 50.*

4.4.2 – Optimisation of the cell labelling protocol

The optimum concentration of Xenolight DiR reagent, and staining buffer and conditions to use were investigated to maximise the intensity of labelled cells. Cell recovery, viability and fluorescence intensity were used as a measure of performance (*Figure 51; A-C*). Downstream in the protocol is a separation of $CD4^+$ cells from homogenised tissues. The kits used for this procedure necessitate the homogenisation of tissue in HBSS, or EasySep™ buffer (which consists of HBSS, 2% FCS, 2mM EDTA). Adoptive transfer to mice requires sterile PBS medium. Several

media were tried as a staining buffer: PBS, PBA (PBS with 0.1% w/v BSA), RPMI-1640, HBSS, and EasySep buffer. $1x10^6$ cells were incubated in 1ml of staining buffer containing varying concentrations of DiR dye, according to the procedure detailed in section 4.3.1. PBA, HBSS and EasySep buffer were all comparable. Cells stained using PBS as the staining buffer resulted in a reduction of cell recovery (*Figure 51; A*). In terms of the viability of the recovered cells, there was no difference between the respective buffers, with viability around 80-95% (*Figure 51; B*). A low intensity of fluorescence resulted when using RPMI1640 medium (*Figure 51; C*). This was the case when using RPMI-1640 alone or supplemented with 5% FCS (data not shown).

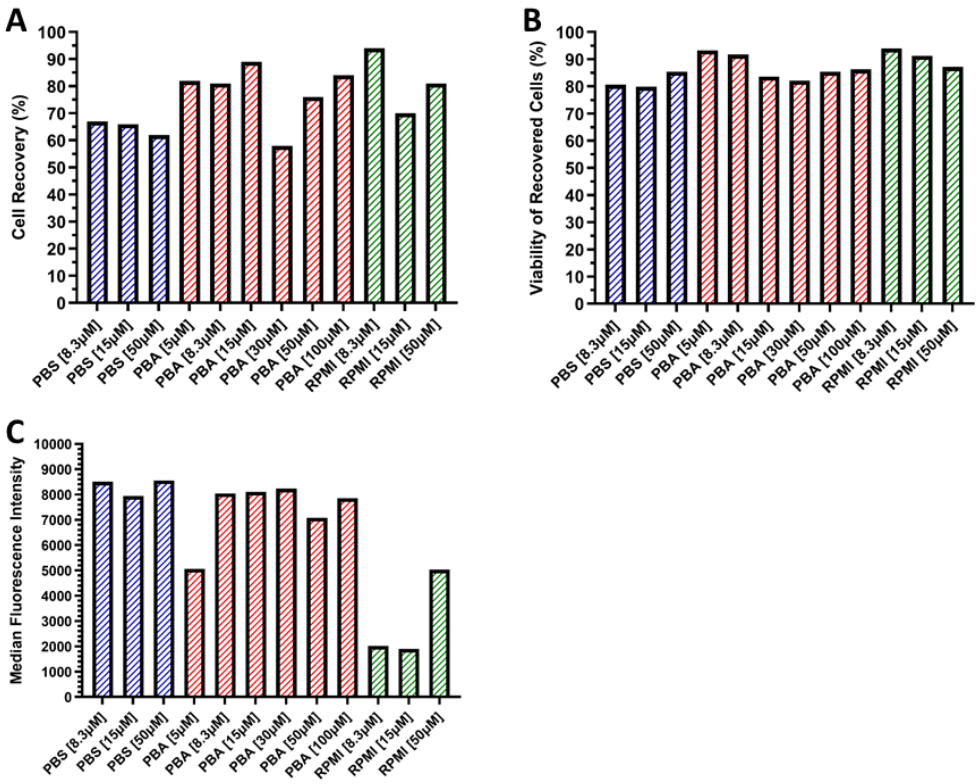

Figure 51 *Recovery and viability of cells under different labelling conditions*

Recovery and viability of cells after staining with Xenolight DiR reagent using different mediums (PBS, red; PBA, blue; RPMI-1640, green) and reagent concentrations. (A) Percent recovery of cells post-labelling. (B) Percent viability of recovered cells determined using Trypan blue.

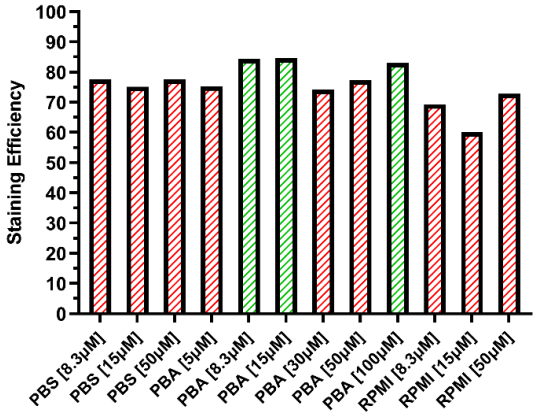

Figure 52 ***Assessment of the optimal conditions for the staining of CD4⁺ T-cells ex vivo***

Scores for the percent recovery, percent viability, and median fluorescent intensity of CD4⁺ T-cells stained using various alternative conditions (concentration, duration, medium) were combined to give a composite score for staining efficiency. Green bars represent the conditions resulting in the best over-all results.

To combine the best conditions from all the above variables, a composite score was assigned by combining the values for the three individual tests, percent recovery of cells after staining, the percent viability of recovered cells, and the median fluorescence intensity of the stained cell solutions measured by flow cytometry. *Figure 52* (above) shows the results from this 'efficiency' of staining. The green bars represent the conditions in which the best results were seen. The optimal conditions were therefore found to be staining in PBA with 8.3-15µM concentration of reagent. For the remaining tests in this study, a concentration of 10µM was used.

Finally, the concentration of cells used in the staining incubation step was considered. For this, cells were resuspended at concentrations between 1 $x10^6.ml^{-1}$ to $18x10^6.ml^{-1}$ (these numbers were solely due to available cell numbers). The staining was performed using the optimised conditions above for 10 minutes at room temperature using PBA with addition of 10µM Xenolight DiR to the staining buffer. There was no noticable difference in the median fluorescence intensity between the concentrations, however it was seen that when using higher cell concentrations some cells remained unstained, or were stained poorly. Further tests found that staining was optimal using cell concentrations of 1-2 $x10^6.ml^{-1}$ (data not shown).

Preceding commencement of the study, an experiment was conducted using the optimised procedures. Additionally, the real study would include a CD4 purification

step. This pilot test allowed a side-by-side comparison of two alternative CD4 selection kits, positive selection, or negative selection, as well as ensuring that cells were still healthy enough post-selection to endure the staining protocol and retain viability prior to injection into animals due to ethical considerations.

A spleen was harvested from a C57BL6 mouse and $CD4^+$ cells were purified using the methods described (*section 4.3.11*). Enriched $CD4^+$ cells were labelled with Xenolight DiR at 10µM in PBA, prior to being counter-stained with anti-CD4:FITC antibody and imaged on a TECAN® fluorescent plate reader (*Figure 53*) at 710-760/80nm.

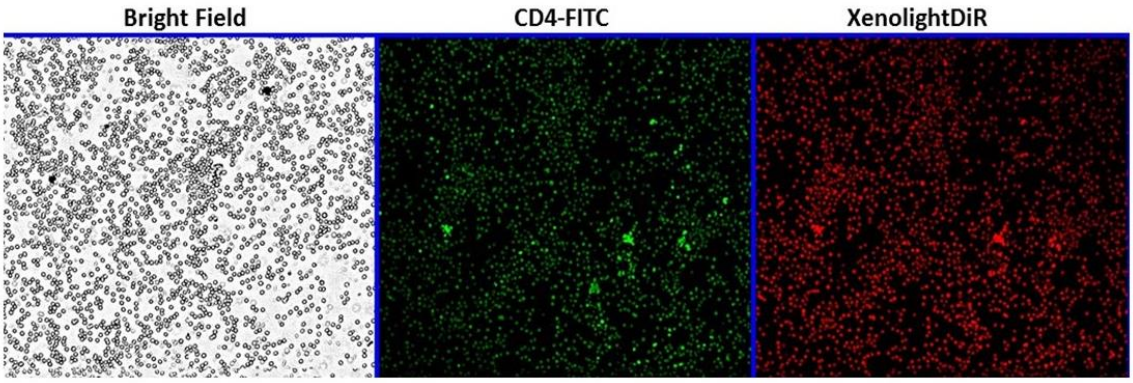

Figure 53 Fluorescence imaging of $CD4^+$ T-cells labelled with Xenolight DiR and anti-CD4:FITC antibody

T-lymphocytes were labelled using Xenolight DiR reagent and co-stained with anti-CD4:FITC antibody. Cells were imaged using a TECAN plate reader. Panels represent bright-field (left), CD4:FITC (centre), and Xenolight DiR (right). >99% of cells were co-stained with both labels.

4.4.3 – EAE $CD4^+$ T-cell migration after adoptive transfer to non-EAE *H. pylori*-infected or uninfected C57BL6 mice.

With an optimised protocol for the labelling of CD4 cells, a pilot study was performed to establish $CD4^+$ EAE T-cell trafficking after adoptive transfer to non-EAE donor mice. This study will inform of the distribution and migration of EAE $CD4^+$ cells after adoptive transfer, and whether this trafficking is differentially regulated between uninfected or *H. pylori*-infected recipient mice.

Two groups (infected/uninfected) of 3 female C57BL6 mice of 5-weeks old were used in this study. 3 mice were administered *H. pylori* strain PMSS1 in PBS by oral gavage,

the control group were administered PBS-only as a sham-infection control. Inoculations were performed as per the methods previously described (*section 4.3.7.2*). Infections were allowed to establish and persist for a period of 10 weeks prior to experimentation.

Meanwhile, EAE was induced in 9 uninfected 5-week-old female C57BL6 mice. Mice were monitored for welfare and weight once daily and were sacrificed at 7 d.p.i. preceding the onset of symptomatic EAE. This time point was chosen as it should immediately precede the onset of EAE symptoms which are usually apparent from 7-9 d.p.i, and thus will have allowed for the induction and propagation of MOG-specific $CD4^+$ EAE T-cells as per the standard EAE induction model. Upon sacrifice, splenocyte cell suspensions were produced and $CD4^+$ cells (containing EAE MOG-primed $CD4^+$ T-cells) were enriched using immunomagnetic separation. Purified EAE $CD4^+$ splenocytes were labelled with Xenolight DiR as described.

A total of $5x10^6$ labelled EAE $CD4^+$ cells were administered to each of the recipient mice. Labelled cells were administered via injection into the tail vein in a 75µl volume of sterile PBS immediately post-labelling. Once administered, mice were monitored for a period of 30 minutes to ensure of their welfare. No adverse events were apparent resulting from the procedure.

At 24-hours post-injection, mice were humanely euthanised using a CO_2 chamber. Cadavers were imaged at various stages of dissection using an IVIS Spectrum™ instrument (Perkin-Elmer). As a pilot study, it was necessary to investigate the ability to detect the Xenolight reagent through the fur and skin to inform of the possibility for longitudinal tracking of cell migration *in vivo* during future studies of this nature. *Figure 54* shows results of this, both with and without the skin. The signal was markedly attenuated through the skin of the animals (top two panels) with a robust boost to the detected signal after removal of the skin (bottom two panels).

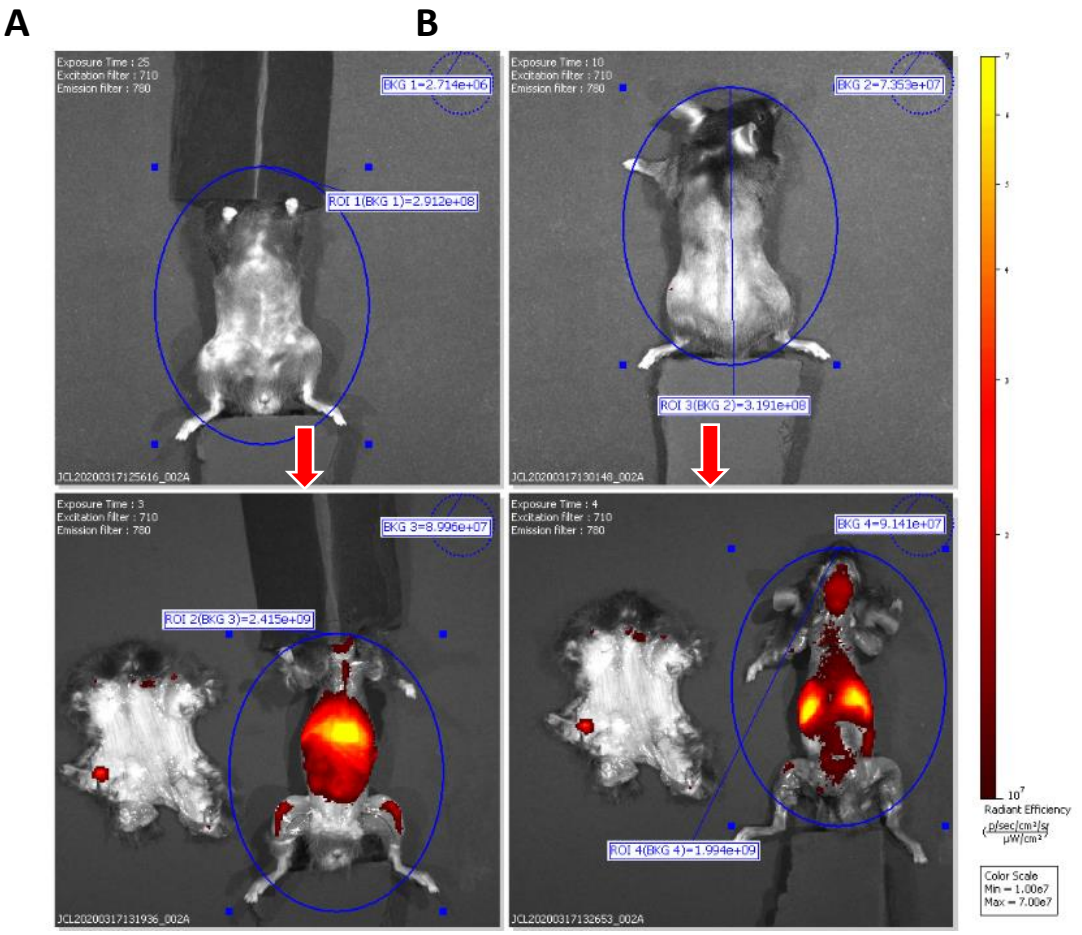

Figure 54 *Quantification of Xenolight DiR-labelled CD4 T-cells adoptively transferred to C57BL6 mice, both with and without fur and skin*

The degree to which fluorescent quenching occurs through the fur and skin of recipient C57BL6 mice. Mice were imaged using an IVIS Spectrum instrument 24-hours after transfer of DiR-labelled EAE $CD4^+$ cells. The label is seen to localise to the abdomen, the long bones of the leg, tonsils, and inaugural lymph nodes. (A) Abdominal view, and (B) back view of recipient mice; top panels: with fur, bottom panel: without fur.

4.4.3.1 – Quantification of the biological distribution of DiR-labelled cells with *in vivo* imaging of recipient mice

The brain, spinal cord, heart, lungs, liver, kidneys, spleen, stomach, and intestines were dissected and arranged for imaging at 710nm excitation/780nm emission along with the remaining carcass. Each organ was assigned a region of interest (ROI) 'gate' and the total radiance ($photons^{-1}.second^{-1}.cm^2.sr^{-1}$) per mouse was quantified in a similar manner. Representative images showing the arrangement and gating of each ROI are shown in *Figure 55*.

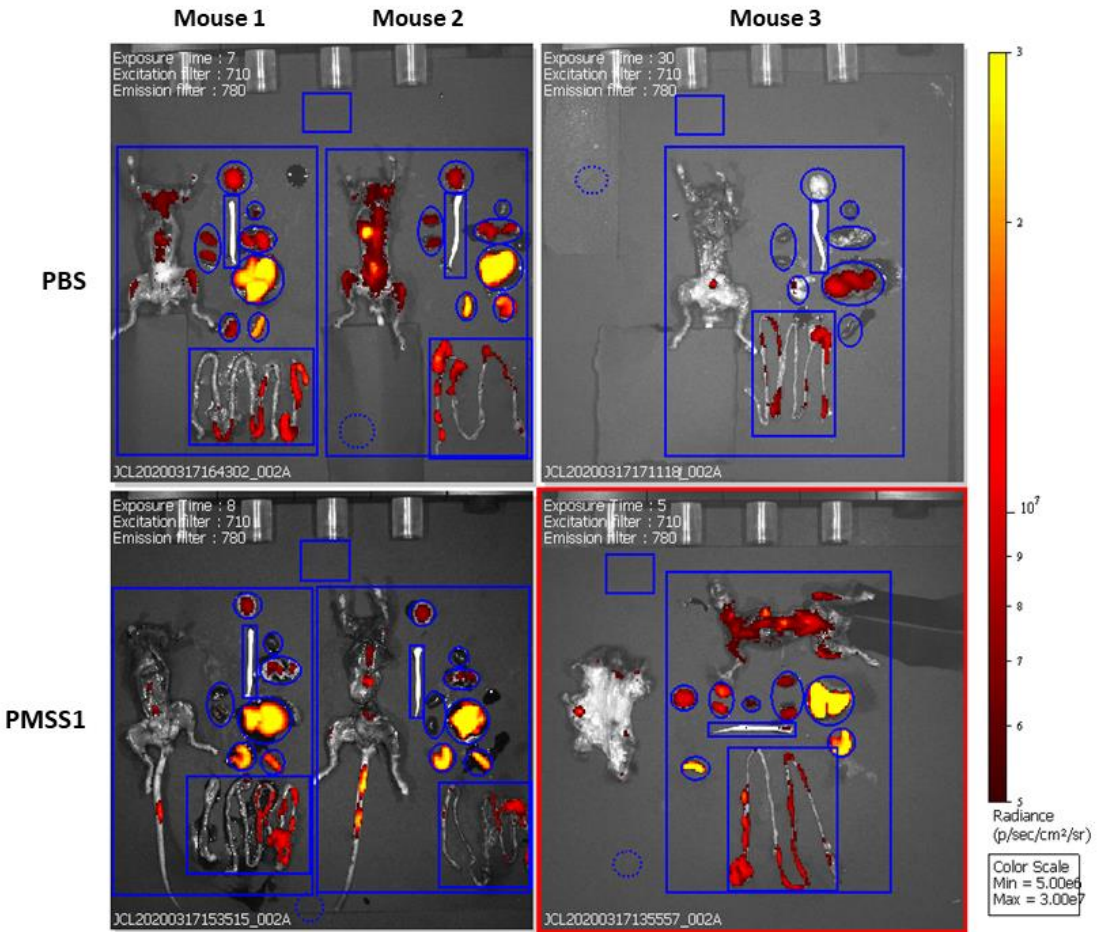

Figure 55 Representative gating strategy for quantification of the distribution of labelled EAE CD4⁺ T-cells adoptively transferred to C57BL6 mice

Three recipient mice per group, either uninfected (PBS, top panels) or *H. pylori* PMSS1-infected (PMSS1, bottom panels) were dissected 24-hours after adoptive transfer of DiR-labelled $CD4^+$ cells from EAE donor mice. Fluorescence was quantified on an IVIS imaging system. After dissection, each organ was assigned a region of interest (ROI) 'gate' for quantification of fluorescence. Average radiance (photons per second per cm^2 per steradian) was determined for each region of interest. To account for variance in the total dose administered to each mouse, the average radiance of each organ ROI was normalised to the total radiance per animal.

To correct for potential confounding differences in the number of cells administered, the total radiance across each mouse was quantified. The total radiance from each mouse was variable (*Figure 56*).

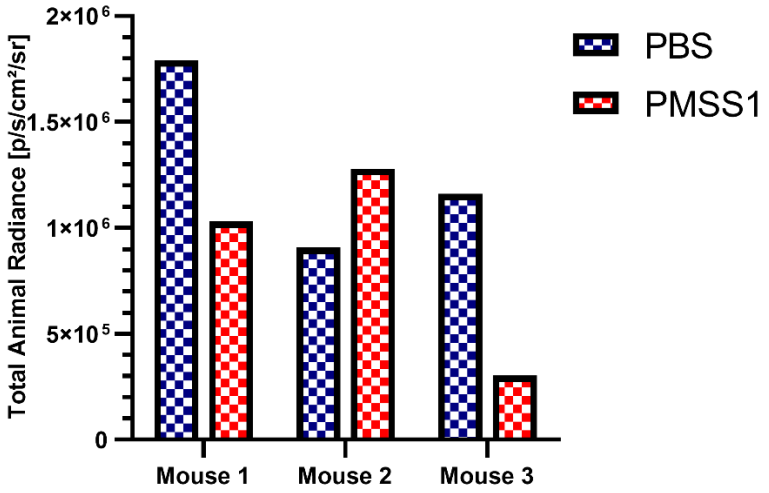

Figure 56 ***Total radiance quantified for each mouse after dosing with 5x10^6 CD4$^+$ cells from EAE mice labelled with Xenolight DiR reagent.***

Mice were imaged post-mortem at 24-hours after adoptive transfer of labelled EAE CD4 cells. The total dose of DiR administered to each mouse was quantified and used to normalise the data derive from individual organs.

The biodistribution of the label in each organ, data was normalised by dividing by the total radiance for the whole mouse. Corrected radiance is presented in *Figure 57*. The brain and spinal cord were markedly lower in labelled cells in the infected group as compared to the uninfected group. The *H. pylori* infected animals had an elevation in the number of labelled cells in the intestines, but interestingly not the stomach.

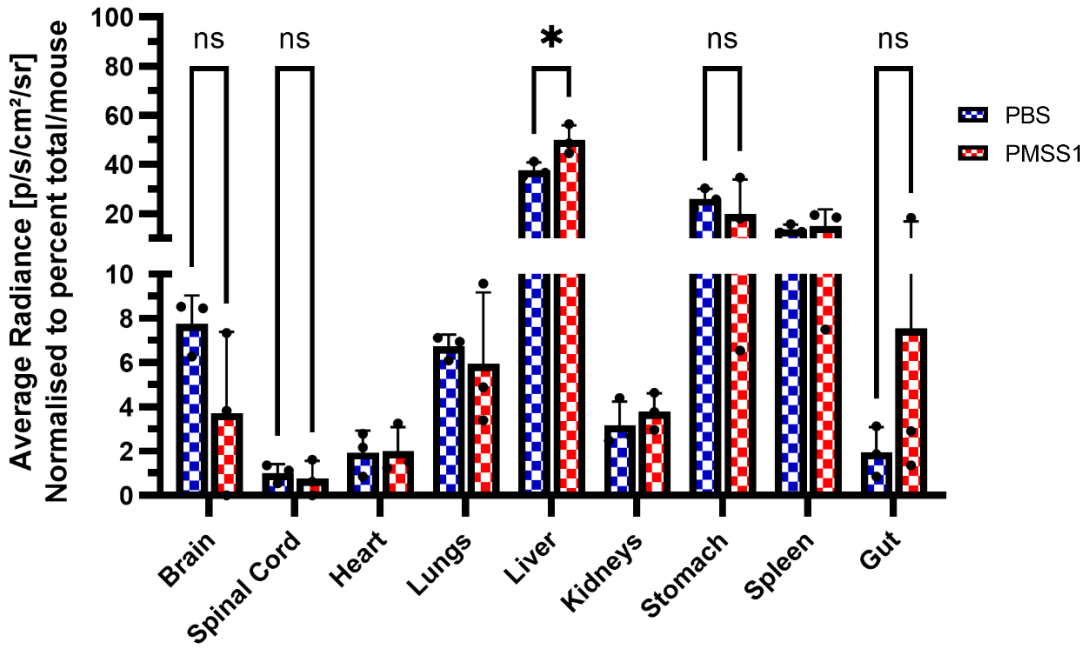

Figure 57 Average radiance quantified for each organ after adoptive transfer of Xenolight DiR labelled EAE CD4⁺ T-cells to C57BL6 mice.

The average radiance measured in photons per second per cm^2 in each organ after dissection at the study endpoint. To correct for confounding variance in the total dose administered to each mouse, the average radiance from each organ is normalised to the total sum of radiance quantified across all tissues. Bars and error represent the mean + SD. ANOVA with Šídák's correction; ** p=0.0037.*

Cells stained with Xenolight DiR (and thus adoptively transferred cells) were found to distribute widely and were detectable in all the measured organs. The major site of their localisation was the liver, followed by the stomach and spleen. In the *H. pylori* infected mice, adoptively transferred EAE CD4 cells were reduced in the central nervous system (both brain and spinal cord) as compared to uninfected mice (brain: 2.1-fold reduction; spinal cord: 1.4-fold reduction, not statistically significant) and elevated 3.1-fold in the gut (not significant), but not in the stomach.

For comparison, previous work in this research group used the radio isotope Indium to label cells prior to adoptive transfer. This was followed by imaging using SPECT-CT nuclear imaging *in vivo*. The migration of CD4 cells after adoptive transfer to *H. pylori* infected or uninfected recipient mice was imaged using SPECT-CT and the data was presented in the PhD thesis of Dr. Katie Cook; University of Nottingham [443]. These data were presented here as a comparison between the two imaging modalities.

Figure 58; A-C, shows the quantification of radioisotope in the spleen, lymph nodes, lungs, stomach, and liver at 1-, 2-, and 3-days post-transfer of labelled cells.

Of the CD4 cells transferred, most of the *in vivo* signal was localised to the spleen, followed by the lymph nodes. Of total injected radioisotope, only 0.33% was recovered in the spleen at 24 hours post-transfer. This number reduced markedly each 24 hours for a period of 72 hours indicating a short stability half-life of the label.

Interestingly, the localisation of cells in the current and previous studies do not agree. The current study found around 50% of fluorescent signal from DiR-stained cells was detected in the liver followed by the gut, in stark contrast to the localisation to the spleen and lymph in the previous study.

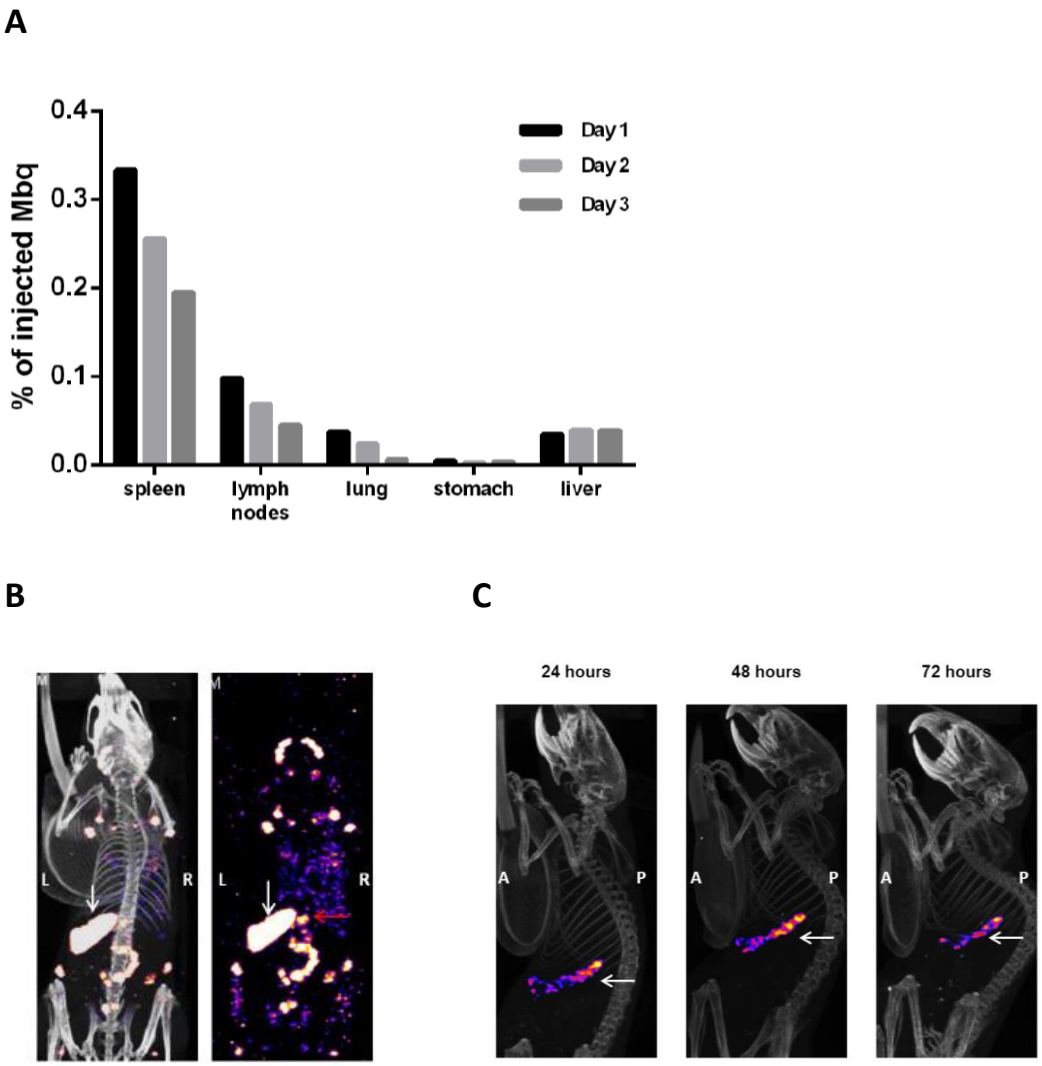

Figure 58 ***Comparative results of the biodistribution of adoptively transferred CD4⁺ cells labelled with Indium^{111} in C57BL6 mice either infected with H. pylori or uninfected***

A previous study performed by Cook *et al.* in this research group used the radioisotope Indium^{111} to label CD4⁺ cells prior to adoptive transfer in infected or uninfected mice. (A) The biodistribution of the label is presented. (B) SPECT-CT images are shown at 24-hours, localisation was seen primarily in the spleen (white arrow), stomach and GI tract (red arrow), and lymph nodes (no arrows). (C) Splenic localisation of labelled CD4 cells at each time point over a 72-hour period. The images and data here were produced by Dr. Kathryn Cook, University of Nottingham and used as a reference, unmodified from her submitted PhD thesis.

One year after the experiment, brain sections and stomachs were removed from the formalin solution where they were stored at 4°C. Tissues were again imaged using the IVIS Spectrum instrument to investigate the long-term stability of the label. Originally these tissues were intended for use with confocal microscopy, but this was

not possible at the time due to the 2019 coronavirus pandemic and closure of this institution.

The brain sections taken into fixation solution on the day of sacrifice were taken out of formalin and imaged using the IVIS Spectrum (*Figure 59*). The imaging of these tissues will provide evidence as to the stability of the label in long term storage which may be pertinent to future studies of this nature. The label was still visible after 12-months storage at 4°C in the dark. No such imaging of this tissue was performed at the time of the study from which to draw comparisons as to longevity of the label.

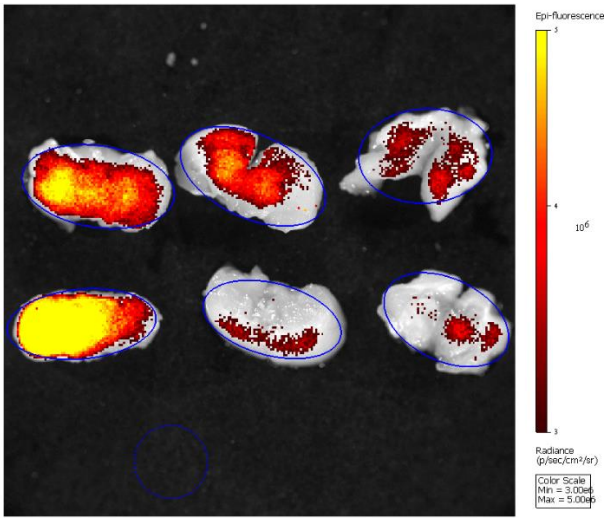

Figure 59 ***Mid-coronal brain sections from the H. pylori infected and uninfected recipient mice after adoptive transfer of labelled CD4⁺ T-cells from EAE donor mice.***

Brain sections from 3 *H. pylori*-infected (top row) and 3 uninfected mice (bottom row) were imaged using the IVIS Spectrum instrument, quantifying average radiance (photons per second per cm^2). Sections were imaged 12 months after the experiment for qualitative not quantitative purposes, to advise on the stability of the reagent for future work.

Half-stomachs which were fixed at the time of sacrifice were analysed in the same manner (*Figure 60; A-C*). Stomach tissue was devoid of dietary matter and washed prior to deposition in formalin fixation solution. Fluorescent signal was still apparent after long term storage, localised to distinct regions of the gastric mucosa which may correlate to regions of inflammation.

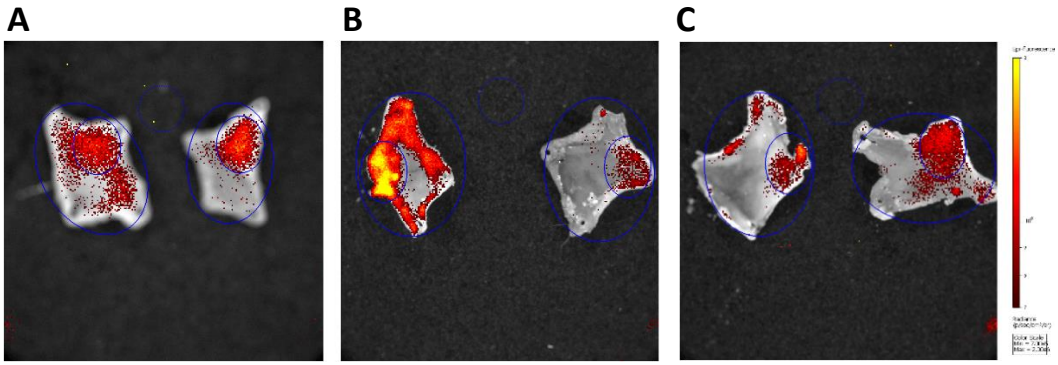

Figure 60 ***Stomach tissue from H. pylori infected or uninfected mice after adoptive transfer of labelled CD4 T-cells from EAE donor mice***

Stomachs from recipient mice were extracted and cleaned of food debris prior to being deposited into formalin solution and stored at 4°C. At a point of 12 months after the experiment, tissues were removed from storage and imaged using the IVIS Spectrum instrument. Panels show stomachs from one mouse for each group (Panel A, Hp1 and PBS1; panel B, Hp2 and PBS2; panel 3. Hp3 and PBS3). Labelled cells can still be visualised after 12 months of storage.

Due to the observations in this study that the intestines were a rich source of fluorescence in the target wavelengths of Xenolight (760-780nm), faecal matter was collected from C57BL6 mice in an unrelated study. Faecal pellets were placed into the IVIS instrument and imaged as described previously (*Figure 61*). A high level of fluorescence was apparent from the faecal pellets suggesting that the dietary matter fed to the study mice may well be confounding the data acquired during this study.

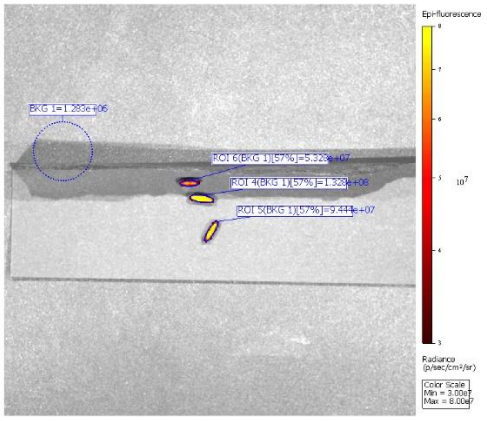

Figure 61 ***Confounding auto-fluorescence from faecal matter of C57BL6 mice fed the standard rodent chow.***

Faecal matter from non-experimental C57BL6 mice fed on a standard rodent chow generates significant amounts of signal detectable in the far-red wavelengths of the Xenolight DiR label (710nm/760-780nm).

4.4.3.2 – Flow cytometry analysis of lymphocyte populations after adoptive transfer of EAE CD4$^+$ cells to *H. pylori* infected or uninfected mice.

Having visualised the biodistribution of DiR using the IVIS system, flow cytometry was performed to confirm the DiR data, and quantify cellular subtypes expressing each marker. After imaging, cell suspensions were produced from the spleen, brain, and spinal cords for use in a flow cytometry analysis staining for identifiable cellular lineage markers. The markers used in the characterisation of the lymphocyte populations across these tissues were CD45 (lymphocytes), CD4 (CD4$^+$ T-cells), CD19 (B-cells), CCR6 (CCL20-responsive cells), CD11c (dendritic cells), F4/80 (macrophage). In addition to T-helper subtype-specific transcription factors; Tbet (Th1), GATA3 (Th2), RORγT (Th17), and FoxP3 (Treg).

Cell preparations from the central nervous system were of very low numbers and poor-quality preps, the resulting cell suspension was predominantly Trypan blue-positive, indicating dead or dying cells. The flow cytometry data here should be taken as a representation of the methods used, and not used to make inferences. CD45, CD4, RORγT, FoxP3, and DiR staining was acceptable; Tbet and CCR6 staining was inefficient and with positive staining from the isotype control. As such, no conclusions should be drawn from the flow cytometry data for these markers. CNS cell suspensions were stained with Zombie NiR viability dye with dead cells excluded from the analysis. A representative gating strategy used in these analyses is presented in *Figure 62; A-E*.

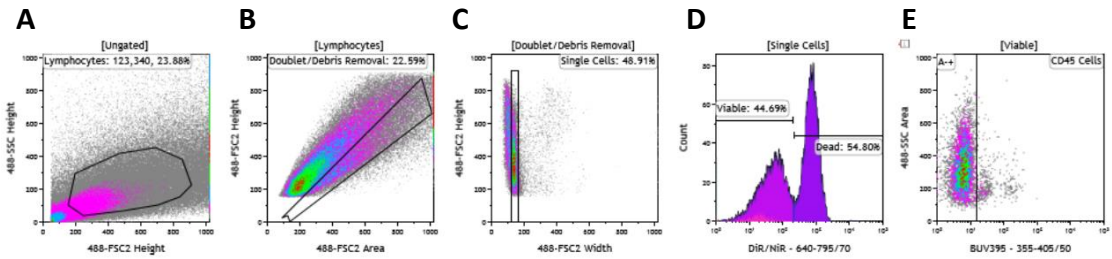

Figure 62 ***Representative gating strategy for the identification and characterisation of central nervous system infiltrating murine lymphocytes***

Lymphocytes are selected from complex mixtures of CNS cells in a series of steps. (A) forward and side-scatter characteristics defining the size and complexity of cells are gated. (B) Debris and doublets are removed by gating the regions in plots B and C. (D) Dead cells are removed from the analysis by gating only those cells not stained with the viability dye. (E) From the resulting population of viable single events, individual markers can be characterised, such as CD45.

Flow cytometry analysis of CNS tissue (*Figure 63*) determined that, despite a 2-fold reduction in the frequency of $CD45^+$ cells in the brain in the *H. pylori* infected group, there was no difference in the proportion of these $CD45^+$ cells expressing either CD4 or CCR6. There was a shift in the proportion of adoptively transferred DiR-labelled cells amongst CD45+CD4+ infiltrating lymphocytes, being 2-fold elevated in the infected group. Similarly, there was a 1.6-fold elevation in the number of CD45+CD4+ cells stained for both CCR6 and DiR. Adoptively transferred DiR+ cells made up a comparable small minority in both groups, accounting for <0.25% of total brain resident $CD45^+$ cells.

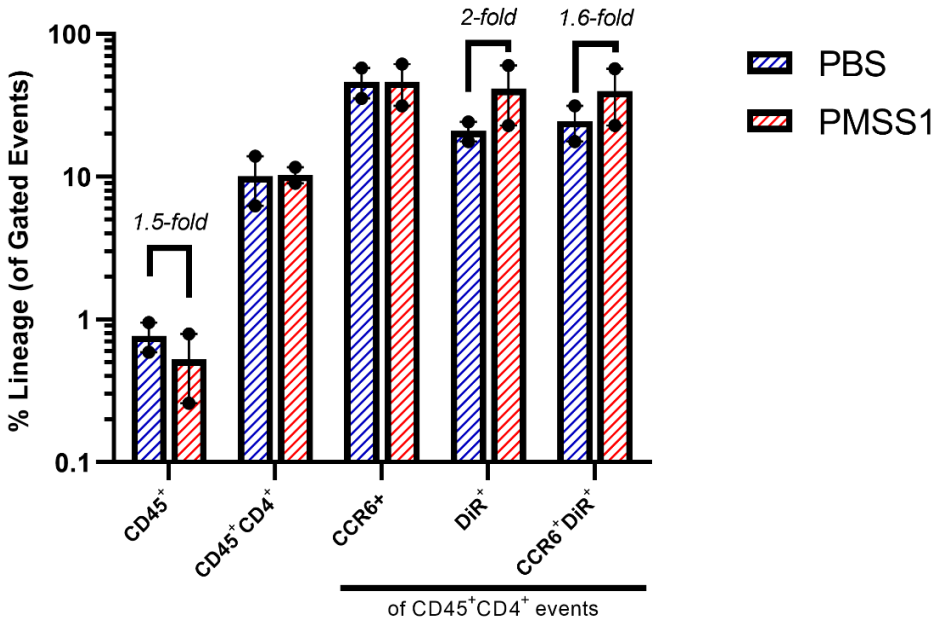

Figure 63 ***Frequency of lymphocytes in the brain after adoptive transfer of EAE CD4⁺ T-cells to H. pylori infected or uninfected EAE mice.***

Staining of cellular markers from cells extracted from the brains of infected and uninfected recipient mice. Proportions of CD45+ and $CD4^+$ cells are expressed as a percentage of total viable cells. Proportions of cells stained for CCR6, DiR, or both, are expressed as the total percentage of CD45+CD4+ cells. Bars and error denote the mean and SD.

In the brain, although the relative proportion of CD45+ amongst total brain cells was reduced by 1.5-fold (not significant), no differences between groups were noted in the proportion of either CD4 T-cells or CD19 B-cells amongst resident lymphocytes. There were however elevations in the frequencies of F4/80+ macrophages and CD11c+ dendritic cells (or microglia) from $CD45^+CD4^-CD19^-$ cells (*Figure 64*).

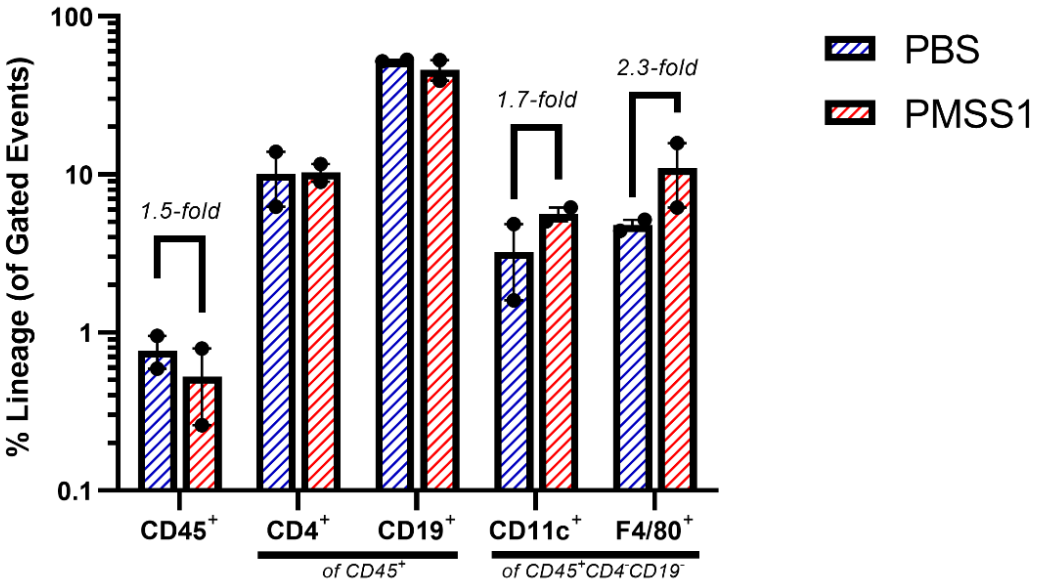

Figure 64 ***Cellular lineages in the brain of H. pylori infected or uninfected mice after adoptive transfer of EAE CD4⁺ T-cells***

Staining of lineage defining markers on cells extracted from the brains of uninfected or infected recipient mice. Doublets and debris were excluded from the analysis. CD45+ cells are expressed as a percentage of total cells. $CD4^+$ T-cells and CD19+ B-cells as a percent of total CD45+ events; CD11c dendritic cells, and F4/80+ macrophage is expressed as a percent of CD45+ but CD4-CD19- events. Bars and error denote the mean and SD.

In contrast to the brain, spinal cord cells from the *H. pylori* infected mice were enriched for CD45+ lymphocytes (1.9-fold, n.s.) with a concurrent reduction in the frequency of these to be $CD4^+$ (1.9-fold, n.s.). Of either CD45+ cells or CD45+CD4+ cells, no differences were seen in the expression of CCR6 between groups. CD19, CD11c and F4/80 were not stained in this panel and may account for the elevation of CD45+ cells (*Figure 65*).

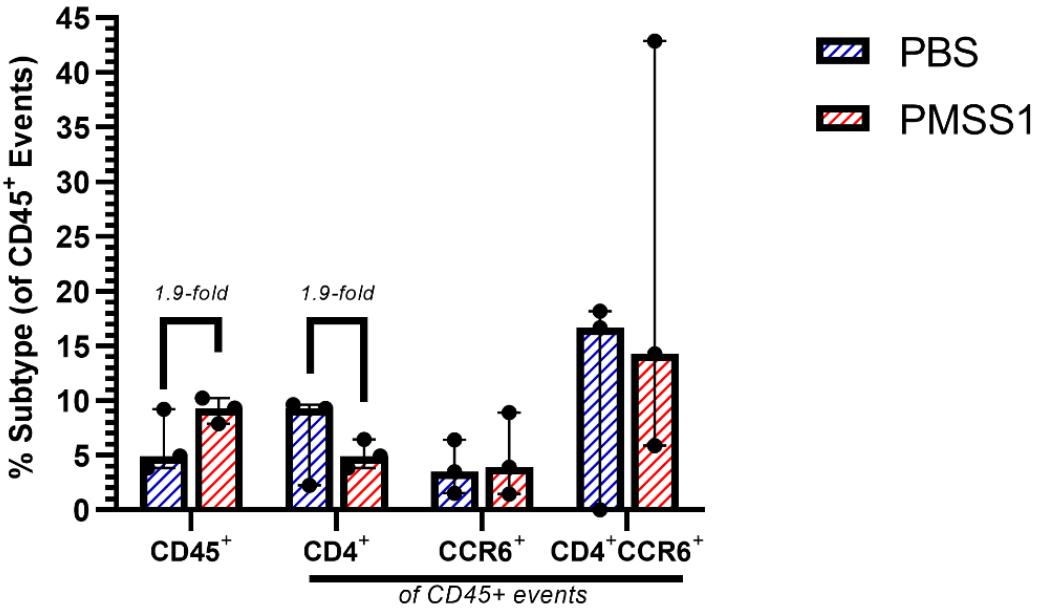

Figure 65 ***Flow cytometry analysis of lymphocyte frequency in the spinal cord of H. pylori infected or uninfected recipient mice 24-hours after adoptive transfer of EAE CD4⁺ T-cells***

Cells from the spinal cords of recipient mice 24-hours after adoptive transfer of labelled CD4⁺ cells were extracted and stained for cellular surface markers CD45, CD4 and the chemokine receptor CCR6; imaged using flow cytometry. Lymphocytes were selected according to forward and side scatter characteristics, excluding debris and doublets, and gated as those cells expressing CD45. CD4⁺ and CCR6⁺ cells are presented as a percentage of total CD45+ cells. Bars represent the group median value; error bars denote the range.

Further to the reductions in the overall frequency of CD4⁺ cells from spinal cord CD45⁺ lymphocytes in the *H. pylori* infected group, there was also a shift in the underlying composition of the CD4⁺ T-helper subtype populations to favour protection. Determined by the major transcription factors for; Th1 (Tbet), Th17 (RORγT), and Treg (FoxP3) cells, the inflammatory Th1 and Th17 subsets were reduced (Th1: 2-fold, n.s.; Th17: 4.5-fold, n.s.) in parallel to an elevated proportion of FoxP3⁺ Tregs (5-fold, *p=0.02*) in the spinal cords of *H. pylori* infected mice 24-hours post adoptive transfer of EAE CD4⁺ cells (*Figure 66*).

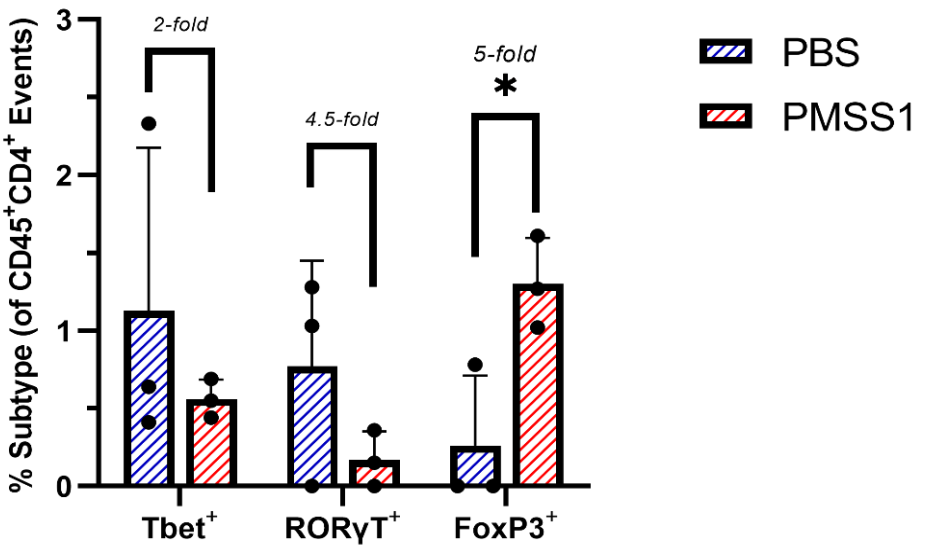

Figure 66Flow cytometry analysis of the frequency of the T-helper subsets; Th1, Th17 and Treg in the spinal cords between uninfected and H. pylori-infected recipient mice after adoptive transfer of labelled EAE CD4⁺ cells

Frequency of inflammatory CD45+CD4+Tbet+ (Th1), CD45+CD4+RORγT+ (Th17), and CD45+CD4+FoxP3+ (Tregs) cells in the spinal cords of *H. pylori* infected or uninfected mice 24 hours following adoptive transfer from EAE donor mice. Proportions expressed as a percentage of total CD45+CD4+ cells. Dots represent individual mice; bars and error represent the group mean + SD. Unpaired t-test; * *p= <0.028.*

Initially, the experimental design included the fixation of tissue and confocal imaging to quantify the labelled cells *in situ* to establish intra-tissue localisation with a finer resolution. Due to the poor viability and recovery of spinal cord cells it was deemed necessary to stain with Zombie NiR viability dye. Zombie NiR emits in the same near-infra-red channel as Xenolight DiR, as such the label cannot be quantified from the spinal cord in this flow cytometry analysis, with the expectation that these data could be attained via microscopy later. Due to the coronavirus pandemic the microscopy was not possible to perform.

As well as characterising the brain and spinal cord infiltrate, splenocytes of the recipient groups were analysed in the same manner (*Figure 67*). There was a modest reduction in CD4⁺ cells stained with the label DiR amongst splenocytes from the *H. pylori* infected mice as compared to uninfected control animals. There was no difference in the proportions of any of the cellular markers stained for in either group in the spleen.

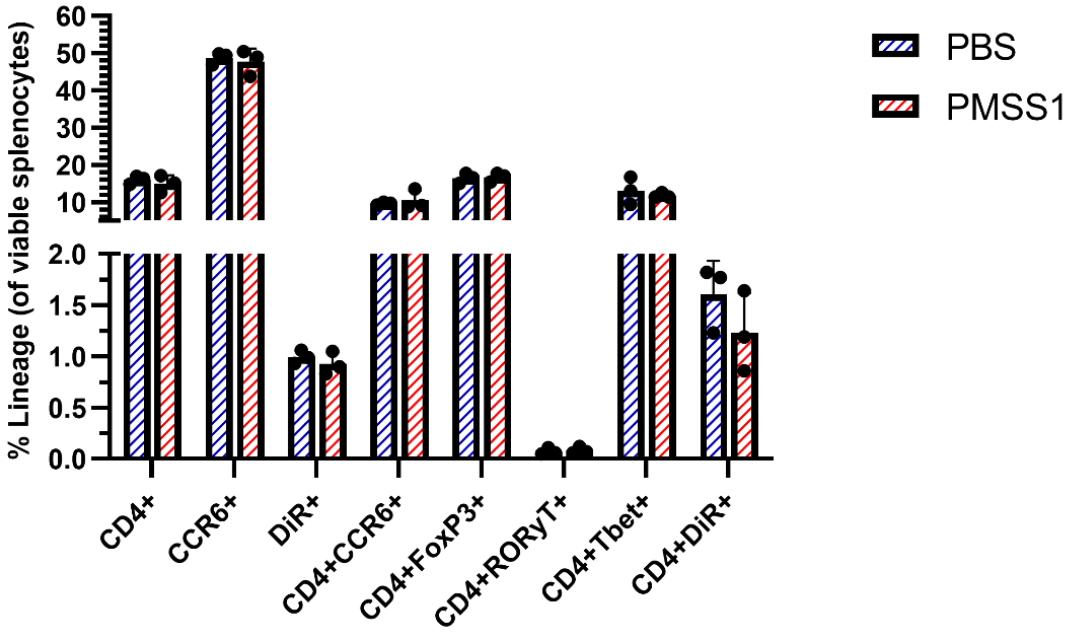

Figure 67 ***Flow cytometry analysis of the frequency of lymphocyte subsets amongst splenocytes after adoptive transfer of EAE CD4⁺ T-cells between H. pylori infected or uninfected recipient mice.***

Splenocytes from recipient mice were stained and analysed using flow cytometry. Cells were labelled with Xenolight reagent prior to adoptive transfer. *Ex vivo*, cells were stained for the surface markers CD4 and CCR6. T-helper subtypes were quantified by staining for the associated transcription factors for Th1 (Tbet), Th17 (RORγT), and Treg (FoxP3). Lymphocytes were gated according to forward and side scatter characteristics; debris and doublets were excluded; viable cells were gated using a viability dye. The proportion of cells expressing each marker are given as a percent of total viable lymphocytes. Bars and error show the mean + SD.

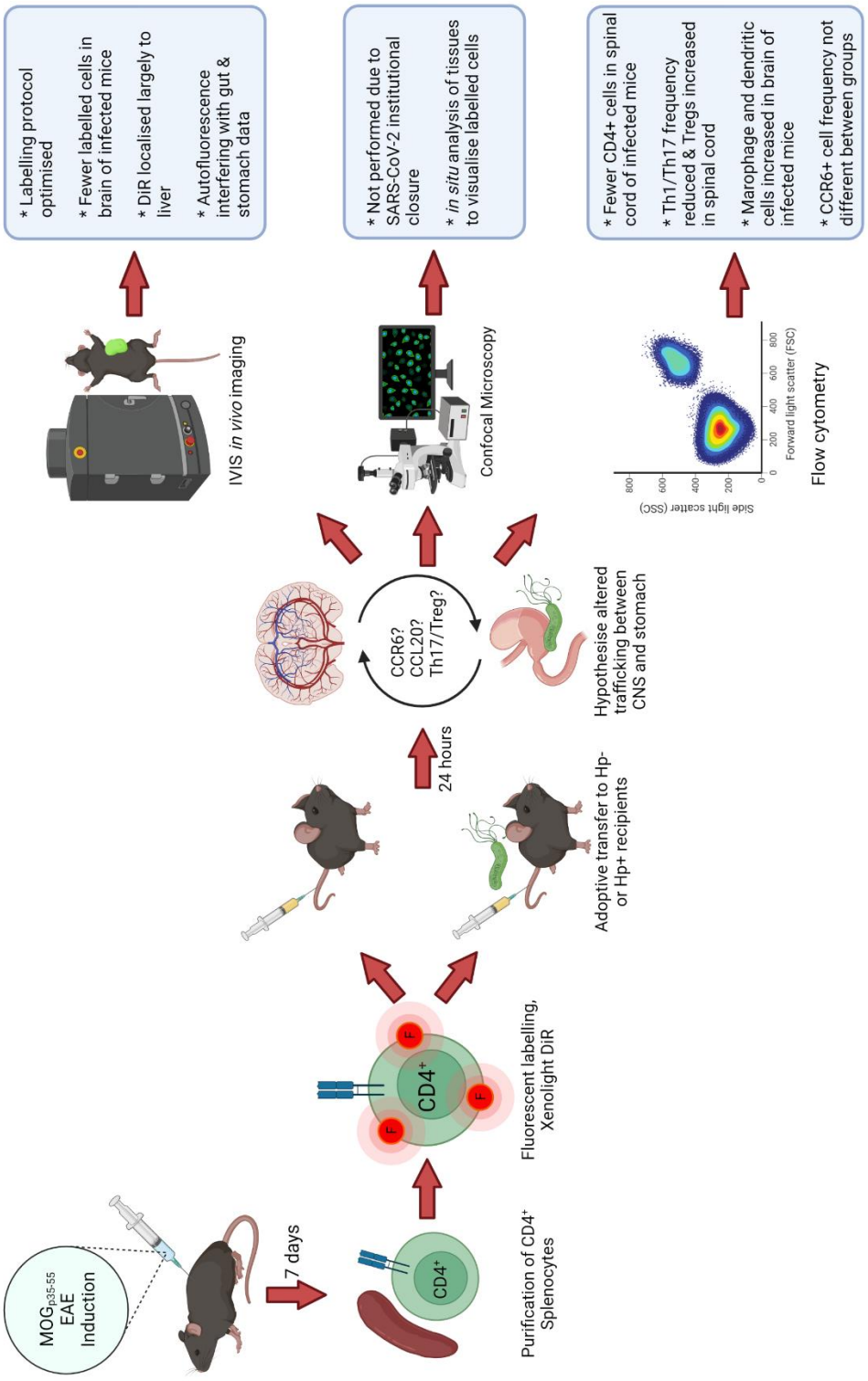

Figure 68 Schematic representation of the T-cell migration study design and summary of the data generated

Experimental design of the migration study. The hypothesised CCR6/CCL20 axis mediating differential trafficking was not confirmed in the current study. However, fewer labelled EAE $CD4^+$ cells migrated to the brain in *H. pylori* infected mice. Of CNS infiltrating cells, infected mice displayed reduced numbers of inflammatory Th1/Th17 cells, and concurrent increase in Tregs. Figure created with BioRender.

4.5 – Discussion

A graphical summary of the study and data generated is given in *Figure 68*.

4.5.1 – Summation of the major findings

- A protocol for the Xenolight DiR reagent was optimised and subsequently used to uniformly label $CD4^+$ lymphocytes enriched from the spleens of EAE mice.

- DiR-labelled cells were adoptively transferred to recipient mice either infected or uninfected with *H. pylori* and were quantifiable from tissues post-mortem.

- C57BL6 mice are not a suitable strain for the purpose of *in vivo* fluorescent imaging using this reagent as observed by a marked attenuation of the signal through the skin and fur.

- The standard rodent chow fed to study animals contributes significantly to autofluorescence in this model as observed from faecal matter; alternative specialised diets may overcome this obstacle.

- The label was primarily detected in the liver of recipient animals, followed by the gut and spleen. Liver tropism may indeed indicate metabolism of the reagent or cellular debris accumulation.

- I do not find evidence that adoptively transferred $CD4^+$ EAE T-cells migrate to the infected gastric mucosa.

- Flow cytometry analysis of cell populations in tissues was hindered by low cell recovery and viability from the brain and spinal cord, and inadequate staining.

- There may be a trend for CD4 cells of the spinal cord to shift towards a predominantly anti-inflammatory phenotype in *H. pylori* infected mice.

- These data do not find clear differences in the expression of CCR6 between groups, nor in shaping differential trafficking as hypothesised.

4.5.2 – Optimising the fluorescent labelling of $CD4^+$ T-cells

The major aim of this preliminary pilot study was to assess the suitability of the Xenolight DiR labelling reagent for use in tracking the migration of murine $CD4^+$ cells *in vivo*. Du, *et al.* [454], and Youniss *et al.* [455] have used this dye successfully to track the homing of T-cells in murine tumour models. In both these reports, labelling of cells had no detrimental impact on their functionality or *in vivo* migration. Furthermore, Du reports the labelled cells were quantifiable in tissues up to 14 days post-adoptive transfer. Youniss demonstrates visualisation of T-cells *in vivo* up to 3 weeks post transfer [455]. Uong used Xenolight to track natural killer T-cells in mice, without detriment to viability and quantifiable up to 21 days [456]. Here, I show that murine $CD4^+$ EAE T-cells were successfully labelled with the reagent without notable loss to either cell recovery or viability. The labelled cells were adoptively transferred to recipient mice and the biodistribution was possible to quantify after 24 hours.

This study has shown that $CD4^+$ cells can be purified from EAE mice and subsequently labelled with Xenolight reagent preceding adoptive transfer EAE (passive EAE), without loss of viability. Trafficking of these cells in recipient animals can be shown experimentally *in vivo*, quantified using the IVIS Spectrum imaging system. It was important to establish an optimised method for labelling prior to commencing the study, various conditions were tested. The best results were seen when using a concentration of 10µM Xenolight DiR reagent incubated with $1x10^6$ cells.ml^{-1} for a duration of 10 minutes at RT/4°C in the dark. Youniss *et al.* use 320µM in culture medium, Uong *et al.* use 40µM in culture media, whereas Du *et al.* use 3.5µM in PBS. I find noticeably fewer cells were recovered when staining was performed in PBS as compared to other staining buffers. Cell numbers were comparable pre- and post-incubation with reagent but were lost during the centrifugation step proceeding this. This may suggest the insertion of reagent has destabilised the membrane and caused lysis resulting from the forces exerted in centrifugation. However, this does not explain why this did not occur using other media to the same extent as in PBS. This

contrasts with other uses of this reagent in the literature and PBS is recommended as the standard media by the manufacturer. The best recovery and viability of cells was achieved when staining was performed using RPMI1640 with between 0-10% foetal calf serum, however this medium markedly attenuated the intensity of the label which may explain the high dye concentrations required by Youniss & Du. Recommended concentrations on the manufacturers' datasheet state from 1-10 µM.

One parameter assessed which was not efficient in this study is the resolution. With the current protocol it would be difficult to accurately define intra-tissue localisation with a refined resolution. However, if tissues were imaged using confocal microscopy to visualise labelled cells *in situ* this may be achievable. Unfortunately, this remains as future work, due to the current (at the time of writing) SARS-CoV-2 pandemic the microscopy was not possible to perform as originally intended in the study design

Together, it must be noted that although Xenolight labelling is cost-effective and easy to undertake, the Indium radiolabelling protocol appears to perform better at the primary aim of tracking cells *in vivo,* especially in the strain of mice we use for the EAE model. Despite these considerations for *in vivo* work, the label was easily quantifiable from tissues post-mortem. There are indications that in a further optimised protocol it could be used in the intended capacity but would likely still be inferior to alternative imaging modalities.

4.5.3 – Distribution of adoptively transferred of EAE $CD4^+$ T-cells to *H. pylori* infected mice

Of note is the large portion of the Xenolight label detected in the liver. During the optimisation of the labelling protocol cell loss was observed under centrifugation which I hypothesised may involve the destabilisation of membranes by insertion of the dye molecule. Although this was mitigated somewhat using the optimised conditions, the intense DiR concentration in the livers may be an accumulation of dead cells or debris containing the dye molecule. This would suggest that a proportion of the transferred cells were not retaining viability post-transfer. However, viability of murine lymphocytes was retained for at least 24 hours after incubation with label and up to 72 hours without notable loss to cell number (not shown).

The same occurrence of liver tropism was observed by Kalchenko *et al.* [457] who showed the liver and spleen to be the primary targets for the homing of Xenolight-labelled murine lymphocytes. The concentration in the liver may also be the accumulation of membranous or particulate matter derived from labelled cells in Kupffer macrophages [458]. Indeed, a major function of these cells is to scavenge foreign matter and debris from blood in the hepatic system [458].

In the work of Kalchenko, injection of free dye to the circulation of mice led to homogenous near infra-red signal developing across the entire animal [457], which was observed in the work here to an extent. I had attributed this to the tissue autofluorescence being higher than expected, however it may indeed be circulating free dye molecules if separated from membranes which may well ultimately be endocytosed by liver macrophages. The dye was still visible in tissue up to 12 months post-labelling suggesting the molecule is stable, although fixation will preserve this substantially. If becoming free *in vivo* it may well bind to and label membranous debris, exosomes, red blood cells, or other cells non-specifically in the recipient mice. However, this is conjecture.

On the other hand, the purity of the initial CD4 enrichments should also be considered as Xenolight is a hydrophobic molecule with no specificity for distinct cellular lineages. The purification of CD4 cells from splenocytes gave a 90-99% pure $CD4^+$ suspension in all instances. However, not only does this leave 1-10% of non-CD4 cells which may have been co-transferred to recipient mice, but also the non-T-cell $CD4^+$ cells which may have been enriched alongside the cells of interest. Although mice do not express CD4 on non-T-cells as widely as humans, there are subsets of dendritic cells which do [459]. However, the method of negative selection we used should have selectively depleted these lineages from the splenocyte suspension.

It was hypothesized due to the nature of CD4 lymphocytes and the homing receptors they express that they should home towards lymphoid tissues such as the spleen and lymph nodes. This was indeed observed in the previous work of Cook [443]. In contrast, my data show the predominant localisation to the liver, but followed by the stomach and spleen at comparable levels. Differences between these studies is not unexpected; the previous study labels with a radioactive tracer ($Indium^{111}$) and tracks

total $CD4^+$ cells from naïve mice in a *H. pylori* infection mouse model. I use cells from EAE donor mice labelled with a near-infrared dye, in a similar *H. pylori* infection model. T-cell trafficking is crucially dependent on the complement of homing receptors expressed on the lymphocytes; of which the difference in backgrounds of naïve and EAE-induced donor mice may likely alter the expression.

Perhaps importantly is that the current study imaged animals at a single timepoint of 24-hours post-transfer. This may not be a sufficient time for injected cells to reach their target compartment, nor enough time for the MOG-specific DiR-labelled cells to reach the CNS if indeed that is their destination. We see from the experimental work using the EAE model (chapter 3) that mice do not present symptoms until around day 7-10, corresponding with mass infiltration of T-cells, macrophages, and neutrophils to the CNS. This will of course be preceded by an initial re-activation of MOG-primed T-cells in the CNS, but 24 hours would be a rapid accumulation not in line with the literature. However, if this study is to be compared to the SPECT-CT study performed by Cook [443], transferred cells administered via the tail vein had localised to the spleen by a timepoint of 6 hours. Originally, this study was designed to image *in vivo* at intervals between 1-hour to 48-hours, however this was not possible with the 2019 coronavirus pandemic forcing a closure of this institution at the crucial time for this work to be performed.

As there was a high background fluorescence in the stomach and gut, the current study cannot conclusively discern between signal from the DiR label on transferred cells, and that of autofluorescence. If it had been possible to perform, the confocal microscopy of tissue sections *ex vivo* would have been able to visualise cellular localisation with a much finer resolution.

4.5.4 - Preliminary evidence of differential trafficking between the stomach and CNS

I hypothesised that an active *H. pylori* infection would induce the production of chemotactic stimuli in the gastric mucosa, which may act to restrain EAE $CD4^+$ T-cells in the periphery and dysregulate the expected trafficking to the central nervous system. This phenomenon was shown by Sewell, Lee, and Lippens to occur in response to *M. bovis* infection [436-438]. Supported by Cooks data showing $CD4^+$ cell

migration to the *H. pylori* infected mucosa mediated by CCL20/CCR6 [448], and the tropism of EAE Th17 cells for the gastrointestinal mucosa shown by Berer [460].

My data conflict, quantifying the biodistribution of radiance across the dissected organs suggested that the infected mice may indeed have a reduction in the number of transferred cells infiltrating the brain and spinal cord. However, upon further analysis imaging the brain, spinal cord, stomach, and spleen in finer detail there was evidence for the opposite to be true. Furthermore, the flow cytometry data suggests a disparity between the brain and spinal cord; with a reduction of CD45+ lymphocytes in the brain but an increase in the spinal cord. In the brain, the reduced frequency of CD45+ cells were not associated with differences of the relative proportion of CD4-expressing cells amongst them. Conversely, in the spinal cord the increase of CD45+ cells were alongside a reduction in the proportion of $CD4^+$ cells. These data do not agree, and this is a paradox which will need resolving. Due to the poor viability and number of dead cells extracted from the CNS, the absolute number of cells in these tissues cannot be presented. Although we know that the pre-symptomatic phase of EAE will involve a large-scale infiltration of monocyte, macrophage, and dendritic cells to the spinal cord immediately preceding symptoms [269,272], which may explain the elevation of CD45+ cells.

Differences in cell migration between the brain and spinal cord may also result from differential expression of adhesion molecules between the T-cell subsets able to induce passive EAE; Th1 and Th17 cells. This is supported in the literature, Rothhammer *et al.* provide evidence of a differential capacity for CNS infiltration between the Th1 and Th17 EAE cells, which can utilise alternative routes of entry to the CNS dependent on the expression of either α4 or αL integrins [461]. Briefly, Th17 EAE cells can enter the brain despite experimental abrogation of the canonical α4β1:VCAM-1 route, Th1 cells cannot.

The studies of Sewell and Lee *et al.* [436,437], report reduced incidence and severity of EAE; increased lymphocytes in the spleens; yet reduced proportions of Th1 and Th17 cells in the CNS in response to infection of C57BL6 mice with *M. bovis* preceding EAE induction; forming a hypothesis that peripheral infection restrained EAE cells in the periphery. Lippens *et al.* suggest the mechanism for this is mediated by dendritic cells

and the induction of Tregs [438]. However, I did not see peripheral changes of Tregs in this study, nor were dendritic cells or alternative antigen presenting cells quantified.

However, the relative contributions of inflammatory or anti-inflammatory T-helper subsets amongst total $CD4^+$ cells were altered in the spinal cord. Here, as a proportion of $CD4^+$ cells *H. pylori* infected mice had elevated frequencies of suppressive Tregs concurrent with a reduced burden of Th1 and Th17 inflammatory subsets.

The adequacy of the Treg response can indeed modify EAE and MS course and severity [230,341]. On the other hand, previous data from this research group (Cook *et al.* 2015 [334]) found no difference in the frequency of FoxP3 expressing $CD4^+$ cells in the CNS to explain the reduction of EAE severity or Th1 and Th17 subtype frequency observed in an actively-induced EAE model in *H. pylori* infected mice [334], nor a CCL20/CCR6 migratory response of FoxP3+ CD4 cells *in vitro* [443], this was restricted to CD4+FoxP3- cells.

The study by Duc *et al.* [427] found adoptively transferred EAE Th17 cells to home primarily to the gut preceding a migration to the CNS. Berer *et al.* also report accumulation of EAE cells within the intestine [460]. Interestingly, we did observe a notable accumulation of fluorescence in the intestines of the study animals. However, in retrospect I believe this signal is more likely to have originated from autofluorescence from the dietary matter. This conclusion is based on the marked fluorescent signal observed when imaging C57BL6 faecal matter from uninfected and non-EAE mice. The lack of a control for this within the study is a confounding factor. Nonetheless, a proportion of this signal may indeed be EAE cells. To assess the contribution of EAE or non-EAE cells, future work could extract cells at the study endpoint and stimulate with MOG peptide to which only EAE cells should be responsive.

4.5.5 – The role of CCR6 in EAE CD4 T-cell migration

In this pilot study, we were not analysing cell migration in animals with dual disease (*H. pylori* infection, and concurrent EAE). This will of course confound the data to an extent, since a robust CNS inflammation would be present with active EAE/MS [272]. Here, no such inflammatory stimuli are present in the CNS and so the major CCL20

gradient and inflammation would be in the *H. pylori*-infected gastric mucosa; shown previously to induce the migration of $CCR6^{+}CD4^{+}$ T-cells in mice [448]. On the other hand, adoptive transfer EAE (passive EAE) is an established model of EAE induction in mice [271,272,391], and these MOG-primed cells must indeed be capable of infiltrating an uninflamed CNS and inducing disease in otherwise healthy mice. Of course, our model is confined to the pre-symptomatic phase of EAE and thus it is not known if mice will have proceeded to develop EAE.

Many published studies agree and some present evidence in disagreement on the contributions of both CCR6 and the various CCR6-expressing cell types in relation to EAE. Therefore, this means our study is highly relevant. The work which has been performed and presented here is focussed on the $CD4^{+}$ T-helper lineages. Flow cytometry showed no significant differences in the frequencies of CCR6+ cells between groups. In the brain there was a modest 1.6-fold increase in the number of both DiR+ CCR6-expressing $CD4^{+}$ cells. This may be taken to suggest a trend for more CCR6+ cells reaching the brain in the *H. pylori* infected group; however, the same trend was observed with unlabelled CD4+CCR6+ cells which infers no difference between EAE or non-EAE cells in this process.

In spinal cords, flow cytometry analysis of T-helper subset transcription factors identified elevations of 5-fold of Tregs from *H. pylori* infected mice, concurrent with similar-scale reductions in Th17 cells, and to a lesser extent Th1 cells. This data would be in support of a protective effect of infection by skewing the balance of inflammation in the spinal cord infiltrates, responsible for disease propagation. On the other hand, it is also an important consideration that extracted cell numbers were very low from the CNS tissue and contained a large majority of Trypan blue-positive (dead or dying) cells. The number of events available for analysis may not fully recapitulate the *in vivo* state, and even a small number of non-specific events can result in a notable change to the percentages derived from the analysis.

Given that the current study found *H. pylori*-infected recipient mice had elevated CD4+FoxP3+ and CCR6+DiR+ cells in the brain and spinal cord, it is a reasonable supposition that CCR6-expressing Tregs may migrate towards the CNS. Not

supported in the *in vitro* work of Cook [443] where this was not observed with FoxP3-expressing cells.

This study did not find differences in any of the $CD4^+$ subtypes, nor of total CCR6+ expressing cells in the spleens.

4.5.6 - Comparison of the current methodology with alternative imaging modalities

Previous work studying the migration of $CD4^+$ cells in *H. pylori* infection models suggests that CD4 cells labelled with $Indium^{111}$ and imaged using SPECT-CT were found to localise in majority to the spleen followed by the lymph nodes. This alternative imaging methodology was intended for use in this study however the required isotope was unavailable for purchase due to Britain's exit from the European Union, and the National Health Service purchasing all available material at the time the work was performed. This necessitated an unexpected redirection to the study design and research outcomes.

It is noteworthy that of the radiolabel administered, the highest accumulation seen (in the spleen) was only 0.33% of the total injected dose, with the vast majority remaining unaccounted for. The current study using fluorescent imaging would appear to retain more of the administered label, at least by 24-hours, however given the high background interference the exact quantification cannot be confidently calculated. It is important to also consider that the half-life of Indium is around 2.8 days [462], however as seen from the current study the Xenolight DiR reagent could still be detected in formalin-fixed tissues around 12 months post staining after storage at 4°C. But of course, as no work was done in the current study to assess the rate of decay of the DiR reagent it cannot be discounted that there will have been a substantial decline over time in storage.

Numerous inefficiencies were highlighted for DiR reagents in this study. There are of course alternatives such as luciferase-based bioluminescence models, reporter mice models can be costly to set up, however.

4.5.7 – Suggested additions or alterations to the method

An aim of this study was to ascertain the efficiency of this reagent for use in longitudinal tracking of transferred cells *in vivo*. There are some noteworthy factors that must be considered, it is apparent from imaging the mice post-mortem (but pre-depilation) that the skin and fur of C57BL6 mice attenuates the signal of the label to an extent which prevents accurate tracking of the cells in the living animal. This is not to say that increasing the concentration of reagent would not overcome this quenching effect to an extent, but perhaps a more suitable alternative would be to use an alternative mouse strain with white fur instead of black. The current project licence for this study did not allow for the removal of fur before imaging or animal sacrifice, this would be an important addition if C57BL6 are to be used again. However, on the other hand there are albino C57BL6 that could be used which should benefit the imaging side of the experiment whilst not potentially abrogating the induction of EAE, which in this thesis has been solely performed in the standard C57BL6 active EAE model, a model for progressive multiple sclerosis.

Confounding these data is the unacceptably high level of background (or autofluorescence) from the mice in the study. A dye in the far-red channel was chosen as it should have been less prone to interference by tissue autofluorescence than those in the green channels [463]. The high background observed here is an occurrence that requires thought before future work is performed building on this pilot study. It would be my recommendation in subsequent work of this nature to feed animals on a specialised chow which is low in constituents including alfalfa that can contribute to emission in the red wavelengths [464], demonstrated by Troy *et al.* [463].

A major oversight in the study design here is the lack of an extra control group, either naïve mice, or mice administered unlabelled cells. Despite *in vitro* tests showing no staining when unlabelled cells were imaged on the IVIS system in the preliminary testing, neither animals nor tissue was imaged in this manner. Signals corresponding to the emission wavelengths of the label were seen widely distributed across all tissues, even present in regions of the carcass after removal of organs. It would be vital for any future work to be able to relate what is seen in the treated groups to the

corresponding tissues in mice to which no DiR was administered, to allow correct normalisation and interpretation of the data.

Previous data from this group [443] analysed the expression of CCR6 amongst total $CD4^+$ cells, FoxP3 Tregs, and RORγT+ Th17 cells isolated from the spleen, mesenteric lymph node (mLN), or Peyer's patches (PP) of mice. Interestingly it was the Peyers patches followed by the lymph node in which the greatest proportions of CCR6+ cells were found, with the lowest frequency in the spleen. In the current study, due to logistical constraints the PP and mLN were not isolated for flow cytometry quantification. On the other hand, although the frequency of CCR6+ cells will be lower in the spleen, the absolute numbers will be far higher. As an ethical consideration for future methods, if the PP and mLN cells are indeed rich in the CCR6-expressing cells of interest then it may require large groups of mice to attain sufficient numbers.

4.5.8 – Future Work

Work by Arnold *et al.* [20] demonstrate that mLN and PP cells extracted from infected mice were able to mitigate exacerbations of experimentally induced asthma when adoptively transferred to recipient mice. Cook *et al.* reports similar [443]. The mLN and PP may indeed be a key site in the immune response to *H. pylori* and accumulation of suppressive immunity, however this may not be similar for EAE cells. In retrospect these may be important tissues to study and should be included in future work.

It also may be of interest to characterise wider panels of homing receptors or associated molecules on cells prior to transfer to provide valuable clues as to their initial destination in the recipient mice.

To the best of my knowledge there are no published studies using albino C57BL6 mice in the EAE model, it would be an interesting future project to assess their suitability for this purpose. Given the notable strain-dependent effect of mice on the course of EAE this may not recapitulate the kinetics of the C57BL6 model.

It may be an interesting inclusion for future work to not just quantify labelled (and thus adoptively transferred EAE cells) reaching the CNS or stomach, but also to perform characterisation of cells within these tissues for reactivity to MOG which would identify EAE cells amongst non-EAE cells co-purified in the CD4 enrichment

step. Functional assays to determine MOG reactivity would benefit future studies and allow a more refined analysis with specificity for the EAE cells of interest.

Furthermore, sorting MOG-specific cells from complex mixtures prior to staining would enable staining of only EAE MOG-specific CD4 cells. The practicalities of this may make this difficult, as gathering sufficient specific cells in this manner whilst retaining their viability and *in vivo* functionality through the extra pre-transfer procedures would be challenging.

For this study, donor mice were subjected to active MOG-EAE induction in the usual manner prior to having CD4 cells harvested from the spleens. This is based on the factually supported assumption that a proportion of these CD4 cells from EAE mice will be reactive against MOG. However, I did not take steps verify the $CD4^+$ cells extracted from the donor spleens were MOG-specific cells or not, however the absence of symptomatic EAE in the donor mice would infer that CNS migration had not yet occurred, the lymph nodes are unaccounted for here.

4.6 – Conclusions

- As preliminary data to ascertain the efficiency of this type of imaging modality for the tracking of cells *in vivo*, the current study has highlighted numerous inefficiencies which require addressing prior to translating these data towards a larger scale study.

- The differences in CCR6 expression and cell trafficking identified in this chapter are small, and sometimes conflicting. Although some comparisons may attain a level of statistical significance, the data presented here are insufficient to either prove or disprove the hypothesis of having a biological relevance. Refined techniques and larger groups would be required to assess this.

Chapter 5

The CD4$^+$ T-cell Response in Murine *H. pylori* Infection as a Modulator of Glial Function and CNS Remyelination

Chapter 5: A study to identify potential communication between CD4$^+$ T-cells, gastric *H. pylori* infection and the differentiation and regenerative capacity of oligodendrocytes – a focus on remyelination.

5.1 – Introduction

Here, I discuss the basic mechanisms of myelination in the central nervous system in both developmental biology and in the context of (re)myelination during demyelinating diseases. A process which is crucial for efficient transduction of action potentials through the CNS and one that is subject to dysfunction in diseases such as multiple sclerosis (MS). In the case of MS, the process of remyelination and repair is compromised increasingly from the onset of disease whereby oligodendrocytes fail to repair the damaged axons and resulting in the hallmark motor and cognitive dysfunction which make MS such a devastating disease to those affected. I will briefly summarise the current understanding of how these processes occur *in vivo* and introduce important factors with influence in these pathways. Of these, are the CD4$^+$ T-cells, both crucial mediators of demyelination and pathology in MS, and participants in the orchestration of inflammation resolution and tissue repair. In line with the theme of this thesis, that *H. pylori* infection can confer a benefit to immune-mediated disease, we hypothesise that immunomodulation by such an infection may indirectly affect these neural repair pathways. Of particular interest in this regard are regulatory T-cells, induced by *H. pylori*, and participants in the remyelination and repair process.

In the CNS, both developmental myelination and remyelination after injury are mediated by CNS-resident glia, oligodendrocytes (OGC). Briefly, oligodendrocytes develop from multipotent progenitors in the neural tube, characterised by the expression of NG2 proteoglycan, DM-20 (an isoform of PLP) and PDGFα receptor [465,466]. These progenitors are named NG2-glia, or O-2A progenitors, named as such as they have the potential to terminally differentiate along the lineage pathway of either oligodendrocytes or type 2 astrocytes [466]. The primary function of OGCs is to produce myelin, the lipid-rich insulation of CNS axons.

5.1.1 – Oligodendrocytes

The first description of myelin in the literature was made as early as 1717 by Leeuwenhoek who reported nerves surrounded by a fatty substance [466]. Oligodendrocytes were first hypothesised in the 1850's by Rudolf Virchow [467], however, they were not first identified until *circa* 1928 by Pı´o del Rı´o-Hortega using novel gold and silver-staining methodology developed with the eminent neuroscientist and Nobel laureate Santiago Ramón y Cajal [468-470]. In so doing, four types of 'oligodendroglia' were identified; types I to IV, classified according to their morphology and the number of axons myelinated by each cell [465,470,471]. A single oligodendrocyte can insulate as many as 50 axons [465]. As we now know, oligodendrocytes are connected both to the axonal body in addition to neighbouring oligodendrocytes and can function in the inter-cell transport of metabolites [471] such as pyruvate and lactate for neuronal ATP generation [466,472]. Vesicles secreted by OGC's support neuronal viability, abrogation of their uptake leads to increased axonal instability and degeneration [473]. OGC-derived vesicles are rich in myelin proteins and readily taken up by microglia possibly as a mechanism of immune surveillance within the CNS in the steady-state [474]. Oligodendrocytes with no primary myelin-wrapping function, termed satellite oligodendrocytes, have been identified which may serve a primary function of regulating inter-oligodendrocyte communication and the local environmental milieu [465,475]. These non-myelinating OGC can however adopt a myelinating phenotype during remyelination in demyelinating diseases [475]. OGCs express cytokine receptors and can regulate activity

according to the environmental stimuli [466]. However, the major function of oligodendrocytes is the production of myelin. In the human brain, between 40-70% of total cells are oligodendrocytes [476], and around 15% of total mouse brain cells [477].

5.1.2 – Myelin

The myelin sheath is comprised of a series of ~12nm layers wrapping each axon to form a compacted insulating architecture [471]. Physically, myelin is a lipid-rich material (70-80% lipid constitution) with a characteristic set of structural proteins and glycoproteins such as myelin associated glycoprotein (MAG), myelin oligodendrocyte glycoprotein (MOG), proteolipid protein (PLP), and myelin basic protein (MBP) [465,471]. Importantly, in MS and EAE these proteins are found to host numerous encephalitogenic epitopes for which T- and B-cell responses are directed. Interestingly, some myelin proteins including MBP, PLP, and CNPase are reported as being expressed in immune cells such as peripheral blood lymphocytes and thymic macrophage [465,478]. The expression of MBP proteins in cells of the immune system can be a result of the Golli gene cluster overlapping with that of MBP protein coding genes such that golli-MBP transcripts are expressed [478]. PLP proteins, and the truncated form DM-20 (expressed in O-2A progenitors) are expressed in the thymus [478]. There is a notable homology between MAG and some immunoglobulin-family proteins, including the neural cell adhesion molecule (NCAM) and the MHC class II molecules, with 28% and 20% homology respectively [465,479]. Parts of the complement system also share a homology to MOG [465]. These may or may not be a contributary factor in the development of autoimmunity against these specific antigens, the exact initiating factor of which is still not understood.

5.1.3 – Myelination

The process of myelination can be summarised as 4 steps; (1) proliferation and migration of oligodendrocyte precursor cells (OPCs), (2) axonal-glia signalling events to stimulate the recognition of a target axon, (3) differentiation of OPCs to mature myelinating OGCs, and (4) myelin production and wrapping of the target axon [465,471]. These steps precede a subsequent functional refinement such as myelin compaction, and the organisation and nodal clustering to produce the nodes of Ranvier [471].

During embryological development, mature myelinating OGCs are acquired around the third trimester and myelination occurs uniformly at a constrained rate from late-gestation and postnatally [480]. The myelination of axons is a dynamic process which occurs predominantly from the developmental stage through to pubescence, but maintains plasticity throughout adult life [481]. In fact, myelination is increased in response to learning new adult skills as new connections are formed within the brain [481-483]. In contrast, socially isolated or unstimulated individuals have a reduced amount of myelin [482,483]. However, despite the evidence of a highly dynamic and plastic function of myelination, the number of OPCs in the brain largely remains stable after the age of around 20 years [481,482]. The number of mature OGCs and indeed of the total brain myelin volume plateaus at around the same age however steadily declines throughout adult life in the absence of stimuli [482]. The decline of oligodendrocyte myelin correlates to reduced cognitive ability into old age and is augmented further in patients with dementia as neural circuits degenerate [482].

Myelin generation is of course a tightly regulated mechanism, which can be influenced by numerous factors. Some of the constituent proteins within myelin itself including MAG have inherent inhibitory activity against further neuronal outgrowth or repair [465]. Efficient clearance of myelin debris is essential to allow for remyelination to occur. Some autophagy-related genes are differentially regulated in MS and EAE [484], and experimentally inhibiting the process leads to exacerbated disease [485]. Indeed, the literature largely supports the proposition of a dysfunction amongst the autophagic pathways as a contributory factor in the progression of MS. Similar influences on remyelination are observed in Schwann cells in peripheral neuropathies [484]. Ineffective autophagy in microglia, astrocytes and neurones results in polarisation towards a reactive phenotype, and elevations in cytotoxic molecules such as ROS [485]. On the other hand, in dendritic cells autophagy can lead to enhanced myelin antigen-presentation to auto-reactive lymphocytes [485].

5.1.4 – Demyelinating Diseases & Infectious triggers

The demyelination of axons results in an inhibited conduction of electrical impulses along the neural pathways. There are several disorders which result from such an occurrence. Perhaps the most frequently referenced of these is multiple sclerosis

(MS), others include neuromyelitis optica (NMO), acute disseminating encephalomyelitis (ADEM), transverse myelitis, and optic neuritis [480,486]. The myelinating Schwann cells of the peripheral nervous system (PNS) can be affected in a related manner, such as in the example of Guillain-Barre Syndrome (GBS), peripheral neuropathy, and Charcot-Marie-Tooth disease [487]. Similarly, to MS, the exact aetiology of such disorders is not fully understood, however recurring trends in the literature would suggest an infectious event preceding disease onset. In the case of Guillain-Barre syndrome, around 60% of incidence is preceded by, or associated with, *Campylobacter jejuni* infection [487]. In other cases, onset has been associated with infection by numerous viruses in the period preceding clinical symptoms, these include; Zika virus [488], Hepatitis E [489], human immunodeficiency virus (HIV) [490], Epstein-Barr virus (EBV) [491], varicella-zoster virus (VZV) [492], and influenza [493]. In fact, the 1976 influenza vaccine to combat swine-flu was halted due to abnormally high reports of GBS presentation associated with the influenza vaccination [493]. Interestingly, the current (at the time of writing) severe acute respiratory syndrome coronavirus 2 (SARS-CoV-2) pandemic has resulted in several reports of post-infectious Guillain-Barre diagnoses in individuals with prior diagnosed COVID-19 [494-496]. The exact mechanisms by which infections such as these can induce GBS are not fully known, however patients are often reported to have autoantibodies against peripheral nerve gangliosides as a result of both *C. jejuni* and Zika virus infection, likely as a result of molecular mimicry between those and microbial constituent molecules [487,497]. Furthermore, GBS has been associated with the elevated presence of *H. pylori* VacA antibodies in cerebrospinal fluid (CSF) suggesting a possible connection between *H. pylori* infection and GBS onset [498]. Further review of this association revealed that *H. pylori* IgG are significantly elevated in CSF and peripheral blood in GBS as compared to healthy controls [499], this contrasts starkly with the reduced *H. pylori* seropositivity in patients with multiple sclerosis. These reports are consistent with the hypotheses of an infectious agents modulating demyelinating diseases, including multiple sclerosis, and suggests the involvement, either in a beneficial or negative manner of *H. pylori* in these processes.

In all such disorders, the patient will experience dysfunction of neural conduction which can lead to the hallmark symptoms of motor and cognitive impairment. The exact presentation of which is differential based upon the regions of the CNS, or indeed the specific peripheral nerves affected. In the case of optic neuritis (ON) the optic nerve is affected and leads to impaired visual processing. The predominant autoimmune target epitopes across the spectrum of these disorders vary and form the different presentations between diseases. In NMO a known molecular target is the aquaporin-4 (AQP4) channel on the optic nerve, whereas in MS, the MOG, MBP and PLP proteins are well-characterised targets. The AQP4 channel protein is known to be expressed on the basal side of gastric parietal cells, and AQP4 autoantibodies are elevated in NMO-spectrum disorders (NMOSD) [500,501]. Interestingly, *H. pylori* seropositivity is significantly higher in patients who are AQP4 autoantibody-positive, but not significantly elevated in MS patients [502,503]. Similarly, in opticospinal MS (OSMS) which has a similar presentation to NMO, *H. pylori* neutrophil activating protein (*Hp*-NAP) antibodies are found to be elevated in concordance with elevated AQP4 autoantibody, not present in conventional MS patients, however there is no notable homology between Hp-NAP and AQP4 to explain this phenomena [501].

5.1.5 – Remyelination

After a demyelinating event such as upon cessation of an MS relapse, the endogenous repair mechanisms are activated. New OPCs (alternatively termed NG2 glia) which make up between 5-10% of total cells in the brain are recruited and populate the site of the lesion [475]. Cells in the oligodendrocyte lineage pathway can be characterised with stage-specific expression of cellular markers.

Briefly, cells from the existing OPC pool within the CNS are mobilised, or in cases whereby this pool is depleted, O-2A progenitors are derived from neural crest stem cells which differentiate to OPCs driven by the upregulated expression of the transcription factor Nkx2.2, the neural-glial antigen 2 (NG2) proteoglycan and PDGFRα [480,504]. Proliferating OPCs upregulate Ki67, and migratory OPCs express the CXCL1 receptor. The chemokine CXCL1 is produced by astrocytes in the vicinity of a lesion and acts to arrest migratory OPCs at the target site [505]. These OPCs express the markers NG2 and platelet-derived growth factor alpha receptor (PDGFRα). After

proliferation and migration to the lesion site, OPCs differentiate into pre-OGCs which make the first contact with viable axons.

Upon differentiation from OPCs to pre-OGCs, cells downregulate these immature markers concurrently with upregulated expression of early differentiation markers such as 2',3'-cyclic nucleotide 3'-phosphodiesterase (CNPase), galactocerebrosidase (GalC), with the O1 and O4 surface markers [466]. When pre-OGCs experience a permissive environment to do so, including signals from a viable target axon, they terminally differentiate into mature myelinating OGCs which will proceed to wrap demyelinated axons [480].

Myelinating OGCs can be identified by the co-expression of the lineage-specific transcription factor Olig2 with the myelin proteins such as MBP, MAG, PLP and MOG [466,480]. Some of the myelin proteins can be used to discern a cells differentiated state, whereby PLP is detected as early as the OPC stage, CNPase is an early differentiation marker, followed by MAG and MBP, and finally MOG is expressed as a late stage marker for terminally differentiated and myelinating cells [466].

5.1.6 – Failure of Remyelination in MS

It is becoming increasingly apparent that repair mechanisms are often inefficient and fail to completely repair the axonal damage incurred through an autoimmune relapse [504,506,507]. Although OPCs are present in lesion sites, the differentiation of these cells is inhibited in chronic MS plaques. In regions where remyelination has occurred, it is restricted to the edges of the lesion [466,475,504,507]. Furthermore, even axons on which remyelination has taken place have an inferior thinner insulation to non-demyelinated axons [466]. Remyelination can be inhibited by numerous factors, including inflammatory cytokines [508], non-receptive axons [507], dysfunction in ECM remodelling [505,509], and the activity and secreted factors of local microglia and astrocytes [510-512]. As described previously, dysregulation of the autophagic machinery of recruited monocyte/macrophage and microglia can lead to an excess of myelin debris which itself can be inhibitory to remyelination [465,512].

Remyelination efficiency can be determined by calculating the G-ratios of the (re)myelinated axons in regions of repair. G-ratios are calculated as the total axon

diameter including myelin relative to the nude axon internal diameter, with thicker myelin resulting in a reduced G-ratio [475]. This can be investigated experimentally using silver stain or Luxol fast-blue stain on sections using microscopy. The uniformity of G-ratios in the steady state (un-demyelinated) suggests that myelination is a tightly regulated process. Indeed, myelin formation occurs in uniform segments along the length of an axon, whereby the regularity and consistency of junctions between these segments are essential in forming the nodes of Ranvier and impulse propagation. This regulation is performed by several contributors including signalling between the OGCs and the axon [481], local glia (microglia & astrocytes) [512], neuronal electrical activity [475,481], and of course the microenvironmental cytokine milieu.

In chronic MS, these processes are inefficient. As most of all approved therapies for MS are targeted to the relapsing-remitting disease stage, novel mechanisms which may augment the natural repair processes are of high value.

5.1.7 – Immunological Factors Regulating Remyelination

5.1.7.1 – The phagocytic Component; Macrophage & Microglia

Microglia are the CNS-resident phagocytes which make up around 10-20% of CNS glia in humans [513]. Microglia can develop from yolk sac-derived monocytes populating the brain parenchyma during development and persisting with self-renewal long-term, they can also be recruited into the CNS from monocytes during inflammation. Microglia develop from a shared precursor to macrophage and are similar in both lineage and function, reviewed by Li, *et al.* (2018) [514]. Discerning between macrophages and microglia can be achieved by characterising the expression of the surface proteins CD45 and CD11b. Macrophages will be of $CD45^{hi}CD11b^{+}$, whilst microglia $CD45^{low}CD11b^{+}$ [514]. Microglia are long-lived cells which will persist for the lifetime of their host [303], constantly extending processes for surveillance in the CNS and interact with neighbouring glia through both contact-dependent mechanisms and secretion of cytokines, growth factors, ROS, proteases, and bioactive molecules [514,515]. The function of microglia in neurodegenerative diseases is complex and difficult to characterise. This is in part due to the heterogenicity of microglial populations (discussed later) and partly due to the wide range of cells they can

directly, or indirectly affect, making delineations of the interaction pathways hard to resolve.

In MS and EAE there would seem to be starkly contrasting roles of microglia in disease progression dependent on the stage of the disease and the lesion they are present around. Indeed, the stages of MS and lesion types can be characterised by the microglial populations, their activation state, and there spatial distribution around the primary lesion [516]. Microglia can be broadly described as having two functional states; polarised to either an inflammatory/activated, or anti-inflammatory/resting phenotype in the same manner as the M1/M2 polarisation of macrophages. Although this is likely a notable understatement to their true plasticity.

When we focus on immunological factors influencing remyelination, it has long been proposed that macrophages and microglia function as regulators in this process. In this regard, we see evidence in the literature that remyelination is somewhat dependent on the presence of myelin-laden macrophages, or perhaps more specifically, the absence of myelin debris from the microenvironment [517,518]. The rationale for this observation is that myelin itself contains factors which inhibit differentiation of OPCs to OGCs [517], this would prevent OGC generation *in situ*ations where an unmyelinated axon was not present [518]. To control the differentiation of OGCs only when active remyelination is required, would necessitate the removal of myelin-breakdown products from the vicinity of the lesion by their engulfment in phagocytes [518]. Nonetheless, the importance of these cells has been demonstrated in loss-of-function studies by the minocycline-mediated inhibition of macrophage/microglial cells in the immediate days after experimental demyelination, in which repair was attenuated [519]. Further still, *vice versa* macrophage/microglia stimulated using Amphotericin B and GM-CSF resulted in an enhanced remyelinating capacity in other studies [519,520].

Indeed, the environmental conditions (either demyelinating/inflammatory, or remyelinating/anti-inflammatory) will see either the M1 or M2-activation state of macrophages predominate respectively [518,519]. It is an important consideration however, that the generalised M1/M2 paradigm is likely over-simplified. The activation states of macrophage/microglia are suggested to be far more of a

spectrum with between 9-14 alternative states of activation being proposed, dependent on factors such as developmental stage, aging, injury, or pathological condition [514,521,522].

Microglia polarisation has a correlation with active lesions in MS and EAE. A simplified view is that chronic active MS lesions are associated with myelin-filled microglia at the lesion edge, and chronic inactive lesions are characterised by few cells but astrocytic glial scar formation [523]. In a similar manner to their developmentally related family members, macrophages; microglial activation is often generalised into the two main states of M1 and M2. The M1 phenotype is associated with neurotoxicity and facilitates oligodendrocyte dysfunction, whereas the M2 state is more supportive of anti-inflammatory repair and regeneration [523]. However, similarly to macrophage the markers used to discern these states can often be co-expressed which would lead to the hypothesis that there is a high level of plasticity and overlap between several different functional states [523]. In terms of characterising the markers for microglial activation, this is not pertinent to studies in this thesis however they have been well reviewed in the literature [514,521,523,524].

Taken together the literature would seem to overwhelmingly support a dynamic role of phagocytes in either the direct orchestration of de- and re-myelination in the CNS, or at least in the provision of crucial signals required for these processes to occur. These may occur because of modulatory effects on the infiltrating T-cells, the cytokine composition of the local microenvironment, or they also may be mediated through undefined effects on neighbouring cell types such as astrocytes or even neurons themselves and providing crucial signals. It would be of great benefit to both the field of MS research as well as neuro-immunology in general to elucidate these diverse functions of microglia.

In addition to their roles in phagocytosis and antigen presentation, microglia/macrophage are also an important source of secreted cytokines which may help shape the pro- or anti-inflammatory landscape necessary for CNS repair to occur. Microglia are increased in number during demyelination, along with the upregulation of the phagocytic machinery. There is also an induction of growth-

regulatory proteins such as epidermal growth factors (EGF) and insulin-like growth factor (IGF) during the remyelination phase [525].

Interestingly, one such cytokine, TGFα secreted by activated microglia has been shown to protect against further lesions and promote repair in the CNS acting through its' receptor ErbB1 receptor on astrocytes [306]. This is especially interesting as the expression of TGFα, amongst others, in microglia can be regulated to some extent by metabolites of tryptophan produced by the intestinal microbiota, transducing signals to microglia via the AhR [306]. Therefore, here we see a link between the gut flora-microglia-astrocytes in which the pathogenesis of CNS inflammatory diseases may be regulated.

5.1.7.2 – Regulatory T-cells in Wound Healing & Tissue Repair

The function of regulatory T-cells in host immunity has been the subject of much research over recent years. Recently, additional roles for Tregs aside from immunosuppression have begun to be elucidated within the literature. Of these, Tregs have been demonstrated to have important functions in wound healing and tissue repair pathways in numerous different tissues [526-528]. Modulation of Tregs either through attenuation or augmentation of their functionality has been observed to regulate tissue repair in numerous tissue types including; skeletal muscle [529], cutaneous wounds [530], myocardial infarction [531], and the CNS [234].

Wound healing and tissue repair is a regulated process that can be summarised to 3 stages; (1) inflammation, aided by recruited neutrophils and monocytes and comprising neutralisation of infection and/or clearance of debris; (2) tissue formation, mediated by angiogenesis and the proliferation and differentiation of cells to close-up a wound; (3) resolution & remodelling, whereby immunity and ECM growth is halted as the repaired tissue is completed [526].

Regulatory T-cells have been shown to play important roles in the orchestration of these processes. FoxP3^{+} Tregs populate the site of injury, depletion of these cells results in attenuated ability for the inflammatory phase to resolve and healing to occur [526,528]. The immunological basis for this effect is understood, Tregs can resolve the pro-inflammatory phase through their well characterised mechanisms including

the ectonucleoside triphosphate diphosphohydrolase-1 (NTPase1, or CD39), or the ecto-5'-nucleotidase (5NTE, or CD73)-mediated conversion of ATP or AMP to anti-inflammatory adenosine [527]. The secretion of suppressive and pro-transformation molecules TGFβ, IL-10, keratinocyte growth factor (KGF), epidermal growth factor (EGF), the EGF-like amphiregulin, the cellular communication network protein 3 (CCN3) [234,526,527,532], via contact-dependent suppression of inflammatory T-helper cells using CTLA4 [526,527], and by facilitating the polarisation of M1-macrophage to a pro-resolving M2-phenotype [528]. In the context of the CNS specifically, CCN3 secretion by Tregs can induce the differentiation of oligodendrocytes to a myelinating phenotype [234].

Taken together, these data start to build a picture of a multimodal and highly adaptable cell, capable of both harnessing and regulating immune response to infection, but also orchestrating the resolution of inflammation and promotion of tissue repair.

5.1.7.3 – Regulatory T-cells in Remyelination

Tregs have diverse functions such as suppression of inflammation, M2-polarisation of macrophages, secretion of TGFβ and neural growth factors, and the promotion of a pro-regenerative environment. The identification of remyelination as a target pathway in which Tregs can exert a pro-repair influence was elucidated in 2017 by Dombrowski *et al.* [234]. Here, Tregs were shown to be important for the ability of oligodendrocytes to differentiate and to remyelinate CNS axonal lesions in mouse models of chemically induced demyelination. These data proposed a candidate molecule by which this may be achieved, based on bioinformatic analysis and network mapping. This candidate molecule is the cellular communication network protein 3 (CCN3), previously and sometimes still referred to as nephroblastoma overexpressed (NOV) in the human and mouse. What the work of Dombrowski *et al.* [234] elegantly demonstrated was that Treg-conditioned media (that is culture medium containing secreted factors after stimulation of purified Treg cells) could induce the differentiation of OPCs to OGCs producing myelin proteins. The targeted ablation of CCN3 within this media using neutralising anti-CCN3 antibodies attenuated the ability of OPCs to differentiate *in vitro* as observed by a reduction in the number of MBP^+

oligodendrocytes. Furthermore, in CCN3-depleted *in vitro* models, supplementation of CCN3 thus rescued the cells' ability to attain this functional state.

5.1.7.4 - The CCN protein family and functions

The CCN proteins CCN1-CCN6 are regulators of cellular growth and communication working both individually and in concert to co-ordinate signalling events [533,534]. CCN3 (NOV) acts in an opposing manner to CCN1/CCN2 and may represent both positive and negative regulation of various signalling cascades [534]. One such case in point is during diabetic renal failure, whereby CCN3 functions in the reciprocal regulation of ECM protein production and fibrosis mediated by CCN2, and thus CCN3 reduces fibrotic scarring [535]. Of the many roles proposed for CCN3, an inhibition of cellular proliferation and induction of transformation have been demonstrated [534]. Pro-healing effects are demonstrated in wound healing of the skin [532]. Indeed, functional roles as an angiogenic regulator are described [536]. In several tumour models, the expression of CCN3 is upregulated and associated with both pro- and anti-tumour effects in different types of cancer [537]. Taken together, CCN3 can be considered a dynamically expressed growth regulatory protein with an array of diverse disease and tissue-specific functions.

5.1.8 – *H. pylori* infection, Regulatory T-cells, and Multiple sclerosis

The hypothesised connection between *H. pylori* infection and MS, and the functions of Tregs in MS and EAE are discussed in detail in chapter 1 and 3, respectively. It has been established that infection with *H. pylori* results in induction of a FoxP3$^+$ Treg response, allowing immune escape and persistence by the pathogen [106,221]. Tregs have also been shown to confer a positive effect on the severity of MS and EAE whereby a depleted or dysfunctional population results in unrestrained inflammatory response and worsening disease [225,341]. Adoptive transfer of Tregs has an efficacy in reducing the severity of EAE in mouse models [538]. Tregs are identified as key mediators of inflammation resolution and tissue repair in numerous models of disease or injury and are a cellular source of many bioactive anti-inflammatory and pro-resolution molecules [527]. Many of these molecules including IL-10, TGFβ, and CCN3 have beneficial roles in both MS and EAE [234,409,539]. Both Tregs and IL-10 are increased during *H. pylori* infection and augment the proposed protection from

allergy and asthma in mouse models [20,219]. Treg-derived CCN3 supports repair by oligodendrocytes using *in vitro* demyelination models [234]. Taken together, tentative links between *H. pylori*, regulatory T-cells, and remyelination are apparent. These links were investigated in further detail in the work presented in this chapter. An overview of the study design is shown in *Figure 69.*

5.1.9 – Aims & Hypotheses.

5.1.9.1 – Hypothesis of the study

It was proposed that a *H. pylori* infection would modulate the host $CD4^+$ T-cell subset response in a manner to enrich the proportion of regulatory T-cells, thereby facilitating a bias towards immunosuppression.

The total $CD4^+$ cell secretome would be enriched for anti-inflammatory secreted factors. Of these factors, it was proposed that CCN3 expression would be higher in infected mice compared to uninfected controls.

A higher number of CCN3-secreting Tregs may augment the capacity for immature oligodendrocytes to differentiate and produce myelin proteins when subjected to a demyelinating insult *in vitro*.

A mechanistic basis for *H. pylori*-mediated protection from MS and EAE severity was proposed, via increasing the number of differentiated myelinating OGCs.

5.1.9.2 – Aims of the study

- To establish a chronic gastric infection with *H. pylori* strain PMSS1 in C57BL/6 mice
- To purify $CD4^+$ T-helper cell subsets from the spleen, mesenteric lymph nodes, and stomachs of infected or uninfected mice
- To perform flow cytometry staining on $CD4^+$ lymphocytes for signature markers for the subsets Th1, Th2, Th17, and Treg cells
- To investigate differences in the secretomes of these $CD4^+$ cells by analysing stimulated culture supernatants for the concentration of signature cytokines by ELISA

- To quantify CCN3 expression at the mRNA level by RT-qPCR from extracted RNA derived from $CD4^+$ cells post-stimulation.
- To determine the amount of CCN3 protein secreted by these cells using ELISA of stimulated $CD4^+$ cell culture supernatants.
- To investigate differential effects of these supernatants between groups, regarding the differentiation of oligodendrocytes to a mature myelinating phenotype, determined by myelin protein (CNPase, MBP) production using immunofluorescence staining of *in vitro* mixed glial cell cultures.

5.2 – Materials and Methods

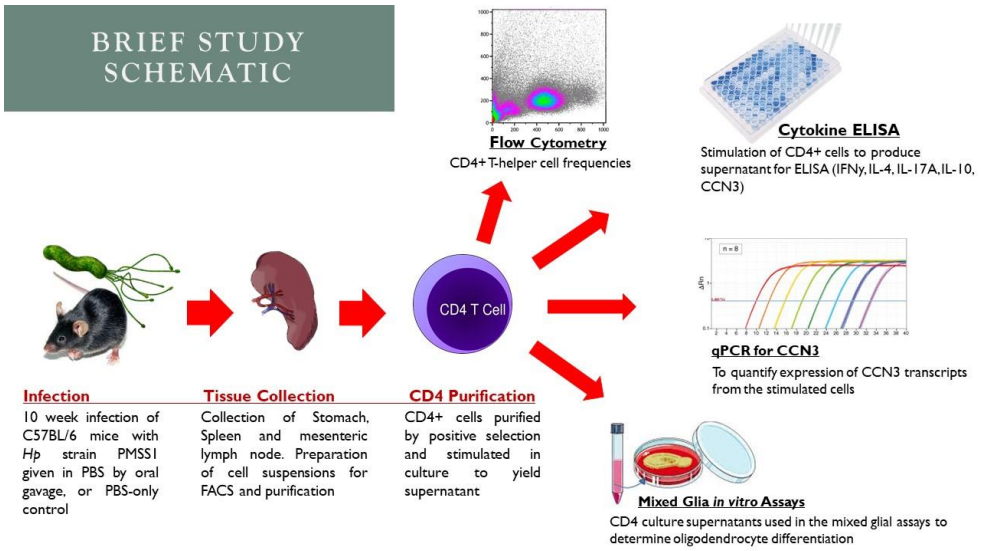

Figure 69 Overview of the remyelination study

For this study, C57BL6 mice were infected with *H. pylori* strain PMSS1 for a period of 10 weeks. *H. pylori* inoculum was delivered by oral gavage in PBS or administered PBS-only as a sham infection control. At 10 weeks post-inoculation cell suspensions were extracted. Here, CD4 cells from these were purified and analysed using flow cytometry, staining for the signature T-helper subset transcription factors; Tbet (Th1), GATA3 (Th2), RORγT (Th17) and FoxP3 (Treg), to investigate the relative compositions of the major T-helper subsets. Total CD4 cells were cultured in the presence of anti-CD3/CD28 beads to activate and induce cytokine production. Supernatants from these cultures had signature cytokines quantified using ELISA and were incubated at 5% *v/v* with murine mixed glia (oligodendrocytes, astrocytes, and microglia) for 5 days, followed by immunofluorescence staining to quantify myelin protein expression (CNPase and MBP) and proliferation (Ki67) of the oligodendrocyte precursor cells. RNA was extracted from stimulated cells and used in qPCR to quantify the relative expression of *Ccn3*.

5.2.1 – *Helicobacter pylori* PMSS1 Culture

The *Helicobacter pylori* strain: pre-mouse SS1 (PMSS1), was recovered from frozen stocks. Bacterial aliquots of 50µl were plated onto blood agar (BA) plates (Oxoid) containing 5% horse blood and rolled to disperse the cultures. Plates were then cultured for 24 hours in a VAIN cabinet at 37°C under microaerophilic conditions. Fresh BA pates were inoculated with growth from the edges of the culturing plates and incubated for a further 48 hours, this was repeated for a further 48 hours. At the final passage, the growth was collected from plates using sterile swabs and suspended in sterile PBS. The final concentration for administration to study animals was determined at the point where a 1:10 dilution (prepared in a 1ml cuvette with sterile PBS) had an optical density of 1.0 at a wavelength of 600nm (which provides an inoculum of $1x10^9$ colony forming units per ml), or $1x10^8$ per 0.1ml dose administered.

Remaining growth on the plates was used to prepare fresh plates for the second round of inoculations 48-hours after the first. This process was repeated for 3 rounds of inoculations. Remaining growth on the plates after the final administration was collected into Iso-sensitest medium (Oxoid®) containing 15% *v/v* glycerol and was frozen at -80°C.

5.2.2 – The animal model of *H. pylori* infection

The study was conducted under the Home Office Licence 40/3399 held by Dr. Karen Robinson, with assistance from Dr. Kazuyo Kaneko, Dr. Darren Letley, and Dr. Jo Rhead (University of Nottingham) in the Bio-support unit of the Queens' Medical Centre Medical School, Nottingham. All experiments were approved by the Animal Welfare and Ethical Review Body, University of Nottingham.

5.2.2.1 – Infection of C57BL/6 Mice with *H. pylori* Strain PMSS1

6-week-old female C57BL/6 mice (Charles River Ltd.) were inoculated with a 0.1ml dose of *H. pylori* PMSS1 suspension in PBS containing $1x10^8$ colony forming units per dose. In each group, 3 mice were infected and 3 administered PBS-only as a sham infection control. Administration of the inoculum was via oral gavage using a 1.5-inch straight gavage needle with a 2.5mm ball. Oral gavage was performed once each 48 hours for a total of 3 treatments. After the infections had been performed, the mice were monitored for 12 weeks, recording their body weight weekly.

5.2.2.2 – Euthanasia & Tissue Collection

At 10 weeks post-infection, mice were humanely euthanised. Spleens and mesenteric lymph nodes (mLN) were collected into washing medium (RPMI-1640 medium containing 2% *v/v* FCS and 100µg.ml^{-1} penicillin/ 100U.ml^{-1} streptomycin (1% p/s)) and homogenised by rubbing through a 70µm cell strainer placed in a petri dish using the end of a sterile 1ml syringe. Solutions were collected using a sterile Pasteur pipette and dishes were washed with a further 5ml of the same medium to collect remaining cells. Cells were collected into a 20ml universal tube and centrifuged at 300x *g* for 5 minutes to pellet cells. The medium was decanted, and the cells were further washed once more with 10ml medium before resuspension for counting in 10ml culture medium (RPMI-1640, 10% FCS, 100µg.ml^{-1} penicillin/100U.ml^{-1} streptomycin)

Stomachs were halved lengthwise comprising a section of the antrum and corpus into each half. Residual food matter was washed out with sterile PBS. Half stomachs were pinned onto cork boards and washed thoroughly with PBS before placing onto blood agar plates (Oxoid; containing 5% horse blood) for *H. pylori* culture. The remaining half stomach was used to extract lymphocytes for analysis using flow cytometry.

5.2.3 - Purification of CD4$^+$ T-cells

To enrich CD4$^+$ cells from total cell suspensions, positive selection kits (StemCell Technologies; Cat No. 18952) were chosen. Total cell suspensions were counted using 3% *v/v* acetic acid with methylene blue (StemCell Technologies; Cat. No. 07060). Cells were pelleted and resuspended in the required volume of EasySep™ buffer (StemCell Technologies; Cat. No. 20144) to a concentration of 1x10^8.ml^{-1} as per the manufacturer's instructions. Between 0.25-2ml (dependent on cell numbers from each spleen) of this suspension were added to 5ml FACS tubes and CD4 cells were purified according to the manufacturers' instructions. After the selection procedure, suspensions were counted using a haemocytometer slide with Trypan blue exclusion of dead cells.

5.2.4 – Stimulation of CD4$^+$ Cells

Purified CD4$^+$ cells from the spleens and mesenteric lymph nodes were counted and plated in 48-well cell culture plates (Greiner Bio-One) to a final well volume of 0.5ml

at a concentration of $1x10^6.ml^{-1}$. Cells were stimulated using a 1:1 bead-to-cell ratio of mouse T-activator anti-CD3/CD28 DynaBeads™ (Gibco™, Cat. No. 11456D) and incubated with beads for a period of 3 days maintained at 37°C with 5% CO_2 in a humidified incubator. After stimulation, the wells were aspirated, and cells were pelleted for RNA extraction. The resultant supernatants were centrifuged at full speed for 5mins to pellet residual debris. These purified supernatants were collected into sterile low protein-binding tubes (Eppendorf; Cat. No. EP0030108094) and frozen at -80°C for subsequent analysis.

5.2.5 – Cell culture Supernatant Cytokine ELISA

The concentration of the signature cytokines for the T-helper subsets Th1, Th2, Th17, and Treg (IFNγ, IL-4, IL-10, and IL-17A, respectively), as well as CCN3, were quantified using commercial ELISA kits (Invitrogen™; *IFNγ*, Cat. No. 88-7314-22; *IL-4*, 88-7044-88; *IL-17A*, 88-7371-22), and (R&D Systems; *IL-10*, Cat. No. DY417; *CCN3*, DY1976). Supernatants were assayed according to the manufacturers' instructions and analysed using a BioTek plate reader.

5.2.6 – Flow Cytometry

Flow cytometry was performed on cells from the spleen, stomach, and mesenteric lymph nodes, extracted and processed as described above. For all conditions, $1x10^6$ cells (or as many as possible if numbers were low) were added to 5ml FACS tube. Cells were centrifuged at 300x *g* for 5 minutes and the medium decanted. The pellet was resuspended by flicking the tube and was washed in duplicate by the addition of 1ml PBA (Sterile PBS, 0.01% *w/v* BSA, 2% *v/v* FCS) before pelleting and decanting the buffer. All tubes were kept on ice throughout the staining procedure.

Cells were first stained for surface markers. Specific antibodies used in *Table 16*. For surface staining, after the PBA washes described above the pellets were loosened and the required amount of antibody added to the residual pellet volume (approximately 100µl). Cells were incubated with antibody for a period of 30 minutes in the dark and kept on ice. After the incubation, 1ml of PBA (2% FCS) was added to each tube and centrifuged at 300x *g* for 5 minutes, the medium was decanted off and

the pellet loosened by flicking the tube. Cells were washed in this manner in duplicate.

For intracellular staining, the Foxp3 Transcription Factor Staining Buffer Set was used (eBioscience, Cat. 00-5523) according to the manufacturer's recommendations. Briefly, tubes were centrifuged at 300x *g* for 5 minutes to pellet cells before resuspending the cells in 1ml of Fixation/Permeablisation reagent and incubating on ice for 20 minutes away from light. After the incubation, cells were washed in duplicate with 2ml of permeablisation buffer and centrifuged at 300x *g* for 5 minutes before decanting the buffer and loosening the pellet. After the final wash step, the required amount (described in *Table 16*) of antibodies for transcription factors were added to the residual pellet volume (around 100µl). Cells were incubated with antibody on ice for a period of 30 minutes away from light. After the incubation, the cells were washed in duplicate with permeablisation buffer. After the final wash, the pellet was loosened and resuspended in 0.5ml PBA. Prior to analysing, all cells' solutions were filtered into 0.22µm filter-capped tubes.

Acquisition was performed using an Astrios™ flow cytometer (Beckmann-Coulter®). A target number of 200,000 events falling into pre-defined lymphocyte gating parameters were recorded, where possible. Analysis was performed using the Beckmann-Coulter, Kaluza™ software package.

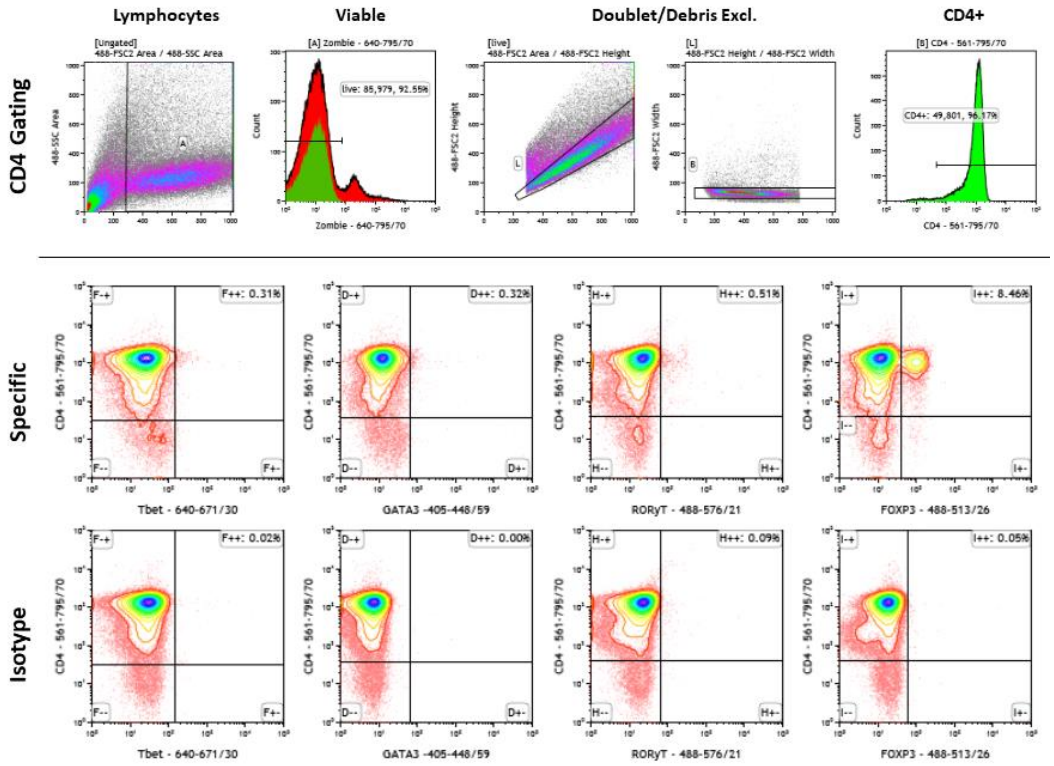

Figure 70 Representative gating strategy for CD4⁺ T-helper subtypes

Gating strategy, dead cells were excluded with a viability dye, debris and doublets were excluded. (Top panel) left to right; Lymphocytes; Viable cells; doublet/debris exclusion; CD4⁺. (Middle panel), specific antibodies gated to CD4, left to right; Tbet (Th1); GATA3 (Th2); RORγT (Th17); Foxp3 (Treg). (Bottom panel), isotype controls, gated to CD4; Th1, Th2, Th17, Treg.

Table 16 Flow cytometry antibodies used

Antibody	Clone	Catalogue Num.	Quantity per test	Excitation	Emission
Zombie NIR	n/a	Biolegend; 423105	1:200	633	795/70
CD4:PE/Cy7	RM4-5	Biolegend; 100547	0.25 µg	405	614/20
CD45:BUV395	30-F11	BD Bioscience; 564279	0.1 µg	355	405/50
Tbet:AF647	4B10	Biolegend; 644803	1 µg	640	671/30
AF647 Isotype	MOPC-21	Biolegend; 400167	1 µg	640	671/30
GATA3:BV421	16E10A23	Biolegend; 653814	0.05 µg	405	448/59
BV421 Isotype	MPC-11	Biolegend; 400341	0.05 µg	405	448/59
RORγT:PE	B2D	eBioscience; 12-6981-82	0.25 µg	488	576/21
PE Isotype	eBRG-1	eBioscience; 12-4301-81	0.25 µg	488	576/21
FoxP3:FITC	FJK-16S	eBioscience; 11-5773-80	0.5 µg	488	513/26
FITC Isotype	RTK2758	Biolegend; 400506	0.5 µg	488	513/26

5.2.7 – RNA Extraction

Cells collected from the stimulated culture supernatants were homogenised using QIAShredder spin columns (QIAGEN; Cat No. 79654), before RNA was extracted using commercial RNeasy extraction kits (QIAGEN; Cat No. 74104) according to the manufacturers' instructions. RNA was eluted into 50µl RNase-free water. Purified RNA solutions were quantified using a NanoDrop spectrophotometer (NanoDrop Technologies).

5.2.8 – cDNA Synthesis

Purified RNA was used at a final mass of 500ng in each 20µl reaction. cDNA synthesis was performed using SuperScript II™ reverse transcriptase (Invitrogen; Cat No. 18064071) according to the manufacturers' instructions with the addition of 1 unit of RNaseOUT (Invitrogen; Cat No. 10777019), 10mM each dNTPs (Promega; Cat No. U1330) and using 125nM random hexamers to prime the reaction (Invitrogen; Cat. No. N8080127).

5.2.9 – Quantitative PCR (qPCR)

RT-qPCR was used to quantify the abundance of *Ccn3* mRNA transcripts from each condition. For these analyses, TaqMan assays were purchased for mouse *Ccn3* and *Gapdh* (Applied Biosystems; *Ccn3*:FAM Cat. No. 4453320, assay ID: Mm00456855_m1; and *Gapdh*:Vic(P/L) 4331182, assay ID: Mm99999915_g1). Primer-limited (P/L) assays were used for *Gapdh* as the expression of *Ccn3* was expected to be substantially lower. Assays were performed according to the manufacturers' recommendations in a 20µl final reaction volume consisting of 500ng template RNA, 1x TaqMan Fast Advanced Master Mix (Applied Biosystems, Cat. No. 4444558), made up to 20µl with RNase-free H_2O (Invitrogen, Cat. No. 10977035). All qPCR reactions were performed over 40 cycles on a RotorGene RG3000 instrument (Corbett Research). Data was analysed using the RotorGene Software package, version 6. Relative expression ratios were determined using the Pfaffl method [360].

5.2.10 – Agarose Gel Electrophoresis

qPCR amplicons were verified using agarose gel electrophoresis. An aliquot of the qPCR reaction was applied to a well of a 100ml gel made using 3% *w/v* agarose with Tris-Borate-EDTA (TBE) buffer. GelRed stain (Biotium; Cat. No. 41003) was included

in each gel to stain nucleic acids. Gels were electrophoresed at a constant voltage of 100v until the products had migrated 75% of the way down the gel. Gels were imaged under UV light.

5.2.11 – Mixed Glia *in vitro* Myelination Assay

Performed by Dr. Marie Dittmer, Queens University Belfast; methods as described by Dombrowski [234]: "Mixed glial cells consisting of a proportion of oligodendrocytes, astrocytes, microglia, and neurones were extracted from the CNS of P2-7 C57BL/6 mouse pups according to the methods described by Dombrowski *et al.* [234]. Briefly, the MACS neural tissue dissociation kit (Miltenyi Biotec; Cat. No. 130-092-628) was used according to the manufacturers' instructions. Isolated mixed glia was cultured in Dulbecco's modified eagles' medium (DMEM) with 2mM L-Glutamine, 1% *v/v* penicillin/streptomycin, 10% *v/v* endotoxin-free FCS, and supplemented with 10ng.ml^{-1} platelet-derived growth factor alpha (PDGFα). After 5 days, media was exchanged for neural media consisting of serum-free XVIVO-15 haematopoietic cell culture medium, with 1% pen/strep, 2mM L-Glutamine, and supplemented with B27/MACS Neuro Brew21 (Miltenyi Biotec) and 10ng.ml^{-1} PDGFαα (PeproTech; Cat. No. XXX). At 7 days, PDGFαα was withdrawn to allow OPC differentiation to occur and CD4^{+}-conditioned supernatants were added at 5% *v/v* to each well. Mixed glia were incubated with treatment media for a further 5 days. At this point, the cells were fixed in 4% paraformaldehyde and stained with immunofluorescent primary and secondary antibodies; DAPI, Ki67 (eBioscience; clone SolA15, 1:200), Olig2 (Millipore; Cat. No. AB9610, 1:200), CNPase, and MBP (Millipore; clone 12, 1:200) according to the methods described previously [234]. Each condition was repeated in duplicate technical replicates, from 3 biological replicates, the experiment was repeated twice giving an *n* of 6 wells over the two experiments. Object counting and area quantification were performed using an automated spot detector (Thermo-Scientific Cellomics® Spot Detector version 4). The number of oligodendrocyte lineage cells (comprising both precursor OPCs and mature OGCs) expressing the lineage-specific transcription factor Olig2 were expressed as a percentage of total DAPI^{+} objects. The number of Ki67, CNPase, and MBP-positive cells were expressed as a percentage of

total Olig2^{+}DAPI^{+} objects. Data was plotted and analysed for statistical significance using GraphPad Prism™. Mann-Whitney *U*-tests were used to ascertain significance. Significant results were determined where *p= <0.05*."

5.3 – Results

5.3.1 – *H. pylori* Colonisation

After administration of either *H. pylori* PMSS1 in PBS, or a sham infection control administering only PBS, all mice were monitored and weighed once weekly. The growth rate in both groups was as expected and no differences in development were apparent in response to infection (data not shown).

To determine the number of mice successfully colonised with *H. pylori*, quantitative culture assays were performed on gastric tissue homogenates harvested at the study endpoint and processed by Dr. Darren Letley. Colonies on plates were counted and tested with urease reagent. No colonies were present on plates inoculated with material from the sham-treated animals as expected, and urease-positive colonies were identified from 4 of the 6 mice given the *H. pylori* PMSS1 inoculum. A colonisation success rate of 67% was determined from the study (*Figure 71*).

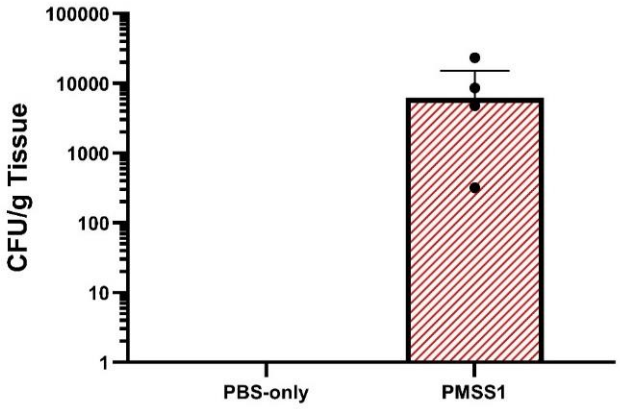

Figure 71 H. pylori PMSS1 Colonisation Density

Colonisation density on half stomachs was determined by verifying urease-positive colonies present and expressed as colony-forming units per gram of tissue. In the infected group, 4 of 6 mice had the presence of *H. pylori* in the gastric tissue giving a colonisation efficiency rate of 67%. Dots represent individual mice; bars represent the median; error bars denote interquartile range.

5.3.2 – Flow cytometry

At the endpoint, animals were dissected and the spleens, mesenteric lymph nodes (mLN), and stomachs were harvested for downstream analysis. Cell suspensions were produced and counted using Trypan blue to exclude dead cells.

In both the spleens and mLN there was a trend for increased numbers of cells in the *H. pylori*-infected animals, perhaps indicative of an increased immune response (data not shown). This trend was not statistically significant in either case (1.2-fold and 1.6-fold increases, respectively).

Very few viable cells were extracted from the gastric tissue. As such the whole sample obtained was used for flow cytometry analysis.

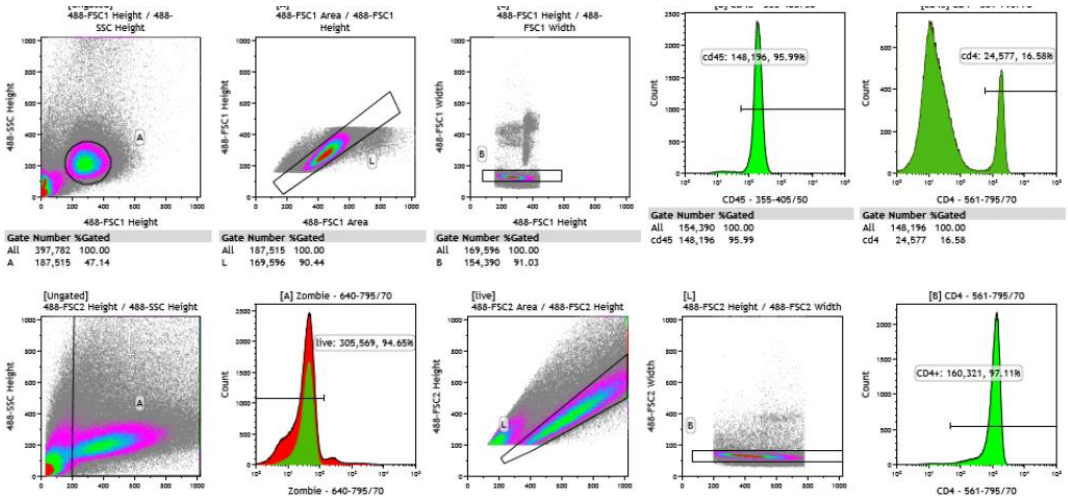

Figure 72 Representative Gating Strategy for Quantification of CD4 Cell Purification

Example gating strategy used to determine $CD4^+$ cell frequency pre- (top row) and post- (bottom row) enrichment of CD4 cells. (A) Lymphocytes were gated according to pre-established forward and side-scatter parameters; (B & C) Doublets and Debris exclusion; (D) CD45+ cells; (E) $CD4^+$ cells expressed as a percentage of total CD45+. Plots F-J describe gating parameters for purified CD4 cells after purification; (F) Total enriched cell solutions, excluding FSC-low debris; (G) live cells were gated as negative for the viability dye; (H & I) Doublet and debris exclusion; (J) $CD4^+$ cells expressed as a frequency of viable cells. In all instances, the $CD4^+$ enrichments reached a purity of >90%.

$CD4^+$ cells in the spleens, mLN, or stomachs of the study animals were quantified using flow cytometry. Forward- and side-scatter characteristics were used to gate single events falling under a pre-defined lymphocyte gating parameter. A viability dye

was used to stain dead or dying cells, of which any events were excluded. For the stomachs, cells were stained for CD45 to identify lymphocytes from the more complex mixture. An example gating strategy is presented in *Figure 72*.

No differences in the frequency of $CD4^+$ cells between the groups in either the spleens or mLN were observed (*Figure 73; A*). There was however a marked increase of 16.7-fold in the frequency of $CD4^+$ cells populating the infected stomach at 10 weeks post-infection (PBS-treated, 0.44% $CD4^+$; c.f. *H. pylori*-infected; 7.4% $CD4^+$) (*Figure 73; B*). These data reaffirm that the model had induced a robust $CD4^+$ T-cell response to *H. pylori* infection in the gastric mucosa.

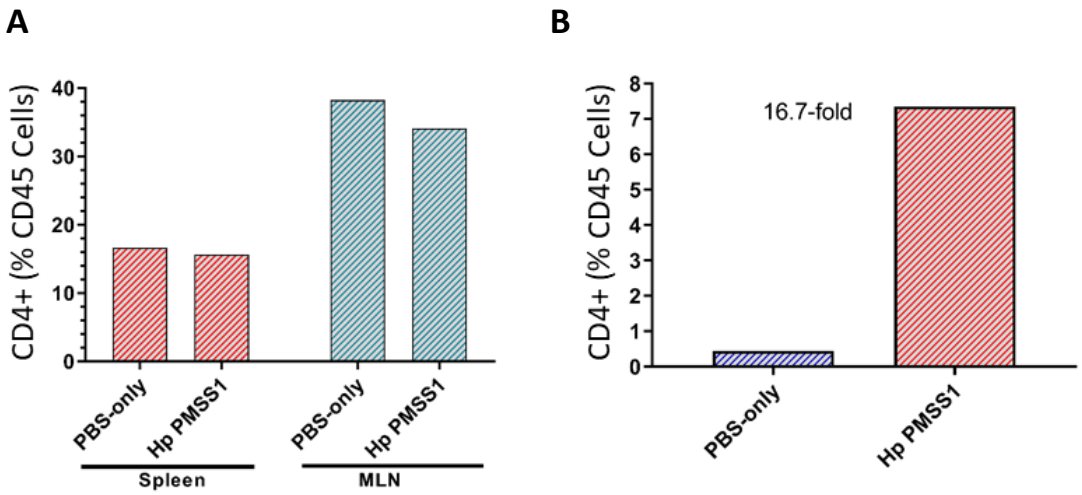

Figure 73 Distribution of $CD4^+$ Cells to the Spleens, mLN, and Stomachs

Flow cytometry was used to quantify cellular markers from samples derived from the spleens, mesenteric lymph nodes (mLN), and stomachs of *H. pylori* infected or uninfected C57BL6 mice. (A) The proportion of CD4 cells as a percentage of viable splenocytes (red) and mLN cells (blue). (B) $CD4^+$ cells as a percentage of total CD45+ lymphocytes in the stomachs.

With this observation, I next aimed to characterise the T-helper subset distribution amongst the $CD4^+$ cells in the spleens, mLN and stomachs. For this, the signature transcription factors of the T-helper subsets; Th1, Th2, Th17 and Treg cells (Tbet, GATA3, RORγT, and FoxP3, respectively) were stained and quantified with flow cytometry.

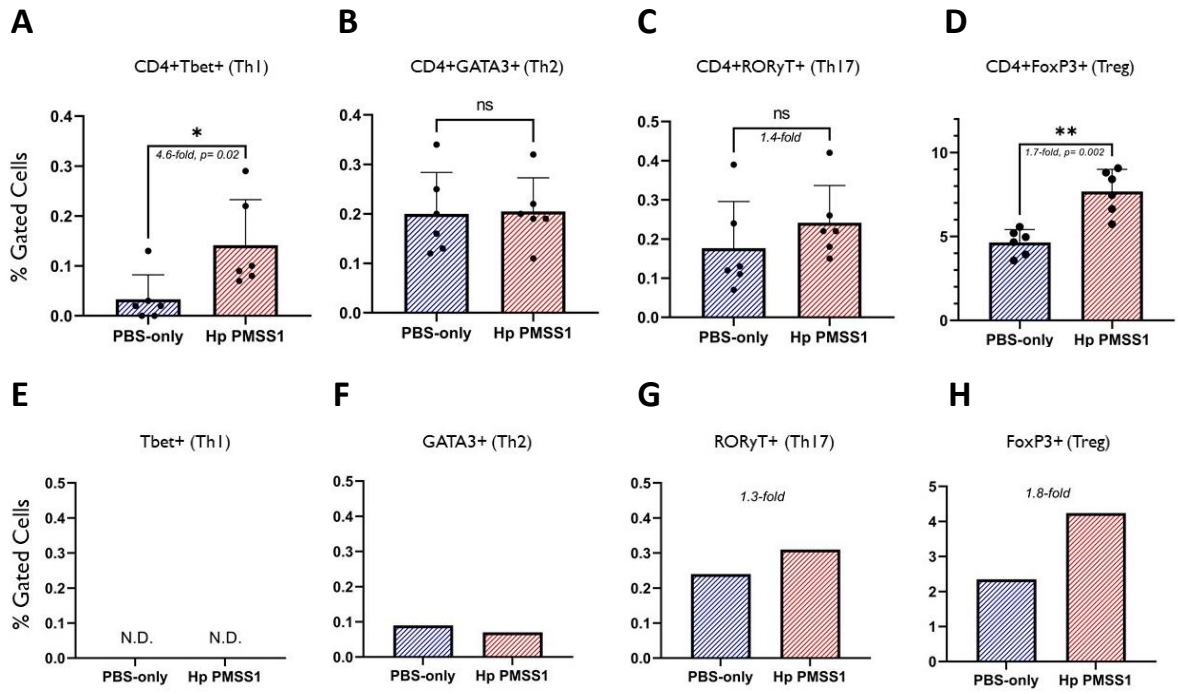

Figure 74 Distribution of T-helper cell subsets in the spleens and mLN of H. pylori-infected or uninfected mice

The T-helper subtypes Th1, Th2, Th17 and Treg, were quantified from the lymphoid tissues of *H. pylori* PMSS1-infected or uninfected mice using flow cytometry. Dead cells, debris, and doublets were excluded from the analysis. The frequency of each T-helper subtype is expressed as the proportion of cells positive for each respective signature transcription factor and expressed as a percentage of viable $CD4^+$ events. *Top row (splenocytes)*: (A) Tbet, Th1; (B) GATA3, Th2; (C) RORγT, Th17; (D) Foxp3, Treg. *Bottom row (mLN-derived cells)*: (E) Tbet, Th1; (F) GATA3, Th2; (G) RORγT, Th17; (H) Treg, Foxp3. Tbet staining (denoting Th1 cells) was not detected (N.D.) from the mLN. *Bars denote the mean ± SD; Mann-Whitney U-test; * p=0.02; ** p=0.002.*

A statistically significant increase in the number of Th1 ($CD4^+Tbet^+$) and Treg ($CD4^+FoxP3^+$) cells in the spleens of the infected mice was observed (Th1: 4.6-fold, *p=0.02*; Treg: 1.7-fold, *p=0.002*). There was also a non-significant increase of Th17 cells ($CD4^+RORγT^+$) in these infected mice (1.7-fold, *n.s.*). No observable difference was seen in the frequency of Th2 cells (*Figure 74; A-D, top panel*).

There was no detectable T-bet staining from cells of the mLN in either group (*Figure 74; E*). Similarly, to splenocytes, the number of Th17 and Treg cells within the mLN were elevated in infected animals (Th17: 1.3-fold, *n.s*; Treg: 1.8-fold, *n.s.*) (*Figure 74; G & H*). There was no difference in Th2 lineage cells (*Figure 74; F*). There were no differences observed in the number of $FoxP3^+RORγT^+$, or $Tbet^+FoxP3^+$ double-positive cells in any tissue from either group (data not shown), but a proportion of

double-positive cells were present in each case. Low numbers of lymphocytes recovered from gastric tissue meant that there were insufficient events collected to determine proportions of T-helper subtypes.

5.3.3 – $CD4^+$ supernatant cytokine ELISA

Cell culture supernatants were derived from stimulated $CD4^+$ cells which were enriched from the spleens and mLN. These were seeded into 48-well plates at a concentration of $1x10^6.ml^{-1}$ in serum-free media. Cells were activated by the addition of anti-CD3/CD28 T-activator beads and incubated for 3 days. At this point, supernatants containing CD4-secreted factors were collected.

The next step was to confirm the flow cytometry data and to characterise the cytokine composition in the culture supernatants by analysing secreted cytokine concentrations using ELISA. The concentrations of the respective signature cytokines for the T-helper subsets Th1 (IFNγ), Th2 (IL-4), Th17 (IL-17A), and Treg (IL-10), in addition to CCN3 were quantified.

In agreement with the flow cytometry data, the concentrations of the Th1, Th17 and Treg-signature cytokines were elevated in the *H. pylori* infected animals as compared to PBS-treated controls in the spleens (*Figure 75; A-D*). A low number of available cells from the mLN meant that the volume of supernatant derived was insufficient to perform ELISA on all the cytokine targets. As Tregs are a particular focus here, ELISA was performed for the Treg factors; IL-10, and CCN3, respectively (*Figure 75; E & F*).

In all samples, the concentration of CCN3 was below the limit of detection for the ELISA kit and obscured by high background interference. This was replicated in subsequent attempts modifying sample diluent with increasing serum concentrations to attempt to block background binding (data not shown).

There was agreement between the flow cytometry and ELISA data. Both the signature transcription factors and the associated cytokines for Th1, Th17, and Treg cells were elevated reciprocally in both the spleen and mLN from *H. pylori* infected as compared to uninfected mice. No differences in either GATA3 or IL-4 were observed between groups. In only a few analyses did the differences between groups

reach statistical significance; CD4+Tbet+ (Th1) and CD4+FoxP3+ (Treg) splenocytes were increased 4.6-fold, *p=0.02*, and 1.7-fold, *p=0.002* respectively from the *H. pylori*-infected mice. IL-17A concentration in supernatants was elevated 7.9-fold (*p=0.01)* from infected c.f. uninfected mice.

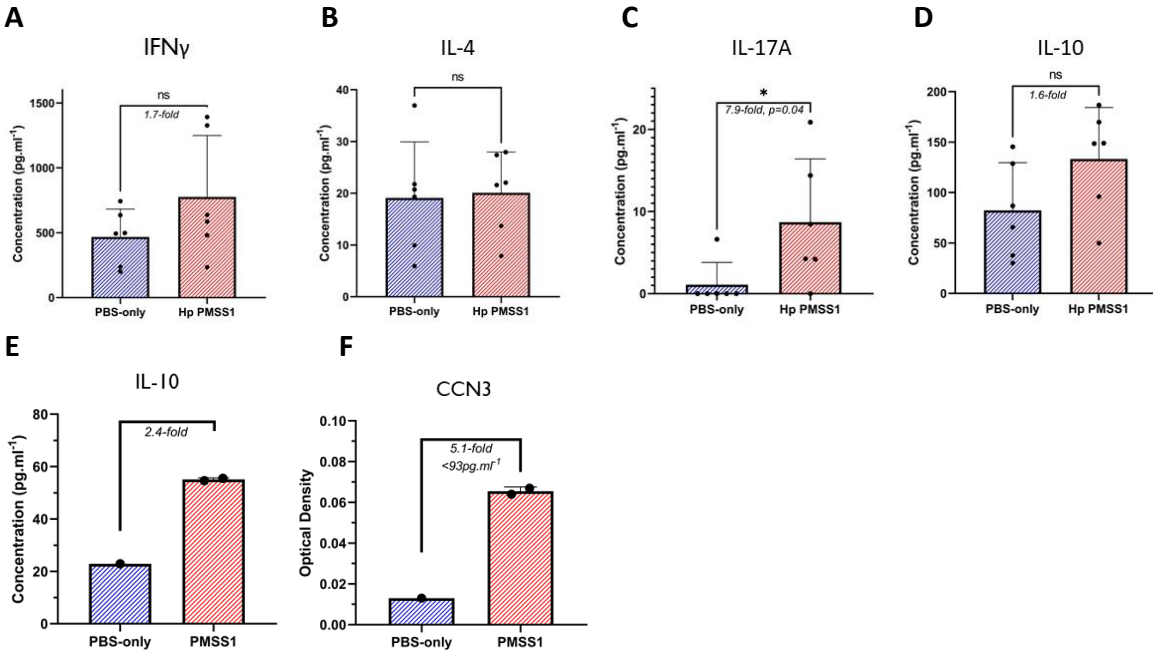

Figure 75 Cytokine concentration in CD4⁺ splenocyte and mLN supernatants from H. pylori infected or uninfected mice

Signature cytokines of the Th1, Th2, Th17 and Treg subsets (IFNγ, IL-4, IL-17A, IL-10 & CCN3, respectively) were quantified by ELISA from CD4⁺ supernatants. *Splenocytes*: (A) Th1, IFNγ; (B) Th2, GATA3; (C) Th17; (D) Treg, IL-10. *mLN cells*: (E) IL-10. (F) CCN3. The concentration of CCN3 was below the lower limit of the ELISA to quantify. Optical density from ELISA is plotted. Dots show individual mice; bars represent the median; error bars denote the interquartile range. *Mann-Whitney U-test; * p=0.04.*

5.3.4 – RT-qPCR analysis of *Ccn3* mRNA expression

CCN3 could not be quantified by ELISA in any of the supernatants tested, therefore an RT-qPCR approach was used to investigate *Ccn3* expression at the mRNA level. Commercial TaqMan primer/probe assays were used for qPCR. *Gapdh* was used as an endogenous control gene (housekeeping gene) to normalise the relative mRNA expression ratios.

Ccn3 transcripts were quantifiable in all samples and groups, from both the spleen and mLN (*Figure 76*). Interestingly, *Ccn3* mRNA expression was found to be markedly

increased in the *H. pylori*-infected mice as compared to PBS-treated controls in both the spleen (5-fold, *p=0.004*) and mLN (4.5-fold, *p=0.0001*). Within the *H. pylori* infected group, *Ccn3* expression was higher (2-fold, *p=0.001*) in cells derived from the mLN as compared to splenocytes.

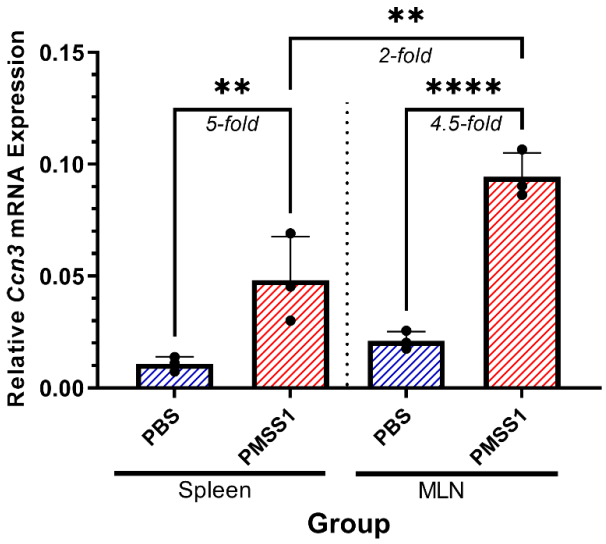

Figure 76 Expression of Ccn3 mRNA in CD4⁺ cells of the spleen & mLN of H. pylori PMSS1 infected or uninfected mice.

RT-qPCR was used to quantify the expression of *Ccn3* mRNA in CD4⁺ T-cells purified from the spleens and mLN's of mice infected with *H. pylori* PMSS1 or sham-infected with PBS. Purified cells from 6 mice per group were pooled in pairs (total n=3) for splenocytes, and to a single pooled sample (n=1) for mLN-derived cells. Cells were stimulated with anti-CD3/CD28 T-activator beads for 3 days. Expression of *Ccn3* was normalised to that of an endogenous control gene; *Gapdh*. Bars denote the mean + S.D. ANOVA; ** *p=0.004*; **p=0.001; **** *p=<0.0001*).

To further investigate the production of CCN3, samples were derived from an EAE experiment occurring in parallel (chapter 3). Here, two groups of mice either infected with *H. pylori* strain SS1 in *Brucella* broth or given *Brucella* broth-only as a sham-infection control group were analysed. Cells from the spleens of these mice at day 21 days post-induction of EAE (at the peak EAE severity) were enriched for CD4⁺ cells using immunomagnetic separation and stimulated with T-activator anti-CD3/CD28 beads. Stimulation was maintained for 3 days at which point cells and supernatants were collected. From the collected cells, equal numbers from each sample were pooled and re-stimulated in fresh media for a further 3 days. This was to better replicate the work of Dombrowski *et al.* [234] in the duration of stimulation, and to

inform on the potential requirements needed to induce *Ccn3* expression in similar cells if future work should require it.

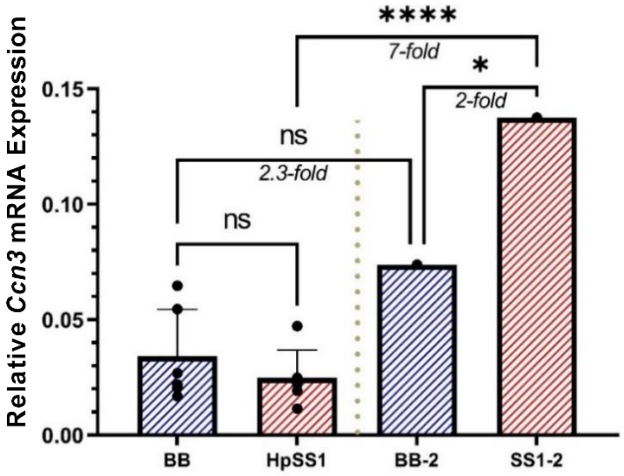

Figure 77 Expression of Ccn3 mRNA in CD4⁺ splenocytes of EAE Mice, either infected with H. pylori SS1 or uninfected sham-treated mice.

Quantitative RT-PCR was used to enumerate the expression of *Ccn3* mRNA in CD4⁺ T-cells purified from the spleens of EAE mice infected with *H. pylori* SS1 (*Hp*SS1) or sham-infected with *Brucella* broth (BB). Cells from groups of 6 mice each were later pooled and restimulated for a further 72 hours (BB-2, and SS1-2). *Ccn3* mRNA expression was normalised to that of an endogenous control gene; *Gapdh*. Bars denote the mean + S.D. ANOVA; * *p=0.02*; **** *p=0.0001.*

Here, from EAE mice *Ccn3* was detected in both groups at similarly low levels (*Figure 77*). The relative expression of *Ccn3* mRNA from splenocytes derived from both experimental groups were of a comparable level after the first stimulation (day 3). However, after a further 3-day stimulation the expression of *Ccn3* had increased in both groups; 2.3-fold (not significant; n.s.) in the control group and 7-fold (*p= <0.0001*) in the infected group. With a second stimulation, the expression was significantly deviated between groups being 2-fold (*p=0.02*) higher in cells from the *H. pylori* SS1 infected EAE mice as compared to sham-infected EAE mice.

With such a marked increase of *Ccn3* after a second stimulation, it was hypothesised that extended stimulation of CD4⁺ cells in this manner may be inadvertently skewing the relative frequencies of each of the T-helper subtypes within the total population. If indeed the case, this may lead to confounding data as cytokine concentrations may not accurately reflect the composition of T-helper cells. Compared to pre-stimulation, Th1 and Th2 lineages both rose markedly in frequency, similarly in both

treatment groups. Th1 cells rose 31-fold in the BB group and 111-fold in the *H. pylori* SS1 infected group. Th2 cells rose 13-fold and 7-fold in the BB and *H. pylori* SS1 groups, respectively. The relative proportion of Tregs dropped substantially in both treatment groups (BB, 19-fold; *H. pylori* SS1, 14-fold) from around 10% to a similar level of <1% after stimulation. Between infected and uninfected groups, there was a marked difference in the proportion of CD4+RORγT+ Th17 cells, only in the SS1 infected cells. These were elevated 6-fold (<1% to 6%) as compared to pre-stimulation; and were 3.6-fold elevated in *H. pylori*-infected as compared to uninfected mice. (*Figure 78; A-D*).

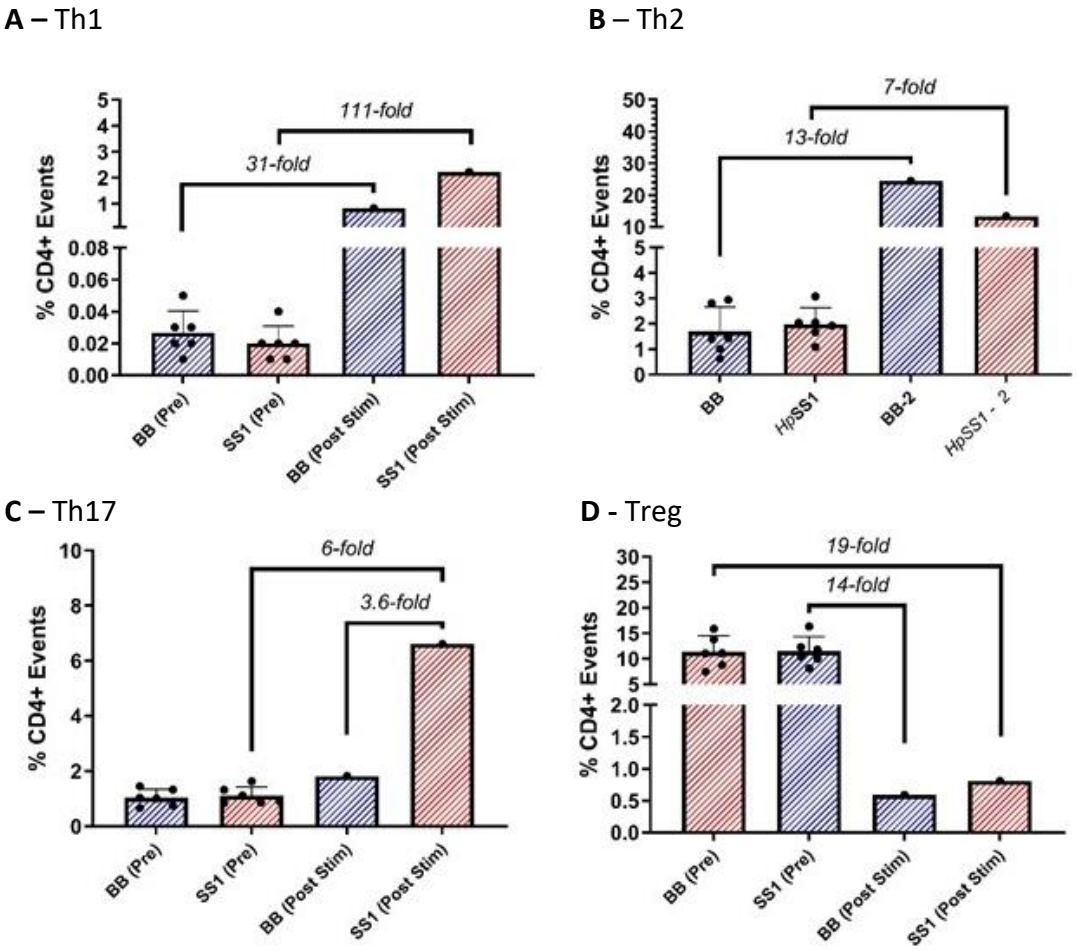

Figure 78 Frequency of the T-helper subsets; Th1, Th2, Th17 and Treg before and after repeated stimulation for a total of 6 days

Flow cytometry was used to determine the proportions of $CD4^+$ subtypes between *H. pylori* infected or uninfected EAE mice. The respective transcription factors for each subtype; (A) Th1 (CD4+Tbet+); (B) Th2 (CD4+GATA3+); (C) Th17 (CD4+RORγT+); (D) Treg (CD4+FoxP3+), before and after stimulation are plotted. Dead cells, debris, and doublets were excluded. The proportion of cells expressing each transcription factor is given as a percentage of $CD4^+$ cells.

When the media from these prolonged stimulations was measured for CCN3 by ELISA it had elevated in both groups, and 2.8-fold higher in cells from *H. pylori* infected EAE mice.

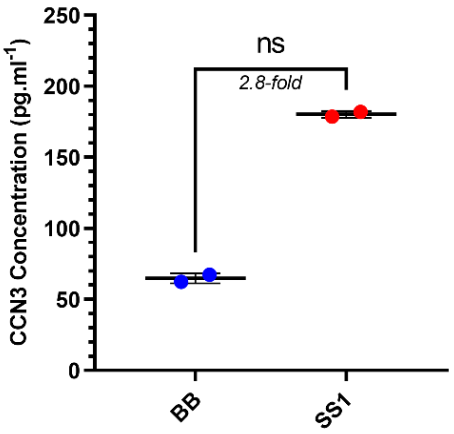

Figure 79 CCN3 concentration in twice stimulated CD4 culture supernatants

CD4 cells from the spleens of infected or uninfected mice were stimulated twice over 6 days. Each time, the media was collected and CCN3 quantified by ELISA. CCN3 was not detectable at day 3 in either group but was by day 6. Concentrations were elevated 2.8-fold in cells from *H. pylori* infected mice.

5.3.6 – Mixed Glial *in vitro* Assays

After characterising the cytokine composition in cell culture supernatants, interest turned to whether differential effects on oligodendrocyte differentiation and myelin protein expression could be exerted *in vitro* using mixed glial cell culture assays. To determine this, aliquots of the supernatants were supplemented at a final concentration of 5% *v/v* into cell culture media containing mixed glia isolated from mouse pups, as described previously by Dombrowski *et al.* [234].

Immunofluorescence staining was performed after the incubation period, staining for cell nuclei (DAPI); the oligodendrocyte (OGC) lineage-specific transcription factor, Olig2; a marker of proliferating cells, Ki67; and 2 distinct myelin protein markers characteristic of early and late differentiation states, CNPase (early marker), and MBP (late marker). The aim of this work was to quantify the total number of oligodendrocytes ($DAPI^+Olig2^+$); changes to the numbers of proliferating OGCs ($DAPI^+Olig2^+Ki67^+$); and differentiated OGCs ($DAPI^+Olig2^+CNPase^+$ and

DAPI⁺Olig2⁺MBP⁺ cells). This process would be indicative that there may be some evidence of a pro-remyelinating effect.

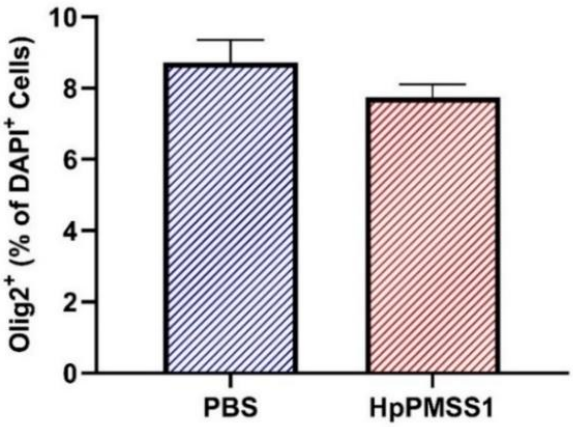

Figure 80 Immunofluorescence staining of Olig2+ oligodendrocyte lineage cells

Mixed glia (oligodendrocytes, astrocytes, and microglia) from 3 mouse pups were incubated with CD4⁺ cell culture supernatants from the spleens and mLN; derived from *H. pylori* PMSS1- infected or uninfected mice. The number of Olig2+ oligodendrocytes (as determined by Olig2 overlayed with DAPI) in each well is expressed as a percentage of the total number of DAPI⁺ events.

There was no difference to the numbers of Olig2⁺DAPI⁺ oligodendrocytes between the infected or uninfected groups (*Figure 80*). These data suggest starting cell number would not account for any difference observed. From Olig2+DAPI+ cells, the percentage that overlayed with Ki67, CNPase or MBP were enumerated using an automated spot counter as described by Dombrowski [234].

In MS, oligodendrocyte precursors migrate to the lesion site but fail to myelinate suggesting a defect in proliferation or differentiation. Cells were stained for Ki67 as a readout of cell proliferation. There were no differences in proliferation in OGCs observed in response to any of the treatments, nor did the CD4-conditioned media affect the rate of proliferation as compared to cells treated with unmodified culture media alone (*Figure 81; A & B*).

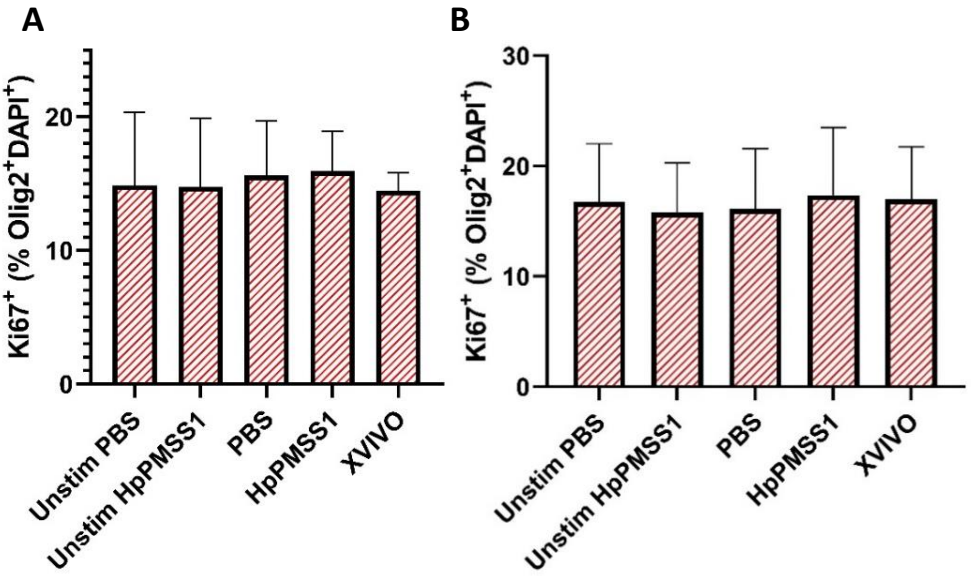

Figure 81 Proliferating Olig2+ oligodendrocytes cells in response to treatment with or without CD4-conditioned media from infected or uninfected mice

Oligodendrocytes were identified by staining for the lineage-specific transcription factor Olig2, overlayed with DAPI+ nuclei. As a readout for the number of proliferating oligodendrocytes, cells co-stained with Ki67 are expressed as the percentage of total Olig2+DAPI+ cells. Supernatants from the PBS-only or PMSS1-infected mice either unstimulated or stimulated were incubated with glia alongside a control consisting of media alone. (A) CD4 supernatants derived from splenocytes; (B) derived from the mesenteric lymph nodes. Bars represent the mean + SD.

Next, the number of oligodendrocytes which had differentiated, as discerned by the positive staining of the myelin proteins CNPase and/or MBP were quantified (*Figure 82; A & B*).

CNPase is an early differentiation marker and is expressed before MBP. As a pilot study, the inclusion of CNPase here acts as a failsafe in this experiment to determine cells which are potentially differentiating but have not progressed sufficiently through this transcriptional program by the experimental endpoint to express MBP.

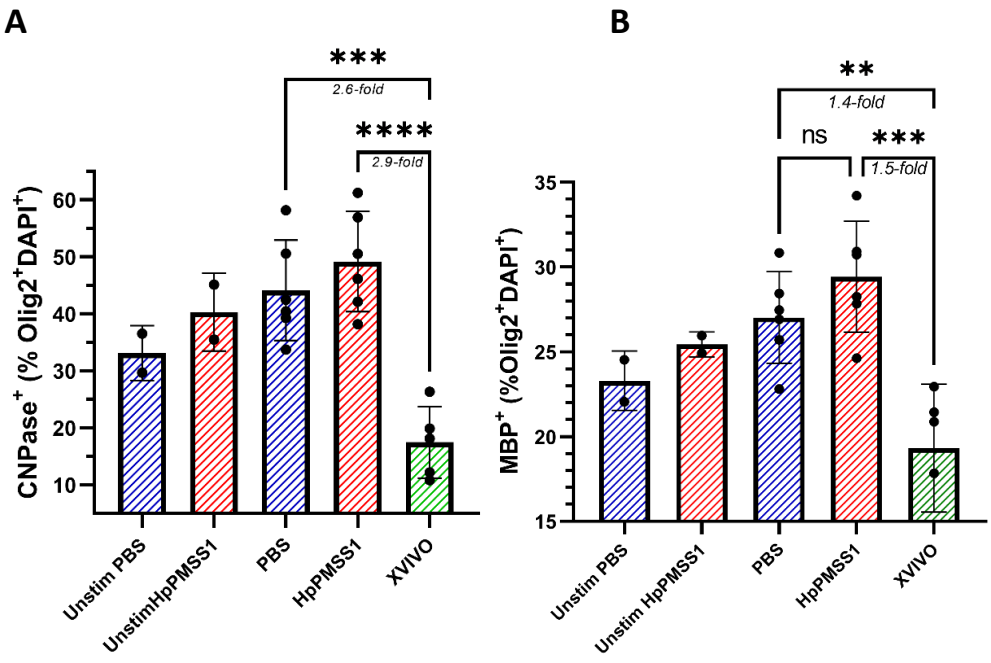

Figure 82 CNPase and MBP myelin protein expression in Olig2+ oligodendrocytes after incubation with splenocyte-derived CD4-conditioned media from H. pylori infected or uninfected mice

Oligodendrocytes (DAPI+Olig2+) were stained for CNPase (A) and MBP (B), representing early and late markers for differentiation, respectively. Glia from 6 mouse pups (dots) were incubated in duplicate with each of 3 supernatants produced from CD4 splenocytes from infected (red) or uninfected (blue) mice. A media-only supplement (XVIVO) was included as a control. Oligodendrocytes expressing each marker is given as a percentage of total OGCs per well. Šídák's ANOVA; CNPase, *** *p=0.0003*; **** *p=<0.0001. MBP, ** p=0.004; *** p=0.0004.*

When glia were incubated with unmodified media, the number of CNPase and MBP positive oligodendrocytes were 17% and 19% of total Olig2+ cells, respectively. In comparison, after incubation with CD4-conditioned media there was a marked induction of myelin protein expression. From supernatants of the infected group the number of CNPase positive cells increased to 49% of total Olig2+ cells (elevated 2.9-fold, *p=<0.0001*), and MBP positive cells to 29% of total Olig2+ cells (elevated 1.5-fold, *p=0.0004*). Both myelin markers were found to be modestly elevated when incubated with supernatants derived from the *H. pylori*-infected splenocytes as compared to PBS-treated controls, however this trend was modest and not statistically significant.

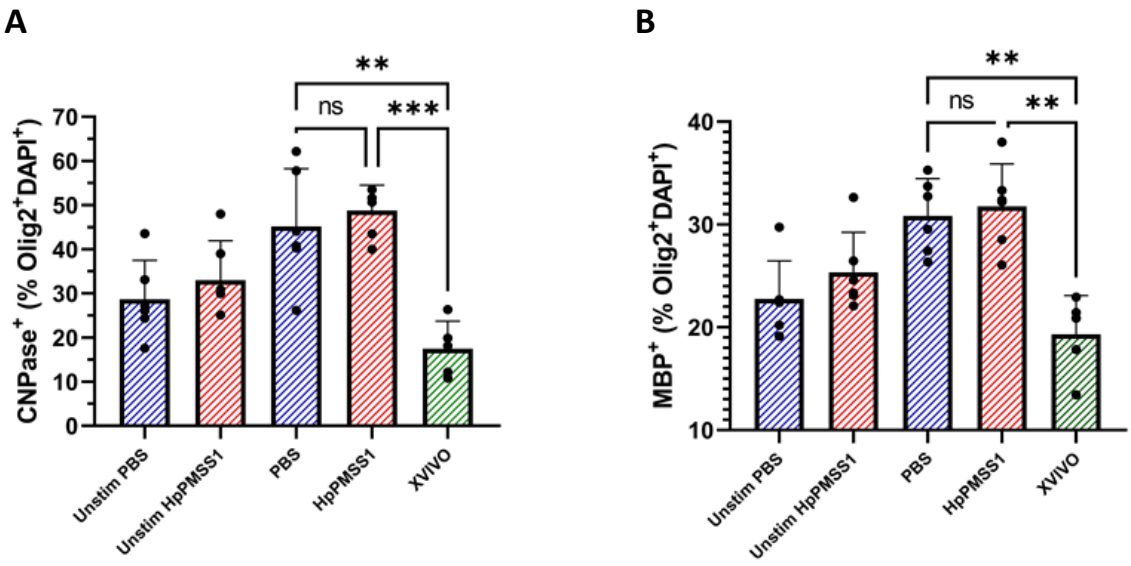

Figure 83 CNPase and MBP myelin proteins in Olig2+ oligodendrocytes after incubation with CD4-conditioned media derived from mLN cells from H. pylori infected or uninfected mice

Oligodendrocyte differentiation determined by staining for myelin proteins CNPase and MBP after incubation of glia with CD4-conditioned media. Supplements were either stimulated or unstimulated CD4 supernatants from infected or uninfected mice. A media-only control was included (XVIVO). CNPase or MBP positive cells are expressed as a percentage of total Olig2+DAPI+ oligodendrocytes. Šídák's ANOVA; ** p= <0.005; *** p= <0.0005.

The mLN-derived cells were comparable to splenocytes with respect to the trends for myelin protein expression (*Figure 83; A & B*). Significant increases of both CNPase and MBP were observed in glia incubated with CD4-conditioned media compared with media alone. There was a modest increase when cells were treated with supplements derived from the *H. pylori* infected mice to uninfected controls (not significant).

Although on a small scale these differences may still be relevant even if not statistically significant. The most notable outcome from these analyses is the marked effect of activated CD4 cell supernatants, irrespective of infection status, on the induction of myelin protein expression in oligodendrocytes. Both CNPase and to a lesser extent MBP were markedly elevated in glia incubated with $CD4^+$ supernatants as compared to incubated with media alone, both from the spleen and mLN cells.

The early differentiation marker CNPase was expressed in <20% of total Olig2+ cells when glia were cultured in unmodified media, however this was elevated to 44% of

total Olig2+ cells in response to CD4-conditioned media, a 2.7-fold (*p=0.0001*) increase, both in splenocyte- and mLN-derived supernatants, comparably (*Figure 84*).

When glia were cultured without supplementation, MBP was expressed in <20% of total Olig2+ cells, similarly to CNPase. Rising to around 30% in response to CD4-derived factors. This elevation was similar in magnitude in both the spleen (*A*) and mLN-derived (*B*) supernatants, giving statistically significant increases of 1.5-fold (*p=0.003*) and 1.6-fold (*p=0.0009*), respectively (*Figure 84; A*, and *Figure 84; B*).

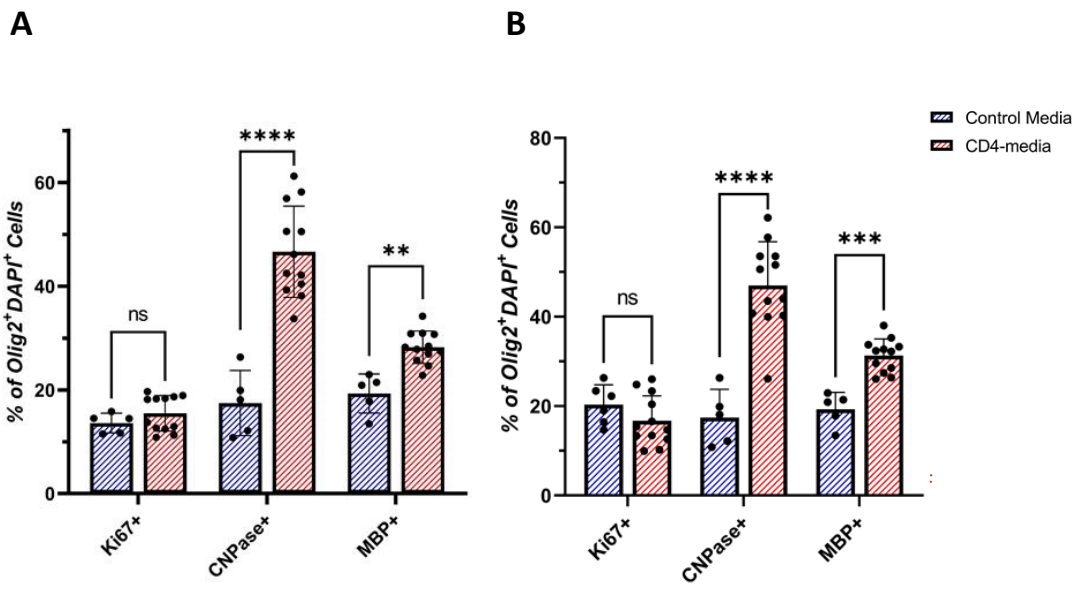

Figure 84 Expression of the myelin proteins CNPase and MBP in oligodendrocytes after incubation with activated CD4 cell-derived supernatants

Murine mixed glia from groups of 6 mice (3 per group, 2 groups, 2 experiments) were incubated with CD4-conditioned media (red bars) or unmodified culture media (blue bars) for 5 days. Proliferating cells are identified by the co-expression of Olig2 with Ki67. Differentiated oligodendrocytes are identified by the co-expression of Olig2 with CNPase and/or MBP. (A) Splenocyte-derived CD4 supplement. (B) mLN-derived CD4 supplement. Dots represent individual wells; bars show the median; error bars show the interquartile range. ANOVA; ** *p=<0.003*; *** *p=<0.0009*; **** *p=<0.0001*.

5.3.7 – Image analysis from Immunostaining of mixed glia

The images were analysed using Perkin-Elmer Columbus software using a custom script to identify cells positive for one or more markers. Nuclei were selected using DAPI. Border objects were removed to exclude duplicate counts. Thresholds for each channel were assigned after correcting for background fluorescence. *Figure 85* shows a representation of the selection criteria. Representative images from the splenocyte-derived supernatants are shown in *Figure 86*. Representative images for the mLN-derived supernatants are shown in *Figure 87.*

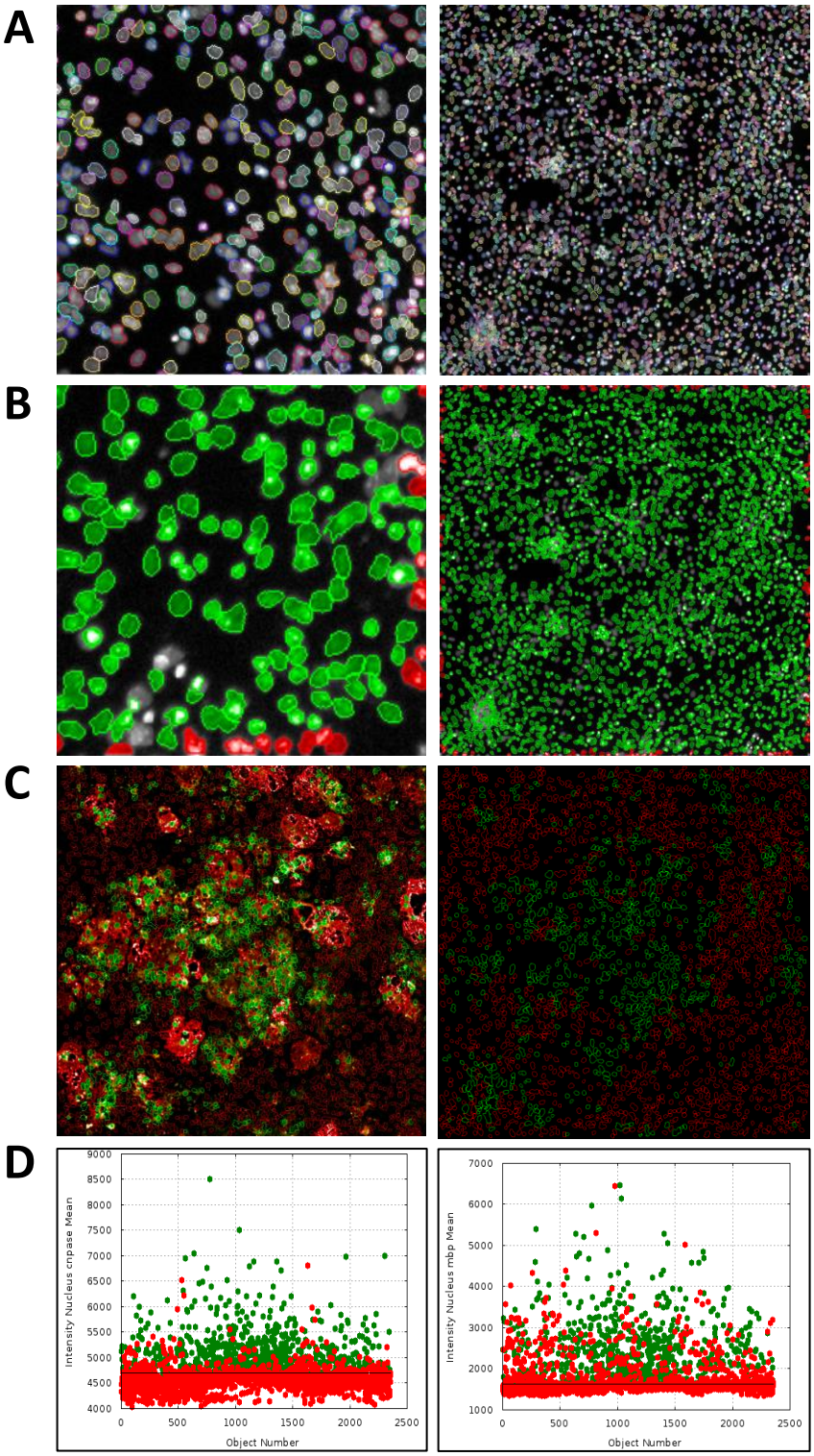

Figure 85 Image segmentation used for high-content analysis using Perkin-Elmer Columbus™ software.

A script was designed to identify individual cells stained positively for the different markers (DAPI, Ki67, Olig2, CNPase, MBP). (A) DAPI was used to identify the nuclei of individual cells in each field of view (FOV). (B) To avoid duplicate counting, border events were removed. (C) The intensity of fluorescence was measured for each channel; thresholds were set manually based on intensity and subtracting the background signal.

Figure 86: Mixed glia with CD4⁺ splenocyte-derived supernatant

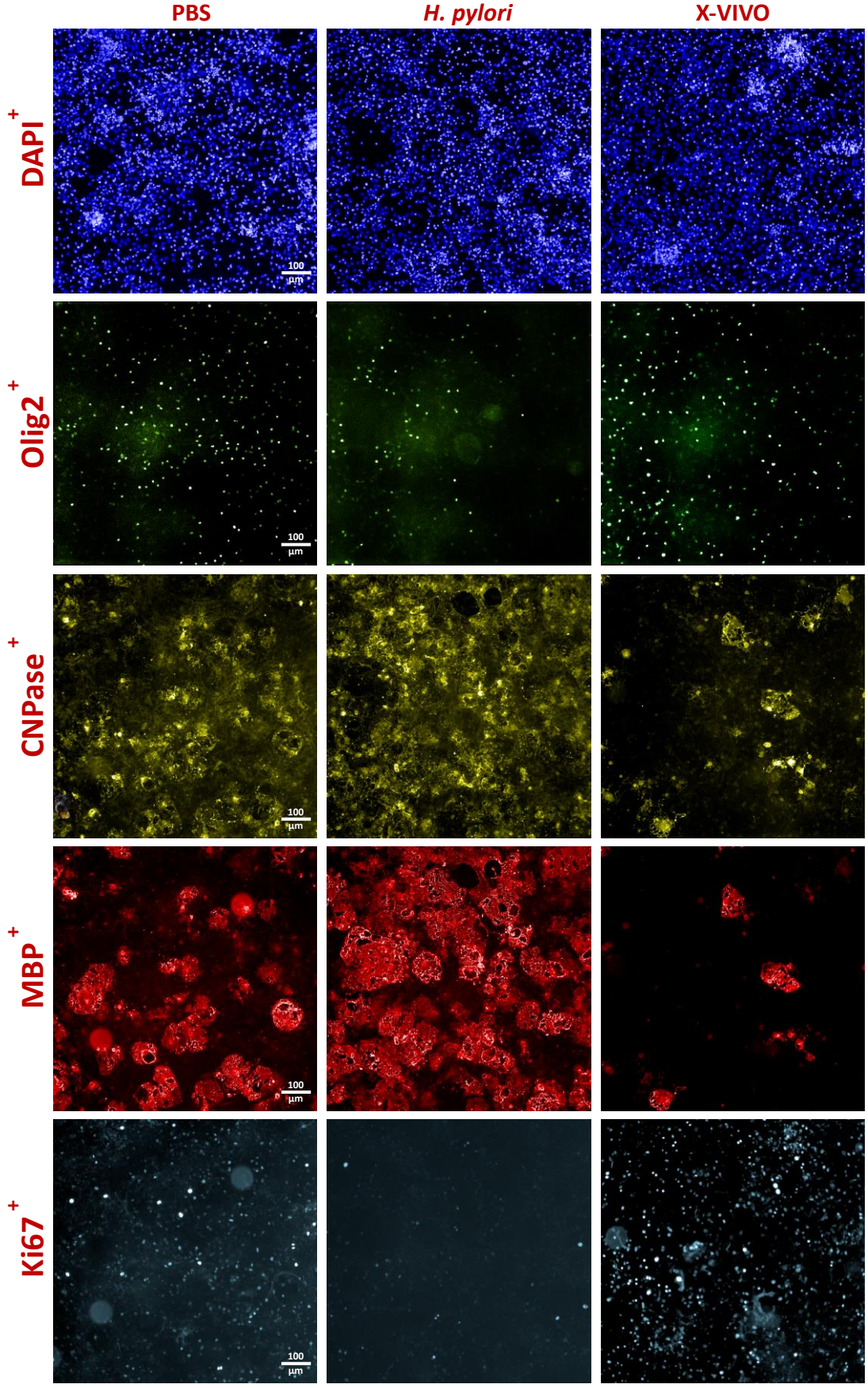

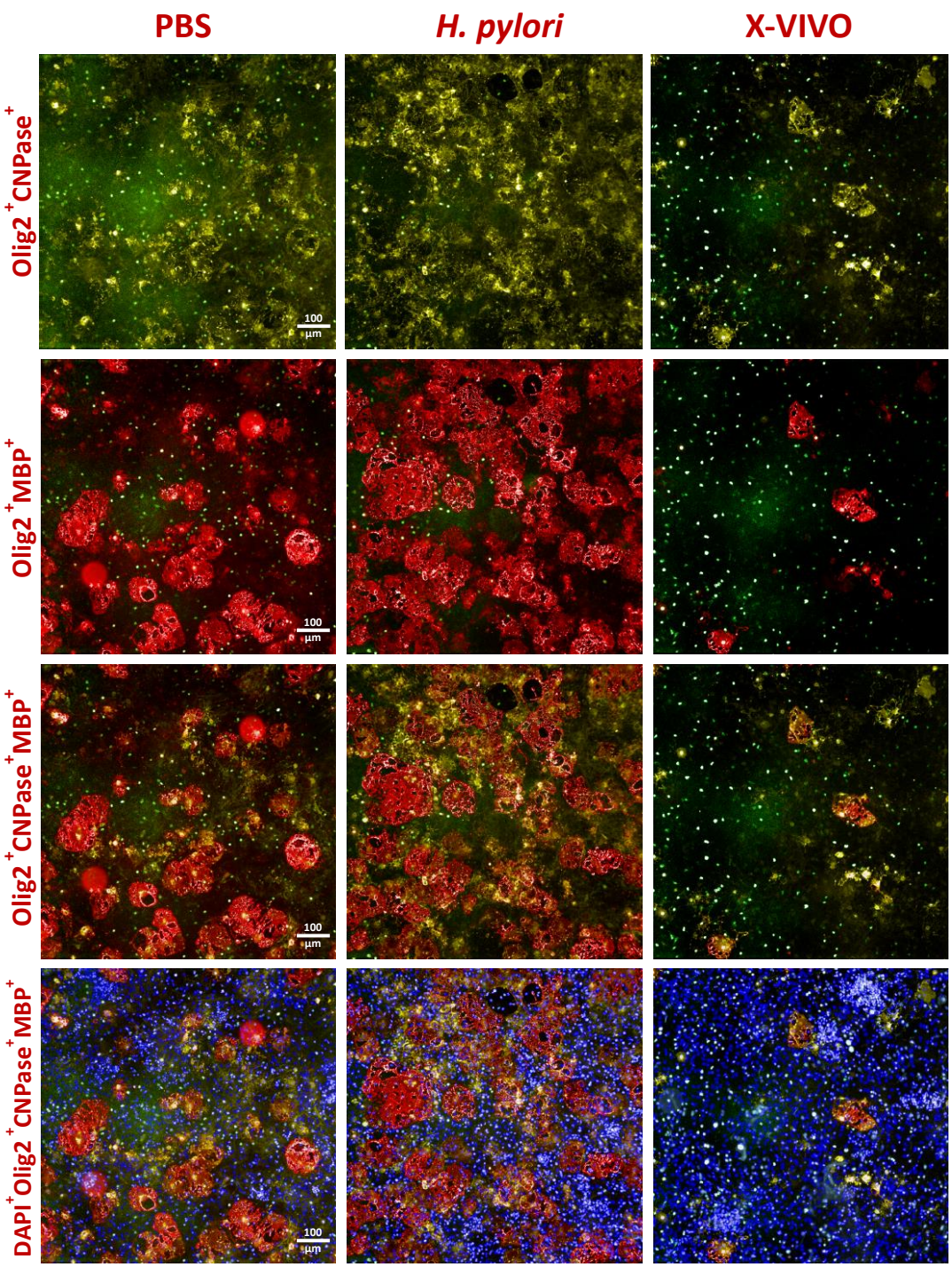

Figure 86 Representative immunostaining images of murine mixed glia after incubation with CD4⁺ T-cell conditioned media derived from splenocytes of H. pylori infected or uninfected mice.

Murine mixed glia incubated with CD4-conditioned supernatant. Cells are stained for nuclei, DAPI (blue); proliferation marker, Ki67 (cyan); oligodendrocyte-specific transcription factor, Olig2 (green); early differentiation marker, CNPase (yellow); and late differentiation marker, MBP (red). Images analysed using Perkin-Elmer® Columbus™ software.

Figure 87: Mixed glia with CD4$^+$ supernatant derived from mesenteric lymph node cells

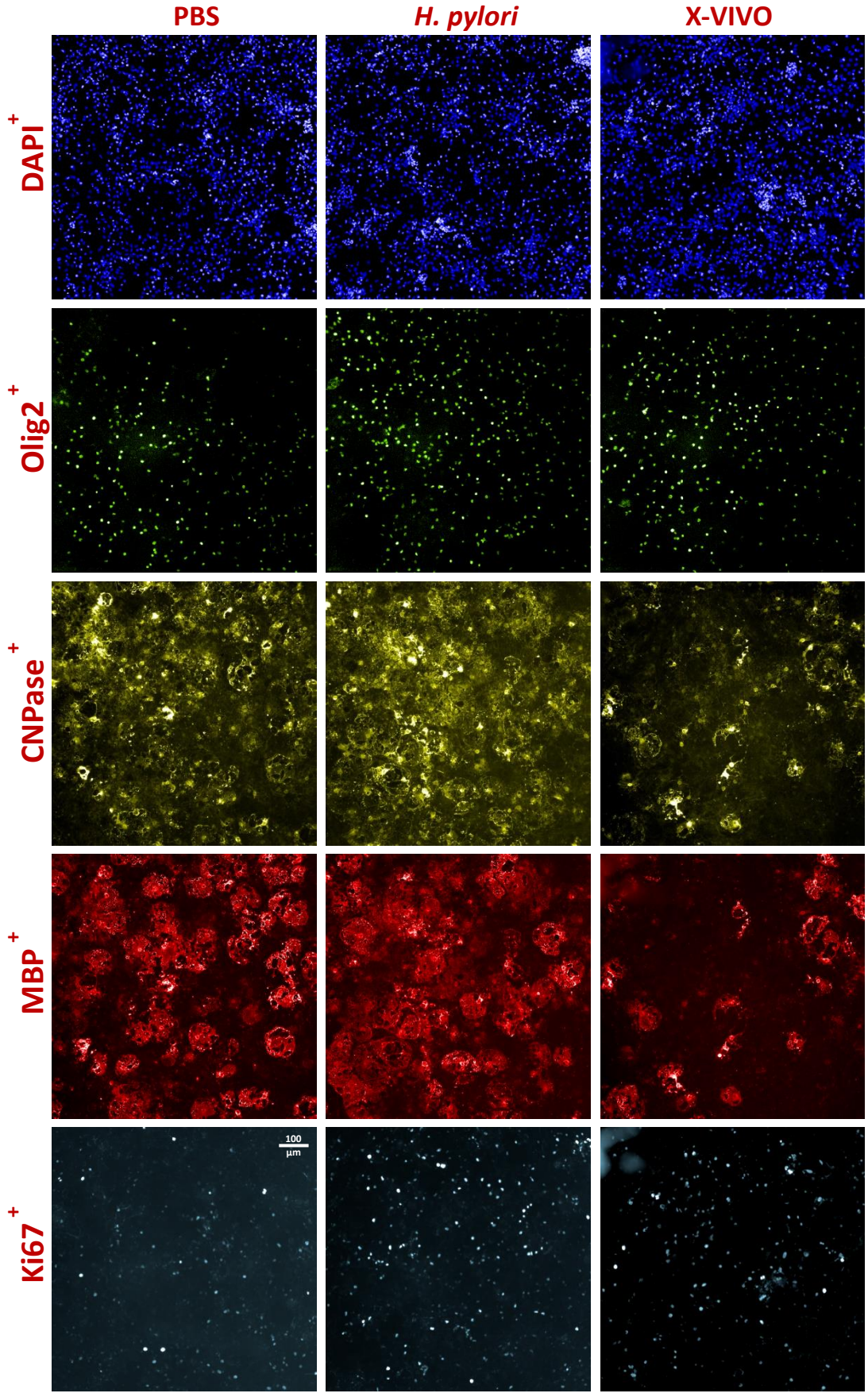

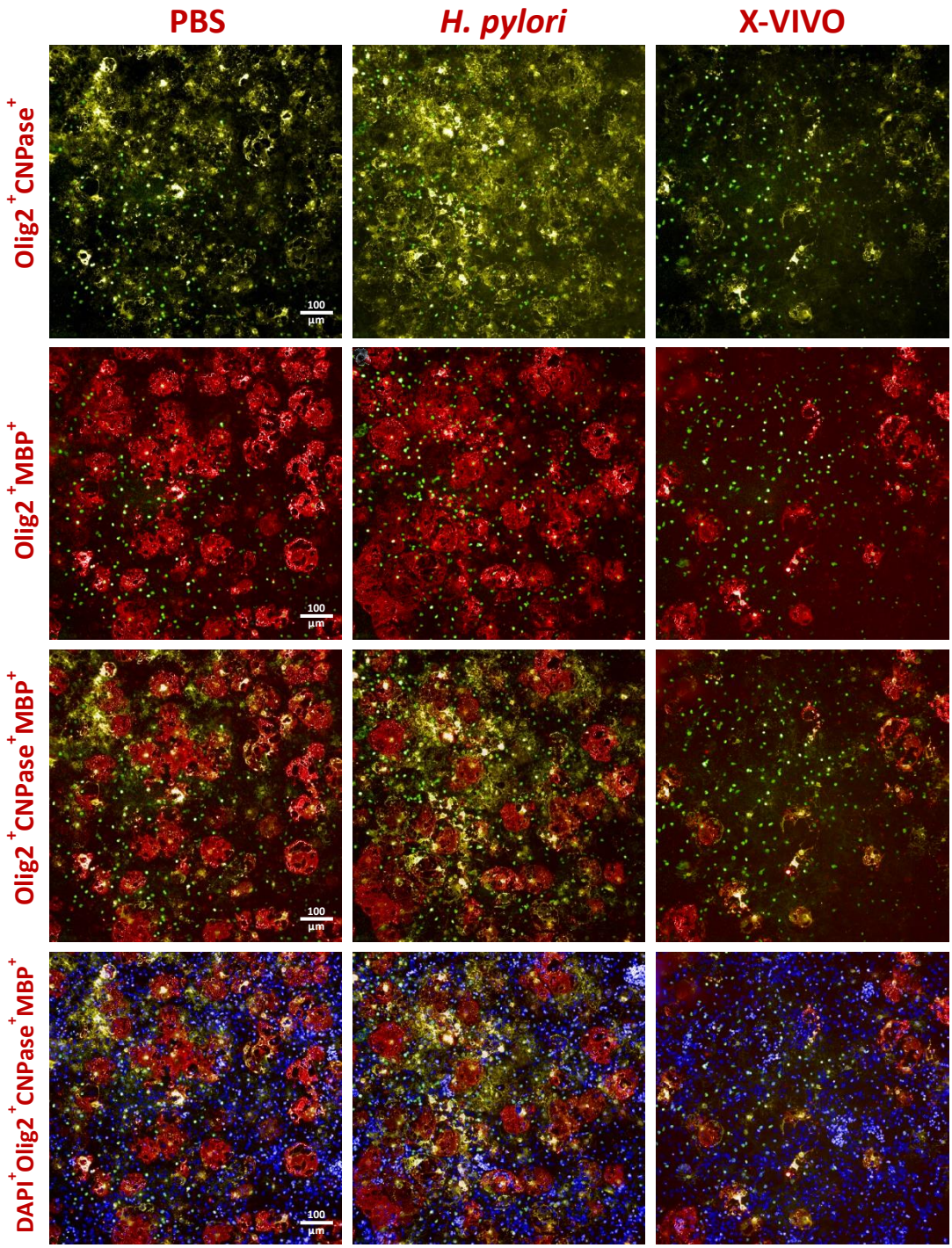

Figure 87 Representative immunostaining images of murine mixed glia after incubation with CD4⁺ T-cell conditioned media derived from mesenteric lymph node cells of H. pylori infected or uninfected mice

Murine mixed glia incubated with CD4-conditioned supernatant. Cells are stained for nuclei, DAPI (blue); proliferation marker, Ki67 (cyan); oligodendrocyte-specific transcription factor, Olig2 (green); early differentiation marker, CNPase (yellow); and late differentiation marker, MBP (red). Images analysed using Perkin-Elmer® Columbus™ software.

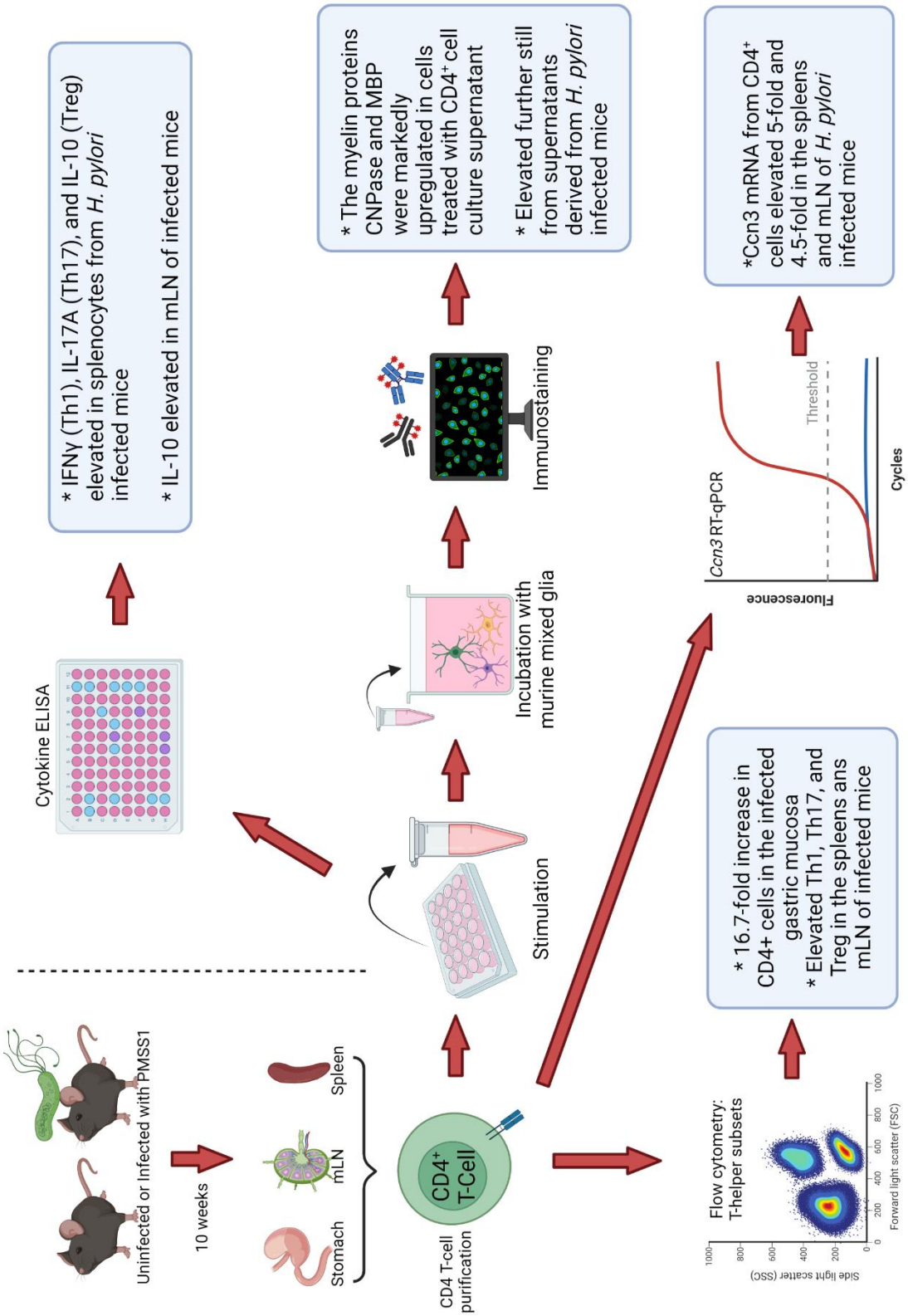

Figure 88 *Schematic representation of the remyelination study design and summary of the data generated*

Experimental design of the remyelination study. The Th1, Th17, and Treg subsets and their respective cytokines, in addition to *Ccn3* mRNA were all elevated in *H. pylori* infected mice. The myelin proteins CNPase and MBP were elevated in glia treated with $CD4^+$ supernatant, and further still in supernatants derived from infected mice. Figure created with BioRender.

5.4 – Discussion

A graphical summary of the study and data generated is given in *Figure 88*.

5.4.1 – Summation of major findings

- Infection of C57BL6 mice with *H. pylori* strain PMSS1 resulted in a substantial 14-fold elevation of $CD4^+$ T-cell migration infiltrating the inflamed gastric mucosa

- Inflammatory and anti-inflammatory T-helper subsets Th1, Th17, and Treg were elevated in the spleens and lesser-so in the mLN of *H. pylori* infected mice.

- $CD4^+$ cells purified from the spleens of infected mice produced greater concentration of the signature cytokines for the Th1, Th17 and Treg subsets by ELISA than those from uninfected mice.

- $CD4^+$ cells purified from the mLN produced greater Th17 and Treg associated cytokines from infected as compared to uninfected mice.

- The pro-regenerative CCN3 was elevated markedly at the mRNA level in cells derived from both the spleen and mLN of *H. pylori* infected mice. But required acute stimulation to be detectable at the protein level in the supernatants.

- There were small increases of myelin protein induction in glia cultured in the presence of CD4 cells from both the spleen and mLN of *H. pylori*-infected mice as compared to uninfected mice.

- There was a marked and significant elevation in both the early and late differentiation markers CNPase and MBP in oligodendrocytes in response to CD4-conditioned supernatant compared to control media, irrespective of infection status

I began this study after the publication of a seminal paper demonstrating a direct role of regulatory T-cells to facilitate re-myelination in a demyelinated CNS [234]. Furthermore CCN3, a candidate molecule through which the regenerative effects can be mediated was also shown to induce oligodendrocyte differentiation using *in vivo*,

in vitro and *ex vivo* approaches. This study was based on the work of Dombrowski *et al.* [234] from the Fitzgerald group at Queen's University Belfast, who have collaborated with this research group for this project.

We have discussed some of the immunological mechanisms by which Tregs can exert a beneficial, and anti-inflammatory influence in the introduction to this chapter. For the most part, they are mediated through the immunosuppressive function of Tregs. Here, they can facilitate protection from diseases such as MS and EAE through suppressing the inflammatory activity of the pathogenic cells which mediate these mechanisms. These include the CD4 T-cells, microglia, macrophage, and neutrophil, all of which contribute to the autoimmune destruction observed in MS [234,481,512,540,541] (discussed in chapter 3)

The authors propose a concept by which a protection can be mediated not by suppression of inflammation and limitation of further disease progression, but by a direct pro-regenerative effect. This effect is suggested to be regulated by a Treg-secreted factor, the central communication network protein 3 (CCN3).

There are many published studies in the literature which support the premise that Tregs exert beneficial effects on neurodegenerative and autoimmune conditions [342]. Susceptibility to, or worsening severity of MS is augmented when a Treg response is absent or inadequate [225]. This is exemplified by IPEX or scurfy as a result of FoxP3 dysfunction [341]. Furthermore, adoptive transfer of Tregs can alleviate symptoms of EAE and MS [342] and may support remyelination either directly [234], or indirectly through the regulation of other contributory cells such as microglia, neutrophils, effector T-cells and macrophages. As discussed in the introduction, recent years have revealed other roles of Tregs facilitating wound healing, and tissue regeneration in muscle, heart, skin, and the CNS [526,528,542]. Indeed, the literature contains evidence that CCN3 is functional in a broad range of biological processes. The previous study has shown that CCN3 derived from Tregs stimulates a robust remyelinating effect on oligodendrocytes *in vitro* [234]. Others report that CCN3 is expressed in regions of the brain, especially neurones, following chemically induced demyelination [543]. However, the mechanisms may not be the same *in vivo,* as $CCN3^{-/-}$ mice did not display defects in myelination [543]. Others show CCN3 levels in human plasma to be comparable

between MS patients and healthy controls, but to be significantly higher in those patients with progressive MS over relapsing MS [544]. Furthermore, two medical interventions for MS (IFNβ and natalizumab) resulted in differential regulation of CCN3 in those patient groups [544]. The idea that CCN3 levels could be augmented by the immunomodulatory effect of *H. pylori*, especially via the induction of Tregs is interesting. The next steps to take this idea forwards towards proof-of-concept for a clinical efficacy are to ascertain how this mechanism may function.

Here, as Tregs and CCN3 might mediate this effect, I investigated how Treg-modulating factors such as *H. pylori* infection may interact with these pathways. If so, it may form one mechanistic basis by which the protection from MS and EAE could be conferred (*Figure 88*).

The previous study used *in vitro* induced Tregs, purified, and stimulated to produce Treg-conditioned media (containing secreted factors). The question I ask, is do naturally arising Tregs show a similar function as those previously produced *in vitro*? And can microbes such as *H. pylori* augment Treg activity and secretions to an extent whereby this can have a biological effect? Of course, stimulating mixed, or total CD4 cells will inevitably lead to the increase of the inflammatory cytokines in parallel. The negative impact the Th1 and Th17 cytokines IFNγ and IL-17 have in the propagation of CNS autoimmunity and myelin pathology is understood. (Discussed in chapter 3). Indeed, for *H. pylori* to confer a positive effect on remyelination, any influence it exerts must be substantial enough to overcome the robust inflammatory responses which characterise MS and EAE.

The current study, I believe, provides some promising preliminary suggestions that infections such as *H. pylori* can modulate $CD4^+$ cell populations in a manner which can potentially regulate activity of CNS glia and remyelination. It would be of benefit to expand on the current work to generate robust experimental evidence to assess this hypothesis adequately. Potential candidate factors which may mediate this effect are not limited to the signature cytokines quantified in this study. Indeed, there are wider lineage-associated cytokines which may also be acting in these pathways which are uncharacterised by these experiments. There are also a wider range of CD4-derived secreted proteins which may also influence glial biology.

We aimed to produce CD4 cell culture supernatants from groups of infected or uninfected mice to prepare and characterise $CD4^+$ cell culture supernatants containing secreted factors. These supernatants, and the cytokines they contain will represent the T-helper subsets in the tissues from which they were derived and may differ between the infected or uninfected groups. I hypothesised that the induction of Tregs by *H. pylori* may enrich the CD4 cell pool with anti-inflammatory cytokines such as IL-10, and pro-regenerative factors; possibly CCN3

To achieve this, C57BL6 mice were inoculated with the *H. pylori* strain PMSS1; this strain has a functional *cag* PaI and can result in greater levels of $CD4^+$ T-cell infiltration into the gastric mucosa, both inflammatory and anti-inflammatory subsets [106]. This should provide the best chance to observe differences conferred by the altered T-helper distributions.

Using flow cytometry and cytokine ELISA, I do show that both $CD4^+Foxp3^+$ cells, and IL-10 concentration in supernatants are elevated in the infected group, both from cells of the spleen and mLN comparably. Conversely, so were markers of the inflammatory subsets Tbet (Th1) and IL-17A (Th17). The mixed Th1, Th17, and Treg response is in line with that expected in the literature where these subsets are found at higher abundance, especially from more virulent strains [106,165].

As the ELISA was unsuitable to quantify CCN3 at the concentrations present in our samples, it was decided to quantify CCN3 at the mRNA level using RT-qPCR. This is a far more sensitive method which can detect down to a single copy per reaction in an ideal circumstance. These qPCR analyses did indeed successfully measure CCN3 in all samples tested. Interestingly, CCN3 was elevated significantly from both the spleen and the mLN cells derived from infected as compared to uninfected mice. This elevation was on the order of 4-fold and 5-fold for the spleen and mLN respectively, being 2-fold higher from cells of the mLN as compared to the spleen. Assuming that CCN3 is biologically active in the process of oligodendrocyte differentiation as was convincingly demonstrated in the original work, we show with the current study that this molecule is upregulated markedly from infected as opposed to uninfected mice.

I found a markedly higher expression of *Ccn3* mRNA these $CD4^+$ cells of infected mice as compared to uninfected mice. This may suggest it is differentially regulated between the two groups, this is not known from the literature. These transcripts may be subject to a post-transcriptional regulation thus preventing an accumulation of the corresponding protein in our samples. However, augmented mRNA expression is itself indicative that there may be underlying differences in the cellular activity or composition between groups. The elevated expression of *Ccn3* from the infected group was present in cells of both the spleens and mesenteric lymph nodes (mLN), but greater in the lymph nodes; where we also show FoxP3, and IL-10 elevated in parallel, suggestive of a Treg signature.

Mixed glia derived from uninfected donor C57BL6 mice were incubated with or without the addition of stimulated CD4 culture supernatant (at 5% of the seeding volume), as described previously [234].

With the cytokine compositions of the supernatants determined, the next step was to analyse the effect of these on the differentiation of mixed glia. The placement which was supposed to support this work being carried out at a collaborating lab was not possible due to the coronavirus pandemic. However, this work was kindly carried out by collaborating colleagues.

The experimental readouts from these *in vitro* experiments inform of the number of Olig2+ oligodendrocyte-lineage cells, the proportion of these which are proliferating (Ki67+), and the number of these expressing markers for early and late differentiation, CNPase and MBP, respectively. We observed no difference between groups in the number of Olig2+Ki67+ proliferating oligodendrocyte progenitor cells. These data would suggest that the supplementation with CD4 cell supernatants is not mediating changes to the proliferation of Olig2+ cells in culture.

There was a substantially increased number of Olig2+ cells counter-stained with CNPase from both the treated groups as compared to media-only control cells. The frequency of Olig2+ cells positive for CNPase rose from <20% in control cells to around 40% in cells from both treated groups. Between the treated groups, there was a modest increase in this frequency in the *H. pylori* infected mouse cells as

compared to sham-infected control cells. The expression of CNPase is expected from an early point in the differentiation of OGCs from OPC precursors and would be expected to precede that of MBP. As such CNPase expression can still be used to identify differentiated cells, however not necessarily of a fully mature and myelinating phenotype.

The frequency of Olig2+ cells co-expressing MBP followed a comparable pattern as CNPase, as expected. There were marked increases in Olig2+MBP+ cells in both the treated groups as compared to control cells cultured in the presence of media only. Between the treated groups, there was again a modest increase in the frequency of MBP+ Olig2+ OGCs in cells from the *H. pylori*-infected group as compared to the sham-infected control group. The scale of this increase was lesser than was observed with the earlier marker, CNPase. This would be expected and suggests that not all the cells had fully differentiated at the study endpoint. Given this, CNPase expression is likely a more suitable marker for this experiment in defining differentiated cells as it cannot be discounted that not all cells will yet have induced MBP, even if they are actively differentiating in response to factors in the supernatants.

Taken together, these data are challenging to interpret. In comparison to mixed glia cultured in the presence of media alone, both the *H. pylori*-infected and uninfected cell supernatants resulted in robust upregulation in the number of differentiated/differentiating oligodendrocytes. This observation suggests that a product of activated $CD4^+$ T-cells in these supernatants, which is present irrespectively of infection status, has the potential to induce remyelination and CNS regeneration. Characterising these supernatants to identify the factor responsible would be of great relevance to expanding this work further. Between the infected and uninfected groups, the differences are slight. However, in all instances, there is a trend for elevated myelin protein expression from the *H. pylori* infected group. This difference did not reach statistical significance; however, group sizes were small.

Importantly, we were also aiming to use *ex vivo* cerebellar brain slices with CD4 supernatants, this experiment was not possible to perform as a direct result of the current (at the time of writing) coronavirus pandemic and the disruption caused as a result. These brain slices comprise a section of cerebellum maintained in media

which will still retain the full 3D architecture of the brain and may be able to clearly show myelination taking place *in situ*. Using mixed glial cultures, not all the resident cells present in the brain will be available in culture, nor will they form 3D structures including the presence of axons in which OGCs may be able to myelinate. It is possible that the lack of neurones in the mixed glia cultures may to some extent prevent the OGCs from synthesizing myelin membranes as there are no supporting signals derived from the nude axon requiring myelination.

Nonetheless, these preliminary data provide us with experimental *in vitro* evidence that $CD4^+$ T-cells secrete factors which can induce the differentiation of oligodendrocytes. This effect may be mediated directly, or it may be indirect through primary effects on the microglia and astrocytes also present in the glial cultures. Indeed, both these glial lineages play intricate roles in the support and regulation of myelination *in vivo*. The previous work of Dombrowski assessed supernatants in purified oligodendrocyte-neurone co-cultures and observed a pro-remyelinating effect. This would infer that the effects seen are likely mediated in a similar manner directly on OGCs. It also supports the premise that the absence of neurones in the mixed glial cultures used in the current study are not confounding the data.

Between the infected or uninfected cell supernatants, the most notable differences in terms of cytokines quantified were that of IL-17A (4-fold) followed by IL-10 (2-fold). Importantly however, *Ccn3* mRNA was elevated 4-fold and 5-fold from splenocyte or mLN-derived CD4 cells from the *H. pylori* infected as compared to PBS-treated group. The elevation of *Ccn3* mRNA corresponds to an elevated number of CNPase/MBP+ Olig2+ OGCs in the infected cell supernatants. However, this difference was only slight, yet the difference in *Ccn3* mRNA between the groups was substantial. For the PBS-treated sham infected group to have induced myelin protein expression in the mixed glia on a scale only slightly reduced from the infected group it does not correlate with CCN3. One may argue that the infected group were markedly higher in CCN3, however also elevated 4-fold in IL-17A therefore these inflammatory and anti-inflammatory pathways may be contributing to a mutual inhibition of each other. The large increase of CCN3 may indeed be sufficient to result in large increases

in the differentiation of OGCs. However, in the presence of a notably elevated concentration of IL-17A, pathogenic in MS and EAE, this may not have occurred.

5.5 – Summary & Future Work

The work presented in this chapter is perhaps the most novel, although we did not see large differences between infected or uninfected groups. However, we must also consider that the assay was not optimised for supernatants of such a low concentration as ours. With some preliminary experiments to optimise the method I think it would be a great and underexplored topic to investigate, especially considering the impact it could have to identify such a factor with so much potential.

- I would like to identify the factor responsible for the profound effect my supernatants had on oligodendrocytes. This could be achieved through knock out of individual cytokines proposed to mediate the effect. For instance, this was shown for CCN3 in the original paper, and reproducing the result will be starting point.
- This could also be done if we fractionate the supernatant and separate the constituent factors that way to narrow down where our molecule is.
- It may be beneficial to purify individual T-helper subtypes as opposed to mixed CD4 solutions. By doing so we could create subtype-specific supernatant by which to characterise separately
- Growth factors are a potential factor secreted by Tregs, and other cells, which may have induced this effect on oligodendrocytes. There are high-sensitivity assays such as the MSD panels that we used to quantify human plasma cytokines in chapter 1. These could simultaneously identify panels of related cytokines and growth factors in each of our samples
- I believe there is a potential that other non-CD4 cells may be very important mediators. Here, especially microglia would be interesting to characterise, such as their polarisation state (M1/M2) in response to our factors.
- Additionally, there are a wide range of regulatory cell subtypes which may play a key role. B-regs, Tr1 cells, Th3 cells, regulatory CD8 cells. Work to

characterise the functions of these in future in our models would be of benefit.

- Myelination assays with neurones (or cones) to check actual myelinating capacity would allow a functional assessment of myelinating capacity aside from phenotyping by myelin marker expression.
- I also think it would be pertinent to assess any differences that there may be between different *H. pylori* strains, just as we saw a strain-specific benefit in the EAE model.

Chapter 6

General Discussion

Chapter 6: An overview of the work presented in this thesis, with observations and discussions relating to the principal hypothesis; can *H. pylori* protect from multiple sclerosis?

6.1 – Objectives and hypotheses

The overarching hypothesis behind the work I present here is that *H. pylori* infection can confer a protection against immune-mediated diseases such as multiple sclerosis. I proposed that this may be mediated via suppression of inflammatory T-helper cell activity, modulation to $CD4^+$ T-cell trafficking, by enhancing the regeneration and repair in the CNS, or by a combination of all these factors. A central paradigm of this research is the ability of *H. pylori* to tip the balance of the $CD4^+$ response toward an anti-inflammatory state driven by regulatory T-cells and IL-10 (*Figure 89*). Therefore, this thesis aimed to investigate the $CD4^+$ T-cell responses to *H. pylori* infection and EAE to identify mechanisms which may help explain the proposed protective associations.

6.2 – Observations and discussion of the major findings

Over the last five chapters I have introduced *H. pylori*, multiple sclerosis, the cellular immunological mechanisms which underlie them, and other contributory factors such as the gut microbiome. The true extent of the interactions between microbes and their human hosts and the intricate influence they can have on our biology is still to be fully elucidated, but the concept is gaining a great deal of attention in the literature. The stark rise of immune-mediated conditions, particularly in developed nations, is a matter of great importance for human health and disease. The 'Old friend's hypothesis' is one which would seem to be supported by a wealth of published literature, and the co-evolution of *H. pylori* with its human hosts is well documented. One must consider whether *H. pylori* really is an 'infection' or would it be more suitably referred to as a colonisation of a once-commensal microbe. Of

course, there are serious implications from harbouring a microbe which is the predominant cause of gastric cancer.

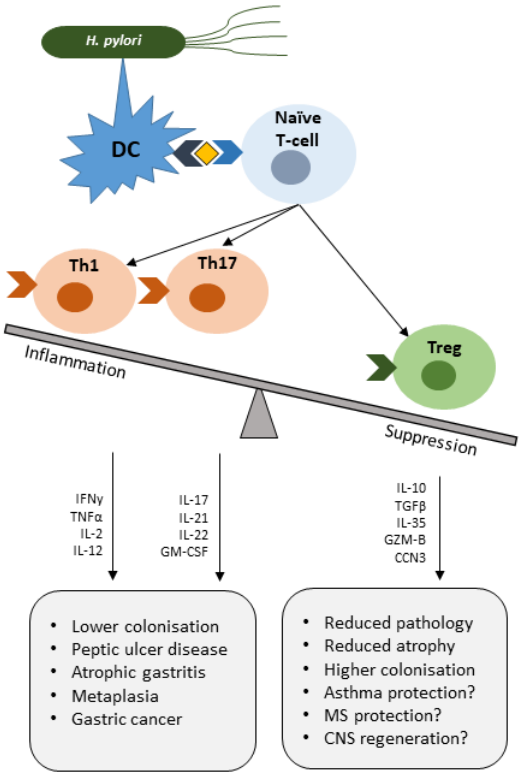

Figure 89 Diagram of the proposed immunomodulatory effect of H. pylori infection on CD4+ T-cells

The balance between inflammatory and anti-inflammatory CD4+ effector function influences the course of *H. pylori* mediated gastric disease and enables the bacterium to subvert host immunity and establish persistent colonisation. The generation of a regulatory T-cell response may also have the potential to mediate the protection from immunological conditions such as asthma, allergy, and autoimmunity.

I have discussed numerous examples in the literature whereby *H. pylori* infection, and the wider microbiota in general can have marked effects on a whole variety of human diseases, both immunological and neurological. Many of these reports are based on correlation, with a paucity of robust mechanistic data to conclusively support cause and effect. Indeed, the work which is presented in this thesis can neither prove, nor disprove, the hypothesis that *H. pylori* may protect people from multiple sclerosis. A better understanding of the underlying cellular mechanisms is crucial to understand the contributory factors driving these responses to guide new therapeutic strategies. A schematic of the overall mechanisms proposed is shown in *Figure 90*.

Much of the experimental work here utilises mouse models, both of *H. pylori* infection and EAE, the animal model of MS. Important differences between human and mouse immunology have been discussed previously, with not all mechanisms fully recapitulated between species. Mouse models are an invaluable tool by which to identify potential novel pathways, especially when human study is difficult, or tissue limited. With this comes a more challenging obstacle; showing a translation of mouse to human data, the downfall of several potential therapeutic strategies for MS showing initial promise in EAE. Furthermore, whilst being able to provide experimental groups not confounded by the high amount of variation in human cohorts, this same factor means that results derived from mouse models may not be comparable in more heterogenous human populations.

6.2.1 – Human immune response to *H. pylori* infection and eradication

Chapter 2 investigated the human immune responses to *H. pylori* based on the peripheral blood of infected and uninfected patients, by stratifying plasma cytokine concentrations with the extent of gastric disease, and quantifying PBMC cytokine mRNA expression (*Figure 28*). One of the major aims of this research was to investigate how eradication of *H. pylori* affects the cytokine profile in the host. It was hypothesised *H. pylori* infection would result in altered $CD4^+$ signatures in peripheral blood which may have prognostic impact for both gastric disease risk and/or extra-gastric protection. As an infection usually acquired in early childhood any protection conferred may be shaped during immunological development which may not depend on persistent infection, on the other hand, eradication of *H. pylori* may inadvertently remove any beneficial consequence. Therefore, we sought to quantify T-helper subsets in human peripheral blood. The variation within the cohorts was marked, and not all the mRNA and protein data agreed, however these two data were derived from different cohorts. It would have been an interesting addition to perform similar high-sensitivity plasma cytokine quantification from the eradication cohort to accompany the mRNA data. The data presented here have identified several statistically significant differences which warrant further investigation.

Most of the published literature has shown that IL-10 and regulatory T-cells play a major role in *H. pylori*-mediated protection from asthma; however, the current studies were not able to confirm such associations. Furthermore, we identify reductions of *IL10* mRNA in human PBMCs as the most sizeable difference that was observed in *H. pylori* infected people. An association between *H. pylori* infection, the severity of disease and plasma concentration of IL-17 was found, however, despite elevated protein concentration in infected individuals, similarly to *IL10*, *IL17A* mRNA was significantly reduced compared to uninfected controls. In contrast, Th1 and Th2 cell-derived cytokines remained comparable between groups following eradication.

The finding that both Th17 and Treg cytokine mRNA expression were markedly decreased in PBMC's from infected individuals was unexpected; it would be of great interest to ascertain the reasons this was observed in our cohort as this has not been reported regularly in the literature. *H. pylori* can downregulate inflammatory T-cell activity by a number of mechanisms, for instance suppression by Tregs, or VacA-mediated inhibition of human T-cell activation. However, neither Th1 or Th2 cells were significantly different between groups implying the Th17 and Treg regulatory pathways are predominantly affected. In humans the different FOXP3 isoforms can have differential effects on the development of Treg or Th17 lineages, and of the suppressive capacity of Tregs; this provides an attractive option to investigate in future. Furthermore, in addition to the CagA serology, which appeared to not influence baseline cytokine expression levels, data on the virulence genotype of the colonising strains, particularly *vacA*-typing may be useful. Gathering microbiome data would be interesting as Th17 and Treg cells are influenced closely by the microbiota, changes to microbial populations or diversity could be expected either as a cause or effect of *H. pylori* infection and antibiotic administration.

One potential impact of this work is the identification of prognostic markers for *H. pylori* disease risk, if *H. pylori* does mediate protection from immunological diseases, then eradicating the infection may inadvertently worsen the presentation of such conditions. This research has identified factors which may be of interest to investigate further, namely IL-17-, IL-10-, and IL-12-family cytokines and their

respective cellular sources. The differences were modest but with additional markers such fingerprints for disease risk would be of great benefit clinically.

Inflammatory signatures in peripheral blood remained largely unchanged for at least 24 months post eradication, but the anti-inflammatory *IL10* increased. Plasma anti-*H. pylori* IgG concentration decreased steadily over the study period, but with most participants still serologically positive at 24 months. Taken together, it may be hypothesised that eradication of *H. pylori* is not expected to cause a worsening of autoimmune or atopic conditions. On the contrary, there may indeed be the opposite effect given the elevation of *IL10* after eradication.

Here, cytokine expression was only quantified from peripheral blood, data from the gastric mucosa or lymphoid tissues, where the immune response to *H. pylori* is likely to be the strongest is lacking. However, with the hypothesis that *H. pylori* infection can modulate extra-gastric disease, differences in the periphery were anticipated. Cytokine transcripts may be low considering the cells were not stimulated prior to analysis. However, I presented evidence previously that stimulation can skew the cellular phenotype and frequencies by a substantial amount.

6.2.2 – The immunomodulatory impact of *H. pylori* infection in EAE

In chapter 3, I investigated the effect of *H. pylori* on the development and severity of the animal model for MS, EAE (*Figure 47*). This research group previously published that *H. pylori* infection protected from EAE severity, a finding which was associated with substantially reduced frequencies of Th1 and Th17 cells and cytokines in the spleen and CNS of mice infected with *H. pylori* strain SS1 [334]. However, no concurrent differences in FoxP3 Tregs were observed to explain this, and further work using the EAE model is crucial to delineate the contributory factors driving this observed protection. Additional tissues would be useful to analyse aside from the spleen and spinal cord. There is evidence from the literature that adoptively transferred $CD4^+$ cells in a passive EAE model possess a tropism for the intestines, preceding migration to the CNS. Furthermore, we have hypothesised differential T-cell trafficking to occur during *H. pylori* infection (as investigated in chapter 4) which may also contribute to the failure of Th1 and Th17 subsets to infiltrate the CNS in the study.

In the current studies, reduced EAE severity was observed in mice colonised with *H. pylori* strain SS1, but not the more virulent PMSS1 strain. This is interesting as the more virulent PMSS1 was hypothesised to have a greater beneficial effect and has been shown previously to exert a greater suppression of total IgE, correlated to increased IL-10. The theory behind this is that more inflammatory strains (possessing the *vacA* type 1 or functional *cag* T4SS virulence factors) augmented the immune response including Tregs. When considering the paradigm that infection may confer a protection, it is encouraging that this was observed to a greater extent with a less virulent SS1 strain, as this may suggest that protection can be achieved with a much-reduced concurrent risk of developing gastric disease. However, I have previously alluded to the inherent differences between animal models of *H. pylori* infection and the human condition, thus the biological effect of VacA and CagA may not result in similar outcomes between these species.

Unfortunately, only mild EAE developed in most of the study animals, which may have affected the ability to observe significant differences in their immune responses. There were no differences in the proportions of T-helper subsets as quantified using flow cytometry between the infected and uninfected mice, nor between PMSS1- or SS1-infected groups. As the severity of EAE is known to correlate with increased immune infiltrates, the failure of the model to reach high EAE severity scores in the mice may be a factor in this. The reasons we observed only a mild EAE severity here are not known, and our previous work using this model, both in our published work and the pilot experiments documented here, developed in a manner more comparable with that expected from the literature. Further work investigating this should be performed to confirm and expand on our previous finding.

The immunological mechanisms of both MS and EAE are well characterised in terms of the cellular contributions to an increasing pathology. In our pilot study, aside from $CD4^+$ T-cells the largest differences observed in CNS-infiltrating cells were of macrophages, and dendritic cells, and a substantial B-cell response in the lymph nodes. Experimentally, these studies have focussed on the $CD4^+$ T-cells but we may be missing crucial determinants of disease course by not quantifying these other

lineages. As has been discussed at length, *H. pylori* can influence the activity of all these lineages, which I would like to observe in similar studies in the future. The work of Muller *et al.* has convincingly demonstrated the crucial interactions between *H. pylori*, dendritic cells, and Tregs in shaping the beneficial immune response in asthma [20,21,354]. The $CD11c^+$ dendritic cells were indeed shown to be elevated markedly in the CNS of EAE mice in the pilot study, and were observed to elevate in correlation with EAE score, hence functional or phenotypical differences in these cells may represent an important mediator in the protection from MS. An important observation was that the predominant source of IL-10 was from B-cells not T-cells. Regulatory B-cells (Bregs) have not been studied here but may have an important role in the immune crosstalk between *H. pylori* infection, and MS/EAE. Indeed, the work of Rojas *et al.* demonstrating that intestinal B-cell/plasma cell recruitment to the CNS could supress EAE, further supports this theory.

During revisions to this manuscript, seminal work was published in Science with the strongest evidence to date of a causal link between MS development and Epstein Barr viral infection [545,546]. Of course, Epstein Barr has been long associated with MS, however also widely prevalent in the general otherwise healthy population. The viral trigger hypothesis is supported from the literature, and we have discussed examples of infectious triggers of demyelinating diseases such as *C. jejuni* and Guillain-Barre syndrome (GBS), associations of MS incidence with endogenous retroviruses, and of course there are virally-induced models of MS utilising Theiler's murine encephalomyelitis virus (TMEV). Furthermore, there are recent reports of demyelination and cellular dysfunction in the brain after SARS-CoV-2 infection [547]. Given the latest finding, the EBV-associated pathways, which of course include the aforementioned B-cells, may be of great interest to revisit.

The reduced cumulative EAE severity observed from the SS1-infected group was interesting, although the EAE scores were comparable in terms of the peak score reached in each group, the SS1-infected group presented with a period of recovery and a reduction of symptoms not observed in the other two groups. This may indicate *H. pylori* strain specific effects and might suggest that an amount of repair and regeneration had occurred in the demyelinated CNS of these mice. A seminal paper

by Dombrowski *et al.* was published in 2017, here the authors demonstrated that Tregs actively and directly facilitate CNS regeneration and repair of demyelination [234]. In chapter 5, I therefore investigated whether the *H. pylori* mediated induction of Tregs could play a role in remyelination or repair of the CNS.

6.2.3 – Alterations to CD4+ T-cell trafficking during *H. pylori* infection

The reduction of EAE severity, and the potential increase in CNS regeneration may both be influenced by T-cell trafficking, whether this should be to divert inflammatory cells away from the CNS, or to direct suppressive Tregs towards it. In chapter 4, a pilot study was performed to investigate the trafficking of EAE T-cells in mice (*Figure 68*). Here we extracted MOG-primed $CD4^+$ cells from pre-symptomatic EAE mice. These cells were labelled *ex vivo* prior to adoptive transfer to non-EAE recipient mice, either infected with *H. pylori* strain PMSS1, or uninfected. As we know, passive EAE is an established method of EAE induction and so a proportion of these cells were hypothesised to naturally infiltrate the CNS. Both EAE and *H. pylori* infection result in the induction of the chemokine CCL20 at the respective sites of inflammation. Our hypothesis here was that gastric *H. pylori* infection influences the CCL20 gradients guiding CCR6-mediated cell trafficking. Indeed, we have published evidence previously that the CCR6/CCL20 axis is important for the migration of CD4 cells to the inflamed *H. pylori*-infected gastric mucosa [448]. Reboldi *et al*. have shown CCR6+ Th17 cells to be critical mediators of EAE induction in both passively and actively induced EAE models [446].

Work for this chapter was disrupted due to the 2019 SARS-CoV-2 pandemic and the subsequent closure of this institution. Nonetheless, some promising findings were observed. Some differences in the homing of transferred EAE cells to the brain and spinal cord between infected and uninfected groups were noted. We hypothesised that *H. pylori* infection may sufficiently divert EAE-$CD4^+$ T-cells away from the CNS and towards the stomach. We did observe fewer labelled EAE $CD4^+$ cells migrating to the brain in the infected group, however no reciprocal accumulation of them was noted in the stomach as hypothesised. Upon characterisation of the $CD4^+$ cells infiltrating the CNS, the proportion of Tregs to Th1/Th17 subsets was elevated in *H. pylori* infected mice, supporting the premise of a more anti-inflammatory

environment. However, a high concentration of the fluorescent label in the liver may suggest that a large amount of the dye is being metabolised and may call into question the validity of the findings. In this same regard, I observed a notable elevation of fluorescent signal in the gut, however subsequent analysis showed that faecal matter from naïve mice unrelated to this study contributed to the radiance in the far-red wavelengths and so this signal cannot be attributed to labelled cells with certainty. A control group consisting of untreated mice, or mice administered unlabelled cells was not included in this small-scale pilot study. Despite this limitation in the study design, the data suggest that there are differences in cellular migration to be investigated in greater depth in future.

Although the data derived from the current study was insufficient from which to draw robust conclusions, there was an indication that trafficking of $CD4^+$ cells may be modulated by *H. pylori* infection as hypothesised. As alluded to previously, there are numerous other lymphocyte subsets which may also be acting in this pathway, such as dendritic cells, macrophage, neutrophil, and B-cells which were not included in these investigations. Indeed, Rojas *et al.* report intestinal IgA plasma cells infiltrating the inflamed CNS could suppress EAE, and Duc *et al.* presented evidence of an unexpected inherent gut-tropism of adoptively transferred EAE Th17 cells in models of passive EAE induction. Taken together, I believe that the hypothesis should be investigated further and will be an exciting future research direction.

6.2.4 – Regulatory T-cells and CNS Remyelination

It was hypothesised that $CD4^+$ T cells from *H. pylori*-infected mice may be enriched in regulatory T-cells and contain pro-regenerative factors supportive of CNS remyelination and repair. Although this study primarily hypothesised that CCN3 was responsible for these effects, the involvement of the other $CD4^+$ T-cell cytokines and other secreted factors are equally important (*Figure 88*).

Higher proportions of oligodendrocytes expressed the myelin proteins CNPase and MBP after incubation with the $CD4^+$ supernatants from infected mice, derived from both the spleen and mesenteric lymph nodes. Perhaps the most interesting finding was that the CNS-regenerative factor *Ccn3* was elevated substantially at the mRNA level in $CD4^+$ cells from *H. pylori*-infected compared to uninfected mice. In the

interim, the group of Fitzgerald, *et al.* have published further work utilising a *Ccn3* knockout mouse model to investigate the importance of this factor to remyelination [543]. Here, they find that *Ccn3* knockout does not have a substantial effect on the capacity for remyelination. However, this is not to say that it cannot participate in the induction of remyelination as elegantly shown in the original paper, but rather that there are other factors and mechanisms able to compensate for its functionality when absent.

What we observed in this study, is the astounding difference in myelin protein expression between murine mixed glia incubated with unconditioned media, and those incubated with media supplemented with $CD4^+$ cell supernatant. The difference between uninfected and infected groups were modest, but with a trend for more myelin protein expression from *H. pylori*-derived supernatants. However, we have identified that factors from stimulated CD4 cells present in the supernatants resulted in profound expression of both CNPase and MBP in oligodendrocytes. Future work characterising these supernatants and the identification of the factors responsible for such an effect could be highly valuable. Indeed, facilitating remyelination could have enormous potential if administered therapeutically. Looking at the ELISA data, the cytokine present in highest abundance was the Th1-associated IFNγ. On the other hand, IL-17A followed by IL-10 were elevated most significantly between groups.

IFNγ and IL-17A were the most dominant cytokines in our supernatants, both known to have detrimental effects in EAE and MS, supporting further disease progression. These are the signature cytokines produced by Th1 and Th17 cells but with a wide range of cellular sources. However, IFNγ is also a potent ligand for the aryl hydrocarbon receptor (AhR). Activation of AhR induces the expression of indoleamine dioxygenase (IDO) which can transduce effects through metabolites such as kynurenine, a product of Tryptophan metabolism. Interestingly, the AhR-IDO axis is pertinent to EAE and MS whereby signalling through this pathway in CNS microglia and astrocytes has been shown to induce remyelination by oligodendrocytes, with potential importance to MS. Furthermore, IDO induction in dendritic cells supports a tolerised phenotype which can be exploited by some

infectious agents to evade immunity, suppressing effector T-cell activation, and promoting the generation of IL-10 and Tregs. No work has been performed here to characterise these mechanisms. However, future work investigating the effect of T-cell-derived cytokines, metabolic products, and the AhR-IDO axis in additional lineages of CNS glia such as microglia and astrocytes would be a fascinating and under-explored avenue of research on which to embark. The gut-brain axis is a rapidly expanding field and one with many secrets still to be revealed.

The original study design included additional models by which to analyse the regenerative potential of the supernatants. For logistical reasons because of the SARS-CoV-2 pandemic, much of this work could not be performed. Optimising the *in vitro* assays would be essential in future and acquiring data from the brain slice models quantifying axonal remyelination after induced demyelination, in addition to the mixed glia or oligodendrocyte-neuron co-culture assays as initially intended may elucidate important mechanisms.

Figure 90: Schematic of the proposed immunological crosstalk between multiple sclerosis and *H. pylori* infection

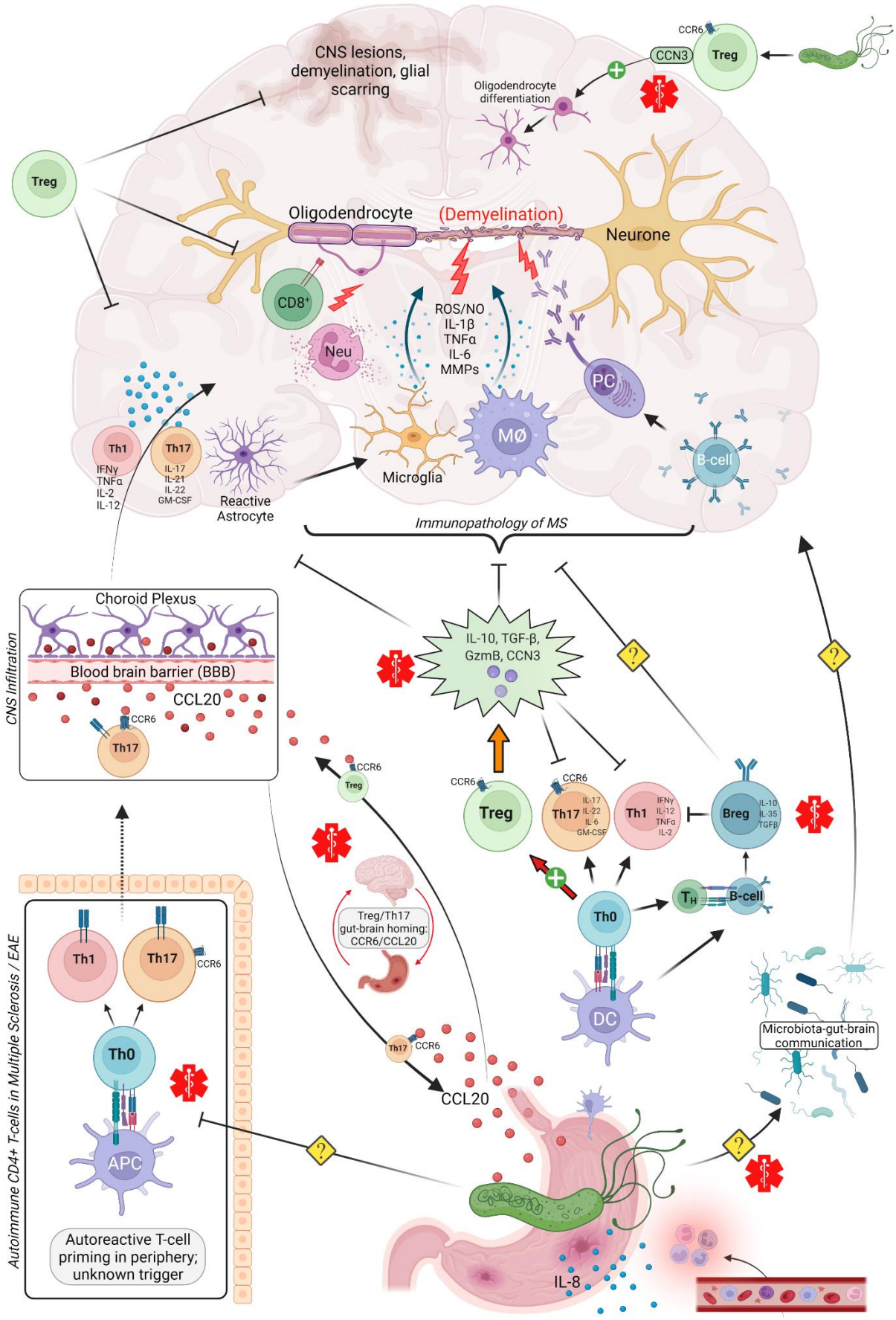

* = *Potential therapeutic intervention*

Figure 90: Schematic representation of the proposed mechanisms H. pylori may exploit to mediate regulatory effects on the immunopathology of multiple sclerosis.

Multiple sclerosis: Autoreactive T-helper subsets are primed in the periphery, sensitised to an unknown initiating stimulus; the $CD4^+$ Th1 and Th17 cells with TCR specific for CNS myelin antigens are major effectors. Infiltration to the CNS requires migration and traversal across the blood-brain barrier (BBB). Reactivation within the CNS induces effector function and the secretion of inflammatory cytokines. The pro-inflammatory milieu that ensues facilitates the infiltration of further innate and adaptive cells; neutrophils, macrophages, activated microglia, reactive astrocytes, B-cells, and $CD8^+$ T-cells amongst others all contribute to tissue damage, propagating further pathogenesis. Epitopes of oligodendrocyte myelin are key targets of the autoimmune response, which results in the characteristic demyelinated lesions observed in MS and EAE. Th17 cells expressing the homing receptor CCR6 may be essential for initial entry to the CNS, navigational cues are derived from the chemokine gradients of CCL20 which is expressed by astrocytes and Kolmer cells on the choroid plexus epithelium. ***Helicobacter pylori***: The expression of chemotactic stimuli such as IL-8 and CCL20 are induced in the infected gastric mucosa which may act to interrupt canonical migratory patterns of cells of the immune system, including CCR6-expressing Th17 and Treg cells. Diversion of Th17 cells to the infected gastric mucosa, or of *H. pylori* specific Tregs to the inflamed CNS is proposed as a potential mechanism to protect against MS severity in infected individuals. *H. pylori* may interfere with the initial priming of autoreactive cells in the periphery or may suppress the functions of these cells through the induction of Tregs and Bregs, producing anti-inflammatory factors such as IL-10 in addition to utilising contact-dependent mechanisms. In MS and EAE, exacerbated disease can develop in those with an inadequate Treg response, and adoptive transfer of Tregs can confer a protection. Tregs can secrete CCN3, a pleiotropic factor with pro-regenerative properties which may enhance the differentiation of oligodendrocyte precursor cells to a mature phenotype with the capacity for remyelination. Regulatory B-cells can express a similar compliment of suppressive cytokines as Tregs, such as IL-10, and B-cell-directed therapies have an efficacy in MS and EAE. Bregs induced by *H. pylori* infection may play a crucial role in these pathways. Dysregulation of the microbiota can have beneficial or deleterious effects on MS and EAE; colonisation with certain gut bacteria such as *Prevotella histocola* can suppress disease severity comparably with leading pharmacological interventions. Both *H. pylori* and the wider microbiome may be able to influence MS pathogenesis through the gut-brin axis; neuroactive molecules, metabolic homeostasis, or direct induction of anti-inflammatory immunity, which may all play a role.

6.3 – Strengths and Limitations

For the human peripheral blood work, the study allowed the exploration of T-cell cytokine responses during the eradication of *H. pylori*. Data of this nature is sparse in the literature and the results derived from our cohort were very interesting. The main caveats of this study were the variation observed within the cohort which may have obscured small differences. The study would also have benefitted from some additional data from the participants on the colonising strains, gut microbiota composition, and a longer-term follow up.

The EAE model provides the best recapitulation of human MS currently possible *in vivo and* investigating the mechanisms of this alongside concurrent *H. pylori* infection has not been widely performed by others, providing unique and novel immunological data. There are however limitations to this model. The EAE induction resulted in a much milder severity than anticipated and this may well have prevented the

observation of significant differences between groups. Of course, the mechanisms of MS and EAE are not totally comparable as discussed previously, and the course of EAE can vary largely with genetic backgrounds of the mice, myelin antigen used to illicit a response (MOG, MBP, PLP, etc), and the microbiota.

The methodology used to track T-cell migration was inferior to the resolution achievable with alternative methods such as the previously used SPECT-CT imaging modality. Tracking of T-helper subset-specific patterns of migration would be very interesting. Of course, we did not verify these cells were reactive against MOG in this study, and given we extract cells at the pre-symptomatic phase, and the failure of EAE to induce effectively in the previous work may call into question how representative of EAE T-cells these were.

The remyelination study was perhaps the most novel of the work performed here. This hypothesis provides a mechanism for MS protection totally aside from the immunosuppression generally proposed. Providing data that there may be a pro-regenerative effect on oligodendrocytes by CD4+ T-cells has great impact for the field of autoimmunity. A caveat of this work was the unavoidable disruption to the planned work as a result of SARS-CoV-2. Furthermore, although indications of oligodendrocyte differentiation was shown, this was not shown to translate directly to remyelination in a demyelinated CNS. Further work quantifying functional remyelination would be a fantastic data set to analyse.

6.4 – Looking ahead to future work

In future, characterisation of human peripheral blood immune responses should be expanded, to account for additional cellular lineages, and a wider array of cytokine markers. We have identified the IL-17, IL-10, and IL-12-family cytokines as promising targets which may be differentially regulated during *H. pylori* infection. A non-invasive prognostic test based on peripheral blood immune signatures would have great clinical impact and better inform physicians on treatment strategies.

I would be interested to investigate regulatory immunity in a wider context in these models. The current work has relied strongly on FoxP3 or IL-10 as a marker for Tregs, and the data I present here does not necessarily show a sizeable difference between

experimental groups. It is important to quantify FoxP3- Tregs (Tr1-like cells), regulatory CD8+ T-cells, or indeed Bregs, or IL-10-secreting dendritic cell subsets which may all contribute to the protection from MS. Furthermore, assessing the suppressive capacity of these cells may inform of functional differences that the quantification of signature transcription factors or cytokines alone may not identify.

As a potential future refinement, there are several alternate models of EAE which result in distinct disease courses. It would be interesting to observe the effect of *H. pylori* infection across these, for instance in the relapsing-remitting MBP-EAE model.

The T-cell migration model should be optimised as although there were indeed indications that the migration of $CD4^+$ T-cells was altered in *H. pylori* infected mice, the current methods were inefficient to quantify them. As suggested above, tracking of additional cellular lineages as well as specific T-helper subtypes would greatly improve the dataset here. Characterising tissue-specific integrins on cells such as the CNS-associated $\alpha_4\beta_1$, or gut-associated $\alpha_4\beta_7$ may reveal important clues in addition to quantifying the chemokine and homing receptor contribution of the CCR6/CCL20 axis. I would like to perform these experiments in larger groups over multiple timepoints as opposed to a single 24-hour endpoint.

I believe that CNS-resident glia aside from oligodendrocytes may be crucial mediators of the immunopathology of MS and EAE. Such cells as microglia and astrocytes can intricately regulate the function of myelinating oligodendrocytes, drive progression of disease, or facilitate a pro-regenerative anti-inflammatory environment. Being modulated through the gut-brain axis, these cells may prove essential in elucidating novel therapeutic strategies to either mitigate severity of disease or to simulate repair.

As elevated expression of myelin proteins was observed from oligodendrocytes in response to $CD4^+$ T-cell-derived factors, the characterisation of these supernatants, and the identification of the factors responsible for this effect may ultimately lead to novel therapeutics. The necessity for CCN3 is controversial, however its expression was substantially elevated from *H. pylori* infected mice and may relate to the increase

of oligodendrocyte differentiation using the *in vitro* models, which may indicate that shared pathways are present.

Immunometabolism has been described more frequently in the literature in recent years, and appreciation of the regulatory potential of both metabolic signalling and nutrient availability is starting to be recognised. We have discussed examples of this such as metabolites of tryptophan, or SCFA's from dietary fibre, produced by the microbiota can exert immunomodulatory effects [303,308,314]. In autoimmunity, T-cells are reported to have defective glucose metabolism [187]. De Rosa *et al*. identify the glycolytic enzyme enolase-1 as a modulator of FOXP3 splice variant expression, able to directly influence FOXP3 regulation and Treg/Th17 responses [188]. As *H. pylori* infection can alter nutrient availability, affect gastric secretions and hormones it is of course a possibility not explored here that *H. pylori*'s protective effects may be in-part influenced immuno-metabolically.

In the published literature, both obesity and plasma levels of Leptin were correlated to differential expression of CCN3 in peripheral blood T-cells, and this expression was further elevated in MS patients as compared to healthy controls, and differential in response to the MS treatments of IFNβ or natalizumab [544]. It is appreciated that leptin can affect glycolytic metabolism in $CD4^+$ T-cells which subsequently modifies inflammatory function. There may be important mechanisms to explore regarding immunometabolism and autoimmune diseases in the future.

In future mouse work, I would include additional groups infected with *H. pylori* expressing the more virulent *vacA* type 1 forms. I would also like to quantify the response occurring in additional tissue such as the gastric mucosa and lymph nodes concurrently with the spleen and CNS. This would necessitate the optimisation of the *H. pylori*/EAE mouse model, or the downstream methods used for analysis, as the extraction of sufficient cells from the stomach and CNS was challenging. Observing the effect of *H. pylori* in alternate MS mouse models such as TMEV may represent a rich source of novel data.

6.5 – Impact Statement

Some of the experimental work presented in this thesis was irrevocably disrupted by national and global events. The lymphocyte trafficking work (chapter 4) had been planned to utilise SPECT-CT imaging to track radiolabelled cells *in vivo*. Immediately prior to beginning the preparatory work for this chapter, the United Kingdom's exit from the European Union led to supply chain shortages of the radioisotope Indium^{111}. The unavailability of this critical reagent led to the necessity to change the experimental design to utilise fluorescent membrane dyes to label the cells of interest. Having not been used previously, the work in this chapter was a pilot experiment to optimise and assess the suitability of the reagent for studies of this nature. The unexpected change of reagent meant that the existing project licence in-place did not permit multiple timepoint imaging, and a single timepoint of 24 hours was chosen.

As this study was concluding in March 2020, the SARS-CoV-2 pandemic caused the closure of this institution meaning the planned microscopy of labelled cells *in situ* from tissue sections could not be performed. With hindsight, due to the inefficiency of the membrane dye and the confounding autofluorescence observed from the dietary matter, this analysis would have proved essential.

The remyelination study work presented in chapter 5 was originally designed to be performed as a placement in the collaborating laboratory of Prof. Denise Fitzgerald at Queens University Belfast. The mixed glia model was intended to be accompanied by related experiments using murine brain slice models to assess remyelination after chemically induced demyelination, maintaining both the cellular composition and 3D architecture of the brain. As a result of the SARS-CoV-2 pandemic, all travel of this nature was prevented and the full set of *in vitro* experiments that had been planned were not possible to conduct. It is with enormous gratitude to both Prof. Fitzgerald and Dr. Marie Dittmer that the $CD4^+$ cell supernatants produced in my mouse model were able to be tested on a smaller scale using the mixed glia model of oligodendrocyte differentiation, resulting in novel and interesting data to explore further in future.

6.6 – Final summary and concluding remarks

In summary, the intricate and overlapping mechanisms which mediate the immunology of both *H. pylori* infection and autoimmunity create a complicated picture (*Figure 90*).

Both in the human cohorts and mouse models, some novel findings have been unveiled which may form the basis for exciting future research. The $CD4^+$ T-cell subsets were hypothesised to mediate the proposed protection from MS, primarily through regulatory T-cells. Experimentally there may be some evidence of this and evaluating this further is crucial. I have shown that the Th17 and Treg T-helper responses were altered between infected and uninfected human individuals. In mice, the trafficking of these subsets can be influenced by concurrent *H. pylori* infection; and these cells may produce factors which can stimulate the differentiation of oligodendrocytes and induce myelin production. Furthermore, particular *H. pylori* strains might differ in their capacity to reduce the severity of EAE.

The hypotheses I present here, if proven, could have great impact. If a protection from *H. pylori* can be shown conclusively, it may be possible to administer non-pathogenic *H. pylori* strains therapeutically to protect people from developing severe MS or other immunological diseases. Indeed, we already see examples of experimental infections with parasitic worms or particular gut bacteria undergoing investigation in this manner. Alternatively, we may be able to identify important factors induced by the bacterium and identify underlying mechanisms, which could both have therapeutic potential.

The correlative data is convincing but needs to be supported by solid mechanism to prove a cause and effect. 4 decades since *Helicobacter pylori* was first discovered, much is still to come.

Chapter 7

Bibliography

1 Salama, N. R., Hartung, M. L. & Muller, A. Life in the human stomach: persistence strategies of the bacterial pathogen *Helicobacter pylori*. *Nat Rev Microbiol* **11**, 385-399, doi:10.1038/nrmicro3016 (2013).

2 Miller, A. K. & Williams, S. M. *Helicobacter pylori* infection causes both protective and deleterious effects in human health and disease. *Genes Immun* **22**, 218-226, doi:10.1038/s41435-021-00146-4 (2021).

3 Kidd M, M. I. A Century of *Helicobacter Pylori*: Paradigms Lost - Paradigms Regained. *Digestion* **59**, 1-15 (1997).

4 Marshall, B. J., Armstrong, J. A., McGechie, D. B. & Glancy, R. J. Attempt to fulfil Koch's postulates for *pyloric* Campylobacter. *Med J Aust* **142**, 436-439, doi:10.5694/j.1326-5377.1985.tb113443.x (1985).

5 Robinwarren, J. Unidentified Curved Bacilli on Gastric Epithelium in Active Chronic Gastritis. *The Lancet* **321**, 1273-1275, doi:10.1016/s0140-6736(83)92719-8 (1983).

6 Marshall, B. J. & Warren, J. R. Unidentified curved bacilli in the stomach of patients with gastritis and peptic ulceration. *Lancet* **1**, 1311-1315, doi:10.1016/s0140-6736(84)91816-6 (1984).

7 Goodwin CS, A. A., et al Transfer of Campylobacter *pylori* and Campylobacter mustelae to *Helicobacter* gen. nov. as *Helicobacter pylori* comb. nov. and *Helicobacter* mustelae comb. nov. Respectively *Int. Jour. of Systematic Bacteriology* **39**, 397-405 (1989).

8 Marshall, B. J. *Barry J. Marshall - Biographical*, <http://www.nobelprize.org/nobel_prizes/medicine/laureates/2005/marshall-bio.html> (2005).

9 IARC. Schistosomes, Liver Flukes and *Helicobacter Pylori IARC Monographs on the Carcinogenic Risks to Humans* **61** (1994).

10 Buck, G. E. Campylobacter *pylori* and gastroduodenal disease. *Clin Microbiol Rev* **3**, 1-12, doi:10.1128/CMR.3.1.1 (1990).

11 Kusters, J. G., van Vliet, A. H. & Kuipers, E. J. Pathogenesis of *Helicobacter pylori* infection. *Clin Microbiol Rev* **19**, 449-490, doi:10.1128/CMR.00054-05 (2006).

12 Dubois, A. *et al.* Transient and persistent experimental infection of nonhuman primates with *Helicobacter pylori*: implications for human disease. *Infect Immun* **64**, 2885-2891, doi:10.1128/iai.64.8.2885-2891.1996 (1996).

13 Brown, L. M. *Helicobacter pylori*: epidemiology and routes of transmission. *Epidemiol Rev* **22**, 283-297, doi:10.1093/oxfordjournals.epirev.a018040 (2000).

14 Leung, W. K. *et al.* Isolation of *Helicobacter pylori* from vomitus in children and its implication in gastro-oral transmission. *Am J Gastroenterol* **94**, 2881-2884, doi:10.1111/j.1572-0241.1999.01431.x (1999).

15 Lin, S. K., Lambert, J. R., Schembri, M. A., Nicholson, L. & Korman, M. G. *Helicobacter pylori* prevalence in endoscopy and medical staff. *J Gastroenterol Hepatol* **9**, 319-324, doi:10.1111/j.1440-1746.1994.tb01249.x (1994).

16 Hooi, J. K. Y. *et al.* Global Prevalence of *Helicobacter pylori* Infection: Systematic Review and Meta-Analysis. *Gastroenterology* **153**, 420-429, doi:10.1053/j.gastro.2017.04.022 (2017).

17 Robinson, K. *Helicobacter pylori*-Mediated Protection against Extra-Gastric Immune and Inflammatory Disorders: The Evidence and Controversies. *Diseases* **3**, 34-55, doi:10.3390/diseases3020034 (2015).
18 Dunn B, C. H., Blaser M *Helicobacter Pylori*. *Clin. Microbiology Reviews* **10**, 720-741 (1997).
19 Bach, J. F. The hygiene hypothesis in autoimmunity: the role of pathogens and commensals. *Nat Rev Immunol* **18**, 105-120, doi:10.1038/nri.2017.111 (2018).
20 Arnold, I. C. *et al. Helicobacter pylori* infection prevents allergic asthma in mouse models through the induction of regulatory T cells. *J Clin Invest* **121**, 3088-3093, doi:10.1172/JCI45041 (2011).
21 Oertli, M. *et al.* DC-derived IL-18 drives Treg differentiation, murine *Helicobacter pylori*-specific immune tolerance, and asthma protection. *J Clin Invest* **122**, 1082-1096, doi:10.1172/JCI61029 (2012).
22 Arnold, I. C., Hitzler, I. & Muller, A. The immunomodulatory properties of *Helicobacter pylori* confer protection against allergic and chronic inflammatory disorders. *Front Cell Infect Microbiol* **2**, 10, doi:10.3389/fcimb.2012.00010 (2012).
23 Koch, K. N. & Muller, A. *Helicobacter pylori* activates the TLR2/NLRP3/caspase-1/IL-18 axis to induce regulatory T-cells, establish persistent infection and promote tolerance to allergens. *Gut Microbes* **6**, 382-387, doi:10.1080/19490976.2015.1105427 (2015).
24 Oertli, M. & Muller, A. *Helicobacter pylori* targets dendritic cells to induce immune tolerance, promote persistence and confer protection against allergic asthma. *Gut Microbes* **3**, 566-571, doi:10.4161/gmic.21750 (2012).
25 Montecucco C, R. R. Living Dangerously: How *Helicobacter Pylori* Survives in the Human Stomach. *Nature Reviews Molecular Cell Biology* **2**, 457-466 (2001).
26 Eppinger, M. *et al.* Who ate whom? Adaptive *Helicobacter* genomic changes that accompanied a host jump from early humans to large felines. *PLoS Genet* **2**, e120, doi:10.1371/journal.pgen.0020120 (2006).
27 Odenbreit, S. *et al.* Outer membrane protein expression profile in *Helicobacter pylori* clinical isolates. *Infect Immun* **77**, 3782-3790, doi:10.1128/IAI.00364-09 (2009).
28 Miftahussurur, M. *et al.* Extremely low *Helicobacter pylori* prevalence in North Sulawesi, Indonesia and identification of a Maori-tribe type strain: a cross sectional study. *Gut Pathog* **6**, 42, doi:10.1186/s13099-014-0042-0 (2014).
29 de Sablet, T. *et al.* Phylogeographic origin of *Helicobacter pylori* is a determinant of gastric cancer risk. *Gut* **60**, 1189-1195, doi:10.1136/gut.2010.234468 (2011).
30 Alm, R. A. *et al.* Comparative genomics of *Helicobacter pylori*: analysis of the outer membrane protein families. *Infect Immun* **68**, 4155-4168, doi:10.1128/IAI.68.7.4155-4168.2000 (2000).
31 Matsuo, Y., Kido, Y. & Yamaoka, Y. *Helicobacter pylori* Outer Membrane Protein-Related Pathogenesis. *Toxins (Basel)* **9**, 1-9, doi:10.3390/toxins9030101 (2017).
32 Goers Sweeney, E. *et al.* Structure and proposed mechanism for the pH-sensing *Helicobacter pylori* chemoreceptor TlpB. *Structure* **20**, 1177-1188, doi:10.1016/j.str.2012.04.021 (2012).
33 Dunn, B. E. *et al.* Localization of *Helicobacter pylori* urease and heat shock protein in human gastric biopsies. *Infect Immun* **65**, 1181-1188, doi:10.1128/iai.65.4.1181-1188.1997 (1997).
34 Phadnis S, P. M., Levy M, Dunn B Surface Localisation of *Helicobacter Pylori* Urease and Heat Shock Protein homologue Requires Bacterial Autolysis. *Infection and Immunity* **64**, 905-912 (1996).

35 Yoshiyama, H. & Nakazawa, T. Unique mechanism of *Helicobacter pylori* for colonizing the gastric mucus. *Microbes Infect* **2**, 55-60, doi:10.1016/s1286-4579(00)00285-9 (2000).
36 Shiotani, A. & Graham, D. Y. Pathogenesis and therapy of gastric and duodenal ulcer disease. *Med Clin North Am* **86**, 1447-1466, viii, doi:10.1016/s0025-7125(02)00083-4 (2002).
37 Sutton, P. & Chionh, Y. T. Why can't we make an effective vaccine against *Helicobacter pylori*? *Expert Rev Vaccines* **12**, 433-441, doi:10.1586/erv.13.20 (2013).
38 Bakshani, C. R. *et al.* Evolutionary conservation of the antimicrobial function of mucus: a first defence against infection. *NPJ Biofilms Microbiomes* **4**, 14, doi:10.1038/s41522-018-0057-2 (2018).
39 McGuckin, M. A., Linden, S. K., Sutton, P. & Florin, T. H. Mucin dynamics and enteric pathogens. *Nat Rev Microbiol* **9**, 265-278, doi:10.1038/nrmicro2538 (2011).
40 Dupont, A., Heinbockel, L., Brandenburg, K. & Hornef, M. W. Antimicrobial peptides and the enteric mucus layer act in concert to protect the intestinal mucosa. *Gut Microbes* **5**, 761-765, doi:10.4161/19490976.2014.972238 (2014).
41 Risso, A. Leukocyte antimicrobial peptides: multifunctional effector molecules of innate immunity. *Journal of Leukocyte Biology* **68**, 785-792, doi:https://doi.org/10.1189/jlb.68.6.785 (2000).
42 Mestas, J. & Hughes, C. C. W. Of Mice and Not Men: Differences between Mouse and Human Immunology. *The Journal of Immunology* **172**, 2731-2738, doi:10.4049/jimmunol.172.5.2731 (2004).
43 Pero, R. *et al.* Beta-defensins and analogs in *Helicobacter pylori* infections: mRNA expression levels, DNA methylation, and antibacterial activity. *PLoS One* **14**, e0222295, doi:10.1371/journal.pone.0222295 (2019).
44 Rokita E, M. A., Presterl E, Rotter ML, Hirschl AM. *Helicobacter pylori* Urease Significantly Reduces Opsonization by Human Complement. *Journal of Infectious Diseases* **178**, 1521-1525 (1998).
45 White, J. R., Winter, J. A. & Robinson, K. Differential inflammatory response to *Helicobacter pylori* infection: etiology and clinical outcomes. *J Inflamm Res* **8**, 137-147, doi:10.2147/JIR.S64888 (2015).
46 Linden, S. K. *et al.* MUC1 limits *Helicobacter pylori* infection both by steric hindrance and by acting as a releasable decoy. *PLoS Pathog* **5**, e1000617, doi:10.1371/journal.ppat.1000617 (2009).
47 Van den Brink, G. R. *et al.* H *pylori* colocalises with MUC5AC in the human stomach. *Gut* **46**, 601-607, doi:10.1136/gut.46.5.601 (2000).
48 Niv, Y. *Helicobacter pylori* and gastric mucin expression: A systematic review and meta-analysis. *World J Gastroenterol* **21**, 9430-9436, doi:10.3748/wjg.v21.i31.9430 (2015).
49 Byrd, J. C. *et al.* Aberrant expression of gland-type gastric mucin in the surface epithelium of *Helicobacter pylori*-infected patients. *Gastroenterology* **113**, 455-464, doi:10.1053/gast.1997.v113.pm9247464 (1997).
50 Byrd, J. C. & Bresalier, R. S. Alterations in gastric mucin synthesis by *Helicobacter pylori*. *World J Gastroenterol* **6**, 475-482, doi:10.3748/wjg.v6.i4.475 (2000).
51 Navabi, N., Johansson, M. E., Raghavan, S. & Linden, S. K. *Helicobacter pylori* infection impairs the mucin production rate and turnover in the murine gastric mucosa. *Infect Immun* **81**, 829-837, doi:10.1128/IAI.01000-12 (2013).
52 Babu, S. D., Jayanthi, V., Devaraj, N., Reis, C. A. & Devaraj, H. Expression profile of mucins (MUC2, MUC5AC and MUC6) in *Helicobacter pylori* infected pre-neoplastic

and neoplastic human gastric epithelium. *Mol Cancer* **5**, 10, doi:10.1186/1476-4598-5-10 (2006).

53 Ota, H. *et al. Helicobacter pylori* infection produces reversible glycosylation changes to gastric mucins. *Virchows Arch* **433**, 419-426, doi:10.1007/s004280050269 (1998).

54 Wen, R., Gao, F., Zhou, C. J. & Jia, Y. B. Polymorphisms in mucin genes in the development of gastric cancer. *World J Gastrointest Oncol* **7**, 328-337, doi:10.4251/wjgo.v7.i11.328 (2015).

55 Kobayashi, M., Lee, H., Nakayama, J. & Fukuda, M. Carbohydrate-dependent defense mechanisms against *Helicobacter pylori* infection. *Curr Drug Metab* **10**, 29-40, doi:10.2174/138920009787048428 (2009).

56 Kobayashi, M., Lee, H., Nakayama, J. & Fukuda, M. Roles of gastric mucin-type O-glycans in the pathogenesis of *Helicobacter pylori* infection. *Glycobiology* **19**, 453-461, doi:10.1093/glycob/cwp004 (2009).

57 Atherton, J. C. The pathogenesis of *Helicobacter pylori*-induced gastro-duodenal diseases. *Annu Rev Pathol* **1**, 63-96, doi:10.1146/annurev.pathol.1.110304.100125 (2006).

58 Amieva, M. & Peek, R. M., Jr. Pathobiology of *Helicobacter pylori*-Induced Gastric Cancer. *Gastroenterology* **150**, 64-78, doi:10.1053/j.gastro.2015.09.004 (2016).

59 Ford, A. C., Yuan, Y. & Moayyedi, P. *Helicobacter pylori* eradication therapy to prevent gastric cancer: systematic review and meta-analysis. *Gut* **69**, 2113-2121, doi:10.1136/gutjnl-2020-320839 (2020).

60 Ford, A. C., Gurusamy, K. S., Delaney, B., Forman, D. & Moayyedi, P. Eradication therapy for peptic ulcer disease in *Helicobacter pylori*-positive people. *Cochrane Database Syst Rev* **4**, CD003840, doi:10.1002/14651858.CD003840.pub5 (2016).

61 Tucci, A. *et al.* Reversal of fundic atrophy after eradication of *Helicobacter pylori*. *Am J Gastroenterol* **93**, 1425-1431, doi:10.1111/j.1572-0241.1998.00454.x (1998).

62 Liou, J. M. *et al.* Screening and eradication of *Helicobacter pylori* for gastric cancer prevention: the Taipei global consensus. *Gut* **69**, 2093-2112, doi:10.1136/gutjnl-2020-322368 (2020).

63 Huang, J. Q., Sridhar, S. & Hunt, R. H. Role of *Helicobacter pylori* infection and non-steroidal anti-inflammatory drugs in peptic-ulcer disease: a meta-analysis. *Lancet* **359**, 14-22, doi:10.1016/S0140-6736(02)07273-2 (2002).

64 Polk, D. B. & Peek, R. M., Jr. *Helicobacter pylori*: gastric cancer and beyond. *Nat Rev Cancer* **10**, 403-414, doi:10.1038/nrc2857 (2010).

65 Graham, D. Y. *Helicobacter pylori* update: gastric cancer, reliable therapy, and possible benefits. *Gastroenterology* **148**, 719-731 e713, doi:10.1053/j.gastro.2015.01.040 (2015).

66 Toh, B. H. Diagnosis and classification of autoimmune gastritis. *Autoimmun Rev* **13**, 459-462, doi:10.1016/j.autrev.2014.01.048 (2014).

67 D'Elios, M. M., Appelmelk, B. J., Amedei, A., Bergman, M. P. & Del Prete, G. Gastric autoimmunity: the role of *Helicobacter pylori* and molecular mimicry. *Trends Mol Med* **10**, 316-323, doi:10.1016/j.molmed.2004.06.001 (2004).

68 D'Elios, M. M., Bergman, M. P., Amedei, A., Appelmelk, B. J. & Del Prete, G. *Helicobacter pylori* and gastric autoimmunity. *Microbes Infect* **6**, 1395-1401, doi:10.1016/j.micinf.2004.10.001 (2004).

69 Taye, B. *et al.* Effect of early and current *Helicobacter pylori* infection on the risk of anaemia in 6.5-year-old Ethiopian children. *BMC Infect Dis* **15**, 270, doi:10.1186/s12879-015-1012-y (2015).

70 DuBois, S. & Kearney, D. J. Iron-deficiency anemia and *Helicobacter pylori* infection: a review of the evidence. *Am J Gastroenterol* **100**, 453-459, doi:10.1111/j.1572-0241.2005.30252.x (2005).

71 Hershko, C. & Skikne, B. Pathogenesis and management of iron deficiency anemia: emerging role of celiac disease, *Helicobacter pylori*, and autoimmune gastritis. *Semin Hematol* **46**, 339-350, doi:10.1053/j.seminhematol.2009.06.002 (2009).

72 Choe, Y. H., Kim, S. K. & Hong, Y. C. *Helicobacter pylori* infection with iron deficiency anaemia and subnormal growth at puberty. *Arch Dis Child* **82**, 136-140, doi:10.1136/adc.82.2.136 (2000).

73 Taye, B. *et al.* Effect of *Helicobacter pylori* infection on growth trajectories in young Ethiopian children: a longitudinal study. *Int J Infect Dis* **50**, 57-66, doi:10.1016/j.ijid.2016.08.005 (2016).

74 Briani, C. *et al.* Cobalamin deficiency: clinical picture and radiological findings. *Nutrients* **5**, 4521-4539, doi:10.3390/nu5114521 (2013).

75 Miller, A., Korem, M., Almog, R. & Galboiz, Y. Vitamin B12, demyelination, remyelination and repair in multiple sclerosis. *J Neurol Sci* **233**, 93-97, doi:10.1016/j.jns.2005.03.009 (2005).

76 Figura, N. *et al.* Extragastric manifestations of *Helicobacter pylori* infection. *Helicobacter* **15 Suppl 1**, 60-68, doi:10.1111/j.1523-5378.2010.00778.x (2010).

77 Cho, I. & Blaser, M. J. The human microbiome: at the interface of health and disease. *Nat Rev Genet* **13**, 260-270, doi:10.1038/nrg3182 (2012).

78 Roubaud Baudron, C., Franceschi, F., Salles, N. & Gasbarrini, A. Extragastric diseases and *Helicobacter pylori*. *Helicobacter* **18 Suppl 1**, 44-51, doi:10.1111/hel.12077 (2013).

79 Suzuki, H., Marshall, B. J. & Hibi, T. Overview: *Helicobacter pylori* and extragastric disease. *Int J Hematol* **84**, 291-300, doi:10.1532/IJH97.06180 (2006).

80 Rokkas, T., Gisbert, J. P., Niv, Y. & O'Morain, C. The association between *Helicobacter pylori* infection and inflammatory bowel disease based on meta-analysis. *United European Gastroenterol J* **3**, 539-550, doi:10.1177/2050640615580889 (2015).

81 Vare, P. O. *et al.* Seroprevalence of *Helicobacter pylori* infection in inflammatory bowel disease: is *Helicobacter pylori* infection a protective factor? *Scand J Gastroenterol* **36**, 1295-1300, doi:10.1080/003655201317097155 (2001).

82 Castano-Rodriguez, N., Kaakoush, N. O., Lee, W. S. & Mitchell, H. M. Dual role of *Helicobacter* and Campylobacter species in IBD: a systematic review and meta-analysis. *Gut* **66**, 235-249, doi:10.1136/gutjnl-2015-310545 (2017).

83 Yu, Y., Zhu, S., Li, P., Min, L. & Zhang, S. *Helicobacter pylori* infection and inflammatory bowel disease: a crosstalk between upper and lower digestive tract. *Cell Death Dis* **9**, 961, doi:10.1038/s41419-018-0982-2 (2018).

84 Ramos, G. P. & Papadakis, K. A. Mechanisms of Disease: Inflammatory Bowel Diseases. *Mayo Clin Proc* **94**, 155-165, doi:10.1016/j.mayocp.2018.09.013 (2019).

85 Strachan, D. P. Hay fever, hygiene, and household size. *BMJ* **299**, 1259-1260, doi:10.1136/bmj.299.6710.1259 (1989).

86 Park, J. H., Peyrin-Biroulet, L., Eisenhut, M. & Shin, J. I. IBD immunopathogenesis: A comprehensive review of inflammatory molecules. *Autoimmun Rev* **16**, 416-426, doi:10.1016/j.autrev.2017.02.013 (2017).

87 Abraham C, C. J. Inflammatory Bowel Disease. *N Engl J Med* **361**, 2066-2078 (2009).

88 Khor, B., Gardet, A. & Xavier, R. J. Genetics and pathogenesis of inflammatory bowel disease. *Nature* **474**, 307-317, doi:10.1038/nature10209 (2011).

89 Tursi, A. Onset of Crohn's disease after *Helicobacter pylori* eradication. *Inflamm Bowel Dis* **12**, 1008-1009, doi:10.1097/01.mib.0000235100.09231.d7 (2006).

90 Umetsu, D. T., McIntire, J. J., Akbari, O., Macaubas, C. & DeKruyff, R. H. Asthma: an epidemic of dysregulated immunity. *Nat Immunol* **3**, 715-720, doi:10.1038/ni0802-715 (2002).

91 Blaser MJ, C. Y., Reibman J. Does *Helicobacter pylori* protect against asthma and allergy? *Gut* **57**, 561-567 (2008).

92 Chen, Y. & Blaser, M. J. Inverse associations of *Helicobacter pylori* with asthma and allergy. *Arch Intern Med* **167**, 821-827, doi:10.1001/archinte.167.8.821 (2007).

93 Chen, Y. & Blaser, M. J. *Helicobacter pylori* colonization is inversely associated with childhood asthma. *J Infect Dis* **198**, 553-560, doi:10.1086/590158 (2008).

94 Reibman, J. *et al.* Asthma is inversely associated with *Helicobacter pylori* status in an urban population. *PLoS One* **3**, e4060, doi:10.1371/journal.pone.0004060 (2008).

95 Charabati, M., Donkers, S. J., Kirkland, M. C. & Osborne, L. C. A critical analysis of helminth immunotherapy in multiple sclerosis. *Mult Scler* **26**, 1448-1458, doi:10.1177/1352458519899040 (2020).

96 Tanasescu, R. *et al.* Hookworm Treatment for Relapsing Multiple Sclerosis: A Randomized Double-Blinded Placebo-Controlled Trial. *JAMA Neurol* **77**, 1089-1098, doi:10.1001/jamaneurol.2020.1118 (2020).

97 White, M. P. J. *et al.* The Helminth Parasite Heligmosomoides polygyrus Attenuates EAE in an IL-4Ralpha-Dependent Manner. *Front Immunol* **11**, 1830, doi:10.3389/fimmu.2020.01830 (2020).

98 Zheng, X. *et al.* Soluble egg antigen from Schistosoma japonicum modulates the progression of chronic progressive experimental autoimmune encephalomyelitis via Th2-shift response. *J Neuroimmunol* **194**, 107-114, doi:10.1016/j.jneuroim.2007.12.001 (2008).

99 Shu, H. *et al.* Interferon characterization associates with asthma and is a potential biomarker of predictive diagnosis. *Biosci Rep* **41**, doi:10.1042/BSR20204210 (2021).

100 Salazar, F., Awuah, D., Negm, O. H., Shakib, F. & Ghaemmaghami, A. M. The role of indoleamine 2,3-dioxygenase-aryl hydrocarbon receptor pathway in the TLR4-induced tolerogenic phenotype in human DCs. *Sci Rep* **7**, 43337, doi:10.1038/srep43337 (2017).

101 Chan FKL, L. W. Peptic-ulcer disease. *Lancet* **360**, 933-941 (2002).

102 El-Omar, E. M. Mechanisms of increased acid secretion after eradication of *Helicobacter pylori* infection. *Gut* **55**, 144-146, doi:10.1136/gut.2005.071779 (2006).

103 Tseng FC, B. E., Maiese E, Hisada M, et al Polymorphisms in Cytokine Genes and Risk of *Helicobacter pylori* Infection among Jamaican Children. *Helicobacter* **11**, 425-430 (2006).

104 Santos JC, L. M., Pedrazzoli J, Ribeiro ML Relationship of IL-1 and TNFα polymorphisms with *Helicobacter pylori* in gastric diseases in a Brazilian population. *Braz J Med Biol Res* **45**, 811-817 (2012).

105 Semper, R. P. *et al. Helicobacter pylori*-induced IL-1beta secretion in innate immune cells is regulated by the NLRP3 inflammasome and requires the cag pathogenicity island. *J Immunol* **193**, 3566-3576, doi:10.4049/jimmunol.1400362 (2014).

106 Robinson, K., Argent, R. H. & Atherton, J. C. The inflammatory and immune response to *Helicobacter pylori* infection. *Best Pract Res Clin Gastroenterol* **21**, 237-259, doi:10.1016/j.bpg.2007.01.001 (2007).

107 El-Omar, E. M. The importance of interleukin 1beta in *Helicobacter pylori* associated disease. *Gut* **48**, 743-747, doi:10.1136/gut.48.6.743 (2001).

108 Roesler, B. M., Rabelo-Goncalves, E. M. & Zeitune, J. M. Virulence Factors of *Helicobacter pylori*: A Review. *Clin Med Insights Gastroenterol* **7**, 9-17, doi:10.4137/CGast.S13760 (2014).

109 Backert, S., Tegtmeyer, N. & Fischer, W. Composition, structure and function of the *Helicobacter pylori* cag pathogenicity island encoded type IV secretion system. *Future Microbiol* **10**, 955-965, doi:10.2217/fmb.15.32 ( ).

110 Bonsor, D. A. *et al.* Integrin engagement by the helical RGD motif of the *Helicobacter pylori* CagL protein is regulated by pH-induced displacement of a neighboring helix. *J Biol Chem* **290**, 12929-12940, doi:10.1074/jbc.M115.641829 (2015).

111 Cover, T. L. Role of *Helicobacter pylori* CagL in modulating gastrin expression. *Gut* **61**, 965-966, doi:10.1136/gutjnl-2012-302142 (2012).

112 Kwok, T. *et al. Helicobacter* exploits integrin for type IV secretion and kinase activation. *Nature* **449**, 862-866, doi:10.1038/nature06187 (2007).

113 Naumann, M., Sokolova, O., Tegtmeyer, N. & Backert, S. *Helicobacter pylori*: A Paradigm Pathogen for Subverting Host Cell Signal Transmission. *Trends Microbiol* **25**, 316-328, doi:10.1016/j.tim.2016.12.004 (2017).

114 Algood, H. M. & Cover, T. L. *Helicobacter pylori* persistence: an overview of interactions between *H. pylori* and host immune defenses. *Clin Microbiol Rev* **19**, 597-613, doi:10.1128/CMR.00006-06 (2006).

115 Peek, R. M., Jr., Fiske, C. & Wilson, K. T. Role of innate immunity in *Helicobacter pylori*-induced gastric malignancy. *Physiol Rev* **90**, 831-858, doi:10.1152/physrev.00039.2009 (2010).

116 Shiota, S., Suzuki, R. & Yamaoka, Y. The significance of virulence factors in *Helicobacter pylori*. *J Dig Dis* **14**, 341-349, doi:10.1111/1751-2980.12054 (2013).

117 Basso, D. *et al.* Clinical relevance of *Helicobacter pylori* cagA and vacA gene polymorphisms. *Gastroenterology* **135**, 91-99, doi:10.1053/j.gastro.2008.03.041 (2008).

118 Hatakeyama, M. Oncogenic mechanisms of the *Helicobacter pylori* CagA protein. *Nat Rev Cancer* **4**, 688-694, doi:10.1038/nrc1433 (2004).

119 Batista, S. A. *et al.* Higher number of *Helicobacter pylori* CagA EPIYA C phosphorylation sites increases the risk of gastric cancer, but not duodenal ulcer. *BMC Microbiol* **11**, 61, doi:10.1186/1471-2180-11-61 (2011).

120 Beltran-Anaya, F. O. *et al.* The EPIYA-ABCC motif pattern in CagA of *Helicobacter pylori* is associated with peptic ulcer and gastric cancer in Mexican population. *BMC Gastroenterol* **14**, 223, doi:10.1186/s12876-014-0223-9 (2014).

121 Jones, K. R. *et al.* Polymorphisms in the intermediate region of VacA impact *Helicobacter pylori*-induced disease development. *J Clin Microbiol* **49**, 101-110, doi:10.1128/JCM.01782-10 (2011).

122 Jones, K. R., Whitmire, J. M. & Merrell, D. S. A Tale of Two Toxins: *Helicobacter Pylori* CagA and VacA Modulate Host Pathways that Impact Disease. *Front Microbiol* **1**, 115, doi:10.3389/fmicb.2010.00115 (2010).

123 Papini, E., Zoratti, M. & Cover, T. L. In search of the *Helicobacter pylori* VacA mechanism of action. *Toxicon* **39**, 1757-1767, doi:10.1016/s0041-0101(01)00162-3 (2001).

124 Kim, I. J. & Blanke, S. R. Remodeling the host environment: modulation of the gastric epithelium by the *Helicobacter pylori* vacuolating toxin (VacA). *Front Cell Infect Microbiol* **2**, 37, doi:10.3389/fcimb.2012.00037 (2012).

125 Papini E, Z. M., Cover TL. In search of the *Helicobacter pylori* VacA mechanism of action . *Toxicon* **39**, 1757-1767 (2001).

126 Blaser, M. J. & Atherton, J. C. *Helicobacter pylori* persistence: biology and disease. *J Clin Invest* **113**, 321-333, doi:10.1172/JCI20925 (2004).
127 Rhead, J. L. *et al.* A new *Helicobacter pylori* vacuolating cytotoxin determinant, the intermediate region, is associated with gastric cancer. *Gastroenterology* **133**, 926-936, doi:10.1053/j.gastro.2007.06.056 (2007).
128 Sinnett, C. G. *et al. Helicobacter pylori* vacA transcription is genetically-determined and stratifies the level of human gastric inflammation and atrophy. *J Clin Pathol* **69**, 968-973, doi:10.1136/jclinpath-2016-203641 (2016).
129 Sundrud, M. S., Torres, V. J., Unutmaz, D. & Cover, T. L. Inhibition of primary human T cell proliferation by *Helicobacter pylori* vacuolating toxin (VacA) is independent of VacA effects on IL-2 secretion. *Proc Natl Acad Sci U S A* **101**, 7727-7732, doi:10.1073/pnas.0401528101 (2004).
130 Oldani, A. *et al. Helicobacter pylori* counteracts the apoptotic action of its VacA toxin by injecting the CagA protein into gastric epithelial cells. *PLoS Pathog* **5**, e1000603, doi:10.1371/journal.ppat.1000603 (2009).
131 Imagawa, S. *et al. Helicobacter pylori* dupA and gastric acid secretion are negatively associated with gastric cancer development. *J Med Microbiol* **59**, 1484-1489, doi:10.1099/jmm.0.021816-0 (2010).
132 Talebi Bezmin Abadi, A. The *Helicobacter pylori* dupA: A Novel Biomarker for Digestive Diseases. *Front Med (Lausanne)* **1**, 13, doi:10.3389/fmed.2014.00013 (2014).
133 Dossumbekova, A. *et al. Helicobacter pylori* HopH (OipA) and bacterial pathogenicity: genetic and functional genomic analysis of hopH gene polymorphisms. *J Infect Dis* **194**, 1346-1355, doi:10.1086/508426 (2006).
134 Liu, J. *et al.* Association of presence/absence and on/off patterns of *Helicobacter pylori* oipA gene with peptic ulcer disease and gastric cancer risks: a meta-analysis. *BMC Infect Dis* **13**, 555, doi:10.1186/1471-2334-13-555 (2013).
135 Teymournejad, O., Mobarez, A. M., Hassan, Z. M., Moazzeni, S. M. & Ahmadabad, H. N. *In vitro* suppression of dendritic cells by *Helicobacter pylori* OipA. *Helicobacter* **19**, 136-143, doi:10.1111/hel.12107 (2014).
136 Muniz, L. R., Knosp, C. & Yeretssian, G. Intestinal antimicrobial peptides during homeostasis, infection, and disease. *Front Immunol* **3**, 310, doi:10.3389/fimmu.2012.00310 (2012).
137 Lavelle, E. C., Murphy, C., O'Neill, L. A. & Creagh, E. M. The role of TLRs, NLRs, and RLRs in mucosal innate immunity and homeostasis. *Mucosal Immunol* **3**, 17-28, doi:10.1038/mi.2009.124 (2010).
138 Fukata, M., Vamadevan, A. S. & Abreu, M. T. Toll-like receptors (TLRs) and Nod-like receptors (NLRs) in inflammatory disorders. *Semin Immunol* **21**, 242-253, doi:10.1016/j.smim.2009.06.005 (2009).
139 Ng, G. Z. *et al.* The MUC1 mucin protects against *Helicobacter pylori* pathogenesis in mice by regulation of the NLRP3 inflammasome. *Gut* **65**, 1087-1099, doi:10.1136/gutjnl-2014-307175 (2016).
140 Muller, A., Oertli, M. & Arnold, I. C. *H. pylori* exploits and manipulates innate and adaptive immune cell signaling pathways to establish persistent infection. *Cell Commun Signal* **9**, 25, doi:10.1186/1478-811X-9-25 (2011).
141 Cadamuro, A. C., Rossi, A. F., Maniezzo, N. M. & Silva, A. E. *Helicobacter pylori* infection: host immune response, implications on gene expression and microRNAs. *World J Gastroenterol* **20**, 1424-1437, doi:10.3748/wjg.v20.i6.1424 (2014).
142 Caruso, R., Warner, N., Inohara, N. & Nunez, G. NOD1 and NOD2: signaling, host defense, and inflammatory disease. *Immunity* **41**, 898-908, doi:10.1016/j.immuni.2014.12.010 (2014).

143 Strober, W., Murray, P. J., Kitani, A. & Watanabe, T. Signalling pathways and molecular interactions of NOD1 and NOD2. *Nat Rev Immunol* **6**, 9-20, doi:10.1038/nri1747 (2006).
144 Viala, J. *et al.* Nod1 responds to peptidoglycan delivered by the *Helicobacter pylori* cag pathogenicity island. *Nat Immunol* **5**, 1166-1174, doi:10.1038/ni1131 (2004).
145 D'Elios MM, A. A., Cappon A, Del Prete G, Bernard MD. The neutrophil activating protein of *Helicobacter pylori* (HP-NAP) as an immune modulating agent. *FEMS Immunol Med Microbiol* **50**, 157-164, doi:10.1111/j.1574-695X.2007.00258x (2007).
146 Ismail, H. F., Fick, P., Zhang, J., Lynch, R. G. & Berg, D. J. Depletion of neutrophils in IL-10(-/-) mice delays clearance of gastric *Helicobacter* infection and decreases the Th1 immune response to *Helicobacter*. *J Immunol* **170**, 3782-3789, doi:10.4049/jimmunol.170.7.3782 (2003).
147 Fu, H. W. *Helicobacter pylori* neutrophil-activating protein: from molecular pathogenesis to clinical applications. *World J Gastroenterol* **20**, 5294-5301, doi:10.3748/wjg.v20.i18.5294 (2014).
148 Ginhoux, F. & Jung, S. Monocytes and macrophages: developmental pathways and tissue homeostasis. *Nat Rev Immunol* **14**, 392-404, doi:10.1038/nri3671 (2014).
149 Theriault, P., ElAli, A. & Rivest, S. The dynamics of monocytes and microglia in Alzheimer's disease. *Alzheimers Res Ther* **7**, 41, doi:10.1186/s13195-015-0125-2 (2015).
150 Zhang, Y. *et al.* Early apoptosis of monocytes induced by *Helicobacter pylori* infection through multiple pathways. *Dev Comp Immunol* **73**, 46-51, doi:10.1016/j.dci.2017.03.010 (2017).
151 Baldari, C. T., Lanzavecchia, A. & Telford, J. L. Immune subversion by *Helicobacter pylori*. *Trends Immunol* **26**, 199-207, doi:10.1016/j.it.2005.01.007 (2005).
152 Lewis, N. D. *et al.* Immune evasion by *Helicobacter pylori* is mediated by induction of macrophage arginase II. *J Immunol* **186**, 3632-3641, doi:10.4049/jimmunol.1003431 (2011).
153 Gobert, A. P. & Wilson, K. T. The Immune Battle against *Helicobacter pylori* Infection: NO Offense. *Trends Microbiol* **24**, 366-376, doi:10.1016/j.tim.2016.02.005 (2016).
154 McGee, D. J. *et al.* Purification and characterization of *Helicobacter pylori* arginase, RocF: unique features among the arginase superfamily. *Eur J Biochem* **271**, 1952-1962, doi:10.1111/j.1432-1033.2004.04105.x (2004).
155 Hardbower, D. M. *et al.* Arginase 2 deletion leads to enhanced M1 macrophage activation and upregulated polyamine metabolism in response to *Helicobacter pylori* infection. *Amino Acids* **48**, 2375-2388, doi:10.1007/s00726-016-2231-2 (2016).
156 Rittig, M. G. *et al. Helicobacter pylori*-induced homotypic phagosome fusion in human monocytes is independent of the bacterial vacA and cag status. *Cell Microbiol* **5**, 887-899, doi:10.1046/j.1462-5822.2003.00328.x (2003).
157 Wunder, C. *et al.* Cholesterol glucosylation promotes immune evasion by *Helicobacter pylori*. *Nat Med* **12**, 1030-1038, doi:10.1038/nm1480 (2006).
158 Du, S. Y. *et al.* Cholesterol glucosylation by *Helicobacter pylori* delays internalization and arrests phagosome maturation in macrophages. *J Microbiol Immunol Infect* **49**, 636-645, doi:10.1016/j.jmii.2014.05.011 (2016).
159 Djekic, A. & Muller, A. The Immunomodulator VacA Promotes Immune Tolerance and Persistent *Helicobacter pylori* Infection through Its Activities on T-Cells and Antigen-Presenting Cells. *Toxins (Basel)* **8**, 1-9, doi:10.3390/toxins8060187 (2016).
160 Lina, T. T. *et al.* Immune evasion strategies used by *Helicobacter pylori*. *World J Gastroenterol* **20**, 12753-12766, doi:10.3748/wjg.v20.i36.12753 (2014).

161 Rescigno, M. Dendritic cell functions: Learning from microbial evasion strategies. *Semin Immunol* **27**, 119-124, doi:10.1016/j.smim.2015.03.012 (2015).

162 Strober, W. Vitamin A rewrites the ABCs of oral tolerance. *Mucosal Immunol* **1**, 92-95, doi:10.1038/mi.2007.22 (2008).

163 Shiu, J. & Blanchard, T. G. Dendritic cell function in the host response to *Helicobacter pylori* infection of the gastric mucosa. *Pathog Dis* **67**, 46-53, doi:10.1111/2049-632X.12014 (2013).

164 Staples, E. *IL-17 and Th17 Responses to Human Helicobacter pylori Infection and their Association with Disease* Doctor of Philosophy thesis, University of Nottingham, (2013).

165 Larussa, T., Leone, I., Suraci, E., Imeneo, M. & Luzza, F. *Helicobacter pylori* and T Helper Cells: Mechanisms of Immune Escape and Tolerance. *J Immunol Res* **2015**, 981328, doi:10.1155/2015/981328 (2015).

166 Robinson, K. *et al. Helicobacter pylori*-induced peptic ulcer disease is associated with inadequate regulatory T cell responses. *Gut* **57**, 1375-1385, doi:10.1136/gut.2007.137539 (2008).

167 Agard, M., Asakrah, S. & Morici, L. A. PGE(2) suppression of innate immunity during mucosal bacterial infection. *Front Cell Infect Microbiol* **3**, 45, doi:10.3389/fcimb.2013.00045 (2013).

168 Kalinski, P. Regulation of immune responses by prostaglandin E_2. *J Immunol* **188**, 21-28, doi:10.4049/jimmunol.1101029 (2012).

169 Toller, I. M., Hitzler, I., Sayi, A. & Mueller, A. Prostaglandin E2 prevents *Helicobacter*-induced gastric preneoplasia and facilitates persistent infection in a mouse model. *Gastroenterology* **138**, 1455-1467, 1467 e1451-1454, doi:10.1053/j.gastro.2009.12.006 (2010).

170 Mellor, A. L. & Munn, D. H. IDO expression by dendritic cells: tolerance and tryptophan catabolism. *Nat Rev Immunol* **4**, 762-774, doi:10.1038/nri1457 (2004).

171 Routy, J. P., Routy, B., Graziani, G. M. & Mehraj, V. The Kynurenine Pathway Is a Double-Edged Sword in Immune-Privileged Sites and in Cancer: Implications for Immunotherapy. *Int J Tryptophan Res* **9**, 67-77, doi:10.4137/IJTR.S38355 (2016).

172 Zelante, T. *et al.* Tryptophan catabolites from microbiota engage aryl hydrocarbon receptor and balance mucosal reactivity via interleukin-22. *Immunity* **39**, 372-385, doi:10.1016/j.immuni.2013.08.003 (2013).

173 Stevens, E. A., Mezrich, J. D. & Bradfield, C. A. The aryl hydrocarbon receptor: a perspective on potential roles in the immune system. *Immunology* **127**, 299-311, doi:10.1111/j.1365-2567.2009.03054.x (2009).

174 Wilson, K. T. & Crabtree, J. E. Immunology of *Helicobacter pylori*: insights into the failure of the immune response and perspectives on vaccine studies. *Gastroenterology* **133**, 288-308, doi:10.1053/j.gastro.2007.05.008 (2007).

175 Segal, I., Ally, R., Sitas, F. & Walker, A. R. P. *Helicobacter pylori*: the African enigma. *Gut* **43**, 300.302-300, doi:10.1136/gut.43.2.300-b (1998).

176 Arachchi, P. S. *et al.* Proinflammatory Cytokine IL-17 Shows a Significant Association with *Helicobacter pylori* Infection and Disease Severity. *Gastroenterol Res Pract* **2017**, 6265150, doi:10.1155/2017/6265150 (2017).

177 Bagheri, N. *et al.* The biological functions of IL-17 in different clinical expressions of *Helicobacter pylori*-infection. *Microb Pathog* **81**, 33-38, doi:10.1016/j.micpath.2015.03.010 (2015).

178 Bagheri, N. *et al.* Up-regulated Th17 cell function is associated with increased peptic ulcer disease in *Helicobacter pylori*-infection. *Infect Genet Evol* **60**, 117-125, doi:10.1016/j.meegid.2018.02.020 (2018).

179 Bettelli E, O. M., Kuchroo VK. TH-17 cells in the circle of immunity and autoimmunity. *Nature Immunology* **8**, 345-350 (2007).
180 Yang, X. O. *et al.* T helper 17 lineage differentiation is programmed by orphan nuclear receptors ROR alpha and ROR gamma. *Immunity* **28**, 29-39, doi:10.1016/j.immuni.2007.11.016 (2008).
181 Gagliani, N. *et al.* Th17 cells transdifferentiate into regulatory T cells during resolution of inflammation. *Nature* **523**, 221-225, doi:10.1038/nature14452 (2015).
182 Omenetti, S. & Pizarro, T. T. The Treg/Th17 Axis: A Dynamic Balance Regulated by the Gut Microbiome. *Front Immunol* **6**, 639, doi:10.3389/fimmu.2015.00639 (2015).
183 Gouirand, V., Habrylo, I. & Rosenblum, M. D. Regulatory T Cells and Inflammatory Mediators in Autoimmune Disease. *J Invest Dermatol*, doi:10.1016/j.jid.2021.05.010 (2021).
184 Luzza, F. *et al.* Up-regulation of IL-17 is associated with bioactive IL-8 expression in *Helicobacter pylori*-infected human gastric mucosa. *J Immunol* **165**, 5332-5337, doi:10.4049/jimmunol.165.9.5332 (2000).
185 Dixon, B. R., Radin, J. N., Piazuelo, M. B., Contreras, D. C. & Algood, H. M. IL-17a and IL-22 Induce Expression of Antimicrobials in Gastrointestinal Epithelial Cells and May Contribute to Epithelial Cell Defense against *Helicobacter pylori*. *PLoS One* **11**, e0148514, doi:10.1371/journal.pone.0148514 (2016).
186 Serelli-Lee, V. *et al.* Persistent *Helicobacter pylori* specific Th17 responses in patients with past *H. pylori* infection are associated with elevated gastric mucosal IL-1beta. *PLoS One* **7**, e39199, doi:10.1371/journal.pone.0039199 (2012).
187 Chapman, N. M. & Chi, H. Metabolic adaptation of lymphocytes in immunity and disease. *Immunity* **55**, 14-30, doi:10.1016/j.immuni.2021.12.012 (2022).
188 De Rosa, V. *et al.* Glycolysis controls the induction of human regulatory T cells by modulating the expression of FOXP3 exon 2 splicing variants. *Nat Immunol* **16**, 1174-1184, doi:10.1038/ni.3269 (2015).
189 Dumitru, C., Kabat, A. M. & Maloy, K. J. Metabolic Adaptations of CD4+ T Cells in Inflammatory Disease. *Frontiers in Immunology* **9**, doi:10.3389/fimmu.2018.00540 (2018).
190 Hecker, M. *et al.* Aberrant expression of alternative splicing variants in multiple sclerosis – A systematic review. *Autoimmunity Reviews* **18**, 721-732, doi:https://doi.org/10.1016/j.autrev.2019.05.010 (2019).
191 Kitz, A., Singer, E. & Hafler, D. Regulatory T Cells: From Discovery to Autoimmunity. *Cold Spring Harb Perspect Med* **8**, 1-18, doi:10.1101/cshperspect.a029041 (2018).
192 Sakaguchi, S. Naturally arising Foxp3-expressing CD25+CD4+ regulatory T cells in immunological tolerance to self and non-self. *Nat Immunol* **6**, 345-352, doi:10.1038/ni1178 (2005).
193 Belkaid, Y. & Tarbell, K. Regulatory T cells in the control of host-microorganism interactions (*). *Annu Rev Immunol* **27**, 551-589, doi:10.1146/annurev.immunol.021908.132723 (2009).
194 Bilate, A. M. & Lafaille, J. J. Induced CD4+Foxp3+ regulatory T cells in immune tolerance. *Annu Rev Immunol* **30**, 733-758, doi:10.1146/annurev-immunol-020711-075043 (2012).
195 Workman, C. J., Szymczak-Workman, A. L., Collison, L. W., Pillai, M. R. & Vignali, D. A. The development and function of regulatory T cells. *Cell Mol Life Sci* **66**, 2603-2622, doi:10.1007/s00018-009-0026-2 (2009).
196 Perniola, R. Twenty Years of AIRE. *Front Immunol* **9**, 98, doi:10.3389/fimmu.2018.00098 (2018).

197 Gershon, R. K. & Kondo, K. Cell interactions in the induction of tolerance: the role of thymic lymphocytes. *Immunology* **18**, 723-737 (1970).
198 Gershon, R. K., Cohen, P., Hencin, R. & Liebhaber, S. A. Suppressor T cells. *J Immunol* **108**, 586-590 (1972).
199 Gershon, R. K. A disquisition on suppressor T cells. *Transplant Rev* **26**, 170-185, doi:10.1111/j.1600-065x.1975.tb00179.x (1975).
200 Sakaguchi, S., Wing, K. & Miyara, M. Regulatory T cells - a brief history and perspective. *Eur J Immunol* **37 Suppl 1**, S116-123, doi:10.1002/eji.200737593 (2007).
201 Sakaguchi S, S. N., Asano M, Itoh M, Toda M. Immunologic self-tolerance maintained by activated T cells expressing IL-2 receptor alpha-chains (CD25). Breakdown of a single mechanism of self-tolerance causes various autoimmune diseases. *J Immunol* **155**, 1151-1164 (1995).
202 Brunkow, M. E. *et al.* Disruption of a new forkhead/winged-helix protein, scurfin, results in the fatal lymphoproliferative disorder of the scurfy mouse. *Nat Genet* **27**, 68-73, doi:10.1038/83784 (2001).
203 Bennett, C. L. *et al.* The immune dysregulation, polyendocrinopathy, enteropathy, X-linked syndrome (IPEX) is caused by mutations of FOXP3. *Nat Genet* **27**, 20-21, doi:10.1038/83713 (2001).
204 Fontenot, J. D., Gavin, M. A. & Rudensky, A. Y. Foxp3 programs the development and function of CD4+CD25+ regulatory T cells. *Nat Immunol* **4**, 330-336, doi:10.1038/ni904 (2003).
205 Roncarolo, M. G. *et al.* Autoreactive T cell clones specific for class I and class II HLA antigens isolated from a human chimera. *J Exp Med* **167**, 1523-1534, doi:10.1084/jem.167.5.1523 (1988).
206 Roncarolo, M. G., Gregori, S., Bacchetta, R., Battaglia, M. & Gagliani, N. The Biology of T Regulatory Type 1 Cells and Their Therapeutic Application in Immune-Mediated Diseases. *Immunity* **49**, 1004-1019, doi:10.1016/j.immuni.2018.12.001 (2018).
207 Sakaguchi, S., Miyara, M., Costantino, C. M. & Hafler, D. A. FOXP3+ regulatory T cells in the human immune system. *Nat Rev Immunol* **10**, 490-500, doi:10.1038/nri2785 (2010).
208 Kunicki, M. A., Amaya Hernandez, L. C., Davis, K. L., Bacchetta, R. & Roncarolo, M. G. Identity and Diversity of Human Peripheral Th and T Regulatory Cells Defined by Single-Cell Mass Cytometry. *J Immunol* **200**, 336-346, doi:10.4049/jimmunol.1701025 (2018).
209 Zhao, H., Liao, X. & Kang, Y. Tregs: Where We Are and What Comes Next? *Front Immunol* **8**, 1578, doi:10.3389/fimmu.2017.01578 (2017).
210 Zhang, S., Liang, W., Luo, L., Sun, S. & Wang, F. The role of T cell trafficking in CTLA-4 blockade-induced gut immunopathology. *BMC Biol* **18**, 29, doi:10.1186/s12915-020-00765-9 (2020).
211 Walker, L. S. Treg and CTLA-4: two intertwining pathways to immune tolerance. *J Autoimmun* **45**, 49-57, doi:10.1016/j.jaut.2013.06.006 (2013).
212 Chambers, C. A., Sullivan, T. J. & Allison, J. P. Lymphoproliferation in CTLA-4-deficient mice is mediated by costimulation-dependent activation of CD4+ T cells. *Immunity* **7**, 885-895, doi:10.1016/s1074-7613(00)80406-9 (1997).
213 Boasso, A., Herbeuval, J. P., Hardy, A. W., Winkler, C. & Shearer, G. M. Regulation of indoleamine 2,3-dioxygenase and tryptophanyl-tRNA-synthetase by CTLA-4-Fc in human CD4+ T cells. *Blood* **105**, 1574-1581, doi:10.1182/blood-2004-06-2089 (2005).

214 Burmeister, Y. *et al.* ICOS controls the pool size of effector-memory and regulatory T cells. *J Immunol* **180**, 774-782, doi:10.4049/jimmunol.180.2.774 (2008).
215 Coyle, A. J. & Gutierrez-Ramos, J. C. The role of ICOS and other costimulatory molecules in allergy and asthma. *Springer Semin Immunopathol* **25**, 349-359, doi:10.1007/s00281-003-0154-y (2004).
216 Zheng, J. *et al.* ICOS regulates the generation and function of human CD4+ Treg in a CTLA-4 dependent manner. *PLoS One* **8**, e82203, doi:10.1371/journal.pone.0082203 (2013).
217 Wikenheiser, D. J. & Stumhofer, J. S. ICOS Co-Stimulation: Friend or Foe? *Front Immunol* **7**, 304, doi:10.3389/fimmu.2016.00304 (2016).
218 Galicia, G. *et al.* ICOS deficiency results in exacerbated IL-17 mediated experimental autoimmune encephalomyelitis. *J Clin Immunol* **29**, 426-433, doi:10.1007/s10875-009-9287-7 (2009).
219 Hussain, K. *et al. Helicobacter pylori*-Mediated Protection from Allergy Is Associated with IL-10-Secreting Peripheral Blood Regulatory T Cells. *Front Immunol* **7**, 71, doi:10.3389/fimmu.2016.00071 (2016).
220 O'Keeffe, J. & Moran, A. P. Conventional, regulatory, and unconventional T cells in the immunologic response to *Helicobacter pylori*. *Helicobacter* **13**, 1-19, doi:10.1111/j.1523-5378.2008.00559.x (2008).
221 Kao, J. Y. *et al. Helicobacter pylori* immune escape is mediated by dendritic cell-induced Treg skewing and Th17 suppression in mice. *Gastroenterology* **138**, 1046-1054, doi:10.1053/j.gastro.2009.11.043 (2010).
222 Bergman, M. P. *et al. Helicobacter pylori* modulates the T helper cell 1/T helper cell 2 balance through phase-variable interaction between lipopolysaccharide and DC-SIGN. *J Exp Med* **200**, 979-990, doi:10.1084/jem.20041061 (2004).
223 Zhang, M., Liu, M., Luther, J. & Kao, J. Y. *Helicobacter pylori* directs tolerogenic programming of dendritic cells. *Gut Microbes* **1**, 325-329, doi:10.4161/gmic.1.5.13052 (2010).
224 Dendrou, C. A., Fugger, L. & Friese, M. A. Immunopathology of multiple sclerosis. *Nat Rev Immunol* **15**, 545-558, doi:10.1038/nri3871 (2015).
225 Viglietta, V., Baecher-Allan, C., Weiner, H. L. & Hafler, D. A. Loss of functional suppression by CD4+CD25+ regulatory T cells in patients with multiple sclerosis. *J Exp Med* **199**, 971-979, doi:10.1084/jem.20031579 (2004).
226 Haas, J. *et al.* Reduced suppressive effect of CD4+CD25high regulatory T cells on the T cell immune response against myelin oligodendrocyte glycoprotein in patients with multiple sclerosis. *Eur J Immunol* **35**, 3343-3352, doi:10.1002/eji.200526065 (2005).
227 Venken, K. *et al.* Secondary progressive in contrast to relapsing-remitting multiple sclerosis patients show a normal CD4+CD25+ regulatory T-cell function and FOXP3 expression. *J Neurosci Res* **83**, 1432-1446, doi:10.1002/jnr.20852 (2006).
228 Costantino, C. M., Baecher-Allan, C. & Hafler, D. A. Multiple sclerosis and regulatory T cells. *J Clin Immunol* **28**, 697-706, doi:10.1007/s10875-008-9236-x (2008).
229 Sakaguchi, S., Yamaguchi, T., Nomura, T. & Ono, M. Regulatory T cells and immune tolerance. *Cell* **133**, 775-787, doi:10.1016/j.cell.2008.05.009 (2008).
230 Korn, T. *et al.* Myelin-specific regulatory T cells accumulate in the CNS but fail to control autoimmune inflammation. *Nat Med* **13**, 423-431, doi:10.1038/nm1564 (2007).
231 Fletcher, J. M. *et al.* CD39+Foxp3+ regulatory T Cells suppress pathogenic Th17 cells and are impaired in multiple sclerosis. *J Immunol* **183**, 7602-7610, doi:10.4049/jimmunol.0901881 (2009).

232 Wang, Y. *et al.* An intestinal commensal symbiosis factor controls neuroinflammation via TLR2-mediated CD39 signalling. *Nat Commun* **5**, 4432, doi:10.1038/ncomms5432 (2014).
233 Nyirenda, M. H. *et al.* TLR2 stimulation regulates the balance between regulatory T cell and Th17 function: a novel mechanism of reduced regulatory T cell function in multiple sclerosis. *J Immunol* **194**, 5761-5774, doi:10.4049/jimmunol.1400472 (2015).
234 Dombrowski, Y. *et al.* Regulatory T cells promote myelin regeneration in the central nervous system. *Nat Neurosci* **20**, 674-680, doi:10.1038/nn.4528 (2017).
235 Sellebjerg, F., Krakauer, M., Khademi, M., Olsson, T. & Sorensen, P. S. FOXP3, CBLB and ITCH gene expression and cytotoxic T lymphocyte antigen 4 expression on CD4(+) CD25(high) T cells in multiple sclerosis. *Clin Exp Immunol* **170**, 149-155, doi:10.1111/j.1365-2249.2012.04654.x (2012).
236 Xu, L., Xu, Z. & Xu, M. Glucocorticoid treatment restores the impaired suppressive function of regulatory T cells in patients with relapsing-remitting multiple sclerosis. *Clin Exp Immunol* **158**, 26-30, doi:10.1111/j.1365-2249.2009.03987.x (2009).
237 Muls, N., Dang, H. A., Sindic, C. J. & van Pesch, V. Fingolimod increases CD39-expressing regulatory T cells in multiple sclerosis patients. *PLoS One* **9**, e113025, doi:10.1371/journal.pone.0113025 (2014).
238 Charcot, J. M. Histologie de la sclérose en plaques. *Gaz Hôp (París)* (1868).
239 Zalc, B. One hundred and fifty years ago Charcot reported multiple sclerosis as a new neurological disease. *Brain* **141**, 3482-3488, doi:10.1093/brain/awy287 (2018).
240 Fletcher, J. M., Lalor, S. J., Sweeney, C. M., Tubridy, N. & Mills, K. H. T cells in multiple sclerosis and experimental autoimmune encephalomyelitis. *Clin Exp Immunol* **162**, 1-11, doi:10.1111/j.1365-2249.2010.04143.x (2010).
241 McDonald, W. I. *et al.* Recommended diagnostic criteria for multiple sclerosis: guidelines from the International Panel on the diagnosis of multiple sclerosis. *Ann Neurol* **50**, 121-127, doi:10.1002/ana.1032 (2001).
242 Dalton, C. M. *et al.* Application of the new McDonald criteria to patients with clinically isolated syndromes suggestive of multiple sclerosis. *Annals of Neurology* **52**, 47-53, doi:https://doi.org/10.1002/ana.10240 (2002).
243 Pugliatti, M. *et al.* The epidemiology of multiple sclerosis in Europe. *Eur J Neurol* **13**, 700-722, doi:10.1111/j.1468-1331.2006.01342.x (2006).
244 Sospedra, M. & Martin, R. Immunology of multiple sclerosis. *Annu Rev Immunol* **23**, 683-747, doi:10.1146/annurev.immunol.23.021704.115707 (2005).
245 Kurtzke, J. F. Rating neurologic impairment in multiple sclerosis. *An expanded disability status scale (EDSS)* **33**, 1444-1444, doi:10.1212/wnl.33.11.1444 (1983).
246 Walton, C. *et al.* Rising prevalence of multiple sclerosis worldwide: Insights from the Atlas of MS, third edition. *Multiple Sclerosis Journal* **26**, 1816-1821, doi:10.1177/1352458520970841 (2020).
247 Mackenzie, I. S., Morant, S. V., Bloomfield, G. A., MacDonald, T. M. & O'Riordan, J. Incidence and prevalence of multiple sclerosis in the UK 1990-2010: a descriptive study in the General Practice Research Database. *J Neurol Neurosurg Psychiatry* **85**, 76-84, doi:10.1136/jnnp-2013-305450 (2014).
248 Wallin, M. T. *et al.* Global, regional, and national burden of multiple sclerosis 1990-2016: a systematic analysis for the Global Burden of Disease Study 2016. *Lancet Neurology* **18**, 269-285, doi:Doi 10.1016/S1474-4422(18)30443-5 (2019).
249 Rook, G. A. & Brunet, L. R. Old friends for breakfast. *Clin Exp Allergy* **35**, 841-842, doi:10.1111/j.1365-2222.2005.02112.x (2005).

250 Rook, G. A. W. *et al.* Mycobacteria and other environmental organisms as immunomodulators for immunoregulatory disorders. *Springer Seminars in Immunopathology* **25**, 237-255, doi:10.1007/s00281-003-0148-9 (2004).
251 Gold, S. M., Willing, A., Leypoldt, F., Paul, F. & Friese, M. A. Sex differences in autoimmune disorders of the central nervous system. *Seminars in Immunopathology* **41**, 177-188, doi:10.1007/s00281-018-0723-8 (2019).
252 Klein, S. L. & Flanagan, K. L. Sex differences in immune responses. *Nature Reviews Immunology* **16**, 626-638, doi:10.1038/nri.2016.90 (2016).
253 Ysrraelit, M. C. & Correale, J. Impact of sex hormones on immune function and multiple sclerosis development. *Immunology* **156**, 9-22, doi:https://doi.org/10.1111/imm.13004 (2019).
254 Ramien, C. *et al.* Sex effects on inflammatory and neurodegenerative processes in multiple sclerosis. *Neuroscience & Biobehavioral Reviews* **67**, 137-146, doi:https://doi.org/10.1016/j.neubiorev.2015.12.015 (2016).
255 Segal, B. M. The Diversity of Encephalitogenic CD4+ T Cells in Multiple Sclerosis and Its Animal Models. *J Clin Med* **8**, doi:10.3390/jcm8010120 (2019).
256 Cusick, M. F., Libbey, J. E. & Fujinami, R. S. Multiple sclerosis: autoimmunity and viruses. *Curr Opin Rheumatol* **25**, 496-501, doi:10.1097/BOR.0b013e328362004d (2013).
257 Olsson, T., Barcellos, L. F. & Alfredsson, L. Interactions between genetic, lifestyle and environmental risk factors for multiple sclerosis. *Nat Rev Neurol* **13**, 25-36, doi:10.1038/nrneurol.2016.187 (2017).
258 Wood, H. Latitude and vitamin D influence disease course in multiple sclerosis. *Nature Reviews Neurology* **13**, 3-3, doi:10.1038/nrneurol.2016.181 (2017).
259 Tao, C. *et al.* Higher latitude is significantly associated with an earlier age of disease onset in multiple sclerosis. *Journal of Neurology, Neurosurgery & Psychiatry* **87**, 1343-1349, doi:10.1136/jnnp-2016-314013 (2016).
260 Smolders, J., Damoiseaux, J., Menheere, P. & Hupperts, R. Vitamin D as an immune modulator in multiple sclerosis, a review. *J Neuroimmunol* **194**, 7-17, doi:10.1016/j.jneuroim.2007.11.014 (2008).
261 Wilkin, T. Autoimmunity: attack, or defence? (The case for a primary lesion theory). *Autoimmunity* **3**, 57-73, doi:10.3109/08916938909043614 (1989).
262 Wilkin, T. J. The primary lesion theory of autoimmunity: a speculative hypothesis. *Autoimmunity* **7**, 225-235, doi:10.3109/08916939009087582 (1990).
263 t Hart, B. A., Hintzen, R. Q. & Laman, J. D. Multiple sclerosis - a response-to-damage model. *Trends Mol Med* **15**, 235-244, doi:10.1016/j.molmed.2009.04.001 (2009).
264 Dolei, A. The aliens inside us: HERV-W endogenous retroviruses and multiple sclerosis. *Mult Scler* **24**, 42-47, doi:10.1177/1352458517737370 (2018).
265 Cossu, D., Yokoyama, K. & Hattori, N. Bacteria-Host Interactions in Multiple Sclerosis. *Front Microbiol* **9**, 2966, doi:10.3389/fmicb.2018.02966 (2018).
266 Voskuhl, R. R., Farris, R. W., Nagasato, K., McFarland, H. F. & Dalcq, M. D. Epitope spreading occurs in active but not passive EAE induced by myelin basic protein. *Journal of Neuroimmunology* **70**, 103-111, doi:10.1016/s0165-5728(96)00054-9 (1996).
267 Smith, P. A. *et al.* Epitope spread is not critical for the relapse and progression of MOG 8-21 induced EAE in Biozzi ABH mice. *J Neuroimmunol* **164**, 76-84, doi:10.1016/j.jneuroim.2005.04.006 (2005).
268 Lehmann, P. V., Forsthuber, T., Miller, A. & Sercarz, E. E. Spreading of T-cell autoimmunity to cryptic determinants of an autoantigen. *Nature* **358**, 155-157, doi:10.1038/358155a0 (1992).

269 Bjelobaba, I., Begovic-Kupresanin, V., Pekovic, S. & Lavrnja, I. Animal models of multiple sclerosis: Focus on experimental autoimmune encephalomyelitis. *J Neurosci Res* **96**, 1021-1042, doi:10.1002/jnr.24224 (2018).
270 Sanabria-Castro, A., Flores-Diaz, M. & Alape-Giron, A. Biological models in multiple sclerosis. *J Neurosci Res* **98**, 491-508, doi:10.1002/jnr.24528 (2020).
271 Procaccini, C., De Rosa, V., Pucino, V., Formisano, L. & Matarese, G. Animal models of Multiple Sclerosis. *Eur J Pharmacol* **759**, 182-191, doi:10.1016/j.ejphar.2015.03.042 (2015).
272 Constantinescu, C. S., Farooqi, N., O'Brien, K. & Gran, B. Experimental autoimmune encephalomyelitis (EAE) as a model for multiple sclerosis (MS). *Br J Pharmacol* **164**, 1079-1106, doi:10.1111/j.1476-5381.2011.01302.x (2011).
273 van Zwam, M. *et al.* Brain antigens in functionally distinct antigen-presenting cell populations in cervical lymph nodes in MS and EAE. *J Mol Med (Berl)* **87**, 273-286, doi:10.1007/s00109-008-0421-4 (2009).
274 van Zwam, M. *et al.* Surgical excision of CNS-draining lymph nodes reduces relapse severity in chronic-relapsing experimental autoimmune encephalomyelitis. *J Pathol* **217**, 543-551, doi:10.1002/path.2476 (2009).
275 Wagner, C. A., Roqué, P. J. & Goverman, J. M. Pathogenic T cell cytokines in multiple sclerosis. *J Exp Med* **217**, doi:10.1084/jem.20190460 (2020).
276 Baecher-Allan, C., Kaskow, B. J. & Weiner, H. L. Multiple Sclerosis: Mechanisms and Immunotherapy. *Neuron* **97**, 742-768, doi:https://doi.org/10.1016/j.neuron.2018.01.021 (2018).
277 Milovanovic, J. *et al.* Interleukin-17 in Chronic Inflammatory Neurological Diseases. *Frontiers in Immunology* **11**, 947, doi:10.3389/fimmu.2020.00947 (2020).
278 Haak, S. *et al.* IL-17A and IL-17F do not contribute vitally to autoimmune neuro-inflammation in mice. *The Journal of clinical investigation* **119**, 61-69 (2009).
279 McGeachy, M. J. *et al.* TGF-β and IL-6 drive the production of IL-17 and IL-10 by T cells and restrain TH-17 cell–mediated pathology. *Nature Immunology* **8**, 1390-1397, doi:10.1038/ni1539 (2007).
280 Pedrini, M. J. *et al. Helicobacter pylori* infection as a protective factor against multiple sclerosis risk in females. *J Neurol Neurosurg Psychiatry* **86**, 603-607, doi:10.1136/jnnp-2014-309495 (2015).
281 Saxena, A., Martin-Blondel, G., Mars, L. T. & Liblau, R. S. Role of CD8 T cell subsets in the pathogenesis of multiple sclerosis. *FEBS Letters* **585**, 3758-3763, doi:https://doi.org/10.1016/j.febslet.2011.08.047 (2011).
282 Yu, X., Graner, M., Kennedy, P. G. E. & Liu, Y. The Role of Antibodies in the Pathogenesis of Multiple Sclerosis. *Front Neurol* **11**, 533388-533388, doi:10.3389/fneur.2020.533388 (2020).
283 Duffy, S. S. *et al.* Regulatory T Cells and Their Derived Cytokine, Interleukin-35, Reduce Pain in Experimental Autoimmune Encephalomyelitis. *J Neurosci* **39**, 2326-2346, doi:10.1523/jneurosci.1815-18.2019 (2019).
284 De Angelis, F., John, N. A. & Brownlee, W. J. Disease-modifying therapies for multiple sclerosis. *BMJ* **363**, k4674, doi:10.1136/bmj.k4674 (2018).
285 Tramacere, I., Del Giovane, C., Salanti, G., D'Amico, R. & Filippini, G. Immunomodulators and immunosuppressants for relapsing-remitting multiple sclerosis: a network meta-analysis. *Cochrane Database Syst Rev*, CD011381, doi:10.1002/14651858.CD011381.pub2 (2015).
286 La Mantia, L. *et al.* Fingolimod for relapsing-remitting multiple sclerosis. *Cochrane Database Syst Rev* **4**, CD009371, doi:10.1002/14651858.CD009371.pub2 (2016).
287 Pucci, E. *et al.* Natalizumab for relapsing remitting multiple sclerosis. *Cochrane Database Syst Rev*, CD007621, doi:10.1002/14651858.CD007621.pub2 (2011).

288 Jakimovski, D., Kolb, C., Ramanathan, M., Zivadinov, R. & Weinstock-Guttman, B. Interferon β for Multiple Sclerosis. *Cold Spring Harb Perspect Med* **8**, doi:10.1101/cshperspect.a032003 (2018).

289 Perumal, J. *et al.* Glatiramer acetate therapy for multiple sclerosis: a review. *Expert Opin Drug Metab Toxicol* **2**, 1019-1029, doi:10.1517/17425255.2.6.1019 (2006).

290 Hooijmans, C. R. *et al.* Remyelination promoting therapies in multiple sclerosis animal models: a systematic review and meta-analysis. *Sci Rep* **9**, 822, doi:10.1038/s41598-018-35734-4 (2019).

291 Mei, F. *et al.* Micropillar arrays as a high-throughput screening platform for therapeutics in multiple sclerosis. *Nat Med* **20**, 954-960, doi:10.1038/nm.3618 (2014).

292 Bove, R. M. & Green, A. J. Remyelinating Pharmacotherapies in Multiple Sclerosis. *Neurotherapeutics* **14**, 894-904, doi:10.1007/s13311-017-0577-0 (2017).

293 Deshmukh, V. A. *et al.* A regenerative approach to the treatment of multiple sclerosis. *Nature* **502**, 327-332, doi:10.1038/nature12647 (2013).

294 Gingele, S. & Stangel, M. Emerging myelin repair agents in preclinical and early clinical development for the treatment of multiple sclerosis. *Expert Opin Investig Drugs* **29**, 583-594, doi:10.1080/13543784.2020.1762567 (2020).

295 Foale, S., Berry, M., Logan, A., Fulton, D. & Ahmed, Z. LINGO-1 and AMIGO3, potential therapeutic targets for neurological and dysmyelinating disorders? *Neural Regen Res* **12**, 1247-1251, doi:10.4103/1673-5374.213538 (2017).

296 Mi, S. *et al.* LINGO-1 antagonist promotes spinal cord remyelination and axonal integrity in MOG-induced experimental autoimmune encephalomyelitis. *Nat Med* **13**, 1228-1233, doi:10.1038/nm1664 (2007).

297 Mi, S. *et al.* LINGO-1 negatively regulates myelination by oligodendrocytes. *Nat Neurosci* **8**, 745-751, doi:10.1038/nn1460 (2005).

298 Mi, S., Sandrock, A. & Miller, R. H. LINGO-1 and its role in CNS repair. *Int J Biochem Cell Biol* **40**, 1971-1978, doi:10.1016/j.biocel.2008.03.018 (2008).

299 Kim, M. J., Kang, J. H., Theotokis, P., Grigoriadis, N. & Petratos, S. Can We Design a Nogo Receptor-Dependent Cellular Therapy to Target MS? *Cells* **8**, 1 (2019).

300 Cadavid, D. *et al.* Safety and efficacy of opicinumab in patients with relapsing multiple sclerosis (SYNERGY): a randomised, placebo-controlled, phase 2 trial. *Lancet Neurol* **18**, 845-856, doi:10.1016/S1474-4422(19)30137-1 (2019).

301 Zhao, Q. & Elson, C. O. Adaptive immune education by gut microbiota antigens. *Immunology* **154**, 28-37, doi:10.1111/imm.12896 (2018).

302 Marinelli, L. *et al.* Identification of the novel role of butyrate as AhR ligand in human intestinal epithelial cells. *Sci Rep* **9**, 643, doi:10.1038/s41598-018-37019-2 (2019).

303 Erny, D. *et al.* Host microbiota constantly control maturation and function of microglia in the CNS. *Nat Neurosci* **18**, 965-977, doi:10.1038/nn.4030 (2015).

304 Duranti, S. *et al.* Bifidobacterium adolescentis as a key member of the human gut microbiota in the production of GABA. *Sci Rep* **10**, 14112, doi:10.1038/s41598-020-70986-z (2020).

305 Kennedy, P. J., Cryan, J. F., Dinan, T. G. & Clarke, G. Kynurenine pathway metabolism and the microbiota-gut-brain axis. *Neuropharmacology* **112**, 399-412, doi:10.1016/j.neuropharm.2016.07.002 (2017).

306 Rothhammer, V. *et al.* Microglial control of astrocytes in response to microbial metabolites. *Nature* **557**, 724-728, doi:10.1038/s41586-018-0119-x (2018).

307 Rothhammer, V. *et al.* Type I interferons and microbial metabolites of tryptophan modulate astrocyte activity and central nervous system inflammation via the aryl hydrocarbon receptor. *Nat Med* **22**, 586-597, doi:10.1038/nm.4106 (2016).

308 Mossad, O. & Erny, D. The microbiota-microglia axis in central nervous system disorders. *Brain Pathol* **30**, 1159-1177, doi:10.1111/bpa.12908 (2020).

309 Raybould, H. E. Gut chemosensing: interactions between gut endocrine cells and visceral afferents. *Auton Neurosci* **153**, 41-46, doi:10.1016/j.autneu.2009.07.007 (2010).

310 Strandwitz, P. *et al.* GABA-modulating bacteria of the human gut microbiota. *Nat Microbiol* **4**, 396-403, doi:10.1038/s41564-018-0307-3 (2019).

311 Prud'homme, G. J., Glinka, Y. & Wang, Q. Immunological GABAergic interactions and therapeutic applications in autoimmune diseases. *Autoimmun Rev* **14**, 1048-1056, doi:10.1016/j.autrev.2015.07.011 (2015).

312 Strandwitz, P. Neurotransmitter modulation by the gut microbiota. *Brain Res* **1693**, 128-133, doi:10.1016/j.brainres.2018.03.015 (2018).

313 Clarke, G. *et al.* Minireview: Gut microbiota: the neglected endocrine organ. *Mol Endocrinol* **28**, 1221-1238, doi:10.1210/me.2014-1108 (2014).

314 Silva, Y. P., Bernardi, A. & Frozza, R. L. The Role of Short-Chain Fatty Acids From Gut Microbiota in Gut-Brain Communication. *Front Endocrinol (Lausanne)* **11**, 25, doi:10.3389/fendo.2020.00025 (2020).

315 Azadegan-Dehkordi, F. *et al.* Increased Indoleamine 2, 3-Dioxygenase expression modulates Th1/Th17/Th22 and Treg pathway in humans with *Helicobacter Pylori*-Infected gastric mucosa. *Hum Immunol* **82**, 46-53, doi:10.1016/j.humimm.2020.10.005 (2021).

316 Larussa, T. *et al.* Downregulation of Interleukin- (IL-) 17 through Enhanced Indoleamine 2,3-Dioxygenase (IDO) Induction by Curcumin: A Potential Mechanism of Tolerance towards *Helicobacter pylori*. *J Immunol Res* **2018**, 3739593, doi:10.1155/2018/3739593 (2018).

317 Raitala, A., Karjalainen, J., Oja, S. S., Kosunen, T. U. & Hurme, M. *Helicobacter pylori*-induced indoleamine 2,3-dioxygenase activity *in vivo* is regulated by TGFB1 and CTLA4 polymorphisms. *Mol Immunol* **44**, 1011-1014, doi:10.1016/j.molimm.2006.03.006 (2007).

318 Berer, K. *et al.* Commensal microbiota and myelin autoantigen cooperate to trigger autoimmune demyelination. *Nature* **479**, 538-541, doi:10.1038/nature10554 (2011).

319 Katz Sand, I. *et al.* Disease-modifying therapies alter gut microbial composition in MS. *Neurol Neuroimmunol Neuroinflamm* **6**, e517, doi:10.1212/NXI.0000000000000517 (2019).

320 Chen, J. *et al.* Multiple sclerosis patients have a distinct gut microbiota compared to healthy controls. *Sci Rep* **6**, 28484, doi:10.1038/srep28484 (2016).

321 Berer, K. *et al.* Gut microbiota from multiple sclerosis patients enables spontaneous autoimmune encephalomyelitis in mice. *Proc Natl Acad Sci U S A* **114**, 10719-10724, doi:10.1073/pnas.1711233114 (2017).

322 Mirza, A. *et al.* The multiple sclerosis gut microbiota: A systematic review. *Mult Scler Relat Disord* **37**, 101427, doi:10.1016/j.msard.2019.101427 (2020).

323 Rothhammer, V. & Quintana, F. J. The aryl hydrocarbon receptor: an environmental sensor integrating immune responses in health and disease. *Nat Rev Immunol* **19**, 184-197, doi:10.1038/s41577-019-0125-8 (2019).

324 Shahi, S. K. *et al.* Prevotella histicola, A Human Gut Commensal, Is as Potent as COPAXONE(R) in an Animal Model of Multiple Sclerosis. *Front Immunol* **10**, 462, doi:10.3389/fimmu.2019.00462 (2019).

325 Shahi, S. K. *et al.* Human Commensal Prevotella histicola Ameliorates Disease as Effectively as Interferon-Beta in the Experimental Autoimmune Encephalomyelitis. *Front Immunol* **11**, 578648, doi:10.3389/fimmu.2020.578648 (2020).

326 Rojas, O. L. *et al.* Recirculating Intestinal IgA-Producing Cells Regulate Neuroinflammation via IL-10. *Cell* **176**, 610-624 e618, doi:10.1016/j.cell.2018.11.035 (2019).
327 Chudnovskiy, A. *et al.* Host-Protozoan Interactions Protect from Mucosal Infections through Activation of the Inflammasome. *Cell* **167**, 444-456 e414, doi:10.1016/j.cell.2016.08.076 (2016).
328 He, B. *et al.* Lactobacillus reuteri Reduces the Severity of Experimental Autoimmune Encephalomyelitis in Mice by Modulating Gut Microbiota. *Front Immunol* **10**, 385, doi:10.3389/fimmu.2019.00385 (2019).
329 Johanson, D. M., 2nd *et al.* Experimental autoimmune encephalomyelitis is associated with changes of the microbiota composition in the gastrointestinal tract. *Sci Rep* **10**, 15183, doi:10.1038/s41598-020-72197-y (2020).
330 Miyauchi, E. *et al.* Gut microorganisms act together to exacerbate inflammation in spinal cords. *Nature* **585**, 102-106, doi:10.1038/s41586-020-2634-9 (2020).
331 Jenkins, T. *et al.* Experimental infection with the hookworm, Necator americanus, promotes gut microbial diversity in human volunteers with relapsing multiple sclerosis. (2020).
332 Jaruvongvanich, V., Sanguankeo, A., Jaruvongvanich, S. & Upala, S. Association between *Helicobacter pylori* infection and multiple sclerosis: A systematic review and meta-analysis. *Mult Scler Relat Disord* **7**, 92-97, doi:10.1016/j.msard.2016.03.013 (2016).
333 Li, W. *et al. Helicobacter pylori* infection is a potential protective factor against conventional multiple sclerosis in the Japanese population. *J Neuroimmunol* **184**, 227-231, doi:10.1016/j.jneuroim.2006.12.010 (2007).
334 Cook, K. W. *et al. Helicobacter pylori* infection reduces disease severity in an experimental model of multiple sclerosis. *Front Microbiol* **6**, 52, doi:10.3389/fmicb.2015.00052 (2015).
335 Yao, G. *et al.* Meta-analysis of association between *Helicobacter pylori* infection and multiple sclerosis. *Neurosci Lett* **620**, 1-7, doi:10.1016/j.neulet.2016.03.037 (2016).
336 Mohebi, N., Mamarabadi, M. & Moghaddasi, M. Relation of *Helicobacter pylori* infection and multiple sclerosis in Iranian patients. *Neurol Int* **5**, 31-33, doi:10.4081/ni.2013.e10 (2013).
337 Gavalas E, K. J., Boziki M, Deretzi G, *et al.* Relationship between *Helicobacter pylori* infection and multiple sclerosis. *Annals of Gastroenterology* **28**, 353-356 (2015).
338 Duffy, S. S., Keating, B. A., Perera, C. J. & Moalem-Taylor, G. The role of regulatory T cells in nervous system pathologies. *J Neurosci Res* **96**, 951-968, doi:10.1002/jnr.24073 (2018).
339 Noori-Zadeh, A. *et al.* Regulatory T cell number in multiple sclerosis patients: A meta-analysis. *Mult Scler Relat Disord* **5**, 73-76, doi:10.1016/j.msard.2015.11.004 (2016).
340 Martinez, N. E. *et al.* Protective and detrimental roles for regulatory T cells in a viral model for multiple sclerosis. *Brain Pathol* **24**, 436-451, doi:10.1111/bpa.12119 (2014).
341 Venken, K., Hellings, N., Liblau, R. & Stinissen, P. Disturbed regulatory T cell homeostasis in multiple sclerosis. *Trends Mol Med* **16**, 58-68, doi:10.1016/j.molmed.2009.12.003 (2010).
342 Duffy, S. S., Keating, B. A. & Moalem-Taylor, G. Adoptive Transfer of Regulatory T Cells as a Promising Immunotherapy for the Treatment of Multiple Sclerosis. *Front Neurosci* **13**, 1107, doi:10.3389/fnins.2019.01107 (2019).

343 Ranjbar, R., Karampoor, S. & Jalilian, F. A. The protective effect of *Helicobacter Pylori* infection on the susceptibility of multiple sclerosis. *J Neuroimmunol* **337**, 577069, doi:10.1016/j.jneuroim.2019.577069 (2019).
344 Razavi, A. *et al.* Comparative Immune Response in Children and Adults with *H. pylori* Infection. *Journal of immunology research* **2015**, 315957-315957, doi:10.1155/2015/315957 (2015).
345 Hugenholtz, F. & de Vos, W. M. Mouse models for human intestinal microbiota research: a critical evaluation. *Cellular and Molecular Life Sciences* **75**, 149-160, doi:10.1007/s00018-017-2693-8 (2018).
346 Lee, A. *et al.* A standardized mouse model of *Helicobacter pylori* infection: introducing the Sydney strain. *Gastroenterology* **112**, 1386-1397, doi:10.1016/s0016-5085(97)70155-0 (1997).
347 Ziegler, S. F. FOXP3: of mice and men. *Annu Rev Immunol* **24**, 209-226, doi:10.1146/annurev.immunol.24.021605.090547 (2006).
348 Mailer, R. K. W. Alternative Splicing of FOXP3—Virtue and Vice. *Frontiers in Immunology* **9**, doi:10.3389/fimmu.2018.00530 (2018).
349 Sellers, R. S. Translating Mouse Models:Immune Variation and Efficacy Testing. *Toxicologic Pathology* **45**, 134-145, doi:10.1177/0192623316675767 (2017).
350 Butcher, L. D., den Hartog, G., Ernst, P. B. & Crowe, S. E. Oxidative Stress Resulting From *Helicobacter pylori* Infection Contributes to Gastric Carcinogenesis. *Cell Mol Gastroenterol Hepatol* **3**, 316-322, doi:10.1016/j.jcmgh.2017.02.002 (2017).
351 Algood, H. M., Gallo-Romero, J., Wilson, K. T., Peek, R. M., Jr. & Cover, T. L. Host response to *Helicobacter pylori* infection before initiation of the adaptive immune response. *FEMS Immunol Med Microbiol* **51**, 577-586, doi:10.1111/j.1574-695X.2007.00338.x (2007).
352 Probstel, A. K. *et al.* Gut microbiota-specific IgA(+) B cells traffic to the CNS in active multiple sclerosis. *Sci Immunol* **5**, eabc7191, doi:10.1126/sciimmunol.abc7191 (2020).
353 Kronsteiner, B., Bassaganya-Riera, J., Philipson, N. & Hontecillas, R. Novel insights on the role of CD8+ T cells and cytotoxic responses during *Helicobacter pylori* infection. *Gut Microbes* **5**, 357-362, doi:10.4161/gmic.28899 (2014).
354 Arnold, I. C. *et al.* NLRP3 Controls the Development of Gastrointestinal CD11b(+) Dendritic Cells in the Steady State and during Chronic Bacterial Infection. *Cell Rep* **21**, 3860-3872, doi:10.1016/j.celrep.2017.12.015 (2017).
355 Lambrecht, B. N. & Hammad, H. The immunology of the allergy epidemic and the hygiene hypothesis. *Nat Immunol* **18**, 1076-1083, doi:10.1038/ni.3829 (2017).
356 Frew, J. W. The Hygiene Hypothesis, Old Friends, and New Genes. *Front Immunol* **10**, 388, doi:10.3389/fimmu.2019.00388 (2019).
357 Rocha, A. M. *et al.* Cytokine profile of patients with chronic immune thrombocytopenia affects platelet count recovery after *Helicobacter pylori* eradication. *Br J Haematol* **168**, 421-428, doi:10.1111/bjh.13141 (2015).
358 Engler, D. B. *et al. Helicobacter pylori*-specific protection against inflammatory bowel disease requires the NLRP3 inflammasome and IL-18. *Inflamm Bowel Dis* **21**, 854-861, doi:10.1097/MIB.0000000000000318 (2015).
359 Papamichael, K., Konstantopoulos, P. & Mantzaris, G. J. *Helicobacter pylori* infection and inflammatory bowel disease: is there a link? *World J Gastroenterol* **20**, 6374-6385, doi:10.3748/wjg.v20.i21.6374 (2014).
360 Pfaffl, M. W. A new mathematical model for relative quantification in real-time RT-PCR. *Nucleic Acids Res* **29**, e45, doi:10.1093/nar/29.9.e45 (2001).
361 White, J. R. Developing new predictors of *Helicobacter pylori* associated disease and its progression. *Ph.D Thesis; University of Nottingham* **4196683** (2016).

362 Zhang, B. *et al.* The prevalence of Th17 cells in patients with gastric cancer. *Biochem Biophys Res Commun* **374**, 533-537, doi:10.1016/j.bbrc.2008.07.060 (2008).
363 Fehlings, M. *et al.* Comparative analysis of the interaction of *Helicobacter pylori* with human dendritic cells, macrophages, and monocytes. *Infect Immun* **80**, 2724-2734, doi:10.1128/IAI.00381-12 (2012).
364 Ma, X. *et al.* Regulation of IL-10 and IL-12 production and function in macrophages and dendritic cells. *F1000Res* **4**, F1000 Faculty Rev-1465, doi:10.12688/f1000research.7010.1 (2015).
365 Detry, S., Skladanowska, K., Vuylsteke, M., Savvides, S. N. & Bloch, Y. Revisiting the combinatorial potential of cytokine subunits in the IL-12 family. *Biochem Pharmacol* **165**, 240-248, doi:10.1016/j.bcp.2019.03.026 (2019).
366 Tait Wojno, E. D., Hunter, C. A. & Stumhofer, J. S. The Immunobiology of the Interleukin-12 Family: Room for Discovery. *Immunity* **50**, 851-870, doi:10.1016/j.immuni.2019.03.011 (2019).
367 Dewayani, A. *et al.* The Roles of IL-17, IL-21, and IL-23 in the *Helicobacter pylori* Infection and Gastrointestinal Inflammation: A Review. *Toxins (Basel)* **13**, 315, doi:10.3390/toxins13050315 (2021).
368 Becher, B., Durell, B. G. & Noelle, R. J. Experimental autoimmune encephalitis and inflammation in the absence of interleukin-12. *J Clin Invest* **110**, 493-497, doi:10.1172/JCI15751 (2002).
369 Mondal, S. *et al.* IL-12 p40 monomer is different from other IL-12 family members to selectively inhibit IL-12Rbeta1 internalization and suppress EAE. *Proc Natl Acad Sci U S A* **117**, 21557-21567, doi:10.1073/pnas.2000653117 (2020).
370 Gran, B. *et al.* IL-12p35-deficient mice are susceptible to experimental autoimmune encephalomyelitis: evidence for redundancy in the IL-12 system in the induction of central nervous system autoimmune demyelination. *J Immunol* **169**, 7104-7110, doi:10.4049/jimmunol.169.12.7104 (2002).
371 Cua, D. J. *et al.* Interleukin-23 rather than interleukin-12 is the critical cytokine for autoimmune inflammation of the brain. *Nature* **421**, 744-748, doi:10.1038/nature01355 (2003).
372 Vonkeman, H. E. *et al.* Assessment of *Helicobacter pylori* eradication in patients on NSAID treatment. *BMC Gastroenterol* **12**, 133, doi:10.1186/1471-230X-12-133 (2012).
373 Best, L. M. *et al.* Non-invasive diagnostic tests for *Helicobacter pylori* infection. *Cochrane Database Syst Rev* **3**, CD012080, doi:10.1002/14651858.CD012080.pub2 (2018).
374 Cutler, A. F., Prasad, V. M. & Santogade, P. Four-year trends in *Helicobacter pylori* IgG serology following successful eradication. *Am J Med* **105**, 18-20, doi:10.1016/s0002-9343(98)00134-x (1998).
375 Savoldi, A., Carrara, E., Graham, D. Y., Conti, M. & Tacconelli, E. Prevalence of Antibiotic Resistance in *Helicobacter pylori*: A Systematic Review and Meta-analysis in World Health Organization Regions. *Gastroenterology* **155**, 1372-1382 e1317, doi:10.1053/j.gastro.2018.07.007 (2018).
376 Onal, I. K., Gokcan, H., Benzer, E., Bilir, G. & Oztas, E. What is the impact of *Helicobacter pylori* density on the success of eradication therapy: a clinico-histopathological study. *Clin Res Hepatol Gastroenterol* **37**, 642-646, doi:10.1016/j.clinre.2013.05.005 (2013).
377 Hopkins, R. J., Girardi, L. S. & Turney, E. A. Relationship between *Helicobacter pylori* eradication and reduced duodenal and gastric ulcer recurrence: a review. *Gastroenterology* **110**, 1244-1252, doi:10.1053/gast.1996.v110.pm8613015 (1996).

378 Kim, N. *et al.* Effect of eradication of *Helicobacter pylori* on the benign gastric ulcer recurrence--a 24 month follow-up study. *Korean J Intern Med* **14**, 9-14, doi:10.3904/kjim.1999.14.2.9 (1999).

379 Tomita, T. *et al.* Successful eradication of *Helicobacter pylori* prevents relapse of peptic ulcer disease. *Aliment Pharmacol Ther* **16 Suppl 2**, 204-209, doi:10.1046/j.1365-2036.16.s2.24.x (2002).

380 Milic, L. *et al.* Altered cytokine expression in *Helicobacter pylori* infected patients with bleeding duodenal ulcer. *BMC Res Notes* **12**, 278, doi:10.1186/s13104-019-4310-4 (2019).

381 Reddiar, D. Regulatory B and T cells in *Helicobacter pylori* infection. *Ph.D thesis; University of Nottingham* (2017).

382 Gibbings, D. & Befus, A. D. CD4 and CD8: an inside-out coreceptor model for innate immune cells. *J Leukoc Biol* **86**, 251-259, doi:10.1189/jlb.0109040 (2009).

383 O'Doherty, U. *et al.* Dendritic cells freshly isolated from human blood express CD4 and mature into typical immunostimulatory dendritic cells after culture in monocyte-conditioned medium. *J Exp Med* **178**, 1067-1076, doi:10.1084/jem.178.3.1067 (1993).

384 Zhen, A. *et al.* CD4 ligation on human blood monocytes triggers macrophage differentiation and enhances HIV infection. *J Virol* **88**, 9934-9946, doi:10.1128/JVI.00616-14 (2014).

385 D'Elios, M. M., Amedei, A., Benagiano, M., Azzurri, A. & Del Prete, G. *Helicobacter pylori*, T cells and cytokines: the "dangerous liaisons". *FEMS Immunol Med Microbiol* **44**, 113-119, doi:10.1016/j.femsim.2004.10.013 (2005).

386 He, H. *et al. Helicobacter pylori* CagA Interacts with SHP-1 to Suppress the Immune Response by Targeting TRAF6 for K63-Linked Ubiquitination. *J Immunol* **206**, 1161-1170, doi:10.4049/jimmunol.2000234 (2021).

387 Tesmer, L. A., Lundy, S. K., Sarkar, S. & Fox, D. A. Th17 cells in human disease. *Immunol Rev* **223**, 87-113, doi:10.1111/j.1600-065X.2008.00628.x (2008).

388 Burrows, D. J. *et al.* Animal models of multiple sclerosis: From rodents to zebrafish. *Mult Scler* **25**, 306-324, doi:10.1177/1352458518805246 (2019).

389 Rao, P. & Segal, B. M. in *Autoimmunity: Methods and Protocols* (ed Andras Perl) 363-380 (Humana Press, 2012).

390 Baxter, A. G. The origin and application of experimental autoimmune encephalomyelitis. *Nat Rev Immunol* **7**, 904-912, doi:10.1038/nri2190 (2007).

391 Glatigny, S. & Bettelli, E. Experimental Autoimmune Encephalomyelitis (EAE) as Animal Models of Multiple Sclerosis (MS). *Cold Spring Harb Perspect Med* **8**, doi:10.1101/cshperspect.a028977 (2018).

392 Gold, R., Linington, C. & Lassmann, H. Understanding pathogenesis and therapy of multiple sclerosis via animal models: 70 years of merits and culprits in experimental autoimmune encephalomyelitis research. *Brain* **129**, 1953-1971, doi:10.1093/brain/awl075 (2006).

393 Koritschoner RS, S. F. Induction of paralysis and spinal cord inflammation by immunizing rabbits with human spinal cord tissue. *Z Immunity Exp Therapy* **42**, 217-283 (1925).

394 Rivers, T. M. & Schwentker, F. F. Encephalomyelitis Accompanied by Myelin Destruction Experimentally Produced in Monkeys. *J Exp Med* **61**, 689-702, doi:10.1084/jem.61.5.689 (1935).

395 Rivers, T. M., Sprunt, D. H. & Berry, G. P. Observations on Attempts to Produce Acute Disseminated Encephalomyelitis in Monkeys. *J Exp Med* **58**, 39-53, doi:10.1084/jem.58.1.39 (1933).

396 Einstein, E. R., Robertson, D. M., Dicaprio, J. M. & Moore, W. The isolation from bovine spinal cord of a homogeneous protein with encephalitogenic activity. *J Neurochem* **9**, 353-361, doi:10.1111/j.1471-4159.1962.tb09461.x (1962).
397 Huseby, E. S., Huseby, P. G., Shah, S., Smith, R. & Stadinski, B. D. Pathogenic CD8 T cells in multiple sclerosis and its experimental models. *Front Immunol* **3**, 64, doi:10.3389/fimmu.2012.00064 (2012).
398 Kuchroo, V. K. *et al.* T cell response in experimental autoimmune encephalomyelitis (EAE): role of self and cross-reactive antigens in shaping, tuning, and regulating the autopathogenic T cell repertoire. *Annu Rev Immunol* **20**, 101-123, doi:10.1146/annurev.immunol.20.081701.141316 (2002).
399 Peng, Y. *et al.* Characterization of myelin oligodendrocyte glycoprotein (MOG)35-55-specific CD8+ T cells in experimental autoimmune encephalomyelitis. *Chin Med J (Engl)* **132**, 2934-2940, doi:10.1097/CM9.0000000000000551 (2019).
400 Kurschus, F. C. T cell mediated pathogenesis in EAE: Molecular mechanisms. *Biomed J* **38**, 183-193, doi:10.4103/2319-4170.155590 (2015).
401 Lassmann, H. Pathology of inflammatory diseases of the nervous system: Human disease versus animal models. *Glia* **68**, 830-844, doi:10.1002/glia.23726 (2020).
402 Caravagna, C. *et al.* Diversity of innate immune cell subsets across spatial and temporal scales in an EAE mouse model. *Sci Rep* **8**, 5146, doi:10.1038/s41598-018-22872-y (2018).
403 Giles, D. A., Duncker, P. C., Wilkinson, N. M., Washnock-Schmid, J. M. & Segal, B. M. CNS-resident classical DCs play a critical role in CNS autoimmune disease. *J Clin Invest* **128**, 5322-5334, doi:10.1172/JCI123708 (2018).
404 Aharoni, R., Globerman, R., Eilam, R., Brenner, O. & Arnon, R. Titration of myelin oligodendrocyte glycoprotein (MOG) - Induced experimental autoimmune encephalomyelitis (EAE) model. *J Neurosci Methods* **351**, 108999, doi:10.1016/j.jneumeth.2020.108999 (2021).
405 Rangachari, M. & Kuchroo, V. K. Using EAE to better understand principles of immune function and autoimmune pathology. *J Autoimmun* **45**, 31-39, doi:10.1016/j.jaut.2013.06.008 (2013).
406 Papenfuss, T. L. *et al.* Estriol Generates Tolerogenic Dendritic Cells *In vivo* That Protect against Autoimmunity. *The Journal of Immunology* **186**, 3346-3355, doi:10.4049/jimmunol.1001322 (2011).
407 Benmamar-Badel, A., Owens, T. & Wlodarczyk, A. Protective Microglial Subset in Development, Aging, and Disease: Lessons From Transcriptomic Studies. *Frontiers in immunology* **11**, 430-430, doi:10.3389/fimmu.2020.00430 (2020).
408 Cua, D. J., Hutchins, B., LaFace, D. M., Stohlman, S. A. & Coffman, R. L. Central nervous system expression of IL-10 inhibits autoimmune encephalomyelitis. *J Immunol* **166**, 602-608, doi:10.4049/jimmunol.166.1.602 (2001).
409 Zhang, X. *et al.* IL-10 is involved in the suppression of experimental autoimmune encephalomyelitis by CD25+CD4+ regulatory T cells. *Int Immunol* **16**, 249-256, doi:10.1093/intimm/dxh029 (2004).
410 O'Brien, K., Fitzgerald, D., Rostami, A. & Gran, B. The TLR7 agonist, imiquimod, increases IFN-beta production and reduces the severity of experimental autoimmune encephalomyelitis. *J Neuroimmunol* **221**, 107-111, doi:10.1016/j.jneuroim.2010.01.006 (2010).
411 Takeuchi, C., Yamagata, K. & Takemiya, T. Variation in experimental autoimmune encephalomyelitis scores in a mouse model of multiple sclerosis. *World* **3** (2013).
412 Gandy, K. A. O., Zhang, J., Nagarkatti, P. & Nagarkatti, M. The role of gut microbiota in shaping the relapse-remitting and chronic-progressive forms of multiple sclerosis in mouse models. *Sci Rep* **9**, 6923, doi:10.1038/s41598-019-43356-7 (2019).

413 Johanson, D. M. *et al.* Experimental autoimmune encephalomyelitis is associated with changes of the microbiota composition in the gastrointestinal tract. *Scientific Reports* **10**, 15183, doi:10.1038/s41598-020-72197-y (2020).
414 Mandal, R. K. *et al.* Temporospatial shifts within commercial laboratory mouse gut microbiota impact experimental reproducibility. *BMC Biol* **18**, 83, doi:10.1186/s12915-020-00810-7 (2020).
415 George E. Rainger, H. M. M. *T-cell Trafficking: Methods and Protocols*. Second Edition edn, Vol. 1591 (Humana Press, 2017).
416 Saxer, F. Primary Wandering Cells. *Anat. Hefte* **xix** (1896).
417 Farber, D. L., Yudanin, N. A. & Restifo, N. P. Human memory T cells: generation, compartmentalization and homeostasis. *Nature Reviews Immunology* **14**, 24-35, doi:10.1038/nri3567 (2014).
418 Krummel, M. F., Bartumeus, F. & Gerard, A. T cell migration, search strategies and mechanisms. *Nat Rev Immunol* **16**, 193-201, doi:10.1038/nri.2015.16 (2016).
419 Zlotnik, A. & Yoshie, O. The chemokine superfamily revisited. *Immunity* **36**, 705-716, doi:10.1016/j.immuni.2012.05.008 (2012).
420 Zlotnik, A. & Yoshie, O. Chemokines: A new classification system and their role in immunity. *Immunity* **12**, 121-127, doi:Doi 10.1016/S1074-7613(00)80165-X (2000).
421 Chen, K. *et al.* Chemokines in homeostasis and diseases. *Cell Mol Immunol* **15**, 324-334, doi:10.1038/cmi.2017.134 (2018).
422 Colobran, R., Pujol-Borrell, R., Armengol, M. P. & Juan, M. The chemokine network. I. How the genomic organization of chemokines contains clues for deciphering their functional complexity. *Clin Exp Immunol* **148**, 208-217, doi:10.1111/j.1365-2249.2007.03344.x (2007).
423 Forster, R., Davalos-Misslitz, A. C. & Rot, A. CCR7 and its ligands: balancing immunity and tolerance. *Nat Rev Immunol* **8**, 362-371, doi:10.1038/nri2297 (2008).
424 Moschovakis, G. L. & Forster, R. Multifaceted activities of CCR7 regulate T-cell homeostasis in health and disease. *Eur J Immunol* **42**, 1949-1955, doi:10.1002/eji.201242614 (2012).
425 Ley, K., Laudanna, C., Cybulsky, M. I. & Nourshargh, S. Getting to the site of inflammation: the leukocyte adhesion cascade updated. *Nat Rev Immunol* **7**, 678-689, doi:10.1038/nri2156 (2007).
426 Engelhardt, B. & Ransohoff, R. M. Capture, crawl, cross: the T cell code to breach the blood-brain barriers. *Trends Immunol* **33**, 579-589, doi:10.1016/j.it.2012.07.004 (2012).
427 Duc, D. *et al.* Disrupting Myelin-Specific Th17 Cell Gut Homing Confers Protection in an Adoptive Transfer Experimental Autoimmune Encephalomyelitis. *Cell Rep* **29**, 378-390 e374, doi:10.1016/j.celrep.2019.09.002 (2019).
428 Kuhbandner, K. *et al.* MAdCAM-1-Mediated Intestinal Lymphocyte Homing Is Critical for the Development of Active Experimental Autoimmune Encephalomyelitis. *Front Immunol* **10**, 903, doi:10.3389/fimmu.2019.00903 (2019).
429 Yago, T. *et al.* Catch bonds govern adhesion through L-selectin at threshold shear. *J Cell Biol* **166**, 913-923, doi:10.1083/jcb.200403144 (2004).
430 Nourshargh, S. & Alon, R. Leukocyte migration into inflamed tissues. *Immunity* **41**, 694-707, doi:10.1016/j.immuni.2014.10.008 (2014).
431 Wilson, E. H., Weninger, W. & Hunter, C. A. Trafficking of immune cells in the central nervous system. *J Clin Invest* **120**, 1368-1379, doi:10.1172/JCI41911 (2010).
432 Wolburg, H., Wolburg-Buchholz, K. & Engelhardt, B. Diapedesis of mononuclear cells across cerebral venules during experimental autoimmune encephalomyelitis leaves tight junctions intact. *Acta Neuropathol* **109**, 181-190, doi:10.1007/s00401-004-0928-x (2005).

433 Alon, R. & Feigelson, S. From rolling to arrest on blood vessels: leukocyte tap dancing on endothelial integrin ligands and chemokines at sub-second contacts. *Semin Immunol* **14**, 93-104, doi:10.1006/smim.2001.0346 (2002).

434 Kim, C. H. Crawling of effector T cells on extracellular matrix: role of integrins in interstitial migration in inflamed tissues. *Cellular & molecular immunology* **11**, 1-4, doi:10.1038/cmi.2013.47 (2014).

435 Engelhardt, B. T cell migration into the central nervous system during health and disease: Different molecular keys allow access to different central nervous system compartments. *Clinical and Experimental Neuroimmunology* **1**, 79-93, doi:10.1111/j.1759-1961.2010.009.x (2010).

436 Sewell, D. L. *et al.* Infection with Mycobacterium bovis BCG diverts traffic of myelin oligodendroglial glycoprotein autoantigen-specific T cells away from the central nervous system and ameliorates experimental autoimmune encephalomyelitis. *Clin Diagn Lab Immunol* **10**, 564-572, doi:10.1128/cdli.10.4.564-572.2003 (2003).

437 Lee, J., Reinke, E. K., Zozulya, A. L., Sandor, M. & Fabry, Z. Mycobacterium bovis bacille Calmette-Guerin infection in the CNS suppresses experimental autoimmune encephalomyelitis and Th17 responses in an IFN-gamma-independent manner. *J Immunol* **181**, 6201-6212, doi:10.4049/jimmunol.181.9.6201 (2008).

438 Lippens, C., Garnier, L., Guyonvarc'h, P. M., Santiago-Raber, M. L. & Hugues, S. Extended Freeze-Dried BCG Instructed pDCs Induce Suppressive Tregs and Dampen EAE. *Front Immunol* **9**, 2777, doi:10.3389/fimmu.2018.02777 (2018).

439 Jackson, S. J., Giovannoni, G. & Baker, D. Fingolimod modulates microglial activation to augment markers of remyelination. *J Neuroinflammation* **8**, 76, doi:10.1186/1742-2094-8-76 (2011).

440 Cao, L. *et al.* Siponimod for multiple sclerosis. *Cochrane Database of Systematic Reviews*, doi:10.1002/14651858.Cd013647 (2020).

441 Kappos, L. *et al.* Siponimod versus placebo in secondary progressive multiple sclerosis (EXPAND): a double-blind, randomised, phase 3 study. *Lancet* **391**, 1263-1273, doi:10.1016/S0140-6736(18)30475-6 (2018).

442 Colombo, E. *et al.* Siponimod (BAF312) Activates Nrf2 While Hampering NFkappaB in Human Astrocytes, and Protects From Astrocyte-Induced Neurodegeneration. *Front Immunol* **11**, 635, doi:10.3389/fimmu.2020.00635 (2020).

443 Cook, K. *The Regulatory T-cell Response to Helicobacter pylori Infection* Doctor of Philosophy thesis, University of Nottingham, (2014).

444 Ambrosini, E., Columba-Cabezas, S., Serafini, B., Muscella, A. & Aloisi, F. Astrocytes are the major intracerebral source of macrophage inflammatory protein-3alpha/CCL20 in relapsing experimental autoimmune encephalomyelitis and *in vitro*. *Glia* **41**, 290-300, doi:10.1002/glia.10193 (2003).

445 Arima, Y. *et al.* Regional neural activation defines a gateway for autoreactive T cells to cross the blood-brain barrier. *Cell* **148**, 447-457, doi:10.1016/j.cell.2012.01.022 (2012).

446 Reboldi, A. *et al.* C-C chemokine receptor 6-regulated entry of TH-17 cells into the CNS through the choroid plexus is required for the initiation of EAE. *Nat Immunol* **10**, 514-523, doi:10.1038/ni.1716 (2009).

447 Singh, S. P., Zhang, H. H., Foley, J. F., Hedrick, M. N. & Farber, J. M. Human T cells that are able to produce IL-17 express the chemokine receptor CCR6. *J Immunol* **180**, 214-221, doi:10.4049/jimmunol.180.1.214 (2008).

448 Cook, K. W. *et al.* CCL20/CCR6-mediated migration of regulatory T cells to the *Helicobacter pylori*-infected human gastric mucosa. *Gut* **63**, 1550-1559, doi:10.1136/gutjnl-2013-306253 (2014).

449 Restorick, S. M. *et al.* CCR6(+) Th cells in the cerebrospinal fluid of persons with multiple sclerosis are dominated by pathogenic non-classic Th1 cells and GM-CSF-only-secreting Th cells. *Brain Behav Immun* **64**, 71-79, doi:10.1016/j.bbi.2017.03.008 (2017).

450 Alt, C., Laschinger, M. & Engelhardt, B. Functional expression of the lymphoid chemokines CCL19 (ELC) and CCL 21 (SLC) at the blood-brain barrier suggests their involvement in G-protein-dependent lymphocyte recruitment into the central nervous system during experimental autoimmune encephalomyelitis. *European Journal of Immunology* **32**, 2133-2144, doi:Doi 10.1002/1521-4141(200208)32:8<2133::Aid-Immu2133>3.0.Co;2-W (2002).

451 Mori, Y. *et al.* Early pathological alterations of lower lumbar cords detected by ultrahigh-field MRI in a mouse multiple sclerosis model. *Int Immunol* **26**, 93-101, doi:10.1093/intimm/dxt044 (2014).

452 Elhofy, A., Depaolo, R. W., Lira, S. A., Lukacs, N. W. & Karpus, W. J. Mice deficient for CCR6 fail to control chronic experimental autoimmune encephalomyelitis. *Journal of neuroimmunology* **213**, 91-99, doi:10.1016/j.jneuroim.2009.05.011 (2009).

453 Mony, J. T., Khorooshi, R. & Owens, T. Chemokine receptor expression by inflammatory T cells in EAE. *Front Cell Neurosci* **8**, 187, doi:10.3389/fncel.2014.00187 (2014).

454 Du, X. *et al.* Dynamic tracing of immune cells in an orthotopic gastric carcinoma mouse model using near-infrared fluorescence live imaging. *Exp Ther Med* **4**, 221-225, doi:10.3892/etm.2012.579 (2012).

455 Youniss, F. M. *et al.* Near-infrared imaging of adoptive immune cell therapy in breast cancer model using cell membrane labeling. *PLoS One* **9**, e109162, doi:10.1371/journal.pone.0109162 (2014).

456 Uong, T. N. T. *et al.* Live cell imaging of highly activated natural killer cells against human hepatocellular carcinoma *in vivo*. *Cytotherapy*, doi:https://doi.org/10.1016/j.jcyt.2020.11.004 (2021).

457 Kalchenko, V. *et al.* Use of lipophilic near-infrared dye in whole-body optical imaging of hematopoietic cell homing. *J Biomed Opt* **11**, 050507, doi:10.1117/1.2364903 (2006).

458 Naito, M., Hasegawa, G., Ebe, Y. & Yamamoto, T. Differentiation and function of Kupffer cells. *Medical Electron Microscopy* **37**, 16-28, doi:10.1007/s00795-003-0228-x (2004).

459 Jardine, L. *et al.* Rapid Detection of Dendritic Cell and Monocyte Disorders Using CD4 as a Lineage Marker of the Human Peripheral Blood Antigen-Presenting Cell Compartment. *Frontiers in Immunology* **4**, doi:10.3389/fimmu.2013.00495 (2013).

460 Berer, K., Boziki, M. & Krishnamoorthy, G. Selective accumulation of pro-inflammatory T cells in the intestine contributes to the resistance to autoimmune demyelinating disease. *PLoS One* **9**, e87876, doi:10.1371/journal.pone.0087876 (2014).

461 Rothhammer, V. *et al.* Th17 lymphocytes traffic to the central nervous system independently of alpha4 integrin expression during EAE. *J Exp Med* **208**, 2465-2476, doi:10.1084/jem.20110434 (2011).

462 Beightol, R. W. & Baker, W. J. Labeling autologous leukocytes with indium-111 oxine. *Am J Hosp Pharm* **37**, 847-850 (1980).

463 Troy, T., Jekic-McMullen, D., Sambucetti, L. & Rice, B. Quantitative comparison of the sensitivity of detection of fluorescent and bioluminescent reporters in animal models. *Mol Imaging* **3**, 9-23, doi:10.1162/153535004773861688 (2004).

464 Inoue, Y., Izawa, K., Kiryu, S., Tojo, A. & Ohtomo, K. Diet and abdominal autofluorescence detected by *in vivo* fluorescence imaging of living mice. *Mol Imaging* **7**, 21-27 (2008).

465 Baumann, N. & Pham-Dinh, D. Biology of oligodendrocyte and myelin in the mammalian central nervous system. *Physiol Rev* **81**, 871-927, doi:10.1152/physrev.2001.81.2.871 (2001).

466 Kuhn, S., Gritti, L., Crooks, D. & Dombrowski, Y. Oligodendrocytes in Development, Myelin Generation and Beyond. *Cells* **8**, 1424, doi:10.3390/cells8111424 (2019).

467 Virchow, R. Ueber das ausgebreitete Vorkommen einer dem Nervenmark analogen substanz in den tierischen Geweben. *Virchows Arch Pathol Anat* **6** (1854).

468 Rı´o-Hortega, P. o. d. Histogenesis y evolucion normal; exodo y distribucion regional de la microglia. *Memor Real Soc Esp Hist Nat* **11**, 213-268 (1921).

469 Rı´o-Hortega, P. o. d. Tercera aportacion al conocimiento morfologico e interpretacion funcional de la oligodendroglia. *Memor Real Soc Esp Hist Nat* **14**, 5-122 (1928).

470 Perez-Cerda, F., Sanchez-Gomez, M. V. & Matute, C. Pio del Rio Hortega and the discovery of the oligodendrocytes. *Front Neuroanat* **9**, 92, doi:10.3389/fnana.2015.00092 (2015).

471 Simons, M. & Nave, K. A. Oligodendrocytes: Myelination and Axonal Support. *Cold Spring Harb Perspect Biol* **8**, a020479, doi:10.1101/cshperspect.a020479 (2015).

472 Philips, T. & Rothstein, J. D. Oligodendroglia: metabolic supporters of neurons. *J Clin Invest* **127**, 3271-3280, doi:10.1172/JCI90610 (2017).

473 Frühbeis, C. *et al.* Oligodendrocyte-derived exosomes promote axonal transport and axonal long-term maintenance. *bioRxiv*, 2019.2012.2020.884171, doi:10.1101/2019.12.20.884171 (2020).

474 Kramer-Albers, E. M. Extracellular vesicles in the oligodendrocyte microenvironment. *Neurosci Lett* **725**, 134915, doi:10.1016/j.neulet.2020.134915 (2020).

475 Dimou, L. & Simons, M. Diversity of oligodendrocytes and their progenitors. *Curr Opin Neurobiol* **47**, 73-79, doi:10.1016/j.conb.2017.09.015 (2017).

476 von Bartheld, C. S., Bahney, J. & Herculano-Houzel, S. The search for true numbers of neurons and glial cells in the human brain: A review of 150 years of cell counting. *J Comp Neurol* **524**, 3865-3895, doi:10.1002/cne.24040 (2016).

477 Valerio-Gomes, B., Guimaraes, D. M., Szczupak, D. & Lent, R. The Absolute Number of Oligodendrocytes in the Adult Mouse Brain. *Front Neuroanat* **12**, 90, doi:10.3389/fnana.2018.00090 (2018).

478 Pribyl, T. M., Campagnoni, C., Kampf, K., Handley, V. W. & Campagnoni, A. T. The major myelin protein genes are expressed in the human thymus. *J Neurosci Res* **45**, 812-819, doi:10.1002/(SICI)1097-4547(19960915)45:6<812::AID-JNR18>3.0.CO;2-X (1996).

479 Salzer, J. L., Holmes, W. P. & Colman, D. R. The amino acid sequences of the myelin-associated glycoproteins: homology to the immunoglobulin gene superfamily. *J Cell Biol* **104**, 957-965, doi:10.1083/jcb.104.4.957 (1987).

480 Galloway, D. A., Gowing, E., Setayeshgar, S. & Kothary, R. Inhibitory milieu at the multiple sclerosis lesion site and the challenges for remyelination. *Glia* **68**, 859-877, doi:10.1002/glia.23711 (2020).

481 Emery, B. Regulation of oligodendrocyte differentiation and myelination. *Science* **330**, 779-782, doi:10.1126/science.1190927 (2010).

482 Yeung, M. S. *et al.* Dynamics of oligodendrocyte generation and myelination in the human brain. *Cell* **159**, 766-774, doi:10.1016/j.cell.2014.10.011 (2014).

483 de Hoz, L. & Simons, M. The emerging functions of oligodendrocytes in regulating neuronal network behaviour. *Bioessays* **37**, 60-69, doi:10.1002/bies.201400127 (2015).
484 Liang, P. & Le, W. Role of autophagy in the pathogenesis of multiple sclerosis. *Neuroscience Bulletin* **31**, 435-444, doi:10.1007/s12264-015-1545-5 (2015).
485 Misrielal, C., Mauthe, M., Reggiori, F. M. & Eggen, B. J. Autophagy in multiple sclerosis: Two sides of the same coin. *Frontiers in cellular neuroscience* **14**, 388 (2020).
486 Mayo, L., Quintana, F. J. & Weiner, H. L. The innate immune system in demyelinating disease. *Immunological Reviews* **248**, 170-187, doi:https://doi.org/10.1111/j.1600-065X.2012.01135.x (2012).
487 Kamil, K., Yazid, M. D., Idrus, R. B. H., Das, S. & Kumar, J. Peripheral Demyelinating Diseases: From Biology to Translational Medicine. *Front Neurol* **10**, 87-87, doi:10.3389/fneur.2019.00087 (2019).
488 Cao-Lormeau, V. M. *et al.* Guillain-Barre Syndrome outbreak associated with Zika virus infection in French Polynesia: a case-control study. *Lancet* **387**, 1531-1539, doi:10.1016/S0140-6736(16)00562-6 (2016).
489 van den Berg, B. *et al.* Guillain-Barre syndrome associated with preceding hepatitis E virus infection. *Neurology* **82**, 491-497, doi:10.1212/WNL.0000000000000111 (2014).
490 Brannagan, T. H., 3rd & Zhou, Y. HIV-associated Guillain-Barre syndrome. *J Neurol Sci* **208**, 39-42, doi:10.1016/s0022-510x(02)00418-5 (2003).
491 Bitan, M. *et al.* Early-onset Guillain-Barre syndrome associated with reactivation of Epstein-Barr virus infection after nonmyeloablative stem cell transplantation. *Clin Infect Dis* **39**, 1076-1078, doi:10.1086/424015 (2004).
492 Islam, B. *et al.* Guillain-Barre syndrome following varicella-zoster virus infection. *Eur J Clin Microbiol Infect Dis* **37**, 511-518, doi:10.1007/s10096-018-3199-5 (2018).
493 Vellozzi, C., Iqbal, S. & Broder, K. Guillain-Barre syndrome, influenza, and influenza vaccination: the epidemiologic evidence. *Clin Infect Dis* **58**, 1149-1155, doi:10.1093/cid/ciu005 (2014).
494 Arnaud, S., Budowski, C., Ng Wing Tin, S. & Degos, B. Post SARS-CoV-2 Guillain-Barre syndrome. *Clin Neurophysiol* **131**, 1652-1654, doi:10.1016/j.clinph.2020.05.003 (2020).
495 Toscano, G. *et al.* Guillain-Barre Syndrome Associated with SARS-CoV-2. *N Engl J Med* **382**, 2574-2576, doi:10.1056/NEJMc2009191 (2020).
496 Zhao, H., Shen, D., Zhou, H., Liu, J. & Chen, S. Guillain-Barre syndrome associated with SARS-CoV-2 infection: causality or coincidence? *Lancet Neurol* **19**, 383-384, doi:10.1016/S1474-4422(20)30109-5 (2020).
497 Ebrahim Soltani, Z., Rahmani, F. & Rezaei, N. Autoimmunity and cytokines in Guillain-Barre syndrome revisited: review of pathomechanisms with an eye on therapeutic options. *Eur Cytokine Netw* **30**, 1-14, doi:10.1684/ecn.2019.0424 (2019).
498 Chiba, S. *et al.* An antibody to VacA of *Helicobacter pylori* in cerebrospinal fluid from patients with Guillain-Barre syndrome. *J Neurol Neurosurg Psychiatry* **73**, 76-78, doi:10.1136/jnnp.73.1.76 (2002).
499 Dardiotis, E. *et al.* Association between *Helicobacter pylori* infection and Guillain-Barre Syndrome: A meta-analysis. *Eur J Clin Invest* **50**, e13218, doi:10.1111/eci.13218 (2020).
500 Fukuhara, S. *et al.* Mucosal expression of aquaporin-4 in the stomach of histamine type 2 receptor knockout mice and *Helicobacter pylori*-infected mice. *J Gastroenterol Hepatol* **29 Suppl 4**, 53-59, doi:10.1111/jgh.12771 (2014).

501 Wei, L. *et al.* Association of anti-*Helicobacter pylori* neutrophil-activating protein antibody response with anti-aquaporin-4 autoimmunity in Japanese patients with multiple sclerosis and neuromyelitis optica. *Multiple Sclerosis Journal* **15**, 1411-1421, doi:10.1177/1352458509348961 (2009).

502 Long, Y. *et al. Helicobacter pylori* infection in Neuromyelitis Optica and Multiple Sclerosis. *Neuroimmunomodulation* **20**, 107-112, doi:10.1159/000345838 (2013).

503 Kountouras, J. *et al.* Aquaporin 4, *Helicobacter pylori* and potential implications for neuromyelitis optica. *J Neuroimmunol* **263**, 162-163, doi:10.1016/j.jneuroim.2013.06.003 (2013).

504 Kuhlmann, T. *et al.* Differentiation block of oligodendroglial progenitor cells as a cause for remyelination failure in chronic multiple sclerosis. *Brain* **131**, 1749-1758, doi:10.1093/brain/awn096 (2008).

505 Motavaf, M., Sadeghizadeh, M. & Javan, M. Attempts to Overcome Remyelination Failure: Toward Opening New Therapeutic Avenues for Multiple Sclerosis. *Cell Mol Neurobiol* **37**, 1335-1348, doi:10.1007/s10571-017-0472-6 (2017).

506 Gruchot, J. *et al.* The Molecular Basis for Remyelination Failure in Multiple Sclerosis. *Cells* **8**, 825, doi:10.3390/cells8080825 (2019).

507 Chang, A., Tourtellotte, W. W., Rudick, R. & Trapp, B. D. Premyelinating oligodendrocytes in chronic lesions of multiple sclerosis. *N Engl J Med* **346**, 165-173, doi:10.1056/NEJMoa010994 (2002).

508 Hartung, H. P. *et al.* Inflammatory mediators in demyelinating disorders of the CNS and PNS. *J Neuroimmunol* **40**, 197-210, doi:10.1016/0165-5728(92)90134-7 (1992).

509 de Jong, J. M., Wang, P., Oomkens, M. & Baron, W. Remodeling of the interstitial extracellular matrix in white matter multiple sclerosis lesions: Implications for remyelination (failure). *J Neurosci Res* **98**, 1370-1397, doi:10.1002/jnr.24582 (2020).

510 Lombardi, M. *et al.* Detrimental and protective action of microglial extracellular vesicles on myelin lesions: astrocyte involvement in remyelination failure. *Acta Neuropathol* **138**, 987-1012, doi:10.1007/s00401-019-02049-1 (2019).

511 Traiffort, E., Kassoussi, A., Zahaf, A. & Laouarem, Y. Astrocytes and Microglia as Major Players of Myelin Production in Normal and Pathological Conditions. *Front Cell Neurosci* **14**, 79, doi:10.3389/fncel.2020.00079 (2020).

512 Baaklini, C. S., Rawji, K. S., Duncan, G. J., Ho, M. F. S. & Plemel, J. R. Central Nervous System Remyelination: Roles of Glia and Innate Immune Cells. *Front Mol Neurosci* **12**, 225, doi:10.3389/fnmol.2019.00225 (2019).

513 Peferoen, L., Kipp, M., van der Valk, P., van Noort, J. M. & Amor, S. Oligodendrocyte-microglia cross-talk in the central nervous system. *Immunology* **141**, 302-313, doi:10.1111/imm.12163 (2014).

514 Li, Q. & Barres, B. A. Microglia and macrophages in brain homeostasis and disease. *Nat Rev Immunol* **18**, 225-242, doi:10.1038/nri.2017.125 (2018).

515 Giunti, D., Parodi, B., Cordano, C., Uccelli, A. & Kerlero de Rosbo, N. Can we switch microglia's phenotype to foster neuroprotection? Focus on multiple sclerosis. *Immunology* **141**, 328-339, doi:10.1111/imm.12177 (2014).

516 Hickman, S., Izzy, S., Sen, P., Morsett, L. & El Khoury, J. Microglia in neurodegeneration. *Nat Neurosci* **21**, 1359-1369, doi:10.1038/s41593-018-0242-x (2018).

517 Kotter, M. R., Li, W. W., Zhao, C. & Franklin, R. J. Myelin impairs CNS remyelination by inhibiting oligodendrocyte precursor cell differentiation. *J Neurosci* **26**, 328-332, doi:10.1523/JNEUROSCI.2615-05.2006 (2006).

518 Franklin, R. J. M. & Ffrench-Constant, C. Regenerating CNS myelin - from mechanisms to experimental medicines. *Nat Rev Neurosci* **18**, 753-769, doi:10.1038/nrn.2017.136 (2017).
519 Rawji, K. S., Mishra, M. K. & Yong, V. W. Regenerative Capacity of Macrophages for Remyelination. *Front Cell Dev Biol* **4**, 47, doi:10.3389/fcell.2016.00047 (2016).
520 Doring, A. *et al.* Stimulation of monocytes, macrophages, and microglia by amphotericin B and macrophage colony-stimulating factor promotes remyelination. *J Neurosci* **35**, 1136-1148, doi:10.1523/JNEUROSCI.1797-14.2015 (2015).
521 Stratoulias, V., Venero, J. L., Tremblay, M. E. & Joseph, B. Microglial subtypes: diversity within the microglial community. *EMBO J* **38**, e101997, doi:10.15252/embj.2019101997 (2019).
522 Wang, J. *et al.* Targeting Microglia and Macrophages: A Potential Treatment Strategy for Multiple Sclerosis. *Front Pharmacol* **10**, 286, doi:10.3389/fphar.2019.00286 (2019).
523 Peferoen, L. A. *et al.* Activation status of human microglia is dependent on lesion formation stage and remyelination in multiple sclerosis. *J Neuropathol Exp Neurol* **74**, 48-63, doi:10.1097/NEN.0000000000000149 (2015).
524 Mitchell, D. M., Sun, C., Hunter, S. S., New, D. D. & Stenkamp, D. L. Regeneration associated transcriptional signature of retinal microglia and macrophages. *Sci Rep* **9**, 4768, doi:10.1038/s41598-019-41298-8 (2019).
525 Voss, E. V. *et al.* Characterisation of microglia during de- and remyelination: can they create a repair promoting environment? *Neurobiol Dis* **45**, 519-528, doi:10.1016/j.nbd.2011.09.008 (2012).
526 Zaiss, D. M., Minutti, C. M. & Knipper, J. A. Immune- and non-immune-mediated roles of regulatory T-cells during wound healing. *Immunology* **157**, 190-197, doi:10.1111/imm.13057 (2019).
527 Zhang, C. *et al.* 'Repair' Treg Cells in Tissue Injury. *Cell Physiol Biochem* **43**, 2155-2169, doi:10.1159/000484295 (2017).
528 Ito, M., Komai, K., Nakamura, T., Srirat, T. & Yoshimura, A. Tissue regulatory T cells and neural repair. *Int Immunol* **31**, 361-369, doi:10.1093/intimm/dxz031 (2019).
529 Burzyn, D. *et al.* A special population of regulatory T cells potentiates muscle repair. *Cell* **155**, 1282-1295, doi:10.1016/j.cell.2013.10.054 (2013).
530 Nosbaum, A. *et al.* Cutting Edge: Regulatory T Cells Facilitate Cutaneous Wound Healing. *J Immunol* **196**, 2010-2014, doi:10.4049/jimmunol.1502139 (2016).
531 Weirather, J. *et al.* Foxp3+ CD4+ T cells improve healing after myocardial infarction by modulating monocyte/macrophage differentiation. *Circ Res* **115**, 55-67, doi:10.1161/CIRCRESAHA.115.303895 (2014).
532 Lin, C. G., Chen, C. C., Leu, S. J., Grzeszkiewicz, T. M. & Lau, L. F. Integrin-dependent functions of the angiogenic inducer NOV (CCN3): implication in wound healing. *J Biol Chem* **280**, 8229-8237, doi:10.1074/jbc.M404903200 (2005).
533 Perbal, B. NOV story: the way to CCN3. *Cell Commun Signal* **4**, 3, doi:10.1186/1478-811X-4-3 (2006).
534 Perbal, B. CCN proteins: A centralized communication network. *J Cell Commun Signal* **7**, 169-177, doi:10.1007/s12079-013-0193-7 (2013).
535 Riser, B. L. *et al.* CCN3/CCN2 regulation and the fibrosis of diabetic renal disease. *J Cell Commun Signal* **4**, 39-50, doi:10.1007/s12079-010-0085-z (2010).
536 Lin, C. G. *et al.* CCN3 (NOV) is a novel angiogenic regulator of the CCN protein family. *J Biol Chem* **278**, 24200-24208, doi:10.1074/jbc.M302028200 (2003).
537 McCallum, L. & Irvine, A. E. CCN3--a key regulator of the hematopoietic compartment. *Blood Rev* **23**, 79-85, doi:10.1016/j.blre.2008.07.002 (2009).

538 Kohm, A. P., Carpentier, P. A., Anger, H. A. & Miller, S. D. Cutting edge: CD4+CD25+ regulatory T cells suppress antigen-specific autoreactive immune responses and central nervous system inflammation during active experimental autoimmune encephalomyelitis. *J Immunol* **169**, 4712-4716, doi:10.4049/jimmunol.169.9.4712 (2002).

539 Lee, P. W., Severin, M. E. & Lovett-Racke, A. E. TGF-beta regulation of encephalitogenic and regulatory T cells in multiple sclerosis. *Eur J Immunol* **47**, 446-453, doi:10.1002/eji.201646716 (2017).

540 Hvilsted Nielsen, H., Toft-Hansen, H., Lambertsen, K. L., Owens, T. & Finsen, B. Stimulation of adult oligodendrogenesis by myelin-specific T cells. *Am J Pathol* **179**, 2028-2041, doi:10.1016/j.ajpath.2011.06.006 (2011).

541 Lloyd, A. F. & Miron, V. E. The pro-remyelination properties of microglia in the central nervous system. *Nat Rev Neurol* **15**, 447-458, doi:10.1038/s41582-019-0184-2 (2019).

542 Panduro, M., Benoist, C. & Mathis, D. Tissue Tregs. *Annu Rev Immunol* **34**, 609-633, doi:10.1146/annurev-immunol-032712-095948 (2016).

543 de la Vega Gallardo, N. *et al.* Dynamic CCN3 expression in the murine CNS does not confer essential roles in myelination or remyelination. *Proc Natl Acad Sci U S A* **117**, 18018-18028, doi:10.1073/pnas.1922089117 (2020).

544 Naughton, M. *et al.* CCN3 is dynamically regulated by treatment and disease state in multiple sclerosis. *J Neuroinflammation* **17**, 349, doi:10.1186/s12974-020-02025-7 (2020).

545 Bjornevik, K. *et al.* Longitudinal analysis reveals high prevalence of Epstein-Barr virus associated with multiple sclerosis. *Science* **375**, 296-301, doi:doi:10.1126/science.abj8222 (2022).

546 Robinson, W. H. & Steinman, L. Epstein-Barr virus and multiple sclerosis. *Science* **375**, 264-265, doi:doi:10.1126/science.abm7930 (2022).

547 Shabani, Z. Demyelination as a result of an immune response in patients with COVID-19. *Acta Neurol Belg* **121**, 859-866, doi:10.1007/s13760-021-01691-5 (2021).